厚生労働科学研究費補助金
化学物質リスク研究事業

発達期における総合的な
遅発性神経毒性試験法の開発
(H28-化学--一般-003)

平成 28 年度総括・分担研究報告書

研究代表者　諫田 泰成

平成 29（2017）年 3 月

目　　次

I.　総括研究報告

厚生労働科学研究費補助金（化学物質リスク研究事業）
総括研究報告書

発達期における統合的な遅発性神経毒性試験法の開発

研究代表者　　国立医薬品食品衛生研究所　薬理部第二室長
諫田　泰成

＜全体要旨＞
近年、自閉症など発達障害が急速に増加し、社会問題となっている。その原因の一つは発達期における化学物質の曝露とされる。発達期の神経系は成体と比較して化学物質に対する感受性が高く、健康被害が長期間あるいは遅発性に生じることが考えられ、子どもの健康影響評価法の確立が強く望まれる。
現在、OECDやEPAによって、妊娠ラットを用いる発達神経毒性試験ガイドラインが制定されているが、試験方法が複雑で、試験期間は1年以上、動物数は720にも及び経費も膨大である。さらに、日本ではこのようなガイドラインは未整備である。そこで我々は、発達期における細胞機能異常と神経回路異常の毒性作用メカニズムに基づいて、新たにスループット性の高い発達神経毒性評価スキームを作製し、評価指標の選定やプロトコルの最適化を行うことにより統合的な発達神経毒性試験法の開発を行っている。
ヒトiPS細胞（神経発生モデル細胞の評価系）やラット小脳皮質およびラット海馬（生後初期における遅発性毒性評価系）を用いて、化学物質の影響評価に関する評価指標の最適化を行った。また、ラット海馬ニューロンを用いた、スループット性の高いスクリーニング系の構築に着手し、新たに、HESI NeuToxと国際バリデーションの議論を開始した。
また、バルプロ酸などのメカニズムを理解する上で、妊娠中の母親への摂取栄養の程度や栄養成分の偏りによって胎児のエピゲノムに影響し生後の発育や疾患の発症に寄与する、というDoHaDについて調査研究を行った。
今後は、最適化された評価指標をもとに統合的な遅発性毒性評価系のプロトコル最適化を行いながら、国際連携のもと試験法開発を目指す。

＜研究課題一覧＞
諫田泰成（国立衛研）
「ヒト幹細胞の分化による評価法の開発」

宇佐見誠（国立衛研）
「神経堤細胞の機能解析による評価法の開発」

山崎大樹（国立衛研）
「海馬ニューロンを用いた神経ネットワークによる評価法の開発」

吉田祥子（豊橋技科大）
「生後小脳の神経回路の機能的影響による評価法の開発」

上野晋（産業医大）
「幼若期海馬の神経回路機能による評価法の開発」

秦健一郎（成育医療センター）
「既存の毒性データおよびヒトデータとの検証」

A. 研究目的

本研究では、胎児期の神経発生モデル細胞を用いたスクリーニングを行い（細胞評価グループ）、さらに生後の成熟期における遅発性神経毒性の早期予測評価法（神経ネットワーク評価グループ）を検証し、統合的な新規試験法として開発を目指す。現在進行中のHESI NeuTox との国際連携をもとに、HESIリストの中から既に評価した化学物質と作用の異なる陽性対照物質および陰性対照物質を選定して検証する。

上記 2 グループに毒性データ検証グループを加えた 3 グループの密な連携により、我々が提案した発達期に対応した化学物質の発達神経毒性に関する新規試験法として提案を目指す。本試験法により化学物質規制行政への応用が期待される。

B. 研究方法

詳細は各分担報告書を参照のこと。

C. 研究結果

以下に、各分担研究者の詳細を記載する。

【①ヒト幹細胞の分化による評価法】

ヒト iPS 細胞を用いて、化学物質の影響評価に関する評価指標の最適化を行った。その結果、遅発性神経毒性が懸念される農薬であるクロルピリホス曝露により、ヒト iPS 細胞における神経分化の抑制が認められた。分化抑制メカニズムとして、Mfn1 分解を介したミトコンドリアの形態異常による ATP 産生の低下を見いだした。この結果はすでに論文として報告済である。以上より、ヒト iPS 細胞におけるミトコンドリア機能を指標にして、成長期における化学物質の発達神経毒性を評価できる可能性が示唆された。

【②神経ネットワークによる評価法】

スループット性および再現性の高い海馬ニューロンを用いた神経スパイクによる神経活動評価系の開発を行うため、米国 EPA の Timothy J Shafer 教授との共同研究体制を構築し各種条件の検討を行った。また、HESI NeuTox の多点電極システム（MEA）サブチームに参加し、プレバリデーションの議論を開始した。これまでに再現性の高い結果が得られていることから、今後は陽性・陰性対照物質を評価し、他の評価系で得られている結果と比較することで評価系の妥当性を検証する。

【③生後小脳の神経回路】

遅発性神経毒性が考えられる化学物質であるバルプロ酸、クロルピリホスを胎生期の動物に投与し、生後の神経回路発達の変化を小脳神経細胞の突起伸展と小脳構造の変化、動物の行動変化から定量化して示した。バルプロ酸に関する結果は、販売元の製薬企業に情報提供した。小脳の形態形成は生後早期の遅発性毒性を予測可能な指標となりうることが示唆された。

【④幼若期海馬の神経回路機能】

遅発性神経毒性試験手法の妥当性を調べる目的で、発達神経毒性の詳細が不明であった産業化学物質である 1BP について検討した結果、神経回路興奮性の亢進をもたらすことから、1BP が発達神経毒性を有する可能性が示唆された。以上より、発達神経毒性を示す化学物質に加えて産業化学物質についても生後早期の海馬神経回路機能評価が発達神経毒性の評価指標として有用となる可能性が確認された。

【⑤既存毒性データ、ヒトデータとの検証】

陽性対照物質バルプロ酸などの作用メカニズムを明らかにするため、動物実験を中心に DoHaD のメカニズムについて文献調査を行った。また、ヒトのエピゲノムデータに関しても調査を開始した。調査研究により、胎児期あるいは新生児期に受けた影響により、ゲノムのメチル化が生じ生後長期に渡って継続し、疾患リスクとなる可能性が示唆された。

D. 考察

本研究では、ヒト iPS 細胞やラット小脳皮質およびラット海馬を用いて、化学物質の影響評価に関する評価指標の最適化を行い、各評価系において化学物質の発達神経毒性を評価できる可能性の高い指標を決定した。

また、ラット海馬ニューロンを用いた、スループット性の高いスクリーニング系の構築は、HESI NeuTox において国際検証試験の議論が進んでおり、我々も国際電話会議、対面会議に参加して議論を行っている。国際連携のもと引き続き MEA プロトコルの最適化を行い、予測性の評価などに取り組む必要がある。

現在、世界的な流れは in vivo から in vitro 試験法となっているが、本研究データと動物データや現行ガイドラインと比較検討し、有用性や検出限界などの検討も必要である。今後、研究班が一体となり統合的な遅発性毒性評価系の構築に向けて取り組みたい。

E. 結論

胎児期、成熟期において陽性対照となる化学物質を用いて、試験法の確立に向けて安定な評価指標を選定した。また、ラット海馬ニューロンを用いた、スループット性の高いスクリーニング系を新たに構築した。また、バルプロ酸のデータをもとに DoHaD の調査研究を行った。

F. 研究発表

分担研究者の報告書に示すように、多数の論文発表および学会発表を行った。

II.　分担研究報告

厚生労働科学研究費補助金（化学物質リスク研究事業）
分担研究報告書

ヒト幹細胞の分化による評価法の開発

研究代表者　　国立医薬品食品衛生研究所薬理部　第二室長
諫田　泰成

要旨
ヒト iPS 細胞を用いて、化学物質の影響評価に関する評価指標の最適化を行った。その結果、遅発性神経毒性が懸念される農薬であるクロルピリホス（CPF）曝露により、ヒト iPS 細胞における神経分化の抑制が認められた。分化抑制メカニズムとして、Mfn1 分解を介したミトコンドリアの形態異常による ATP 産生の低下を見いだした。以上より、ヒト iPS 細胞におけるミトコンドリア機能を指標にして、成長期における化学物質の発達神経毒性を評価できる可能性が示唆された。

A. 研究目的

近年、子供の学習障害や自閉症などの発達障害が増加しているが、その原因の一つとして環境中の化学物質の関与が指摘されている（Landrigan et al., *Environ. Health Perspect. Med.*, 2012）。ヒト iPS 細胞はヒト発生過程を in vitro で模倣できることから、化学物質の神経毒性を検出できる可能性が考えられる。しかし、評価系としての手法は確立されていない。

本研究では、化学物質の発達期における毒性を評価するために、ヒト iPS 細胞を用いて発達神経毒性を評価できるか検討を行った。評価系の構築には、HESI と共有している発達毒性が懸念される陽性対照物質のリストから、農薬であるクロルピリホスを選択した。

本年度は、ヒト iPS 細胞における毒性メカニズムの検討を行い、毒性評価における有用性を検証した。また、HESI NeuTox のメンバーとなり、国際検証試験の議論を開始した。

B. 研究方法

1. 細胞

ヒト iPS 細胞株 253G1（Nakagawa et al., *Nat. Biotechnol.*, 2008）は、TeSR-E8 培地（Stem Cell Technologies）にてフィーダーフリー[マトリゲル（BD Biosciences）コート]の条件で培養した。

2. ミトコンドリアの形態

細胞を 4%PFA で固定後、ミトコンドリアを 50 nM の MitoTracker Red CMXRos (Cell Signaling Technology) および核を DAPI により染色し、confocal 顕微鏡（Nikon A1）で観察した。点状のミトコンドリアが 10%未満の細胞数を計測した（Fan et al., *Free Radic. Biol. Med.*, 2010）。

3. ミトコンドリア膜電位

細胞を JC10（Life Technologies）で染色したのち FACS ARIAII（BD Biosciences）を用いて計測した。

4. ATP 量

ルシフェラーゼ法に基づいて定量した。

5. qPCR

TRIzol 試薬（Life Technologies）を用いて RNA を抽出した。QuantiTect SYBR Green RT-PCR Kit（QIAGEN）、ABI PRISM 7900HT を用いて qPCR を行った。

6. shRNA を用いたノックダウン

shRNA 導入はレンチウイルス（SIGMA）を用いた。ヒト iPS 細胞にウイルスを moi 1 で感染させた。さらに 24 時間後にピューロマイシンを添加して感染細胞のセレクションを行った。

7. 神経分化誘導

Dual smad 阻害法（Chambers et al., *Nat. Biotechnol.*, 2012）を用いて、BMP シグナル阻害剤 LDN193189（Wako）及び Activin シグナル阻害剤 SB431542（Wako）により iPS 細胞を神経外胚葉から神経前駆細胞へと分化させた。

C. 研究結果

1. ヒト iPS 細胞のミトコンドリア機能に対する CPF の作用

発達神経毒性が懸念される CPF を用いて iPS 細胞への影響を検討した。CPF 曝露は細胞内 ATP 含量の低下、ミトコンドリア膜電位の低下およびミトコンドリア形態異常を引き起こした（図 1）。したがって、iPS 細胞において CPF はミトコンドリア機能異常を引き起こすことが示唆された。

次に、ミトコンドリアの形態制御因子の発現について検討した。分裂因子（Drp1, Fis1）および融合因子（Mfn1, Mfn2, Opa1）の遺伝子発現には影響がなかった（図 2A）。一方で、CPF 暴露によって Mfn1 のタンパク分解が誘導されることを見出した（図 2B, C）。すでに報告したように shRNA を用いて Mfn1 をノックダウンするとミトコンドリア形態異常が観察されることから、CPF によるミトコンドリア機能の低下はミトコンドリア融合タンパク質の分解によって誘導されることが示唆された。

2. ヒト iPS 細胞の神経分化に対する CPF の作用

CPF が iPS 細胞の分化に及ぼす影響を調べるために、Dual smad 阻害法を用いて、iPS 細胞の神経分化誘導を行った。CPF 曝露した iPS 細胞に神経分化刺激を与えた結果、神経外胚葉のマーカーである PAX6（Manuel et al., *Front. Cell Neurosci.*, 2015）, FOXG1（Shen et al., *Hippocampus*, 2006）や神経前駆細胞のマーカーである NCAM1（Polo-Parada et al., *J. Neurosci.*, 2004）の発現低下が認められた（図 3）。したがって、CPF は iPS 細胞の初期の神経分化誘導を阻害することが明らかとなった。

次に CPF による神経分化の阻害がミトコンドリアの機能異常を介しているかを明らかにするために、Mfn1 をノックダウンした iPS 細胞を用いて、神経分化誘導を行った（図 4）。その結果、Mfn1 ノックダウンにより、CPF 曝露と同様に、PAX6, FOXG1, NCAM1 の発現低下が認められた（図 4D）。したがって、CPF による神経分化の阻害は、Mfn1 分解を介したミトコンドリア機能異常により引き起こされることが示唆された。

3. CPF の神経分化阻害における Erk シグナルの関与

ミトコンドリア機能の破綻は Erk のリン酸化を引き起こすことが報告されている（Yu et al., *Toxicol. Appl. Pharmacol.*, 2012）。一方、Erk のリン酸化によって PAX6 の発現が抑制され神経分化が阻害されるという報告もある（Greber et al., *EMBO J.*, 2011）。したがって、CPF による神経分化阻害の経路として Erk シグナルの関与が考えられる。まず CPF の作用に対する Erk シグナルの関与を調べるために、ヒト iPS 細胞に CPF を曝露した結果、Erk のリン酸化レベルの亢進が認められた。またこのリン酸化は Erk 阻害剤 U0126 処理により消失した（図 5A, B）。さらに CPF 曝露による PAX6 の低下は U0126 処理により回復した（図 5C）。

次に CPF により引き起こされる Erk シグナルがミトコンドリアの機能異常を介しているかを明らかにするために、Mfn1 をノックダウンした iPS 細胞において Erk のリン酸化を調べた。その結果、Mfn1 ノックダウンにより、Erk リン酸化レベルの亢進が認められた。またこのリン酸化は U0126 処理で消失した（図 6A, B）。さらに Mfn1 ノックダウンによる PAX6 の低下は U0126 処理により回復した（図 6C）。したがって、CPF によるミトコンドリア機能異常を介した神経分化の阻害は Erk シグナルが関与していることが示唆された（図 7）。

以上より、iPS 細胞において TBT と同様に、CPF はミトコンドリア機能異常を引き起こすことが明らかになった。また、iPS 細胞で ATP 量、ミトコンドリア膜電位・形態さらには神経分化といった指標を用いることにより、発達神経毒性を評価できる可能性が示唆された。

D. 考察

本研究では、ヒト iPS 細胞を用いて、これまで見出した指標（ATP 産生量、ミトコンドリア膜電位・形態）により発達神経毒性が懸念される化学物質の影響を評価できることを明らかにした。特に、iPS 細胞で使用した CPF は血中に存在しうる濃度（Huen et al., *Environ. Res.*, 2012）がアッセイに使用した 30 μM であり、本アッセイ系は非常に好感度であると考えられた。

今回、iPS 細胞を用いて CPF の毒性作用点として、Mfn1 分解を介したミトコンドリアの分裂による ATP 産生の低下を見出し、TBT と同様のミトコンドリア毒性を示すことを明らかにした（論文発表 1, 2）。発達神経毒性を示す化学物質の毒性評価においてミトコンドリアの機能異常は有効であり、幅広く

応用できる可能性が期待される。今後もiPS細胞において、発達神経毒性が懸念される被験物質を増やすことで、こうしたミトコンドリアを指標とした毒性マーカーの探索や評価法の検討を行い、簡便で再現性のある評価法の確立を目指す。

また、研究代表者として、HESI NeuTox の国際検証試験の議論を新たに開始して、連携を取りながら試験法の確立に取り組みたい。

E. 結論

ヒトiPS細胞のミトコンドリア機能や分化を指標に、成長期における化学物質の発達神経毒性を評価できる可能性が示唆された。

F. 研究発表

1. 論文発表

[1] Yamada S., Kubo Y., Yamazaki D., Sekino Y. and Kanda Y. "Chlorpyrifos inhibits neural induction via Mfn1-mediated mitochondrial dysfunction in human induced pluripotent stem cells." *Sci. Rep.* (2017) 7:40925

[2] Yamada S., Asanagi M., Hirata N., Itagaki H., Sekino Y. and Kanda Y. "Tributyltin induces mitochondrial fission through Mfn1 degradation in human induced pluripotent stem cells." *Toxicol. In Vitro.* (2016) 34:257-263

[3] Asanagi M., Yamada S., Hirata N., Itagaki H., Kotake Y., Sekino Y. and Kanda Y. "Tributyltin induces G2/M cell cycle arrest via NAD(+)-dependent isocitrate dehydrogenase in human embryonic carcinoma cells." *J. Toxicol. Sci.* (2016) 41:207-215

[4] Hirata N., Yamada S., Asanagi M., Sekino Y. and Kanda Y. "Nicotine induces mitochondrial fission through mitofusin degradation in human multipotent embryonic carcinoma cells." *Biochem. Biophys. Res. Commun.* (2016) 470:300-305

2. 学会発表

[1] 山田茂、麻薙美紀、平田尚也、板垣宏、関野祐子、諫田泰成：ヒトiPS細胞のミトコンドリアダイナミクスを用いた細胞毒性評価、第89回日本薬理学会、2016 横浜

[2] Yasunari Kanda, Shigeru Yamada, Naoya Hirata, Daiju Yamazaki, and Yuko Sekino. Role of mitochondrial dynamics in neural toxicity assessment in human iPS cells. 5th Annual Meeting of the American Society for Cellular and Computational Toxicology. US EPA Building Research Triangle Park, NC. 2016.9.29-30

[3] 麻薙美紀、山田茂、平田尚也、板垣宏、関野祐子、諫田泰成：ヒト多能性幹細胞を用いた発達神経毒性評価の試み、第89回日本薬理学会、2016 横浜

[4] 山田茂、関野祐子、諫田泰成：ヒトiPS細胞のミトコンドリア機能に基づいたクロルピリホスの毒性評価、第134回日本薬理学会関東部会、2016 大田原

[5] 山田茂、久保祐亮、犬塚隆志、関野祐子、諫田泰成：ヒトiPS細胞のミトコンドリア機能による医薬品の毒性評価、第43回日本毒性学会、2016 名古屋

[6] 山田茂、関野祐子、諫田泰成：ミトコンドリアを指標としたヒトiPS細胞毒性評価系の検討、第2回次世代を担う若手のためのレギュラトリーサイエンスフォーラム、2016 東京

[7] 山田茂、関野祐子、諫田泰成：ミトコンドリア機能を介した新規神経誘導メカニズム、第39回日本分子生物学会、2016 横浜

G. 知的財産権の出願・登録状況

該当なし

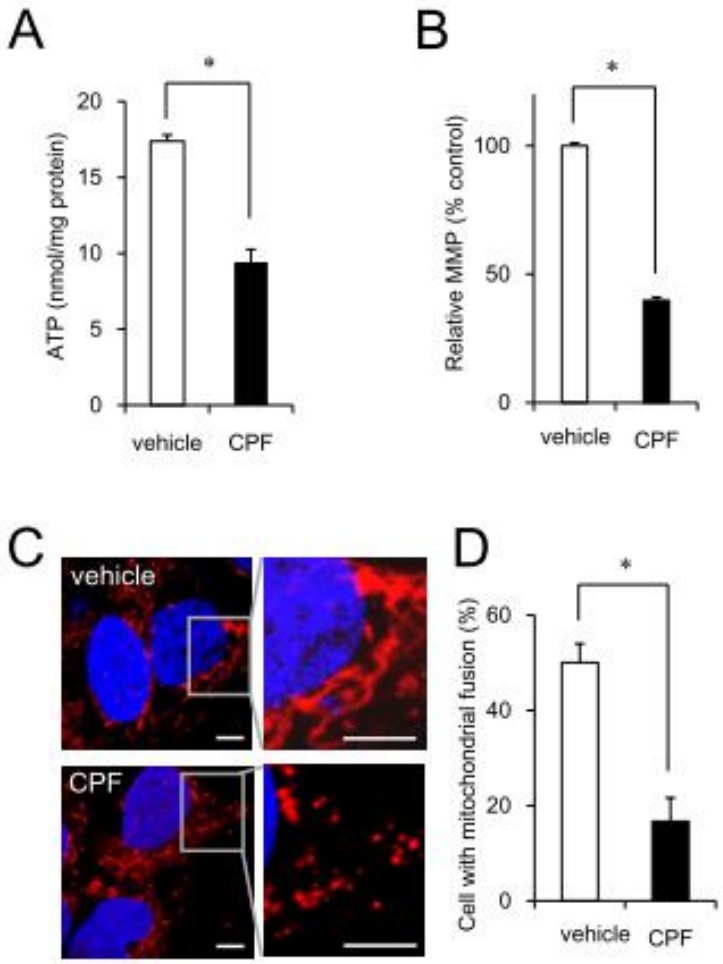

図 1　CPF によるミトコンドリアの機能異常

A) ヒト iPS 細胞において、CPF（30 μM）の暴露によって ATP 産生低下が認められた。
B) ヒト iPS 細胞において、CPF の暴露によってミトコンドリア膜電位の低下が認められた。
C) ヒト iPS 細胞において、CPF の暴露によってミトコンドリアの分裂が誘導された。
D) C)の結果を定量的に評価した。

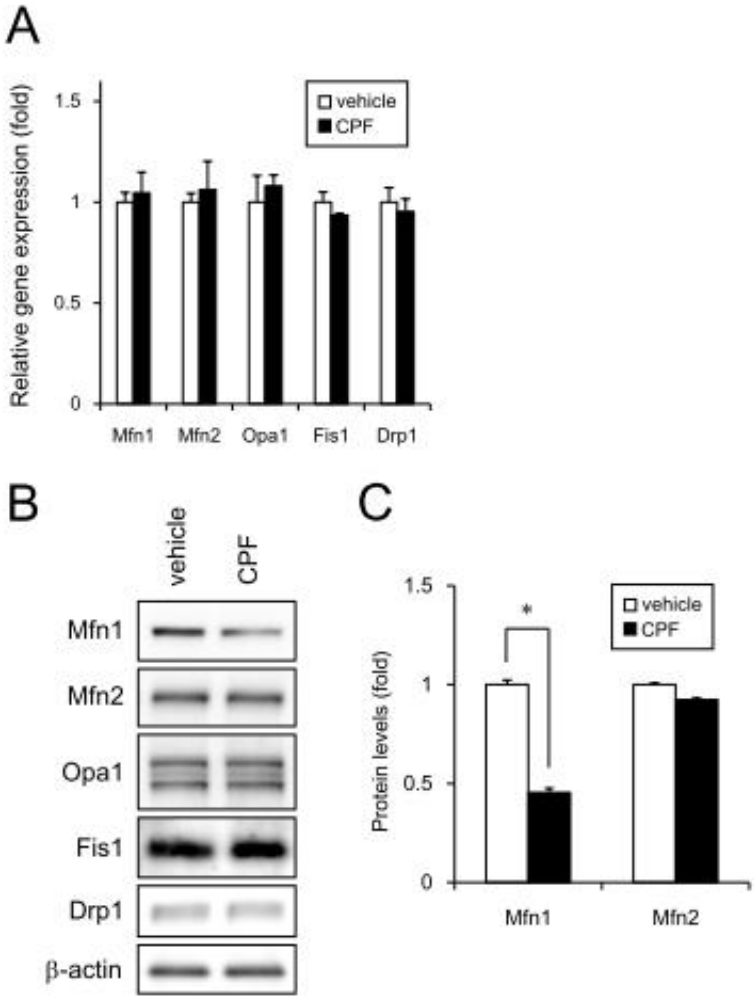

図 2　CPF による Mfn1 の分解

A) 30 μM の CPF を曝露したヒト iPS 細胞から RNA を抽出し、Mfn1、Mfn2、Opa1、Fis1、Drp1 遺伝子の qPCR を行った。

B) 30 μM の CPF を曝露したヒト iPS 細胞から cell lysate を作成し、Mfn1、Mfn2、Opa1、Fis1、Drp1 蛋白質の発現をウエスタン法によって調べた。

C) B)の Mfn1、Mfn2 蛋白質の発現を定量的に評価した。

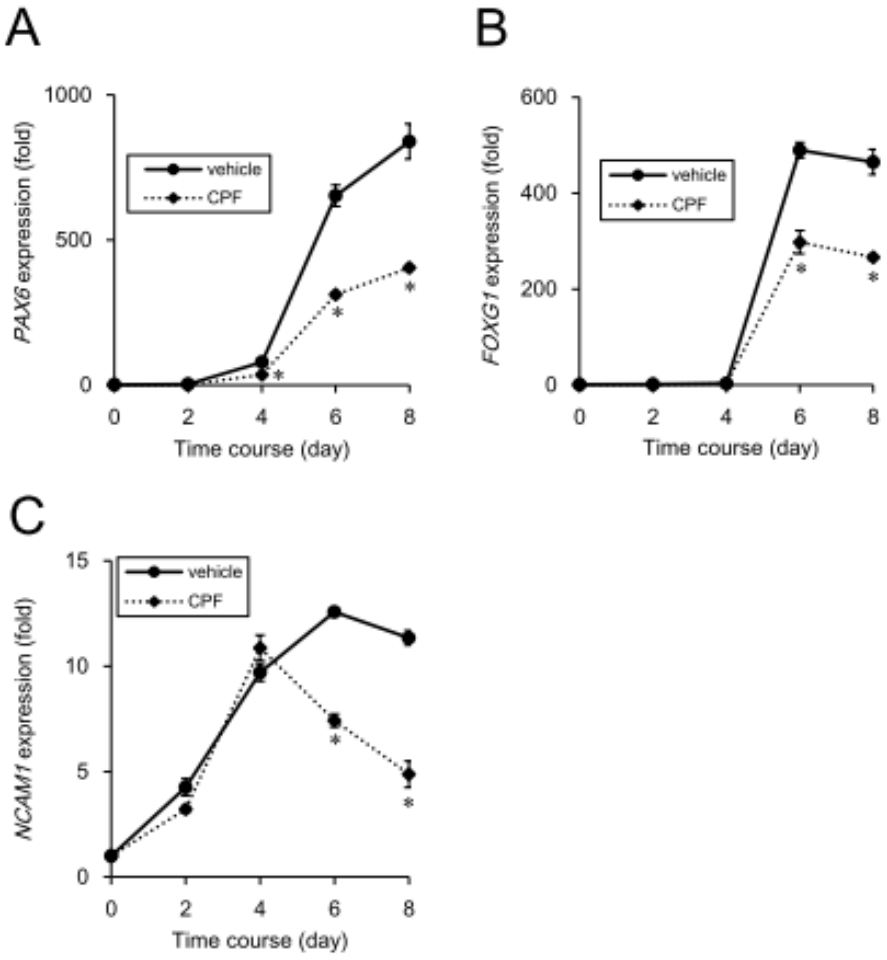

図 3　CPF による神経分化誘導の阻害

30 μM の CPF を曝露したヒト iPS 細胞に神経分化刺激を与えた後、タイムコースをとって神経分化マーカーの遺伝子発現を qPCR で調べた。

A) 神経外胚葉マーカーPAX6 遺伝子の発現変化

B) 神経外胚葉マーカーFOXG1 遺伝子の発現変化

C) 神経前駆細胞マーカーNCAM1 遺伝子の発現変化

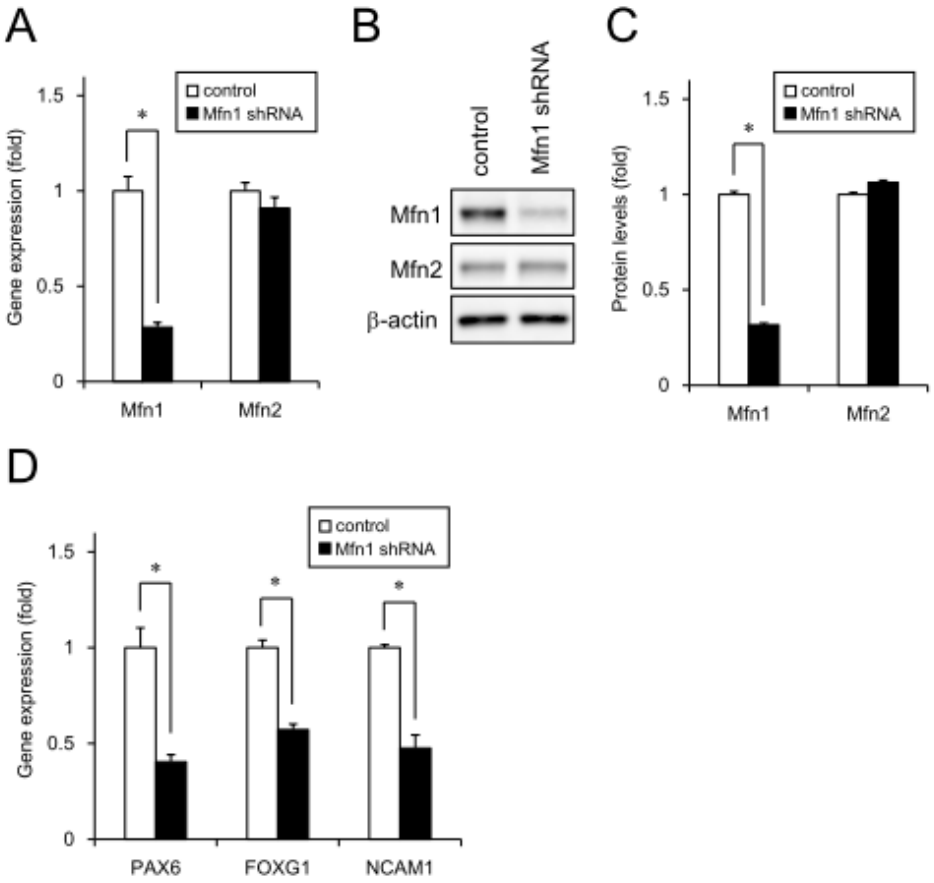

図 4　Mfn1 ノックダウンによる神経分化誘導の阻害

A) Mfn1-shRNA を導入したヒト iPS 細胞における Mfn1, Mfn2 の遺伝子発現を qPCR で調べた。
B) Mfn1-shRNA を導入したヒト iPS 細胞における Mfn1, Mfn2 の蛋白発現をウェスタンブロット法で調べた。
C) B)の結果を定量的に評価した。
D) Mfn1 をノックダウンしたヒト iPS 細胞を用いて神経分化誘導を行い、神経分化マーカー（PAX6, FOXG1, NCAM1）の遺伝子発現を qPCR で調べた。

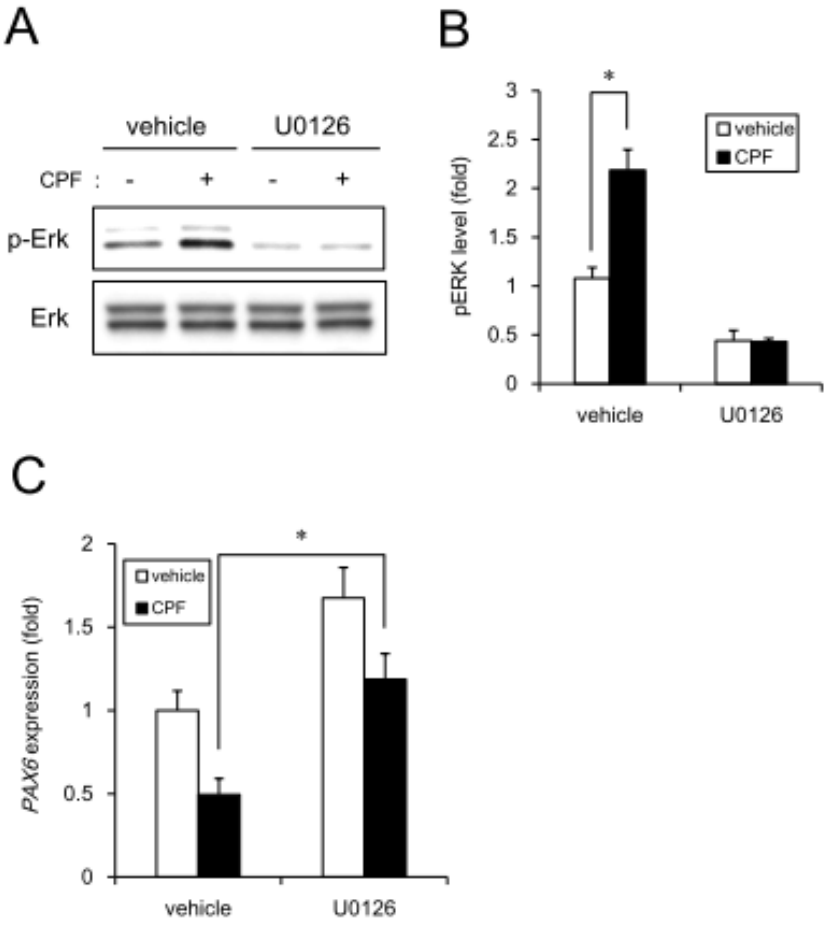

図 5　CPF の神経誘導阻害における Erk シグナルの関与

A) 30 μM の CPF を曝露したヒト iPS 細胞から cell lysate を作成し、Erk のリン酸化レベルをウエスタン法によって調べた結果、Erk リン酸化の亢進が認められた。このリン酸化レベルの亢進は Erk 阻害剤である U0126 処理により消失した。

B) A)の結果を定量的に評価した。

C)ヒト iPS 細胞の神経分化誘導において、CPF 曝露による PAX6 の発現低下は、U0126 処理により回復した。

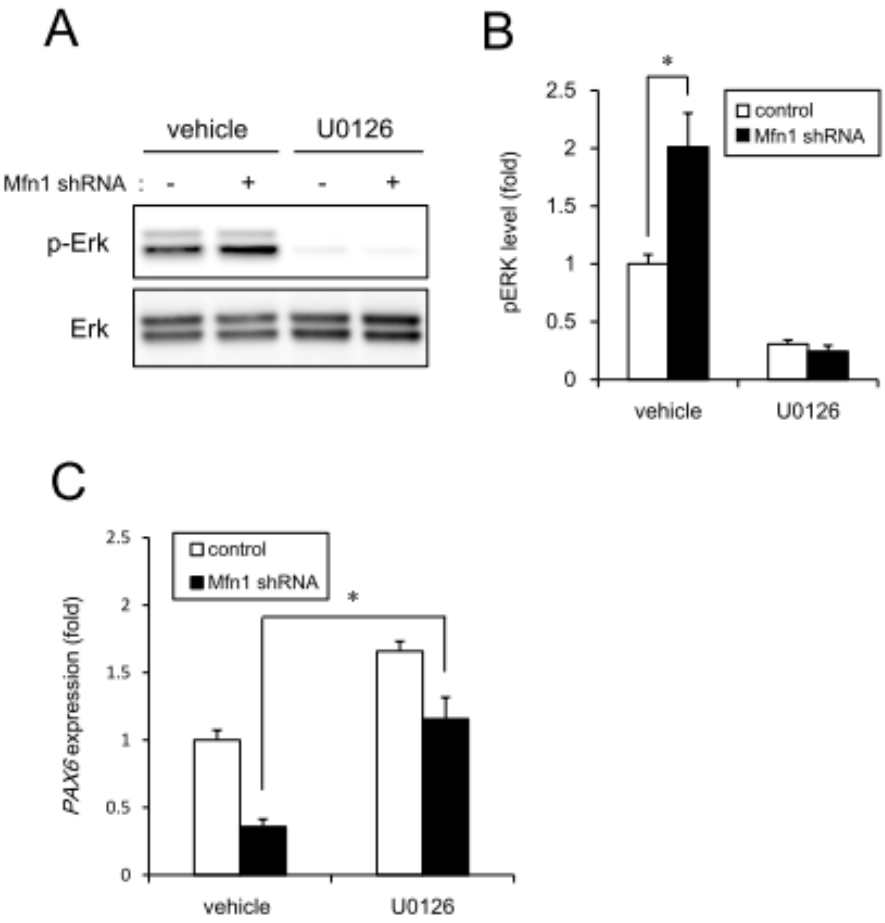

図 6　Mfn1 ノックダウンによる神経誘導阻害における Erk シグナルの関与

A) Mfn1 をノックダウンしたヒト iPS 細胞から cell lysate を作成し、Erk のリン酸化レベルをウエスタン法によって調べた結果、Erk リン酸化の亢進が認められた。このリン酸化レベルの亢進は Erk 阻害剤である U0126 処理により消失した。

B) A)の結果を定量的に評価した。

C)ヒト iPS 細胞の神経分化誘導において、Mfn1 ノックダウンによる PAX6 の発現低下は、U0126 処理により回復した。

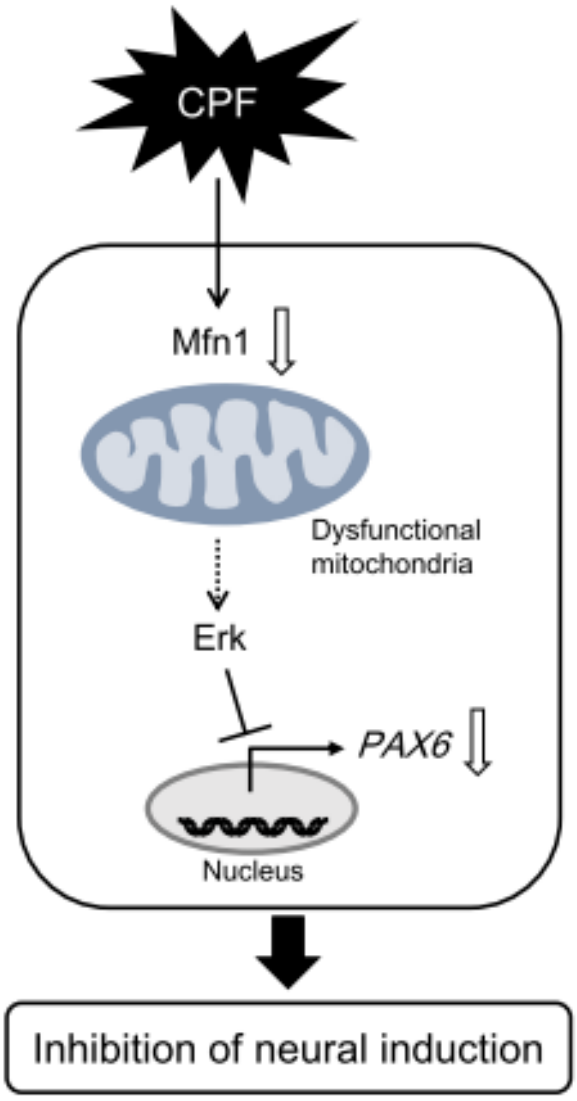

図 7　CPF の神経分化阻害作用（模式図）

厚生労働科学研究費補助金（化学物質リスク研究事業）
分担研究報告書

神経堤細胞の機能解析による評価法の開発

研究分担者　国立医薬品食品衛生研究所薬理部第四室長
宇佐見　誠
研究協力者　簾内　桃子
研究協力者　入江　智彦
研究協力者　日本バイオアッセイ研究センター 試験管理部
奥田　裕計

要旨
ラット神経堤細胞の遊走等に及ぼす影響について、メカニズムに関する実験系としてタンパクリン酸化パスウェイの関与を調べる方法を検討した。ラット 10.5 日胚から頭部又は腹部の神経管を摘出して培養して、神経管から遊出する神経堤細胞の広がりを測定することにより、神経堤細胞の遊走を調べた。その結果、ピルビン酸を含まない培養液では、神経堤細胞の遊走は少ないことを示した。また、RNA 干渉実験の条件を検討し、リポフェクタミン RNAiMAX トランスフェクション試薬を用いる方法を確立した。さらに、確立した RNA 干渉実験法により、Rho キナーゼである Rock1 および Rock2 を同時に抑制して培養時間を延ばすことにより、神経堤細胞の遊走が促進されることを示した。本実験法は、Rho パスウェイが関与する毒性発現メカニズムに基づいた化学物質の発達神経毒性評価法として有用であると考えられた。

A. 研究目的

近年、子供の学習障害や自閉症などの発達障害が増加しているが、その原因として化学物質の関与が指摘されている。神経提細胞は、脊椎動物における個体発生の限られた時期に存在し、胚の隅々に遊走した後に末梢神経、グリア細胞などの神経系細胞を含む様々な細胞に分化することにより、個体の機能発育および形態形成に重要な役割を果たす。そのため、発生過程における神経提細胞の誘導、遊走、分化などにおける異常は、神経提症と総称される神経芽細胞腫などの神経系の異常を含むさまざまな疾患を引き起こす。

また、神経提細胞のうち、頭部神経管に由来する頭部神経提細胞の異常では、顔面の奇形などの形態形成に及ぼす影響も認められる。神経提症による顔面奇形と同様の奇形は、胚のレチノイン酸への過剰暴露においても生じることから、神経提細胞は化学物質による毒性の標的組織となり得ると考えられている。しかし、適切な実験法が確立されていないため、化学物質の神経提細胞機能に及ぼす影響は、ほとんど調べられていない。

本研究では、神経提細胞の特徴的な機能である細胞遊走を主な指標とする、形態形成期に重要な役割を果たす神経堤細胞の機能に及ぼす化学物質の影響を調べる方法を確立し、個体の成長期における化学物質の健康影響評価法の一つとして用いることを目的とする。神経提細胞実験法としては、初期着床胚をまるごと培養するラット全胚培養法との比較実験が可能であり、解析が容易な、ラット神経提細胞を用いた実験法の確立を目指した。

本実験法を利用することにより、神経堤細胞遊走に影響する化学物質とそのメカニズムを同定し、ヒトにおける当該化学物質に対する高暴露集団およびメカニズムに関与する遺伝子疾患等を有する集団などの、ハイリスク集団について、疫学的調査の基盤的情報を提供すると共に、健康影響の予防のための方策となる情報を得られることが期待される。

初年度は、神経堤細胞の機能に関与することが報告されている、タンパクリン酸化パスウェイである Rho パスウェイを介した化学

物質の影響を調べることが可能な、ラット神経堤細胞遊走実験法について検討した。

B. 研究方法

1. 動物

ウィスターラット（Crlj:WI, 日本チャールスリバー）を用いた。発情前期の雌ラットを雄と終夜同居させ、妊娠ラットを得た。同居中の深夜を妊娠 0 日として起算した。妊娠 10.5 日に、妊娠ラットから初期着床胚を摘出して実験に用いた。

2. ラット神経堤細胞の培養

頭部神経堤細胞を用いる場合は、摘出したラット初期着床胚から、電解研磨したタングステン針を用いて、菱脳部を切り出し、物理的に神経管を取り出した。腹部神経堤細胞を用いる場合は、前肢芽の部位から神経管を同様の方法で取り出した。取り出した神経管を、培養シャーレ（Becton, Dickinson and Company）に培養液（10% Fetal Bovine Serum を含む Dulbecco's Modified Eagle Medium, GIBCO）と共に入れ、炭酸ガスインキュベーター内で、5% CO_2、37℃にて培養した。

3. ラット神経堤細胞の観察

培養 24 時間及び 48 時間に、神経管から遊走した細胞すべてを含む領域を、位相差顕微鏡（BZ-900、株式会社キーエンス）で撮影し、神経管の培養容器底面への付着及び遊走細胞の広がりを観察した。

4. データの解析

細胞の撮影画像ファイルを画像解析ソフト ImageJ （Rasband, W.S. ImageJ, U. S. National Institutes of Health, Bethesda, Maryland, USA, http://rsb.info.nih.gov/ij/, 1997-2009）で開き、最外側の神経提細胞をポリゴンツールでつないでできる図形を円とみなして、そのピクセル数で表される面積から計算した半径を神経堤細胞の遊走距離として解析した。

（倫理面への配慮）

動物の使用にあたっては国立医薬品食品衛生研究所の「動物実験に関する指針」を遵守した。

C. 研究結果

ラット神経堤細胞遊走に及ぼす化学物質の影響に関するカニズムを調べる方法としての感度を改善するために、基本培養液中のピルビン酸の影響を調べた。その結果、ピルビン酸を含まない培養液では、頭部および腹部のいずれの神経堤細胞においても遊走が少ない傾向が認められ、二元配置分散分析では、ピルビン酸の有無による差は統計学的に有意であった。ラット胚の部位による神経堤細胞の起源とピルビン酸の影響との間に相互作用は認められなかった （図 1）。

Rho パスウェイを介した化学物質の影響を調べる方法として RNA 干渉実験の条件を確立するために、種々のトランスフェクション試薬について検討した結果、リポフェクタミン RNAiMAX 試薬を単独で用いた場合が効果的であった。さらに RNAiMAX 試薬の無毒性量を確認したところ、シャーレ一枚の培養液（2 ml）あたり 4 □l においても神経堤細胞の遊走に影響は認められなかった（図 2）。

確立した RNA 干渉実験法により、Rho キナーゼである Rock1 の発現抑制が神経堤細胞の遊走に及ぼす影響を調べた。その結果、神経堤細胞の遊走に影響は認められなかった（図 3）。しかし、Rock1 および Rock2 の発現を同時に抑制して、培養 48 時間から 72 時間まで観察した場合には、神経堤細胞の遊走が促進された（図 4）。

D. 考察

本実験系で用いるラット胚は、嫌気的条件から好気的条件に移る時期である。そのため、嫌気的エネルギー産生系である解糖系と、好気的エネルギー産生系であるトリカルボン酸サイクルの接点であるピルビン酸の有無は、実験結果に影響を及ぼす可能性が考えられた。本実験の結果、ピルビン酸を含む培養液の方が、神経堤細胞の遊走が大きいことから、ダイナミックレンジが広くなり、実験系としての感度が良いと考えられる。

RNA 干渉実験法では、神経堤細胞遊走の観察時間を 48～72 時間に遅らせることおよび Rock1 および Rock2 の発現を同時に抑制することにより siRNA の効果を観察することが出来た。この観察時間は、一般的な RNA 干渉実験における mRNA の減少には 48 時間程度を要することと一致しており、神経堤細胞における mRNA のターンオーバーは一般的な速さであると考えられる。また、Rock1 および Rock2 の発現を同時に抑制した場合に神経堤細胞の遊走が促進されたことから、Rock1 と Rock2 の役割の違いなどについて調べる必要がある。

以上の結果から、本実験法は Rho パスウェイが関与する毒性発現メカニズムに基づ

いた化学物質の発達神経毒性評価法として有用であると考えられる。

E. 結論

ラット神経堤細胞の遊走等に及ぼす影響について、メカニズムに関する実験系としてタンパクリン酸化パスウェイの関与を調べる方法を検討した。その結果、ピルビン酸を含む培養液の方が、実験系としての感度が良いと考えられた。また、RNA 干渉実験の条件を確立した。確立した RNA 干渉実験法により、Rho キナーゼである Rock1 および Rock2 を同時に抑制することにより、神経堤細胞の遊走が促進されることを示した。本実験法は、Rho パスウェイが関与する毒性発現メカニズムに基づいた化学物質の発達神経毒性評価法として有用であると考えられた。

F. 研究発表

1. 論文発表

該当なし

2. 学会発表

[1] 宇佐見誠、満長克祥、奥田裕計、土井守：クロルピリホスが培養ラット神経堤細胞の遊走に及ぼす影響に関する 研究、第 43 回日本毒性学会学術年会、2016 名古屋

G. 知的財産の出願・登録状況

該当なし

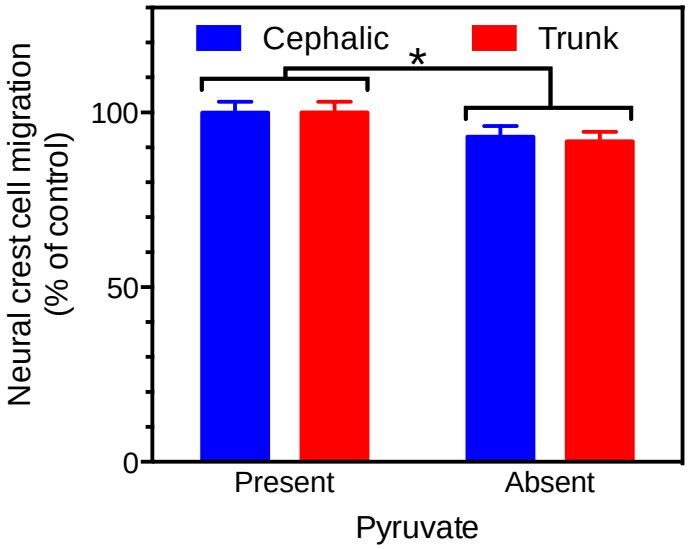

図 1　ラット頭部（cephalic）および腹部（trunk）神経堤細胞の遊走に及ぼすピルビン酸の影響

ラット 10.5 日の神経管から遊走する神経堤細胞をピルビン酸を含む培養液（1 mM）または含まない培養液で 48 時間培養した。「*」は統計学的な有意差があることを示す　（* $p < 0.05$）。

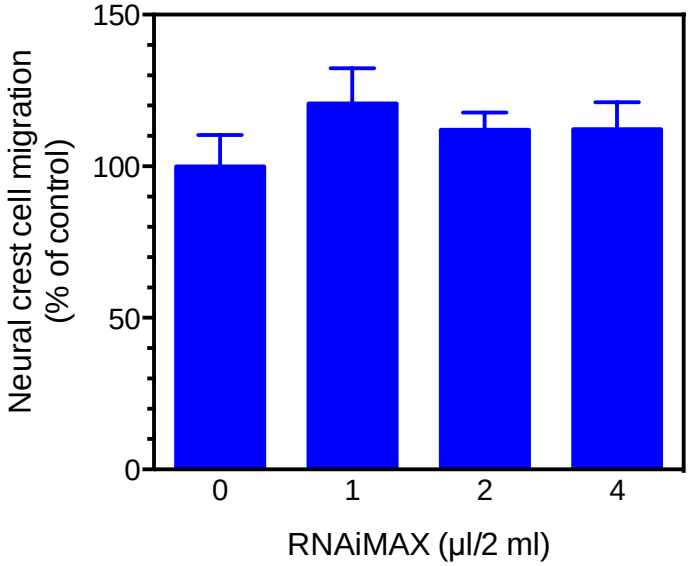

図 2　ラット神経堤細胞の遊走に及ぼすリポフェクタミン RNAiMAX トランスフェクション試薬の影響

ラット 10.5 日の神経管から遊走する神経堤細胞を 48 時間培養した。神経管を培養 18 時間目に除去した。

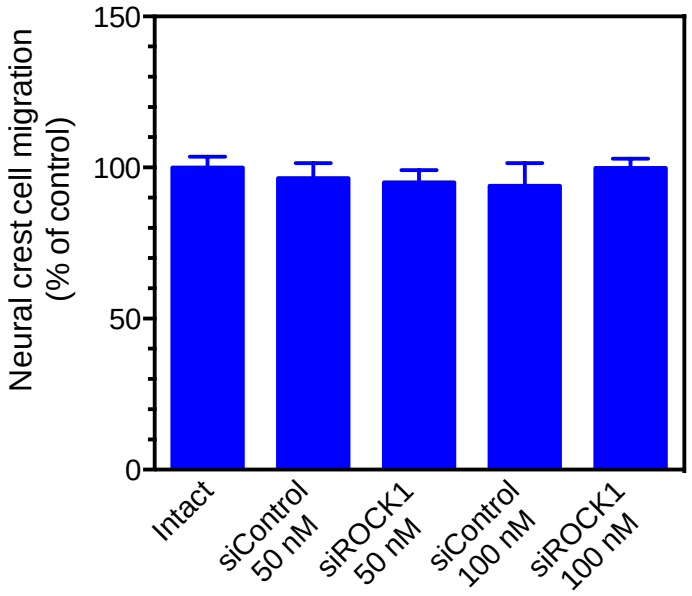

図 3　ラット神経堤細胞の遊走に及ぼす Rock1 発現抑制の影響

ラット 10.5 日の神経管から遊走する神経堤細胞を 48 時間培養した。平均値と標準誤差を示す。神経管を培養 18 時間目に除去した。

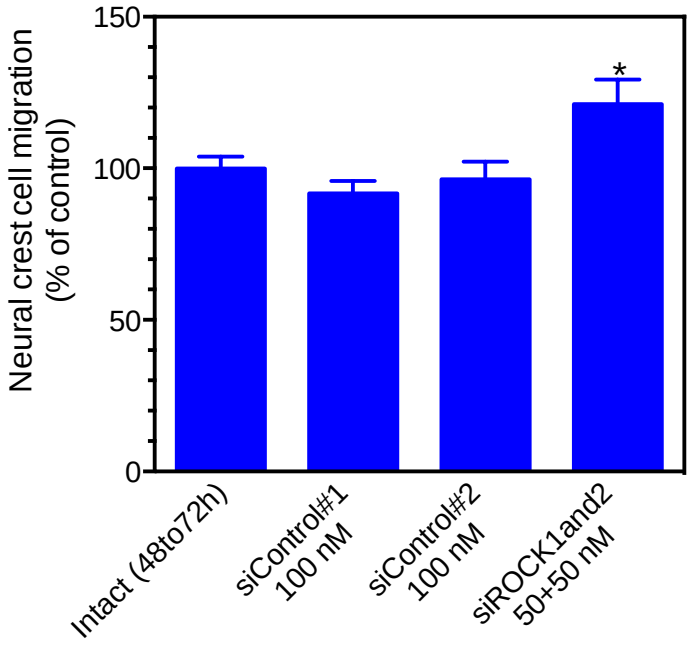

図 4　ラット神経堤細胞の遊走に及ぼす Rock1 および Rock2 発現抑制の影響

ラット 10.5 日の神経管から遊走する神経堤細胞を 72 時間培養した。平均値と標準誤差を示す。神経管を培養 18 時間目に除去した。「*」は無処置群と比較して統計学的な有意差があることを示す（* $p < 0.05$）。

厚生労働科学研究費補助金（化学物質リスク研究事業）
分担研究報告書

海馬ニューロンを用いた神経ネットワークによる評価法の開発

研究分担者　国立医薬品食品衛生研究所薬理部　主任研究官
山崎　大樹
研究協力者　群馬大学大学院医学研究科　教授
白尾　智明

要旨
本研究では、神経ネットワーク形成過程およびネットワーク形成後の化学物質の毒性評価系の開発を目的として、以下の 2 つの内容に取り組んだ。第一に、高い再現性を目指すための条件検討項目として、プレートのコーティング方法、播種細胞密度、AraC の添加、培地交換の量について検証を行った。各々の条件検討の結果から、最適条件を得ることができ、その条件において再現性の高い結果が得られた。今後、本研究で得られた最適条件により化学物質の毒性評価を実施する予定である。第二に、化学物質の投与方法について溶媒として主に用いられる DMSO で検証を行った。その結果、高濃度の DMSO が細胞に対して直接接触することで測定パラメーターに大きく影響することが明らかとなった。DMSO を 10 倍に薄めて投与する方法は測定パラメーターへ影響を与えないことから、今後の化学物質を評価する際の投与方法については、上記方法を採用することとした。また今回のプロトコル整備にあたり、米国環境保護庁の Timothy J Shafer 教授との共同研究体制を構築した。さらに、HESI NeuTox の MEA サブチームにおけるプレバリデーション試験に関する議論に参加して、条件設定に関する有益な情報を得ることができた。
以上の経緯を以って開発した評価法により、今後は陽性・陰性対照物質の発達神経毒性に対する影響を効率よく評価していけるものと考えられる。

A. 研究目的

近年、自閉症など発達障害が急速に増加し社会問題となっており、その原因の一つは発達期における化学物質の曝露とされている。発達期の神経系は成体と比較して化学物質に対する感受性が高く、健康被害が長期間あるいは遅発性に生じることが考えられ、子どもの健康への影響に対する評価法の確立が強く望まれている。現在の発達神経毒性を評価するガイドライン（OECD および EPA）は、妊娠ラットを用いた複雑な試験系であり、試験期間が 1 年以上、動物数が 720 にも及び経費も膨大であるため、これまでにわずかな化学物質しか評価できていない。本邦においては、このようなガイドラインも未整備である。個体の成長期の高感受性の時期に一時的に曝露しただけで生涯にわたり脳神経機能に影響をもたらすような危険な化学物質を優先的に選定するためには、新規試験法の開発が喫緊の課題となっている。そこで、我々は発達期の細胞評価系および生後初期における神経ネットワーク形成評価系を組み合わせた統合的な新規試験法の開発を行っている。

神経ネットワーク形成過程およびネットワーク形成後において、化学物質の毒性評価が可能な系として期待されているのが、多点電極（MEA, multi-electrode array）システムを用いたげっ歯類神経細胞の評価である。これは、電極が多数パターニングされた平面に神経細胞を播種し、そこで長期間の培養を行うとともに神経活動（スパイクとよばれる電気活動）を記録するものである。

本研究では、神経ネットワーク形成過程およびネットワーク形成後の化学物質の毒

性評価系の開発を目指した。さらには、開発した評価系を用いて複数の陽性・陰性対照物質を評価し、これまで我々が開発してきた他の評価系で得られた結果と比較し、評価法の妥当性を検証する。

B. 研究方法

1. 細胞

細胞は研究協力者である群馬大学・白尾智明教授の研究室で作製された凍結ラット胎仔海馬神経細胞（SKY Neuron）を用いた。この細胞は胎生 18 日目のラット胎仔海馬より単離されたものである。

2. プレートコーティング

AxionBiosystems 社製 Maestro プレート（48 ウェルタイプ）の各ウェルに 100 µl の 0.1%ポリエチレンイミン（PEI）（0.1 % PEI in 0.1 M Boric asid buffer solution（pH 8.5））を添加し、インキュベーター内に 1 時間静置した。その後、滅菌水で 3 回リンスし、クリーンベンチ内で 1 時間乾燥させた。乾燥後、フタをしてアルミホイルで遮光し、4ºC に保管した。PEI コートしたプレートは原則 1 週間以内に使用した。

3. 細胞の解凍および播種

細胞が入ったバイアルを液体窒素保存容器から取り出し、速やかに 37ºC の温浴に 3 分間浸した。その後、クリーンベンチ内で細胞懸濁液を 50 ml チューブに移し、バイアル内を播種用培地（10% FBS, 1.14 mM Pyruvic acid, 0.7% Glucose in Minimum Essential medium）でリンスし、細胞懸濁液にゆっくりと滴下した。合計 6 ml となるように播種用培地を細胞懸濁液に一定の速度で滴下し、よく混合した後に細胞数を計測した。200 x g で 5 分間遠心し、一定の細胞密度になるよう laminin（20 µg/ml）を含んだ播種用培地を添加し、10 µl/ウェルでプレートに播種した。2 時間後、500 µl の培養用培地（0.25% GlutaMAX, 1% Penicillin-Streptomycin, 2% B27 in Neurobasal medium-A）を添加し、1 日おきあるいは 2 日おきに測定し、3 日おきあるいは 4 日おきに培地交換を行った。

4. MEA システム

評価系は AxionBiosystems 社製の Maestro を用いた。使用した 48 ウェルプレートの各ウェルには、4 x 4 の合計 16 個の電極がパターニングされている。このプレートで細胞を培養した状態で MEA システムにセットすると、各電極における自発的なスパイク発生をアクティビティマップにて可視化することができる（図 1A）。MEA システムではスパイクの検出閾値をノイズレベルの 6～8 倍に設定することでノイズの検出を防いでおり、検出閾値を超えたスパイクはラスタープロットとして表される（図 1B）。神経細胞の成熟とともにスパイクの発生頻度は増加し、やがて神経細胞の突起同士がシナプスを形成することで神経ネットワークを構築する。神経ネットワークの構築により各神経細胞で独立に発生しているスパイクが同期し、最終的にはバーストやネットワークスパイクと呼ばれる連続的でウェル中の複数の電極で同期した電位変化が起こるようになる（図 1C）。

5. 解析

評価系の開発にあたり、実験条件の検討や再現性の検証には、平均発火頻度と活性化電極数（1 分間に 5 回以上のスパイクを生じた電極）の 2 つのパラメーターを用いた。平均発火頻度は 1 ウェルで 1 分間に発生したスパイク数を活性化電極数で割った値である。

C. 研究結果

1. 細胞の解凍

通常、ラット等げっ歯類の胎児から単離した神経細胞は、そのまま分散培養して各種実験に供する。しかしながら、状態の良い細胞を単離するには熟練した技術が必要であり、またそのための単離・培養設備を準備しなければならない。神経細胞を凍結することで同一ロットの細胞バイアルを大量に作成することができ、事前に当該ロットの状態をグルタミン酸に対する反応性などで確認することが可能なことから、再現性の高い結果が期待できる。一方で、細胞の凍結・融解は細胞に対してダメージを与えることが知られているため、凍結・融解による細胞の生存率への影響について検証した。表 1 にまとめたように生細胞数と死細胞数はほぼ半々であり、生存率としては平均 50%強であった。ロットや実験者（融解の際の）に依存した差はほとんどなかった。

2. コーティングに関する検討

Axion 社が提供している Maestro 用プロトコルでは、0.1% PEI によるプレートコーティングを推奨している。一方で、SKY

neuron 用のコーティングは PLL（Poly-L lysine）コーティングが実施されている。そこで、PEI コーティングと PLL コーティングを 1 枚のプレートに施し、その他の条件を全く同一にして実験を行った。その結果、平均発火頻度、活性化電極ともに PLL コーティングよりも PEI コーティングにおいて、値が上昇していた。電極がパターニングされていないプレートによる細胞観察では、培養開始 2 日後には細胞の凝集が PLL コーティングの方で観察されている一方で、PEI コーティングでは、細胞が接着していないことによる隙間が極端に少なかった。次に PEI コーティングがどの程度有効なのかを調べるため、PEI コーティング直後、約 3 週間後および約 4 週間後のプレートを用いて実験を行った。その結果、コーティング 3 週間以降のプレートでは、活性化電極数はコーティング直後のものと大差ない変化を示すものの、平均発火頻度の時間依存的な上昇は AraC の有無にかかわらずコーティング直後に比べて低い値で推移することが明らかとなった（図 2）。活性化電極数については、コーティング期間の長さには影響されなかった。

以上より、Maestro による MEA システムにおいては、PEI コーティングの方が適しており、コーティングの効果は 3 週間保存することで低減することが示唆された。

3. 細胞播種密度の検討

MEA システムの性質上、電極部分に細胞が存在しなければスパイクの計測は不可能である。我々は再現性の高い結果を得るため、細胞播種密度の検討を行った。これまでに他の研究室ではラット大脳皮質神経細胞における検討が行われており、その際の細胞播種密度は 150,000 細胞/25 µl である。今回の検討では、播種する細胞懸濁液量を全電極が覆うことのできる最小量 10 µl とした。これまでの論文における細胞播種密度に関する情報と最小量 10 µl を鑑みた上で細胞播種密度以外の条件を揃えて 6,000、12,500、25,000、50,000 細胞/10 µl の 4 条件にて計測を行ったところ、12,500 細胞/10 µl 以下では平均発火頻度および活性化電極数のいずれもほとんど増加しなかった。25,000 細胞/10 µl の条件では、50,000 細胞/10 µl の条件と比較して、平均発火頻度の増加が緩やかであり、また最高値も低かった（図 3A）。活性化電極数については、50,000 細胞/10 µl では 16 電極全てが活性化する一方で、25,000 細胞/10 µl では最高で 12～14 電極が活性化した（図 3B）。細胞数を増やすことで 16 電極全てを確実に覆うことが可能になるものと考察される。以上より、細胞播種密度は、50,000 細胞/10 µl が妥当との結論に至った。

4. AraC の添加

神経細胞単離の際、グリア細胞の混入は避けられない。また、培養によりグリア細胞は増殖するため、グリア細胞の割合によって化学物質に対する応答も異なる可能性が考えられる。

そこで、グリア細胞の増殖による神経ネットワーク形成への影響を検討するため、グリア細胞の増殖抑制剤である 0.5 µM AraC を培養開始 5 日目に添加し 7 日目に除去する群（0.5 AraC）と AraC を添加しない群（0 AraC）の 2 群について比較した。その結果、0 AraC および 0.5 AraC のいずれにおいても培養開始 7 日後から急激な平均発火頻度の上昇が観察された（図 4A）。平均発火頻度の最高値は 0 AraC の方が高かった。これは、グリア細胞の増殖が抑制されなかったことにより、神経細胞間のネットワーク形成が亢進した可能性が考えられた。両群で活性化電極数の経時的変化に大きな差はなく（図 4B）、いずれの群においても培養開始 12～19 日目において平均発火頻度の値が安定していたことから、化学物質の急性投与実験を行うタイミングとしては、培養開始 16 日目が最適だと考えられる。

培地を全量交換ではなく半量るいは 1/3 量で交換することで AraC の濃度を徐々に薄くしていく方法もある。しかし、Maestro プレートはウェル間で培地の蒸発量が異なっていることから、AraC の濃度を徐々に薄める方法では、同一の条件とはなり得ない。従って今回は培養 7 日目に AraC を培地の全量交換によって除去した。神経細胞の単離（ロット）ごとにどの程度グリア細胞が混入しているかは不明であることから、AraC 非添加の場合にグリア細胞と神経細胞の割合がどの程度なのかは全く予想できない。AraC の添加によってグリア細胞の増殖がある程度抑制されれば、培養期間を通じてのグリア細胞が混入している割合はそれほど大きくばらつかないのではないかと考えられる。現段階では、定量的にどちらが最良か判断できないため、引き続き条件

検討を続けることが必要である。

5. 培地交換量

本研究では、最大で 28 日間の培養を行うが、その間 3 日あるいは 4 日おきに培地交換を行う。その際、ウェル中のすべての培地を除去して新たに培地を添加すると、細胞が乾燥してしまい結果に影響することが予想された。そこで、培地交換の量を半量あるいは全量の 2 条件について検討を行った。その結果、0 AraC の半量交換が全量交換に比べて顕著に高い平均発火頻度だったが、0.5 AraC では半量交換と全量交換に大きな差はなかった（図 5A）。活性化電極数にも半量交換と全量交換で大きな差はなかった（図 5B）。

3 日あるいは 4 日おきに培地交換を行うと、インキュベーター内の湿度が十分であっても各ウェルより培地が蒸発していく。しかもウェルごとに蒸発量が異なるため培地量を一定に保つことが困難だと考えられる。0.5 AraC の場合、半量交換と全量交換で大差なかったことから全量交換によって毎回ウェル中の培地を一定量に保つことが最適だと考えられる。

6. 急性投与の投与操作の検討

上述したように、化学物質の急性投与実験を行うタイミングとしては、培養開始 16 日目付近が最適だと考えられる。急性投与実験では、化学物質の投与前後でのパラメーターの比較を行うことから、化学物質による作用のみを抽出する必要があり、溶媒や投与操作によるパラメーター変動は避けたい。そこで、溶媒に最も多く用いられる培地と DMSO に関して、投与操作の検討を行った。DMSO の最終濃度を 0.1%に抑えたいため、500 µl の培地に対して 5% DMSO を 10 µl 投与した。

10 µl の培地および DMSO を 1 ショットで投与した場合、培地では平均発火頻度の大きな変化は観察されなかったものの、DMSO の投与により平均発火頻度の値が大きく変化し時にはまったくスパイクが観察されない時間帯もあった（図 6）。これは高濃度の DMSO が神経細胞に対して直接作用したためだと考えられる。次に高濃度の DMSO が細胞に直接作用することを避けるため、以下の 4 つの投与方法を検討した。①10 µl の 5% DMSO を 1 ショットではなく、ゆっくりと時間をかけてウェル中に投与、②96 ウェルプレートに配置した 10 µl の 5% DMSO に細胞を培養している実際のマエストロプレートのウェルから培地を 50 µl 抜いて混合し、元のウェルに戻す方法、③②における培地量を 100 µl にした方法、④②における培地量を 200 µl にした方法。①は 1 ショットで投与した場合と同じように、平均発火頻度が大きく変動した（図 7A）。②では添加直後に平均発火頻度がゼロとなる時間帯も観察された（図 7B）。③④はウェルに投与する DMSO の濃度が大幅に薄くなっていることから、投与による影響はほぼ消失した（図 7B-D）。以上より 100 µl 以上の培地と 5% DMSO を混合し、ウェルに投与することが最適だと考えられる。

7. その他

上記の条件検討を行うにあたり非常に役立ったのが、米国環境保護庁（EPA）の Timothy J Shafer 教授との共同研究体制である。EPA を訪問し、実際に作業を行っている実験補助の方を交えて直接話をすることで技術的な問題が解決できるとともに、プロトコルの最適化を加速することができた。特に、プレートのコーティングおよび細胞播種について、コーティング剤である Laminin を培地に混合しそこに細胞を懸濁させて播種することで、コーティング時間の短縮と電極上への確実な細胞播種を実現することができ、再現性が飛躍的に向上した。また、HESI（Health and Environmental Sciences Institute）の NeuTox サブチームにも参加し、プレバリデーションに関する議論を進めている。

D. 考察

本研究では、神経ネットワーク形成過程およびネットワーク形成後の化学物質の毒性評価系の開発を目指し、プレートのコーティング方法、播種細胞密度、AraC の添加、培地交換の量について検証を行った。その結果、最適だと考えられる条件が選択でき、より高い再現性が得られた。今後、化学物質の毒性評価に望む予定である。また、化学物質の投与方法についても溶媒である DMSO を用いて検証した。DMSO を 10 倍に薄めて投与する方法は測定パラメーターへ影響を与えないことから、今後の化学物質を評価する際の投与方法については、上記方法を採用することとした。今年度開発した評価法をもとに、性・陰性対照物質の発達神経毒性に対する影響を効率よく評価

する予定である。

E. 結論

海馬ニューロンを用いて神経ネットワーク形成過程およびネットワーク形成後の化学物質の毒性評価系の開発を行い、再現性が高く最適な評価系を構築した。また、対照物質の投与方法についても適切な方法を見出した。

F. 研究発表

1. 論文発表

[1] Yamada S., Kubo Y., Yamazaki D., Sekino Y. and Kanda Y. “Chlorpyrifos inhibits neural induction via Mfn1-mediated mitochondrial dysfunction in human induced pluripotent stem cells.” *Sci. Rep.* (2017) 7:40925

2. 学会発表

[1] Yasunari Kanda, Shigeru Yamada, Naoya Hirata, Daiju Yamazaki, and Yuko Sekino. Role of mitochondrial dynamics in neural toxicity assessment in human iPS cells. 5th Annual Meeting of the American Society for Cellular and Computational Toxicology. US EPA Building Research Triangle Park, NC. 2016.9.29-30

G. 知的財産権の出願・登録状況

なし

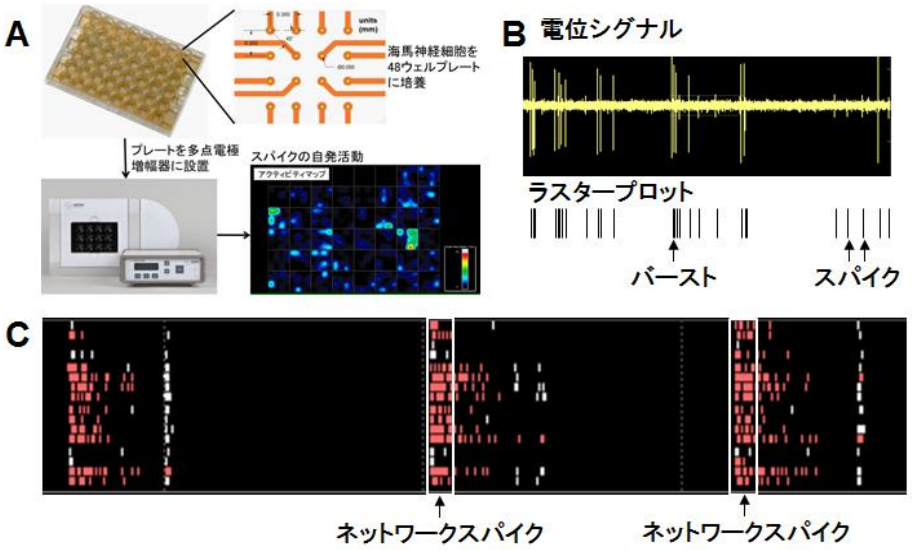

図 1　神経細胞を用いた多点電極システムについて

A. 各ウェルに 16 個の電極が埋め込まれている 48 ウェルプレートに対して凍結ラット胎仔海馬神経細胞を 1 ウェルあたり 50,000 細胞を播種・培養し、 Axion 社製多点電極システムに設置し、神経活動を記録する。神経活動（スパイク）がアクティビティマップとして疑似カラー表示される。B. 1 電極ごとに電位シグナルが検出され、検出閾値よりも大きなシグナルはラスタープロットとして表示される。ラスタープロット 1 本 1 本はスパイクを表しており、スパイクがまとまって発生した場合にはバーストと呼ばれる。C. 1 ウェル（16 電極）のラスタープロット。同期したスパイクをネットワークスパイクと呼ぶ。白のラスタープロットは単一のスパイク、赤のラスタープロットはバーストを表している。

表 1　細胞融解時の生存率について

回数	生細胞数	死細胞数	生存率（%）	総細胞数
1	0.86 x 10^6	0.66 x 10^6	56.6	1.52 x 10^6
2	0.73 x 10^6	0.85 x 10^6	46.2	1.58 x 10^6
3	0.9 x 10^6	0.7 x 10^6	56.3	1.60 x 10^6
4	1.05 x 10^6	0.9 x 10^6	53.8	1.95 x 10^6
5	2.2 x 10^6	2.2 x 10^6	50.0	4.4 x 10^6
6	1.9 x 10^6	2.1 x 10^6	47.5	4.0 x 10^6
7	0.78 x 10^6	0.69 x 10^6	53.1	1.47 x 10^6
8	1.56 x 10^6	0.78 x10^6	66.7	2.34 x10^6
9	0.53 x 10^6	0.68 x 10^6	43.4	1.21 x 10^6
10	0.81 x 10^6	0.54 x 10^6	60.0	1.35 x 10^6
11	1.8 x 10^6	1.35 x10^6	57.1	3.15 x 10^6
12	1.13 x 10^6	0.95 x 10^6	54.3	2.08 x 10^6
13	0.81 x 10^6	0.66 x 10^6	55.1	1.47 x10^6
14	0.98 x 10^6	0.68 x 10^6	59.1	1.65 x10^6
15	0.80 x 10^6	0.72 x 10^6	52.3	1.52 x10^6
平均			54.1	

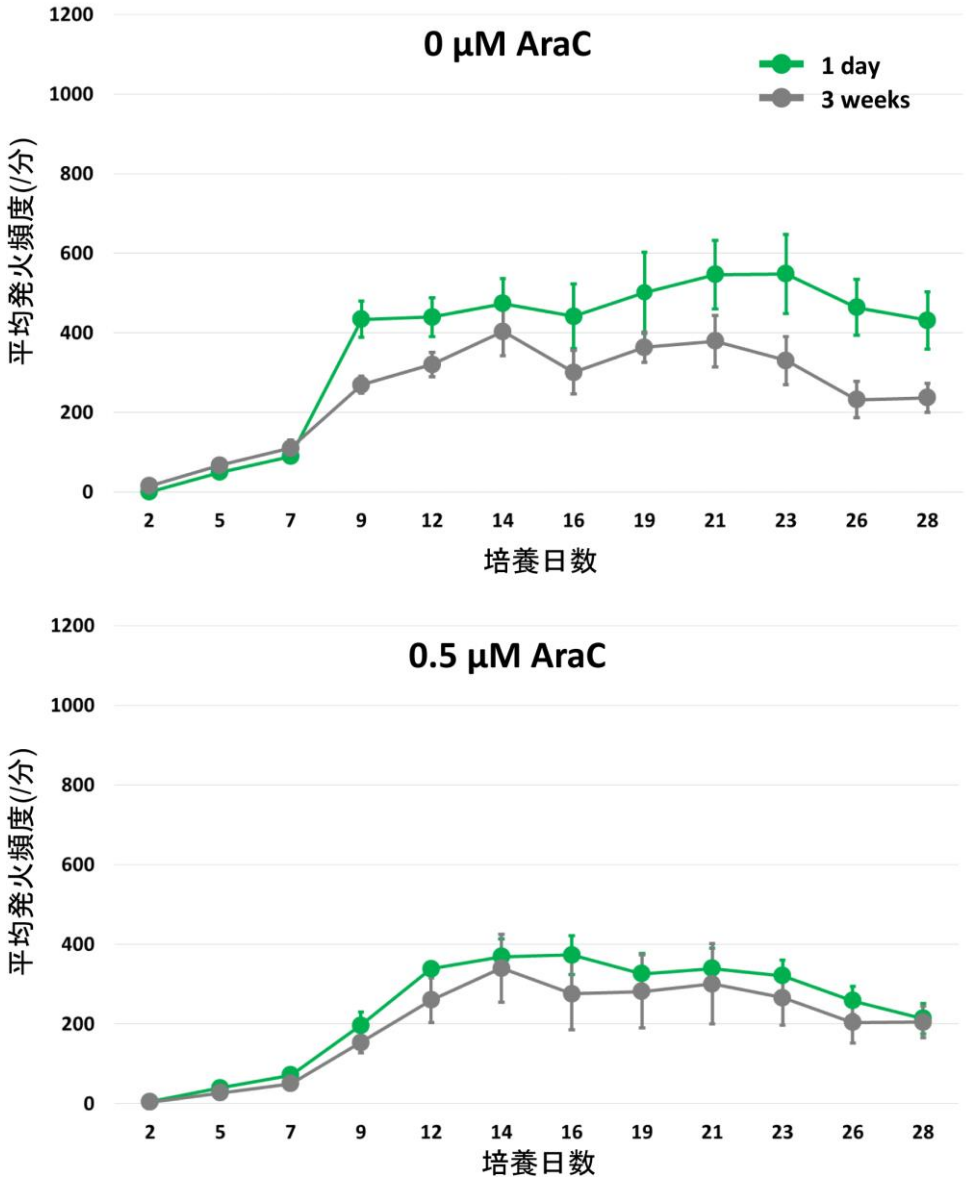

図 2　コーティング後の保存期間の検討

マエストロプレートに対して 0.1% PEI コーティングを行った後、1 日（1 day）あるいは 3 週間（3 weeks）後に細胞を播種し、28 日後まで計測を行った。AraC を適用しない場合（上段）には、3 weeks に比べて 1 day の方が平均発火頻度は高値であった。一方で、0.5 μM AraC の適用（下段）では、1 day および 3 weeks に大きな差はなかったものの、コーティングから時間が経過すると、若干低い平均発火頻度で推移する傾向があった。

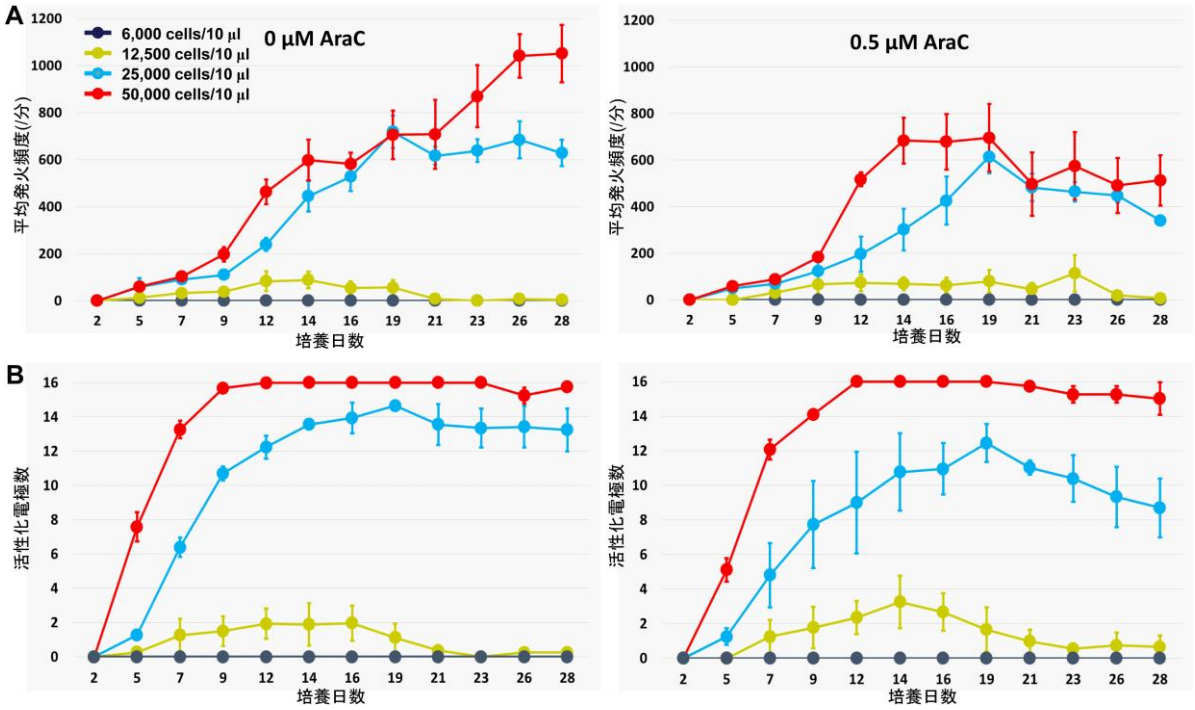

図 3　播種細胞密度の検討

播種細胞密度について 6,000、12,500、25,000、50,000 細胞/10 µl で検討を行った。0 µM AraC（左）および 0.5 µM AraC（右）を適用した際の平均発火頻度（A）および活性化電極数（B）について 28 日まで計測した。6,000 細胞/10 µl および 12,500 細胞/10 µl では、培養期間が 9 日を過ぎたところで平均発火頻度が上昇せず、28 日目まで低値であった。活性化電極数も 12,500 細胞/10 µl や 25,000 細胞/10 µl ではほとんどの電極が活性化しなかった。25,000 細胞/10 µl では、50,000 細胞/10 µl に比べてわずかに遅れて平均発火頻度が上昇したものの、すべての電極が活性化しなかったことから全電極を覆うことができないものと考えられる。

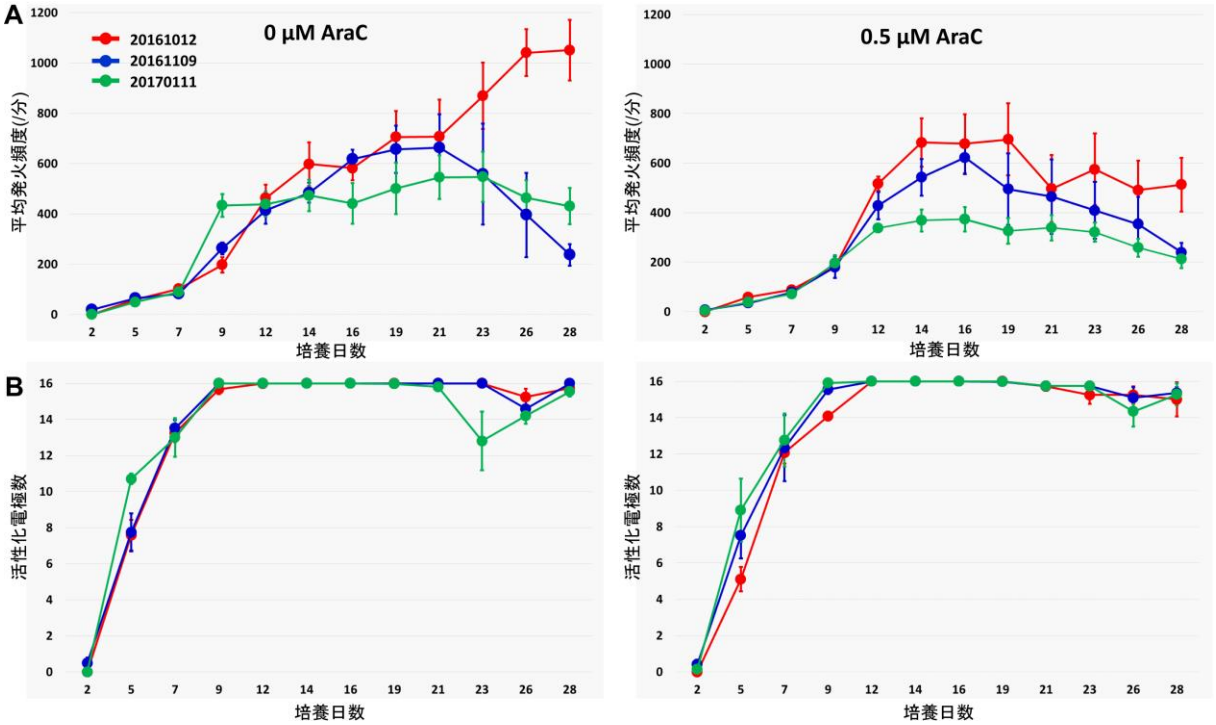

図 4　AraC 濃度の検討

Day 5 から Day 7 の 3 日間に培地に AraC を加えるかどうかの検討を行った。0 μM AraC（左）および 0.5 μM AraC（右）を適用した際の平均発火頻度（A）および活性化電極数（B）について 28 日まで計測した。それぞれ同一ロット、同一条件にて 3 回行った結果を示した。AraC の添加、非添加のいずれにおいても平均発火頻度は Day 7 あるいは Day 9 から上昇し、一部を除いて Day 21 あたりから下降を始めた。活性化電極数については、いずれも Day 12 では最大値まで到達し、Day 19 まではそれを維持した。

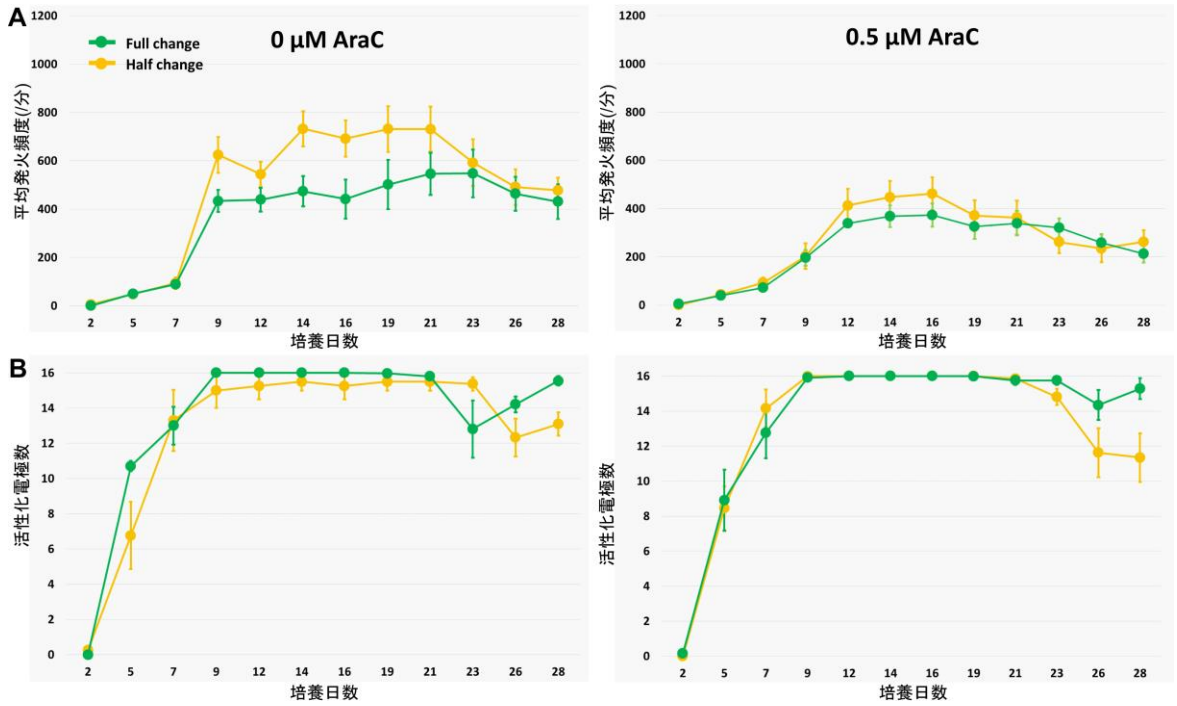

図 5　培地交換量の検討

3 日あるいは 4 日おきに実施している培地交換に関して、交換する培地の量を全量（緑）あるいは半量（黄色）か検討を行った。0 µM AraC（左）および 0.5 µM AraC（右）を適用した際の平均発火頻度（A）および活性化電極数（B）について 28 日まで計測した。平均発火頻度については、0 µM AraC の半量交換を除いて他の 3 条件はほぼ同じような値で変化した。活性化電極数についても 0 µM AraC の半量交換のみ最大値に到達しなかった。半量交換の条件では、培養期間後半の Day 23 あたりから活性化電極数の下降が目立った。

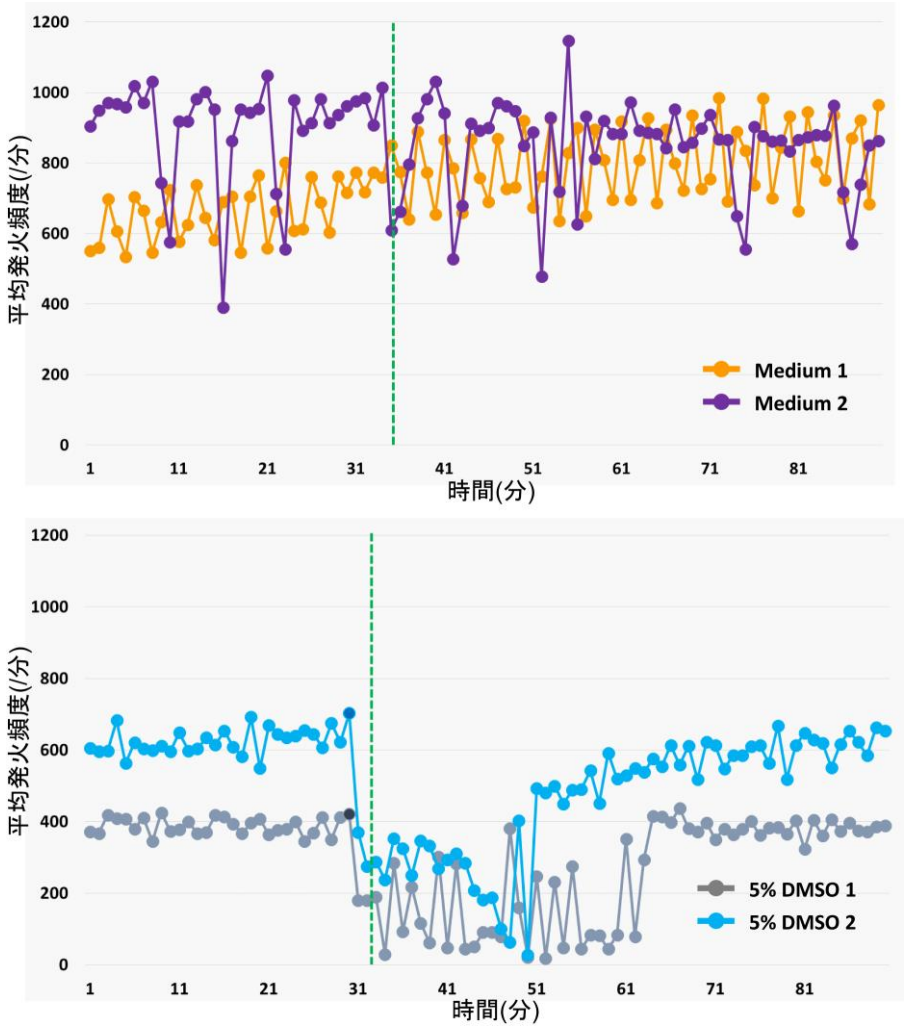

図 6　投与方法に関する検討 1

化学物質の投与方法に関する検討。およそ 30 分間の測定後に 10 µl の medium（上段）および 5% DMSO（下段）を 1 ショットでウェル中に投与し、その後 60 分間平均発火頻度を記録した。1 分間ごとの総平均発火頻度をプロットした。緑色の点線がそれぞれ投与したタイミングである。Medium を投与した細胞は培養 26 日目、DMSO を投与した細胞は培養 16 日目である。Medium の投与では、平均発火頻度に大きな乱れは観察されなかったが、5% DMSO の投与によって急激な平均発火頻度の下降が観察され、その後 30 分間元の値に戻らなかった。

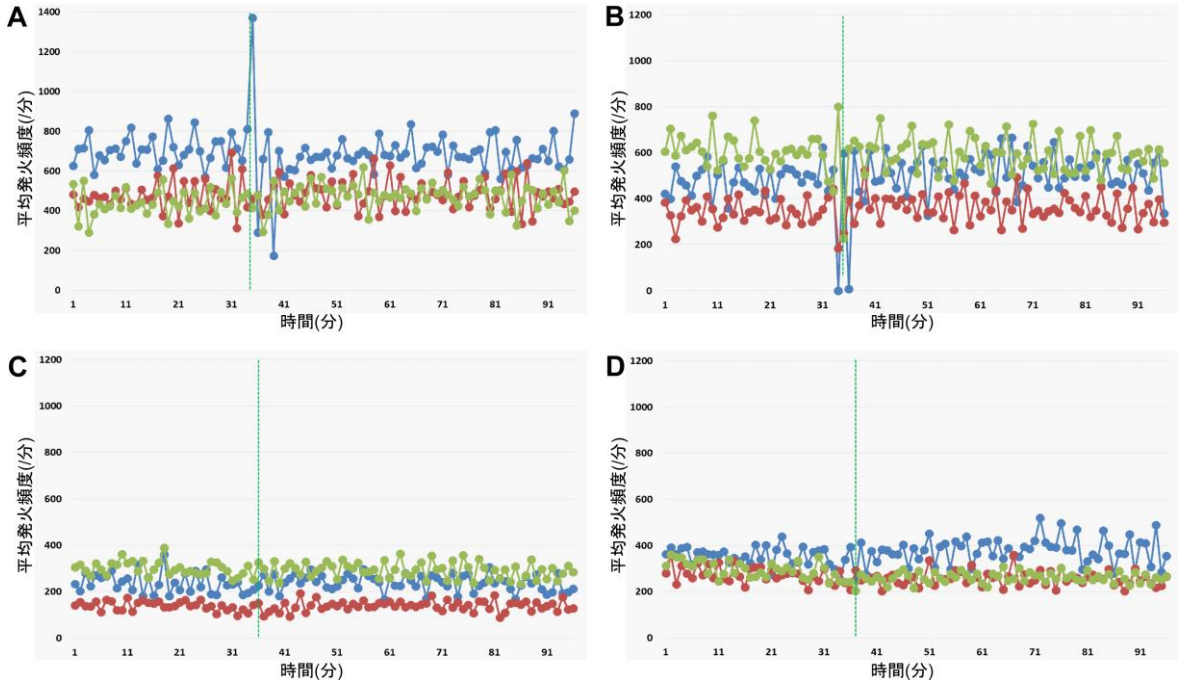

図 7　投与方法に関する検討 2

化学物質の投与方法に関する検討。およそ 30 分間の測定後に 5% DMSO をウェルにゆっくりと添加（A)、96 ウェルプレートに分注した 10 µl の 5% DMSO に記録するウェルから 50 µl の培地を抜いて混合しその混合液を記録するウェルに添加（B)、96 ウェルプレートに分注した 10 µl の 5% DMSO に記録するウェルから 100 µl の培地を抜いて混合しその混合液を記録するウェルに添加（C）および 96 ウェルプレートに分注した 10 µl の 5% DMSO に記録するウェルから 200 µl の培地を抜いて混合しその混合液を記録するウェルに添加（D）した。添加の後 60 分間平均発火頻度を記録した。1 分間ごとの総平均発火頻度をプロットした。緑色の点線がそれぞれ投与したタイミングである。100 µl 以上の培地に 5% DMSO を混合した場合に添加による影響が観察されなくなった。

厚生労働科学研究費補助金（化学物質リスク研究事業）
分担研究報告書

生後小脳の神経回路の機能的影響による評価法の開発

研究分担者　豊橋技術科学大学　環境・生命工学系
吉田　祥子
研究協力者　国立医薬品食品衛生研究所　薬理部長
関野　祐子

要旨
本年度は、化学物質に対して感受性の高いラット小脳皮質を用いて、化学物質曝露による神経突起進展、神経回路形成への影響を検討し、最も適切な定量化方法を決定することを目的として実施した。ヒト自閉症誘発が報告されているバルプロ酸、およびクロルピリホスに加え，同様の薬理作用機序が考えられる SAHA、MS-275、環境毒性物質の有機スズについて、神経細胞レベルおよび小脳組織レベルでの変化を観察し、定量化を試みた。さらにバルプロ酸について、投与時期と投与濃度を変化させその効果を検討した。本年度は、化学物質投与による神経伸長変化の定量化、小脳虫部第一裂の過剰な褶曲の定量化、行動観察の定量化を行った。その結果、遅発性神経毒性が考えられる化学物質であるバルプロ酸、クロルピリホスが、生後の神経回路発達の変化を小脳神経細胞の突起伸展と小脳構造の変化、動物の行動変化を引き起こすことを定量的に示した。これにより投与量依存性、投与時期依存性が明瞭になり、さらに遺伝子レベル、たんぱく質レベルでの発達期神経毒性の定量化につなげることが期待される。

A. 研究目的

ヒト自閉症誘発が報告されているバルプロ酸（VPA）、VPA と同様にヒストン脱アセチル化酵素（HDAC）阻害剤であるスベロイルアニリドヒドロキサム酸（SAHA）、MS-275、ヒト自閉症誘発が報告されているクロルピリホス（CPF）、および環境毒性物質のトリブチルスズ（TBT）投与による小脳発達への影響を、免疫組織化学的手法による神経の形態的変化、およびヘマトキシリン–エオシン染色（HE 染色）による小脳虫部全体の構造変化を観察した。さらに個体の行動に及ぼす変化を確認するために、発達期個体の行動観察を行った。

B. 研究方法

近年自閉症の変異部位であることが報告されている小脳を研究試料として用いた。各化学物質を妊娠動物に投与し、出生動物の小脳を摘出してその効果を観察した。妊娠 16 日のラットに、600 mg/kg の VPA（経口）、50 mg/kg の SAHA（腹腔内）、4 mg/kg の MS-275（経口）、10 mg/kg の CPF（経口）、20 mg/kg の TBT（経口）をそれぞれ投与した。VPA については、妊娠 14 日、18 日にそれぞれ 600 mg/kg の投与することを試験した。また，妊娠 16 日に 200 mg/kg、300 mg/kg、400　mg/kg の VPA 投与を試験した。

各投与動物を生後 2 から 3 週で灌流固定後、小脳虫部の矢状面スライスを調整し、抗カルビンジン抗体による蛍光染色を行った。さらにスライス全体を HE 染色し、皮質層の変化を観察した。また各投与動物の任意に選んだ 3 匹について、生後 4 日から 10 日にかけて、温度維持した明環境下での 3 分間の自由行動の観察を行った。

抗カルビンジン抗体染色によってプルキンエ細胞の樹状突起長を測定し，化学物質投与による神経伸長変化の定量化を行った。

小脳虫部スライスの第 V/VI 小葉間にある primary fissure（第一裂）について、プルキンエ層の長さと裂の深さの比を計算し、投与動

物と対照動物を比較して化学物質投与の影響の定量化を行った。

行動観察では，震えのような不随意運動の出現率を計測し、定量化を行った。

C. 研究結果

VPA投与動物、SAHA投与動物では,プルキンエ細胞の樹状突起伸長が対照動物より早く著しく、生後2週で1.6倍、生後3週でも1.3倍の伸長を示した。この現象はCPF投与動物でも観察されるが、MS-275投与動物、TBT投与動物では観察されなかった（図1、図2）。

VPA投与動物では、小脳虫部第一裂に過剰な褶曲ができることが観察された。これにより、プルキンエ層が長くなり，対照動物よりも1.2倍のプルキンエ層を持つに至った。この変化はCPF投与動物でも観察され、1.05倍のプルキンエ層を示した。一方MS-275、TBT投与動物では観察されず、神経突起伸展異常と同様の傾向を示した。妊娠14日にVPAを投与した動物では1.25倍のプルキンエ層が観察されたが、妊娠18日投与動物は対照動物と差を示さなかった。この変化はVPAの投与量に正の相関を示した（図3、図4）。

行動観察の結果、VPA投与動物では,P4で多くの不随意運動を確認したが、成長するにつれて減少する傾向にあった。SAHA投与動物では,対照動物やVPA投与動物と比較して多くの不随意運動を確認し、且つP4～P8にかけ増加する傾向が見られた。MS-275投与動物では対照動物より若干の不随意運動の増加が確認されたが,著しい変化は確認できなかった。TBT投与動物では,対照動物と比較して多くの不随意運動を確認することができた。また, P4～P7にかけて不随意運動が増加する傾向にあった（図5）。

D. 考察

今回提案した小脳変化の定量法によって、自閉症誘発が疑われる化学物質の神経毒性の定量化の可能性を示した。小脳の広い範囲に及ぶ変異は、SHH 遺伝子の発現変異や発生制御たんぱく質、神経栄養因子などの発現変異を示唆しているものと考えられる。動物を用いた試験法から得られた神経回路レベル、行動レベルでの変化を細胞レベルの変化につなげて行くことが必要であると考えられる。

E. 結論

本研究において、遅発性神経毒性が考えられる化学物質であるバルプロ酸、クロルピリホスを胎生期の動物に投与し、生後の神経回路発達の変化を小脳神経細胞の突起伸展と小脳構造の変化、動物の行動変化から定量化して示した。定量化により投与量依存性、投与時期依存性が明瞭になり、さらに遺伝子レベル、たんぱく質レベルでの発達期神経毒性の定量化につなげることが期待される。

F. 研究発表

1. 論文発表

[1] Mabuchi H., Ong HY., Watanabe K., Yoshida S. and Hozumi N. “Visualization of Spatially Distributed Bioactive Molecules Using Enzyme-Linked Photo Assay.” *IEEJ Transactions on Fundamentals and Materials*, (2016) Vol.136, No.2, pp.99-104

2. 学会発表

[1] 冨田達朗、岩本早起、笛田由紀子、上野晋、関野祐子、Roman Maev、穂積直裕、吉田祥子、Alteration of cerebellar lobules in Valproate-induced autistic model rat、第39回日本神経科学大会、2016　横浜

[2] 西川ちひろ、高橋信人、冨田達朗、重本−最上由香里、佐藤薫、関野祐子、馬渕光、穂積直裕、吉田祥子、Interaction between neurosphere and cultured glial cell、第39回日本神経科学大会、2016　横浜

[3] 三上哲理、渡邊一徳、笛田由紀子、上野晋、関野祐子、穂積直裕、吉田祥子、Fast glutamate release detection in normal and valproate- administrated rat cerebellum、第39回日本神経科学大会、2016　横浜

[4] 高橋信人，馬渕光，重本−最上由香里，佐藤薫，関野祐子，穂積直裕，吉田祥子，Visualization of neurotransmitter release in the developing neuroshere cells using the enzyme-linked photo-assay、第39回日本神経科学大会，　2016　横浜

[5] 中嶋さりい、冨田達朗、笛田由紀子、上野晋、関野祐子、吉田祥子、Alteration of neuronal development by Autism-induce drugs and recovery effects with bumetanide in developing rat cerebellum、第39回日本神経科学大会、2016　横浜

[6] Hikaru Mabuchi, Nobuto Takahashi, Kaoru Sato, Yuko Sekino, Naohiro Hozumi and

Sachiko Yoshida. Visualization of neurotransmitter released from cultured granule cells and the neuroshere cells using enzyme-linked photo-assay combined with ICA. 46th Neuroscience meeting, 2016 San Diego

[7] Sari Nakajima, Tatsuro Tomida, Koichiro Ikai, Yukiko Fueta, Susumu Ueno, Naohiro Hozumi, Yuko Sekino and Sachiko Yoshida. Alteration of Purkinje cells by autism-inducing drugs, and recovery effects with bumetanide or oxytocin administration in developing rat cerebellum. 46th Neuroscience meeting, 2016 San Diego

[8] 佐藤誠太、中嶋さりい、笛田由紀子、上野晋、関野祐子、吉田祥子、抗てんかん薬バルプロ酸の曝露期・曝露濃度による発達期神経毒性の変化、第 47 回中部化学関係学協会連合会秋季大会、2016　豊橋

G. 知的財産の出願・登録状況

1. 特許出願

吉田祥子，穂積直裕，氏家雅彦，光学観察装置，特願 2016-221213

2. 実用新案登録

なし。

3. その他

なし。

(Bar = 100μm)

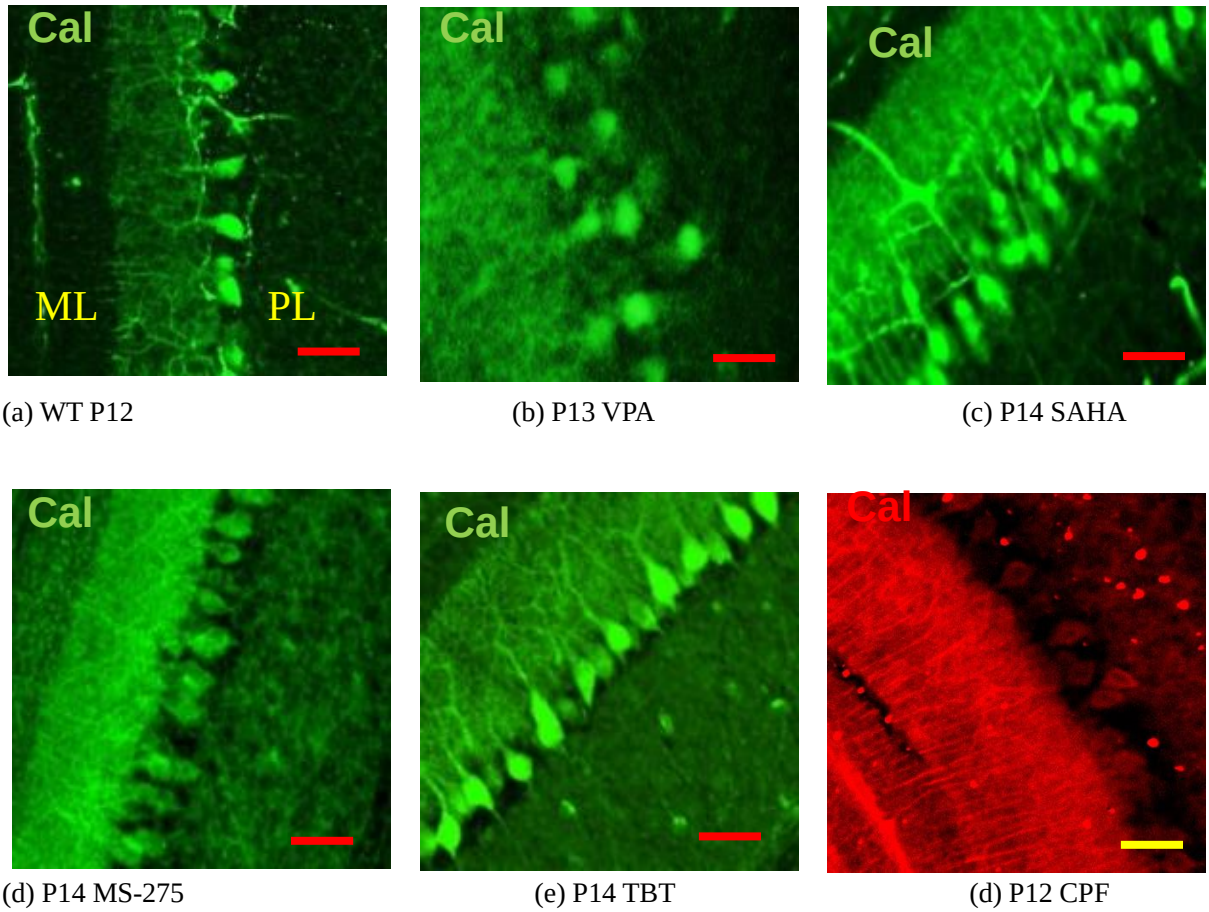

(a) WT P12　(b) P13 VPA　(c) P14 SAHA

(d) P14 MS-275　(e) P14 TBT　(d) P12 CPF

図 1　各種物質投与動物の小脳プルキンエ細胞。抗 Calbindin D-28k 抗体染色。

WT:対照動物、VPA:バルプロ酸投与動物、SAHA:　スベロイルアニリドヒドロキサム酸投与動物、MS-275:MS-275 投与動物、TBT:トリブチルスズ投与動物、CPF:クロルピリフォス投与動物のそれぞれ小脳。

VPA 投与動物、および SAHA 投与動物では、細胞体が一列に並ばず，樹状突起の乱れが観察された。

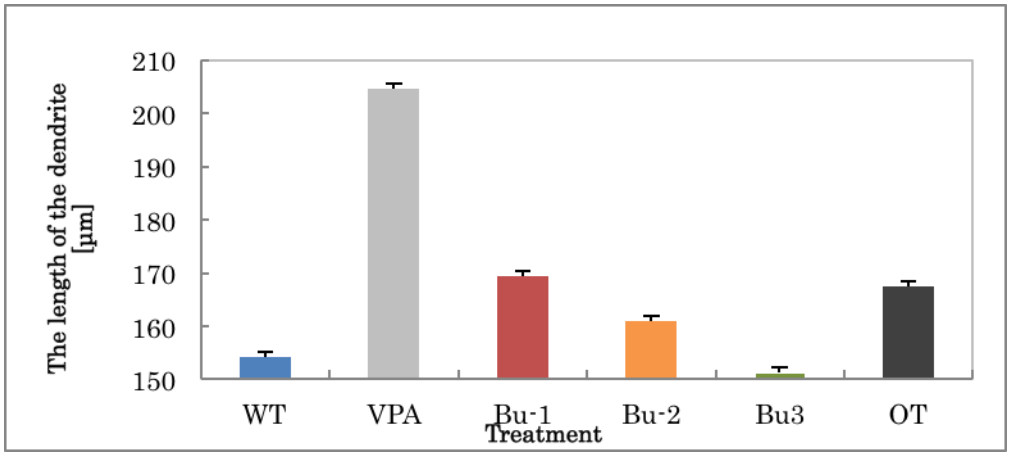

図 2　各種物質投与動物の生後 21 日における小脳プルキンエ細胞樹状突起の長さ

WT:対照動物、VPA:バルプロ酸投与動物、Bu-1、Bu-2、Bu-3、OT:VPA 投与動物にブメタニド(Bu)またはオキシトシン(OT)を追加投与した動物

生後 21 日では、バルプロ酸投与動物に著しい樹状突起伸長が観察された。これらの伸長は、ブメタニド，またはオキシトシンの追加投与で改善された。

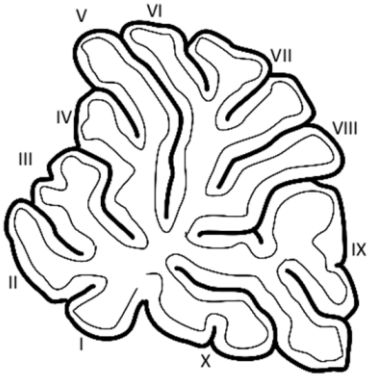

生後 16 日　対照動物小脳

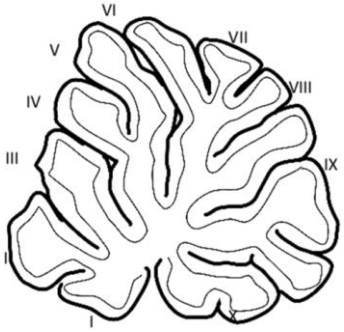

VPA 200 ㎎/kg 投与動物小脳　(P15)

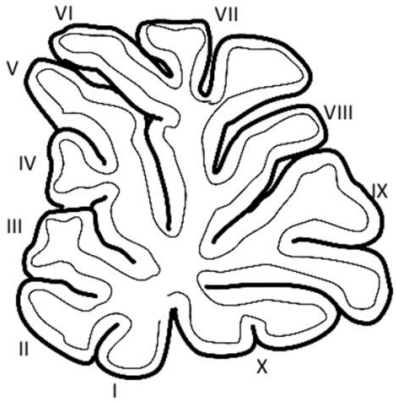

VPA 400 ㎎/kg 投与動物小脳　(P16)

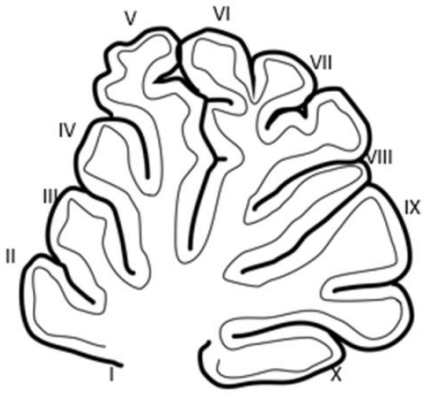

VPA 600 ㎎/kg 投与動物小脳　(P16)

図 3　各条件で VPA を投与した動物の小脳虫部の褶曲構造の変化

(a)

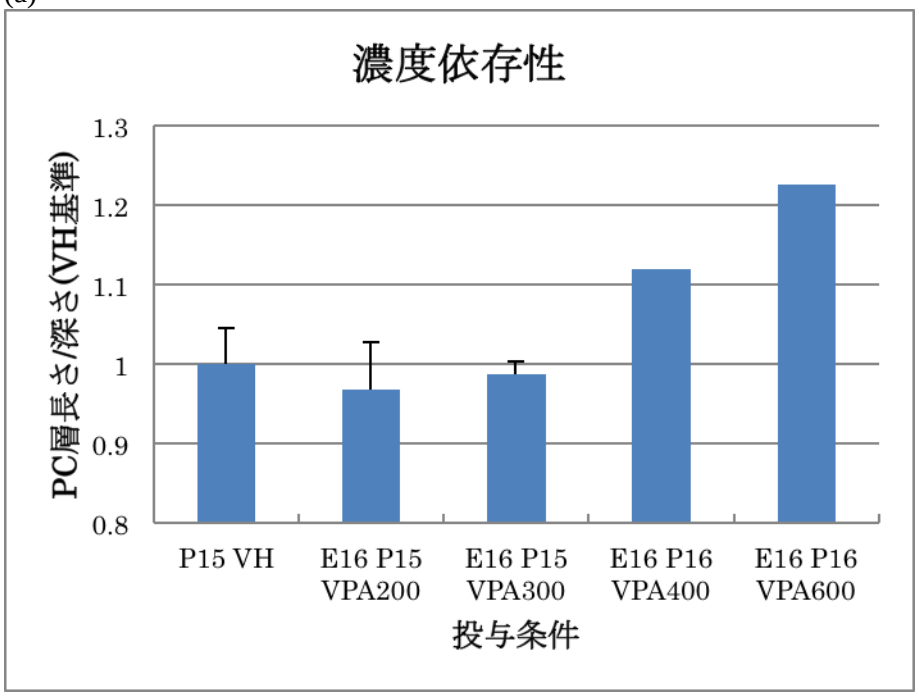

(b)

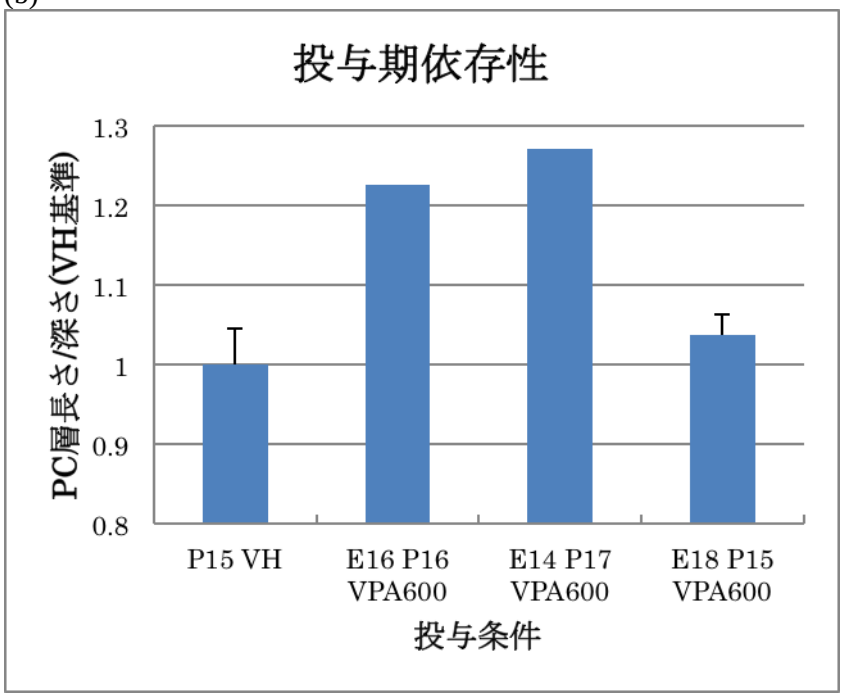

図 4　VPA の投与濃度(a)、投与時期(b)による小脳虫部の褶曲度の変化

(a)

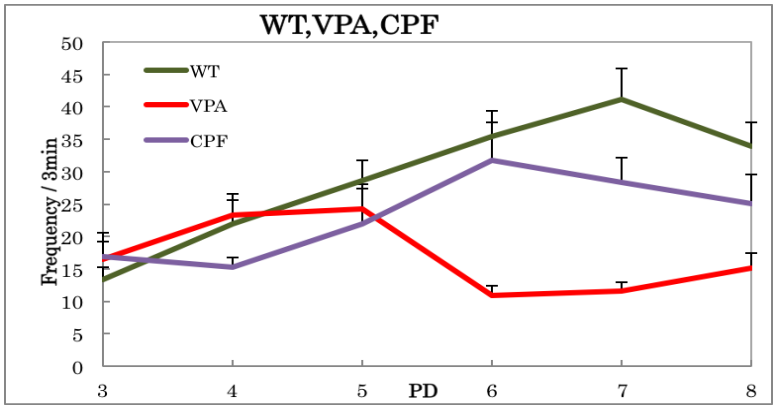

(b)

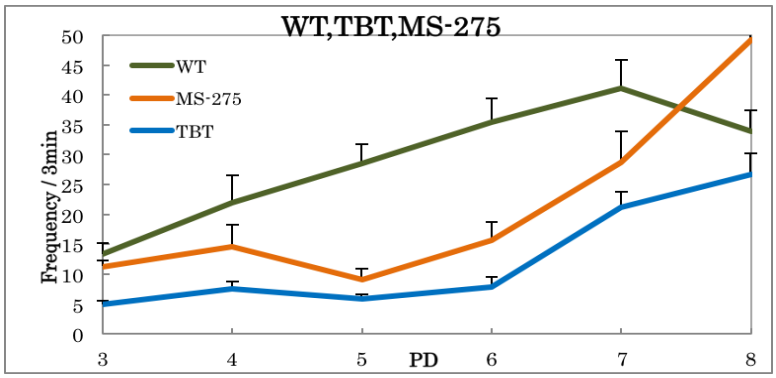

(c)

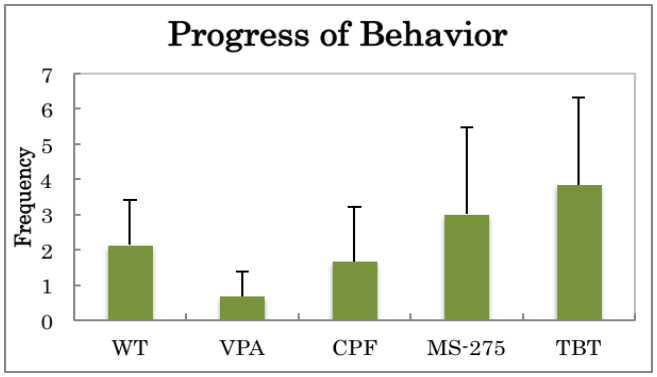

図 5　VPA,CPF,TBT,MS-275 投与動物の生後１０日程度の不随意運動の発生頻度
(a)VPA は対照動物よりも早く不随意運動の低下が見られる。
(b)TBT や MS-275 ではむしろ遅くなる。
(c)運動の頻度変化をしめす。

厚生労働科学研究費補助金（化学物質リスク研究事業）
分担研究報告書

幼若期海馬の神経回路機能による評価法の開発

研究分担者　産業医科大学　産業生態科学研究所　教授
上野　晋
研究協力者　産業医科大学　産業保健学部　講師
笛田由紀子
研究協力者　豊橋技術科学大学　環境・生命工学系　講師
吉田祥子

要旨
本研究班が提案してきた遅発性神経毒性試験手法の妥当性を調べる目的で、産業化学物質 1-ブロモプロパン（1BP）を対象として検討した。1BP では生殖毒性や神経毒性などが報告されているが、発達神経毒性は不明であり、ヒトにおける事例も報告されていない。そこで妊娠ラットに対して 1BP の吸入曝露を行い、産まれた仔ラットの授乳期である 2 週齢、離乳後である 5 週齢、性成熟後の 8 週齢および 13 週齢にわたって、海馬の神経回路機能を検討した。その結果、1BP 胎生期曝露により 2 週齢で神経回路機能の興奮性が亢進することが認められた。このことから、バルプロ酸の胎生期曝露と同様に、1BP 胎生期曝露も神経発達期において神経回路興奮性の亢進をもたらすことが判明した。一方、8 週齢および 13 週令において、海馬神経回路における抑制系回路の指標となるフィードバック抑制が減弱することが認められ、性成熟後では抑制系回路機能の減弱によって神経回路興奮性が変化する可能性が示唆された。以上の結果から 1BP は遅延性発達神経毒性を有する可能性が示唆され、産業化学物質についても生後早期の海馬神経回路機能の評価が発達神経毒性の評価指標として有用となる可能性が確認された。

A. 研究目的

我々はこれまでに胎生期・神経発達期の化学物質曝露に起因する生後の遅発性神経毒性を評価する in vitro 試験法の開発を目指し、作用の異なる神経毒性物質（自閉症モデル動物作製に用いられるバルプロ酸、内分泌かく乱作用を示す有機スズ化合物、有機リン系農薬の一つであるクロルピリホス）を用いて、海馬神経回路機能の変化の有無を指標とした発達期の神経毒性評価を行ってきた。この知見をもとに、本申請課題の初年度、当分担研究班では発達神経毒性が不明な産業化学物質 1-ブロモプロパン（1BP）を用い、妊娠ラットに吸入曝露して産まれた仔ラットの脳スライス標本を採取し、授乳期、離乳後、性成熟後の神経回路異常の有無について電気生理学的手法による検証を行った。

B. 研究方法

1. 1BP の吸入曝露（研究協力者　笛田由紀子）

Wistar 系妊娠ラット（株式会社九動より購入）に対して、曝露チャンバー内で 1BP を濃度 200、400、700 ppm で 1 日 6 時間、妊娠 1～20 日目まで 20 日間の反復吸入曝露を行った。対照群には同様のチャンバーで新鮮空気を供与した。

2. 体重測定（研究協力者　笛田由紀子）

仔ラットの体重は毒性を評価する最も簡便な指標となる。よって、授乳期である生後 2、7、14、18 日にわたって体重を測定した。

3. 電気生理学的評価のための脳スライス標本の作製（研究協力者　笛田由紀子）

生後 2、5、8、13 週齢の雄性仔ラットをエーテルで深麻酔下断頭したのち海馬スライス標本を作製した。母ラットへの吸入曝露お

よび仔ラット出生後にスライスを作製する時期は、バルプロ酸胎生期曝露モデルを作製した時の実験プロトコルに順じた（図 1）。バルプロ酸胎生期曝露モデルでは、神経回路機能に変化が認められたのが開眼前であったことから、今回の 1BP 胎生期曝露モデルでは、あらかじめ予備実験で開眼時期を検討しており、その結果開眼時期に対する 1BP 胎生期曝露の影響は認められなかった（平均開眼日、対照群 : 生後 15.6 日 ; 700 ppm : 15.7 日）。そこで、2 週齢のラットについては生後 13、14 日齢を開眼前期、生後 15 日齢を開眼期とする 3 種類の日齢に分けて解析した。

4. 刺激応答性とフィードバック抑制の電気生理学的評価法（研究協力者　笛田由紀子）

バルプロ酸胎生期曝露モデルでの検討と同様に、刺激電極と記録電極を海馬スライスに設置した後（図 2）、CA1 領野の錐体細胞層からは集合スパイク電位を、シナプス層から集合興奮性シナプス後電位を記録して神経回路興奮性および興奮性シナプス強度を評価した（図 3）。

評価法は、まず単一の電気刺激を与えたときの神経細胞の応答性の発達に伴う変化を、対照群、200 ppm 群、400 ppm 群および 700 ppm 群に分けて解析した。

フィードバック抑制は 2 連続刺激で誘発される電位を用いて評価した。すなわちフィードバック抑制が形成されていれば、2 回目の応答は 1 回目の応答よりも小さくなる。つまり、2 回目の応答の大きさを 1 回目の応答の大きさで除した比（ペアパルス比）が 1 よりも小さい値となる。この解析手法により、ペアパルス比が 1 よりも小さい場合では、抑制系の強さを簡便にかつ定量的に評価できる。

さらに離乳後の仔ラットを用いて、成長に伴う 1BP 胎生期曝露による影響の出現についても検討することとしたが、この検討には対照群と 700 ppm 群での比較を行った。

（倫理面への配慮）

本研究の遂行にあたっては、産業医科大学に定められた、関係する遵守すべき指針等を把握して、十分な管理体制のもと、倫理面に万全の配慮をしながらそれぞれの研究が進められた。

C. 研究結果

これまで検討してきたバルプロ酸の胎生期曝露による神経発達への影響と類似して、1BP の胎生期曝露でも、神経回路の刺激応答性の亢進（図 4）と興奮性シナプス強度の増強（図 5）が開眼前期である生後 14 日齢で認められた。

授乳期のラットの体重増加については、出産時は対照群と 700 ppm 群で有意差が認められないものの、生後 18 日齢までの評価によって 1 割程度の体重増加抑制が 700 ppm 群で見られた（図 6）。

離乳後 5 週齢の単一刺激への神経細胞の応答については、対照群と 700 ppm 群に有意差は認められず（図 7）、性成熟後の 8、13 週齢においても 1BP 胎生期曝露の影響は認められなかった。

しかしながら、2 連続刺激による誘発電位の変化については、性成熟後でも 1BP 胎生期曝露の影響が認められた（図 8）。対照群では、授乳期ではペアパルス比が約 2.0 となる、いわゆる促通効果が認められたが、離乳後（5 週齢以降）にはペアパルス比は著しく小さい値となりフィードバック抑制が形成されていることが認められた。一方、700 ppm 群ではすでに授乳期において、軽度ではあるもののフィードバック抑制（ペアパルス比 <1.0）が認められた。5 週齢では対照群と同程度のペアパルス比を示したが、8 週齢以降、すなわち性成熟後のペアパルス比は対照群と比較して有意に大きく、フィードバック抑制が減弱していることが判明した。

D. 考察

産業化学物質 1BP の胎生期曝露ラットにおいて、バルプロ酸の胎生期曝露ラットで見出した現象と類似した、生後 2 週齢、特に開眼前期での海馬神経回路興奮性の亢進が認められた。このことから、1BP も発達神経毒性を有する化学物質である可能性が示唆される。しかしながら 1BP の胎生期曝露ラットが離乳後あるいは性成熟後にバルプロ酸胎生期曝露ラット、すなわち自閉症モデルラットと類似した社会行動異常を示すかは今後の検討課題として、本研究では電気生理学的手法による神経回路興奮性のみを指標として性成熟後まで検討した。その結果、700 ppm 群では、対照群に比べてフィードバック抑制が有意に減弱することが判明した。フィードバック抑制の減弱は神経回路興奮性

の変化を示す素因となり得ることがヒトやてんかんモデル動物において示されている。本研究は動物実験ではあるが、妊娠ラットに吸入曝露させた 1BP が、成長後の仔ラット脳の神経回路興奮性に影響を及ぼすという発達神経毒性を有する可能性を示唆するものである。さらにこの 1BP がもたらす遅発性神経毒性が、本研究で用いた我々の発達神経毒性評価法により、授乳期に予測できる可能性が示唆された。

1BP については日本産業衛生学会許容濃度等委員会より許容濃度（0.5ppm）がすでに勧告されているものの、その提案理由の中に発達神経毒性はもとより発達毒性も考慮されていない。一方、米国産業衛生専門家会議（ACGIH）が設定した許容濃度（0.1ppm）には、ヒトの事例は認められないものの動物実験データに基づく発達毒性は考慮されているが、発達神経毒性については検討されていない。また母性保護のために、生殖機能などに有害な化学物質が発散する場所での女性労働者の就業を禁止する「女性労働基準規則（女性則)」において、現在対象となっているのはわずか 25 物質に留まっている。日本の労働現場で取り扱われている化学物質は約 60,000 種類あり、毎年約 1,200 物質は新規に届出がなされている。発達毒性あるいは発達神経毒性を有する化学物質は女性則の対象物質になり得ると考えられるが、これら毒性の情報あるいは評価が十分行われているとは言い難い。産業化学物質の発達神経毒性評価にも本研究で用いた評価手法が応用できれば、個々の化学物質の許容濃度の提案、あるいは女性則の対象物質として提案に向けた評価などに対して、有益な情報を提供できることが期待される。

今回の曝露条件については、1BP の産業現場における曝露様式を想定して吸入曝露という経路を選択し、また曝露濃度および曝露期間については、先行研究（論文発表［1]）の中で作製した 1BP 胎生期曝露ラットにおける濃度を最高濃度としてさらに濃度を低く設定した。また妊娠した女性の就業を模して曝露期間は 20 日間を選択した。バルプロ酸や有機スズ化合物の評価を行った時のように妊娠後期における単回曝露という様式でも産業化学物質が評価できるかどうかは今後の検討課題である。

また、授乳期の神経回路興奮性の亢進には抑制性神経伝達物質 GABA のトランスポーターの分布が関連している可能性を研究協力者の笛田と吉田が見出しており、現在その詳細について検討中である。

E. 結論

発達神経毒性の詳細が不明であった産業化学物質である 1BP について検討した結果、胎生期曝露によって神経回路興奮性の亢進をもたらすことから、1BP が発達神経毒性を有する可能性が示唆された。

F. 研究発表

1. 論文発表

[1] Ishidao T., Fueta Y., Ueno S., Yoshida Y. and Hori H. “A cross-fostering analysis of bromine ion concentration in rats that inhaled 1-bromopropane vapor.” *J Occup Health* (2016) 58:241-246

[2] Fueta Y., Sekino Y., Yoshida S., Kanda Y. and Ueno S. “Prenatal exposure to valproic acid alters the development of excitability in the postnatal rat hippocampus.” 論文投稿中

[3] Fueta Y., Ishidao T., Ueno S., Yoshida Y., Kanda Y. and Hori H. “Prenatal exposure to 1-bromopropane causes delayed adverse effects on hippocampal neuronal excitability in the CA1 subfield of rat offspring.” 論文投稿中

[4] Igarashi T., Wilson DJ. and Ueno S. “Acute exposure to toluene and xylene decrease the expression of connexin43 in human cardiac myocytes.” 論文投稿中

2. 学会発表

[1] 笛田由紀子、関野祐子、吉田祥子、上野晋、胎生期トリブチルスズあるいは酢酸スズ単回投与による授乳期ラットの行動と興奮・抑制系の変化、 第43回日本毒性学会学術年会、2016　名古屋

[2] Sari Nakajima, Tatsuro Tomida, Yukiko Fueta, Susumu Ueno, Yuko Sekino and Sachiko Yoshida. **Alteration of neuronal development by autism-induce drugs and recovery effects with bumetanide in developing rat cerebellum. The 39th annual meeting of the Japan Neuroscience Society, 2016　横浜**

[3] **Tatsuro Tomida, Saki Iwamoto, Yukiko Fueta, Susumu Ueno, Yuko Sekino,**

Roman Maev, Naohiro Hozumi and SachikoYoshida. Alteration of cerebellar lobules in Valproate-induced autistic model rat. **The 39th annual meeting of the Japan Neuroscience Society, 2016　横浜**

[4] Yukiko Fueta, Yuko Sekino, Sachiko Yoshida and Susumu Ueno. Novel approaches for electrophysiological and pharmacological evaluation of developmental neurotoxicity of chemicals using juvenile rat brain slices. 5th Prenatal Programming of Toxicology, 2016　北九州

[5] Tatsuro Tomida, Yukiko Fueta, Susumu Ueno, Naohiro Hozumi, Yuko Sekino and Sachiko Yoshida. Alteration of Purkinje ce4lls by autism-inducing drugs, and recovery effects with bumetanide or oxytocin administration in developing rat cerebellum. The 44th Annual Meeting of Society for Neuroscience, 2016　San Diego

G. 知的財産の出願・登録状況

（該当なし）

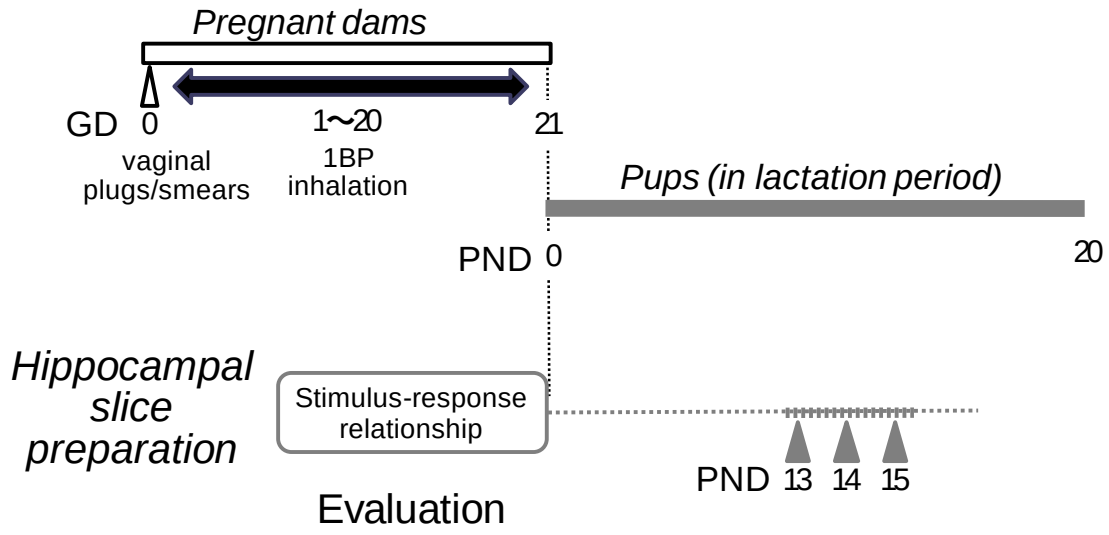

図 1　海馬スライスを用いた電気生理学的手法による発達神経毒性評価のためのプロトコル
ラットの妊娠期 1-20 日の 20 日間、産業化学物質 1BP を吸入曝露した。開眼前の生後 13、14 日および開眼が始まる生後 15 日の 3 日間に、連続して海馬スライス標本を作製して発達神経毒性の評価を行った。

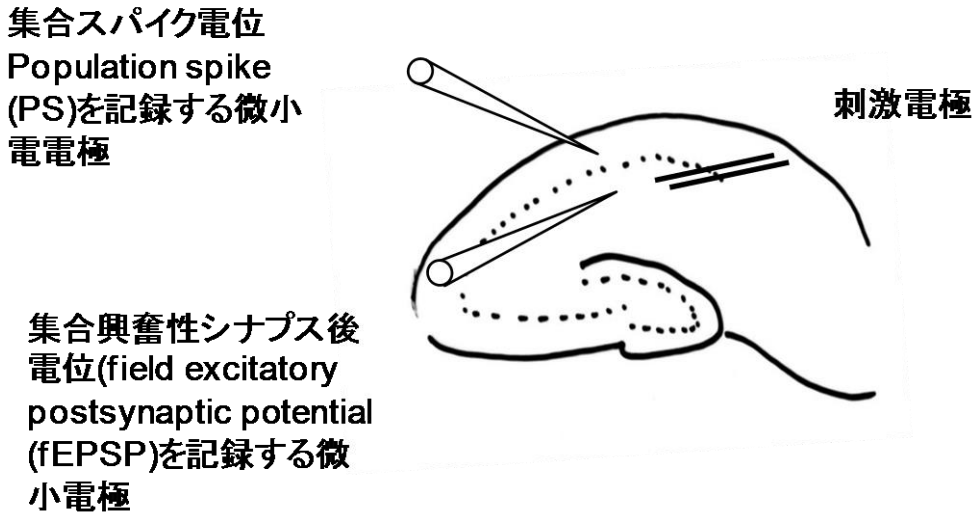

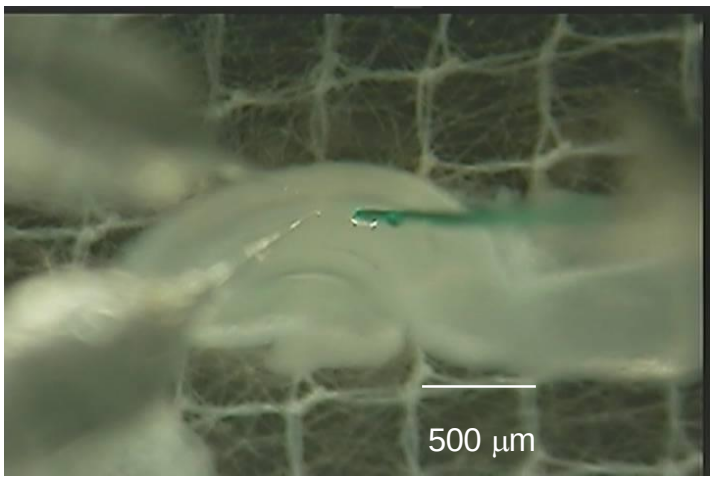

実体顕微鏡下に観察される海馬スライスと
2本の記録電極と刺激電極(緑)

図 2　発達神経毒性評価法のための海馬スライスを用いた電気生理学的手法

上図：海馬スライスにおける双極性電気刺激電極の位置と 2 つの記録用ガラス微小電極を示す。下図：実体顕微鏡下に撮影した生の海馬スライスと、刺激電極（左）および記録用ガラス微小電極（左）の配置。

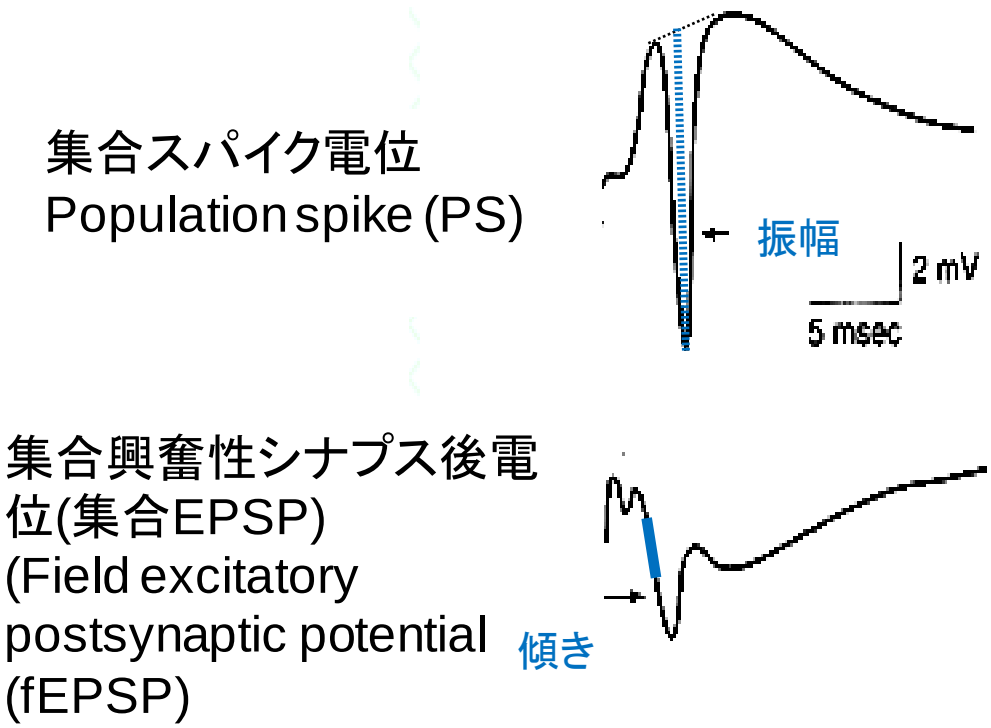

図 3　発達神経毒性評価の指標とする集合スパイク電位(PS)の振幅～回路興奮性を反映～と集合興奮性シナプス後電位の傾き(fEPSP slope)～興奮性シナプス強度を反映～の計測方法

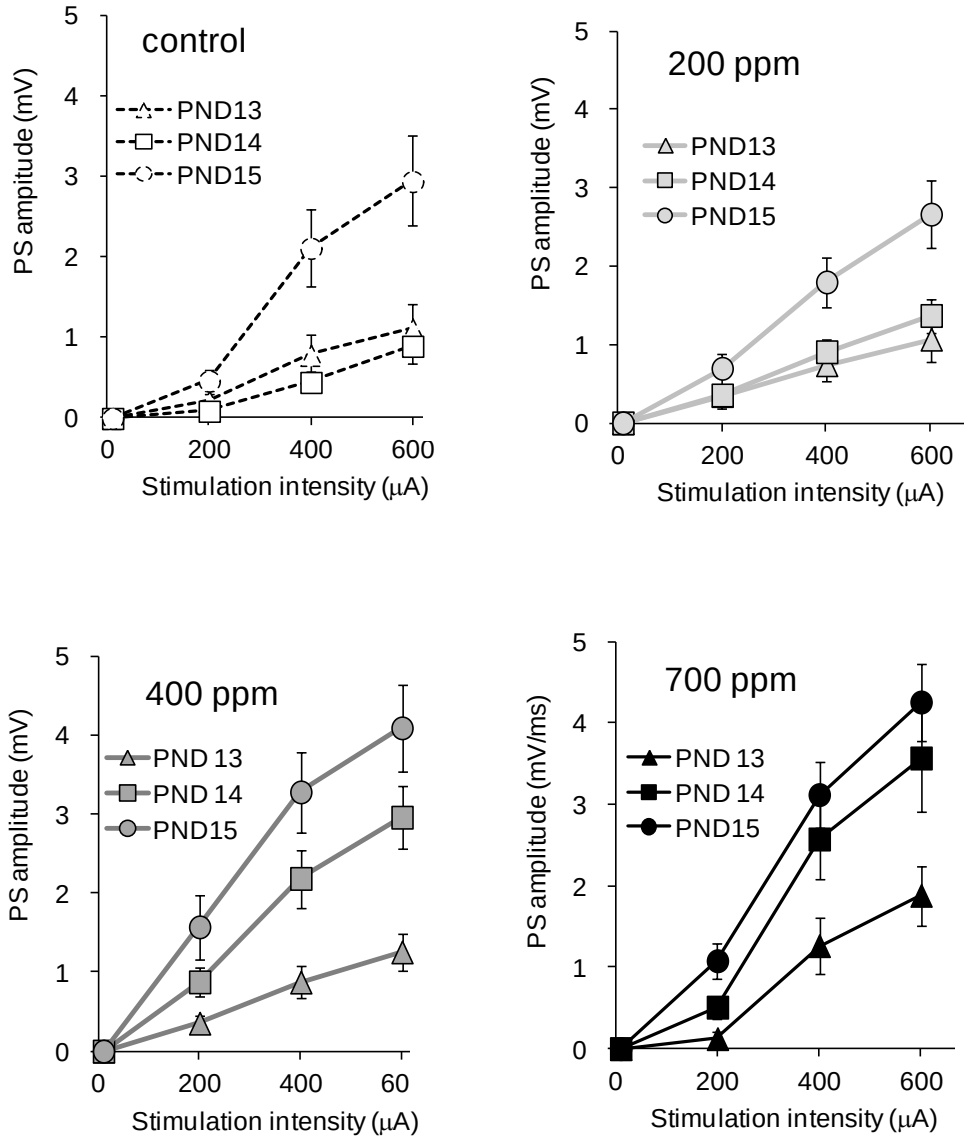

図 4　妊娠 1 日目から 20 日目まで 1BP を吸入曝露した母ラットから生まれた仔ラットの海馬 CA1 領野における電気刺激に対する集合スパイク電位の大きさ
吸入曝露濃度は、0（対照群）、200、400、700 ppm とした。刺激電極は CA1 領野への入力シナプスのある放線状層に置き、記録用微小電極は錐体細胞層に置いた。電気刺激の強度は 10、200、400、600 μA に設定した。曝露濃度 400 ppm 群および 700 ppm 群で、開眼前の PND14 において刺激応答性の亢進が認められた。データは平均値±SEM で表している。

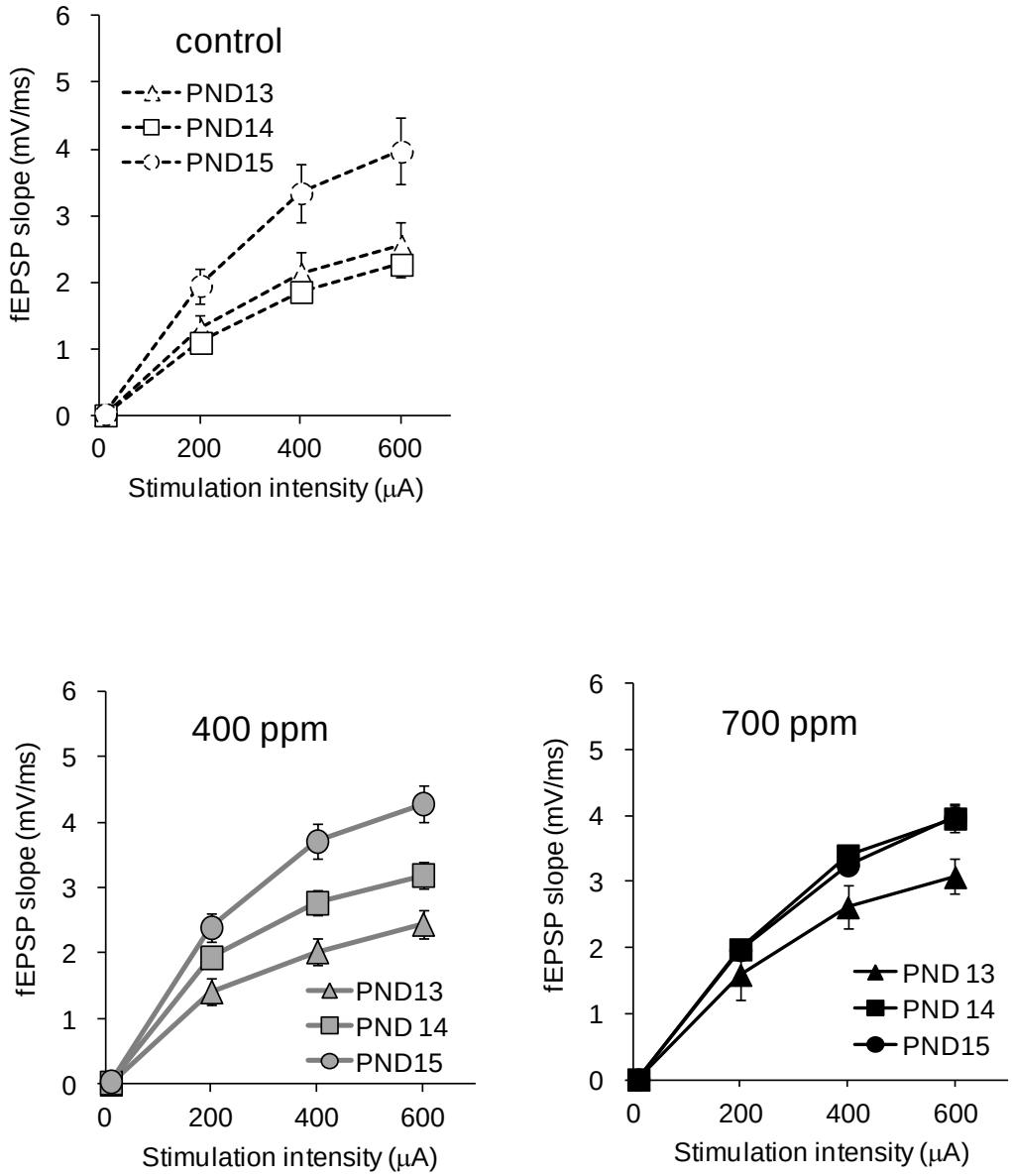

図 5　妊娠 1 日目から 20 日目まで 1BP を吸入曝露した母ラットから生まれた仔ラットの海馬 CA1 領野における電気刺激に対する興奮性シナプス強度の変化

図 4 において、対照群と比べて集合スパイク電位の振幅が亢進していた、400、700 ppm 曝露群について解析した。400 ppm 群と 700 ppm 群において、集合スパイク電位の亢進と同様に、開眼前の PND14 において興奮性シナプス強度の増強が認められた。*p<0.05, repeated measure ANOVA

刺激電極と記録用微小電極は CA1 領野への入力シナプスのある放線状層においた。データは平均値±SEM で表している。

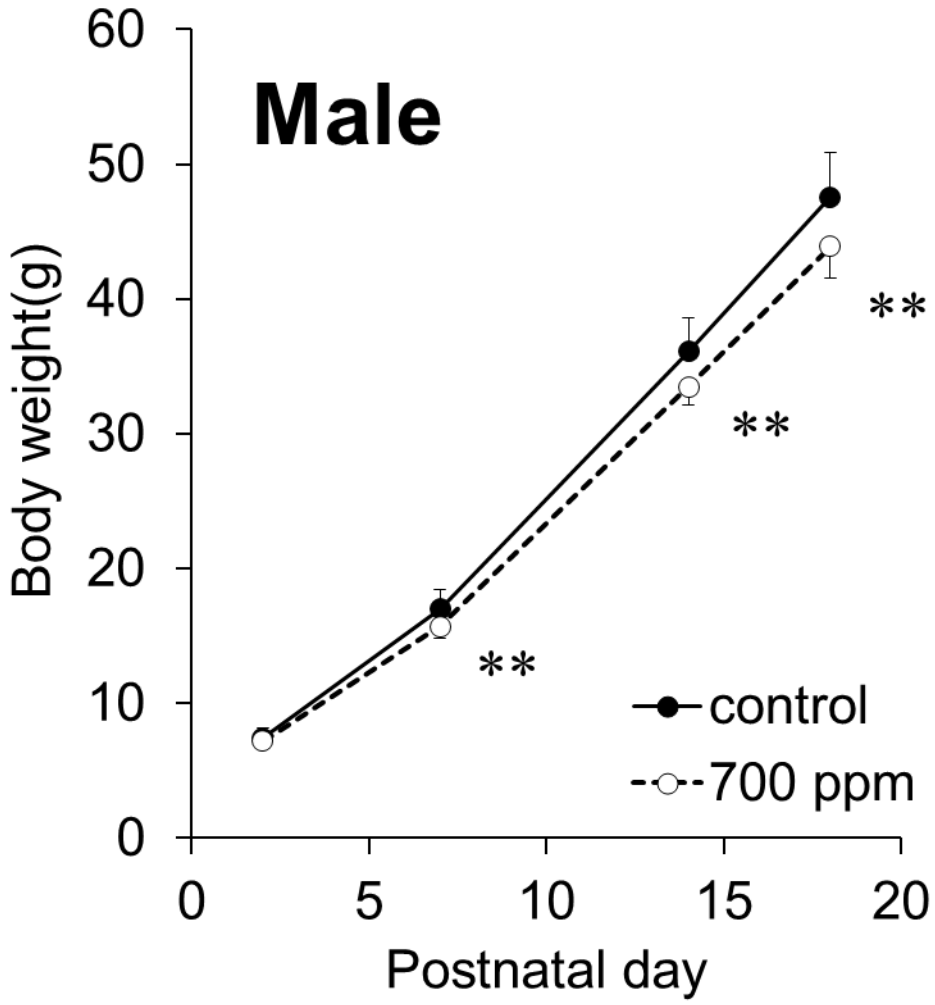

図 6　妊娠期に 20 日間 1BP を吸入曝露した母ラットから生まれた仔ラットの授乳期の体重変化

対照群と比較して、700 ppm 群では生後 2 日目では有意差が認められなかったものの、生後 7 日から 18 日までの計測において体重増加の有意な抑制が認められた。データは平均値±SD で表している。**p<0.01, Student's t-test

5 w Male

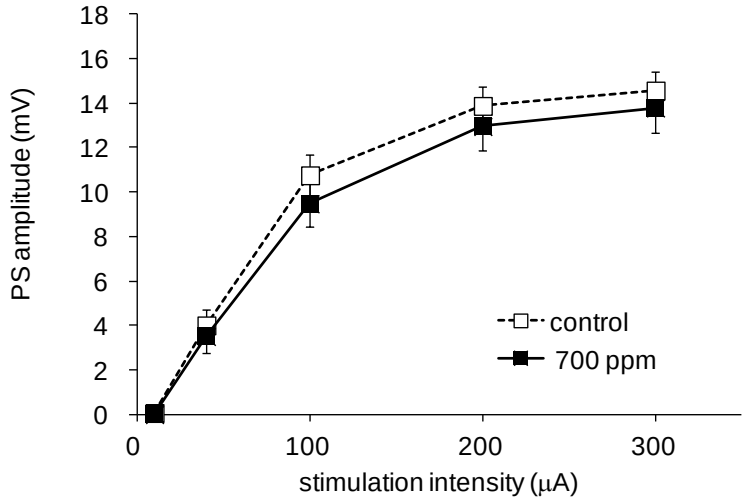

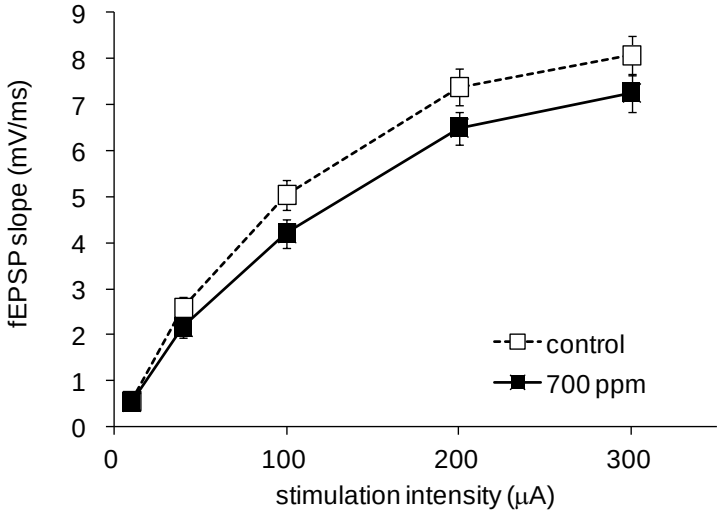

図 7　妊娠期に 1BP を吸入曝露した母ラットから生まれた雄性仔ラットの 5 週齢における海馬 CA1 領野の刺激応答性

集合スパイク電位の振幅、集合興奮性シナプス後電位の傾きのいずれにおいても、対照群と 700 ppm 群との間に有意差は認められなかった。(PS amplitude: p=0.52; fEPSP slope: p=0.22, repeated measure ANOVA)

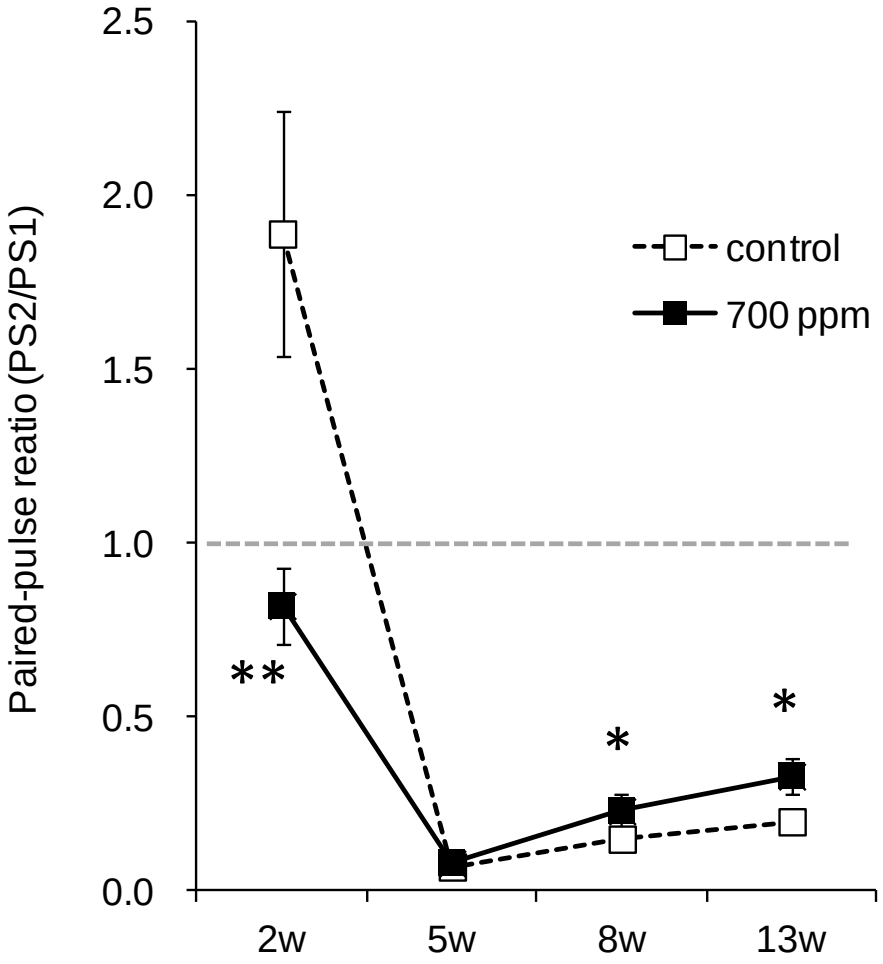

図 8　妊娠期に 1BP を吸入曝露した母ラットから生まれた雄性仔ラットにおける海馬 CA1 領野のペアパルス比の成長に伴う変化

対照群において、2 週齢では促通効果（ペアパルス比＞1.0）が認められたが、5，8，13 週齢でのペアパルス比は 0.2 以下となり、著明なフィードバック抑制の形成が示唆された。これに対して、1BP 胎生期曝露群では、2 週齢でペアパルス比＜1.0 となり、軽度ではあるがフィードバック抑制が形成されていることが判明した。さらに性成熟後の 8 週齢、13 週齢には対照群と比べてペアパルス比が有意に増加しており、フィードバック抑制が減弱していることが示唆された。破線はペアパルス比＝1 .0 を示しており、これは 2 連続刺激に対する 2 つの応答（誘発電位）が独立事象、すなわち 1 回目の刺激応答と 2 回目の刺激応答とが完全に独立していることを意味する値である。

厚生労働科学研究費補助金（化学物質リスク研究事業）
分担研究報告書

既存の毒性データおよびヒトデータとの検証

研究分担者　　国立研究開発法人国立成育医療研究センター研究所
周産期病態研究部・産婦人科学　部長
秦　健一郎

要旨
近年、妊娠中の母親の摂取栄養の程度や栄養成分の偏りが、胎児のエピゲノムに影響し、生後の発育や疾患の発症に寄与するという Developmental Origins of Health and Disease、DOHaD という概念が提唱されており、そのメカニズムについても明らかになりつつある。本研究では動物実験を中心に DOHaD のメカニズムについて文献調査を行った。また、ヒトのエピゲノムデータに関しても調査を開始した。

A. 研究目的

出生前後の環境が数十年後の疾患発症に関連していることが、疫学研究により明確に示されている。この現象を司る分子機構の一つとして、エピジェネティックな制御が示唆されており、それを裏付けるデータも集積してきている。これらの知見を背景に DOHaD（Developmental Origins of Health and Disease）学説が提唱され、予防医学や先制医療の観点からも注目されている。また、このメカニズムを介して疾患発症を引き起こす出生前後の環境要因についても、栄養環境だけではなく、様々な要因の関与が示唆されている。本研究では、DOHaD のメカニズム解明を目的に行われたこれまでの動物実験の報告より、とくに化学物質の影響に着目した報告を取りまとめることを目的とした。さらに、ヒトを対象とした研究で報告されている、児のエピゲノムに影響を及ぼす出生前後の環境要因についてこれまで明らかになっているものを整理する目的で文献調査を行った。

B. 研究方法

DOHaD 学説をもとに、動物実験によりメカニズムの解析を行っている文献を調査した。同じく、同学説に基づきヒトのエピゲノムデータを解析している文献についても調査研究を行った。

C. 研究結果

エピゲノムすなわちエピジェネティックな情報とは、ゲノムを変化させずにはたらきを決め、しかもゲノム（DNA の塩基配列）を介さないにもかかわらず「遺伝」する情報のことである。エピゲノムを担う代表的な分子的実体として、ヒストンのメチル化・アセチル化や、DNA のシトシンのメチル化が挙げられる。哺乳類の初期発生時には特に、これらのエピゲノムがダイナミックに変化して消去と再構築されることが知られている。具体的には、受精直後に精子由来のメチル化は速やかに消去され（能動的脱メチル化）、卵子由来のメチル化はそれに遅れ、DNA 複製依存的に維持されずに失われていく（受動的脱メチル化）。親由来の DNA メチル化修飾情報はこのように、大部分が一度消去され、その後胚盤胞期まで低メチル化状態にある。着床後、それぞれの細胞は複数の DNA メチル化酵素によって、発生段階特異的かつ組織特異的な DNA メチル化修飾を確立する。このように、受精後から発生初期に観察されるエピゲノムの初期化と再構築の時期は、可塑性に富んでいると考えられ、この時期の環境負荷により DNA メチル化状態の違いが生じれば、その違いは長期にわたりそのまま残っている可能性が考えられる。もともと DNA メチル化は、細胞が分裂しても安定して娘細胞に情報が維持される性質を有しており、そのような特徴もこの可能性を支持する点である。したがって、DOHaD 学説はこの時期のエピジェネティックな制御に注目している。さらに、DOHaD 学説が注目する受精時，胎児期、新生児乳幼児期の環境には、栄養環

境だけではなく、内分泌かく乱物質などの影響や、喫煙や飲酒の影響、母体の精神状態に起因する内分泌の乱れ、等も含まれる。

（1）妊娠中の神経内分泌異常の胎児への影響について

妊婦の精神的ストレスが、胎児の内分泌系にかかわる遺伝子のエピゲノム変化を誘導する可能性は、検証数を重ねることで確実性を増してきている。胎児の視床下部－下垂体－副腎の神経内分泌系、いわゆる HPA axis は、妊娠 22 週目より発達し 2 歳までの間は可塑性があることが知られている。したがって、妊娠中の母体のストレス経験が胎児の HPA axis をプログラムし永久的にその機能を変化させる可能性がある。Palma-Gudiel らによる 7 論文に基づく 977 人の被験者のメタ解析の結果は、妊娠中の不安状態やうつ傾向が、児のグルココルチコイドレセプター（GR）遺伝子プロモーター領域の DNA メチル化レベルと有意に相関することを示している。メタ解析で対象とした 7 論文のうち 3 論文は 136 名、25 名あるいは 74 名分の臍帯血 DNA メチル化値を測定しており、残り 4 論文は、胎盤（482 名分）、生後 2 か月前後の口腔粘膜（56 名分）、14 か月時前後の唾液（181 名分）、14 歳前後の末梢血（23 名分）を解析している（Palma-Gudiel H et al. Epigenetics 2015）。この領域の DNA メチル化が上昇していると、GR 遺伝子の発現抑制によるグルココルチコイド不応性、抵抗性、が亢進するため、社会心理的ストレスに脆弱性を示す可能性が示唆されている。

（2）外因性内分泌かく乱物質の胎児、新生児脳発達への影響について

主にポリカーボネート樹脂、エポキシ樹脂などの原料として使用され、広く環境中に存在する合成エストロゲンのビスフェノール A（BPA）を含み、外因性内分泌かく乱物質である環境ホルモンなどの化学物質への暴露が、自閉症など社会的障害に分類される神経行動障害の発症に関与している可能性が示唆されている。BPA はアメリカ人の 93%の尿中で検出されており（Calafat et al. Environ. Health Perspect. 2008）、胎盤を通過することより胎児血清や、母乳中にも検出される。ヒト血中レベルの BPA の妊娠期間中マウスへの暴露は、出生直前（E18.5）の雌胎仔マウスの脳内の DNA メチル化酵素 Dnmt1 と Dnmt3a 量減少とグルタミン酸トランスポーター Slc1a1 発現を上昇させた（Wolstenholme et al. PLoS One. 2011）。子宮内の BPA 暴露によって生後 28 日目の雌仔マウスの海馬 Bdnf の発現が上昇し、一方で雄仔マウスが減少。この影響は雌雄ともに生後 60 日目まで確認され、雄マウスの発現低下は Bdnf プロモータの高メチル化と連動していた。さらに、ヒトにおいても妊娠中の血中の BPA 濃度が高かった母親から生まれた男児の臍帯血 DNA で BDNF のメチル化が高くなった（Kundakovic et al. Proc Natl Acad Sci U S A. 2014）。最近の報告では、人体に影響はないといわれている濃度以下での動物実験において、妊娠中の BPA 暴露が新生仔の脳内の遺伝子発現を変化させている。影響に性差が認められる結果は一致しており、新生雌ラットでは、視床下部におけるエストロゲンレセプターα、β の発現と、海馬と視床下部のオキシトシンの発現が上昇していた。一方新生雄ラットでは海馬のオキシトシンの発現が減少していた（Arambula et al. Endocrinology. 2016）。妊娠中の BPA 暴露の影響は、孫世代の仔の行動異常にも認められた（Wolstenholme et al. Horm Behav. 2013）。

（3）胎児期の外因性内分泌かく乱物質暴露が成人期の生殖能に及ぼす影響について

胎仔期・新生仔期の外因性内分泌かく乱物質への暴露が精子のインプリント領域 DNA メチル化異常を誘引し、その精子で受精した胚は最終的に流産あるいは不妊・不育症の原因となることが動物実験で報告されている（Guerrero-Bosagna et al. Curr Opin Genet Dev. 2014）。ゲノムインプリンティングは哺乳類が進化する過程で獲得した機構と考えられている。インプリンティング遺伝子とは、片親のアレル特異的に発現する遺伝子を指し、およそ数百個のインプリンティング遺伝子が存在すると推測されている。片親アレル特異的発現を制御する機構として、インプリンティング遺伝子の周辺領域には、片親のみでメチル化されているゲノム領域、すなわち、父親性あるいは母親性インプリント領域（インプリンティングの分子的実体であるインプリントを有する領域）が存在する。インプリント領域で認められる DNA メチル化は、一般の遺伝子で認められる遺伝子の発現抑制のみではなく発現誘導にも機能する。インプリンティング遺伝子は、片親のアレルのみから発現することで、発生段階において厳密な発現量を保ちその機能が過剰に働くことを回避している。稀な先天奇形症候群である

インプリンティング疾患は、インプリンティング遺伝子にジェネティックな変異を持つか、インプリント領域にエピジェネティックな変異を持つことを原因とする疾患であり、胎児と胎盤の発生異常を特徴とすることが知られている。これまでに、原因不明と診断された習慣性流産を呈す父親の精子ゲノムにおいて H19 インプリント領域の有意な低メチル化が報告されている。精子ゲノムの H19 インプリント領域の低メチル化は不育症、乏精子症、精子無力症の患者においても認められている。

インプリント領域の DNA メチル化は、ゲノム全体のエピジェネティック情報の書き換えが行われる初期胚発生時において、受精直後のゲノム全体の脱メチル化から免れる機構を持っており、母親性あるいは父親性それぞれのインプリントメチル化情報が受精後も胚組織に維持される。母親性・父親性インプリントメチル化情報はそれぞれ卵子精子とも、生殖細胞の発生時期に確立される。DNA メチル化修飾のない始原生殖細胞から、雄性生殖細胞系列では胎児期にインプリント領域を含めメチル化修飾がゲノムに入り、出生前の精原細胞ではすでにゲノム全体が高メチル化されている。一方、雌性生殖細胞系列では、出生後の卵母細胞成長期にメチル化修飾が入る。したがって、少なくとも精子においては、胎児期のエピゲノム修飾獲得が鍵となり、その修飾状態が生涯にわたり維持され、妊孕能、胚発生・分化能に関与している可能性が示唆される。父親自身の胎児期環境が、この機構の確立に影響を及ぼし、次世代に影響する可能性が示唆されている。

新生仔期の BPA への暴露により、H19 インプリント領域の有意な低メチル化と遺伝子発現異常が認められ、かつこのラットの精子で受精した胚は着床後胚損失が生じた（Doshi et al. Mol Biol Rep. 2013）。農業用の防カビ剤の成分であるビンクロゾリンの胎仔の生殖腺の性分化が行われる時期の妊娠中雌ラットへの暴露は、胎仔の精子エピジェネティック異常と精子形成細胞のアポトーシスが 3 世代後まで遺残する（Anway et al. Science. 2005）。世代を超えたエピジェネティクス異常がいくつかのインプリント領域で生じる一方、世代を超えるごとに徐々に正常化する（Stouder et al. Reproduction. 2010）。ビンクロゾリン暴露による精子エピジェネティックへの影響は、胎仔期の中でも始原生殖細胞ゲノムの DNA メチル化が一度すべて消去される時期での暴露が顕著（Skinner et al. PLoS ONE. 2013）であったことより、始原生殖細胞における親由来の DNA メチル化情報の消去が正常に行われることが生殖能力に重要であることも示唆されている。

（4）世代を超えて遺残する環境の影響

環境の影響は、本人のみではなく、世代を超えた影響がありうることと、その分子機構の解明が、近年多数報告されている。つまりは、ここまで述べてきた対象者の胎児期や新生児・乳幼児期だけでなく、対象者の親が若い頃の環境や、祖父母が経験した環境の影響にも注目が集まっている。

慢性的な高脂肪食下にあるオスのラットを親とするメスは、適正な食餌を与えても糖代謝異常とβ細胞機能不全が認められ、対照群に比べ膵島で多くの遺伝子の発現量が異なっており、プロモーターの DNA メチル化状態が異なっている遺伝子も同定された(Ng et al. Nature 2010)。また、若い時にタンパク質欠乏食を与えられたオスは、その後適正な食餌を与えても、自身の仔の肝臓で代謝にかかわる多くの遺伝子の発現が異常を呈し、脂質代謝のマスターレギュレーターである Ppara の DNA メチル化が異なっていた（Carone et al. Cell 2010）。これらの報告が 2010 年に共に発表されて以来、父親の生活環境が次世代に影響する現象とその分子機構の解明に関する報告がこれまでに集積してきている。不適切な食事負荷により糖尿病予備軍にあるマウスでは、精子の DNA メチル化パターンが健常のそれと異なっており、この異常メチル化パターンが世代を超えて仔の膵島でも確認され、仔世代の代謝異常を引き起こしていると報告された（Wei et al. Proc Natl Acad Sci U S A. 2014）。一方で、世代を超えて食事の乱れの影響が伝わるメカニズムは、DNA メチル化そのものの遺残ではないという報告もある。解析対象となるマウス（第 3 世代）の父（第 2 世代）が、父自身の母親（すなわち解析対象から見ると祖母、第 1 世代）の胎内にいる時期に栄養不良に曝されると、その時期の父（第 2 世代）の生殖細胞に DNA メチル化変化が起き、出生後も精子メチル化パターンの変化が遺残し、その影響が解析対象（すなわち、栄養不良だった妊娠マウスから見ると孫、第 3 世代）の代謝異常を引き起こしている可能性が示された（Radford et al.　Science 2014）。この論文で

は、父（第 2 世代）の異常精子メチル化パターンは、仔（第 3 世代）の脳と肝臓には伝わっておらず、直接の代謝異常の原因ではないことが示唆される。前述したように、胚の発生初期には親由来のエピジェネティックな情報は一旦消去されて再構築されるため、これは理にかなっている。ところが、解析対象マウスの体組織において異常な発現が認められる遺伝子は、解析対象（第 3 世代）から見て祖母（第 1 世代）の栄養不良に伴い父（第 2 世代）の精子で観察される DNA メチル化異常領域の近傍にある遺伝子であり、やはり何らかの因果関係があることが強く示唆される。DNA メチル化以外の分子機構、例えばヒストン修飾の異常による伝達が候補に挙げられるが、実際にヒストン修飾の乱れが世代を超えて伝わる可能性も報告されており（Siklenka et al. Science 2015）、あるいはオスの食環境の乱れが精子内の RNA 分子を介した伝達をする可能性も示され（Sharma et al. Science 2016）、今後の研究発展が注目される。現在のところ、これらの分子機構は動物モデルにおける検証にとどまっているが、ヒトでも同様の分子機構が存在する可能性は十分に考えられる。

（5） 妊娠中の喫煙はヒト臍帯血の解毒や免疫機能に関わる遺伝子（AHRR、MYO1G、CYP1A1、CNTNAP2 など）のメチル化を変化させ、この変化は 17 歳時点の血液中でも継続した（Richmond et al. Hum Mol Genet. 2015）。

D. 考察

上記の調査研究により、以下のことが示唆された。

・胎仔期・新生仔期の環境要因の影響が出生後も持続して認められる。

・ヒトでも同様に、胎児期・新生児期はエピゲノムがダイナミックに変化する時期であると考えられ、環境の影響を受けやすい可能性が十分に予見される。

・発生段階の脳では、一過性の発現変化も結果的に不可逆的な脳機能変化を引き起こし、これは初期エピジェネティックな調節異常が遺残するためである。

・発生段階の脳において、外因性内分泌かく乱物質暴露によるエピジェネティック異常に伴う機能異常が生じる。

・始原生殖細胞における親由来 DNA メチル化情報の消去が正常に行われることが生殖能力に重要である。

・発生初期の子宮内における環境要因の影響が、脳の発達においてエピジェネティックな制御を介し生後遺残する可能性が示されている。

・親の生活環境が生殖細胞のエピゲノムを介して、子に影響する可能性がある。

・祖母の妊娠中の環境が、親が祖母の子宮内で発生する段階で生殖細胞のエピゲノムを変化させ、孫に影響する可能性がある。

E. 結語

調査研究により、胎児期あるいは新生児期はエピゲノム確立に重要な時期であり、かつ、可塑性の高い時期であるため、この時期のエピゲノムは環境の影響を受けやすく、生じたエピゲノム変化は生後長期に渡って継続し、疾患リスクとなる可能性が示唆された。環境因子は、生殖細胞のエピゲノムを介し、次世代に変化を引き起こす現象も認められており、生殖細胞のエピゲノム確立期、並びに成熟生殖細胞のエピゲノムに変化を及ぼすような環境が、次世代で脳を含めた各臓器でどのような影響を及ぼすのか解明する必要がある。

F. 研究発表

1. 論文発表

[1] Kasuga Y., Hata K., Tajima A., Ochiai D., Saisho Y., Matsumoto T., Arata N., Miyakoshi K. and Tanaka M. “Association of common polymorphisms with gestational diabetes mellitus in Japanese women: A case-control study.” *Endocr J.* (2017) in press

[2] Sakaki M., Ebihara Y., Okamura K., Nakabayashi K., Igarashi A., Matsumoto K., Hata K., Kobayashi Y. and Maehara K. “Potential roles of DNA methylation in the initiation and establishment of replicative senescence revealed by array-based methylome and transcriptome analyses.” *PLoS One.* (2017) 12:e0171431.

[3] Liao H., Sato H., Chiba R., Kawai T., Nakabayashi K., Hata K., Akutsu H., Fujiwara S. and Nakamura H. “Human cytomegalovirus downregulates SLITRK6 expression through IE2.” *J Neurovirol.* (2017) 23:79-86.

[4] Ito Y., Maehara K., Kaneki E., Matsuoka K.,

Sugahara N., Miyata T., Kamura H., Yamaguchi Y., Kono A., Nakabayashi K., Migita O., Higashimoto K., Soejima H., Okamoto A., Nakamura H., Kimura T., Wake N., Taniguchi T. and Hata K. “Novel Nonsense Mutation in the NLRP7 Gene Associated with Recurrent Hydatidiform Mole.” *Gynecol Obstet Invest.* (2016) 81:353-358.

[5] Nohara K., Okamura K., Suzuki T., Murai H., Ito T., Shinjo K., Takumi S., Michikawa T., Kondo Y. and Hata K. “Augmenting effects of gestational arsenite exposure of C3H mice on the hepatic tumors of the F2 male offspring via the F1 male offspring.” *J Appl Toxicol.* (2016) 36:105-112.

2. 学会発表

該当なし

G. 知的財産の出願・登録状況

該当なし

III.　研究成果の刊行に関する一覧表

研究成果の刊行に関する一覧表

雑誌

発表者氏名	論文タイトル名	発表誌名	巻号	ページ	出版年
Yamada S., Kubo Y., Yamazaki D., Sekino Y., Kanda Y.	Chlorpyrifos inhibits neural induction via Mfn1-mediated mitochondrial dysfunction in human induced pluripotent stem cells.	Sci. Rep.	7	40925	2017
Yamada S., Asanagi M., Hirata N., Itagaki H., Sekino Y., Kanda Y.	Tributyltin induces mitochondrial fission through Mfn1 degradation in human induced pluripotent stem cells.	Toxicol. In Vitro.	34	257-263	2016
Asanagi M., Yamada S., Hirata N., Itagaki H., Kotake Y., Sekino Y., Kanda Y.	Tributyltin induces G2/M cell cycle arrest via NAD(+)-dependent isocitrate dehydrogenase in human embryonic carcinoma cells.	J. Toxicol. Sci.	41	207-215	2016
Hirata N., Yamada S., Asanagi M., Sekino Y., Kanda Y.	Nicotine induces mitochondrial fission through mitofusin degradation in human multipotent embryonic carcinoma cells.	Biochem. Biophys. Res. Commun.	470	300-305	2016
Mabuchi H., Ong HY, Watanabe K., Yoshida S., Hozumi N.	Visualization of Spatially Distributed Bioactive Molecules Using Enzyme-Linked Photo Assay.	IEEJ Transactions on Fundamentals and Materials	136	99-104	2016
Ishidao T., Fueta Y., Ueno S., Yoshida Y., Hori H.	A cross-fostering analysis of bromine ion concentration in rats that inhaled 1-bromopropane vapor.	J Occup Health	58	241-246	2016
Fueta Y., Sekino Y., Yoshida S., Kanda Y., Ueno S.	Prenatal exposure to valproic acid alters the development of excitability in the postnatal rat hippocampus.	論文投稿中			
Fueta Y., Ishidao T., Ueno S., Yoshida Y., Kanda Y., Hori H.	Prenatal exposure to 1-bromopropane causes delayed adverse effects on hippocampal neuronal excitability in the CA1 subfield of rat offspring.	論文投稿中			
Igarashi T., Wilson DJ., Ueno S.	Acute exposure to toluene and xylene decrease the expression of connexin43 in human cardiac myocytes.	論文投稿中			
Kasuga Y., Hata K., Tajima A., Ochiai D., Saisho Y., Matsumoto T., Arata N., Miyakoshi K., Tanaka M.	Association of common polymorphisms with gestational diabetes mellitus in Japanese women: A case-control study.	Endocr J. in press			
Sakaki M., Ebihara Y., Okamura K., Nakabayashi K., Igarashi A., Matsumoto K., Hata K., Kobayashi Y., Maehara K.	Potential roles of DNA methylation in the initiation and establishment of replicative senescence revealed by array-based methylome and transcriptome analyses.	PLoS One.	12	e0171431	2017

Liao H., Sato H., Chiba R., Kawai T., Nakabayashi K., Hata K., Akutsu H., Fujiwara S., Nakamura H.	Human cytomegalovirus downregulates SLITRK6 expression through IE2.	J Neurovirol.	23	79-86	2017
Ito Y., Maehara K., Kaneki E., Matsuoka K., Sugahara N., Miyata T., Kamura H., Yamaguchi Y., Kono A., Nakabayashi K., Migita O., Higashimoto K., Soejima H., Okamoto A., Nakamura H., Kimura T., Wake N., Taniguchi T., Hata K.	Novel Nonsense Mutation in the NLRP7 Gene Associated with Recurrent Hydatidiform Mole.	Gynecol Obstet Invest.	81	353-358	2016
Nohara K., Okamura K., Suzuki T., Murai H., Ito T., Shinjo K., Takumi S., Michikawa T., Kondo Y., Hata K.	Augmenting effects of gestational arsenite exposure of C3H mice on the hepatic tumors of the F2 male offspring via the F1 male offspring.	J Appl Toxicol.	36	105-112	2016

IV.　研究成果の刊行物・別刷

The Journal of Toxicological Sciences (J. Toxicol. Sci.)
Vol.41, No.2, ***-***, 2016

Original Article

Tributyltin induces G2/M cell cycle arrest via NAD$^+$-dependent isocitrate dehydrogenase in human embryonic carcinoma cells

Miki Asanagi[1,2,*], Shigeru Yamada[1,*], Naoya Hirata[1], Hiroshi Itagaki[2], Yaichiro Kotake[3], Yuko Sekino[1] and Yasunari Kanda[1]

[1]*Division of Pharmacology, National Institute of Health Sciences*
[2]*Faculty of Engineering, Department of Materials Science and Engineering, Yokohama National University*
[3]*Department of Xenobiotic Metabolism and Molecular Toxicology, Graduate School of Biomedical and Health Sciences, Hiroshima University*

(Received November 16, 2015; Accepted December 28, 2015)

ABSTRACT — Organotin compounds, such as tributyltin (TBT), are well-known endocrine-disrupting chemicals (EDCs). We have recently reported that TBT induces growth arrest in the human embryonic carcinoma cell line NT2/D1 at nanomolar levels by inhibiting NAD$^+$-dependent isocitrate dehydrogenase (NAD-IDH), which catalyzes the irreversible conversion of isocitrate to α-ketoglutarate. However, the molecular mechanisms by which NAD-IDH mediates TBT toxicity remain unclear. In the present study, we examined whether TBT at nanomolar levels affects cell cycle progression in NT2/D1 cells. Propidium iodide staining revealed that TBT reduced the ratio of cells in the G1 phase and increased the ratio of cells in the G2/M phase. TBT also reduced cell division cycle 25C (cdc25C) and cyclin B1, which are key regulators of G2/M progression. Furthermore, apigenin, an inhibitor of NAD-IDH, mimicked the effects of TBT. The G2/M arrest induced by TBT was abolished by NAD-IDHα knockdown. Treatment with a cell-permeable α-ketoglutarate analogue recovered the effect of TBT, suggesting the involvement of NAD-IDH. Taken together, our data suggest that TBT at nanomolar levels induced G2/M cell cycle arrest via NAD-IDH in NT2/D1 cells. Thus, cell cycle analysis in embryonic cells could be used to assess cytotoxicity associated with nanomolar level exposure of EDCs.

Key words: Embryonic carcinoma cells, Tributyltin, Cell cycle, Isocitrate dehydrogenase

INTRODUCTION

Organotin compounds, such as tributyltin (TBT) are typical environmental contaminants and are categorized as endocrine-disrupting chemicals (EDCs), which cause neurodevelopmental defects including behavioral abnormality and teratogenicity (Dopp *et al*., 2004; Gårdlund *et al*., 1991). Although the use of TBT has already been restricted, butyltin compounds, including TBT, can still be found in human blood at concentrations between 50 and 400 nM. There is still concern about TBT toxicity for human health (Whalen *et al*., 1999).

Several studies have revealed that TBT activates retinoid X receptor (RXR) and/or peroxisome proliferator-activated receptor γ (PPARγ) (Kanayama *et al*., 2005). TBT at nanomolar levels has the ability to bind with higher affinity than the intrinsic ligands and these genomic transcriptional activations have been reported to mediate neurodevelopmental defects in *Xenopus* (Yu *et al*., 2011). In contrast, TBT elicits non-genomic pathway in mature rat neurons and brain tissues at nearly micromolar levels. For instance, TBT induces neuronal death by inhibiting mammalian target of rapamycin (mTOR) in rat cortical neurons (Nakatsu *et al*., 2010). TBT also induces neuronal degeneration via the generation of reactive oxygen species along with marked reduction of GSH/GSSG levels in the rat brain (Mitra *et al*., 2013).

Cell stress is known to trigger a checkpoint that arrests cells in the G1 or G2 phase (Gabrielli *et al*., 2012). The cell cycle is tightly regulated by spatial and temporal

Correspondence: Yasunari Kanda (E-mail: kanda@nihs.go.jp)
*These authors equally contributed to this work.

expression of cell cycle proteins and divided into p53-dependent and p53-independent regulations (Shackelford *et al*., 1999). In the p53-independent regulations, cdc25C phosphatase, a mitotic inducer, plays a central role in G2/M phase regulation. Cdc25C activates cyclin B1/cyclin-dependent kinase (Cdk) 1 complex, which triggers mitosis (Donzelli and Draetta, 2003) and cyclin B1 accumulates during the S and G2 phases, followed by nuclear translocation and association with Cdk1. Protein levels of these cell cycle regulators are strictly regulated during cell cycle progression. Ultraviolet irradiation or toxic drugs are known to cause G2 arrest by the inactivation of cyclin B1/Cdk1 via p53 induction followed by the upregulation of p21, a Cdk inhibitor and/or cdc25C downregulation by degradation (Chaudhary *et al*., 2013; Kawabe, 2004; Nam *et al*., 2010; Ouyang *et al*., 2009).

We have previously reported that nanomolar levels of TBT induce growth arrest of neuronal precursor NT2/D1 cells as a model of neurodevelopmental stage (Yamada *et al*., 2013). We found that TBT causes growth arrest via mitochondrial NAD^+-dependent isocitrate dehydrogenase (NAD-IDH), which catalyzes the irreversible conversion of isocitrate to α-ketoglutarate in the tricarboxylic acid (TCA) cycle (Yamada *et al*., 2014). Based on these observations, we hypothesized that nanomolar levels of TBT could also affect cell cycle progression via NAD-IDH in NT2/D1 cells.

In the present study, we investigated the effect of TBT on cell cycle progression in NT2/D1 cells. We found that exposure to 100 nM TBT reduced the protein levels of cell cycle regulators and induced G2/M cell cycle arrest through an NAD-IDH-dependent mechanism. Thus, cell cycle regulation via NAD-IDH is a novel target of TBT-induced toxicity in human embryonic carcinoma cells.

MATERIALS AND METHODS

Cell culture

NT2/D1 cells were obtained from the American Type Culture Collection (Manassas, VA, USA). The cells were cultured in Dulbecco's modified Eagle's medium (DMEM; Sigma-Aldrich, St. Louis, MO, USA) supplemented with 10% fetal bovine serum (FBS; Biological Industries, Ashrat, Israel) and 0.05 mg/mL penicillin-streptomycin mixture (Life Technologies, Carlsbad, CA, USA) at 37°C in 5% CO_2.

Cell cycle analysis

The cells were trypsinized and harvested in phosphate buffered saline. Then the cells were resuspended in 70% ethanol for 30 min at -20°C. The fixed cells were collected by centrifugation and resuspended in propidium iodide (PI)/RNase Staining Buffer (BD Biosciences, San Jose, CA, USA) followed by incubation at room temperature for 30 min in the dark. Cell cycle distribution was determined by flow cytometric analysis of the DNA content using the BD FACS Aria II system (BD Biosciences). Data were analyzed by Modfit LT 4.0 (Verity Software House, Topsham, ME, USA).

Real-time PCR

Total RNA was extracted from NT2/D1 cells using TRIzol reagent (Life Technologies), and quantitative real-time reverse transcription (RT)-PCR was performed with QuantiTect SYBR Green RT-PCR Kit (QIAGEN, Valencia, CA, USA) using an ABI PRISM 7900HT sequence detection system (Applied Biosystems, Foster City, CA, USA) as previously reported (Hirata *et al*., 2014). The relative change in transcript amounts was normalized to the expression levels of glyceraldehyde-3-phosphate dehydrogenase (GAPDH). The following primer sequences were used for real-time PCR analysis: human cdc25C: forward, 5′-AGGCAGCCTTGAGTTGCATAGAGA-3′, reverse, 5′-AGAGTTGGCTGGCTTGTGAGAAGA-3′;humancyclin B1:forward,5′-CGGGAAGTCACTGGAAACAT-3′,reverse, 5′-AAACATGGCAGTGACACCAA-3′; human GAPDH: forward, 5′-GTCTCCTCTGACTTCAACAGCG-3′, reverse, 5′-ACCACCCTGTTGCTGTAGCCAA-3′.

Western blot analysis

Western blot analysis was performed as previously reported (Kanda *et al*., 2011). Briefly, cells were lysed with Cell Lysis Buffer (Cell Signaling Technology, Danvers, MA, USA). The proteins were then separated by sodium dodecyl sulfate-polyacrylamide gel electrophoresis (SDS-PAGE) and electrophoretically transferred to Immobilon-P membrane (Millipore, Billerica, MA, USA). The membranes were probed with an anti-cdc25C monoclonal antibody (1:1,000; Cell Signaling Technology), an anti-cyclin B1 monoclonal antibody (1:1,000; Cell Signaling Technology), and an anti-GAPDH polyclonal antibody (1:2,500; Abcam, Cambridge, UK) followed by incubation with horseradish peroxidase-conjugated secondary antibodies against rabbit or mouse IgG (Cel Signaling Technology). The bands were visualized using the ECL Western Blotting Analysis System (GE Healthcare, Buckinghamshire, UK), and images were acquired using a LAS-3000 Imager (FUJIFILM UK Ltd., Systems, Bedford, UK).

NAD-IDH activity assay

NAD-IDH activity was determined using the

Isocitrate Dehydrogenase Activity Colorimetric Assay Kit (Biovision, Mountain View, CA, USA), according to the manufacturer's instructions. Briefly, NT2/D1 cells were lysed in an assay buffer provided in the kit. The lysate was centrifuged at 14,000 *g* for 15 min, and the cleared supernatant was used for the assay.

NAD-IDHα knockdown

Knockdown studies were performed using NAD-IDHα shRNA lentiviruses from Sigma-Aldrich (MISSION shRNA) according to the manufacturer's protocol. A scrambled hairpin sequence was used as a negative control. Briefly, the cells were infected with the viruses at a multiplicity of infection of 10 in presence of 8 μg/mL hexadimethrine bromide (Sigma-Aldrich) for 24 hr, and were then subjected to selection with 0.5 μg/mL puromycin for 72 hr for further functional analyses.

Chemicals and reagents

Tributyltin Chloride was obtained from Tokyo Chemical Industry (Tokyo, Japan). Tin acetate (TA), apigenin, and dimethyl α-ketoglutarate (DMKG) were obtained from Sigma-Aldrich.

Statistical analysis

All data were presented as mean ± S.D. Analysis of variance (ANOVA) followed by post hoc Tukey's test was used to analyze the data in Figs. 1C, 1D, 1E, 2A, 2B, 3C, 4E, 5A, 5B, 6A and 6B. Student's t test was used to analyze the data in Figs. 3A, 3B, 4A, 4B and 4C. P-values less than 0.05 were considered to be statistically significant.

RESULTS

Effect of TBT on cell cycle progression

We have previously found that 100 nM TBT induced growth arrest in NT2/D1 cells (Yamada *et al*., 2013). Here we investigated whether TBT affects cell cycle progression. Exposure to 100 nM TBT for 48 hr decreased the proportion of cells in the G1 phase (51.9% decrease) and increased of the proportion of cells in the G2/M phase (79.6% increase), compared with untreated control cells (Figs. 1A-E). In contrast, TBT did not affect the proportion of cells in the S phase. Moreover, exposure to tin acetate (TA), which is less toxic, did not affect cell cycle progression. These data suggest that TBT induces G2/M cell cycle arrest in the cells.

TBT exposure reduces G2/M cell cycle regulators, cdc25C and cyclin B1

To examine the molecular mechanism by which TBT induces G2/M cell cycle arrest, we assessed the protein levels of p53, a major cell cycle regulator. We found that p53 protein level was reduced after 24 hr of TBT treatment, whereas cisplatin, which is known to cause p53-dependent G2/M cell cycle arrest (Pani *et al*., 2007), increased p53 levels (Supplementary Fig. 1). Since we could not observe p53-dependency in TBT-induced G2/M cell cycle arrest, we assessed cdc25C and its downstream factor, cyclin B1, which are also involved in G2/M progression of cell cycle. Western blot analysis revealed that cdc25C and cyclin B1 protein levels were reduced after 24 hr of TBT treatment (Fig. 2A). In contrast, exposure to TA did not affect cdc25C and cyclin B1 protein levels. Equal GAPDH protein expression levels were confirmed as a loading control. Next, we assessed the gene expression of cdc25C and cyclin B1. However, real-time PCR analysis showed that gene expression was not significantly altered by TBT exposure for both 24 and 48 hr (Fig. 2B). These data suggest that TBT-induced G2/M cell cycle arrest is caused by reduction of cdc25C and cyclin B1 proteins.

TBT induces G2/M cell cycle arrest via NAD-IDH

To investigate the molecular mechanisms by which cdc25C is degraded and G2/M cell cycle arrest is induced, we examined the effect of the PPARγ agonist rosiglitazone (RGZ), which is the genomic target of TBT. We found that RGZ did not induce G1 phase reduction and G2/M phase increase (Figs. 3A and B). RGZ at 100 nM induced PPARγ gene expression at similar level to 100 nM TBT in NT2/D1 cells (Fig. 3C), confirming the agonistic effect of RGZ on PPARγ expression described in previous report (Benkirane *et al*., 2006). These data suggest that TBT induces G2/M cell cycle arrest in NT2/D1 cells through a non-genomic pathway. We next examined the involvement of the non-genomic target NAD-IDH. We used an NAD-IDH inhibitor apigenin (Arango *et al*., 2013) at 10 μM, which reduced NAD-IDH activity to a level (22.4%) (Fig. 4A). As previously reported, 100 nM TBT had a similar inhibitory effect (24.4%; Yamada *et al*., 2014). Treatment with apigenin (10 μM, 48 hr) decreased G1 phase ratio (58.6% decrease) and increased G2/M phase ratio (98.1% increase) (Figs. 4B and C). Similar to TBT, apigenin reduced protein expression of cdc25C and cyclin B1 without affecting gene expression (Figs. 4D and E). To further confirm the effect of apigenin, we performed knockdown (KD) experiments of NAD-IDHα, the catalytic subunit of NAD-IDH, using lentivirus-delivered shRNAs. Real-time PCR analysis showed that KD efficiency was approximately 40% (Yamada *et al*., 2014). We could not obtain more highly KD cells because of cell

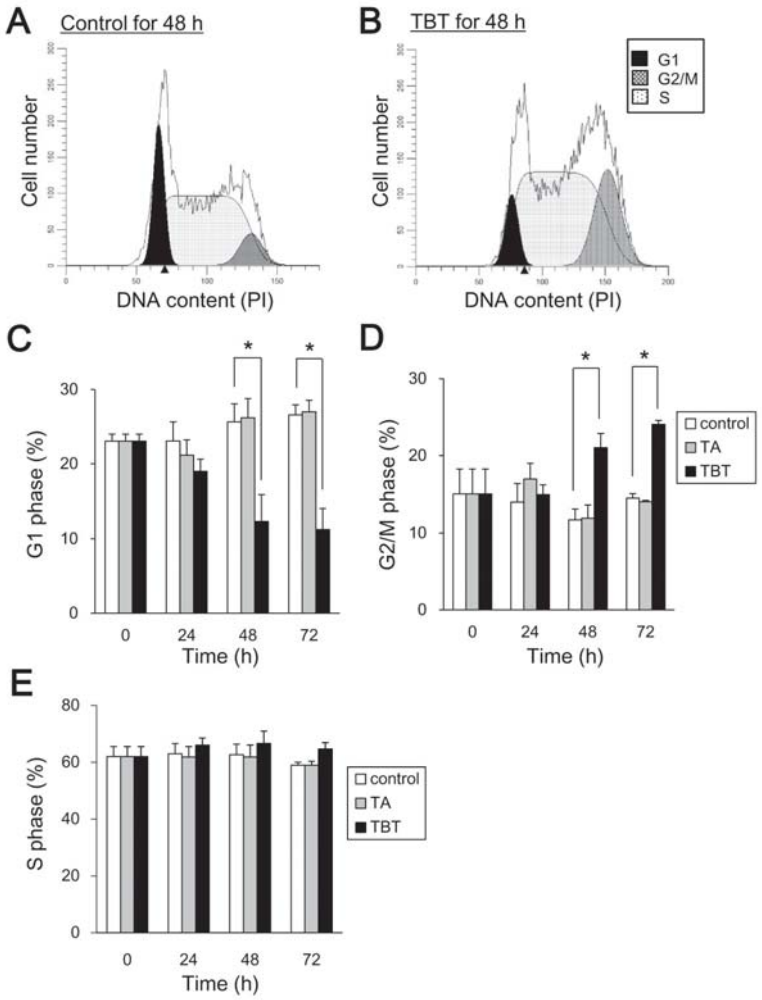

Fig. 1. Effect of TBT on cell cycle progression in NT2/D1 cells. Cells were exposed to 100 nM TA or TBT for 24, 48 or 72 hr. Cells were stained with propidium iodide (PI). Cell cycle distribution was determined by flow cytometric analysis of the DNA content on BD FACS Aria II. Representative cell cycle data in control (A) and TBT (B)-treated cells. The area ratio of G1 (C), G2/M (D) and S (E) phases was determined by Modfit LT 4.0. Data represent mean ± S.D. (n = 3). *P < 0.05.

death. Due to partial KD of the NAD-IDHα gene, NAD-IDH activity decreased by 22%, which is comparable to its decreased levels by TBT. In our previous studies, we observed that NAD-IDHα KD recovered the inhibitory effect of TBT on ATP content (Yamada *et al*., 2014). This might be because the TBT target NAD-IDHα was already inhibited by shRNA and further inhibition by TBT was not observed in the knockdown cells. Similar to these data, NAD-IDHα KD abolished the TBT-induced G1 phase reduction and G2/M phase increase (Figs. 5A and B), suggesting the involvement of NAD-IDH on TBT effects. NAD-IDHα KD tended to decrease the proportion of cells in the G1 phase (24.1% ± 0.55 to 23.2% ± 0.34) and increase the proportion of cells in the G2/M phase (17.5% ± 1.6 to 20.3% ± 0.62), compared with control (Figs. 5A and B). Moreover, NAD-IDHα KD also abolished the TBT-induced reduction of cdc25C and cyclin B1 proteins (Fig. 5C). NAD-IDHα KD reduced the basal levels of cdc25C and cyclin B1 proteins, compared with control (Fig. 5C). These data suggest that NAD-IDH mediates TBT-induced G2/M cell cycle arrest in NT2/D1 cells. To further confirm the involvement of NAD-IDH, we treated the cells with dimethyl α-ketoglutarate (DMKG), a cell-permeable analog of α-ketoglutarate (Willenborg *et al*., 2009). Incubation with DMKG prevented TBT-induced G2/M cell cycle arrest in NT2/D1 cells and

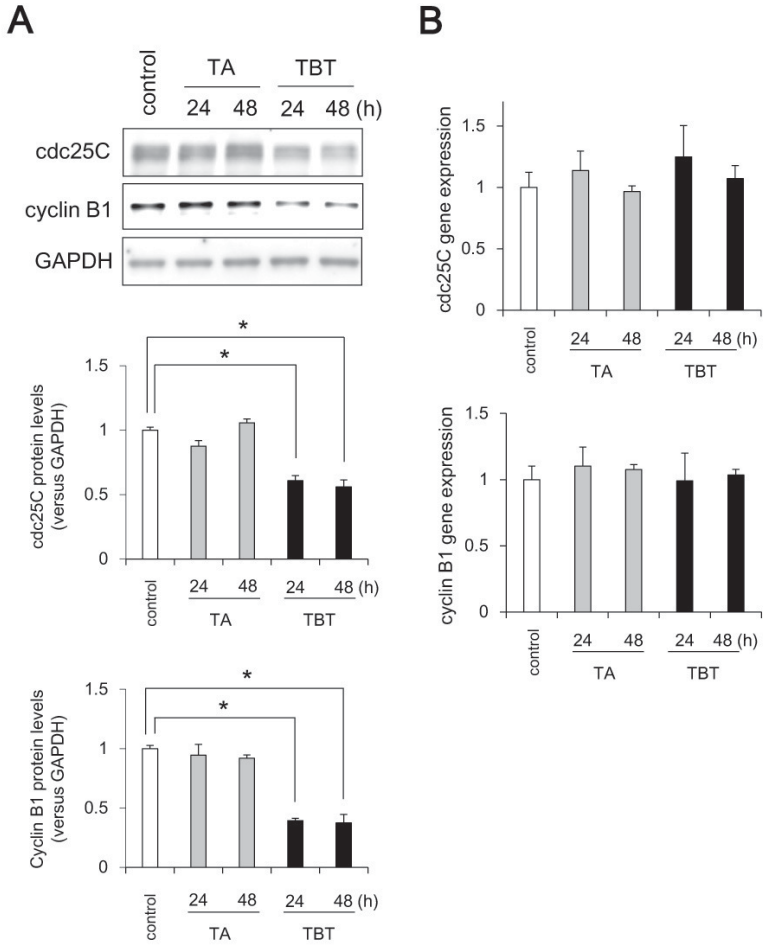

Fig. 2. Effect of TBT on expression levels of G2/M cell cycle regulators in NT2/D1 cells. After TBT exposure for 24 and 48 hr, protein expression was analyzed by western blot using anti-cdc25C, cyclin B1, or GAPDH antibodies (A). After TBT exposure for 24 or 48 hr, the expression of G2/M cell cycle regulators was analyzed by real time PCR (B). The gene expression was not significantly altered by TBT exposure. Data represent mean ± S.D. (n = 3).

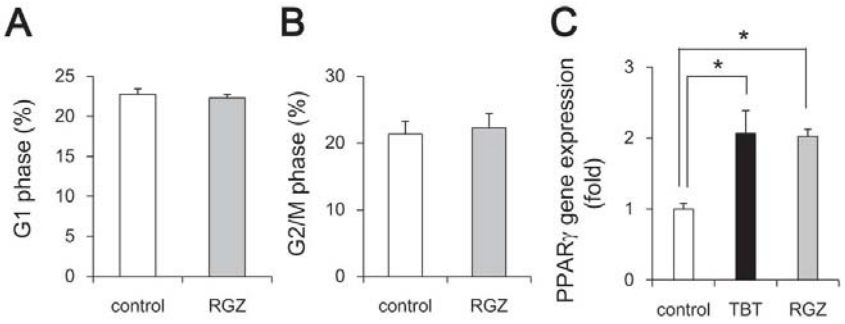

Fig. 3. Effect of RGZ on cell cycle progression in NT2/D1 cells. After RGZ exposure for 48 hr, cells were stained with propidium iodide (PI). The cell cycle distribution was determined by flow cytometric analysis of the DNA content using BD FACS Aria II. The ratio of G1 (A) and G2/M (B) phases was determined by Modfit LT 4.0. After exposure to TBT or RGZ, the expression of PPARγ was analyzed by real time PCR (C). The gene expression was comparably increased upon TBT or RGZ exposure. Data represent mean ± S.D. (n = 3). *P < 0.05.

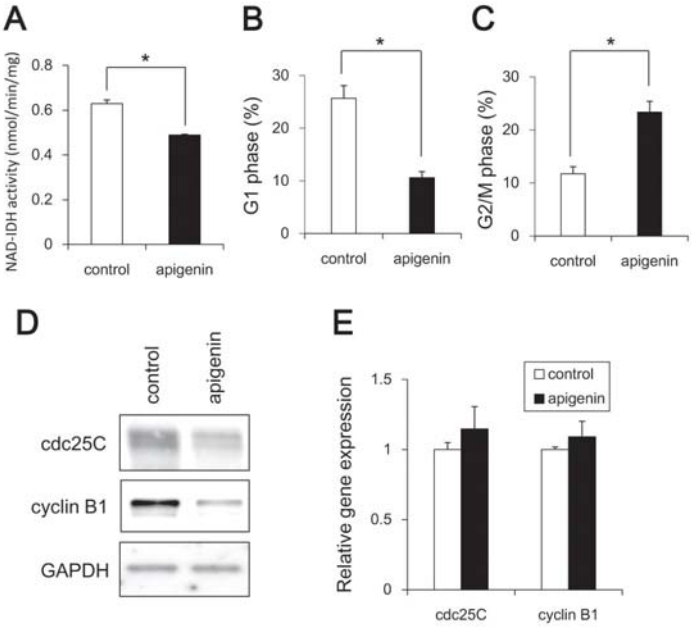

Fig. 4. Effect of apigenin on cell cycle progression in NT2/D1 cells. Cells were exposed to 10 μM apigenin for 24 hr and then determined NAD-IDH activity (A). Moreover, after exposure to apigenin for 48 hr, the cell cycle distribution was determined by flow cytometric analysis of the DNA content using BD FACS Aria II. The ratio of G1 (B) and G2/M (C) phases was determined by Modfit LT 4.0. The protein expressions in the cell lysate were analyzed by western blot using anti-cdc25C, cyclin B1, or GAPDH antibodies (D). The expression of G2/M cell cycle regulators was analyzed by real time PCR (E). The gene expression was not significantly altered upon apigenin exposure. Data represent mean ± S.D. (n = 3). *P < 0.05.

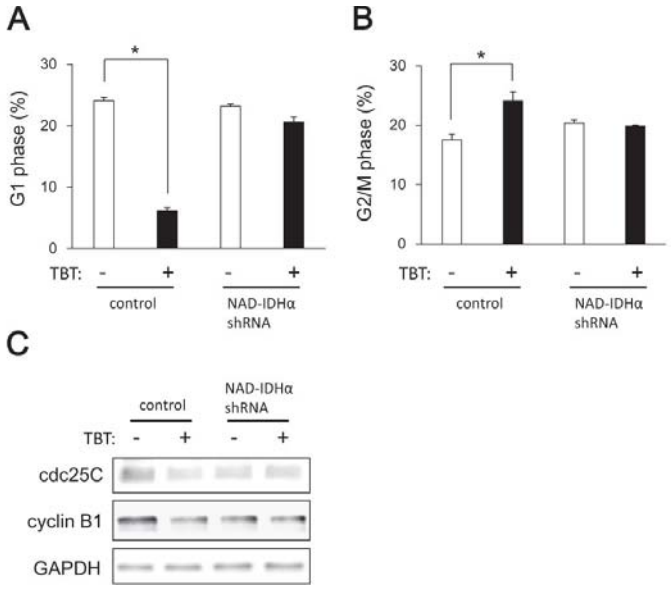

Fig. 5. Effect of NAD-IDH knockdown on cell cycle progression in NT2/D1 cells. Cells were infected with lentiviruses to express a shRNA against NAD-IDHα or a scrambled sequence shRNA (control). The infected cells were subjected to selection with 0.5 μg/mL puromycin for 72 hr and were then exposed to TBT at 100 nM for 48 hr. After staining with PI, cell cycle distribution was determined by flow cytometric analysis of the DNA content using BD FACS Aria II. The ratio of G1 (A) and G2/M (B) phases was analyzed by Modfit LT 4.0. The protein expressions in cell lysates were analyzed by western blot using anti-cdc25C, cyclin B1, or GAPDH antibodies (C). Data represent mean ± S.D. (n = 3). *P < 0.05.

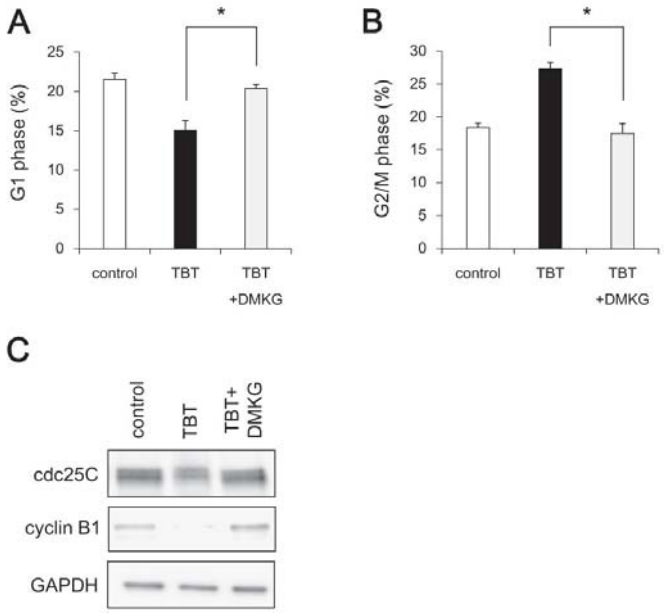

Fig. 6. Effect of dimethyl α-ketoglutarate (DMKG) on TBT-induced G2/M cell cycle arrest in NT2/D1 cells. Cells were exposed to 100 nM TBT and 7 mM DMKG for 48 hr. Cells were then stained with propidium iodide (PI) and cell cycle distribution was determined by flow cytometric analysis of the DNA content using BD FACS Aria II. The ratio of G1 (A) and G2/M (B) phases was analyzed by Modfit LT 4.0. Next, the protein expressions in cell lysates were analyzed by western blot using anti-cdc25C, cyclin B1, or GAPDH antibodies (C). Data represent mean ± S.D. (n = 3). *P < 0.05.

recovered the ratio of G1 and G2/M phases to the basal level (Figs. 6A and B). DMKG treatment also recovered TBT-induced protein reduction of cdc25C and cyclin B1 (Fig. 6C). Taken together, these data suggest that NAD-IDH mediates TBT-induced G2/M cell cycle arrest via cdc25C reduction in NT2/D1 cells.

DISCUSSION

Our data suggest that nanomolar TBT levels induce G2/M cell cycle arrest through the protein reduction of cdc25C and thereafter cyclin B1 (Figs. 1 and 2). Since the protein expression of p53 is decreased after TBT exposure, TBT-induced G2/M cell cycle arrest seems to be p53 independent. Consistent with our data, recent study has reported that nearly micromolar TBT levels induce G2/M cell cycle arrest in human amniotic cells via protein phosphatase (PP) 2A inhibition-mediated extracellular-signal-regulated kinase (ERK) inactivation (Zhang *et al*., 2014). Since we did not observe the reduction of phospho-ERK in NT2/D1 cells after nanomolar levels of TBT exposure (data not shown), the mechanism of inducing G2 arrest may differ depending on the TBT levels and cell type. Moreover, several chemical stressors have been reported to cause G2/M cell cycle arrest through the protein reduction of cell cycle regulators (Chaudhary *et al*., 2013; Nam *et al*., 2010; Ouyang *et al*., 2009). For instance, 4-Hydroxynonenal, an inducer of oxidative stress, causes DNA damage and induces G2/M cell cycle arrest in hepatocellular carcinoma HepG2 and Hep3B cells, following reduction of cdc25C and thereafter cyclin B1 proteins in a p53-independent manner (Chaudhary *et al*., 2013). Reduction of cdc25C protein may be mediated by the ubiquitin-proteasome system in NT2/D1 cells. Cdc25C has been reported to be degraded via ubiquitination by BRCA1 during G2/M cell cycle arrest in breast cancer cell lines (Shabbeer *et al*., 2013). During G2/M cell cycle arrest, another cell cycle regulators, such as Plk1, cdc25A and CDK1, are also known to be degraded by ubiquitin ligases, such as multi-subunit E3 ubiquitin ligases, Skp1-Cullin1-F-box Complex (SCF) or Anaphase Promoting Complex (APC) (Bassermann and Pagano, 2010). Further studies should determine whether ubiquitin ligases are involved in TBT-induced cdc25C reduction and subsequent G2/M cell cycle arrest in embryonic cells.

Our data using apigenin showed that TBT-induced G2/M cell cycle arrest is caused by NAD-IDH inhibition

(Fig. 4) and the data were verified by NAD-IDH knockdown and DMKG experiments (Figs. 5, 6). We used apigenin as a NAD-IDH inhibitor. We also confirmed the data by knockdown experiments. Since Apigenin has been reported to inhibit not only NAD-IDH but also hnRNPA2 and NF-κB (Arango *et al*., 2013), we can not rule out the possibility that apigenin-induced G2/M cell cycle arrest was induced by other targets. Our previous report indicates that TBT induces mitochondrial dysfunction, such as impaired mitochondrial morphological dynamics and reduced ATP production via NAD-IDH in embryonic carcinoma cells (Yamada *et al*., 2015). Considering that NAD-IDH is a mitochondrial enzyme, TBT-induced G2/M cell cycle arrest is caused by mitochondrial dysfunction through NAD-IDH inhibition. NAD-IDH catalyzes the reduction of NAD to NADH, which is oxidized by the electron transport chain and is required to generate proton electrochemical gradients across the inner mitochondrial membrane (Saraste, 1999). Thus, inhibition of NAD-IDH by TBT may reduce the NADH supply, thereby dissipating the proton electrochemical gradient. Intracellular Ca^{2+} may be also involved in mitochondrial dysfunction. Previous reports have shown that several anticancer drugs induce G2/M cell cycle arrest and apoptosis by depolarizing mitochondrial membrane potential and increasing intracellular Ca^{2+} (Fang *et al*., 2014; Guo *et al*., 2014). With respect to intracellular Ca^{2+}, there has been also reported that TBT induces mobilization of Ca^{2+} from intracellular stores and results in phosphorylation of MAPKs because its suppression by chelation of intracellular Ca^{2+} in human T lymphoblastoid cells (Yu *et al*., 2000). Thus, Ca^{2+} release from depolarized mitochondria may induce G2/M cell cycle arrest after TBT exposure. Further studies should determine how the downstream signaling of NAD-IDH induces reduction of the cdc25C protein and subsequent G2/M cell cycle arrest after TBT exposure in embryonic cells.

In our previous studies, we have observed that TBT degrades mitofusin proteins and induces mitochondrial fission via the NAD-IDH inhibition. Moreover, we have also shown that TBT results in growth arrest by targeting the glycolytic systems (Yamada *et al*., 2014). Both mitochondrial fission and glycolysis have been reported to be linked to cell cycle alterations (Yamamori *et al*., 2015; Zhai *et al*., 2013). Thus, we are currently investigating whether TBT-induced mitochondrial fission or glycolytic inhibition are linked to G2/M cell cycle arrest or not.

In summary, we demonstrate that TBT mediates G2/M cell cycle arrest through inhibition of NAD-IDH, representing a novel non-genomic pathway of TBT-induced toxicity (Fig. 7). These negative effects of TBT on the cell cycle could result in direct inhibition of cell growth. Thus, TBT-induced G2/M cell cycle arrest via NAD-IDH in embryonic cells may represent a novel mechanism of cytotoxicity associated with nanomolar level exposure of EDCs.

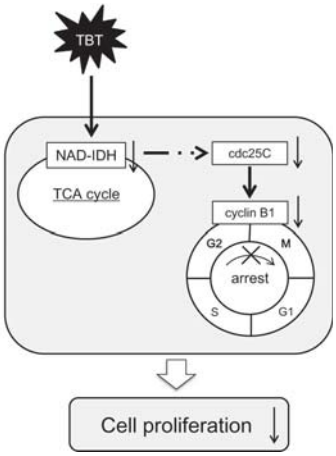

Fig. 7. Proposed model of TBT toxicity through non-genomic pathways in human embryonic carcinoma cells. Nanomolar TBT levels inhibit NAD-IDH activity. TBT induces G2/M cell cycle arrest via the protein reduction of cdc25C and its downstream target, cyclin B1. This TBT-induced G2/M cell cycle arrest may mediate cell growth inhibition.

ACKNOWLEDGMENTS

This work was supported by a Health and Labour Sciences Research Grant from the Ministry of Health, Labour and Welfare, Japan (#H25-Kagaku-Ippan-002 to Y. Kanda), a Grant-in-Aid for Scientific Research from the Ministry of Education, Culture, Sports, Science, and Technology, Japan (#26293056, #26670041 to Y. Kanda), the Research on Regulatory Harmonization and Evaluation of Pharmaceuticals, Medical Devices, Regenerative and Cellular Therapy Products, Gene Therapy Products, and Cosmetics from Japan Agency for Medical Research and development, AMED (To Y. Sekino), and a grant from the Smoking Research Foundation (Y. Kanda).

Conflict of interest---- The authors declare that there is no conflict of interest.

REFERENCES

Arango, D., Morohashi, K., Yilmaz, A., Kuramochi, K., Parihar, A., Brahimaj, B., Grotewold, E. and Doseff, A.I. (2013): Molecular basis for the action of a dietary flavonoid revealed by the com-

prehensive identification of apigenin human targets. Proc. Natl. Acad. Sci. USA, **110**, E2153-E2162.

Bassermann, F. and Pagano, M. (2010): Dissecting the role of ubiquitylation in the DNA damage response checkpoint in G2. Cell Death Differ., **17**, 78-85.

Benkirane, K., Amiri, F., Diep, Q.N., El Mabrouk, M. and Schiffrin, E.L. (2006): PPAR-gamma inhibits ANG II-induced cell growth via SHIP2 and 4E-BP1. Am. J. Physiol. Heart Circ. Physiol., **290**, H390-H397.

Chaudhary, P., Sharma, R., Sahu, M., Vishwanatha, J.K., Awasthi, S. and Awasthi, Y.C. (2013): 4-Hydroxynonenal induces G2/M phase cell cycle arrest by activation of the ataxia telangiectasia mutated and Rad3-related protein (ATR)/checkpoint kinase 1 (Chk1) signaling pathway. J. Biol. Chem., **288**, 20532-20546.

Donzelli, M. and Draetta, G.F. (2003): Regulating mammalian checkpoints through Cdc25 inactivation. EMBO Rep., **4**, 671-677.

Dopp, E., Hartmann, L.M., Florea, A.M., Rettenmeier, A.W. and Hirner, A.V. (2004): Environmental distribution, analysis, and toxicity of organometal(loid) compounds. Crit. Rev. Toxicol., **34**, 301-333.

Fang, C., Zhang, J., Qi, D., Fan, X., Luo, J., Liu, L. and Tan, Q. (2014): Evodiamine induces G2/M arrest and apoptosis via mitochondrial and endoplasmic reticulum pathways in H446 and H1688 human small-cell lung cancer cells. PLoS One, **9**, e115204.

Gabrielli, B., Brooks, K. and Pavey, S. (2012): Defective cell cycle checkpoints as targets for anti-cancer therapies. Front. Pharmacol., **3**, 9.

Gårdlund, A.T., Archer, T., Danielsen, K., Danielsson, B., Frederiksson, A., Lindquist, N.G., Lindström, H. and Luthman, J. (1991): Effects of prenatal exposure to tributyltin and trihexyltin on behaviour in rats. Neurotoxicol. Teratol., **13**, 99-105.

Guo, J., Zhao, W., Hao, W., Ren, G., Lu, J. and Chen, X. (2014): Cucurbitacin B induces DNA damage, G2/M phase arrest, and apoptosis mediated by reactive oxygen species (ROS) in leukemia K562 cells. Anticancer Agents Med. Chem., **14**, 1146-1153.

Hirata, N., Yamada, S., Shoda, T., Kurihara, M., Sekino, Y. and Kanda, Y. (2014): Sphingosine-1-phosphate promotes expansion of cancer stem cells via S1PR3 by a ligand-independent Notch activation. Nat. Commun., **5**, 4806.

Kanayama, T., Kobayashi, N., Mamiya, S., Nakanishi, T. and Nishikawa, J. (2005): Organotin compounds promote adipocyte differentiation as agonists of the peroxisome proliferator-activated receptor gamma/retinoid X receptor pathway. Mol. Pharmacol., **67**, 766-774.

Kanda, Y., Hinata, T., Kang, S.W. and Watanabe, Y. (2011): Reactive oxygen species mediate adipocyte differentiation in mesenchymal stem cells. Life Sci., **89**, 250-258.

Kawabe, T. (2004): G2 checkpoint abrogators as anticancer drugs. Mol. Cancer Ther., **3**, 513-519.

Mitra, S., Gera, R., Siddiqui, W.A. and Khandelwal, S. (2013): Tributyltin induces oxidative damage, inflammation and apoptosis via disturbance in blood–brain barrier and metal homeostasis in cerebral cortex of rat brain: an *in vivo* and *in vitro* study. Toxicology, **310**, 39-52.

Nakatsu, Y., Kotake, Y., Takai, N. and Ohta, S. (2010): Involvement of autophagy via mammalian target of rapamycin (mTOR) inhibition in tributyltin-induced neuronal cell death. J. Toxicol. Sci., **35**, 245-251.

Nam, C., Doi, K. and Nakayama, H. (2010): Etoposide induces G2/M arrest and apoptosis in neural progenitor cells via DNA damage and an ATM/p53-related pathway. Histol. Histopathol., **25**, 485-493.

Ouyang, G., Yao, L., Ruan, K., Song, G., Mao, Y. and Bao, S. (2009): Genistein induces G2/M cell cycle arrest and apoptosis of human ovarian cancer cells via activation of DNA damage checkpoint pathways. Cell Biol. Int., **33**, 1237-1244.

Pani, E., Stojic, L., El-Shemerly, M., Jiricny, J. and Ferrari, S. (2007): Mismatch repair status and the response of human cells to cisplatin. Cell Cycle, **6**, 1796-1802.

Saraste, M. (1999): Oxidative phosphorylation at the fin de siècle. Science, **283**, 1488-1493.

Shabbeer, S., Omer, D., Berneman, D., Weitzman, O., Alpaugh, A., Pietraszkiewicz, A., Metsuyanim, S., Shainskaya, A., Papa, M.Z. and Yarden, R.I. (2013): BRCA1 targets G2/M cell cycle proteins for ubiquitination and proteasomal degradation. Oncogene, **32**, 5005-5016.

Shackelford, R.E., Kaufmann, W.K. and Paules, R.S. (1999): Cell cycle control, checkpoint mechanisms, and genotoxic stress. Environ. Health Perspect., **107**, 5-24.

Whalen, M.M., Loganathan, B.G. and Kannan, K. (1999): Immunotoxicity of environmentally relevant concentrations of butyltins on human natural killer cells *in vitro*. Environ. Res., **81**, 108-116.

Willenborg, M., Panten, U. and Rustenbeck, I. (2009): Triggering and amplification of insulin secretion by dimethyl alpha-ketoglutarate, a membrane permeable alpha-ketoglutarate analogue. Eur. J. Pharmacol., **607**, 41-46.

Yamada, S., Kotake, Y., Sekino, Y. and Kanda, Y. (2013): AMP-activated protein kinase-mediated glucose transport as a novel target of tributyltin in human embryonic carcinoma cells. Metallomics, **5**, 484-491.

Yamada, S., Kotake, Y., Demizu, Y., Kurihara, M., Sekino, Y. and Kanda, Y. (2014): NAD-dependent isocitrate dehydrogenase as a novel target of tributyltin in human embryonic carcinoma cells. Sci. Rep., **4**, 5952.

Yamada, S., Kotake, Y., Nakano, M., Sekino, Y. and Kanda, Y. (2015): Tributyltin induces mitochondrial fission through NAD-IDH dependent mitofusin degradation in human embryonic carcinoma cells. Metallomics, **7**, 1240-1246.

Yamamori, T., Ike, S., Bo, T., Sasagawa, T., Sakai, Y., Suzuki, M., Yamamoto, K., Nagane, M., Yasui, H. and Inanami, O. (2015): Inhibition of the mitochondrial fission protein dynamin-related protein 1 (Drp1) impairs mitochondrial fission and mitoticcatastrophe after X-irradiation. Mol. Biol. Cell, **26**, 4607-4617.

Yu, L., Zhang, X., Yuan, J., Cao, Q., Liu, J., Zhu, P. and Shi, H. (2011): Teratogenic effects of triphenyltin on embryos of amphibian (*Xenopus tropicalis*): a phenotypic comparison with the retinoid X and retinoic acid receptor ligands. J. Hazard Mater., **192**, 1860-1868.

Yu, Z.P., Matsuoka, M., Wispriyono, B., Iryo, Y. and Igisu, H. (2000): Activation of mitogen-activated protein kinases by tributyltin in CCRF-CEM cells: role of intracellular Ca(2+). Toxicol. Appl. Pharmacol., **168**, 200-207.

Zhai, X., Yang, Y., Wan, J., Zhu, R. and Wu, Y. (2013): Inhibition of LDH-A by oxamate induces G2/M arrest, apoptosis and increases radiosensitivity in nasopharyngeal carcinoma cells. Oncol. Rep., **30**, 2983-2991.

Zhang, Y., Go, Z. and Xu, L. (2014): Tributyltin induces a G2/M cell cycle arrest in human amniotic cells via PP2A inhibition-mediated inactivation of the ERK1/2 cascades. Environ. Toxicol. Pharmacol., **37**, 812-818.

SCIENTIFIC REPORTS

OPEN

Chlorpyrifos inhibits neural induction via Mfn1-mediated mitochondrial dysfunction in human induced pluripotent stem cells

Received: 21 October 2016
Accepted: 13 December 2016
Published: 23 January 2017

Shigeru Yamada[1,2], Yusuke Kubo[1], Daiju Yamazaki[1], Yuko Sekino[1] & Yasunari Kanda[1]

Organophosphates, such as chlorpyrifos (CPF), are widely used as insecticides in agriculture. CPF is known to induce cytotoxicity, including neurodevelopmental toxicity. However, the molecular mechanisms of CPF toxicity at early fetal stage have not been fully elucidated. In this study, we examined the mechanisms of CPF-induced cytotoxicity using human induced pluripotent stem cells (iPSCs). We found that exposure to CPF at micromolar levels decreased intracellular ATP levels. As CPF suppressed energy production that is a critical function of the mitochondria, we focused on the effects of CPF on mitochondrial dynamics. CPF induced mitochondrial fragmentation via reduction of mitochondrial fusion protein mitofusin 1 (Mfn1) in iPSCs. In addition, CPF reduced the expression of several neural differentiation marker genes in iPSCs. Moreover, knockdown of *Mfn1* gene in iPSCs downregulated the expression of *PAX6*, a key transcription factor that regulates neurogenesis, suggesting that Mfn1 mediates neural induction in iPSCs. Taken together, these results suggest that CPF induces neurotoxicity via Mfn1-mediated mitochondrial fragmentation in iPSCs. Thus, mitochondrial dysfunction in iPSCs could be used as a possible marker for cytotoxic effects by chemicals.

Growing evidence suggests the involvement of environmental chemicals in neurodevelopmental toxicity, leading to neurobehavioral outcomes such as learning disabilities, attention deficit hyperactivity disorder, cognitive impairment, and autism[1,2]. As the fetal brain is inherently more susceptible to chemical-induced toxicity compared to the adult brain, exposure to neurotoxic chemicals during early prenatal period can cause delayed neural disorders at lower doses than in adults[3,4].

Organophosphates, such as chlorpyrifos (CPF), are well known to affect brain structure and neurodevelopmental outcome, resulting in delayed neural disorders[5,6]. In regard to this, previous studies using magnetic resonance imaging have shown that prenatal exposure to CPF caused abnormalities in the structure, size, and thickness of cerebral cortex, where was responsible for several higher-order brain functions such as attention, cognition, and emotion[7]. Several reports indicate that CPF causes neurotoxicity in the developing brain of animals. In the developing brain of neonatal rats, CPF exposure impairs neurite outgrowth by inhibiting choline acetyltransferase activity[8]. Maternal exposure to CPF suppresses neurogenesis in the hippocampal dentate gyrus of rat offspring[9]. In addition to *in vivo* effects, there has been reported the cytotoxic effects of micromolar CPF levels *in vitro*. For example, CPF inhibited mitochondrial oxidative phosphorylation[10] and induced apoptosis in human neuroblastoma SH-SY5Y cells[11] or human neural precursor cells[12]. As micromolar CPF levels were detected in the blood of human newborns living in an agricultural community[13], the observations made using micromolar levels of CPF *in vitro* could potentially reflect the biological reactions in a living body. However, the effect of CPF on neurodevelopment has not been precisely elucidated.

[1]Division of Pharmacology, National Institute of Health Sciences, Tokyo, Japan. [2]Pharmacological Evaluation Institute of Japan (PEIJ), Kanagawa, Japan. Correspondence and requests for materials should be addressed to Y.K. (email: kanda@nihs.go.jp)

Morphological changes of mitochondria are known to contribute to homeostasis[14,15]. Under normal circumstances, mitochondria fuses together and forms excessive tubular networks (mitochondrial fusion). These fusion is regulated by fusion factors mitofusin 1 and 2 (Mfn1, Mfn2) and optic atrophy 1 (Opa1)[16,17]. In contrast, under stress conditions, mitochondrial networks convert into large numbers of small fragments with spherical and punctate morphology (mitochondrial fission), and are regulated by fission factors, such as fission protein 1 (Fis1) and dynamin-related protein 1 (Drp1)[18,19]. This morphological dynamics contributes to the maintenance of mitochondrial functions, including energy generation[14]. Moreover, several studies have shown the relationship between mitochondrial fragmentation and cellular and neurodevelopmental defects. For example, Mfn1 or Mfn2 knockout mice die in midgestation embryo, accompanying with developmental delay. In addition, embryonic fibroblasts from these knockout mice display distinct types of fragmented mitochondria, a phenotype due to a severe reduction in mitochondrial fusion[20]. Thus, Mfn1 is considered to be functionally different from Mfn2. In support to this, Mfn1, not Mfn2, is reported to contribute to Opa1-mediated fusion of mitochondrial inner membrane[16].

In the present study, we investigated the effect of CPF on neural differentiation using human induced pluripotent stem cells (iPSCs) as a model of human organ development. We focused on the effects of micromolar levels of CPF on mitochondrial dynamics, examining the molecular mechanisms of the process. Our results show that micromolar CPF levels inhibited ATP production through Mfn1 reduction, followed by mitochondrial fragmentation. Moreover, Mfn1-mediated mitochondrial dysfunction suppressed early neural induction by decreasing levels of *PAX6*, a key transcription factor that regulates neurogenesis. These data suggest that CPF-induced neurodevelopmental toxicity is based on impairment of mitochondrial functions in human iPSCs.

Results

Effect of CPF on neural differentiation of iPSCs. To investigate whether CPF affects early neurodevelopment, we examined neural differentiation capability of iPSCs, which was induced by dual SMAD inhibition protocol[21] (Fig. 1A). First, we determined the critical CPF concentration, affecting neural differentiation. At day 4 after neural induction with different concentrations of CPF, the expression of *PAX6*, an early neuroectodermal marker that regulates neurogenesis[22], was analyzed using real-time PCR. We found that exposure to 30 μM CPF significantly decreased *PAX6* gene expression (Fig. 1B). Next, we performed time course experiments for expression of several neural differentiation markers at days 2, 4, 6, and 8 after exposure to 30 μM CPF. At day 9, almost all cells exposed by CPF (30 μM) were detached from the culture dish. Real-time PCR analysis revealed upregulated expression of *PAX6* by day 4, and *FOXG1*, a neuroectodermal marker that also regulates neurogenesis[23], thereafter (Fig. 1C and D). Representative neural maturation marker *NCAM1*[24] continuously increased, confirming that further neural differentiation occurred (Fig. 1E). In addition, CPF exposure reduced the expression of these neural induction markers by day 6 (Fig. 1C–E). These data suggest that CPF has an inhibitory effect on early neural differentiation of iPSCs.

Mitochondrial function of iPSCs exposed to CPF. As neural differentiation process requires ATP as a source of energy[25], we examined intracellular ATP content in iPSCs. Treatment with 30 μM CPF significantly reduced the ATP content of the cells (Fig. 2A). We have previously shown that 0.1 μM carbonyl cyanide m-chlorophenyl hydrazone (CCCP), which functions as a mitochondrial uncoupler[26], decreased ATP levels in iPSCs. Because CPF inhibited ATP production, we focused on several mitochondrial functions. Mitochondrial membrane potential (MMP) was decreased by exposure to 30 μM CPF for 24 h (Fig. 2B and C). As a positive control, exposure to 0.1 μM CCCP reduced MMP (Figure S1). In addition, CPF exposure increased the number of cells with fragmented mitochondria displaying punctate morphology (Fig. 2D) and decreased the number of cells exhibiting mitochondrial fusion (Fig. 2E). We have already confirmed that 0.1 μM CCCP also increased the occurrence of fragmented mitochondria. These results suggest that CPF induces mitochondrial dysfunction, including MMP depolarization and mitochondrial fragmentation, in iPSCs.

Expression of mitochondrial fission and fusion factors in iPSCs exposed to CPF. To examine the molecular mechanisms by which CPF induces mitochondrial fragmentation in iPSCs, we assessed the expression levels of mitochondrial fission (*Fis1* and *Drp1*) and fusion genes (*Mfn1*, *Mfn2*, and *OPA1*). Real-time PCR analysis showed that the gene expression of the factors was not altered after CPF exposure (Fig. 3A). Interestingly, western blot analysis revealed that CPF significantly decreased Mfn1 protein levels. In contrast, protein expression levels of other factors, including Mfn2, were not changed (Fig. 3B and C). These data suggest that CPF-induced mitochondrial fragmentation is caused by reduction of Mfn1 protein levels.

Effects of CPF in iPSC-derived neural progenitor cells. To investigate whether the effects of CPF selectively occur in the early stage of neural differentiation in iPSCs, we used iPSC-derived neural progenitor cells (NPCs), which were induced by dual SMAD inhibition protocol[21] (Figure S1A). Treatment with 30 μM CPF had little effect on ATP content (Figure S1B). Similarly, exposure to 30 μM CPF had little effect on mitochondrial morphology (Figure S1C and D), which was confirmed by the fact that CPF did not alter the protein levels of mitochondrial fission and fusion factors containing Mfn1 (Figure S1E). These data suggest that iPSCs, not NPCs, are sensitive to CPF exposure.

Effect of Mfn1 knockdown on neural induction of iPSCs. To further investigate the involvement of Mfn1 in the effects of CPF on neural induction, we performed knockdown (KD) of Mfn1, using lentivirus-delivered shRNAs. Real-time PCR analysis showed that KD was selective for *Mfn1*, not *Mfn2*, and that the efficiency was approximately 70% (Fig. 4A). The KD effects were also confirmed by protein levels (Fig. 4B and C). The Mfn1 KD cells were used to perform neural induction. Real-time PCR analysis revealed that Mfn1 KD

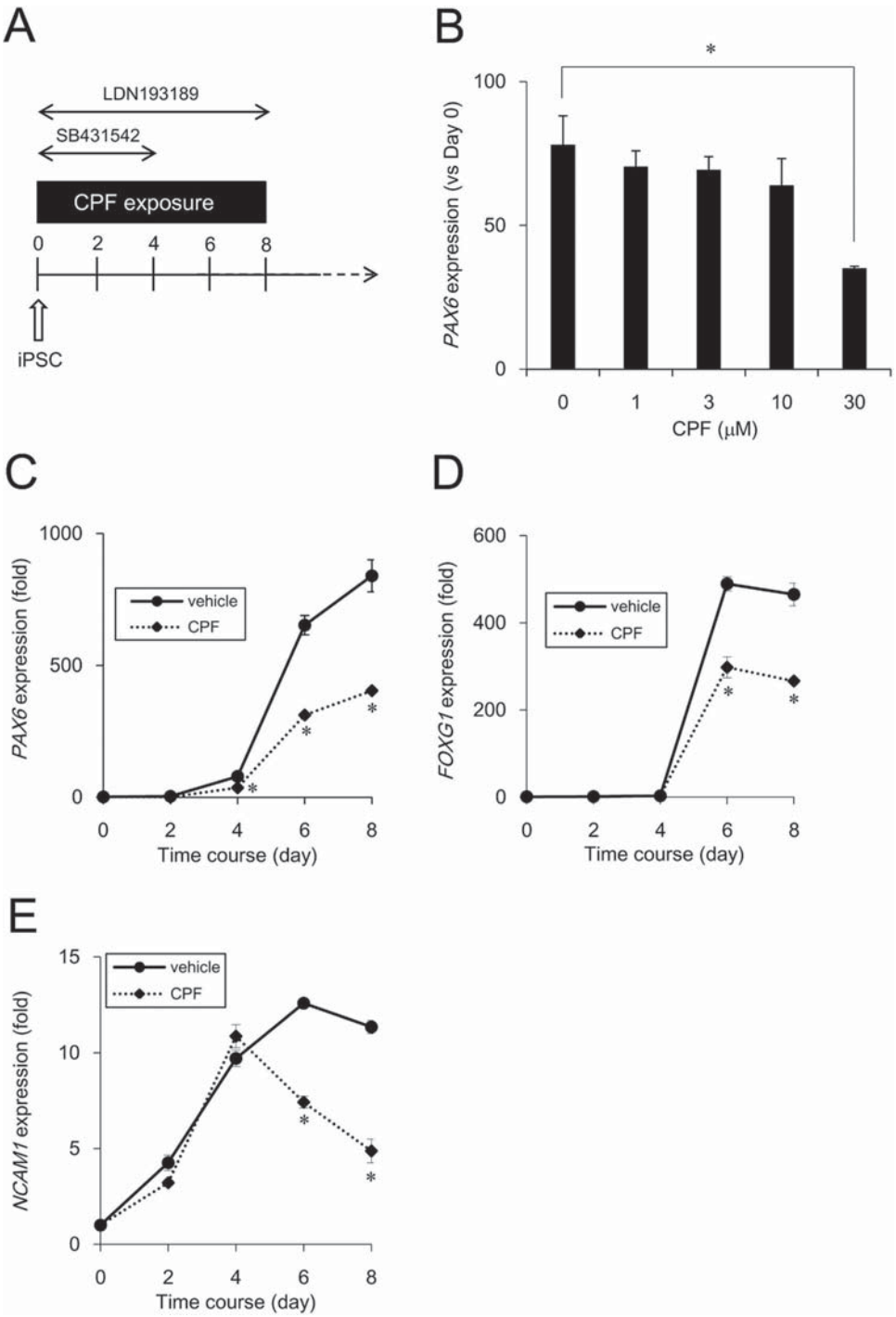

Figure 1. Time course studies of neural induction in iPSCs exposed to CPF. (**A**) Schematic time course of induction from iPSCs to NPCs by dual SMAD inhibition. Neural induction was initiated after exposure to CPF for 24 h. The cells were continuously exposed to CPF throughout neural differentiation. (**B**) At day 4 after neural induction with CPF (0–30 μM), expression of the neural differentiation marker *PAX6* was examined using real-time PCR analysis. (**C–E**) At days 2, 4, 6, and 8 after neural induction with CPF (30 μM), expression of neural differentiation markers, *PAX6*, *FOXG1*, and *NCAM1* was examined using real-time PCR analysis. Data are represented as means ± SD (n = 3). $^*P < 0.05$.

decreased the expression of *PAX6* (day 4), *FOXG1* (day 6) and *NCAM1* (day 6) (Fig. 4D). These data suggest that Mfn1 is involved in CPF-mediated negative effects on neural induction of iPSCs.

Negative regulation of neural induction by CPF exposure. A previous report indicates that ERK signaling inhibits neural induction via *PAX6* silencing in human embryonic stem cells[27]. ERK has been reported to be activated after depletion of Mfn1[28]. We focused on ERK signaling in the effect of CPF on neural induction.

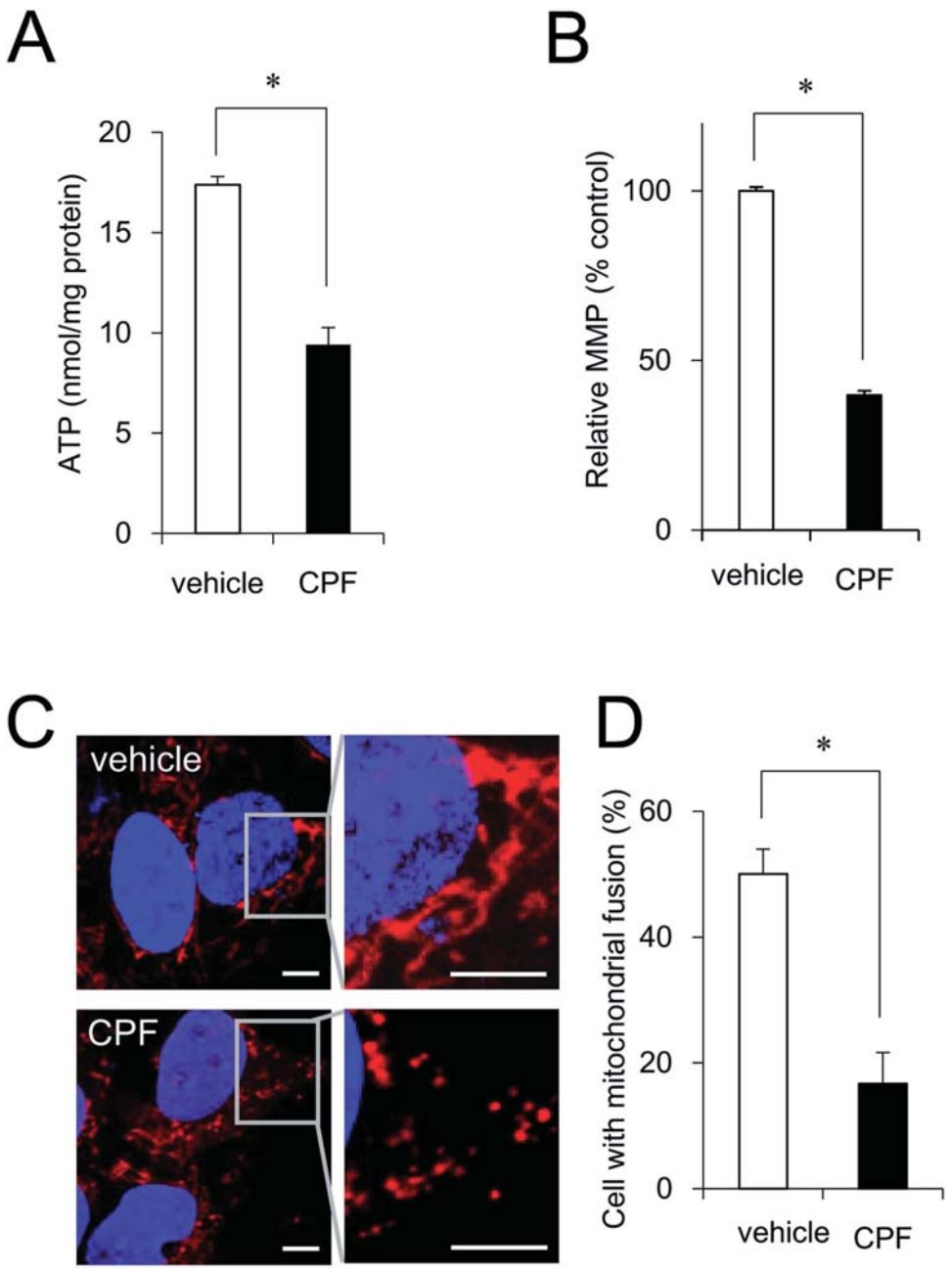

Figure 2. Mitochondrial function of iPSCs exposed to CPF. (**A**) Cells were exposed to CPF (30 μM) for 24 h. Intracellular ATP content was determined in the lysed cells (n = 3). (**B**) Cells were exposed to CPF for 24 h and stained with JC-10 for 20 min. MMP of JC-10 labeled cells was analyzed by flow cytometry. The histogram represents the ratio of JC-aggregate (F-590) to JC-monomer (F-535) fluorescence (n = 3). (**C**) Cells were exposed to CPF for 72 h and stained with MitoTracker Red CMXRos and Hoechst33342. Mitochondrial morphology was observed by confocal laser microscopy. Bar = 5 μm. (**D**) The number of cells with mitochondrial fusion (<10% punctiform) was determined in each image (n = 5). Data are represented as means ± SD. $^*P < 0.05$.

We found that CPF exposure significantly increased basal ERK phosphorylation levels, which were abolished by treatment with the ERK inhibitor U0126 (Fig. 5A and B). To further study whether *PAX6* downregulation in CPF-exposed cells occurred through ERK signaling, we examined the effect of U0126 on *PAX6* expression. Incubation with U0126 recovered the expression levels of *PAX6* (Fig. 5C). These data suggest that CPF activates ERK and prevents neural induction via *PAX6* downregulation.

Effect of Mfn1 knockdown on neural induction. To confirm the involvement of Mfn1 in the inhibition of neural induction by CPF, we used Mfn1 KD cells. Mfn1 KD significantly increased basal ERK phosphorylation levels that were abolished by treatment with the ERK inhibitor U0126 (Fig. 6A and B). To further study

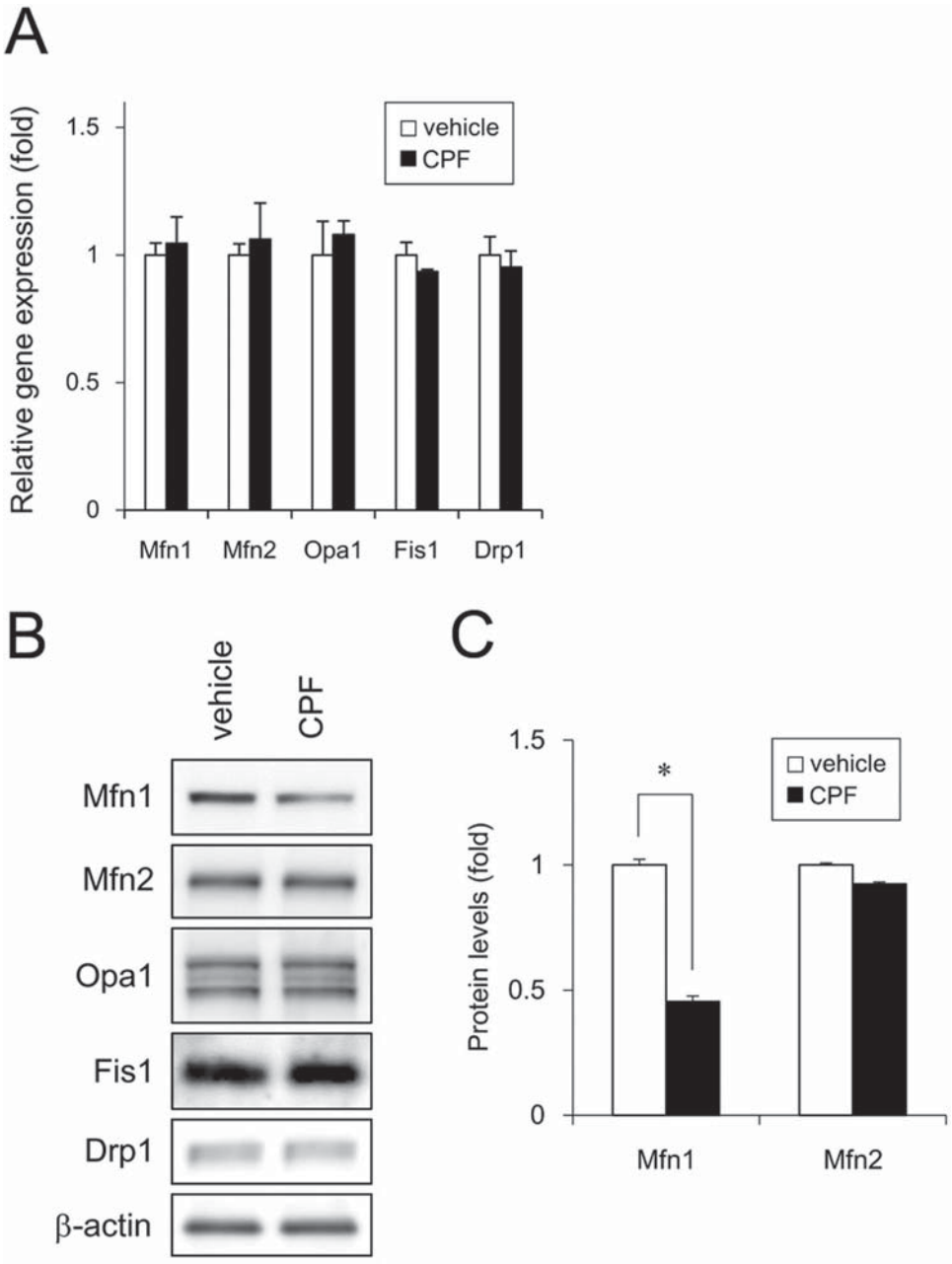

Figure 3. Expression of mitochondrial fission and fusion factors of iPSCs exposed to CPF. (**A**) After exposure to CPF (30 μM) for 24 h, expression of mitochondrial genes was analyzed by real-time PCR. (**B**) After exposure to CPF for 24 h, expression of mitochondrial proteins was analyzed by western blotting using anti-Drp1, anti-Fis1, anti-Mfn1, anti-Mfn2, anti-Opa1, or anti-β-actin antibodies. (**C**) Relative densities of bands were quantified with ImageJ software. Relative changes in expression were determined by normalization to β-actin. Data are represented as means ± SD (n = 3). $^{*}P < 0.05$.

whether *PAX6* downregulation in Mfn1 KD cells occurred through ERK signaling, we examined the effect of U0126 on *PAX6* expression. Mfn1 KD decreased *PAX6* by 64% by in the vehicle-treated cells. In contrast, Mfn1 KD decreased *PAX6* by 30% in the U0126-treated cells. Thus, incubation with U0126 partially recovered the *PAX6* expression in the Mfn1 KD cells (Fig. 6C). Taken together, these data suggest that Mfn1 reduction by CPF exposure activates ERK and prevents neural induction via *PAX6* downregulation.

Discussion

In the present study, we demonstrated that exposure to micromolar CPF targeted mitochondrial quality control in human iPSCs. We showed that CPF induced Mfn1 reduction, thereby promoting mitochondrial fragmentation. These negative effects of CPF on mitochondrial quality control could suppress ATP production and neural

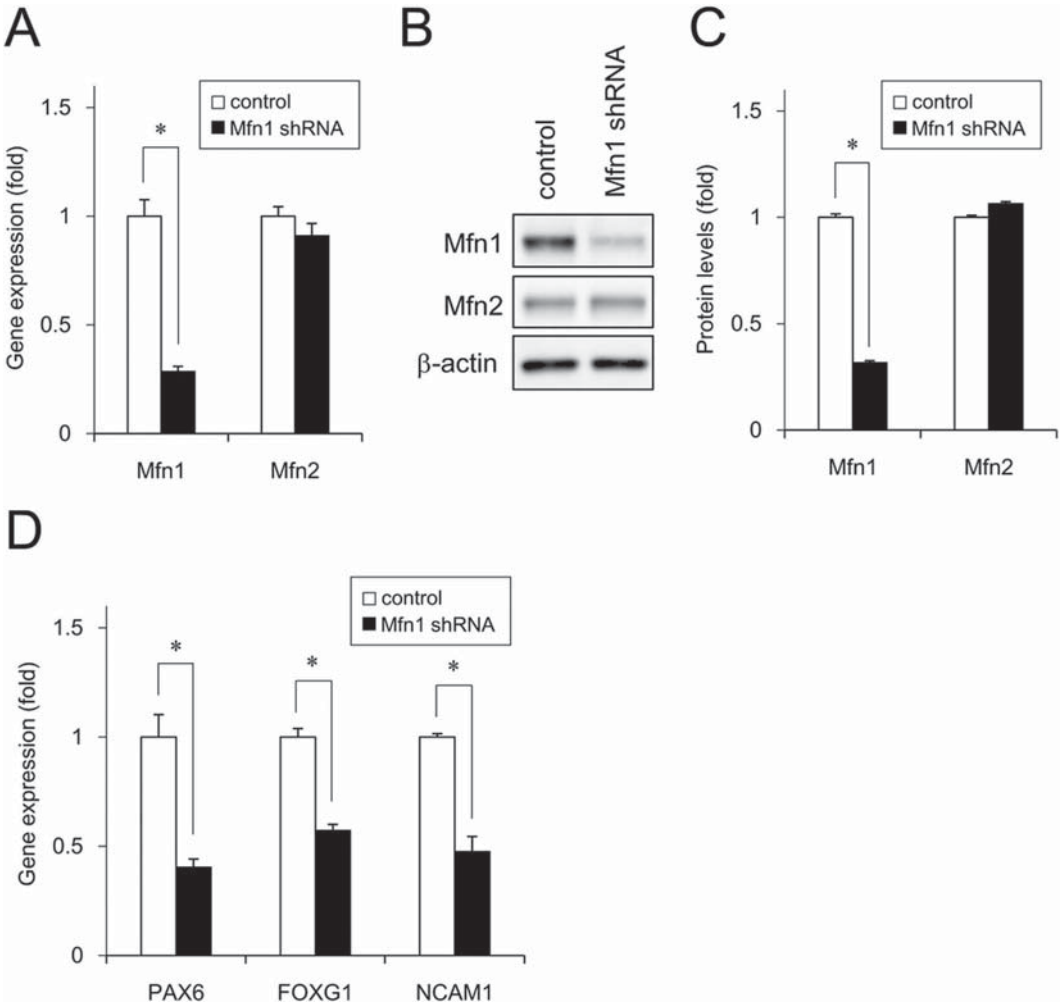

Figure 4. Effect of Mfn1 knockdown on neural induction of iPSCs. Cells were infected with lentiviruses containing a vector encoding a shRNA directed against *Mfn1* or a scrambled sequence shRNA (control) for 24 h. The infected cells were subjected to selection with puromycin (1 μg/ml) for 24 h and cultured for an additional 72 h prior to functional analyses. (**A**) The expression of *Mfn1* and *Mfn2* genes was analyzed by real-time PCR. (**B**) The expression of Mfn1 and Mfn2 proteins was analyzed by western blotting using anti-Mfn1, anti-Mfn2, or anti-β-actin antibodies. (**C**) Relative densities of bands were quantified with ImageJ software. Relative changes in expression were determined by normalization to β-actin. (**D**) Expression of neural differentiation markers *PAX6* (day 4), *FOXG1* (day 6), and *NCAM1* (day 6) was examined with real-time PCR. Data are represented as means ± SD (n = 3). $^*P < 0.05$.

differentiation. Based on the data observed in our study, Fig. 7 shows a proposed mechanism of CPF cytotoxicity via mitochondrial dysfunction.

Our studies showed that treatment with micromolar CPF levels caused mitochondrial dysfunction of human iPSCs (Fig. 2). We observed that iPSCs were sensitive to CPF exposure, unlike iPSC-derived NPCs (Figure S1). Previous reports support this difference in CPF sensitivity. The inhibitory effect of CPF on DNA synthesis in undifferentiated C6 glioma cells is found to be much higher than in differentiated cells[29]. *In vivo* studies indicate that immature organisms are more susceptible to CPF-induced toxicity compared to adults due to lower levels of CPF metabolizing enzymes[30]. Thus, the difference in CPF sensitivity between iPSCs and NPCs may be dependent on the maturation of CPF detoxification pathways. We are currently conducting experiments to determine the mechanism causing the differences in sensitivity to CPF.

We showed that CPF induced mitochondrial fragmentation via Mfn1 reduction (Figs 2 and 3). Consistent with this, our previous knockdown studies indicated that Mfn1 reduction was sufficient to promote mitochondrial dysfunction[31]. CPF-induced Mfn1 reduction might mediate mitochondrial fragmentation, decrease ATP levels, and inhibit iPSC growth. Although Mfn2 is also involved in mitochondrial fission and energy supply processes[32,33], our results indicated that CPF specifically targeted Mfn1, not Mfn2. Regarding this apparent CPF specificity, E3 ubiquitin ligase membrane-associated RING-CH 5 (MARCH5) has been reported to selectively bind to Mfn1 dependent on its acetylation, and degrade among all mitochondrial proteins, including Mfn2[34]. In addition, we have reported that organotin compounds induced Mfn1 degradation through MARCH5,

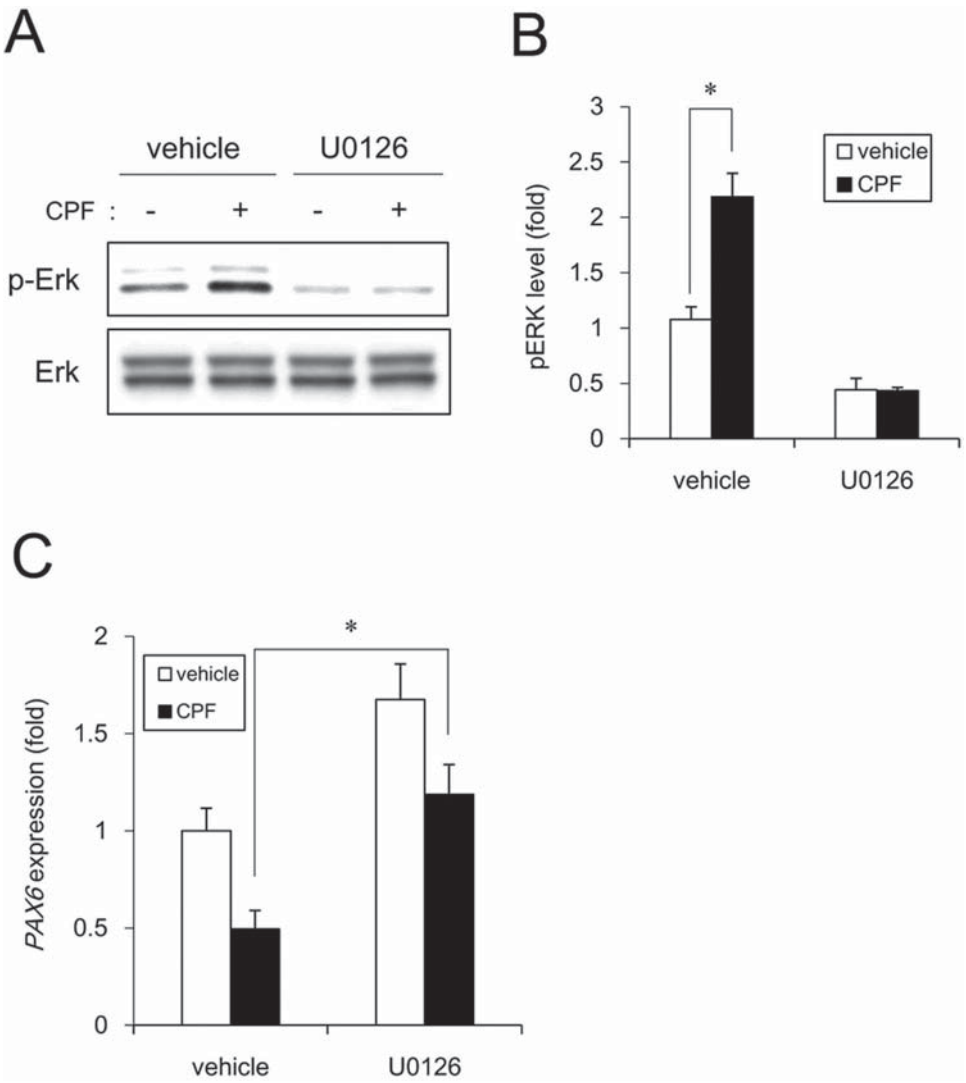

Figure 5. Negative regulation of neural induction by CPF exposure. (**A**) Cells were exposed to CPF (30 μM) or CPF + U0126 (5 μM) for 24 h. ERK phosphorylation was analyzed by western blotting using anti-phospho-ERK antibodies. (**B**) Relative densities of bands were quantified with ImageJ software. Relative changes in expression were determined by normalization to total ERK protein level. (**C**) At day 4 after neural induction with CPF or CPF + U0126, the expression of *PAX6* gene was analyzed by real-time PCR. Data are represented as means ± SD (n = 3). $^{*}P < 0.05$.

thereby promoting mitochondrial fragmentation in iPSCs[31]. Thus, CPF may specifically target Mfn1 protein via MARCH5 in iPSCs without affecting mRNA levels. Furthermore, the difference in CPF sensitivity between iPSCs and NPCs may be dependent on Mfn1 and MARCH5 expression levels or MARCH5 activity. Further studies should determine whether CPF reduces Mfn1 via MARCH5-mediated degradation in iPSCs.

We demonstrated that ERK phosphorylation mediated the negative effects of CPF on early neural differentiation (Figs 1, 4 and 5). A previous report indicates that Mfn1 directly binds Ras and Raf, resulting in the inhibition of Ras-Raf-ERK signaling by the biochemical analysis[35,36]. Mfn1 reduction by CPF or shRNA may reverse this ERK signaling inhibition. Mobilization of Ca^{2+} from intracellular stores, including mitochondria was reported to result in phosphorylation of MAPKs, as the process was suppressed by chelation of intracellular Ca^{2+} in human T lymphoblastoid cells[37]. As mitochondria are known to uptake into the matrix of any Ca^{2+} that has accumulated in the cytosol, dependent on MMP[38], mitochondrial dysfunction by CPF exposure may cause an overload of Ca^{2+}, resulting in ERK activation. Moreover, ERK signaling was reported to inhibit neural induction by *PAX6* silencing via upregulation of stemness factors *NANOG/OCT4* and downregulation of homeobox transcription factor *OTX2*[27]. NANOG and OCT4 act as repressors of *PAX6* induction, whereas OTX2 is a positive inducer of *PAX6*[27]. Therefore, ERK signaling evoked by CPF could affect the expression of these transcriptional network, including *NANOG*, *OCT4* and *OTX2*, *by* regulating *PAX6*. In future studies, we should further investigate the mechanisms of CPF-induced negative regulation of neural induction via ERK.

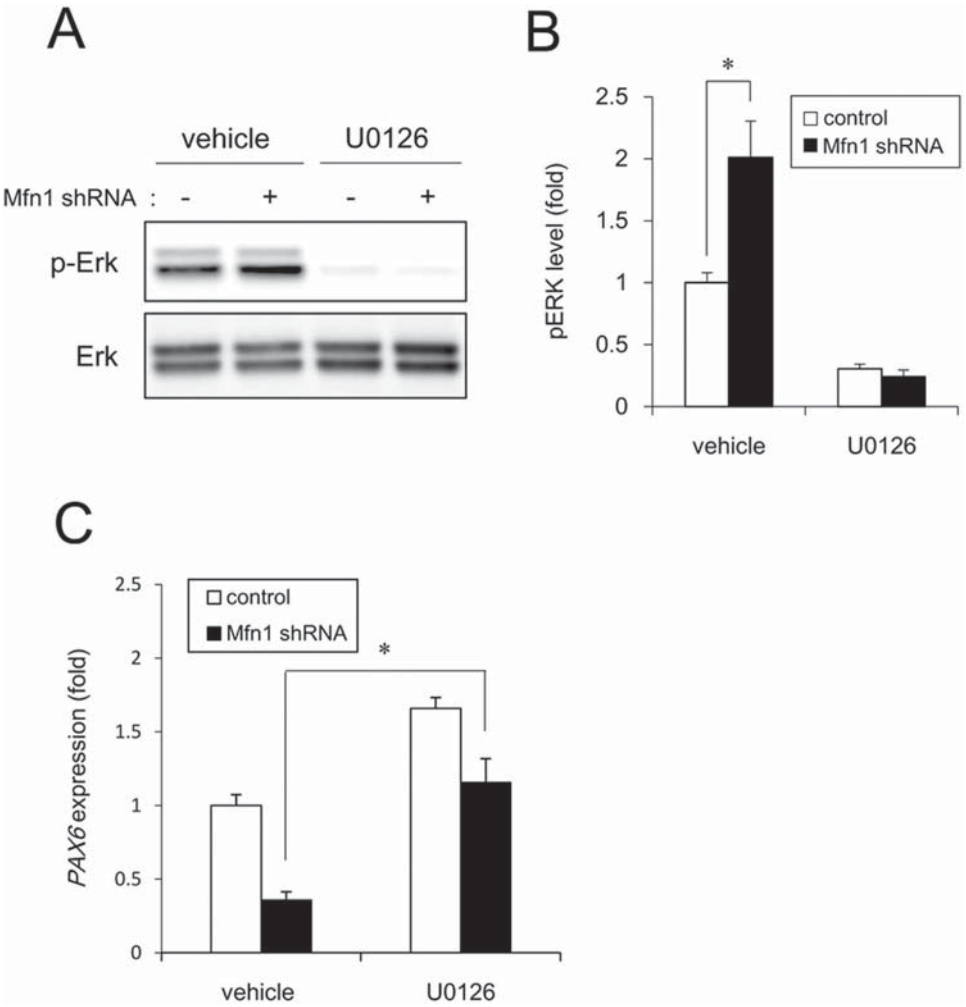

Figure 6. Negative regulation of neural induction by Mfn1 knockdown. The cells were infected with lentiviruses containing a vector encoding a shRNA directed against Mfn1 or a scrambled sequence shRNA (control) for 24 h. The infected cells were subjected to selection with 1 μg/ml puromycin for 24 h and cultured for an additional 72 h prior to functional analyses. (**A**) After incubation with U0126 for 24 h, ERK phosphorylation was analyzed by western blotting using anti-phospho-ERK antibodies. (**B**) Relative densities of bands were quantified with ImageJ software. Relative changes in expression were determined by normalization to total ERK protein level. (**C**) At day 4 after neural induction with U0126, the expression of *PAX6* gene was analyzed by real-time PCR. Data are represented as means ± SD (n = 3). $^{*}P < 0.05$.

We further demonstrated that Mfn1 reduction mediated cytotoxic effects of CPF on iPSCs via *PAX6* down-regulation (Figs 5 and 6). *FOXG1* was downregulated, along with *PAX6*, during neural differentiation of iPSCs exposed to CPF. *PAX6* and *FOXG1* act as transcriptional regulators during forebrain development in vertebrates[39,40]. Targeted disruption of *PAX6* and *FOXG1* in rodents led to the loss of anterior neural tissues, suggesting the central role of these genes in forebrain development[41,42]. CPF causes various defects in the development of hippocampus and cortex of rodents[43]. Thus, CPF-induced defects of forebrain architecture may be caused by transcriptional silencing of anterior neural markers during early neurogenesis. As *NCAM1* was downregulated during neural differentiation of iPSCs exposed to CPF, further studies using NPCs are required to reveal how CPF affects neural maturation processes.

In summary, our results demonstrate a novel mechanism underlying cytotoxicity, including neurodevelopmental toxicity of CPF in iPSCs. Recently, significant progress has been made in the induction of differentiation of pluripotent stem cells into a variety of cell types[44]. Further studies are needed to evaluate the developmental effects of CPF on various types of iPSC-derived cells. Moreover, we show that CPF toxicity is caused by Mfn1-mediated mitochondrial dysfunction, which is involved in the cytotoxicity of organotin compounds[31]. Thus, mitochondrial functions influenced by Mfn1 might be a good starting point for investigating toxic mechanisms induced by exposure to other chemicals.

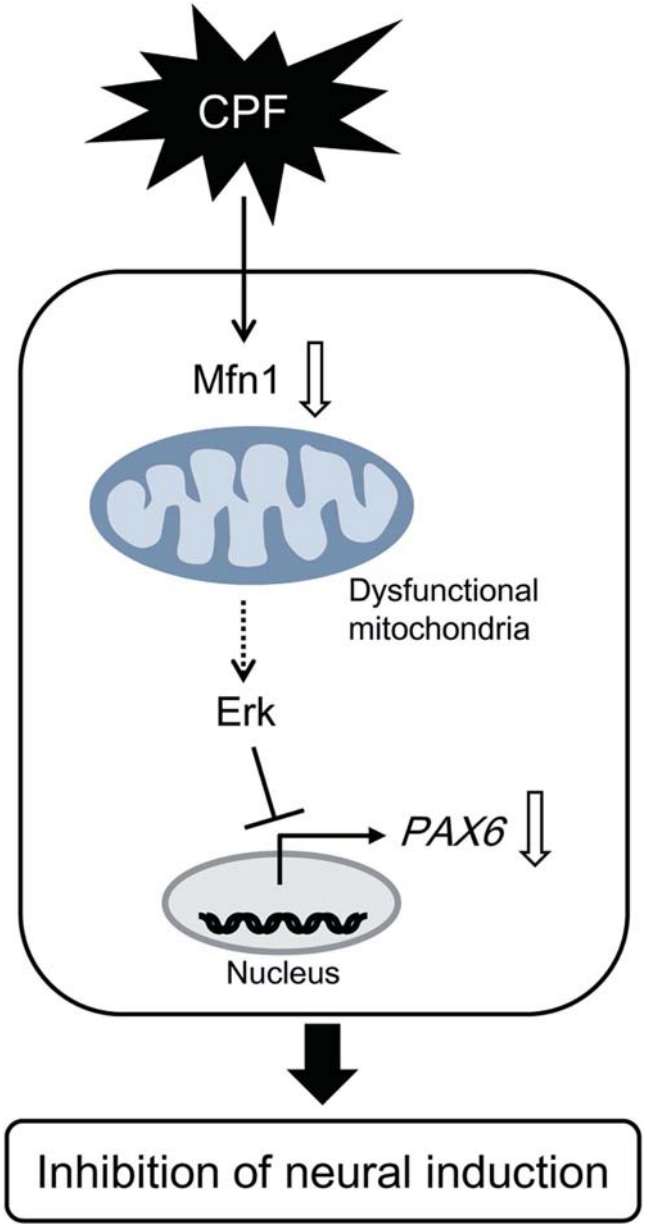

Figure 7. Proposed mechanism of CPF cytotoxicity in human iPSCs. CPF exposure causes Mfn1 reduction, which induces mitochondrial dysfunction, including mitochondrial fragmentation and decreased ATP levels. Mitochondrial dysfunction in turn evokes ERK phosphorylation, leading to the suppression of *PAX6*, which is an early marker of neurogenesis.

Methods

Chemicals. Chlorpyrifos (CPF), Y-27632, SB431542, and LDN193189 were obtained from Wako (Tokyo, Japan). Penicillin-streptomycin mixture (PS) was obtained from Thermo Fisher Scientific (Waltham, MA, USA). U0126 was obtained from Enzo Life Sciences (Farmingdale, NY, USA). Poly-L-ornithine, 2-mercaptoethanol (2-ME), and carbonylcyanide *m*-chlorophenylhydrazone (CCCP) were obtained from Sigma-Aldrich (St. Louis, MO, USA). All other reagents were of analytical grade and obtained from commercial sources.

Cell culture. Human iPSC line 253G1 (Riken BRC Cell Bank, Tsukuba, Ibaraki, Japan) was established through retroviral transduction of *OCT4*, *SOX2*, and *KLF4* into adult human dermal fibroblasts[45]. The cells were cultured under feeder-free conditions using human embryonic stem cell (ESC)-qualified Matrigel (BD Biosciences, San Jose, CA, USA) and TeSR-E8 medium (Stemcell Technologies, Vancouver, BC, Canada) at 37 °C in an atmosphere containing 5% CO_2. For passage, iPSC colonies were dissociated into single cells using Accumax (Innovative Cell Technologies, San Diego, CA, USA) and cultured in TeSR-E8 medium supplemented with Y-27632 (ROCK inhibitor, 10 μM). The NPCs derived from iPSCs were cultured on poly-L-ornithine and Laminin (Thermo Fisher Scientific) coated dishes at 37 °C in an atmosphere containing 5% CO_2. The culture

medium was Neural maintenance medium [NMM; a 1 : 1 mixture of DMEM/F12 (Thermo Fisher Scientific) and Neurobasal (Thermo Fisher Scientific) containing N2 (Thermo Fisher Scientific), B27 (Thermo Fisher Scientific), GlutaMAX (Thermo Fisher Scientific), non-essential amino acids (NEAA; Thermo Fisher Scientific), 2-ME, PS]. For passage, NPCs were dissociated into single cells using Accumax and cultured in NMM supplemented with EGF (20 ng/ml), FGF2 (20 ng/ml) and Y-27632.

Neural differentiation procedure. For the induction of neuronal lineages, dual SMAD inhibition protocol was used as previously described[21] with modifications. Briefly, iPSC colonies were dissociated into single cells with Accumax. The cells were seeded at a density of 7×10^4 cells/cm^2 in TeSR-E8 medium on Matrigel-coated plates in order to reach nearly confluent within two days after seeding. The initial differentiation medium was knockout serum replacement (KSR) medium [Knockout DMEM (Thermo Fisher Scientific) containing KSR (Thermo Fisher Scientific), L-glutamine, NEAA, 2-ME, PS] with SB431542 (TGFβ inhibitor, 10 μM) and LDN193189 (BMP inhibitor, 1 μg/ml). After 4 days, N2 medium [Neurobasal containing N2, B27, GlutaMAX, PS] was added to the KSR medium with LDN193189 every two days.

Measurement of intracellular ATP levels. Intracellular ATP content was measured using an ATP Determination Kit (Thermo Fisher Scientific), according to the manufacturer's protocol. Briefly, the cells were washed and lysed with 0.1% Triton X-100/PBS. The resulting cell lysates were added to a reaction mixture containing 0.5 mM D-luciferin, 1 mM DTT, and 1.25 μg/mL luciferase and incubated for 30 min at room temperature. Luminescence was measured using a Fluoroskan Ascent FL microplate reader (Thermo Fisher Scientific). The luminescence intensities were normalized to the total protein content.

Measurement of MMP. A Cell Meter JC-10 Mitochondrial Membrane Potential Assay Kit (AAT Bioquest, Sunnyvale, CA, USA) was used to detect MMP. Briefly, the cells were suspended in staining buffer containing JC-10 and incubated for 20 min at room temperature. After the cells were treated with CPF, a FACS Aria II cell sorter (BD Biosciences) was used to measure the fluorescence intensity ratio, JC-aggregate (F-590)/JC-monomer (F-535).

Assessment of mitochondrial fusion. After treatment with CPF (30 μM, 72 h), the cells were fixed with 4% paraformaldehyde and stained with 50 nM MitoTracker Red CMXRos (Cell Signaling Technology, Danvers, MA, USA) and 5 μg/mL Hoechst 33342 (Sigma-Aldrich). Changes in mitochondrial morphology were observed using a confocal laser microscope (Nikon A1). Images ($n = 5$) of random fields were taken, and the number of cells displaying mitochondrial fusion (<10% punctiform) was determined in each image, as previously reported[46].

Real-time polymerase chain reaction (PCR). Total RNA was isolated from iPSCs using TRIzol reagent (Thermo Fisher Scientific), and quantitative real-time reverse transcription (RT)-PCR was performed using a QuantiTect SYBR Green RT-PCR Kit (Qiagen, Valencia, CA, USA) on an ABI PRISM 7900HT sequence detection system (Applied Biosystems, Foster City, CA, USA) as previously reported[47]. Relative changes in transcript levels were normalized to the mRNA levels of glyceraldehyde-3-phosphate dehydrogenase (*GAPDH*). The following primer sequences were used for real-time PCR analysis: *Fis1*, forward, 5′-TACGTCCGCGGGTTGCT-3′ and reverse, 5′-CCAGTTCCTTGGCCTGGTT-3′; *Drp1*, forward, 5′-TGGGCGCCGACATCA-3′ and reverse, 5′-GCTCTGCGTTCCCACTACGA-3′; *Mfn1*, forward, 5′-GGCATCTGTGGCCGAGTT-3′ and reverse, 5′-ATTATGCTAAGTCTCCGCTCCAA-3′; *Mfn2*, forward, 5′-GCTCGGAGGCACATGAAAGT-3′ and reverse, 5′-ATCACGGTGCTCTTCCCATT-3′; *Opa1*, forward, 5′-GTGCTGCCCGCCTAGAAA-3′ and reverse, 5′-TGACAGGCACCCGTACTCAGT-3′; *PAX6*, forward, 5′-ATGTGTGAGTAAAATTCTGGGCA-3′ and reverse, 5′-GCTTACAACTTCTGGAGTCGCTA-3′; *FOXG1*, forward, 5′-GCCACAATCTGTCCCTCAACA-3′ and reverse, 5′-GACGGGTCCAGCATCCAGTA-3′; *NCAM1*, forward, 5′-GGCATTTACAAGTGTGTGGTTAC-3′ and reverse, 5′-TTGGCGCATTCTTGAACATGA-3′; *GAPDH*, forward, 5′-GTCTCCTCTGACTTCAACAGCG-3′ and reverse, 5′-ACCACCCTGTTGCTGTAGCCAA-3′.

Western blot analysis. Western blot analysis was performed as previously reported[48]. Briefly, the cells were lysed with Cell Lysis Buffer (Cell Signaling Technology). The proteins were then separated by sodium dodecyl sulfate-polyacrylamide gel electrophoresis (SDS-PAGE) and electrophoretically transferred to Immobilon-P membranes (Millipore, Billerica, MA, USA). The membranes were probed with anti-Drp1 monoclonal antibodies (1:1000; Cell Signaling Technology), anti-Fis1 polyclonal antibodies (1:200; Santa Cruz Biotechnology, Santa Cruz, CA, USA), anti-Mfn1 polyclonal antibodies (1:1000; Cell Signaling Technology), anti-Mfn2 monoclonal antibodies (1:1000; Cell Signaling Technology), anti-Opa1 monoclonal antibodies (1:1000; BD Biosciences), anti-ERK1/2 polyclonal antibodies (1:1000; Cell Signaling Technology), anti-phospho ERK1/2 (Thr202/Tyr204) monoclonal antibodies (1:2000; BD Biosciences), and anti-β-actin monoclonal antibodies (1:5000; Sigma-Aldrich). The membranes were then incubated with secondary antibodies against rabbit or mouse IgG conjugated to horseradish peroxidase (Cell Signaling Technology). The bands were visualized using an ECL Western Blotting Analysis System (GE Healthcare, Buckinghamshire, UK). Images were acquired using an LAS-3000 Imager (FUJIFILM, Tokyo, Japan).

Gene knockdown by shRNA. Knockdown experiments were performed using *Mfn1* shRNA lentiviruses from Sigma-Aldrich (MISSION shRNA), as previously reported[49]. A scrambled hairpin sequence was used as a negative control. Briefly, the cells were infected with the viruses at a multiplicity of infection of 1 in the presence

of 8 μg/mL hexadimethrine bromide (Sigma-Aldrich) for 24 h. After medium exchange, the cells were subjected to selection with 1 μg/mL puromycin for 24 h and cultured for an additional 72 h prior to functional analyses.

Statistical analysis. All data are presented as means ± standard deviation (SD). Analysis of variance (ANOVA) followed by post-hoc Bonferroni test was used to analyze data in Figs 1, 3C, 4, 5, and 6. Student's t test was used to analyze data in Figs 2, 3A, S1, and S2. *P*-values < 0.05 were considered statistically significant.

References

1. Landrigan, P. J., Lambertini, L. & Birnbaum, L. S. A research strategy to discover the environmental causes of autism and neurodevelopmental disabilities. *Environ. Health Perspect.* **120,** a258–a260 (2012).
2. Ross, E. J., Graham, D. L., Money, K. M. & Stanwood, G. D. Developmental consequences of fetal exposure to drugs: what we know and what we still must learn. *Neuropsychopharmacology* **40,** 61–87 (2015).
3. Rodier, P. M. Developing brain as a target of toxicity. *Environ. Health Perspect.* **103,** 73–76 (1995).
4. Rice, D. & Barone, S. Jr. Critical periods of vulnerability for the developing nervous system: evidence from humans and animal models. *Environ. Health* Perspect.**108,** 511–533 (2000).
5. Brown, M. A. & Brix, K. A. Review of health consequences from high-, intermediate- and low-level exposure to organophosphorus nerve agents. *J. Appl. Toxicol.* **18,** 393–408 (1998).
6. Ray, D. E. & Richards, P. G. The potential for toxic effects of chronic, low-dose exposure to organophosphates. *Toxicol. Lett.* **120,** 343–351 (2001).
7. Rauh, V. A. *et al.* Brain anomalies in children exposed prenatally to a common organophosphate pesticide. *Proc. Natl. Acad. Sci. USA* **109,** 7871–7876 (2012).
8. Slotkin, T. A., Levin, E. D. & Seidler, F. J. Comparative developmental neurotoxicity of organophosphate insecticides: effects on brain development are separable from systemic toxicity. *Environ. Health Perspect.* **114,** 746–751 (2006).
9. Ohishi, T. *et al.* Reversible effect of maternal exposure to chlorpyrifos on the intermediate granule cell progenitors in the hippocampal dentate gyrus of rat offspring. *Reprod. Toxicol.* **35,** 125–136 (2013).
10. Salama, M., El-Morsy, D., El-Gamal, M., Shabka, O. & Mohamed, W. M. Mitochondrial complex I inhibition as a possible mechanism of chlorpyrifos induced neurotoxicity. *Ann. Neurosci.* **21,** 85–89 (2014).
11. Lee, J. E., Park, J. H., Jang, S. J. & Koh, H. C. Rosiglitazone inhibits chlorpyrifos-induced apoptosis via modulation of the oxidative stress and inflammatory response in SH-SY5Y cells. *Toxicol. Appl. Pharmacol.* **278,** 159–171 (2014).
12. Lee, J. E., Lim, M. S., Park, J. H., Park, C. H. & Koh, H. C. Nuclear NF-κB contributes to chlorpyrifos-induced apoptosis through p53 signaling in human neural precursor cells. *Neurotoxicology* **42,** 58–70 (2014).
13. Huen, K. *et al.* Organophosphate pesticide levels in blood and urine of women and newborns living in an agricultural community. *Environ. Res.* **117,** 8–16 (2012).
14. Youle, R. J. & van der Bliek, A. M. Mitochondrial fission, fusion, and stress. *Science* **337,** 1062–1065 (2012).
15. van der Bliek, A. M., Shen, Q. & Kawajiri, S. Mechanisms of mitochondrial fission and fusion. *Cold Spring Harb. Perspect. Biol.* **5,** pii: a011072 (2013).
16. Cipolat, S., De Brito, O. M., B. Dal Zilio, B. & Scorrano, L. OPA1 requires mitofusin 1 to promote mitochondrial fusion. *Proc. Natl. Acad. Sci. USA* **101,** 15927–15932 (2004).
17. Koshiba, T. *et al.* Structural basis of mitochondrial tethering by mitofusin complexes. *Science* **305,** 858–862 (2004).
18. Smirnova, E., Griparic, L., Shurland, D.-L. & van der Bliek, A. M. Dynamin-related protein Drp1 is required for mitochondrial division in mammalian cells. *Mol. Biol. Cell* **12,** 2245–2256 (2001).
19. Yoon, Y., Krueger, E. W., Oswald, B. J. & McNiven, M. A. The mitochondrial protein hFis1 regulates mitochondrial fission in mammalian cells through an interaction with the dynamin-like protein DLP1. *Mol. Biol. Cell* **23,** 5409–5420 (2003).
20. Chen, H. *et al.* Mitofusins Mfn1 and Mfn2 coordinately regulate mitochondrial fusion and are essential for embryonic development. *J. Cell Biol.* **160,** 189–200 (2003).
21. Chambers, S. M. *et al.* Highly efficient neural conversion of human ES and iPS cells by dual inhibition of SMAD signaling. *Nat. Biotechnol.* **27,** 275–280 (2009).
22. Manuel, M. N., Mi, D., Mason, J. O. & Price, D. J. Regulation of cerebral cortical neurogenesis by the Pax6 transcription factor. *Front. Cell Neurosci.* **9,** 70 (2015).
23. Shen, L., Nam, H. S., Song, P., Moore, H. & Anderson, S. A. FoxG1 haploinsufficiency results in impaired neurogenesis in the postnatal hippocampus and contextual memory deficits. *Hippocampus* **16,** 875–890 (2006).
24. Polo-Parada, L., Bose, C. M., Plattner, F. & Landmesser, L. T. Distinct roles of different neural cell adhesion molecule (NCAM) isoforms in synaptic maturation revealed by analysis of NCAM 180 kDa isoform-deficient mice. *J. Neurosci.* **24,** 1852–1864 (2004).
25. Cheng, A., Hou, Y. & Mattson, M. P. Mitochondria and neuroplasticity. *ASN. Neuro.* **2,** e00045 (2010).
26. Tanaka, A. *et al.* Proteasome and p97 mediate mitophagy and degradation of mitofusins induced by Parkin. *J. Cell Biol.* **191,** 1367–1380 (2010).
27. Greber, B. *et al.* FGF signalling inhibits neural induction in human embryonic stem cells. *EMBO J.* **30,** 4874–4884 (2011).
28. Son, M. J. *et al.* Mitofusins deficiency elicits mitochondrial metabolic reprogramming to pluripotency. *Cell Death Differ.* **22,** 1957–1969 (2015).
29. Garcia, S. J., Seidler, F. J., Crumpton, T. L. & Slotkin, T. A. Does the developmental neurotoxicity of chlorpyrifos involve glial targets? Macromolecule synthesis, adenylyl cyclase signaling, nuclear transcription factors, and formation of reactive oxygen in C6 glioma cells. *Brain Res.* **891,** 54–68 (2001).
30. Basha, M. & Poojary, A. Cold stress offered modulation on chlorpyrifos toxicity in aging rat central nervous system. *Toxicol. Int.* **19,** 173–181 (2012).
31. Yamada, S. *et al.* Tributyltin induces mitochondrial fission through Mfn1 degradation in human induced pluripotent stem cells. *Toxicol. In Vitro.* **34,** 257–263 (2016).
32. Leboucher, G. P. *et al.* Stress-induced phosphorylation and proteasomal degradation of mitofusin 2 facilitates mitochondrial fragmentation and apoptosis. *Mol. Cell* **47,** 547–557 (2012).
33. Yue, W. *et al.* A small natural molecule promotes mitochondrial fusion through inhibition of the deubiquitinase USP30. *Cell Res.* **24,** 482–496 (2014).
34. Park, Y. Y., Nguyen, O. T., Kang, H. & Cho, H. MARCH5-mediated quality control on acetylated Mfn1 facilitates mitochondrial homeostasis and cell survival. *Cell Death Dis.* **5,** e1172 (2014).
35. Chen, K. H. *et al.* Dysregulation of HSG triggers vascular proliferative disorders. *Nat. Cell Biol.* **6,** 872–883 (2004).
36. Chen, K. H. *et al.* Role of mitofusin 2 (Mfn2) in controlling cellular proliferation. *FASEB J.* **28,** 382–394 (2014).
37. Yu, Z. P., Matsuoka, M., Wispriyono, B., Iryo, Y. & Igisu, H. Activation of mitogen-activated protein kinases by tributyltin in CCRF-CEM cells: role of intracellular Ca(2+). *Toxicol. Appl. Pharmacol.* **168,** 200–207 (2000).
38. Pizzo, P., Drago, I., Filadi, R. & Pozzan, T. Mitochondrial Ca^{2+} homeostasis: mechanism, role, and tissue specificities. *Pflugers Arch.* **464,** 3–17 (2012).

39. Danesin, C. & Houart, C. A. Fox stops the Wnt: implications for forebrain development and diseases. *Curr. Opin. Genet. Dev*. **22,** 323–330 (2012).
40. Georgala, P. A., Carr, C. B. & Price, D. J. The role of Pax6 in forebrain development. *Dev. Neurobiol.* **71,** 690–709 (2011).
41. Tuoc, T. C. *et al.* Selective cortical layering abnormalities and behavioral deficits in cortex-specific Pax6 knock-out mice. *J. Neurosci.* **29,** 8335–8349 (2009).
42. Tian, C. *et al.* Foxg1 has an essential role in postnatal development of the dentate gyrus. *J. Neurosci.* **32,** 2931–2949 (2012).
43. Chen, X. P., Chen, W. Z., Wang, F. S. & Liu, J. X. Selective cognitive impairments are related to selective hippocampus and prefrontal cortex deficits after prenatal chlorpyrifos exposure. *Brain Res.* **1474,** 19–28 (2012).
44. Li, K. *et al.* Differentiation of pluripotent stem cells for regenerative medicine. *Biochem. Biophys. Res. Commun.* **471,** 1–4 (2016).
45. Nakagawa, M. *et al.* Generation of induced pluripotent stem cells without Myc from mouse and human fibroblasts. *Nat. Biotechnol.* **26,** 101–106 (2008).
46. Fan, X., Hussien, R. & Brooks, G. A. H_2O_2-induced mitochondrial fragmentation in C2C12 myocytes. *Free Radic. Biol. Med.* **49,** 1646–1654 (2010).
47. Hirata, N. *et al.* Sphingosine-1-phosphate promotes expansion of cancer stem cells via S1PR3 by a ligand-independent Notch activation. *Nat. Commun.* **5,** 4806 (2014).
48. Kanda, Y. *et al.* Reactive oxygen species mediate adipocyte differentiation in mesenchymal stem cells. *Life Sci.* **89,** 250–258 (2011).
49. Yamada, S. *et al.* NAD-dependent isocitrate dehydrogenase as a novel target of tributyltin in human embryonic carcinoma cells. *Sci. Rep*. **4,** 5952 (2014).

Acknowledgements

This work was supported by a Health and Labour Sciences Research Grant from the Ministry of Health, Labour, and Welfare, Japan (#H25-Kagaku-Ippan-002 and #H28-Kagaku-Ippan-003 to Y.Ka.), a Grant-in-Aid for Scientific Research from the Ministry of Education, Culture, Sports, Science, and Technology, Japan (#26293056 and #26670041 to Y.Ka.), the Japan Agency for Medical Research and Development, AMED (#15mk0104053h0101 and #16mk0104027j0002 to Y.S.), and a grant from the Smoking Research Foundation (Y.Ka.).

Author Contributions

Y.S. and Y.Ka. planned the project. S.Y. performed most of the experiments. S.Y. and Y.Ka. wrote the manuscript. Y.Ku. and D.Y. provided technical advices. All authors reviewed the manuscript.

Additional Information

Supplementary information accompanies this paper at http://www.nature.com/srep

Competing financial interests: The authors declare no competing financial interests.

How to cite this article: Yamada, S. *et al.* Chlorpyrifos inhibits neural induction via Mfn1-mediated mitochondrial dysfunction in human induced pluripotent stem cells. *Sci. Rep.* **7**, 40925; doi: 10.1038/srep40925 (2017).

Publisher's note: Springer Nature remains neutral with regard to jurisdictional claims in published maps and institutional affiliations.

Toxicology in Vitro 34 (2016) 257–263

Contents lists available at ScienceDirect

Toxicology in Vitro

journal homepage: www.elsevier.com/locate/toxinvit

Tributyltin induces mitochondrial fission through Mfn1 degradation in human induced pluripotent stem cells

Shigeru Yamada [a], Miki Asanagi [a,b], Naoya Hirata [a], Hiroshi Itagaki [b], Yuko Sekino [a], Yasunari Kanda [a,*]

[a] Division of Pharmacology, National Institute of Health Sciences, Japan
[b] Faculty of Engineering, Department of Materials Science and Engineering, Yokohama National University, Japan

ARTICLE INFO

Article history:
Received 31 October 2015
Received in revised form 2 March 2016
Accepted 24 April 2016
Available online 29 April 2016

Keywords:
Induced pluripotent stem cells
Mitochondrial fission
Mitofusin
Tributyltin

ABSTRACT

Organotin compounds, such as tributyltin (TBT), are well-known endocrine disruptors. TBT is also known to cause various forms of cytotoxicity, including neurotoxicity and immunotoxicity. However, TBT toxicity has not been identified in normal stem cells. In the present study, we examined the effects of TBT on cell growth in human induced pluripotent stem cells (iPSCs). We found that exposure to nanomolar concentrations of TBT decreased intracellular ATP levels and inhibited cell viability in iPSCs. Because TBT suppressed energy production, which is a critical function of the mitochondria, we further assessed the effects of TBT on mitochondrial dynamics. Staining with MitoTracker revealed that nanomolar concentrations of TBT induced mitochondrial fragmentation. TBT also reduced the expression of mitochondrial fusion protein mitofusin 1 (Mfn1), and this effect was abolished by knockdown of the E3 ubiquitin ligase membrane-associated RING-CH 5 (MARCH5), suggesting that nanomolar concentrations of TBT could induce mitochondrial dysfunction via MARCH5-mediated Mfn1 degradation in iPSCs. Thus, mitochondrial function in normal stem cells could be used to assess cytotoxicity associated with metal exposure.

1. Introduction

Human induced pluripotent stem cells (iPSCs), which possess self-renewal and multipotent differentiation properties, are expected to have applications in drug discovery and drug safety assessment (Nakamura et al., 2014; Takahashi et al., 2007). Growing evidence suggests that iPSCs can also provide a unique platform for assessing chemical-induced toxicities in various tissues, such as the brain (He et al., 2012; Kumar et al., 2015). Thus, it is necessary to elucidate the mechanisms mediating the cytotoxic effects of different chemicals during embryonic development in stem cells.

Organotin compounds, such as tributyltin (TBT), are also associated with various developmental, neurological, immunological, and metabolic effects (Kotake, 2012). Although the use of TBT has already been restricted, butyltin compounds, including TBT, have been reported to be still present at concentrations between 50 and 400 nM in human blood (Whalen et al., 1999). Therefore, the mechanisms through which nanomolar concentrations of TBT cause cytotoxicity should be elucidated using undifferentiated normal stem cells, which is the most suitable platform for toxicological analysis.

Several studies have revealed the cytotoxic effects of nanomolar concentrations of TBT in stem cells. For example, nanomolar concentrations of TBT activate retinoid X receptor (RXR) and/or peroxisome proliferator-activated receptor γ (PPARγ), thereby enhancing adipocyte differentiation in adipose-derived stromal stem cells (ADSCs) (Kirchner et al., 2010). In rat mesencephalic neural stem cells, transcriptome analysis after induction of TBT-dependent apoptosis revealed changes in the expression levels of genes involved in Ca^{2+} mobilization, retinoic acid signaling, and apoptosis (Suzuki and Ishido, 2011). We previously reported that nanomolar concentrations of TBT mediate mitochondrial dysfunction and inhibit the growth of human embryonic carcinoma NT2/D1 cells (Yamada et al., 2015). Thus, we hypothesized that nanomolar concentrations of TBT could also affect mitochondria in human iPSCs.

Mitochondria exhibit continuous changes in morphology through fusion and fission (van der Bliek et al., 2013; Youle and van der Bliek, 2012). Under normal circumstances, mitochondria fuse together, forming excessive tubular networks (mitochondrial fusion). In contrast, under stress conditions, mitochondrial networks convert into large numbers of small fragments with punctate morphology (mitochondrial fission). These mitochondrial dynamics play a key role in the maintenance of mitochondrial functions, such as ATP production. Mitochondrial morphology is strictly regulated by fission (fission protein 1 [Fis1] and dynamin-related protein 1 [Drp1]) and fusion (mitofusin 1 and 2 [Mfn1, Mfn2] and optic atrophy 1 [Opa1]) factors (Fischer et al., 2012). Several reports have described mitochondrial fragmentation induced by chemical exposure. For example, CGP37157, an inhibitor of mitochondrial calcium efflux, mediates mitochondrial fission through Mfn1 degradation via the E3 ubiquitin ligase membrane-associated RING-CH 5

* Corresponding author at: 1-18-1, Kamiyoga, Setagaya-ku, 158-8501, Japan.
E-mail address: kanda@nihs.go.jp (Y. Kanda).

http://dx.doi.org/10.1016/j.tiv.2016.04.013
0887-2333/

(MARCH5) in prostate cancer cells (Choudhary et al., 2014). Another study showed that doxorubicin induces proteasomal degradation of Mfn2, which facilitates mitochondrial fragmentation and apoptosis in sarcoma U2OS cells (Leboucher et al., 2012).

In the present study, we investigated the cytotoxic effects of nanomolar concentrations of TBT in iPSCs. Our results showed that exposure to 50 nM TBT decreased intracellular ATP levels and inhibited cell growth. Moreover, TBT exposure induced Mfn1 degradation and mitochondrial fragmentation through a MARCH5-dependent mechanism. Thus, nanomolar concentrations of TBT induce toxicity through impairment of mitochondrial quality control in human iPSCs.

2. Materials and methods

2.1. Chemicals and reagents

TBT was obtained from Tokyo Chemical Industry (Tokyo, Japan). Tin acetate (TA), rosiglitazone (RGZ), and carbonyl cyanide m-chlorophenyl hydrazone (CCCP) were obtained from Sigma-Aldrich (St. Louis, MO, USA). All other reagents were of analytical grade and were obtained from commercial sources.

2.2. Cell culture

We used the human iPSC line 253G1 (Riken BRC Cell Bank, Tsukuba, Ibaraki, Japan), which was established through retroviral transduction of Oct3/4, Sox2, and Klf4 into adult human dermal fibroblasts (Nakagawa et al., 2008). The cells were cultured under feederless conditions using human embryonic stem cell (ESC)-qualified Matrigel (BD Biosciences, San Jose, CA, USA) and TeSR-E8 medium (Stemcell Technologies, Vancouver, BC, Canada) at 37 °C in an atmosphere containing 5% CO_2. For passage, iPSC colonies were dissociated into single cells using Accumax (Innovative Cell Technologies, San Diego, CA, USA) and cultured in a TeSR-E8 medium supplemented with the Rho-kinase (ROCK) inhibitor Y-27632 (Wako, Tokyo, Japan).

2.3. Cell proliferation assay

Cell viability was measured using CellTiter 96 AQueous One Solution Cell Proliferation Assays (Promega, Madison, WI, USA), according to the manufacturer's instructions. Briefly, iPSCs were seeded into 96-well plates and exposed to different concentrations of TBT. After exposure to TBT, One Solution Reagent was added to each well, and the plate was incubated at 37 °C for another 2 h. Absorbance was measured at 490 nm using an iMark microplate reader (Bio-Rad, Hercules, CA, USA).

2.4. Measurement of intracellular ATP levels

The intracellular ATP content was measured using an ATP Determination Kit (Life Technologies, Carlsbad, CA, USA), according to the manufacturer's protocol. Briefly, the cells were washed and lysed with 0.1% Triton X-100/PBS. The resulting cell lysates were added to a reaction mixture containing 0.5 mM D-luciferin, 1 mM DTT, and 1.25 μg/mL luciferase and incubated for 30 min at room temperature. Luminescence was measured using a Fluoroskan Ascent FL microplate reader (Thermo Fisher Scientific, Waltham, MA, USA). The luminescence intensities were normalized to the total protein content.

2.5. Measurement of mitochondrial membrane potential (MMP)

A Cell Meter JC-10 Mitochondrial Membrane Potential Assay Kit (AAT Bioquest, Sunnyvale, CA, USA) was used to detect MMP. Briefly, the cells were suspended in a staining buffer containing JC-10 and incubated for 20 min at room temperature. After treatment of the cells with chemicals, a FACS Aria II cell sorter (BD Biosciences) was used to measure the fluorescence intensity ratio, that is, JC-aggregate (F-590)/JC-monomer (F-535).

2.6. Assessment of mitochondrial fusion

After the cells were treated with TBT (50 nM, 72 h), they were fixed with 4% paraformaldehyde and stained with 50 nM MitoTracker Red CMXRos (Cell Signaling Technology, Danvers, MA, USA) and 5 μg/mL Hoechst 33342 (Sigma-Aldrich). Changes in mitochondrial morphology were observed using a confocal laser microscope (Nikon A1). Images ($n = 5$) were taken of random fields, and the number of cells displaying mitochondrial fusion (<10% punctiform) was counted in each image, as previously reported (Fan et al., 2010).

2.7. Real-time polymerase chain reaction (PCR)

Total RNA was isolated from iPSCs using TRIzol reagent (Life Technologies), and quantitative real-time reverse transcription (RT)-PCR was performed using a QuantiTect SYBR Green RT-PCR Kit (Qiagen, Valencia, CA, USA) on an ABI PRISM 7900HT sequence detection system (Applied Biosystems, Foster City, CA, USA) as previously reported (Hirata et al., 2014). Relative changes in transcript levels were normalized to the mRNA levels of glyceraldehyde-3-phosphate dehydrogenase (*GAPDH*). The following primer sequences were used for real-time PCR analysis: *Nanog*, forward, 5′-CAGAAGGCCTCAGCACCTAC-3′ and reverse, 5′-ATTGTTCCAGGTCTGGTTGC-3′; *Oct3/4*, forward, 5′-ACATCAAAGCTC TGCAGAAAGAA-3′ and reverse, 5′-CCAGTTCCTTGGCCTGGTT-3′; *Drp1*, forward, 5′-TGGGCGCCGACATCA-3′ and reverse, 5′-GCTCTGCGTTCCCA CTACGA-3′; *Fis1*, forward, 5′-TACGTCCGCGGGTTGCT-3′ and reverse, 5′-CCAGTTCCTTGGCCTGGTT-3′; *Mfn1*, forward, 5′-GGCATCTGTGGCCG AGTT-3′ and reverse, 5′-ATTATGCTAAGTCTCCGCTCCAA-3′; *Mfn2*, forward, 5′-GCTCGGAGGCACATGAAAGT-3′ and reverse, 5′-ATCACGGTGC TCTTCCCATT-3′; *Opa1*, forward, 5′-GTGCTGCCCGCCTAGAAA-3′ and reverse, 5′-TGACAGGCACCCGTACTCAGT-3′; *GAPDH*, forward, 5′-GTCTCC TCTGACTTCAACAGCG-3′ and reverse, 5′-ACCACCCTGTTGCTGTAGCC AA-3′.

2.8. Western blot analysis

Western blot analysis was performed as previously reported (Kanda et al., 2011). Briefly, the cells were lysed with a Cell Lysis Buffer (Cell Signaling Technology). The proteins were then separated by sodium dodecyl sulfate-polyacrylamide gel electrophoresis (SDS-PAGE) and electrophoretically transferred to Immobilon-P membranes (Millipore, Billerica, MA, USA). The membranes were probed with anti-Drp1 monoclonal antibodies (1:1000; Cell Signaling Technology), anti-Fis1 polyclonal antibodies (1:200; Santa Cruz Biotechnology, Santa Cruz, CA, USA), anti-Mfn1 polyclonal antibodies (1:1000; Cell Signaling Technology), anti-Mfn2 monoclonal antibodies (1:1000; Cell Signaling Technology), anti-Opa1 monoclonal antibodies (1:1000; BD Biosciences), and anti-β-actin monoclonal antibodies (1:5000; Sigma-Aldrich). The membranes were then incubated with secondary antibodies against rabbit or mouse IgG conjugated to horseradish peroxidase (Cell Signaling Technology). The bands were visualized using an ECL Western Blotting Analysis System (GE Healthcare, Buckinghamshire, UK), and images were acquired using an LAS-3000 Imager (Fujifilm, Tokyo, Japan).

2.9. Gene knockdown by shRNA

Knockdown experiments were performed using Mfn1 shRNA lentiviruses from Sigma-Aldrich (MISSION shRNA), as previously reported (Yamada et al., 2014). A scrambled hairpin sequence was used as a negative control. Briefly, the cells were infected with the viruses at a multiplicity of infection of 1 in the presence of 8 mg/mL hexadimethrine bromide (Sigma-Aldrich) for 24 h. The cells were then subjected to

selection with 1 μg/mL puromycin for 24 h and cultured for an additional 72 h prior to functional analyses.

2.10. Gene knockdown by siRNA

Double-stranded RNA oligonucleotides (siRNAs) against MARCH5 and appropriate control scrambled siRNA were purchased from Life Technologies. The siRNAs were transfected into iPSCs using DharmaFECT1 (Dharmacon, Lafayette, CO, USA) as previously described (Kinehara et al., 2013).

2.11. Statistical analysis

All data were presented as means ± standard deviations (SDs). Analysis of variance (ANOVA) followed by post-hoc Tukey test was used to analyze data involving more than two samples. For comparisons between two samples, Student's *t*-tests were used. Differences with *P*-values of less than 0.05 were considered statistically significant.

3. Results

3.1. Cytotoxic effects of TBT in iPSCs

To examine whether TBT was cytotoxic in iPSCs, we studied the effects of TBT on cell proliferation in iPSCs. Treatment with TBT reduced cell viability in a dose-dependent manner (Fig. 1A and B). The LC_{50} for TBT was 77 nM in iPSCs. Moreover, almost all cells were detached from the culture dish at more than 200 nM TBT. In contrast, exposure to TA, which is less toxic, had little effect at any concentration tested (Fig. 1A and B). We next examined whether TBT affected pluripotency. The expression levels of the undifferentiated markers Nanog and Oct3/4 were not changed by TBT (Fig. 1C). Because cell growth requires ATP as a source of energy in iPSCs, we examined intracellular ATP content in the cells. We found that treatment with 50 nM TBT reduced the ATP content of the cells (Fig. 1D). We confirmed that 0.1 μM CCCP, which functions as a mitochondrial uncoupler, also decreased ATP levels. In contrast, TA had little effect. These data suggest that exposure to 50 nM TBT reduces cell growth without inhibiting iPSC pluripotency.

3.2. Effects of TBT on mitochondrial function in iPSCs

Because TBT inhibited ATP production, we investigated MMP, as an important parameter of mitochondrial function, during TBT treatment in iPSCs. MMP was decreased by 50 nM TBT for 1 h (Fig. 2A). In contrast, TA had little effect on MMP. We further examined the generation of reactive oxygen species (ROS), which affect MMP and are related to mitochondrion-mediated cell damage (Park et al., 2005), using 2′,7′-dichlorodihydrofluorescein (DCFH). TBT at 50 nM did not affect the ROS level (Fig. S1). In contrast, hydrogen peroxide (H_2O_2) as a positive control promoted the generation of ROS, which was attenuated by *N*-acetylcysteine treatment. Because morphological changes in mitochondria are closely related to energy supply and MMP maintenance (Youle and van der Bliek, 2012), we focused on mitochondrial dynamics in iPSCs. After TBT exposure, we observed fragmented mitochondria with punctate morphology (Fig. 2B). Furthermore, TBT significantly decreased the number of cells exhibiting mitochondrial fusion (Fig. 2C). As expected, fragmented mitochondria were also observed following CCCP treatment (Fig. S2). In contrast, TA exposure did not affect mitochondrial morphology. Taken together, these results suggest that nanomolar concentrations of TBT induce mitochondrial dysfunction, such as MMP depolarization and mitochondrial fragmentation, in iPSCs.

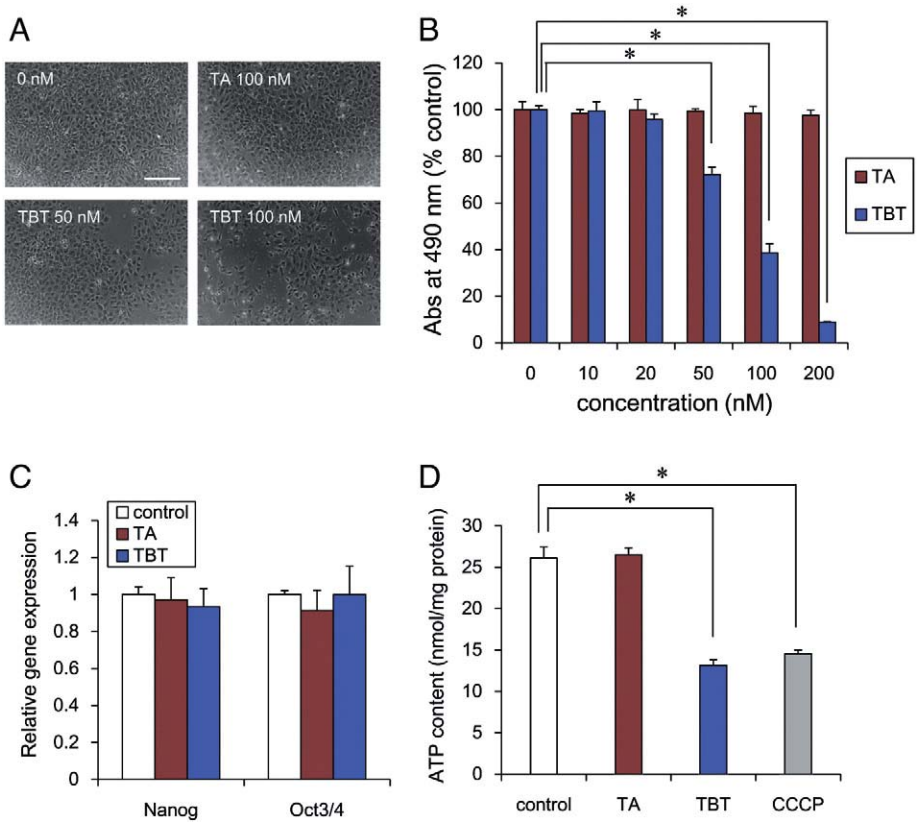

Fig. 1. TBT induces cytotoxic effects in iPSCs. (A) Cells were seeded in 96-well plates and exposed to different concentrations of TBT for 72 h. Phase-contrast photomicrographs of iPSCs were captured after exposure to TBT or TA at 0, 50, and 100 nM. Bar = 100 μm. (B) Cell viability in the presence of TBT or TA was examined using CellTiter 96 AQueous One Solution Cell Proliferation Assays. (C) After exposure to 50 nM TBT or TA for 72 h, the expression of undifferentiated marker genes (*Nanog* and *Oct3/4*) was analyzed by real-time PCR. (D) The intracellular ATP content was determined in the lysed cells. Data represent the mean ± SD (n = 3). *$P < 0.05$ using ANOVA with post-hoc Tukey test.

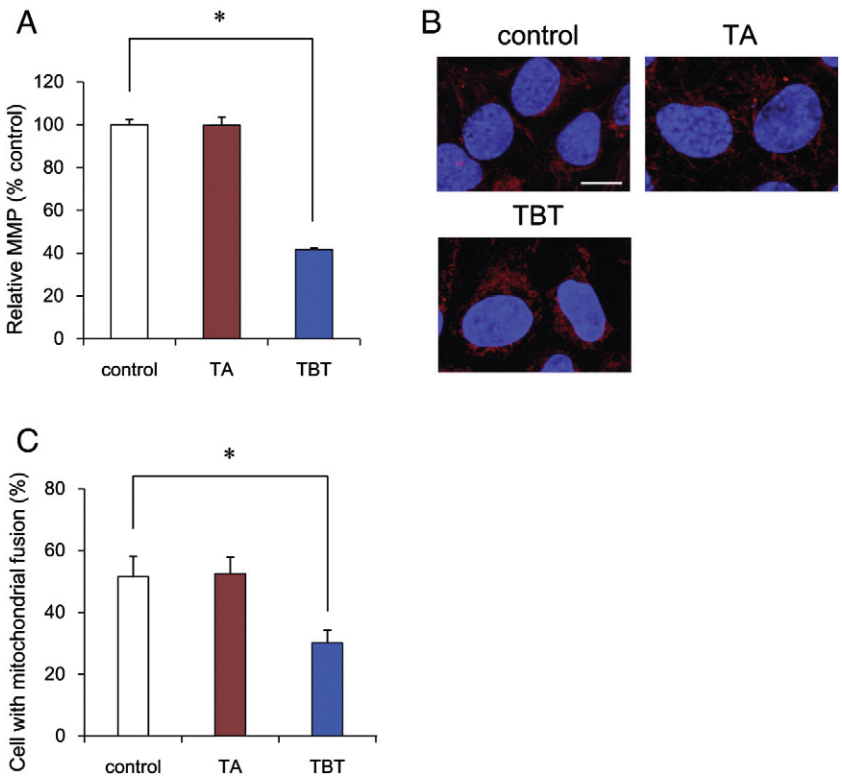

Fig. 2. TBT affects several mitochondrial functions in iPSCs. (A) Cells were stained with JC-10 for 20 min and exposed to 50 nM TBT or TA for an additional 1 h. The MMP of JC-10-labeled cells was analyzed by flow cytometry. (B) Cells were exposed to 50 nM TBT or TA for 72 h and then stained with MitoTracker Red CMXRos and Hoechst 33342. Mitochondrial morphology was observed by confocal laser microscopy. Bar = 10 μm. (C) The number of cells with mitochondrial fusion (<10% punctiform) was counted in each image. Data represent the mean ± SD (n = 5). *$P < 0.05$ using ANOVA with post-hoc Tukey test.

3.3. TBT exposure induced mitochondrial fission via the reduction of Mfn1 protein in iPSCs

To examine the molecular mechanisms through which TBT induces mitochondrial fragmentation, we assessed the effects of TBT on the expression of mitochondrial fission (*Fis1* and *Drp1*) and fusion genes (*Mfn1*, *Mfn2*, and *OPA1*). Real-time PCR analysis showed that the expression of each gene was not altered by TBT exposure (Fig. 3A). Interestingly, western blot analysis revealed that TBT significantly decreased only Mfn1 protein levels. In contrast, the expression levels of other factors, including Mfn2, were not changed (Fig. 3B and C). To confirm the involvement of Mfn1 in the fragmentation of mitochondria, we performed knockdown (KD) of *Mfn1* using lentivirus-delivered shRNAs. Real-time PCR analysis showed that the KD efficiency was approximately 60% (Fig. 3D), which was similar to that reported in previous KD studies (Son et al., 2015). Similar to TBT exposure, Mfn1 KD induced mitochondrial fragmentation (Fig. 3E and F). These data suggest that TBT-induced mitochondrial fragmentation is caused by reduction of Mfn1 protein levels.

3.4. MARCH5 KD abolished TBT-induced Mfn1 reduction in iPSCs

To investigate whether Mfn1 reduction triggered by TBT occurred through an E3 ubiquitin ligase-dependent mechanism, we performed KD of MARCH5 by siRNA. Real-time PCR analysis showed that the KD efficiency of MARCH5 was approximately 70% (Fig. 4A). Western blot analysis revealed that MARCH5 KD increased basal Mfn1 levels and further abolished TBT-induced Mfn1 reduction (Fig. 4B and C). In contrast, Mfn2 protein levels were not recovered by MARCH5 KD. Because the gene expression of Mfn1 was not affected by TBT exposure, Mfn1 reduction was thought to be caused by MARCH5-mediated degradation, independent of gene downregulation. Taken together, these data suggest that MARCH5 mediates TBT-induced Mfn1 degradation in iPSCs.

4. Discussion

In the present study, we demonstrated that nanomolar concentrations of TBT targeted mitochondrial quality control in human iPSCs. We showed that exposure to nanomolar concentrations of TBT induced Mfn1 degradation through the E3 ubiquitin ligase MARCH5, thereby promoting mitochondrial fragmentation. These negative effects of TBT on mitochondrial quality control could inhibit ATP production and cell growth.

Our results showed that treatment with more than 200 nM TBT caused almost complete detachment of human iPSCs from the culture dish (Fig. 1). Previous studies have shown that micromolar concentrations of TBT induce apoptosis in various cell types, such as human amnion cells (Zhu et al., 2007), hepatocytes (Grondin et al., 2007), and neutrophils (Lavastre and Girard, 2002). Compared to somatic cells, immature cells tend to be highly sensitive to TBT exposure. Therefore, analysis of TBT sensitivity using iPSCs, iPSC-neural progenitor cells, and iPSC-neurons might provide interesting insights into the mechanisms of TBT toxicity. Previous reports have shown that iPSC-derived cells are immature compared with human naïve neural cells and do not form neural networks (Belinsky et al., 2011). Therefore, further studies are required to elucidate the mechanisms of TBT neurotoxicity using iPSCs and to optimize the types of iPSC-derived cells.

We also showed that the stemness properties of iPSCs were maintained after TBT exposure, whereas cell growth was reduced (Fig. 1). Mitochondria have been reported to be in a morphologically and functionally immature state in iPSCs, with poorly developed cristae and more fragmented structures than those observed in somatic cells (Wanet et al., 2015). Mfn1 and Mfn2 have been shown to constitute a new barrier to reprogramming because Mfn1/2 ablation facilitates the

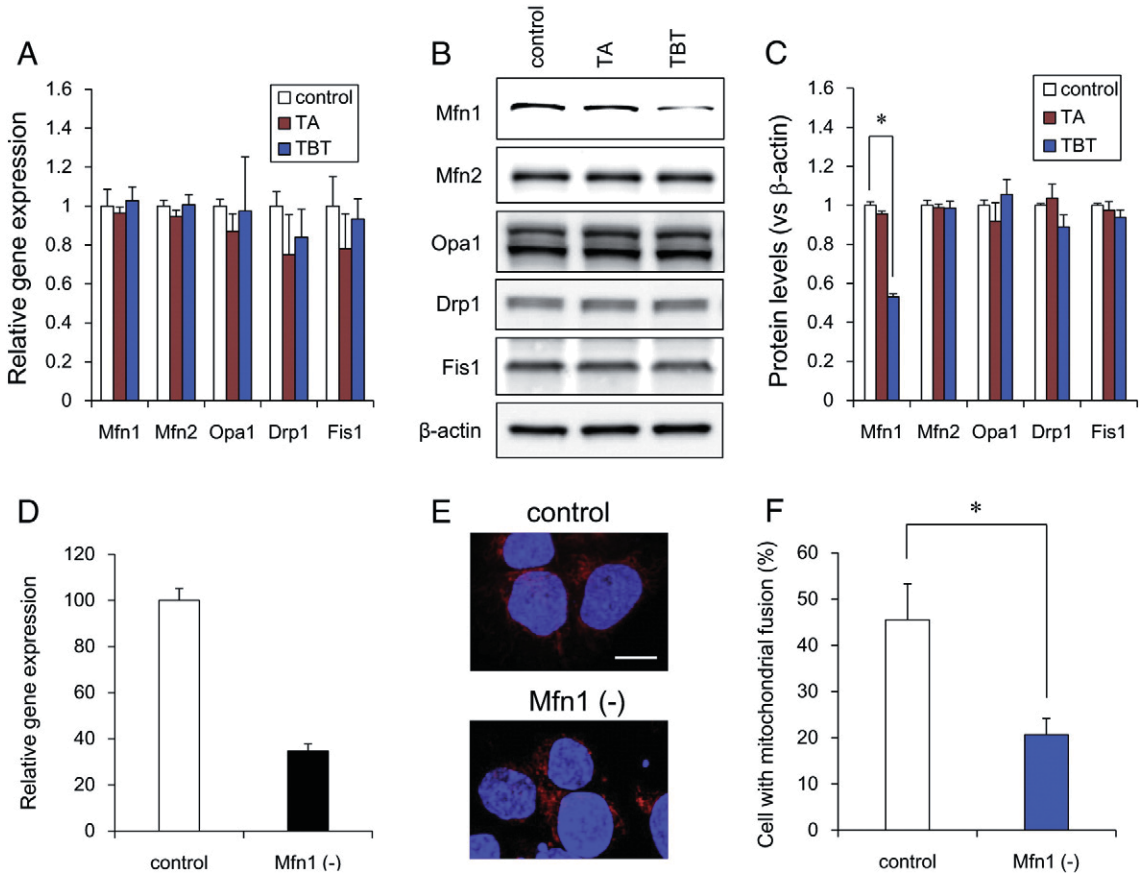

Fig. 3. TBT induces mitochondrial fission via decreased Mfn1 protein levels in iPSCs. (A) After exposure to 50 nM TBT or TA for 72 h, the expression of mitochondrial genes was analyzed by real-time PCR. (B) After exposure to 50 nM TBT or TA for 72 h, the expression of mitochondrial proteins was analyzed by western blotting using anti-Drp1, anti-Fis1, anti-Mfn1, anti-Mfn2, anti-Opa1, or anti-β-actin antibodies. (C) The relative densities of bands were quantified with ImageJ software. Relative changes in expression were determined by normalization to β-actin. (D) After introduction of lentivirus-delivered shRNAs against *Mfn1* to the cells, the expression of *Mfn1* was analyzed by real-time PCR. (E) Mfn1-KD cells were stained with MitoTracker Red CMXRos and Hoechst 33342. Mitochondrial morphology was observed by confocal laser microscopy. Bar = 10 μm. (F) The number of cells with mitochondrial fusion (<10% punctiform) was counted in each image. Data represent the mean ± SD (n = 5). *$P < 0.05$ using ANOVA with post-hoc Tukey test.

induction of pluripotency through the restructuring of mitochondrial dynamics and bioenergetics (Son et al., 2015). Moreover, MARCH5 has been shown to be involved in maintaining the pluripotency of mouse embryonic stem cells through protein kinase A (PKA)-extracellular signal-regulated kinase (ERK) signaling (Gu et al., 2015). Thus, MARCH5-Mfn1 might be involved in maintenance of embryonic stemness through mitochondrial fragmentation in iPSCs. Previous study has reported that Mfn1 knockout results in embryonic lethality of homozygous mutants (Chen et al., 2003). Moreover, Mfn1-deficient embryonic cells have dramatically fragmented mitochondria. Taken together, these data indicate that Mfn1-mediated mitochondrial dynamics might regulate embryonic development. Further studies are needed to determine whether MARCH5-mediated Mfn1 degradation plays a role in the maintenance of stemness properties.

Our data suggest that nanomolar concentrations of TBT could induce mitochondrial fission through MARCH5-mediated Mfn1 degradation (Figs. 2–4). Consistent with our data, chemical stressors have been reported to cause mitochondrial fission through proteasomal degradation of Mfn1 and/or Mfn2 (Choudhary et al., 2014; Leboucher et al., 2012). In addition, Mfn1 or Mfn2 deficiency in cells is known to result in severe cellular defects, including decreased ATP content and poor cell growth (Chen et al., 2005; Yue et al., 2014). Our Mfn1 KD studies indicated that Mfn1 degradation was sufficient to promote mitochondrial dysfunction; therefore, TBT-induced Mfn1 degradation might mediate mitochondrial fragmentation, decrease ATP levels, and inhibit iPSC growth. Although Mfn2 is also involved in mitochondrial fission and energy supply (Chen et al., 2005; Leboucher et al., 2012; Yue et al., 2014), our results indicated that TBT specifically targeted Mfn1, not Mfn2. Regarding this apparent TBT specificity, MARCH5 has been reported to selectively degrade Mfn1 among all mitochondrial proteins, including Mfn2 (Park et al., 2014). This selectivity of MARCH5 toward Mfn1 was also confirmed by our recovery studies of TBT-induced Mfn1 degradation using MARCH5-KD cells. Thus, exposure to nanomolar concentrations of TBT might specifically target Mfn1 via MARCH5 in iPSCs. In future studies, it will be necessary to investigate the specific mechanisms underlying TBT-induced Mfn1 degradation via MARCH5, a process that results in mitochondrial fission and dysfunction.

Herein, we found that TBT targeted the mitochondrial energy supply in iPSCs. Although mitochondrial energy production is more efficient than glycolysis, embryonic cells such as iPSCs are known to rely mainly on glycolysis rather than the mitochondrial system for ATP production (Varum et al., 2011). We previously reported that nanomolar concentrations of TBT inhibit glucose uptake and cause growth arrest in human embryonic carcinoma NT2/D1 cells (Yamada et al., 2013). Further studies should determine whether glycolysis is also targeted by TBT in iPSCs.

In summary, our results demonstrated a novel mechanism underlying the cytotoxicity of nanomolar TBT levels in iPSCs. Recently, significant progress has been made in the induction of differentiation of pluripotent stem cells into a variety of cell types (Li et al., 2016). Thus, further studies are needed to evaluate the toxicities and developmental effects of TBT on somatic cells present in human adults. The chemical sensitivity and broad utility of iPSCs in toxicological studies of TBT may enable the discovery of versatile toxicity evaluation markers,

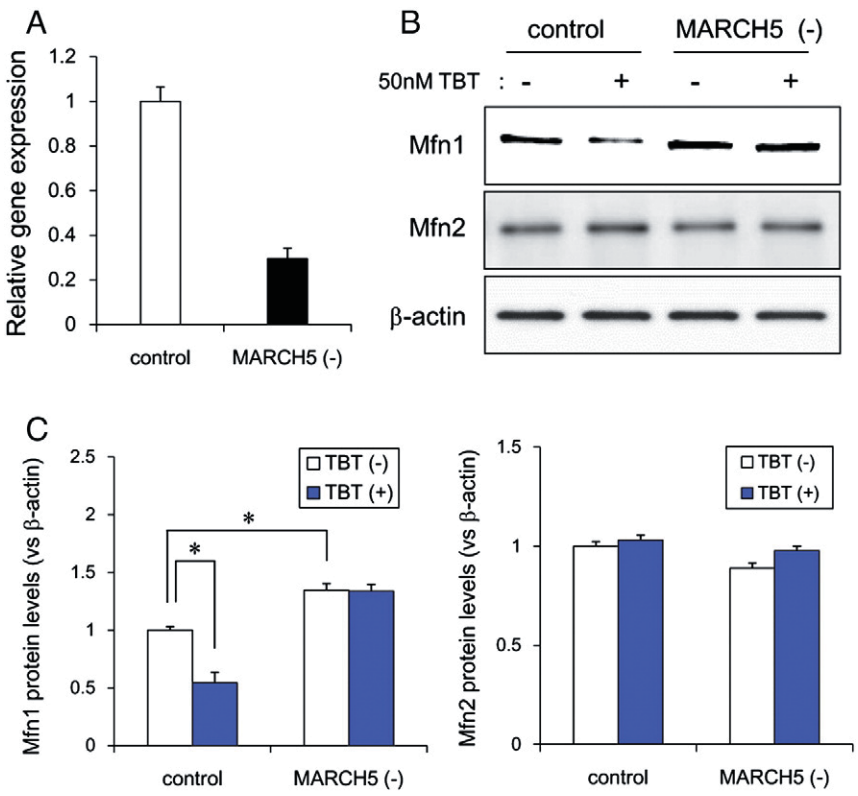

Fig. 4. MARCH5 KD abolishes TBT-induced Mfn1 degradation in iPSCs. (A) Cells were transfected with siRNA targeting MARCH5 or a scrambled siRNA (control), and the relative expression of MARCH5 was measured using real-time PCR. (B) After exposure to 50 nM TBT or TA for 72 h in siRNA-transfected cells, protein levels of Mfn1 and Mfn2 were examined by western blotting using anti-Mfn1, anti-Mfn2, or anti-β-actin antibodies. (C) The relative densities of bands were quantified with ImageJ software. Relative changes in expression were determined by normalization to β-actin. Data represent the mean ± SD (n = 3). $^{*}P < 0.05$ using Student's *t*-tests (A) or ANOVA with post hoc Tukey tests (C).

which could facilitate the development of a platform for chemical validation by providing simple, reproducible, and cost-effective tools.

Conflict of interest

The authors declare that there are no conflicts of interest.

Transparency document

The Transparency document associated with this article can be found, in online version.

Acknowledgments

This work was supported by a Health and Labour Sciences Research Grant from the Ministry of Health, Labour, and Welfare, Japan (#H25-Kagaku-Ippan-002 and #H28-Kagaku-Ippan-003 to Y. Kanda), a Grant-in-Aid for Scientific Research from the Ministry of Education, Culture, Sports, Science, and Technology, Japan (#26293056 and #26670041 to Y. Kanda), the Research on Regulatory Harmonization and Evaluation of Pharmaceuticals, Medical Devices, Regenerative and Cellular Therapy Products, Gene Therapy Products, and Cosmetics from Japan Agency for Medical Research and Development, AMED (#15mk0104053h0101 to Y. Sekino), and a grant from the Smoking Research Foundation (Y. Kanda).

Appendix A. Supplementary data

Supplementary data to this article can be found online at http://dx.doi.org/10.1016/j.tiv.2016.04.013.

References

Belinsky, G.S., Moore, A.R., Short, S.M., Rich, M.T., Antic, S.D., 2011. Physiological properties of neurons derived from human embryonic stem cells using a dibutyryl cyclic AMP-based protocol. Stem Cells Dev. 20, 1733–1746.

Chen, H., Detmer, S.A., Ewald, A.J., Griffin, E.E., Fraser, S.E., Chan, D.C., 2003. Mitofusins Mfn1 and Mfn2 coordinately regulate mitochondrial fusion and are essential for embryonic development. J. Cell Biol. 160, 189–200.

Chen, H., Chomyn, A., Chan, D.C., 2005. Disruption of fusion results in mitochondrial heterogeneity and dysfunction. J. Biol. Chem. 280, 26185–26192.

Choudhary, V., Kaddour-Djebbar, I., Alaisami, R., Kumar, M.V., Bollag, W.B., 2014. Mitofusin 1 degradation is induced by a disruptor of mitochondrial calcium homeostasis, CGP37157: a role in apoptosis in prostate cancer cells. Int. J. Oncol. 44, 1767–1773.

Fan, X., Hussien, R., Brooks, G.A., 2010. H_2O_2-induced mitochondrial fragmentation in C2C12 myocytes. Free Radic. Biol. Med. 49, 1646–1654.

Fischer, F., Hamann, A., Osiewacz, H.D., 2012. Mitochondrial quality control: an integrated network of pathways. Trends Biochem. Sci. 37, 284–292.

Grondin, M., Marion, M., Denizeau, F., Averill-Bates, D.A., 2007. Tributyltin induces apoptotic signaling in hepatocytes through pathways involving the endoplasmic reticulum and mitochondria. Toxicol. Appl. Pharmacol. 222, 57–68.

Gu, H., Li, Q., Huang, S., Lu, W., Cheng, F., Gao, P., Wang, C., Miao, L., Mei, Y., Wu, M., 2015. Mitochondrial E3 ligase March5 maintains stemness of mouse ES cells via suppression of ERK signalling. Nat. Commun. 6, 7112.

He, X., Imanishi, S., Sone, H., Nagano, R., Qin, X.Y., Yoshinaga, J., Akanuma, H., Yamane, J., Fujibuchi, W., Ohsako, S., 2012. Effects of methylmercury exposure on neuronal differentiation of mouse and human embryonic stem cells. Toxicol. Lett. 212, 1–10.

Hirata, N., Yamada, S., Shoda, T., Kurihara, M., Sekino, Y., Kanda, Y., 2014. Sphingosine-1-phosphate promotes expansion of cancer stem cells via S1PR3 by a ligand-independent Notch activation. Nat. Commun. 5, 4806.

Kanda, Y., Hinata, T., Kang, S.W., Watanabe, Y., 2011. Reactive oxygen species mediate adipocyte differentiation in mesenchymal stem cells. Life Sci. 89, 250–258.

Kinehara, M., Kawamura, S., Tateyama, D., Suga, M., Matsumura, H., Mimura, S., Hirayama, N., Hirata, M., Uchio-Yamada, K., Kohara, A., Yanagihara, K., Furue, M.K., 2013. Protein kinase C regulates human pluripotent stem cell self-renewal. PLoS One 8, e54122.

Kirchner, S., Kieu, T., Chow, C., Casey, S., Blumberg, B., 2010. Prenatal exposure to the environmental obesogen tributyltin predisposes multipotent stem cells to become adipocytes. Mol. Endocrinol. 24, 526–539.

Kotake, Y., 2012. Molecular mechanisms of environmental organotin toxicity in mammals. Biol. Pharm. Bull. 35, 1876–1880.

Kumar, V., Jahan, S., Singh, S., Khanna, V.K., Pant, A.B., 2015. Progress toward the development of in vitro model system for chemical-induced developmental neurotoxicity: potential applicability of stem cells. Arch. Toxicol. 89, 265–267.
Lavastre, V., Girard, D., 2002. Tributyltin induces human neutrophil apoptosis and selective degradation of cytoskeletal proteins by caspases. J. Toxic. Environ. Health A 65, 1013–1024.
Leboucher, G.P., Tsai, Y.C., Yang, M., Shaw, K.C., Zhou, M., Veenstra, T.D., Glickman, M.H., Weissman, A.M., 2012. Stress-induced phosphorylation and proteasomal degradation of mitofusin 2 facilitates mitochondrial fragmentation and apoptosis. Mol. Cell 47, 547–557.
Li, K., Kong, Y., Zhang, M., Xie, F., Liu, P., Xu, S., 2016. Differentiation of pluripotent stem cells for regenerative medicine. Biochem. Biophys. Res. Commun 471, 1–4.
Nakagawa, M., Koyanagi, M., Tanabe, K., Takahashi, K., Ichisaka, T., Aoi, T., Okita, K., Mochiduki, Y., Takizawa, N., Yamanaka, S., 2008. Generation of induced pluripotent stem cells without Myc from mouse and human fibroblasts. Nat. Biotechnol. 26, 101–106.
Nakamura, Y., Matsuo, J., Miyamoto, N., Ojima, A., Ando, K., Kanda, Y., Sawada, K., Sugiyama, A., Sekino, Y., 2014. Assessment of testing methods for drug-induced repolarization delay and arrhythmias in an iPS cell-derived cardiomyocyte sheet: multisite validation study. J. Pharm. Sci. 124, 494–501.
Park, M.T., Kim, M.J., Kang, Y.H., Choi, S.Y., Lee, J.H., Choi, J.A., Kang, C.M., Cho, C.K., Kang, S., Bae, S., Lee, Y.S., Chung, H.Y., Lee, S.J., 2005. Phytosphingosine in combination with ionizing radiation enhances apoptotic cell death in radiation-resistant cancer cells through ROS-dependent and -independent AIF release. Blood 105, 1724–1733.
Park, Y.Y., Nguyen, O.T., Kang, H., Cho, H., 2014. MARCH5-mediated quality control on acetylated Mfn1 facilitates mitochondrial homeostasis and cell survival. Cell Death Dis. 5, e1172.
Son, M.J., Kwon, Y., Son, M.Y., Seol, B., Choi, H.S., Ryu, S.W., Choi, C., Cho, Y.S., 2015. Mitofusins deficiency elicits mitochondrial metabolic reprogramming to pluripotency. Cell Death Differ. 10, 1–13.
Suzuki, J.S., Ishido, M., 2011. Transcriptome of tributyltin-induced apoptosis of the cultured rat mesencephalic neural stem cells. Toxicology 287, 61–68.
Takahashi, K., Tanabe, K., Ohnuki, M., Narita, M., Ichisaka, T., Tomoda, K., Yamanaka, S., 2007. Induction of pluripotent stem cells from adult human fibroblasts by defined factors. Cell 131, 861–872.
van der Bliek, A.M., Shen, Q., Kawajiri, S., 2013. Mechanisms of mitochondrial fission and fusion. Cold Spring Harb. Perspect. Biol. 5 (pii: a011072).
Varum, S., Rodrigues, A.S., Moura, M.B., Momcilovic, O., Easley IV., C.A., Ramalho-Santos, J., Van Houten, B., Schatten, G., 2011. Energy metabolism in human pluripotent stem cells and their differentiated counterparts. PLoS One 6, e20914.
Wanet, A., Arnould, T., Najimi, M., Renard, P., 2015. Connecting mitochondria, metabolism, and stem cell fate. Stem Cells Dev. 24, 1957–1971.
Whalen, M.M., Loganathan, B.G., Kannan, K., 1999. Immunotoxicity of environmentally relevant concentrations of butyltins on human natural killer cells in vitro. Environ. Res. 81, 108–116.
Yamada, S., Kotake, Y., Sekino, Y., Kanda, Y., 2013. AMP-activated protein kinase-mediated glucose transport as a novel target of tributyltin in human embryonic carcinoma cells. Metallomics 5, 484–491.
Yamada, S., Kotake, Y., Demizu, Y., Kurihara, M., Sekino, Y., Kanda, Y., 2014. NAD-dependent isocitrate dehydrogenase as a novel target of tributyltin in human embryonic carcinoma cells. Sci. Rep. 4, 5952.
Yamada, S., Kotake, Y., Nakano, M., Sekino, Y., Kanda, Y., 2015. Tributyltin induces mitochondrial fission through NAD-IDH dependent mitofusin degradation in human embryonic carcinoma cells. Metallomics 7, 1240–1246.
Youle, R.J., van der Bliek, A.M., 2012. Mitochondrial fission, fusion, and stress. Science 337, 1062–1065.
Yue, W., Chen, Z., Liu, H., Yan, C., Chen, M., Feng, D., Yan, C., Wu, H., Du, L., Wang, Y., Liu, J., Huang, X., Xia, L., Liu, L., Wang, X., Jin, H., Wang, J., Song, Z., Hao, X., Chen, Q., 2014. A small natural molecule promotes mitochondrial fusion through inhibition of the deubiquitinase USP30. Cell Res. 24, 482–496.
Zhu, X., Xing, M., Lou, J., Wang, X., Fu, W., Xu, L., 2007. Apoptotic related biochemical changes in human amnion cells induced by tributyltin. Toxicology 230, 45–52.

Biochemical and Biophysical Research Communications xxx (2016) 1–6

Contents lists available at ScienceDirect

Biochemical and Biophysical Research Communications

journal homepage: www.elsevier.com/locate/ybbrc

Nicotine induces mitochondrial fission through mitofusin degradation in human multipotent embryonic carcinoma cells

Naoya Hirata [a, 1], Shigeru Yamada [a, 1], Miki Asanagi [a, b], Yuko Sekino [a], Yasunari Kanda [a, *]

[a] Division of Pharmacology, National Institute of Health Sciences, Japan
[b] Faculty of Engineering, Department of Materials Science and Engineering, Yokohama National University, Japan

ARTICLE INFO

Article history:
Received 5 January 2016
Accepted 10 January 2016
Available online xxx

Keywords:
Embryonic cells
Cigarette smoking
Nicotine
Mitochondrial fission
Mitofusin

ABSTRACT

Nicotine is considered to contribute to the health risks associated with cigarette smoking. Nicotine exerts its cellular functions by acting on nicotinic acetylcholine receptors (nAChRs), and adversely affects normal embryonic development. However, nicotine toxicity has not been elucidated in human embryonic stage. In the present study, we examined the cytotoxic effects of nicotine in human multipotent embryonal carcinoma cell line NT2/D1. We found that exposure to 10 μM nicotine decreased intracellular ATP levels and inhibited proliferation of NT2/D1 cells. Because nicotine suppressed energy production, which is a critical mitochondrial function, we further assessed the effects of nicotine on mitochondrial dynamics. Staining with MitoTracker revealed that 10 μM nicotine induced mitochondrial fragmentation. The levels of the mitochondrial fusion proteins, mitofusins 1 and 2, were also reduced in cells exposed to nicotine. These nicotine effects were blocked by treatment with mecamylamine, a nonselective nAChR antagonist. These data suggest that nicotine degrades mitofusin in NT2/D1 cells and thus induces mitochondrial dysfunction and cell growth inhibition in a nAChR-dependent manner. Thus, mitochondrial function in embryonic cells could be used to assess the developmental toxicity of chemicals.

1. Introduction

Growing evidence suggest that maternal smoking during pregnancy is related to adverse neurodevelopmental outcomes in the offspring, including lower intelligence quotients and deficits in learning and memory [1,2]. Nicotine is a naturally occurring alkaloid that is present in tobacco leaves and is considered to contribute to the negative 98effects of cigarette smoking on health [2,3]. Nicotine exerts its cellular functions by activating nicotinic acetylcholine receptors (nAChRs), which are heterodimers composed of combinations of different types of α subunit (α1–α10) and β subunit (β1–β4) [4]. α8-nAChR has not been identified in human. Recent studies have shown that nAChRs are present in a variety of cells, such as cancer cells, vascular smooth muscle, and neural cells [3–6]. Activation of nAChRs by nicotine promotes the release of various neurotransmitters (including dopamine, norepinephrine, acetylcholine, glutamate) [7]. Altered regulation of neurotransmitter levels can adversely affect key events in normal brain development, such as the formation of neural circuits and neurotransmitter systems [7,8]. Therefore, it is necessary to elucidate the cytotoxic effects of nicotine on embryonic development.

Nicotine toxicity has been reported to affect mitochondrial function both *in vitro* and *in vivo*. For example, nicotine exposure alters mitochondrial membrane potential (MMP), increases an oxidative stress, and induces apoptosis in colon adenocarcinoma HCT-116 cell [9]. Another study has shown that nicotine exposure reduced the activity of an enzyme in the pancreatic mitochondrial respiratory chain, and impaired glucose-stimulated insulin secretion in neonatal rats [10]. However, the precise mechanisms underlying the effects of nicotine on mitochondrial function remain largely unknown.

Growing evidence suggest that mitochondria undergo continuous morphological dynamics involving fusion and fission cycles. These dynamics play a key role in maintenance of normal mitochondrial functions, such as ATP production [11]. Mitochondrial fusion and fission are regulated by several GTPases. Mitofusin 1 and 2 (Mfn1, 2) and optic atrophy 1 (Opa1) induce fusion of the outer and inner mitochondrial membranes, respectively [12,13]. In contrast, dynamin-related protein 1 (Drp1) is a cytoplasmic protein that assembles into rings surrounding the outer mitochondrial

* Corresponding author. 1-18-1, Kamiyoga, Setagaya-ku, 158-8501, Japan.
E-mail address: kanda@nihs.go.jp (Y. Kanda).
[1] Equally contributed.

http://dx.doi.org/10.1016/j.bbrc.2016.01.063
0006-291X/

membrane, where it interacts with fission protein 1 (Fis1) to promote fission [14,15]. For example, pigment epithelium-derived factor is reported to improve mitochondrial function by stabilizing mitochondrial fusion in retinal pigment epithelial cells [16]. In contrast, the anti-tumor agent, doxorubicin, facilitates mitochondrial fragmentation and apoptosis by promoting Mfn2 degradation in sarcoma U2OS cells [17].

In the present study, we hypothesized a possible link between nicotine toxicity and mitochondrial function in human mulitpotent NT2/D1 cells, which have neural differentiation capability. Our results showed that exposure to 10 μM nicotine decreased intracellular ATP levels and inhibited cell growth. Moreover, nicotine exposure induced Mfn degradation and mitochondrial fragmentation via nicotinic acetylcholine receptors (nAChRs). Thus, nicotine induces toxicity through impairment of mitochondrial quality control in human NT2/D1 cells.

2. Materials and methods

2.1. Cell culture

The human multipotent embryonal carcinoma NT2/D1 cells were obtained from the American Type Culture Collection (Manassas, VA, USA). SH-SY5Y cells were obtained from European Collection of Animal Cell Culture (Salisbury, Wiltshire, UK). The cells were cultured in Dulbecco's modified Eagle's medium (DMEM; Sigma–Aldrich, St. Louis, MO, USA) supplemented with 10% fetal bovine serum (FBS; Biological Industries, Ashrat, Israel) and 0.05 mg/ml penicillin-streptomycin mixture (Life Technologies, Carlsbad, CA, USA) at 37 °C in the presence of 5% CO_2.

2.2. Cell proliferation assay

Cell viability was measured using the CellTiter 96 AQueous One Solution Cell Proliferation Assay (Promega, Madison, WI, USA), as previously described [18]. Briefly, NT2/D1 cells were seeded into 96-well plate and exposed to different concentrations of nicotine. After exposure to nicotine, One Solution Reagent was added to each well, and the plate was incubated at 37 °C for another 2 h. Absorbance was measured at 490 nm by iMark microplate reader (Bio-Rad, Hercules, CA, USA).

2.3. Measurement of intracellular ATP levels

The intracellular ATP content was measured using the ATP Determination Kit (Life Technologies), as previously described [19]. Briefly, the cells were washed and lysed with phosphate-buffered saline containing 0.1% Triton X-100. The resulting cell lysates were added to a reaction mixture containing 0.5 mM D-luciferin, 1 mM dithiothreitol, and 1.25 μg/ml luciferase and incubated for 30 min at room temperature. Luminescence was measured using a Wallac1420ARVO fluoroscan (Perkin–Elmer, Waltham, MA, USA). The luminescence intensities were normalized to the total protein content.

2.4. Assessment of mitochondrial fusion

After treatment with nicotine (10 μM, 24 h), cells were fixed with 4% paraformaldehyde and stained with 50 nM MitoTracker Red CMXRos (Cell Signaling Technology, Danvers, MA, USA) and 0.1 μg/ml 4′,6-diamidino-2-phenylindole (DAPI; Dojin, Kumamoto, Japan). Changes in mitochondrial morphology were observed using a confocal laser microscope (Nikon A1). Images (n 3–7) of random fields were taken, and the number of cells displaying mitochondrial fusion (<10% punctiform) was counted in each image, as previously described [20]. The number of cells showing mitochondrial fission was calculated by subtracting the number of cells with mitochondrial fusion from the total cell number.

2.5. Real-time PCR

Total RNA was isolated from NT2/D1 cells using TRIzol reagent (Life Technologies), and quantitative real-time reverse transcription (RT)-PCR with QuantiTect SYBR Green RT-PCR Kit (QIAGEN, Valencia, CA, USA) was performed using an ABI PRISM 7900HT sequence detection system (Applied Biosystems, Foster City, CA, USA) as previously described [21]. The relative change in the amount of transcript was normalized to the mRNA levels of glyceraldehyde-3-phosphate dehydrogenase (GAPDH). The following primer sequences were used for real-time PCR analysis: *nAChRα1*, forward, 5′-CTGGACCTACGACGGCTCT-3′ and reverse, 5′-CGCTGCATGACGAAGTGGT-3′; *nAChRα2*, forward, 5′-ACACTTCAGACGTGGTGATTG-3′ and reverse, 5′-CCACTCCTGTTTTAGCCAGAC-3′; *nAChRα3*, forward, 5′-ACCTGTGGCTCAAGCAAATCT-3′ and reverse, 5′-GCAGGGACACGCATGAACT-3′; *nAChRα4*, forward, 5′-GGAGGGCGTCCAGTACATTG-3′ and reverse, 5′-GAAGATGCGGTCGATGACCA-3′; *nAChRα5*, forward, 5′-AGATGGAACCCTGATGACTATGGT-3′ and reverse, 5′-AAACGTCCATCTGCATTATCAAAC-3′; *nAChRα6*, forward, 5′-GGCAGGGATTCCTTCATGGG-3′ and reverse, 5′-GCCTCTCCTCAGTTGCACAG-3′; *nAChRα7*, forward, 5′-CATGGCCTTCTCGGTCTTCA-3′ and reverse, 5′-CACGGCCTCCACGAAGTT-3′; *nAChRα10*, forward, 5′-CAGATGCCTACCTACGATGGG-3′ and reverse, 5′-GGGAAGGCTGCTACATCCA-3′; *nAChRβ1*, forward, 5′-TGAGACCTCACTATCAGTACCCA-3′ and reverse, 5′-AGAACCACGACACTAAGGATGA-3′; *nAChRβ2*, forward, 5′-GGTGACAGTACAGCTTATGGTG-3′ and reverse, 5′-AGGCGATAATCTTCCCACTCC-3′; *nAChRβ3*, forward, 5′-TGCTGGTTCTCATCGTCCTTG-3′ and reverse, 5′-GCATCTTCATTTTCGGCGATTGA-3′; *nAChRβ4*, forward, 5′-CAGCTTATCAGCGTGAATGAGC-3′ and reverse, 5′-GTCAGGCGGTAATCAGTCCAT-3′; *Drp1*, forward, 5′-TGGGCGCCGACATCA-3′ and reverse, 5′-GCTCTGCGTTCCCACTACGA-3′; *Fis1*, forward, 5′-TACGTCCGCGGGTTGCT-3′ and reverse, 5′-CCAGTTCCTTGGCCTGGTT-3′; *Mfn1*, forward, 5′-GGCATCTGTGGCCGAGTT-3′ and reverse, 5′-ATTATGCTAAGTCTCCGCTCCAA-3′; *Mfn2*, forward, 5′-GCTCGGAGGCACATGAAAGT-3′ and reverse, 5′-ATCACGGTGCTCTTCCCATT-3′; *Opa1*, forward, 5′-GTGCTGCCCGCCTAGAAA-3′ and reverse, 5′-TGACAGGCACCCGTACTCAGT-3′; *GAPDH*, forward, 5′-GTCTCCTCTGACTTCAACAGCG-3′ and reverse, 5′-ACCACCCTGTTGCTGTAGCCAA-3′.

2.6. Western blot analysis

Western blot analysis was performed as previously reported [22]. Briefly, the cells were lysed with Cell Lysis Buffer (Cell Signaling Technology). The proteins were then separated by sodium dodecyl sulfate-polyacrylamide gel electrophoresis (SDS-PAGE) and electrophoretically transferred to Immobilon-P (Millipore, Billerica, MA, USA). The membranes were probed with anti-Drp1 monoclonal antibodies (1:1000; Cell Signaling Technology), anti-Fis1 polyclonal antibodies (1:200; Santa Cruz Biotechnology, Santa Cruz, CA, USA), anti-Mfn1 polyclonal antibodies (1:1000; Cell Signaling Technology), anti-Mfn2 monoclonal antibodies (1:1000; Cell Signaling Technology), anti-Opa1 monoclonal antibodies (1:1000; BD Biosciences), and anti-β-actin monoclonal antibodies (1:5000; Sigma–Aldrich). The membranes were then incubated with secondary antibodies against rabbit or mouse IgG conjugated to horseradish peroxidase (Cell Signaling Technology). The bands were visualized using the ECL Western Blotting Analysis System (GE

Please cite this article in press as: N. Hirata, et al., Nicotine induces mitochondrial fission through mitofusin degradation in human multipotent embryonic carcinoma cells, Biochemical and Biophysical Research Communications (2016), http://dx.doi.org/10.1016/j.bbrc.2016.01.063

Healthcare, Buckinghamshire, UK), and images were acquired using a LAS-3000 Imager (FUJIFILM UK Ltd., Systems, Bedford, UK).

2.7. Chemicals and reagents

Nicotine was obtained from Wako Pure Chemicals (Osaka, Japan). Mecamylamine hydrochloride (MCA) and m-chlorophenylhydrazone (CCCP) were obtained from Sigma–Aldrich.

2.8. Statistical analysis

All data were presented as means ± S.D. ANOVA followed by post hoc Fisher test was used to analyze data in Fig. 1A and B and Figs. 2–4B. Student's *t*-test was used to analyze data in Fig. 4C. *P*-values less than 0.05 were considered to be statistically significant.

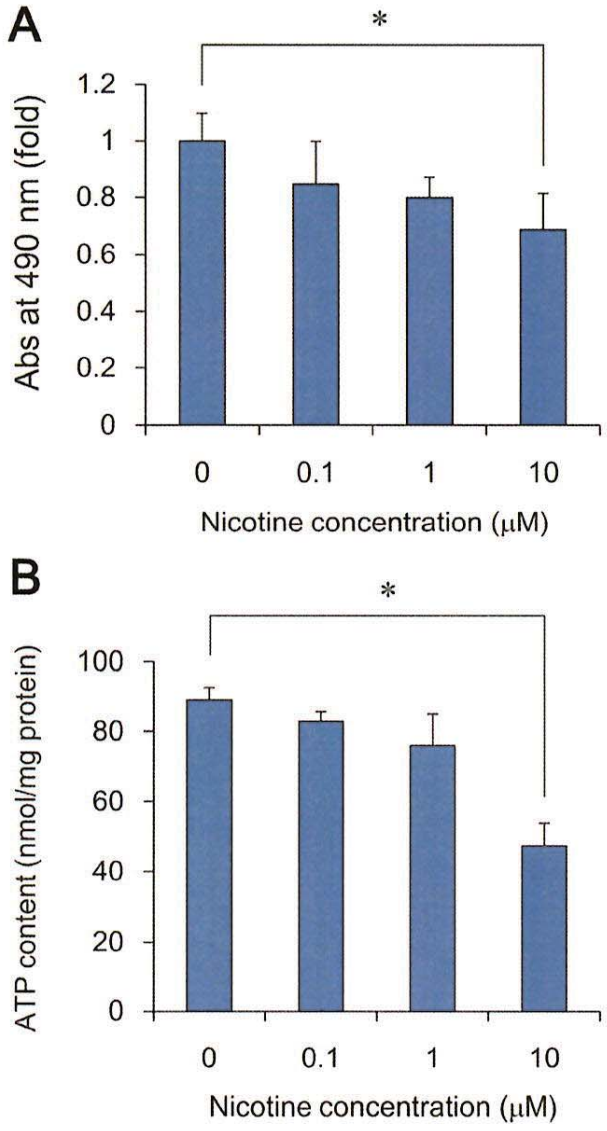

Fig. 1. Nicotine inhibits cell proliferation via intracellular ATP decrease in NT2/D1 cells. A. Cells were exposed to different concentrations of nicotine for 72 h. Cell viability was examined using the CellTiter 96 AQueous One Solution Cell Proliferation Assay. B. After treatment with different concentrations of nicotine for 24 h, intracellular ATP content was determined in cell lysates. Data represent the mean ± SD (n 3). *P < 0.05.

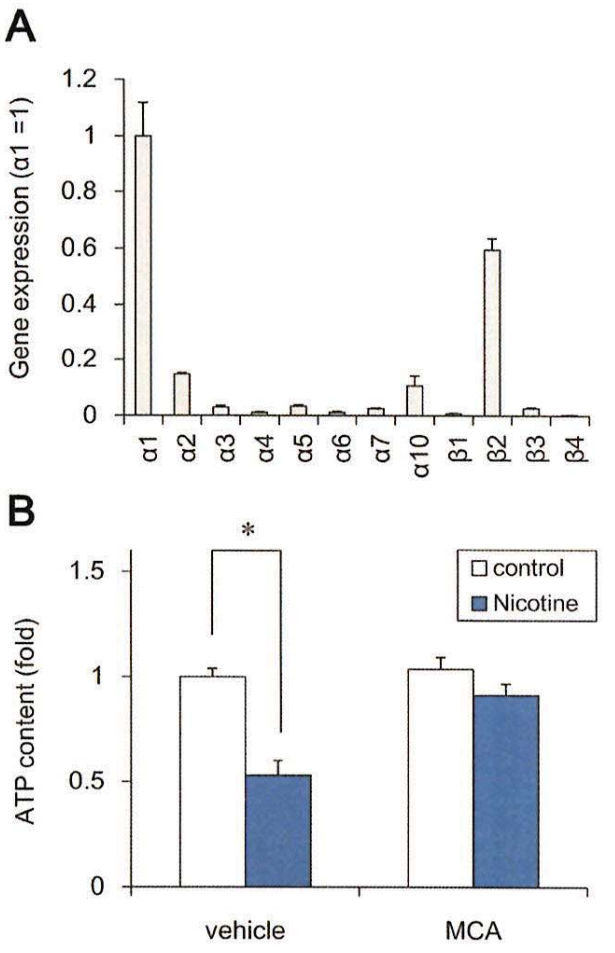

Fig. 2. Nicotine reduces intracellular ATP levels via nAChRs in NT2/D1 cells. A. Expression of AChR subtypes was analyzed by real-time PCR in NT2/D1 cells. The relative changes were determined by normalizing with GAPDH. B. After treatment with 10 μM nicotine and/or 30 μM MCA for 24 h, intracellular ATP content was determined in cell lysates. Data represent the mean ± SD (n 3). *P < 0.05.

3. Results

3.1. Cytotoxic effects of nicotine in NT2/D1 cells

To examine the effects of nicotine on human multipotent embryonic cells, we exposed the cells to different concentrations of nicotine for 72 h and measured cell viability by MTT assay using human multipotent embryonic carcinoma NT2/D1 cells, which have an ability to differentiate into neuronal cells. We found that treatment with 10 μM nicotine significantly inhibited cell proliferation (Fig. 1A). Similarly, exposure to 10 μM nicotine significantly reduced the ATP content of the cells (Fig. 1B). To further investigate whether the nicotine effects are selective for undifferentiated cells, we used human SH-SY5Y neuroblastoma cells. We found that exposure to 10 μM nicotine had little effect on proliferation and ATP content of SH-SY5Y cells (Fig. S1).

We next examined the nAChR mRNA levels by real-time PCR and confirmed that nAChR subtypes except α9-nAChR were expressed in NT2/D1 cells (Fig. 2A). To examine whether the inhibition of ATP

Please cite this article in press as: N. Hirata, et al., Nicotine induces mitochondrial fission through mitofusin degradation in human multipotent embryonic carcinoma cells, Biochemical and Biophysical Research Communications (2016), http://dx.doi.org/10.1016/j.bbrc.2016.01.063

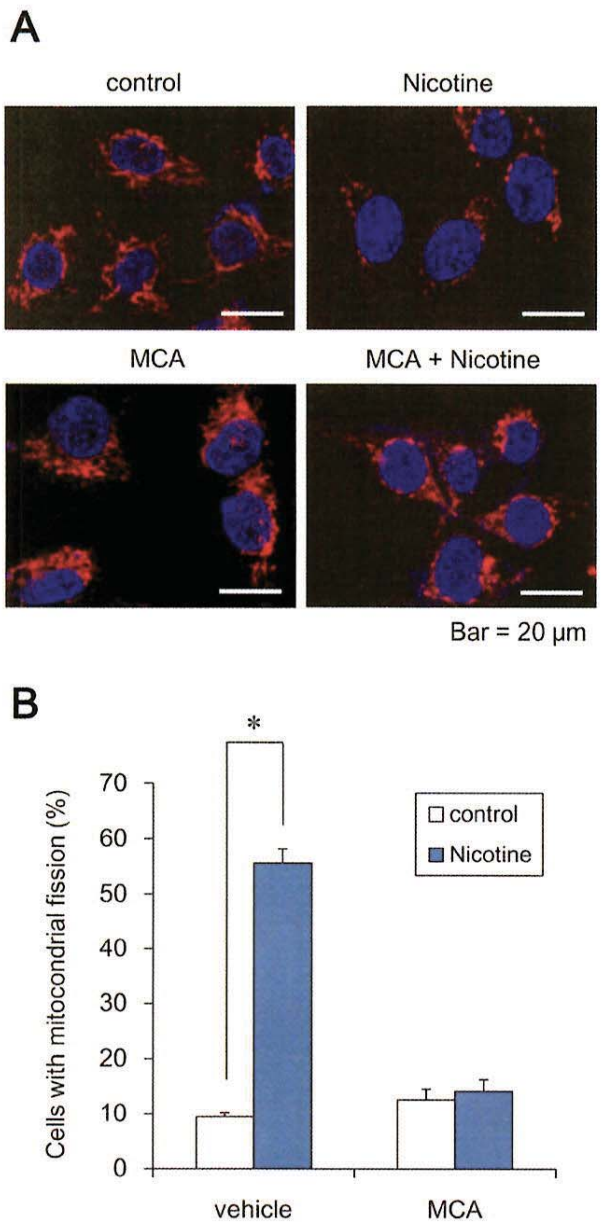

Fig. 3. Nicotine induces mitochondrial fission via nAChRs in NT2/D1 cells. A. Cells were exposed to 10 μM nicotine, in the presence or absence of 30 μM MCA, for 24 h. The cells were stained with MitoTracker Red CMXRos and DAPI and mitochondrial morphology was observed by confocal laser microscopy. Bar 20 μm. B. The number of cells showing mitochondrial fusion (<10% punctiform) was counted in three independent captured images. The number of cells showing mitochondrial fission was calculated by subtracting the number of cells with mitochondrial fusion from the total cell number. *$P < 0.05$.

production is mediated via the nAChRs, we tested the effect of nAChR antagonist on the ATP content. As shown in Fig. 2B, a non-selective nAChR antagonist mecamylamine (MCA) abolished the nicotine-induced reduction of ATP content. MCA alone did not affect the ATP level. These data suggest that nicotine decreases the ATP content via its nAChR and inhibits cell proliferation in NT2/D1 cells.

3.2. Effects of nicotine on mitochondrial morphology in NT2/D1 cells

Mitochondrial function, including ATP production, are maintained by mitochondrial fusion and fission [11]. Since nicotine reduced intracellular ATP levels, we next focused on the mitochondrial dynamics in NT2/D1 cells. Nicotine exposure (10 μM, 24 h) significantly increased the number of fragmented mitochondria with punctate morphology, as compared to the level observed in untreated control cells (Fig. 3). Moreover, MCA abolished this nicotine-induced mitochondrial fragmentation (Fig. 3). MCA alone did not affect mitochondrial dynamics. In contrast to NT2/D1 cells, nicotine did not significantly affect the mitochondrial dynamics in SH-SY5Y neuroblastoma cells (Fig. S1). These results suggest that nicotine induces mitochondrial fission via nAChRs in NT2/D1 cells.

3.3. Nicotine reduces Mfn1 and Mfn2 protein levels in NT2/D1 cells

To examine the molecular mechanism by which nicotine induces mitochondrial fragmentation, we assessed its effects on mitochondrial fission (Fis1, Drp1) and fusion genes (Mfn1, Mfn2, Opa1). Real-time PCR analysis showed that each gene expression was not significantly altered by nicotine exposure (Fig. 4A). Interestingly, western blot analysis revealed that nicotine did significantly decrease the levels of Mfn1 and Mfn2 proteins (Fig. 4B and C). In contrast, the levels of other proteins, including Fis1, Drp1, and Opa1, were not affected by nicotine. These data suggest that nicotine-induced mitochondrial fragmentation is caused by the degradation of Mfn1 and Mfn2 proteins.

4. Discussion

In the present study, we demonstrated that exposure to micromolar levels of nicotine impairs mitochondrial quality control in human multipotent embryonic carcinoma cells. Exposure to nicotine induces nAChR-dependent degradation of Mfn1 and Mfn2, thereby promoting mitochondrial fragmentation. These negative nAChR-mediated effects of nicotine on mitochondrial quality control could inhibit ATP production and cell viability.

Undifferentiated embryonic cells may tend to be sensitive to the growth inhibitory effects of nicotine, whereas proliferative and protective effects of nicotine have been described in more developed somatic cells [23–27]. Our studies showed that treatment with 10 μM nicotine reduces cell growth in human embryonic cells (Fig. 1), whereas the growth of human neuroblastoma SH-SY5Y cells is not affected (Fig. S1). Previous study has also shown that exposure to more than 1.8 μM nicotine inhibits cell adhesion and induces apoptosis in human embryonic stem cells [28]. The concentrations of nicotine tested in our study were relevant to the circulating levels of nicotine in cigarette smokers, which have been reported to range from 10 nM to 10 μM [29]; these have the potential to inhibit the growth of embryonic cells. In contrast to these growth inhibitory effects, nicotine is known to stimulate the proliferation of hematopoietic and neuronal progenitors [23–25]. In addition, nicotine is reported to protect rat basal forebrain neurons or rat hippocampal neurons from the cytotoxicity of β-amyloid protein [26,27]. Taken together, nicotine effects in undifferentiated embryonic cells contains different mechanisms from developed somatic cells. Therefore, further studies are required to elucidate the mechanism of cell stage-specific effects using embryonic and differentiated cells.

Our data suggest that nicotine induces mitochondrial fission through the degradation of Mfn1 and Mfn2 (Figs. 3 and 4). Consistent with this finding, chemical stressors have been reported

Please cite this article in press as: N. Hirata, et al., Nicotine induces mitochondrial fission through mitofusin degradation in human multipotent embryonic carcinoma cells, Biochemical and Biophysical Research Communications (2016), http://dx.doi.org/10.1016/j.bbrc.2016.01.063

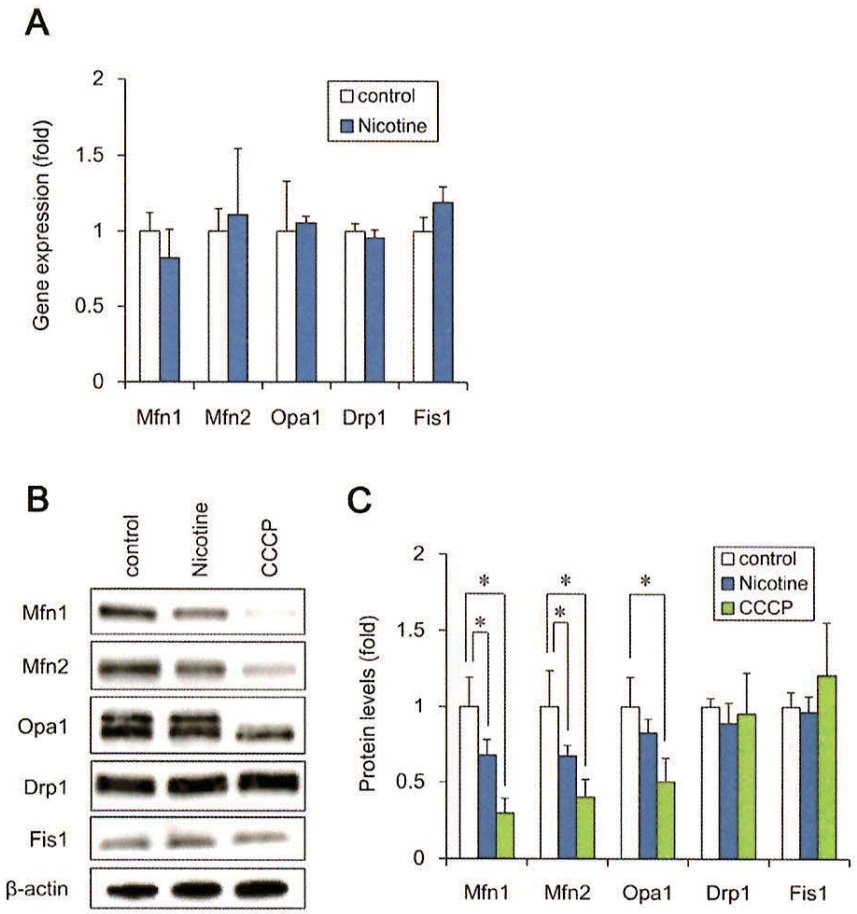

Fig. 4. Nicotine reduces Mfn1 and Mfn2 protein levels in NT2/D1 cells. A. After exposure to 10 μM nicotine for 24 h, the expression of the indicated mitochondrial genes was analyzed by real-time PCR. The relative changes were determined by normalizing with GAPDH. B. After exposure to 10 μM nicotine or 10 μM CCCP for 24 h, the expression of mitochondrial proteins was analyzed by western blot using anti-Drp1, anti-Fis1, anti-Mfn1, anti-Mfn2, anti-Opa1, or anti-β-actin antibodies. C. The band densities were analyzed by ImageJ software. Relative changes in expression were determined by normalization to β-actin. Data represent the mean ± SD (n 3). *P < 0.05.

to cause mitochondrial fission via Mfn degradation. For example, organotin compounds such as tributyltin induce proteasomal degradation of Mfn1 and Mfn2, which facilitates mitochondrial fragmentation and growth arrest in NT2/D1 cells [30,31]. Since nicotine showed similar effects in NT2/D1 cells, nicotine exposure may also degrade Mfn1 and Mfn2 via proteasome. Moreover, an inhibitor of mitochondrial calcium efflux, CGP37157, is reported to degrade Mfn1 via E3 ubiquitin ligase and induce mitochondrial fission in prostate cancer LNCaP cells [32]. Further studies will be necessary to determine whether ubiquitin ligases are involved in nicotine-induced Mfn1 and Mfn2 degradation in embryonic cells.

Our data suggest that nicotine toxicity is mediated by dysfunctional mitochondrial quality control, which occurs via a nAChR-dependent mechanism (Figs. 2 and 3). Nicotine has been reported to evoke extracellular calcium influx through plasma membrane nAChRs [4]. Moreover, a transient increase in intracellular calcium levels is known to cause mitochondrial calcium overload, which is followed by the depolarization of the mitochondrial membrane, resulting in a loss of MMP [33,34]. In other cell lines, MMP reduction is reported to induce the mitochondrial translocation of the E3 ubiquitin ligase, Parkin, which targets the Mfn protein for proteasomal degradation [35]. Therefore, nicotine may increase intracellular calcium entry via nAChRs, thus reducing the MMP and inducing mitochondrial translocation of E3 ubiquitin ligases; this increases the proteasomal degradation of Mfn1 and Mfn2. Several reports indicate that knockdown of Mfn1 and Mfn2 in the cells induces mitochondrial fragmentation and shows severe cellular defects, including decreased ATP content and poor cell growth [36,37]. Especially, Mfn2 has been reported to be necessary for striatal axonal projections of midbrain dopamine neurons by the studies using dopamine neuron-specific Mfn2 knockout mice [38]. Taken together, Mfn1 and Mfn2 might be involved in several nAChR-mediated effects of nicotine, such as the reduction of ATP content, growth inhibition, and modulation of synaptic transmission. In future studies, it will be necessary to investigate the precise mechanism involved in nicotine-induced Mfn degradation, which results in mitochondrial fission and impaired function.

Conflict of interest

The authors declare that there are no conflicts of interest.

Acknowledgments

This work was supported by a Health and Labour Sciences Research Grant from the Ministry of Health, Labour and Welfare,

Please cite this article in press as: N. Hirata, et al., Nicotine induces mitochondrial fission through mitofusin degradation in human multipotent embryonic carcinoma cells, Biochemical and Biophysical Research Communications (2016), http://dx.doi.org/10.1016/j.bbrc.2016.01.063

Japan (#H25-Kagaku-Ippan-002 to Y. Kanda), a Grant-in-Aid for Scientific Research from the Ministry of Education, Culture, Sports, Science, and Technology, Japan (#26293056, #26670041 to Y. Kanda), the Research on Regulatory Harmonization and Evaluation of Pharmaceuticals, Medical Devices, Regenerative and Cellular Therapy Products, Gene Therapy Products, and Cosmetics from Japan Agency for Medical Research and development, AMED (to Y. Sekino), and a grant from the Smoking Research Foundation (Y. Kanda).

Transparency document

Transparency document related to this article can be found online at http://dx.doi.org/10.1016/j.bbrc.2016.01.063.

Appendix A. Supplementary data

Supplementary data related to this article can be found at http://dx.doi.org/10.1016/j.bbrc.2016.01.063.

References

[1] V.S. Knopik, Maternal smoking during pregnancy and child outcomes: real or spurious effect? Dev. Neuropsychol. 34 (2009) 1–36.
[2] C.M. Tiesler, J. Heinrich, Prenatal nicotine exposure and child behavioural problems, Eur. Child. Adolesc. Psychiatry 23 (2014) 913–929.
[3] B.M. Conti-Fine, D. Navaneetham, S. Lei, A.D. Maus, Neuronal nicotinic receptors in non-neuronal cells: new mediators of tobacco toxicity? Eur. J. Pharmacol. 393 (2000) 279–284.
[4] E.X. Albuquerque, E.F. Pereira, M. Alkondon, S.W. Rogers, Mammalian nicotinic acetylcholine receptors: from structure to function, Physiol. Rev. 89 (2009) 73–120.
[5] Y. Kanda, Y. Watanabe, Nicotine-induced vascular endothelial growth factor release via the EGFR-ERK pathway in rat vascular smooth muscle cells, Life Sci. 80 (2007) 1409–1414.
[6] N. Hirata, Y. Sekino, Y. Kanda, Nicotine increases cancer stem cell population in MCF-7 cells, Biochem. Biophys. Res. Commun. 403 (2010) 138–143.
[7] N.L. Benowitz, Pharmacology of nicotine: addiction, smoking-induced disease, and therapeutics, Annu. Rev. Pharmacol. Toxicol. 49 (2009) 57–71.
[8] J.B. Dwyer, S.C. McQuown, F.M. Leslie, The dynamic effects of nicotine on the developing brain, Pharmacol. Ther. 122 (2009) 125–139.
[9] C.L. Crowley-Weber, K. Dvorakova, C. Crowley, H. Bernstein, C. Bernstein, H. Garewal, C.M. Payne, Nicotine increases oxidative stress, activates NF-kappaB and GRP78, induces apoptosis and sensitizes cells to genotoxic/xenobiotic stresses by a multiple stress inducer, deoxycholate: relevance to colon carcinogenesis, Chem. Biol. Interact. 145 (2003) 53–66.
[10] J.E. Bruin, M.A. Petre, S. Raha, K.M. Morrison, H.C. Gerstein, A.C. Holloway, Fetal and neonatal nicotine exposure in wistar rats causes progressive pancreatic mitochondrial damage and beta cell dysfunction, PLoS One 3 (2008) e3371.
[11] R.J. Youle, A.M. van der Bliek, Mitochondrial fission, fusion, and stress, Science 337 (2012) 1062–1065.
[12] T. Koshiba, S.A. Detmer, J.T. Kaiser, H. Chen, J.M. McCaffery, D.C. Chan, Structural basis of mitochondrial tethering by mitofusin complexes, Science 305 (2004) 858–862.
[13] S. Cipolat, O.M. De Brito, B. Dal Zilio, L. Scorrano, OPA1 requires mitofusin 1 to promote mitochondrial fusion, Proc. Natl. Acad. Sci. U. S. A. 101 (2004) 15927–15932.
[14] E. Smirnova, L. Griparic, D.-L. Shurland, A.M. van der Bliek, Dynamin-related protein Drp1 is required for mitochondrial division in mammalian cells, Mol. Biol. Cell 12 (2001) 2245–2256.
[15] Y. Yoon, E.W. Krueger, B.J. Oswald, M.A. McNiven, The mitochondrial protein hFis1 regulates mitochondrial fission in mammalian cells through an interaction with the dynamin-like protein DLP1, Mol. Biol. Cell 23 (2003) 5409–5420.
[16] Y. He, K.W. Leung, Y. Ren, J. Pei, J. Ge, J. Tombran-Tink, PEDF improves mitochondrial function in RPE cells during oxidative stress, Investig. Ophthalmol. Vis. Sci. 55 (2014) 6742–6755.
[17] G.P. Leboucher, Y.C. Tsai, M. Yang, K.C. Shaw, M. Zhou, T.D. Veenstra, M.H. Glickman, A.M. Weissman, Stress-induced phosphorylation and proteasomal degradation of mitofusin 2 facilitates mitochondrial fragmentation and apoptosis, Mol. Cell 47 (2012) 547–557.
[18] S. Yamada, Y. Kotake, Y. Sekino, Y. Kanda, AMP-activated protein kinase-mediated glucose transport as a novel target of tributyltin in human embryonic carcinoma cells, Metallomics 5 (2013) 484–491.
[19] S. Yamada, Y. Kotake, Y. Demizu, M. Kurihara, Y. Sekino, Y. Kanda, NAD-dependent isocitrate dehydrogenase as a novel target of tributyltin in human embryonic carcinoma cells, Sci. Rep. 4 (2014) 5952.
[20] X. Fan, R. Hussien, G.A. Brooks, H_2O_2-induced mitochondrial fragmentation in C2C12 myocytes, Free Radic. Biol. Med. 49 (2010) 1646–1654.
[21] N. Hirata, S. Yamada, T. Shoda, M. Kurihara, Y. Sekino, Y. Kanda, Sphingosine-1-phosphate promotes expansion of cancer stem cells via S1PR3 by a ligand-independent Notch activation, Nat. Commun. 5 (2014) 4806.
[22] Y. Kanda, T. Hinara, S.W. Kang, Y. Watanabe, Reactive oxygen species mediate adipocyte differentiation in mesenchymal stem cells, Life Sci. 89 (2011) 250–258.
[23] M.V. Skok, R. Grailhe, F. Agenes, J.P. Changeux, The role of nicotinic receptors in B-lymphocyte development and activation, Life Sci. 80 (2007) 2334–2336.
[24] L.M. Koval, A.S. Zverkova, R. Grailhe, Y.N. Utkin, V.I. Tsetlin, S.V. Komisarenko, M.V. Skok, Nicotinic acetylcholine receptors alpha4beta2 and alpha7 regulate myelo- and erythropoiesis within the bone marrow, Int. J. Biochem. Cell Biol. 40 (2008) 980–990.
[25] N. He, Z. Wang, Y. Wang, H. Shen, M. Yin, ZY-1, a novel nicotinic analog, promotes proliferation and migration of adult hippocampal neural stem/progenitor cells, Cell Mol. Neurobiol. 33 (2013) 1149–1157.
[26] C.N. Guo, L. Sun, G.L. Liu, S.J. Zhao, W.W. Liu, Y.B. Zhao, Protective effect of nicotine on the cultured rat basal forebrain neurons damaged by β-Amyloid (Aβ)25-35 protein cytotoxicity, Eur. Rev. Med. Pharmacol. Sci. 19 (2015) 2964–2972.
[27] Q. Liu, B. Zhao, Nicotine attenuates beta-amyloid peptide-induced neurotoxicity, free radical and calcium accumulation in hippocampal neuronal cultures, Br. J. Pharmacol. 141 (2004) 746–754.
[28] T. Zdravkovic, O. Genbacev, N. LaRocque, M. McMaster, S. Fisher, Human embryonic stem cells as a model system for studying the effects of smoke exposure on the embryo, Reprod. Toxicol. 26 (2008) 86–93.
[29] E.R. Gritz, V. Baer-Weiss, N.L. Benowitz, M.E. Van VunakisHjarvik, Plasma nicotine and cotine concentrations in habitual smokeless tobacco users, Clin. Pharmacol. Ther. 30 (1981) 201–209.
[30] S. Yamada, Y. Kotake, M. Nakano, Y. Sekino, Y. Kanda, Tributyltin induces mitochondrial fission through NAD-IDH dependent mitofusin degradation in human embryonic carcinoma cells, Metallomics 7 (2015) 1240–1246.
[31] M. Asanagi, S. Yamada, N. Hirata, H. Itagaki, Y. Kotake, Y. Sekino, Y. Kanda, Tributyltin induces G2/M cell cycle arrest via NAD^+-dependent isocitrate dehydrogenase in human embryonic carcinoma cells, J. Toxicol. Sci. (2016) in press. Q4
[32] V. Choudhary, I. Kaddour-Djebbar, R. Alaisami, M.V. Kumar, W.B. Bollag, Mitofusin 1 degradation is induced by a disruptor of mitochondrial calcium homeostasis, CGP37157: a role in apoptosis in prostate cancer cells, Int. J. Oncol. 44 (2014) 1767–1773.
[33] M.R. Duchen, Mitochondria and calcium: from cell signalling to cell death, J. Physiol. 529 (2000) 57–68.
[34] N. Demaurex, D. Poburko, M. Frieden, Regulation of plasma membrane calcium fluxes by mitochondria, Biochim. Biophys. Acta 1787 (2009) 1383–1394.
[35] A. Tanaka, M.M. Cleland, S. Xu, D.P. Narendra, D.F. Suen, M. Karbowski, R.J. Youle, Proteasome and p97 mediate mitophagy and degradation of mitofusins induced by Parkin, J. Cell Biol. 191 (2010) 1367–1380.
[36] H. Chen, A. Chomyn, D.C. Chan, Disruption of fusion results in mitochondrial heterogeneity and dysfunction, J. Biol. Chem. 280 (2005) 26185–26192.
[37] W. Yue, Z. Chen, H. Liu, C. Yan, M. Chen, D. Feng, C. Yan, H. Wu, L. Du, Y. Wang, J. Liu, X. Huang, L. Xia, L. Liu, X. Wang, H. Jin, J. Wang, Z. Song, X. Hao, Q. Chen, A small natural molecule promotes mitochondrial fusion through inhibition of the deubiquitinase USP30, Cell Res. 24 (2014) 482–496.
[38] S. Lee, F.H. Sterky, A. Mourier, M. Terzioglu, S. Cullheim, L. Olson, N.G. Larsson, Mitofusin 2 is necessary for striatal axonal projections of midbrain dopamine neurons, Hum. Mol. Genet. 21 (2012) 4827–4835.

Please cite this article in press as: N. Hirata, et al., Nicotine induces mitochondrial fission through mitofusin degradation in human multipotent embryonic carcinoma cells, Biochemical and Biophysical Research Communications (2016), http://dx.doi.org/10.1016/j.bbrc.2016.01.063

電気学会論文誌 A（基礎・材料・共通部門誌）
IEEJ Transactions on Fundamentals and Materials
Vol.136 No.2 pp.99-104 DOI: 10.1541/ieejfms.136.99

Paper

Visualization of Spatially Distributed Bioactive Molecules using Enzyme-Linked Photo Assay

Hikaru Mabuchi* Student Member, HongYao Ong* Associate
Kazunori Watanabe* Non-member, Sachiko Yoshida* Non-member
Naohiro Hozumi*a) Senior Member

(Manuscript received March 18, 2015, revised Oct. 4, 2015)

In this paper, we propose a new simple device for visualizing bioactive molecules with a fine spatial resolution by using a membrane in which a specific enzyme is immobilized. The layer produces fluorescence after association with a specific substance. The layer, on which a biological tissue is to be mounted, is deposited on a quartz substrate that is used as a light guide to introduce UV light to the layer. Substance release is observed by a CCD camera from the opposite side of the substrate. In order to shorten the experiment time, we had automated the optical device. The paper also describes the reduction of background fluorescence by means of image processing technique. Images were acquired by employing two UV-LEDs with slightly different angle. Image processing was performed to separate background and target fluorescence by means of independent component analysis. Finally the release of GABA(γ-aminobutyric acid) and glutamate from specific layers in rat cerebellum was successfully observed. It is expected that, using this method, both real-time transmitter release and its response to medicine can be observed.

Keywords : bioactive molecules, enzyme-linked photo assay, independent component analysis

1. Introduction

Light guide is composed of a dielectric material that can enclose the light propagation. In addition to being applied to communication, it is useful for sensing as well. In chemical sensing the surface of the light guide has to be coated with some specific chemical that may change its optical property depending on chemical reactions. Such a function can be applied to chemical imaging, if the light guide has a flat surface. This study proposes an application of two-dimensional light guide, of which surface is chemically modified, to biochemical imaging.

Neurotransmitter molecules released from neurons are not only regulators of neuronal transduction but also indicators of neuronal conditions. Glutamate and γ-aminobutyric acid (GABA) are known as typical transmitters in brain cortex that play important roles as stimulator and suppresser, respectively. Lack of balance in the release of glutamate and GABA may lead to autism, epilepsy or Parkinson's disease[1][2].

In order to observe the spatio-temporal release in cerebellar cortex, we have newly proposed the enzyme-linked photo assay system, which is realized even using normal CCD camera, and observed GABA release in developing cerebellar slice using either new or authorized methods[3].

In this paper, we propose a new simple device for this purpose by using a reactive layer in which a specific enzyme is immobilized, and produces fluorescence after association with a specific substance released from mounted slice. This layer is bound a quartz substrate that is used as a light guide for UV light excitation. Fluorescence derived from a substance is observed by a CCD camera from the opposite side of the substrate.

The paper describes the reduction of background fluorescence by means of image processing technique. Finally it will be shown that the release of transmitters from specific layers in rat cerebellum was successfully observed.

2. Specimen Preparation and Photo Excitation System

Imaging of neurotransmitter release was monitored the reaction of oxidoreductases generating reduced nicotinamide adenine dinucleotide (NAD^+) or diphosphonucleotide ($NADP^+$). For glutamate and GABA, we used glutamate dehydrogenase and GABA disassembly enzyme (GABase), respectively.

Enzymes were covalently immobilized on the quartz glass substrate using a silane coupling agent and a crosslink agent. The substrate was as thick as 1 mm. Stoichiometrically generated NADH or NADPH emits 480 nm fluorescence after excitation at 340-365 nm.

Existence of glutamate and GABA lead to fluorescence when co-existing with specific enzyme and co-enzyme. A glass substrate on which specific enzyme is coated is in contact with the biological specimen. A chamber space is created around the specimen. The space is filled with buffer liquid and co-enzyme. On the glass substrate therefore, the specimen is in contact with both enzyme and co-enzyme.

Consequently glutamate or GABA, that is released from the tissue spontaneously by stimulation, makes an oxidation-reduction reaction on the substrate. Although both glutamate and GABA do not produce fluorescence by themselves, NAD(P)H that is created as the result of the above chemical reaction makes fluorescence. As the ratio of glutamate or GABA and NAD(P)H is 1:1, the

a) Correspondence to: Naohiro Hozumi. E-mail: hozumi@icceed.tut.ac.jp
* Toyohashi University of Technology
1-1, Hibarigaoka, Tenpaku, Toyohashi 441-8580, Japan

fluorescence can be correlated to the amount of released glutamate or GABA.

In the experiment, rat cerebellum was sliced sagittally at 400 μm thick and incubated in oxygen-aerated HEPES-Na^+ buffer for 40 min. The slice was placed on the quartz glass substrate with both $NADP^+$ and α-ketoglutarate. Figure 1 shows the schematic diagram of the observation system including the device. The enzyme was immobilized covalently on the glass as shown in Fig. 2. Figure 3 shows chemical reactions taking place on the substrate. $NADP^+$ (nicotinamide adenine dinucleotide phosphate) changes into NADPH (reduced nicotinamide adenine dinucleotide phosphate) just as glutamate and GABA degeneration. Synthesized NADPH was illuminated by 360 nm surface UV-LED, and emitted the 480 nm fluorescent light observed by cooled CCD (ORCA ER, Hamamatsu Photonics). The quartz substrate can be recognized as a light guide to illuminate the surface of the substrate.

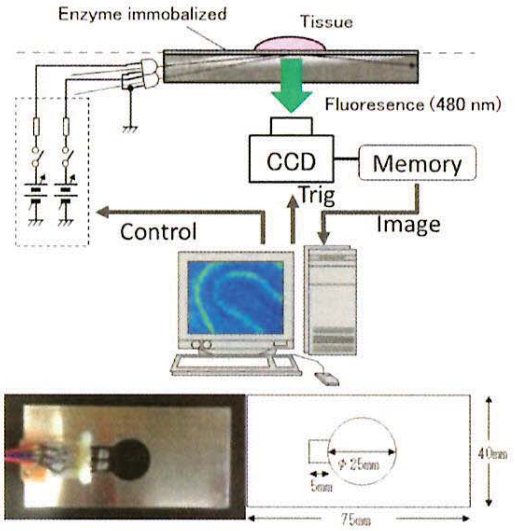

Fig. 1. Schematic diagram of the observation system including the device and its outlook

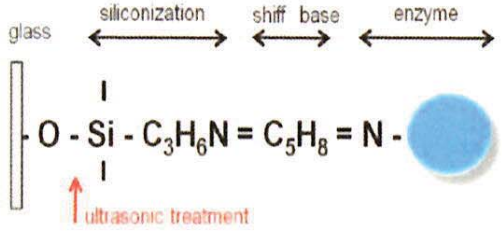

Fig. 2. Immobilized enzyme

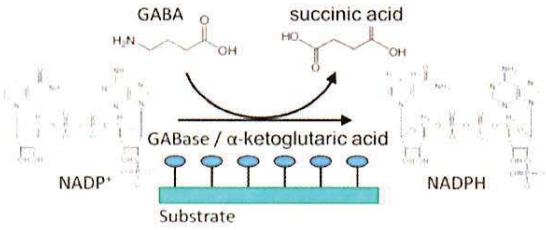

Fig. 3. Chemical reaction on the substrate

3. Image Processing

The fluorescent light detected by the CCD camera is divided into target light and background light. As significant intensity of background light is detected, it is assumed that fluorescence is excited by the light that is refracted on the interface between the substrate and tissue system including the layer. The light, being generated by LEDs and propagates though the substrate, can be decomposed into plane waves with different angles of propagation. Each plane wave transfers across the enzyme layer and comes into the tissue. We assume that both target and background light were predominantly excited by normal light. As the background light significantly damage the quality of the image, it should be reduced as much as possible. Making use of the evanescent light may be a solution, however, it may make the system complicated, and the target light may be not as significant as this case. Therefore we tried to reduce the background by means of a simple image processing.

Assuming that the light is a plane wave and scatter can be neglected, wave propagation and detected fluorescence can be illustrated as Fig. 4. In the figure, fluorescence, attributed to the layer where the enzyme is fixed, is represented as I_0. This is

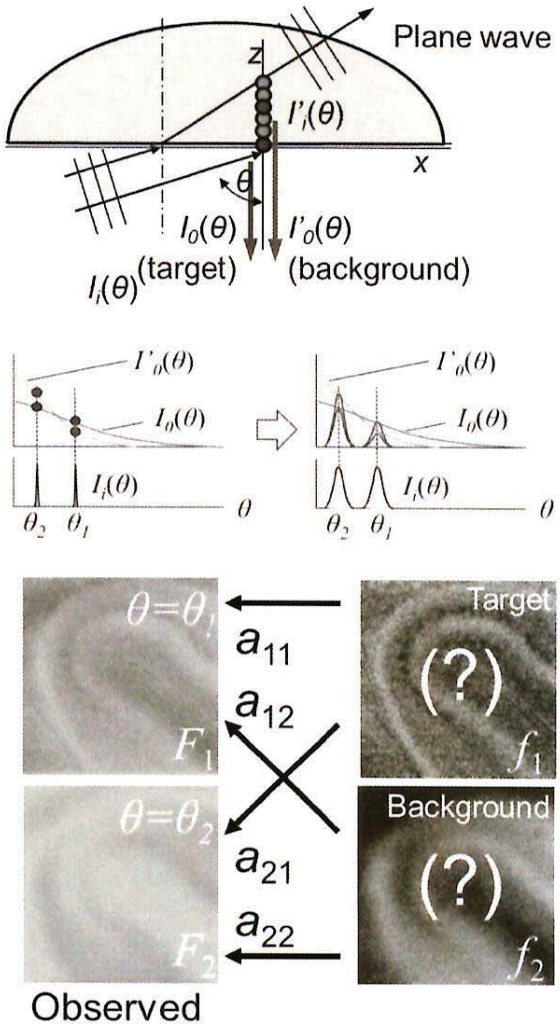

Fig. 4. Fluorescence detected by CCD camera

defined as to be the target. The fluorescence attributed to the tissue is represented as I'_0. This is defined as to be the background. Both I_0 and I'_0 depends on the incident angle θ. The thickness of the quartz plate, which is used as a light guide, is as thick as 1 mm. As it is much thicker than the diameter of normal optical fiber it is relatively easy to introduce two kinds of lights of which angles of center axes are significantly different. In addition, in practice, they depend differently on the incident angle. As the result, the proportion (I_0/I'_0) is not the same along θ. This is true even if the incident angle has distributed.

As the result, the captured fluorescence with different angle of optical axis is composed of target and background fluorescence with different mixture ratios. This can be represented as:

$$\begin{pmatrix} F_1 \\ F_2 \end{pmatrix} = \begin{pmatrix} a_{11} & a_{12} \\ a_{21} & a_{22} \end{pmatrix} \begin{pmatrix} f_1 \\ f_2 \end{pmatrix} \quad \cdots\cdots (1)$$

where $F_1(x,y)$ and $F_2(x,y)$ are captured fluorescence image, $f_1(x,y)$ and $f_2(x,y)$ are spatial distributions of fluorescence as the target and background, a_{11}, a_{12}, a_{21}, a_{22} are constants. Although the image acquisition is sequential, ICA is performed by assuming that two images, $F_1(x,y)$ and $F_2(x,y)$ are acquired with a negligible time lag. Reproduced images $f'_1(x,y)$ and $f'_2(x,y)$ are calculated from F_1 and F_2. As the result of periodical acquisitions of F_1 and F_2, time dependent images of f'_1 and f'_2 are calculated. Eq. (1) can also be described using a matrix expression as:

$$\mathbf{F} = \mathbf{A} \cdot \mathbf{f} \quad \cdots\cdots (2)$$

The target and background fluorescence distribution can be calculated by applying $\mathbf{A}^{-1}$ to $\mathbf{F}$. In practice, only contrast of the image would be enough to recognize the distribution. In such a case $\mathbf{A}^{-1}$ can be represented as:

$$\begin{pmatrix} 1 & \alpha \\ \beta & 1 \end{pmatrix} \quad \cdots\cdots (3)$$

After capturing two images $\mathbf{F}_1$ and $\mathbf{F}_2$ by changing the angle of optical axis, the target and background images can be separated by finding appropriate numbers for α and β. α and β can be tuned manually by monitoring the quality of reproduced image, however, the theory of independent component analysis (ICA) may be powerful for solving such a problem[4].

Stochastic distribution of pixel intensity in images f'_1 and f'_2 are represented as $p(y_{1i})$ and $p(y_{2j})$, where y_{1i} and y_{2j} represent the intensity.

$$\left.\begin{aligned} p(y_1) &\equiv \{p(y_{11}), \cdots, p(y_{1i}), \cdots p(y_{1n})\} \\ p(y_2) &\equiv \{p(y_{21}), \cdots, p(y_{2j}), \cdots p(y_{2n})\} \end{aligned}\right\} \quad \cdots\cdots (4)$$

$p(y_{1i}, y_{2j})$ represents the probability that the intensity of a pixel in image f'_1 is y_{1i} and that of the corresponding point in image f'_2 is y_{2j}. In other words $p(y_1)$ and $p(y_2)$ are probabilities that cases y_1 and y_2 take place, respectively, and $p(y_1, y_2)$ is the probability that cases y_1 and y_2 takes place simultaneously. Variables y_1 and y_2 are considered to be independent when

$$p(y_1, y_2) = p(y_1)p(y_2) \quad \cdots\cdots (5)$$

is established. Kullback-Leibler (K-L) parameter is often employed to indicate the independency of variables:

$$KL \equiv \sum_{i,j} p(y_{1i}, y_{2j}) \log \frac{p(y_{1i}, y_{2j})}{p(y_{1i})p(y_{2j})} \quad \cdots\cdots (6)$$

The K-L parameter is zero when two sets of variables y_1 and y_2 are completely independent together. In practice, α and β in Eq. (3), which determine the probabilities $p(y_1)$, $p(y_2)$ and $p(y_1, y_2)$, can be tuned so that the K-L parameter indicates the minimum.

The process of ICA is illustrated in Fig. 5. The equation described in the form of matrix indicates that two images, F_1 and F_2, derive from linear combination of unknown original images f_1 and f_2. If an appropriate inverse matrix can be found then the original images can be reproduced. However as the matrix to describe the linear combination is unknown as well, ICA algorithm is applied to find the most appropriate matrix (as the inverse matrix). In the

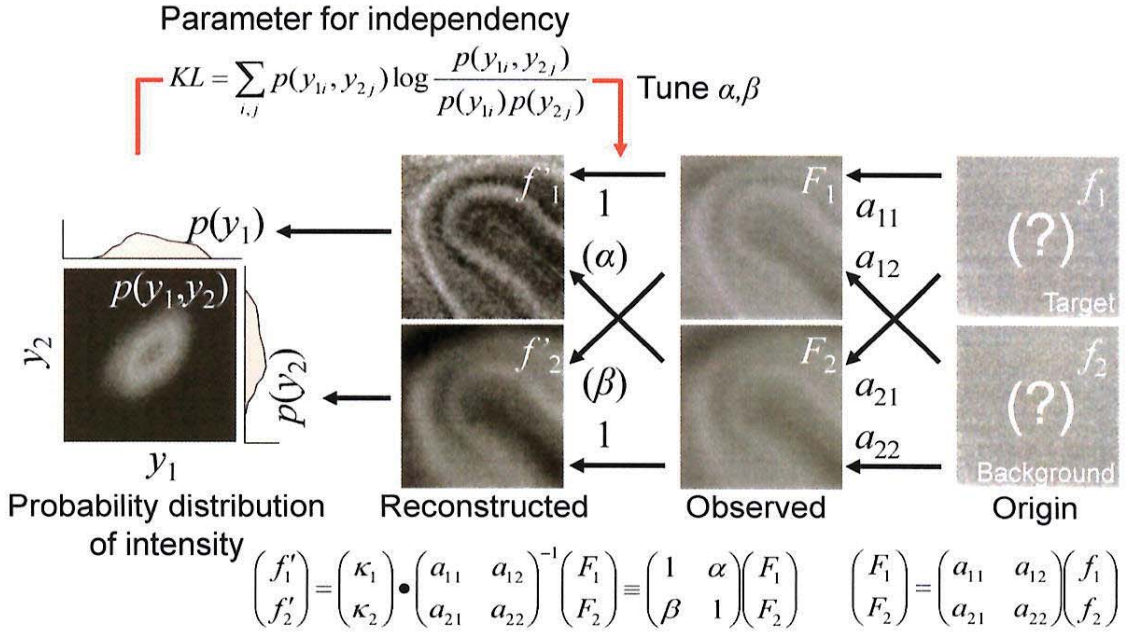

Fig. 5. Illustration for image processing based on independent component analysis

ICA process K-L parameter is calculated in order to evaluate the probabilistic independency of images f'_1 and f'_2. It can be considered that in the reproduction algorithm the core process is the calculation of the K-L parameter. In this preliminary study K-L parameter is successively calculated by manually changing the inverse matrix, and images are assumed to be reproduced when the K-L parameter indicates the minimum.

4. Results and Discussion

4.1 Image Processing using the ICA Figure 6 (a) shows visible light image of the cerebellum with postnatal 21 days. In developing cerebellum, granule cells, small input neurons, proliferate and migrate down from the external granular layer (EGL) to the internal granular layer (IGL). As the development proceeds, EGL turns into molecular layer (ML) whereas IGL remains. Purkinje cells, big output neurons, develop their dendrites and associate neuronal connections between granule cells and other interneurons. Neuronal circuit layer forms the ML. As the cerebellum shown in Fig. 6 (a) is mature, ML, PL, IGL are clearly visible. Note that ML is on the outer side of the cerebellum, and a wrinkle surrounded by the ML is seen in Fig. 6 (a).

As for fluorescence observation, three different images were acquired. Two were with different inclination of the excitation light source, and one was with no excitation light. Each of the two images with excitation light was subtracted with the image with no excitation light, in order to reduce the background light from the outside. These two images after the subtraction were defined as images A and B.

Figure 6 (b) shows these images for a rat cerebellum. Both images are very unclear, because of the background fluorescence. Figure 6 (c) shows the result of image processing. It is clearly shown in the image entitled as "target" that the fluorescence intensity is high in two layers, whereas that entitled as "background" is not clear. By morphological inspection these layers are recognized as ML and IGL. These layers are known that GABAergic neurons distribute in mature cerebellum. Studies using HPLC and electrophysiological method have shown that GABA is released from the postnatal cerebellar cortex even before synaptogenesis, and that GABA receptors act on the developing cerebellar Purkinje cells[4][5]. However, dynamic GABA release could not be observed unless the enzyme-linked photo assay is used. In addition, because cytoplasmic autofluorescence becomes noisy background light, it is useful that the image processing system extracted the image of GABA release from the autofluorescence-contained image. Using this method, both real-time transmitter release and its response to medicine can be observed.

4.2 Transition after Chemical Stimulation In relatively developed cerebellum, cells distributed in the ML and IGL are only the neurons of glutamate release, so that both layers showed fluorescent activities. Figure 7 indicates release distribution of glutamate in comparison with normal optical image illuminated with visible light. The fluorescent image, indicating glutamate release, is after the ICA processing. Figure 7 (c) indicates the regions of interest for analysis. Regions highlighted as ML and IGL have relatively strong intensity in fluorescence. They have a contrast to the region highlighted as PL. Release from white matter (WM), which is mostly composed of fatty materials, is much less significant.

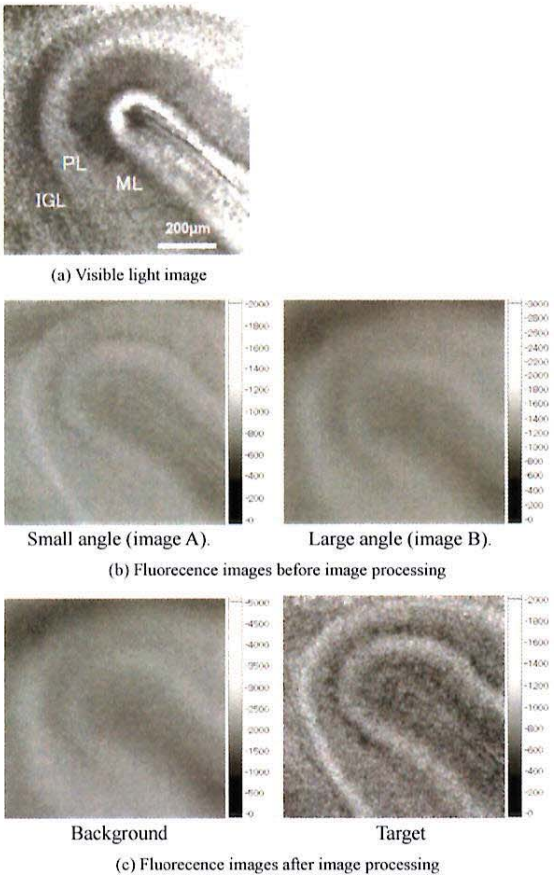

(a) Visible light image

(b) Fluorecence images before image processing

(c) Fluorecence images after image processing

Fig. 6. Cross sectional mages of cerebellar cortex: (a) Visible light image, (b) original fluorescent images with different angle of optical axes, and (c) fluorescent images after the image processing. Scales are indicated in arbitrary unit. Specimen: rat cerebellum (postnatal 21 days), target: GABA

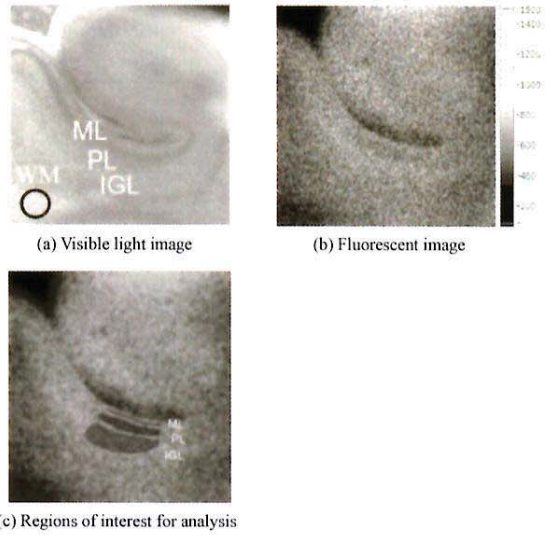

(a) Visible light image

(b) Fluorescent image

(c) Regions of interest for analysis

Fig. 7. Cerebellum with postnatal 7 days observed with visible light and fluorescent light indicating glutamate release. 0.9 mm × 0.9 mm. Gray scale is arbitrary. ML: molecular layer, PL: Purkinje layer, IGL: internal granular layer, WM: white matter. Specimen: rat cerebellum (postnatal 7 days)

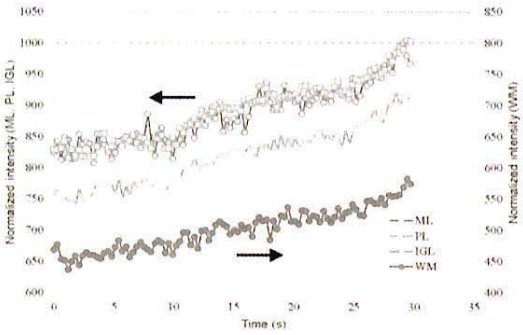

Fig. 8. Transition in fluorescence intensity in each layer (normalized by the intensity of ML 30 s after stimulation that is indicated as 1000). Specimen: rat cerebellum (postnatal 7 days), target: glutaminate

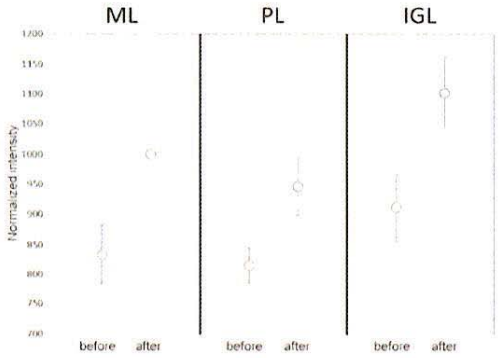

Fig. 9. Change in fluorescence intensity before and after AMPA stimulation (normalized by the intensity of ML 30 s after stimulation that is indicated as 1000). Specimen: rat cerebellum (postnatal 7 days), target: glutaminate

Our system can visualize both spontaneous and responsive transmitter release with about 0.2 s time resolution. Figure 8 shows the transition of glutamate release in response to 100 μmol/ℓ (S)-alpha-Amino-3-hydroxy- 5 methylisoxazole-4-propionic acid (AMPA) application in cerebellar slices. All values are normalized by the intensity of ML 30 s after stimulation that is indicated as 1000. Fluorescence, as indication glutamate release, was intense in both the IGL and ML, whereas the PL was indicated with lower intensity. As shown in Fig. 8, a clear increase in fluorescence was observed after stimulation. Transition in fluorescence was similar for ML and IGL, suggesting that these layers are activated. However PL, which was not expected to release glutamate, showed fluorescence as well although it was less intense than ML and IGL. As this specimen was taken from relatively young rat (postnatal 7 days), the cerebellar development was not totally completed, and the layers were not separated enough. It is hence considered that diffusion from ML and IGL to PL would take place, leading to an increase in fluorescence in this layer. The increase in fluorescence in WM suggests that glutamate might have been diffused into WM as well, although the absolute value was much lower than ML and IGL.

Figure 9 compares the fluorescence in each layer before and after stimulation. Four different specimens were used for the observation, in order to confirm reproducibility. It is clear that the AMPA stimulation brought a significant glutamate release from ML and IGL, although the increase is also seen with PL.

5. Conclusions

A new method for visualization of spatially distributed bioactive molecules using enzyme-linked photo assay has been proposed. It is based on fluorescent reaction assisted by an enzyme immobilized on the substrate, however, background fluorescence disturbs the observation. In order to reduce the background fluorescence, two images were acquired by changing the optical axis of UV illumination. Image processing based on independent component analysis made the target image clear. Observation of rat cerebellum was successfully performed and GABA and glutamate release from two specific layers was clearly indicated.

Acknowledgement

The study was partially supported by grants from Scientific Research (C) 23500516, 26350498 and Health Labor Sciences Research.

References

(1) N. C. Danbolt : "Glutamate Uptake", *Neurobiology*, Vol.65, pp.1-105 (2001)
(2) N. Kasai, Y. Jimbo, O. Niwa, T. Matsue, and K. Torimitsu : "Rea-time Multisite Observation of Glutamate Release in Rat Hippocampal Slices", *Neurosdence Lett.*, Vol.304, pp.112-116 (2001)
(3) T. Morishima, M. Uematsu, T. Furukawa, Y. Yanagawa, A. Fukuda, and S. Yoshida : "GABA Imaging in Brain Slices Using Enzyme-linked Photo Analysis", *Neurosci. Res.*, Vol.67, pp.347-353 (2001)
(4) V. Calhoun, G. Pearlson, and T. Adali : "Independent Component Analysis to fMRI Data, A Generative Model for Validating Results", VLSI Signal Processing, Vol.37, pp.281-291 (2004)
(5) F. F. Trigo, M. Chat, and A. Marty : "Enhancement of GABA Release through Endogenous Activation of Axonal GABA(A) Receptors in Juvenile Cerebellum", *J. Neurosci.*, Vol.27, No.46, pp.12452-63 (2007)
(6) K. Obata : "Excitatory and Trophic Action of GABA and Related Substances in Newborn Mice and Organotypic Cerebellar Culture", *Dev Neurosci*, Vol.19, No.1, pp.117-119 (1997)

Hikaru Mabuchi

(Student Member) was born in Hokkaido, Japan on July 25, 1992. He is 1st-year student in Graduate School of Toyohashi University of Technology. His major is electric and electronic information. He has been engaged in research on bio-sensing by means of optical measurement. He is a student member of IEEJ.

HongYao Ong

(Associate) was born in Malaysia on June 30, 1990. He received his B.S degree in 2014 from Toyohashi University of Technology, Japan. His major is electric and electronic information. He is currently engaged in GS Reality Sdn. Bhd., Malaysia. His major is electric and electronic information. He is an associate member of IEEJ.

Kazunori Watanabe

(Non-member) was born in Asahikawa, Japan on February 3, 1992. He is 2nd-year student in Graduate School of Toyohashi University of Technology. His research focuses both the optimization of surface modification for biosensor, and detection of neurotransmitters. He is a member of Japan neuroscience Society.

Sachiko Yoshida

(Non-member) was born in Toyama, Japan on January 24, 1961. She received her B.S., M.S. and Ph.D. degrees in 1983, 1986 and 1990 from University of Tokyo. She was engaged in JSPS Postdoctoral Researcher from 1990 to 1992, JST PRESTO Researcher from 1992 to 1994, and Research Associate at Toyohashi University of Technology from 1995 to 1996. Since 1996, she has been a lecturer of Toyohashi University of Technology. Her research interests focus the physiological interaction and morphological transformation through brain differentiation, and these detections. She is a member of a member of IEEE, International Brain Research Organization, Society for neuroscience, Japan neuroscience Society, and the Physiological Society of Japan.

Naohiro Hozumi

(Senior Member) was born in Kyoto, Japan on April 2, 1957. He received his B.S., M.S. and Ph.D. degrees in 1981, 1983 and 1990 from Waseda University. He was engaged in Central Research Institute of Electric Power Industry (CRIEPI) from 1983 to 1999. He was an associate professor of Toyohashi University of Technology from 1999 to 2006, and a professor of Aichi Institute of Technology from 2006 to 2011. Since 2011, he has been a professor of Toyohashi University of Technology. He has been engaged in the research in insulating materials and diagnosis for high voltage equipment, acoustic measurement for biological and medical applications, etc. He was awarded in 1990 and 1999 from IEE of Japan for his outstanding research papers. He is a member of IEEE, IEE of Japan and the Acoustic Society of Japan.

J Occup Health 2016; 58: 241-246

Journal of Occupational Health

Original

A cross-fostering analysis of bromine ion concentration in rats that inhaled 1-bromopropane vapor

Toru Ishidao[1], Yukiko Fueta[1], Susumu Ueno[2], Yasuhiro Yoshida[3] and Hajime Hori[1]

[1]Department of Environmental Management, School of Health Sciences, University of Occupational and Environmental Health, Japan, [2]Department of Occupational Toxicology, Institute of Industrial Ecological Sciences, University of Occupational and Environmental Health, Japan and [3]Department of Immunology and Parasitology, School of Medicine, University of Occupational and Environmental Health, Japan

Abstract: Objective: Inhaled 1-bromopropane decomposes easily and releases bromine ion. However, the kinetics and transfer of bromine ion into the next generation have not been clarified. In this work, the kinetics of bromine ion transfer to the next generation was investigated by using cross-fostering analysis and a one-compartment model. **Methods:** Pregnant Wistar rats were exposed to 700 ppm of 1-bromopropane vapor for 6 h per day during gestation days (GDs) 1-20. After birth, cross-fostering was performed between mother exposure groups and mother control groups, and the pups were subdivided into the following four groups: exposure group, postnatal exposure group, gestation exposure group, and control group. Bromine ion concentrations in the brain were measured temporally. **Results:** Bromine ion concentrations in mother rats were lower than those in virgin rats, and the concentrations in fetuses were higher than those in mothers on GD20. In the postnatal period, the concentrations in the gestation exposure group decreased with time, and the biological half-life was 3.1 days. Conversely, bromine ion concentration in the postnatal exposure group increased until postnatal day 4 and then decreased. This tendency was also observed in the exposure group. A one-compartment model was applied to analyze the behavior of bromine ion concentration in the brain. By taking into account the increase of body weight and change in the bromine ion uptake rate in pups, the bromine ion concentrations in the brains of the rats could be estimated with acceptable precision.

Received October 21, 2015; Accepted December 18, 2015
Published online in J-STAGE April 22, 2016
Correspondence to: Toru Ishidao, Department of Environmental Management, School of Health Sciences, University of Occupational and Environmental Health, 1-1 Iseigaoka, Yahatanishi-ku, Kitakyushu, 807-8555, Japan (e-mail: ishidao@health.uoeh-u.ac.jp)

(J Occup Health 2016; 58: 241-246)
doi: 10.1539/joh.15-0284-OA

Key words: 1-Bromopropane inhalation, Cross-fostering, Bromine ion concentration, One-compartment model, Animal experiment

1-Bromopropane (1-BP, CAS no. 106-94-5) is widely used as a substitute for chlorofluorocarbons, which destroy the ozone layer. The toxicity of 1-BP has been reviewed[1], and the Japan Society for Occupational Health recommends an occupation exposure limit of 0.5 ppm[2]. Previously, we studied the effects of inhaled 1-BP vapor in male rats on the nervous[3-8] and immune systems[9,10].

We also studied the effects of inhaled 1-BP vapor on metabolism in male rats and reported that 1-BP rapidly decomposes and releases bromine ion in the blood[11], indicating that bromine ion is a major index of 1-BP exposure. Recently, because of the health effects reported in female workers exposed to 1-BP[12-14], there is concern regarding the health effects of 1-BP exposure on the next generation. Some researchers have reported results of experiments in female animals[15-17]; however, the kinetics of bromine ion distribution to the next generation has not been elucidated. In this study, pregnant rats were exposed to 700 ppm of 1-BP vapor, and the concentration of bromine ion in the rat brain was measured. The distribution of bromine in fetuses and cross-fostered pups was investigated. A one-compartment model was employed to analyze the behavior of bromine ion in rats.

Methods

Animals

Female (9-week-old) and male (10-week-old) Wistar rats were purchased from Kyudo Co., Ltd. (Saga, Japan). After acclimation in polycarbonate cages with dry chips,

Table 1. Experimental groups and ages of adult and fetal rats exposed to 700 ppm of 1-BP and of pups on sampling day

Groups (n)		Age (n) on sampling day
Virgin female	Exposure (5)	GD21 (2)
Mother	Exposure (11)	GD20 (3)
	Control (5)	
Fetus	Exposure	GD20 (13)
Pup†	Exposure	PND1 (10), PND3 (10), PND5 (5), PND7 (5)
	Postnatal exposure	PND2 (5), PND4 (5), PND8 (5)
	Gestation exposure	PND4 (5), PND8 (5)
	Control	PND3 (5)

1-BP: 1-bromopropane, GD: gestation day, PND: postnatal day, †: Exposure=1-BP exposed pups were raised by their birth mother exposed to 1-BP, Postnatal exposure=control pups were raised by 1-BP exposed mother, Gestation exposure=1-BP exposed pups were raised by control mother, Control=control pups were raised by control mother

they were housed in pairs in animal rooms under 12-h light-dark cycle conditions at 22 ± 1℃ and 55 ± 5% relative humidity, with free access to food and water. The presence of sperm in the vaginal smear was defined as day 0 of gestation (GD0; female rats were 11 weeks old). In the inhalation study, the female rats were divided into three groups: 1-BP-exposed virgin female group (n=5), 1-BP-exposed mother group (n=11), and the control mother group (n=5). After the final exposure of mother rats on GD20, they were housed in an animal room for the onset of birth. Postnatal day (PND) i.e., the day after birth, was defined as day 0 (PND0=GD21). On PND1, a litter size of eight pups was assembled and cross-fostering[17,18] of pups was performed between mother exposure groups (n=3) and mother control groups (n=3). The pups were subdivided into four groups: (1) exposure group (1-BP-exposed pups were raised by their birth mother exposed to 1-BP), (2) postnatal exposure group (control pups were raised by 1-BP-exposed mother), (3) gestation exposure group (1-BP-exposed pups were raised by control mother), and (4) control group (control pups were raised by their control mother). The experimental groups are summarized in Table 1. Body weight was measured periodically. The experiments were conducted per the guidance of the Ethics Committee of Animal Care and Experimentation in accordance with The Guiding Principle for Animal Care Experimentation, University of Occupational and Environmental Health, Japan (AE03-065), which conforms to the National Institutes of Health Guide for the Care and Use of Laboratory Animals and the Japanese Law for Animal Welfare and Care.

Exposure

Reagent-grade 1-BP was obtained from Kanto Chemical Co., Ltd. (Tokyo, Japan). 1-BP vapor was introduced into a 400-*l* stainless-steel exposure chamber. Details of this apparatus and procedure have been given elsewhere[11]. In order to study change in bromine ion in blood and brain when the condition of dysfunction of feedback inhibition (i.e., disinhibition) was confirmed, exposure concentration was designed to be 700 ppm, which was higher than LOAEL (400 ppm) for disinhibition[7]. The actual concentration of 1-BP vapor in the chamber was 701.3 ± 5.2 ppm. In the control group, only clean air was introduced into the chamber. The exposure period was 6 h per day between 9 a.m. and 3 p.m. throughout gestation or GD 1-20 (virgin female group was exposed until GD21). Table 1 displays the age of the rats on sampling day. They were deeply anesthetized with diethyl ether and then decapitated. The brains and the stomachs with milk from only the exposure group on PND1 were gently removed and stored in a freezer.

Measurement of bromine ion concentration

The brains (cerebrum and diencephalon) and stomachs (0.25 g) were homogenized with water (1.5 m*l*) at 0℃. The sample (1 m*l*) was dispensed into a vial, and 0.1 m*l* of dimethyl sulfate was added to convert bromine ion to methyl bromide. Then, 0.1 m*l* of an aqueous solution of isopropyl alcohol (0.5 volume percent) was added as an internal standard. The vial was heated at 50℃ for 1 h. The bromine ion concentration was determined by measuring peak area of methyl bromide vapor in the headspace by using a gas chromatograph mass spectrometer (GC/MS, QP-5050; Shimadzu, Kyoto, Japan)[11].

Estimation method of bromine ion concentration

As previously described, inhaled 1-BP was metabolized and bromine ions were released. In this study, the behavior of released bromine ion concentration in the brain was analyzed by using a one-compartment model[19]. We assumed the bromine ion uptake rate, i.e., the genera-

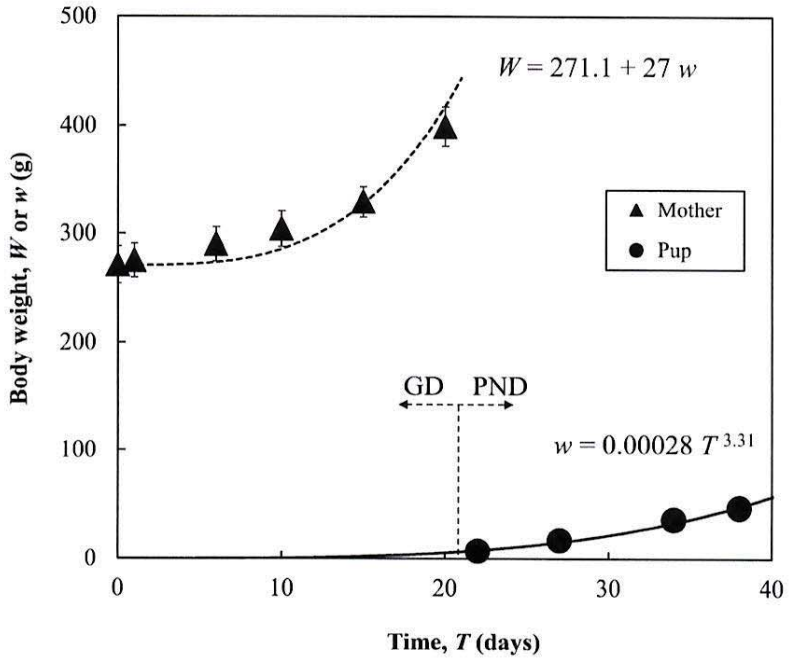

Fig. 1. The average body weight of mothers (W) exposed to 700 ppm of 1-BP up to GD20 and that of pups (w) after exposure. 1-BP: 1-bromopropane; GD: gestation day; PND: postnatal day

tion rate of bromine ion, is equal to the 1-BP uptake rate because 1-BP is decomposed quickly[11] and releases bromine ion. Under this assumption, mass balance equations of bromine ion during exposure and clearance periods respectively were as follows:

$$\frac{dx}{dt}=R-kx \tag{1}$$

$$\frac{dx}{dt}=-kx \tag{2}$$

where x is the amount of bromine ion (μg); t is time (h); R is the generation rate of bromine ion (μg/h), which corresponds to the 1-BP uptake rate; and k is the excretion rate constant (1/h). From equations (1) and (2), the bromine ion concentrations C (μg/g) during exposure and clearance respectively were obtained as follows:

$$C=\frac{R}{\rho Vk}(1-e^{-kt}) \tag{3}$$

$$C=C_0e^{-kt} \tag{4}$$

where V is the volume of the compartment (ml), ρ is the density of the compartment (g/ml), and C_0 is the initial concentration during clearance (μg/g). The excretion rate constant k is given by the biological half-life, $t_{1/2}$ (h) or $T_{1/2}$ (days).

$$k=\frac{\ln 2}{t_{1/2}\text{ (h)}}=\frac{0.693}{T_{1/2}\text{ (days)}\times 24} \tag{5}$$

Experimental Results

Fig. 1 shows the change in the average body weight of mother rats exposed to 700 ppm of 1-BP up to GD20 and that of the pups after the exposure. The time, T (on the horizontal axis), includes the GDs and PNDs. Litter sizes of exposed mothers and control mothers were 15.0 ± 2.8 and 14.9 ± 2.5 pups, respectively. The body weight of both mothers and pups increased rapidly. This tendency was also observed in the control group, and there was no significant difference between the exposure group and the control group. For the virgin female group, body weight did not change significantly (271.1 ± 17.0 g) during GD1-20.

Bromine ion concentration in the rat brain (μg/g-brain) exposed to 700 ppm of 1-BP on GDs is presented as symbols in Fig. 2. The bromine ion concentration in mother rats was lower than that in virgin rats, and the concentration in fetuses was higher than that in mothers. Fig. 3 shows changes in bromine ion concentration in pup brain for PNDs. The concentration in the gestation exposure group decreased between PND4 and PND8, whereas that in the postnatal exposure group increased from PND2 to PND4 and then decreased. This tendency was also ob-

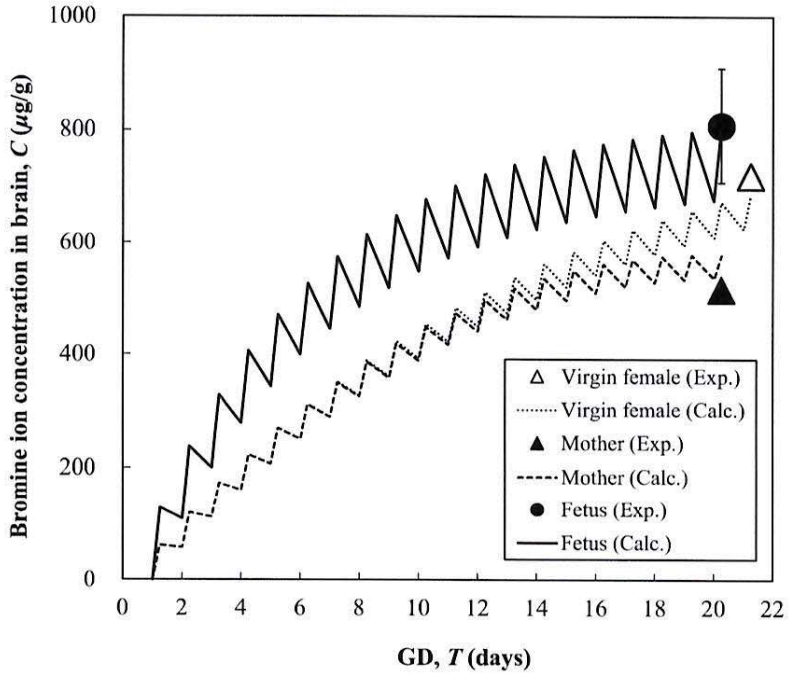

Fig. 2. Change in bromine ion concentration in rat brain exposed to 700 ppm of 1-BP on GDs. Symbols represent experimental data: ●, fetus; ▲, mother; △, virgin female. Solid, broken, and dotted lines indicate calculated lines for fetuses, mothers, and virgin females, respectively. 1-BP: 1-bromopropane; GD: gestation day

served in the exposure group, although the concentration on PND1 was lower than that on GD20 (fetus in Fig. 2). Specifically, the concentration in the exposure group was the highest just after birth, but decreased at PND1. The concentration then increased from PND1 to PND3, but decreased again with time. In the control pups, the bromine ion concentration was 11.2 ± 7.7 μg/g-brain on PND3.

The bromine ion concentration in pup stomachs with milk from the exposure group on PND1 was 830.6 ± 188.8 μg/g-stomach, which was about twice as much as that in the mother brain at GD20 (Fig. 2).

Discussion

The one-compartment model was applied to analyze the bromine ion concentration in the brains of virgin females, mothers, fetuses, and pups. Equations (3) and (4) have two parameters, the excretion rate constant k and the 1-BP uptake rate R. The excretion rate constant, k, can be easily calculated from equation (5) by using the biological half-life $T_{1/2}$ (days). In our previous work[11], $T_{1/2}$ for male rats was 4.7-15.0 days in blood and 5.0-7.5 days in urine. Therefore, $T_{1/2}$=7.0 days was used for mothers and virgin females in this study. $T_{1/2}$ in pups was 3.1 days, obtained by experimental data. Equation (4) was applied to the data from PND1 for the exposure group and from PND4 and PND8 for the gestation exposure group as shown in Fig. 3. $T_{1/2}$=3.1 days was also used for fetuses. The half-lives of between GD20 for fetuses and PND1 for the exposure group were excluded from the calculation because of the time lag due to birth.

As shown in Fig. 2, the bromine ion concentration in the brains of mothers was lower than that in the brains of virgin females. A reason for this might be that the bromine ion concentration was diluted because of increasing body weight. The average body weight of pups, w (g), was expressed using the following equation (Fig. 1):

$$w=0.00028T^{3.31} \quad (6)$$

The average body weight of mothers, W (g), was calculated as the sum of that of virgin females (ρV=271.1 g) and of pups, w, (interpolated value for GDs):

$$W=271.1+27w \quad (7)$$

where 27 is the constant, which was determined to give the best fit for the experimental data as shown in Fig. 1.

For virgin females, the uptake rate, R, of 2853 μg/h was obtained to give the best fit of equations (3) and (4) for the experimental data on GD21 in Fig. 2. Therefore, $R/\rho V=R/W$=2853/271.1=10.5 μg/(h·g) for virgin females, and $R/\rho V$=2853/(271.1 + 27w) for mother rats was used in equation (3). For fetuses, R (bromine ion uptake rate from mothers) was assumed to be proportional to body weight,

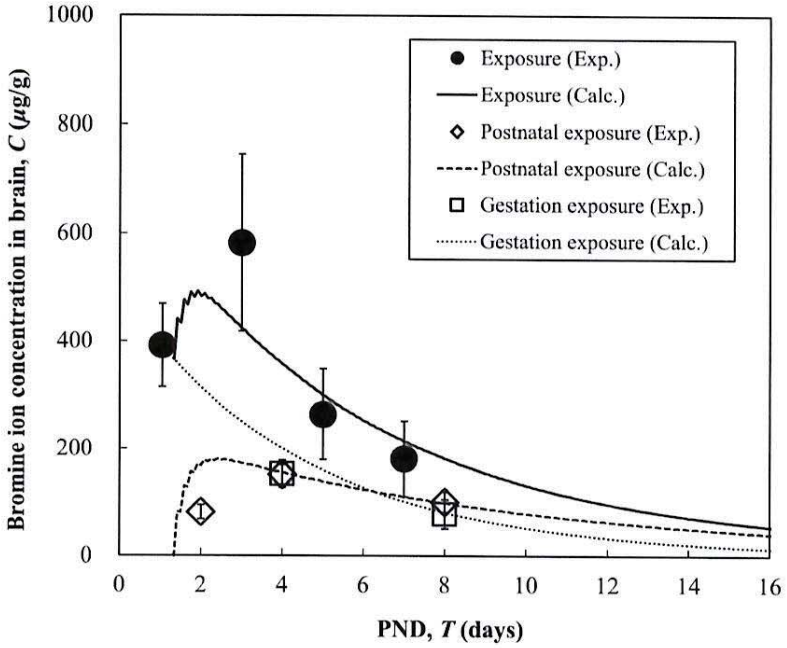

Fig. 3. Change in bromine ion concentration in pup brain during PNDs. Symbols represent experimental data: ●, exposure group (1-BP exposed pups were raised by their birth mother exposed to 1-BP); ◇, postnatal group (control pups were raised by 1-BP exposed mother); □, gestation exposure (1-BP exposed pups were raised by control mother). Solid, broken, and dotted lines indicate calculated lines for exposure, postnatal exposure, and gestation exposure groups, respectively. 1-BP: 1-bromopropane; PND: postnatal day

and $R/\rho V=R/w$=22.0 μg/(h・g) was applied, which was obtained to give the best fit for the experimental data on GD 20 in Fig. 2. On PNDs, suckling (exposure to bromine ion from milk) was assumed to occur at 2-h intervals. As shown in Fig. 3, the curve of bromine ion concentration in the brains of the postnatal exposure group is convex. In addition, on PND 1, the concentration in pup stomachs with milk was high, and the level was higher than that in the mother brain, as calculated using the one-compartment model (486.2 μg/g-brain). Therefore, we assume that the uptake rate R of pups is high at first and then decreases. In this work, R in the postnatal exposure group can be expressed by the following equation:

$$R=388e^{-0.126(t-32)} \quad (8)$$

where 32 is the initial suckling (h) and 388 and 0.126 are the constants determined experimentally. The bromine ion concentration in the exposure group was calculated as the sum of the concentrations in the gestation exposure and postnatal exposure groups. Conditions of the one-compartment model and the values of parameters obtained are listed in Table 2. Solid, broken, and dotted lines in Fig. 2 indicate calculated lines for fetuses, mothers, and virgin females, respectively. In Fig. 3, solid, broken, and dotted lines indicate calculated lines of exposure, postnatal exposure, and gestation exposure groups, respectively. The lines calculated using the proposed model could be estimated from the experimental data with acceptable precision as shown in both figures.

The calculated bromine ion uptake rates per weight, $R/\rho V$, for adults and fetuses were 10.5 and 22 μg/(h・g), respectively. This result suggests that the bromine ion easily transfers from mothers to fetuses, and the concentration in fetuses was higher than that in mothers. R in postnatal exposure group was expressed as an exponential function, and $R/\rho V$ of 55 μg/(h・g) was obtained at initial suckling time. This value was large compared to 22 μg/(h・g), the calculated value at GD20, before birth. This suggests that uptake rate of bromine ion via milk was higher than that via the placenta, and the bromine ion concentration in the exposure group could be explained as the sum of that in the gestation and postnatal exposure groups, which is shown in Fig. 3.

In summary, the results of this study suggest (1) the concentration of bromine ion in mother rats was lower than that in virgin female rats, (2) bromine ion easily transferred from mothers to fetuses and accumulated before birth, (3) bromine ion was concentrated more in milk than in the brains of the mothers, and (4) bromine ion up-

Table 2. Parameters of the one-compartment model

	Groups	$T_{1/2}$ (days)	ρV (g)	R (μg/h)	Results
GD	Virgin female	7.0	271.1	2853	Fig. 2
	Mother	7.0	271.1+27w	2853	Fig. 2
	Fetus	3.1	w	22w	Fig. 2
PND	Gestation exposure	3.1			Fig. 3
	Postnatal exposure	3.1	w	$388e^{-0.126(t-32)}$	Fig. 3
	Exposure	Gestation exposure+Postnatal exposure			Fig. 3
	Mother	7.0			Text†

†: the concentration in mother brain corresponding to PND1 (486.2 μg/g-brain), w=0.000287$^{3.31}$ by equation (6)

take rate in pups was high immediately after birth.

Acknowledgments: The authors thank Ms. Tomoko Tanaka, Kana Hayashi, Erika Ito, and Ai Kanemaru for technical help and Dr. Sumiyo Ishimatsu for her critical comments on our experiments.

Conflict of Interest: None declared.

References

1) Ichihara G. Neuro-reproductive toxicities of 1-bromopropane and 2-bromopropane. Int Arch Occup Environ Health 2005; 78: 79-96.
2) The Japan Society for Occupational Health. Recommendation of occupational exposure limits (2013-14). J Occup Health 2013; 55: 422-441.
3) Ohnishi A, Ishidao T, Kasai T, Arashidani K, Hori H. Neurotoxicity of 1-bromopropane in rats. J UOEH 1999; 21: 23-28.
4) Fueta Y, Ishidao T, Kasai T, Hori H, Arashidani K. Decreased paired-pulse inhibition in the dentate gyrus of the brain in rats exposed to 1-bromopropane vapor. J Occup Health 2000; 42: 149-151.
5) Fueta Y, Ishidao T, Arashidani K, Endo Y, Hori H. Hyperexcitability of the hippocampal CA1 and the dentate gyrus in rats subchronically exposed to a substitute for chlorofluorocarbons, 1-bromopropane vapor. J Occup Health 2002; 44: 156-165.
6) Fueta Y, Fukuda T, Ishidao T, Hori H. Electrophysiology and immunohistochemistry in the hippocampal CA1 and the dentate gyrus of rats chronically exposed to 1-bromopropane, a substitute for specific chlorofluorocarbons. Neuroscience 2004; 124: 593-603.
7) Fueta Y, Ishidao T, Ueno S, Yoshida Y, Kunugita N, Hori H. New approach to risk assessment of central neurotoxicity induced by 1-bromopropane using animal models. Neurotoxicology 2007; 28: 270-273.
8) Ueno S, Yoshida Y, Fueta Y, et al. Changes in the function of the inhibitory neurotransmitter system in the rat brain following subchronic inhalation exposure to 1-bromopropane. Neurotoxicology 2007; 28: 415-420.
9) Yoshida Y, Liu JQ, Nakano Y, et al. 1-BP inhibits NF-kB activity and Bcl-xL expression in astrocytes in vitro and reduces Bcl-xL expression in the brains of rats in vivo. Neurotoxicology 2007; 28: 381-386.
10) Yoshida Y, Nakano Y, Ueno S, et al. Effects of 1-bromopropane, a substitute for chlorofluorocarbons, on brain-derived neurotrophic factor (BDNF) expression. Int Immunopharmacol 2009; 9: 433-438.
11) Ishidao T, Kunugita N, Fueta Y, Arashidani K, Hori H. Effects of inhaled 1- bromopropane vapor on rat metabolism. Toxicol Lett 2002; 134: 237-243.
12) Ichihara G, Miller JK, Ziolkowska A, Itohara S, Takeuchi Y. Neurological disorders in three workers exposed to 1-bromopropane. J Occup Health 2002; 44: 1-7.
13) Ichihara G, Li W, Ding X, et al. A survey on exposure level, health status, and biomarkers in workers exposed to 1-bromopropane. Am J Ind Med 2004; 45: 63-75.
14) Li W, Shibata E, Zhou Z, et al. Dose-dependent neurologic abnormalities in workers exposed to 1-bromopropane. J Occup Environ Med 2010; 52: 769-777.
15) Sekiguchi S, Suda M, Zhai YL, Honma T. Effects of 1-bromopropane, 2-bromopropane, and 1,2-dichloropropane on the estrous cycle and ovulation in F344 rats. Toxicol Lett 2002; 126: 41-49.
16) Yamada T, Ichihara G, Wang H, et al. Exposure to 1-bromopropane causes ovarian dysfunction in rats. Toxicol Sci 2003; 71: 96-103.
17) Furuhashi K, Kitoh J, Tsukamura H, et al. Effects of exposure of rat dams to 1-bromopropane during pregnancy and lactation on growth and sexual maturation of their offspring. Toxicology 2006; 224: 219-228.
18) Lau C, Thibodeaux JR, Hanson RG, et al. Exposure to perfluorooctane sulfonate during pregnancy in rat and mouse. II: postnatal evaluation. Toxicological Sci 2003; 74: 382-392.
19) Hori H, Hyakudo T, Oyabu T, Ishimatsu S, Yamato H, Tanaka I. Effects of inhaled methyl bromide gas on the metabolic system and kinetics of bromine ion in rats. J UOEH 2002; 24: 151-160.

E-mail addresses;

yukiko@med.uoeh-u.ac.jp (Yukiko FUETA)

yukos@nihs.go.jp (Yuko SEKINO)

syoshida@ens.tut.ac.jp (Sachiko YOSHIDA)

kanda@nihs.go.jp (Yasunari KANKDA)

susumu@med.uoeh-u.ac.jp (Susumu UENO)

Corresponding author

Susumu UENO

Department of Occupational Toxicology, Institute of Industrial Ecological Sciences, University of Occupational and Environmental Health, Japan

1-1 Iseigaoka, Yahatanishi-ku, Kitakyushu 807-8555, Japan.

Tel: +81-93-691-7404

Fax: +81-93-692-4790

E-mail: susumu@med.uoeh-u.ac.jp

Abstract

Prenatal valproic acid (VPA) exposure is a well-known animal model of autism spectrum disorder (ASD) that produces alterations in embryonic and adult neurogenesis as well as adolescent/adulthood neurobehavioral phenotypes. However, the effects of prenatal VPA exposure on neural network excitability, especially during the synaptogenic period around eye opening, are not fully understood. In this study, we orally administered VPA (300 mg/kg) to pregnant Wistar rats on gestation day 15 and subsequently performed field potential recording in the CA1 area of hippocampal slices obtained from control (saline-exposed) and VPA-exposed rat pups between postnatal day (PND) 13 and PND18. In control slices, we observed an abrupt enhancement of stimulation-dependent responses including population spike (PS) amplitudes and field excitatory postsynaptic potential (fEPSP) slopes at PND16, which coincided with the average day of eye opening. In contrast, VPA-exposed pups exhibited delayed eye opening (PND17) and gradual rather than abrupt increases in PS amplitudes and fEPSP slopes over the duration of the synaptogenic period. We next investigated the involvement of ambient GABA in PS generation using bicuculline methiodide (BMI), a γ-aminobutyric acid type A ($GABA_A$) receptor antagonist. In control slices, BMI enhanced PS amplitudes during PND14–15 (before eye opening) and had little effect

thereafter during PND16–17; a subsequent regression model analysis of BMI ratios (the ratio of PS amplitudes in the presence and absence of BMI) indicated a possible developmental change between these periods. In contrast, almost identical regression models were obtained for BMI ratios during PND14–15 and PND16–17 in the VPA-exposed group, indicating the absence of a developmental change. Our results suggest that prenatal VPA exposure accelerates the development of hippocampal excitability before eye opening. Moreover, our experimental model can be used as a novel approach for the evaluation of developmental neurotoxicity.

Key words:

developmental neurotoxicity; valproic acid; prenatal exposure; hippocampus; slice preparation; electrophysiology

1. Introduction

The impact of exogenous chemical substances on childhood neural development, also known as developmental neurotoxicity, is an important social issue (Andersen et al., 2000; Grandjean and Landrigan, 2006). Valproic acid (VPA) is an antiepileptic drug and mood stabilizer that has been reported to increase the risk of autism spectrum disorders (ASD) in children when women take VPA during early pregnancy (Chomiak et al., 2013). Similarly, rodent models of ASD have been established using prenatal exposure to VPA; in VPA exposure-based models, offspring exhibit autism-like behaviors including impaired social interactions and repetitive behaviors (Markram et al., 2008; Rodier et al., 1997; Roullet et al., 2013; Schneider and Przewlocki, 2005). In addition to neurobehavioral phenotypes, ASD model animals exhibit alterations in embryonic and adult neurogenesis (Juliandi et al., 2015). However, it is not well known whether prenatal exposure to VPA also affects neurogenesis in developmental stages occurring prior to adulthood, especially during the synaptogenic period.

Neural activity is a critical regulator of neural network development. It was recently demonstrated that spine density is remarkably increased in the hippocampal CA1 area of mice between postnatal day (PND) 11 and PND21, i.e. during the synaptogenic period (Johnson-Venkatesh et al., 2015). Interestingly, when intrinsic neural activity was

suppressed by overexpression of Kir2.1, an inwardly rectifying K^+ channel, increases in spine density during the synaptogenic period were abolished. Thus, neural network activity in the hippocampal CA1 area is necessary for healthy neural development during the synaptogenic period including around eye opening.

Chloride conductance due to ambient concentrations of GABA (γ-aminobutyric acid) also plays a role in regulating neural network excitability during postnatal neural development (Cellot and Cherubini, 2013; Kilb et al., 2013). Ambient GABA originates from the spillover of neurotransmitter escaping the synaptic cleft and from astrocytes via a non-vesicular Ca^{2+}-independent process and mediates tonic inhibition via extrasynaptic $GABA_A$ receptors. However, there is little evidence demonstrating effects of prenatal exposure to toxicants including VPA on ambient GABA-mediated inhibition of neural network excitability.

In the present study, we used a model of prenatal VPA exposure and evaluated effects on neural network activity in the hippocampal CA1 area during the synaptogenic period using hippocampal slices from PND13–18 rat pups. We not only observed the ability of prenatal VPA exposure to abolish development-associated enhancements in stimulation-dependent neural responses, but also confirmed the ability of prenatal exposure to influence ambient GABA-mediated inhibition even prior to eye opening.

2. Material and Methods

2.1 Animals

Adult Wistar/ST rats were purchased from Japan SLC *Inc*. (Japan). Rats were housed in plastic cages on paper chip bedding (ALPHA-dri, Shepherd Specialty Papers, USA) and maintained on a 12-h light/dark cycle (light period: 07:00–19:00) in a room with controlled temperature (23 ± 1°C) and relative humidity (50 ± 15%). Animals were given free access to food (CE2, CLEA Japan Inc., Japan) and filtered water (TCW-PPS filter, Advantech Co., LTD., Japan) dispensed in glass water supply bottles.

The proestrus stage was verified with an impedance checker (MK-10B, Muromachi Kikai Co., Ltd., Japan). When the observed impedance was > 3 kΩ female rats were provided with a male rat for mating. The presence of a vaginal plug or sperm in the vaginal smear the following morning confirmed coition, and it was regarded as gestation day (GD) “zero” (Fig. 1). Pregnant rats were randomly divided into two groups: a control group and a VPA exposure group.

VPA was purchased from Wako Pure Chemical Industries, Ltd. (Japan), dissolved in physiological saline (Otsuka Pharmaceutical Co., Ltd, Japan), and orally administered to dams (300 mg/kg) on GD15 under 5% isoflurane gas anesthesia (Pfizer Japan Inc., Japan).

All dams gave birth on GD21, and the date of birth was defined as PND0. If there were more than 10 pups in a litter, the litter size was adjusted to 10 pups on PND1. Litters of less than 10 pups were not adjusted. All pups were housed with their dams during the lactation period. Rat pup body weights were measured on PND1, PND7, PND14, and PND21. The day of eye opening was determined by checking the eyes of pups at 14:00 on each day from PND15–18.

For the electrophysiological study, the control group included pups from 16 control dams and the VPA-exposed group included pups from 17 VPA-exposed dams. All studies were approved by the Ethics Committee on Animal Care and Experimentation and performed in accordance with the guidelines of the University of Occupational and Environmental Health, Japan.

2.2 Slice preparation and recordings

Hippocampal slices (600 μm thickness) were prepared from male pups on each postnatal day between PND13–18 as previously described (Fueta et al., 2004; Fueta et al., 2002). Slices were perfused with artificial cerebrospinal fluid (ACSF) containing 124 mM NaCl, 2 mM KCl, 2 mM $MgSO_4$, 2 mM $CaCl_2$, 1.25 mM KH_2PO_4, 26 mM $NaHCO_3$, and 10 mM glucose; saturated with an O_2 95%/CO_2 5% gas mixture; and

stored in a thermostatic bath (27.6°C). The perfusion rate of ACSF was 1 ml/min for all experiments.

Population spikes (PSs) and field excitatory synaptic potentials (fEPSPs) were simultaneously recorded from the CA1 area of hippocampal slices using glass microelectrodes (Fig. 2A). For slices obtained during the period from PND13–15, PSs were recorded from the area between the pyramidal cell layer and the alveus. The recording positions for PSs and fEPSPs were similar between the control and VPA-exposed groups. Bipolar stimulation electrodes made of stainless wires (50 μm in diameter) were placed on Shaffer collateral/commissural fibers at a distance of about 250 μm from the fEPSP recording electrodes. Stimulation-response relationships were observed with stimulation intensities from 10–600 μA. The stimulation interval was 2 min in order to avoid the measurement of overlapping stimulation effects.

Between PND14–17, experiments evaluated the effects of bicuculline methiodide (BMI, Tocris Bioscience, U.K.), a $GABA_A$ receptor antagonist, on the generation of PSs. Average PS amplitudes in response to 600 μA stimulation were recorded in triplicate (with 2-min intervals) in the absence and presence of BMI; after PS measurements in the absence of BMI, slices were perfused with ACSF containing BMI (1 μM) for 10 min and subsequently tested. A total of 3–4 slices per rat pup were tested.

2.3 Distribution analysis

Histogram distribution and nonlinear regression analyses of BMI ratios (PS amplitude in the presence of BMI divided by that in the absence of BMI) were conducted using GraphPad Prism software (GraphPad Software, Inc., USA).

2.4 Statistical analysis

Litter sizes and sex ratios as well as pup body weights and the day of eye opening are expressed as the mean ± standard deviation (SD). Electrophysiological results are expressed as the mean ± standard error of mean (SEM). Statistical differences between the control and VPA-exposed groups were determined using two-sided Student's *t*-tests or Mann-Whitney U tests at a significance level of $P < 0.05$.

3. Results

For the purpose of our study, the time of eye opening in our rat models was needed to confirm. In consequence, the average day of eye opening was significantly delayed in the VPA-exposed group compared to the control group ($P<0.01$, Table 1). We also examined general toxicity induced by one-time prenatal VPA exposure at GD15, and found that there were no significant differences between the control and VPA-exposed groups in terms of litter size, litter sex ratio, or changes in pup body weight. Moreover, the number of pups that died before experimentation or weaning was not significantly different between groups (control group, 2 of 206 pups; VPA-exposed group, 4 of 195 pups).

Next, to investigate neural network excitability during the synaptogenic period, we studied stimulation-response (S/R) relationships for fEPSP slopes and PS amplitudes using hippocampal slice preparations, in which the cytoarchitecture and synaptic circuits of the hippocampus are largely retained. S/R relationships exhibited two different stages; similar degrees of stimulation-dependent responses were observed in control pups between PND13–15. However, responses (fEPSP slopes and PS amplitudes) were suddenly augmented on PND16, which seemed to correspond with eye opening. Responses were maintained at an enhanced level for fEPSP slopes and

slightly enhanced for PS amplitudes between PND17–18 (Fig. 2B, C).

In contrast, a gradual enhancement of S/R relationships was observed between PND13–18 in the VPA-exposed group, and did appear to correspond with eye opening. Therefore, we reanalyzed fEPSP slopes and PS amplitudes in response to a stimulation intensity of 600 μA, which evoked the maximal responses. PS amplitudes obtained from the control group showed an abrupt increase between PND15–16, whereas those from the VPA-exposed group again demonstrated a gradual increase over the period examined, with significant differences at PND14 and PND15 compared to the control group. A similar but smaller developmental change was observed in the fEPSP slope, with a significant difference between the control and VPA-exposed groups on PND15 (Fig. 3).

Next we investigated the effect of BMI on PS generation in order to elucidate the role of ambient GABA in postnatal PS generation. Fig. 4 shows the effect of BMI on PS amplitudes in the control group before eye opening (PND14–15) and after eye opening (PND16–17). PS amplitudes were enhanced in the presence of BMI during PND14–15 (Fig. 4A, left), but this enhancement was attenuated during PND16–17 (Fig. 4B, left). The mean BMI ratios (ratio of the PS amplitude in the presence of BMI to that in the absence of BMI) were 1.80 ± 0.17 (n = 13) for PND14–15 and 1.14 ± 0.04 (n = 10)

for PND16–17. Histograms of BMI ratios (Figs. 4A and 4B, right) and nonlinear regression analyses revealed a clear developmental change in the probability distribution of BMI ratios for PS amplitudes (Fig. 6, left).

In contrast, for the VPA-exposed group, PS amplitudes generated in the presence of BMI showed small or little increases during both the PND14–15 and PND16–17 periods (Figs. 5A and 5B, left). The mean BMI ratios were 1.34 ± 0.14 (n = 17) for PND14–15 and 1.14 ± 0.05 (n = 17) for PND16–17. Moreover, histograms of BMI ratios and nonlinear regression analyses (Figs. 5A and 5B, right) were almost identical between the PND14–15 and PND16–17 periods, suggesting attenuation of the developmental change observed in the control group (Fig. 6, right). We also investigated the responses to BMI for fEPSP slopes, but minimal (non-significant) BMI responses and alterations in developmental change were observed.

4. Discussion

In this study, we investigated the effect of prenatal VPA exposure on the development of neural network activity in the hippocampal CA1 area during the synaptogenic period, including during the period of eye opening. A single dose of VPA (300 mg/kg) was orally administered to dams on GD15 and was not noted to affect dam maternal behavior or fetal/neonatal mortality. In animal models of ASD, VPA is often administered repeatedly or earlier than GD11.5 prior to closure of the neural tube (Rodier et al., 1997). Therefore, the most effective period for observing the effects of prenatal VPA exposure as it relates to ASD may be earlier than GD15.

Brain slice preparation is a well-known laboratory technique for electrophysiology and pharmacology research. Since local neuronal circuits remain intact in brain slices, this neurophysiological preparation is useful for studying neurotoxicity (Fountain et al., 1992) as well as the specific effects of neurotoxic agents on synaptic transmission and plasticity (Varela et al., 2012; Wiegand and Altmann, 1994). The electrophysiological strategy used in the present work has been previously implemented to study the effects of prenatal/perinatal ethanol exposure (Puglia and Valenzuela, 2010), lead (Carpenter et al., 2002; Sui et al., 2000), polychlorinated biphenyl exposure (Altmann et al., 1998; Carpenter et al., 2002; Kim and Pessah, 2011), and toluene exposure (Chen et al., 2011).

Thus, we deemed the present model to be useful for evaluating excitatory/inhibitory function and developmental neurotoxicity after VPA exposure.

Our first main finding was that stimulation-dependent responses for fEPSPs and PSs in the hippocampal CA1 area showed two different periods of development in normal pups; one from PND13–15 before eye opening on PND16, and another after eye opening from PND16–18. S/R relationships for neural excitability in the CA1 area exhibited drastic enhancements after eye opening. Alternatively, we did not observe clear discrimination between stimulation-dependent responses before and after eye opening in the VPA-exposed group; enhancements in stimulation-dependent CA1 excitability were observed on PND14 and/or PND15 in the VPA-exposed group compared to the control group, and gradual changes were observed in the subsequent postnatal days. In other words, prenatal VPA exposure appeared to accelerate developmental changes in neural excitability that otherwise appeared in association with eye opening in healthy pups.

Ambient GABA is a critical factor that regulates neural network excitability. Therefore, we also investigated the involvement of ambient GABA in PS generation using BMI, a $GABA_A$ receptor antagonist. On PND14 and PND15 before eye opening, PS amplitudes evoked in the presence of BMI were greater than those in the control

condition, suggesting a possible role for PS inhibition by ambient GABA. On PND 16 and PND17 on or after eye opening, BMI had little effect on PS amplitudes. These results indicated that ambient GABA was involved in suppressing neural excitability in the CA1 area during neural development prior to eye opening. The centering of this developmental change around the event of eye opening is consistent with a previous report that demonstrated notable increases in spine density on PND15 (Johnson-Venkatesh et al., 2015).

In contrast, BMI had little effect on PS generation before or after eye opening in the VPA-exposed group. Indeed, nonlinear regression models of distribution histograms obtained during PND14–15 and PND16–17 were virtually identical. These results suggest that prenatal exposure to VPA may eliminate ambient GABA suppression of neural excitability prior to eye opening, and are consistent with the observation of enhanced stimulation-dependent responses at PND14 and PND15 in the VPA-exposed group. Accordingly, prenatal exposure to VPA may accelerate neural development in CA1 area during the synaptogenic period.

Ambient GABA-mediated tonic inhibition in hippocampal neurons is synergistically modulated by two GABA transporters (GATs): GAT-1 located on presynaptic membranes and GAT-3 on astrocytes (Egawa and Fukuda, 2013; Kersante et al., 2013).

GAT-1 is predominantly responsible for GABA reuptake under resting conditions; alternatively, GAT-3 plays an important role in controlling hippocampal cell excitability during neural activation (Kersante et al., 2013). Therefore, our findings raise the question of whether developmental changes in evoked PS responses to BMI were related to alterations in the expression and/or function of GATs in the CA1 area during development. Further investigations are in progress to address this issue.

Among several hypothetical mechanisms underlying ASD, the disruption of excitation/inhibition (E/I) balance in neuronal circuits has been proposed as a unifying explanation for the complexity and diversity of ASD presentations arising from genetic (Gkogkas et al., 2013; Gogolla et al., 2009; Rubenstein, 2010; Rubenstein and Merzenich, 2003) and environmental factors (Rubenstein and Merzenich, 2003). Although the precise mechanisms of altered E/I balance after prenatal exposure to VPA have not been fully elucidated, this effect has been replicated in several rodent studies. Rinaldi et al. showed that prenatal injection of VPA (500 mg/kg, intraperitoneally) increased N-methyl-D-aspartate (NMDA) receptor subunit protein expression in the whole brains of pups and enhanced NMDA receptor-mediated synaptic currents in neocortical slices obtained from pups during PND12–16 (Rinaldi et al., 2007). These authors further reported that prenatal VPA exposure induced local circuits

hyperconnectivity and enhancements in both excitatory and inhibitory systems in the sensory cortex (Rinaldi et al., 2008). Banerjee et al. reported that a single intraperitoneal injection of VPA (600 mg/kg) at GD11.5 impaired postnatal GABAergic synaptic transmission using slice preparations of the auditory cortex from PND23–45 offspring (Banerjee et al., 2013).

To the best of our knowledge, this is the first report to describe a possible role for GABA-mediated inhibition in the development of evoked PSs during the synaptogenic period around eye opening. Moreover, our data suggest that prenatal exposure to VPA and potentially other developmental neurotoxicants at specific points of the gestation period can accelerate this developmental change. Changes in PS amplitudes evoked from hippocampal slices during prenatal development, especially in the presence of BMI, may be useful as an index for the normal development of neural circuits; to this end, our assay may have utility for screening other candidate neurodevelopmental toxicants. Studies with other known toxicants including organometallic compounds and pesticides are in progress to determine whether similar developmental alterations can be observed using the current experimental approach.

5. Conclusions

In summary, we report that one-time prenatal exposure to VPA at GD 15 produced enhancements in stimulation-dependent responses for fEPSP slopes and PS amplitudes in the CA1 area of offspring, and moreover altered offspring PS amplitude responses to BMI. Taken together, prenatal VPA exposure may transiently alter E/I balance, resulting in the acceleration of neural development before eye opening. This effect corresponds with the hypothetical mechanisms underlying ASD; that is, the disruption of E/I balance in developing brain circuits. Although further investigations are required, our results provide an alternative approach for the evaluation of developmental neurotoxicity.

Funding information

This study was supported by Health and Labor Sciences Research Grants of the Ministry of Health, Labour and Welfare in Japan.

Conflict of interest statement

The authors declare that there is no conflict of interest.

Acknowledgement

The authors would like to thank Kaoru Sato, Seiichi Ishida, and Daiju Yamazaki for helpful discussion.

Table 1. Litter sizes and sex ratios as well as pup weight gain and the day of eye opening for the control and VPA-exposed groups.

	control		VPA-exposed	
litter size of dams	12.0 ± 2.0	(21)	13.0 ± 3.0	(20)
sex ratio of pups (male/female, %)	48.5 ± 0.1	(21)	49.5 ± 0.1	(20)
male pup weight (g)				
PND1	6.0 ± 0.6	(55)	5.7 ± 0.4	(53)
PND7	14.9 ± 1.6	(54)	14.1 ± 1.3	(47)
PND14	30.1 ± 1.9	(47)	28.6 ± 2.2	(45)
PND21	50.2 ± 4.3	(20)	46.9 ± 3.7	(23)
Day of eye opening	16.5 ± 0.6	(67)	17.3 ± 0.7**	(77)

Data represent the mean ± standard deviation. Numbers in parentheses are total numbers of dams/pups examined. **P<0.01, compared to the control. Abbreviations: PND, postnatal day; VPA, valproic acid.

References

Altmann, L., Lilienthal, H., Hany, J., Wiegand, H., 1998. Inhibition of long-term potentiation in developing rat visual cortex but not hippocampus by in utero exposure to polychlorinated biphenyls. Brain Res. Dev. Brain Res. 110, 257-260.

Andersen, H.R., Nielsen, J.B., Grandjean, P., 2000. Toxicologic evidence of developmental neurotoxicity of environmental chemicals. Toxicology 144, 121–127.

Banerjee, A., Garcia-Oscos, F., Roychowdhury, S., Galindo, L.C., Hall, S., Kilgard, M.P., Atzori, M., 2013. Impairment of cortical GABAergic synaptic transmission in an environmental rat model of autism. Int. J. Neuropsychopharmacol. 16, 1309–1318.

Carpenter, D.O., Hussain, R.J., Berger, D.F., Lombardo, J.P., Park, H.Y., 2002. Electrophysiologic and behavioral effects of perinatal and acute exposure of rats to lead and polychlorinated biphenyls. Environ. Health Perspect. 110 Suppl 3, 377–386.

Cellot, G., Cherubini, E., 2013. Functional role of ambient GABA in refining neuronal circuits early in postnatal development. Front. Neural Circuits 7, 136.

Chen, H.H., Lin, Y.R., Chan, M.H., 2011. Toluene exposure during brain growth spurt and adolescence produces differential effects on N-methyl-D-aspartate

receptor-mediated currents in rat hippocampus. Toxicol. Lett. 205, 336–340.

Chomiak, T., Turner, N., Hu, B., 2013. What We Have Learned about Autism Spectrum Disorder from Valproic Acid. Patholog. Res. Int. 2013, 712758.

Egawa, K., Fukuda, A., 2013. Pathophysiological power of improper tonic GABA(A) conductances in mature and immature models. Front. Neural Circuits 7, 170.

Fountain, S.B., Ting, Y.L., Teyler, T.J., 1992. The in vitro hippocampal slice preparation as a screen for neurotoxicity. Toxicol. In Vitro 6, 77–87.

Fueta, Y., Fukuda, T., Ishidao, T., Hori, H., 2004. Electrophysiology and immunohistochemistry in the hippocampal ca1 and the dentate gyrus of rats chronically exposed to 1-bromopropane, a substitute for specific chlorofluorocarbons. Neuroscience 124, 593–603.

Fueta, Y., Ishidao, T., Arashidani, K., Endo, Y., Hori, H., 2002. Hyperexcitability of the Hippocampal CA1 and the Dentate Gyrus in Rats Subchronically Exposed to a Substitute for Chlorofluorocarbons, 1-Bromopropane Vapor. J. Occup. Health 44, 156–165.

Gkogkas, C.G., Khoutorsky, A., Ran, I., Rampakakis, E., Nevarko, T., Weatherill, D.B., Vasuta, C., Yee, S., Truitt, M., Dallaire, P., Major, F., Lasko, P., Ruggero, D., Nader, K., Lacaille, J.C., Sonenberg, N., 2013. Autism-related deficits via dysregulated

eIF4E-dependent translational control. Nature 493, 371–377.

Gogolla, N., Leblanc, J.J., Quast, K.B., Sudhof, T.C., Fagiolini, M., Hensch, T.K., 2009. Common circuit defect of excitatory-inhibitory balance in mouse models of autism. J. Neurodev. Disord. 1, 172–181.

Grandjean, P., Landrigan, P.J., 2006. Developmental neurotoxicity of industrial chemicals. Lancet 368, 2167–2178.

Johnson-Venkatesh, E.M., Khan, M.N., Murphy, G.G., Sutton, M.A., Umemori, H., 2015. Excitability governs neural development in a hippocampal region-specific manner. Development 142, 3879–3891.

Juliandi, B., Tanemura, K., Igarashi, K., Tominaga, T., Furukawa, Y., Otsuka, M., Moriyama, N., Ikegami, D., Abematsu, M., Sanosaka, T., Tsujimura, K., Narita, M., Kanno, J., Nakashima, K., 2015. Reduced Adult Hippocampal Neurogenesis and Cognitive Impairments following Prenatal Treatment of the Antiepileptic Drug Valproic Acid. Stem Cell Reports 5, 996–1009.

Kersante, F., Rowley, S.C., Pavlov, I., Gutierrez-Mecinas, M., Semyanov, A., Reul, J.M., Walker, M.C., Linthorst, A.C., 2013. A functional role for both -aminobutyric acid (GABA) transporter-1 and GABA transporter-3 in the modulation of extracellular GABA and GABAergic tonic conductances in the rat hippocampus. J. Physiol. 591,

2429–2441.

Kilb, W., Kirischuk, S., Luhmann, H.J., 2013. Role of tonic GABAergic currents during pre- and early postnatal rodent development. Front. Neural Circuits 7, 139.

Kim, K.H., Pessah, I.N., 2011. Perinatal exposure to environmental polychlorinated biphenyls sensitizes hippocampus to excitotoxicity ex vivo. Neurotoxicology 32, 981–985.

Markram, K., Rinaldi, T., La Mendola, D., Sandi, C., Markram, H., 2008. Abnormal fear conditioning and amygdala processing in an animal model of autism. Neuropsychopharmacology 33, 901–912.

Puglia, M.P., Valenzuela, C.F., 2010. Repeated third trimester-equivalent ethanol exposure inhibits long-term potentiation in the hippocampal CA1 region of neonatal rats. Alcohol 44, 283–290.

Rinaldi, T., Kulangara, K., Antoniello, K., Markram, H., 2007. Elevated NMDA receptor levels and enhanced postsynaptic long-term potentiation induced by prenatal exposure to valproic acid. Proc. Natl. Acad. Sci. U. S. A. 104, 13501–13506.

Rinaldi, T., Perrodin, C., Markram, H., 2008. Hyper-connectivity and hyper-plasticity in the medial prefrontal cortex in the valproic Acid animal model of autism. Front.

Neural Circuits 2, 4.

Rodier, P.M., Ingram, J.L., Tisdale, B., Croog, V.J., 1997. Linking etiologies in humans and animal models: studies of autism. Reprod. Toxicol. 11, 417–422.

Roullet, F.I., Lai, J.K., Foster, J.A., 2013. In utero exposure to valproic acid and autism--a current review of clinical and animal studies. Neurotoxicol. Teratol. 36, 47–56.

Rubenstein, J.L., 2010. Three hypotheses for developmental defects that may underlie some forms of autism spectrum disorder. Curr. Opin. Neurol. 23, 118–123.

Rubenstein, J.L., Merzenich, M.M., 2003. Model of autism: increased ratio of excitation/inhibition in key neural systems. Genes Brain. Behav. 2, 255–267.

Schneider, T., Przewlocki, R., 2005. Behavioral alterations in rats prenatally exposed to valproic acid: animal model of autism. Neuropsychopharmacology 30, 80–89.

Sui, L., Ge, S.Y., Ruan, D.Y., Chen, J.T., Xu, Y.Z., Wang, M., 2000. Age-related impairment of long-term depression in area CA1 and dentate gyrus of rat hippocampus following developmental lead exposure in vitro. Neurotoxicol. Teratol. 22, 381–387.

Varela, C., Llano, D.A., Theyel, B.B., 2012. An Introduction to In Vitro Slice Approaches for the Study of Neuronal Circuitry, in: Fellin, T., Halassa, M. (Eds.),

Neuronal Network Analysis: Concepts and Experimental Approaches. Humana Press, Totowa, pp. 103–125.

Wiegand, H., Altmann, L., 1994. Neurophysiological aspects of hippocampal neurotoxicity. Neurotoxicology 15, 451–458

Figure legends

Figure 1. Scheme of the experimental design.

Figure 2. Stimulation/response (S/R) relationships for population spike (PS) amplitudes and field excitatory postsynaptic potential (fEPSP) slopes recorded from the hippocampal CA1 area of rats that were prenatally exposed to valproic acid (VPA). (A) Illustration depicting the procedure of fEPSP and PS recordings from CA1. Responses were evoked with a stimulating electrode placed in the stratum radiatum. Thick lines on the left traces indicate how measurements of fEPSP slopes and PS amplitudes were taken. (B, C) In control rats (left graphs), the S/R relationships for both fEPSP slopes and PS amplitudes were enhanced between PND15–16. Data were collected from 14–19 slices obtained from pups of 4–5 different litters. In VPA-exposed rats (right graphs), these relationships were gradually enhanced between PND13–18. Data were gathered from 10–17 slices obtained from pups of 5–6 different litters. The x-axis is stimulation intensity and the y-axis is size of the fEPSP slope or PS amplitude. Data represent the mean ± standard error of the mean.

Figure 3. Developmental changes in population spike (PS) amplitudes and field

excitatory postsynaptic potentials (fEPSPs) slopes in the control and valproic acid (VPA)-exposed groups. One-time prenatal exposure to VPA (300 mg/kg) led to postnatal increases in PS amplitude and fEPSP slope during PND14–15 and PND15, respectively. There were no between-group differences in excitability between PND16–18. The stimulation intensity was 600 μA. * indicates $P < 0.05$ using a Student's *t*-test. ++ indicates $P < 0.01$ using a Mann-Whitney U test.

Figure 4. Development-associated changes in population spike (PS) amplitude responses to BMI in the control group. (A) At PND14–15, application of the $GABA_A$ receptor antagonist BMI to hippocampal slices during recording remarkably increased PS amplitudes; the mean BMI ratio was 1.80 (95% confidence interval = 1.44–2.16). (B) Increased PS amplitudes in response to BMI application were not observed at PND16–17; the mean ratio was 1.14 (95% confidence interval = 1.04–1.24).

Figure 5. Development-associated changes in population spike (PS) amplitude responses to BMI in the valproic acid (VPA)-exposed group. Hippocampal slices from the VPA-exposed group were virtually insensitive to BMI during both the PND14–15 (A) and PND16–17 (B) periods; the mean BMI ratios were 1.34 (95% confidence

interval = 1.04–1.64) and 1.14 (95% confidence interval = 1.04–1.25), respectively.

Figure 6. Developmental alterations in nonlinear regression models of BMI ratios for population spike (PS) responses. Data from right figure panels of 4 and 5 were re-plotted and summarized for the control (left panel) and VPA-exposed groups (right panel).

Fig.1

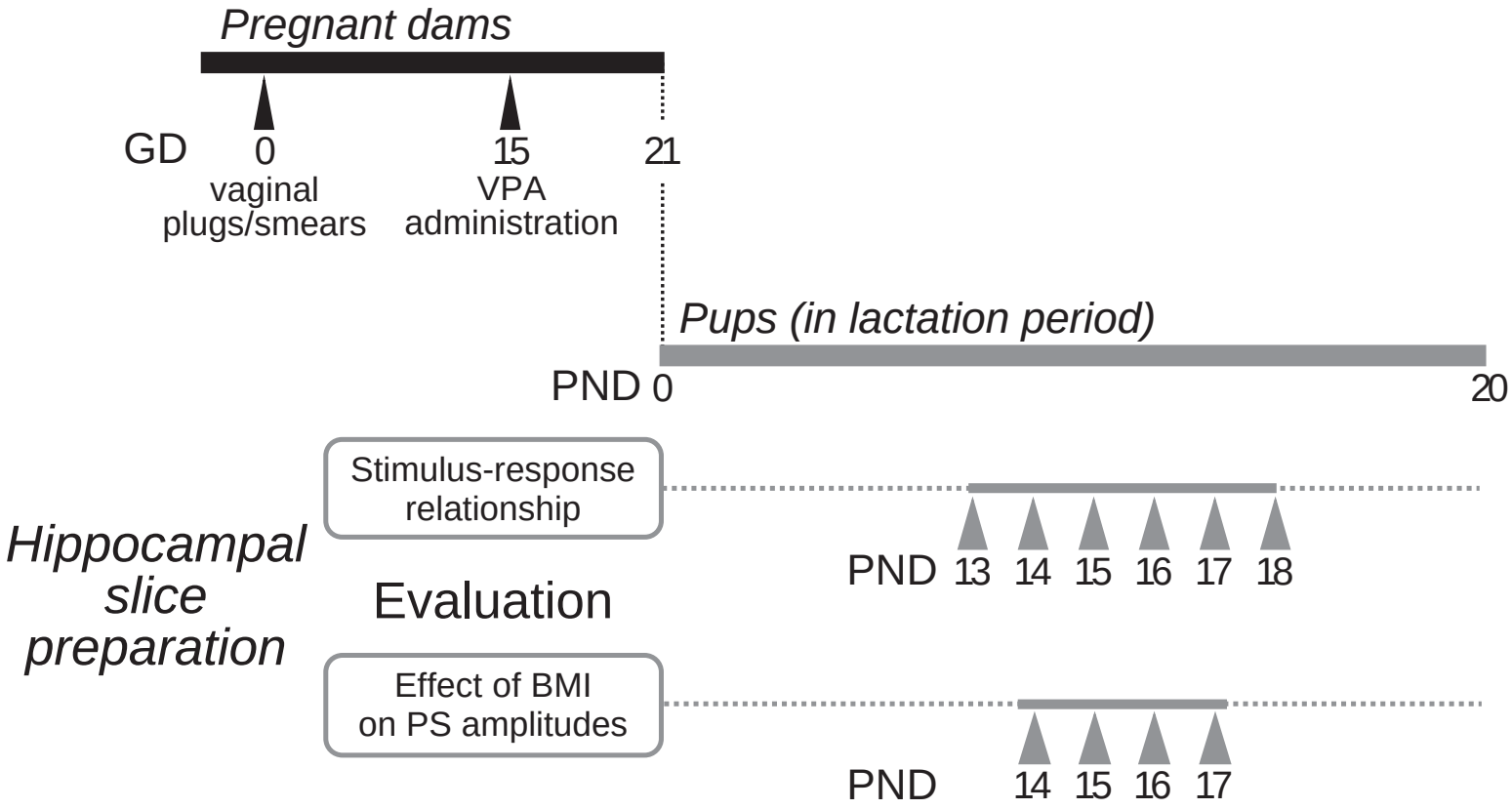
Pregnant dams
GD
0
vaginal plugs/smears
15
VPA administration
21
Pups (in lactation period)
PND 0
20
Hippocampal slice preparation
Stimulus-response relationship
PND 13 14 15 16 17 18
Evaluation
Effect of BMI on PS amplitudes
PND 14 15 16 17

Fig.2

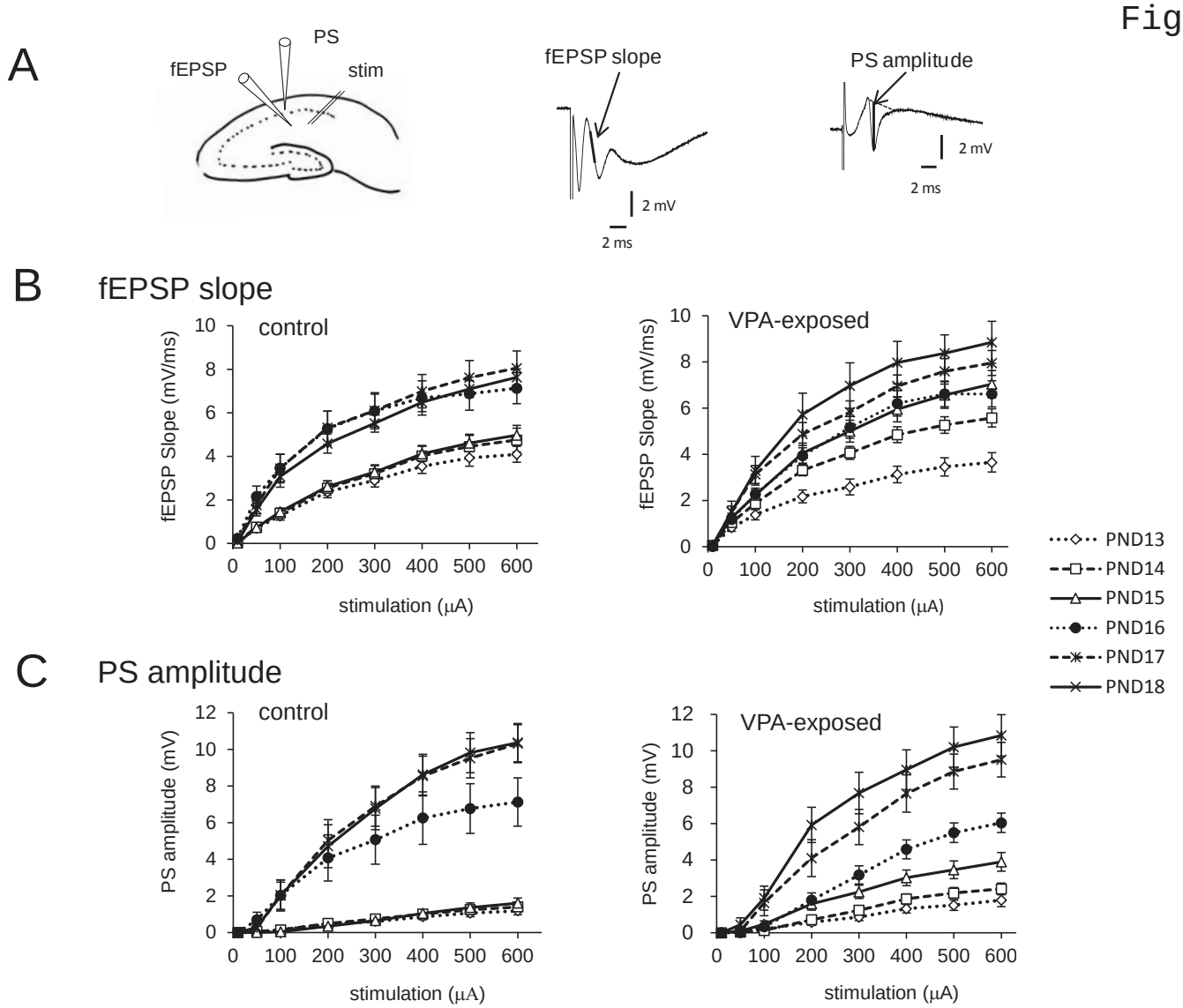
A
PS
fEPSP
stim
fEPSP slope
2 mV
2 ms
PS amplitude
2 mV
2 ms
B
fEPSP slope
control
VPA-exposed
fEPSP Slope (mV/ms)
stimulation (μA)
PND13
PND14
PND15
PND16
PND17
PND18
C
PS amplitude
control
VPA-exposed
PS amplitude (mV)
stimulation (μA)

Fig.3

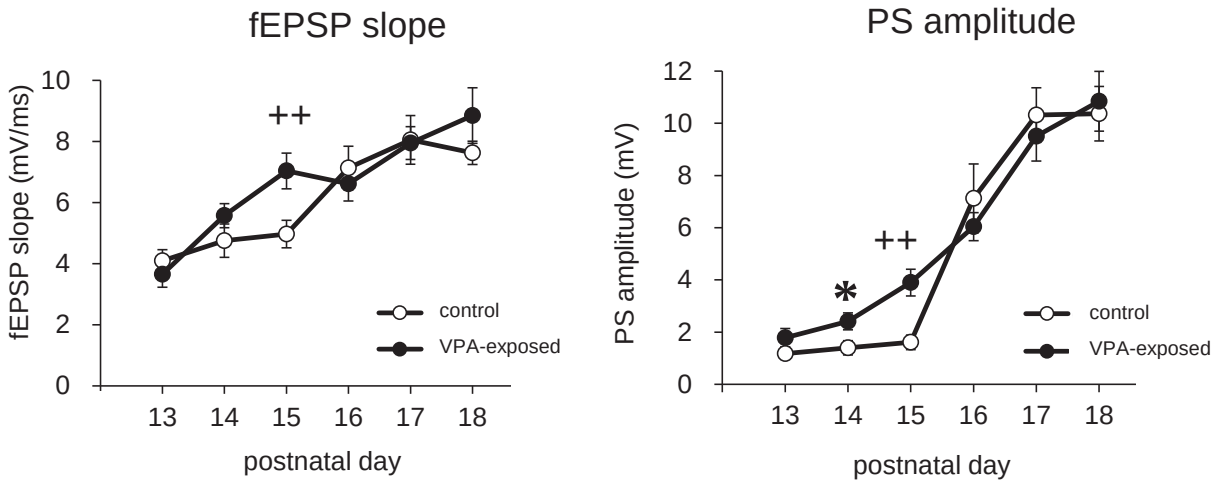
fEPSP slope
fEPSP slope (mV/ms)
0
2
4
6
8
10
++
control
VPA-exposed
13
14
15
16
17
18
postnatal day
PS amplitude
PS amplitude (mV)
0
2
4
6
8
10
12
*
++
control
VPA-exposed
13
14
15
16
17
18
postnatal day

Fig.4

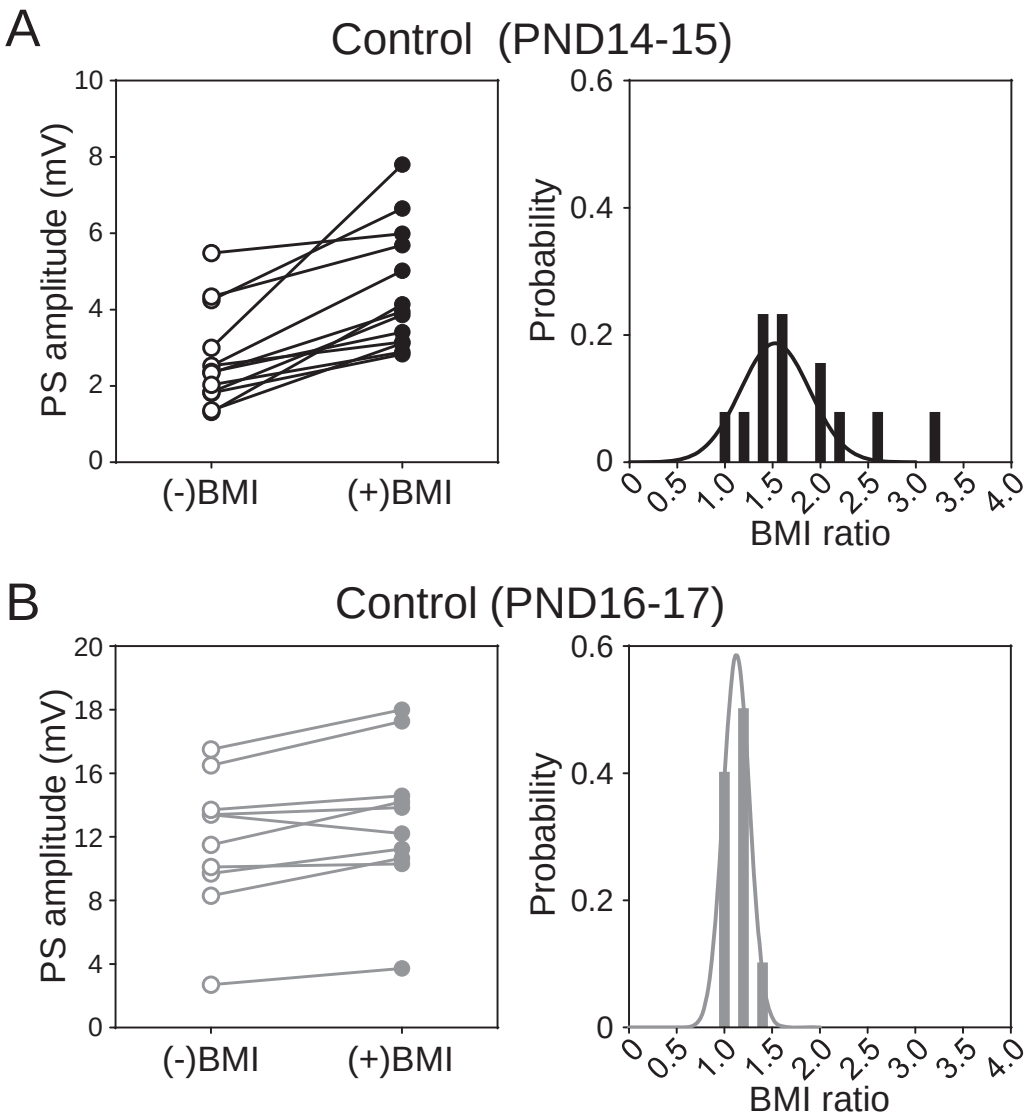
A
Control (PND14-15)
PS amplitude (mV)
10
8
6
4
2
0
(-)BMI
(+)BMI
Probability
0.6
0.4
0.2
0
0
0.5
1.0
1.5
2.0
2.5
3.0
3.5
4.0
BMI ratio
B
Control (PND16-17)
PS amplitude (mV)
20
18
16
12
8
4
0
(-)BMI
(+)BMI
Probability
0.6
0.4
0.2
0
0
0.5
1.0
1.5
2.0
2.5
3.0
3.5
4.0
BMI ratio

Fig.5

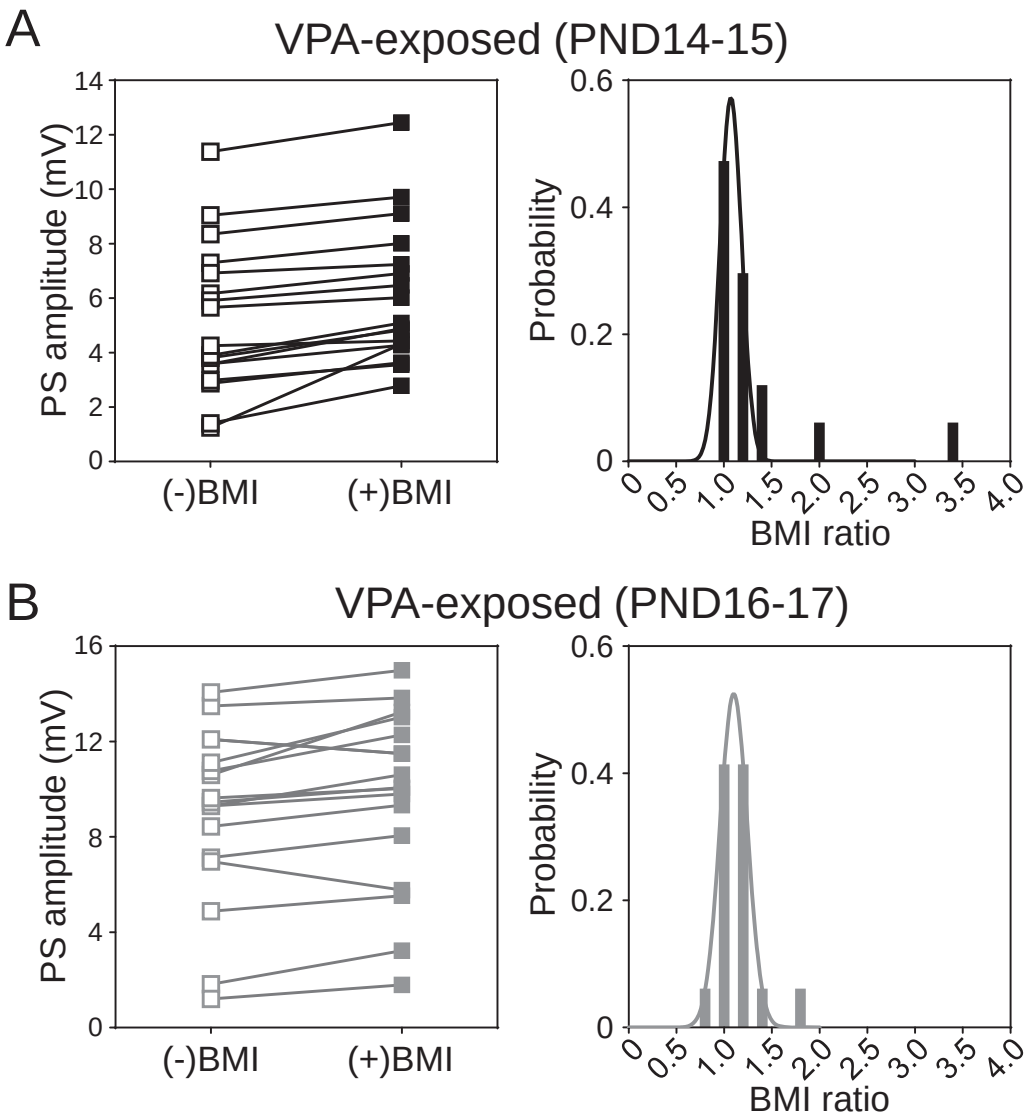
A
VPA-exposed (PND14-15)
PS amplitude (mV)
14
12
10
8
6
4
2
0
(-)BMI
(+)BMI
Probability
0.6
0.4
0.2
0
0
0.5
1.0
1.5
2.0
2.5
3.0
3.5
4.0
BMI ratio
B
VPA-exposed (PND16-17)
PS amplitude (mV)
16
12
8
4
0
(-)BMI
(+)BMI
Probability
0.6
0.4
0.2
0
0
0.5
1.0
1.5
2.0
2.5
3.0
3.5
4.0
BMI ratio

Fig.6

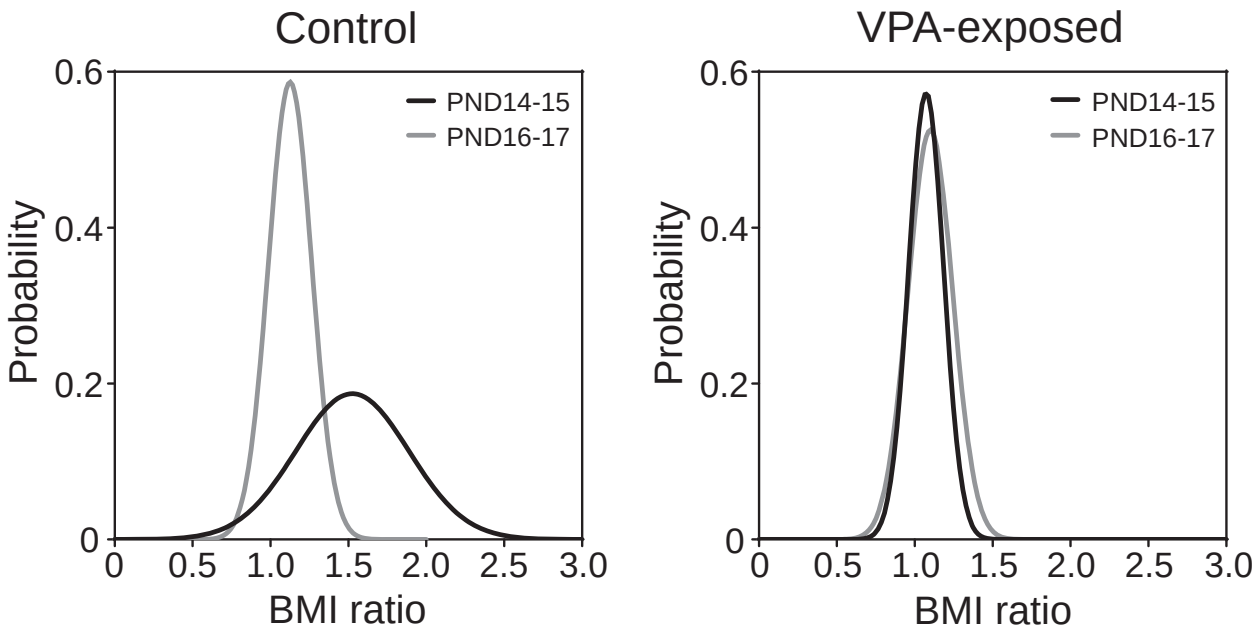
Control
VPA-exposed
PND14-15
PND16-17
Probability
BMI ratio
0
0.2
0.4
0.6
0.5
1.0
1.5
2.0
2.5
3.0

Brief Report

Prenatal Exposure to 1-Bromopropane Causes Delayed Adverse Effects on Hippocampal Neuronal Excitability in the CA1 Subfield of Rat Offspring

Yukiko Fueta[1,*], Toru Ishidao[1], Susumu Ueno[2], Yasuhiro Yoshida[3], Yasunari Kanda[4], Hajime Hori[1]

[1]Department of Environmental Management and Control, School of Health Sciences, University of Occupational and Environmental Health, Kitakyushu, Japan

[2]Department of Occupational Toxicology, University of Occupational and Environmental Health, Kitakyushu, Japan

[3]Department of Immunology and Parasitology, School of Medicine, University of Occupational and Environmental Health, Kitakyushu, Japan

[4]Division of Pharmacology, National Institute of Health Sciences, Tokyo, Japan

*Corresponding Author: Yukiko Fueta, Department of Environmental Management, School of Health Sciences, University of Occupational and Environmental Health, Yahatanishi-ku, Kitakyushu 807-8555, Japan. Tel: +81-93-603-1611. Fax: +81-93-691-2694. E-mail: yukiko@med.uoeh-u.ac.jp.

Running title: Delayed Neurotoxicity in Rats Prenatally Exposed to 10-BP

Number of words in the abstract: 195

Number of words in the text: 2234

Number of figures: 2

Field: Toxicology

Abstract

Objectives: Neurotoxicity of 1-bromopropane (1-BP) has been reported in occupational exposure, but whether the chemical exerts developmental neurotoxicity is unknown. We studied the effects of prenatal 1-BP exposure on neuronal excitability in rat offspring. **Methods:** We exposed dams to 1-BP (700 ppm, 6 h a day for 20 days), and examined hippocampal slices obtained from the offspring at 2, 5, 8, and 13 weeks of age. We measured the stimulation/response (S/R) relationship and paired-pulse ratios (PPRs) of the population spike (PS) at the interpulse intervals (IPIs) of 5 and 10 ms in the CA1 subfield. **Results:** Prenatal 1-BP exposure enhanced S/R relationships of PS at 2 weeks of age; however, the enhancement diminished at 5 weeks of age until it reached control levels. Prenatal 1-BP exposure decreased PPRs of PS at 2 weeks of age. After sexual maturation, however, the PPRs of PS increased at a 50-ms IPI in male rats aged 8 and 13 weeks, and at 50- and 100-ms IPIs in female rats aged 13 weeks. **Conclusions:** Our findings indicate that prenatal 1-BP exposure in dams can cause delayed adverse effects on excitability of pyramidal cells in the hippocampal CA1 subfield of offspring.

Keywords: 1-Bromopropane, Delayed adverse effect, Electrophysiology, Excitability, Prenatal exposure, Rat hippocampal slices

Introduction

Social concerns have been raised regarding the developmental neurotoxicity of prenatally absorbed environmental chemicals, which may exert delayed adverse effects on brain function after birth. It is now recognized that some industrial chemicals (e.g., lead, methylmercury, polychlorinated biphenyls, arsenic, and toluene) can exert developmental neurotoxicity, which results in clinical or subclinical brain dysfunction in humans and in laboratory animals[1]. Many neurotoxic chemicals are present in industrial work settings, and it is not known whether a prenatal exposure to industrial chemicals can cause developmental neurotoxicity.

1-Bromopropane ($CH_3CH_2CH_2Br$; 1-BP), one substitute for specific chlorofluorocarbons, is currently used as a solvent in a variety of industrial and commercial applications. Products containing 1-BP include degreasers and cleaners, spray adhesives, spot removers, coin cleaners, paintable mold release agents, automotive refrigerant flushes, and lubricants[2]. Adverse effects on the central and peripheral nervous system have been found in industrial workers who used 1-BP[3-5]. Adult rats exposed to 1-BP have also shown central neurotoxicity, alteration of mRNA levels of brain neurotransmitter receptors[6], and hippocampal disinhibition caused by a decrease in γ-aminobutyric acid (GABA)-mediated function[7]. In *in vitro* studies using rat hippocampal slices, 1-BP directly suppressed the synaptic plasticity, referred to as a long-term potentiation, in the granule cells of the dentate

gyrus[8].

Developmental toxicity is one reason for the threshold limit value set by the American Conference of Governmental Industrial Hygienists for 1,3-BP[9]. We recently reported that prenatal exposure to 1,3-BP suppressed the occurrence of kainite (KA)-induced "wet dog shake" behavior in 20-week-old rat pups[10]. However, whether prenatal 1,3-BP exposure can change neuronal function at the cellular level in the brain of the offspring is unknown. We therefore studied the effects of prenatal 1,3-BP exposure on neuronal excitability after birth. In studying neuronal excitability, population spikes (PS) were recorded in the CA1 subfield of hippocampal slices. For comparison, the same inhalation concentration was used in this study. We analyzed stimulation-dependent responses, stimulation/response (S/R) relationships, and the ratio of responses to double-pulse stimulations, paired-pulse ratios (PPRs). PPRs have been used as a simple method for assessing excitability in neuronal networks[7),11] In this study, we evaluated rats at 2, 5, 8, and 13 weeks of age, to determine whether prenatal 1,3-BP exposure can exert delayed effects after birth.

Materials and Methods

Animals and exposure protocol

Preparation of rats and 1,3-BP inhalation were made according to our previous study[10].

Briefly, adult male and female Wistar rats were purchased from Kyudo Co., Ltd. (Tosu, Japan). The rats were housed in plastic cages with paper-made chips (ALPHA-dri, Shepherd Specialty Papers, Richland, MI, USA) on a 12-h light/dark cycle (light period: 7 AM–7 PM). The temperature was controlled at 22–23°C. The relative humidity was approximately 50–70%. The animals had free access to food (CE2, CLEA Japan Inc., Tokyo, Japan) and filtered water (TCW-PPS filter, Advantech Co., Ltd., Tokyo, Japan). Female rats at the proestrus stage were mated with male rats. On the morning of the following day, the existence of sperm in the vaginal plug or vaginal smear was verified as gestation day (GD) 0. 1-BP was purchased from Kanto Chemical Co., Ltd. (Tokyo, Japan). Dams were exposed to 1-BP vapor at a concentration of 700 ppm (6 h/day) for 20 days from GD 1 to GD 20 in an exposure chamber, whereas the other dams were provided fresh air in the same type of chamber. Rats were not allowed access to food and water during the inhalation period. Until the experimental days, male and female rat pups were housed separately after weaning. Some pups in the control and prenatally 1-BP-exposed groups were sourced from pups that were not injected with KA in our previous study[10]. The prenatally 1-BP-exposed groups are abbreviated as the 1-BP group. The number of dams was 15 in the control group and 12 in the 1-BP group. The total number of pups was 34 in the control group and 25 in the 1-BP group.

The experiments were conducted under the guidance of the Ethics Committee of Animal Care and Experimentation in accordance with the Guiding Principle for Animal Care

Experimentation, University of Occupational and Environmental Health, Japan, which conforms to the National Institutes of Health Guide for the Care and Use of Laboratory Animals and the Japanese Law for Animal Welfare and Care.

Hippocampal slice preparation

The electrophysiological tests were conducted in male rats at 2, 5, 8, and 13 weeks of age. Female rats were also used for the test at the 13 weeks of age. The female rats at the proestrus stage were deselected for the present experiment, since it is known that estradiol levels can influence the morphology of synaptic boutons and may affect neuron excitability[12]. The total number of tested slices was 135 in the control group and 102 in the 10BP group. The slices were made following previously reported methods[7]. Briefly, the rats were deeply anesthetized with a diethyl ether vapor. After decapitation, the brain was removed and dipped in an ice-cooled artificial cerebrospinal fluid (ACSF) (3–4°C) saturated with an O_2/CO_2 mixture (95%:5%). The ACSF was composed of 124 mM NaCl, 2 mM KCl, 1.25 mM KH_2PO_4, 2 mM $CaCl_2$, 2 mM $MgSO_4$, 26 mM $NaHCO_3$, and 10 mM glucose. The bilateral hippocampi were separated from other brain regions. Next, transverse slices were obtained from the middle third region of the hippocampus with a McIlwain tissue chopper (Mickle Laboratory Engineering, Co., Ltd., Guildford, UK). The thickness of the slice was 600 Lm for 20-week-old rats and 450 Lm for 50, 80, and 130-week-old rats. The slices were transferred to an interface-type recording chamber, which was controlled at 32 ± 0.2°C, and perfused with

ACSF saturated with a mixture of O_2/CO_2 (95%:5%) at a flow rate of 1 ml/min.

All the chemicals used in this study were of reagent grade and purchased from commercial sources.

Stimulation and recordings

After a stabilizing period of 1–2 h, bipolar stimulation electrodes made with stainless steel wires (50 Lm in diameter) were placed on the stratum radiatum, where the Schaffer collateral and commissural fibers run up in the CA1 subfield (Figure 1A). PS was recorded from the pyramidal cell layer in the CA1 subfield using glass microelectrodes (1–2 MN). Stimulations consisted of square0wave pulses (200 Ls) from a stimulator (SEN7203, Nihon Koden Co., Tokyo, Japan) via an isolator (SS202J, Nihon Koden Co.). Stimulation intensities were 10 and 50 LA and increased by 100 LA every 2 min from 100 LA to a current of 600 LA in the slices from the 20week0old rats. In the slices from the 50, 80and 130week0old rats, the stimulation was delivered every 30 sec with intensities of 20, 40, 60, 80, 100, 140, 200, and 300 LA. The S/R relationship in the extracellular recording configuration represents basic excitability of the local area responding to electrical stimulation, and the responses are prefigured to increase as the stimulation strengthens. For the paired0pulse configuration, after the S/R relationship experiment, the current amplitude was adjusted so as to give the almost0maximum PS, 600 LA for slices from the 20week0old rats, and 300 LA for slices from the 50, 80, and 130week0old rats. Interpulse intervals (IPIs) of the paired0pulse stimulation were 5 and 10 ms and delivered

every 2 min for slices from the 20-week-old rats and every 1 min for slices from older rats. Electrophysiological signals were amplified with a high-impedance amplifier (Axoclamp 2B, Molecular Devices, Sunnyvale, CA, USA). The signals were then digitized with an AD converter (Digidata 1200, Molecular Devices) and stored on a computer using pCLAMP software (Molecular Devices).

Electrophysiological analysis

PS amplitude was measured as described in our previous study[7] (Figure 1B). Calculation of the PPRs was done as follows:

PPR of PS = second PS amplitude / first PS amplitude

In our previous inhalation studies using adult rats[7], PPRs of PS evoked with paired-pulse stimulation at IPIs of 5 and 10 ms in the CA1 subfield were less than 1 in the hippocampal CA1 of control adult rats, representing the presence of feedback inhibition. Compared to adult rats, PPRs of PS in immature rats can be 1 or higher[13]. Thus, in either case of inhibition or facilitation, paired-pulse configuration in extracellular recordings in the slices is useful to examine the excitability of the local area responding to double-pulse stimulations.

Statistical analysis

Statistical significance was evaluated by a repeated-measure analysis of variance (ANOVA) or an unpaired Welch's *t*-test for a difference between the 10-BP and control groups, when the

data were normally distributed. Otherwise, the Mann0Whitney U test was applied. p values < 0.05 (two0tailed) were considered statistically significant. Data represent mean ± standard error of the mean (SEM). Statistical tests were performed in Ekuseru0Toukei 2010 for Windows (Social Survey Research Information Co., Ltd., Tokyo, Japan)

Results

As shown in Figure 1C, the PS amplitude was four times greater in the 10BP group than in the control group at 600 LA of stimulation intensity in 20week0old rats. In 50week0old rats, the enhancement disappeared and the levels decreased to the control level of the S/R relationship of the PS amplitude (Figure 1D). No difference was observed either between the 10BP and control groups at 8 and 13 weeks of age (data not shown). Increased excitability of pyramidal neurons was a transient change.

[Insert Figure 1 here.]

Figure 2A shows examples of paired0pulse responses recorded from the hippocampal CA1 subfield of the control and 10BP groups at 2 weeks of age. As shown in Figure 2B, the averaged PPR was approximately 2 at 2 weeks of age in the control group, suggesting a facilitatory effect. In contrast, inhibition rather than facilitation was observed at the 50ms IPI in the 10BP group. At the 100ms IPI, PPRs showed a slight facilitation, but significantly

decreased compared to PPRs in the control group. At 5 weeks of age, PPRs were lower than 0.2, displaying an apparent feedback inhibition in both groups (data not shown), and the effects of prenatal 10BP exposure on PS PPRs disappeared. At 8 and 13 weeks of age, PPRs were still lower than 1, but increased significantly at 5 ms of IPI in the 10BP group compared with the control group (Figures 2C and 2D). In female rats aged 13 weeks, the increase in PPRs was observed at both 100ms and 50ms IPIs (Figure 2E).

[Insert Figure 2 here.]

Discussion

The present study found that prenatal exposure to 10BP enhanced the excitability of CA1 pyramidal neurons and caused a decrease in PPRs of PS amplitude in hippocampal slices from 20week0old rats. The lactation period after birth is considered the period of synaptogenesis in rat brains[14]; so neuronal development during the lactation period may be sensitive to prenatal chemical exposures. In a previous study[10], we reported that prenatal exposure to 10BP suppressed KA0induced "wet dog shake" behaviors in 20week0old rats. Prenatal 10BP exposure rendered the hippocampal CA1 subfield highly responsive to a single stimulation but suppressive to double stimulations. Prenatal 10BP exposure appears to prevent hyperexcitability of CA1 pyramidal neurons induced by repetitive stimulation. Nevertheless,

this is quite different from normal brain development.

Though a decrease in PPRs of PS amplitude was observed in the 10BP group at 2 weeks of age, the difference diminished at 5 weeks of age, as did the S/R relationship. In contrast with the 20week0old pups, the 80and 130week0old groups displayed an increase in PPRs of the PS, termed disinhibition. Thus, prenatal exposure to 10BP can exert developmental effects linked to the excitatory function of neurons and network excitability. Disinhibition has been reported in relation to subclinical and clinical changes in brain excitability in epileptic patients and animals[15], as well as in anxiety disorders[16]. We did not observe any spontaneous abnormal behaviors in the 10BP group during breeding. To date, developmental neurotoxic effects caused by 10BP exposure have not been reported in children whose mothers were exposed occupationally during pregnancy. However, because disinhibition can be related to the hyperexcitable brain and to epilepsy, it should not be concluded that disinhibition is merely a phenomenon restricted to rats. Since disinhibition is interpreted as a disturbance of the excitation/inhibition balance in the hippocampal CA1 area, a disinhibitory effect can be classified as an adverse effect.

The enhancement of excitability induced by prenatal 10BP exposure was observed only in the 20week0old group, and may therefore have been only a transient effect. Alternately, one could argue that the excess basal excitability during synaptogenesis is not coincidental with disinhibition after maturation. If so, the PS S/R relationship can be useful as a new index

marker for developmental neurotoxicity of chemicals before the appearance of neurophysiological changes in the brain after maturation. To validate this method for assessing the developmental neurotoxicity of industrial chemicals, we should test chemicals that are already known to exert developmental neurotoxicity. To this end, we are currently investigating valproic acid (VPA), an antiepileptic drug used in an established animal model of the developmental disorder autism[17]. Synaptic transmission generates action potentials; we are also studying field excitatory postsynaptic potentials.

In conclusion, we demonstrated that prenatal 10BP exposure can cause delayed neurotoxicity, although the underlying mechanism is not known yet, and requires further study.

Acknowledgements

We gratefully acknowledge the animal care of K. Egashira. This study was partly supported by the Grants-in-Aid Program of the Japan Society for the Promotion of Science (no. 23510084 to S.U. and no. 18510064 to Y.F.) and a Health and Labour Sciences Research Grant from the Ministry of Health, Labour and Welfare, Japan (to Y.K.).

References

1) Grandjean P, Landrigan P. Developmental neurotoxicity of industrial chemicals. Lancet 2006; 368: 2167-2178.

2) US Environmental Protection Agency: Fact sheet: 1-Bromopropane (1-BP).[Online]. 2016version [cited 2016 Mar 3]; Available from : URL: https://www.epa.gov/assessing-and-managing-chemicals-under-tsca/fact-sheet-1-bromopropane-1-bp#product

3) Ichihara G, Kitoh J, Li W, Ding X, Ichihara S, Takeuchi Y. Neurotoxicity of 1-bromopropane: Evidence from animal experiments and human studies. J Adv Res 2012; 3: 91-98.

4) Samukawa M, Ichihara G, Oka N, Kusunoki S. A case of severe neurotoxicity associated with exposure to 1-bromopropane, an alternative to ozone-depleting or global-warming solvents. Arch Intern Med 2012; 172: 1257-1260.

5) Wang T, Wu M, Wu Y, Tsai W, Lin K, Wang C, et al. Neurotoxicity associated with exposure to 1-bromopropane in golf-club cleansing workers. Clin Toxicol 2015; 53: 823-826.

6) Ueno S, Yoshida Y, Fueta Y, Ishidao T, Liu J, Kunugita N, et al. Changes in the function of the inhibitory neurotransmitter system in the rat brain following subchronic inhalation exposure to 1-bromopropane. Neurotoxicology 2007; 28: 415-420.

7) Fueta Y, Fukuda T, Ishidao T, Hori H. Electrophysiology and immunohistochemistry in the hippocampal CA1 and the dentate gyrus of rats chronically exposed to 1-bromopropane, a substitute for specific chlorofluorocarbons. Neuroscience 2004; 124: 593-603.

8) Kanemitsu M, Fueta Y, Ishidao T, Aou S, Hori H. Development of a direct exposure system for studying the mechanisms of central neurotoxicity caused by volatile organic compounds. Ind Health 2016; 54: 42-49.

9) ACGIH: 1-Bromopropane: TLV(R) Chemical Substances 7th Edition Documentation. [Online]. 2014; Available from : URL: https://www.acgih.org/forms/store/ProductFormPublic/1-bromopropane-tlv-r-chemical-substances-7th-edition-documentation

10) Fueta Y, Kanemitsu M, Egawa S, Ishidao T, Ueno S, Hori H. Prenatal exposure to 1-bromopropane suppresses kainate-induced wet dog shakes in immature rats. J UOEH 2015; 37: 255-261.

11) Waldbaum S, Dudek FE. Single and repetitive paired-pulse suppression: A parametric analysis and assessment of usefulness in epilepsy research. Epilepsia 2009; 50: 904-916.

12) .Woolley CS. Effects of estrogen in the CNS. Curr Opin Neurobiol 1999; 9: 3490354.

13) Papatheodoropoulos C, Kostopoulos G. Development of a transient increase in recurrent inhibition and paired0pulse facilitation in hippocampal CA1 region. Dev Brain Res 1998; 108: 2730285.

14) Ben0Ari Y. Developing networks play a similar melody. Trends Neurosci 2001; 24: 3530360.

15) Shumate MD, Lin DD, Gibbs III JW, Holloway KL, A. Coulter D. GABA(A) receptor function in epileptic human dentate granule cells: Comparison to epileptic and control rat. Epilepsy Res 1998; 32: 1140128.

16) Bäckström T, Haage D, Löfgren M, Johansson IM, Strömberg J, Nyberg S, et al. Paradoxical effects of GABA0A modulators may explain sex steroid induced negative mood symptoms in some persons. Neuroscience 2011; 191: 46054

17) Schneider T, Przewłocki R. Behavioral alterations in rats prenatally to valproic acid: Animal model of autism. Neuropsychopharmacology 2005; 30: 80089.

291

292 **Figure legends**

293 **Figure 1 Recording of population spike (PS) from the hippocampal CA1 field and PS**

294 **stimulus/response (S/R) relationships**

295 (A) Stimulation electrode and recording electrode set on the CA1 subfield of the hippocampal

296 slice. The stimulation electrode was set in the stratum radiatum, supplying stimulation to

297 Schaffer collateral and commissural fibers. The PS recording electrode was set in the

298 pyramidal cell layer. (B) Typical PS recorded in the CA1 field of the hippocampal slice

299 obtained from a 20week0old control rat. The thick line represents the PS amplitude

300 measurement. Stimulation intensity was 600 LA. (C) At 2 weeks of age, S/R relationships of

301 the PS amplitude obtained from the 10BP0exposed rats were significantly enhanced compared

302 to S/R relationships in control rats ($p < 0.001$ by repeated0measure ANOVA). (D) At 5 weeks,

303 the enhancement observed in the 10BP0exposed rats disappeared, and the S/R relationship

304 decreased to control levels (PS amplitude: $p = 0.5$ by repeated0measure ANOVA). The

305 horizontal axis represents the stimulation intensity; the vertical axis represents the PS

306 amplitude. Data from 16–19 slices were averaged.

307

308 **Figure 2 Paired-pulse ratios (PPRs) of the population spikes (PSs) evoked with a double**

309 **stimulation of 5 and 10 ms interpulse intervals (IPIs) in the CA1 subfield of hippocampal**

slices obtained from 2-, 8-, and 13-week-old male rats and 13-week-old female rats

(A) Paired-pulse responses evoked with a 600-μA stimulation intensity at 10 ms IPI in the hippocampal CA1 subfield of 20-week-old rats. (B) At 2 weeks of age, PPRs decreased substantially in the 10-BP group (++$p < 0.01$ vs. the control group at the 50-ms IPI, +$p < 0.05$ vs. the control group at the 100-ms IPI by Welch's *t*-test). (C) At 8 weeks of age, PPRs were lower than 1 in both groups, indicating an apparent inhibition. At the 50-ms IPI, the PPR of the 10-BP group increased compared with that of the control group (#$p < 0.05$ by Mann-Whitney U test). (D) Similar to the 50-ms IPI at 8 weeks of age, PPR of male rats in the 10-BP group increased compared with that of the control male rats at 13 weeks of age (+$p < 0.05$ by Welch's *t*-test). (E) At 13 weeks, female rats in the 10-BP group showed an increase in PPRs at 50- and 100-ms IPIs compared with control female rats (##$p < 0.01$ by Mann-Whitney U test; ++$p < 0.01$ by Welch's *t*-test). The horizontal axis represents the IPIs; the vertical axis represents the PPRs of PS amplitude. Data from 16–25 slices were averaged.

Fig. 1

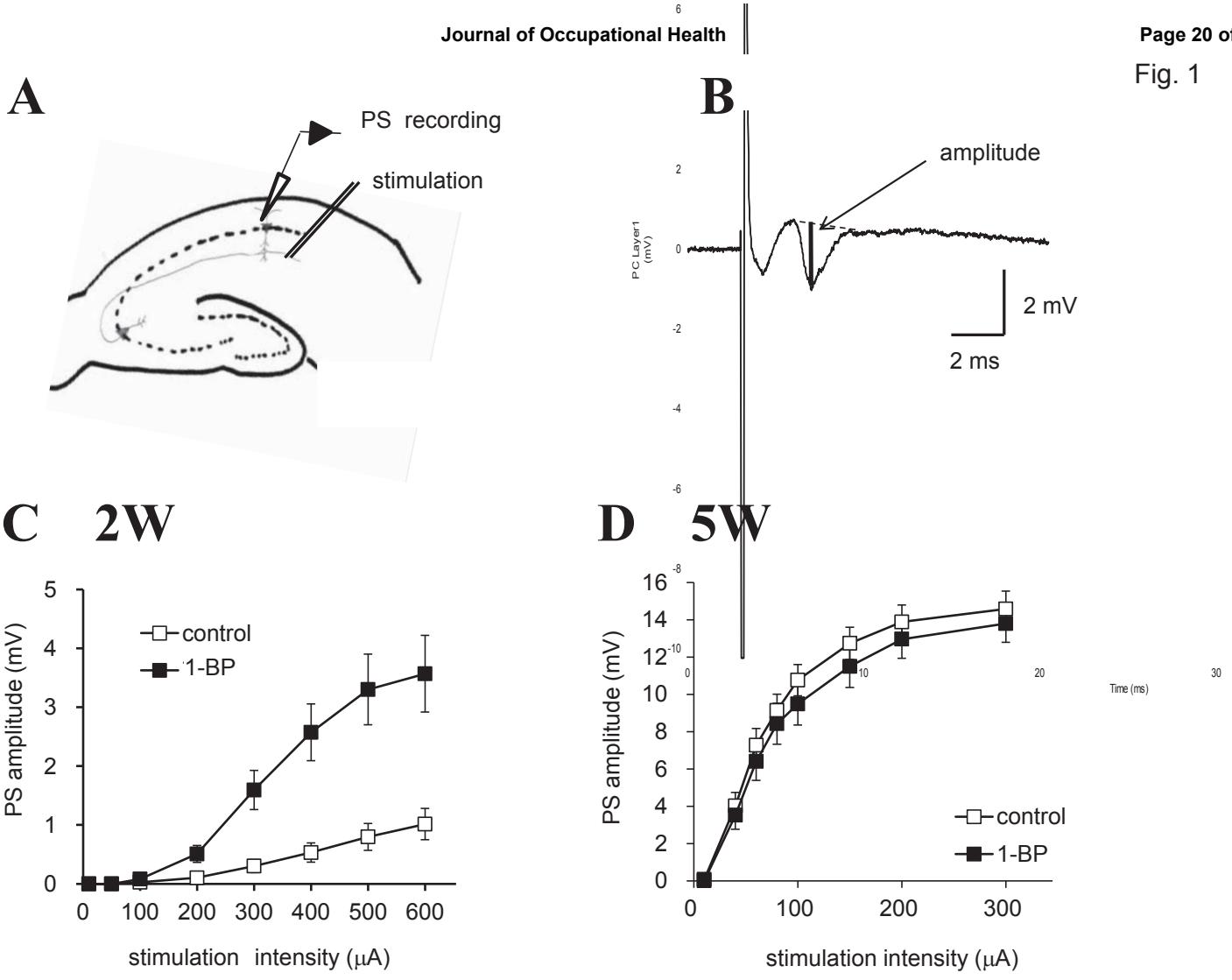
A
PS recording
stimulation
B
amplitude
2 mV
2 ms
PC Layer1 (mV)
C 2W
control
1-BP
PS amplitude (mV)
stimulation intensity (μA)
D 5W
control
1-BP
PS amplitude (mV)
stimulation intensity (μA)
Time (ms)

Fig. 2

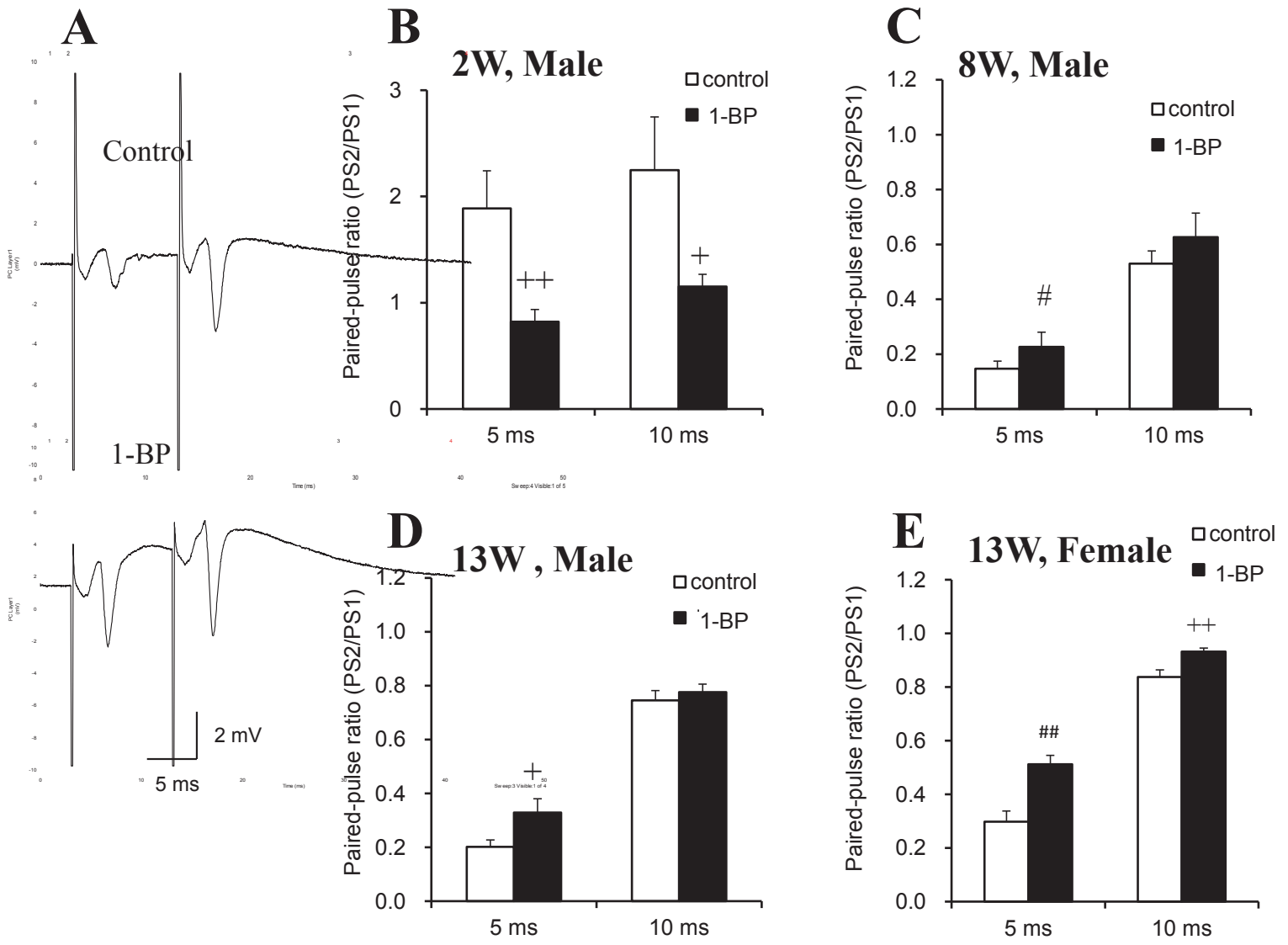
A
Control
1-BP
2 mV
5 ms
B
2W, Male
control
1-BP
Paired-pulse ratio (PS2/PS1)
++
+
5 ms
10 ms
C
8W, Male
control
1-BP
Paired-pulse ratio (PS2/PS1)
#
5 ms
10 ms
D
13W , Male
control
1-BP
Paired-pulse ratio (PS2/PS1)
+
5 ms
10 ms
E
13W, Female
control
1-BP
Paired-pulse ratio (PS2/PS1)
##
++
5 ms
10 ms

Acute exposure to toluene and xylene decrease the expression of connexin43 in human cardiac myocytes

Tomonori Igarashi[a,*], Donald John Wilson[a,b], Susumu Ueno[a]

[a] Department of Occupational Toxicology, Institute of Industrial Ecological Sciences, University of Occupational and Environmental Health Japan, 1-1 Iseigaoka, Yahatanishi-ku, Kitakyushu, 807-8555, Japan

[b] Department of Public Health and Primary Care, College of Medicine, Nursing and Health Sciences, Fiji National University, Lakeba Street, Samabula, Fiji

* Corresponding author:

Tomonori Igarashi

Department of Occupational Toxicology, Institute of Industrial Ecological Sciences, University of Occupational and Environmental Health Japan, 1-1, Iseigaoka, Yahatanishi-ku, Kitakyushu, 807-8555, Japan. Phone: +81-93-691-7404, Fax: +81-93-692-4790, E-mail address: igarashi@med.uoeh-u.ac.jp (T. Igarashi).

ABSTRACT

Organic solvents are widely used in various factories and their use is strictly controlled by official guidelines. Inhalation of organic solvents can cause sudden cardiac death; however, the detailed mechanism of their cardiac toxicity remains unclear. Connexin43 (Cx43) is a principle gap junction protein located in the intercalated disk (IC-D) of cardiac myocytes and associated with a susceptibility to arrhythmia. We hypothesized that acute exposure to organic solvents could affect the expression of gap junction proteins and exposed human cardiac myocytes to doses of toluene and xylene for different times. The cytotoxicity assay revealed that toluene and xylene caused cytotoxicity in a dose-dependent manner. The western blot analysis showed that the expression of Cx43 was significantly decreased after exposure to toluene and xylene (0.56 ± 0.08 AU, $p < 0.05$) in dose-dependent and time-dependent manners. Furthermore, the immunohistochemical study revealed that the expression of Cx43 in the IC-D was significantly decreased and lower in cells that had been exposed to toluene and xylene than it was in the control cells (1.32 ± 0.06AU, $p < 0.05$). Toluene and xylene showed toxic effects on the human cardiac myocytes and decreased the expression of Cx43 in the IC-D.

Keywords: connexin43; toluene; xylene; gap junction protein; cardiotoxicity.

1. Introduction

Organic solvents are widely used in industrial factories and their use is strictly controlled by official guidelines. Several previous studies have reported that organic solvents can affect cardiac function and cause malformations of the heart (Kurppa et al., 1983; Kurppa et al., 1984; Tikkanen and Heinonen, 1991). It has been reported that the early stage following exposure to trichloroethylene is characterized by the induction of atrial and septal defects, whereas chronic exposure to trichloroethylene leads to congestive heart failure (Makwana et al., 2013; Rufer et al., 2010; Watson et al., 2006). Furthermore, trichloromethane (chloroform) has been noted to shorten action potential duration and induce bradycardia and ventricular fibrillation due to the inhibition of multiple ionic currents such as calcium, sodium, and potassium (Tibon-Fisher et al., 1992; Zhou et al., 2011). Another study has reported that inhalation of butane gas causes sudden cardiac death, possibly due to myocardial hypoxia such as is found in the absence of atherosclerotic heart disease (Novosel et al., 2011). Epidemiologic analyses have revealed that a high level of occupational exposure to organic solvents increases the risk of myocardial infarction during at least one year of work. The findings of the abovementioned previous studies imply that organic solvents may affect cardiac function; however, the detailed mechanism of the cardiac toxicity caused by organic solvents remains unclear. As a result, we developed a novel paradigm to understand the relationship between cardiac toxicity and exposure to organic solvents.

Gap junction proteins are expressed in the intercalated disks (IC-Ds) of cardiomyocytes and play an important role in impulse propagation in the heart. Connexin43 (Cx43) is a principle gap junction protein associated with susceptibility to arrhythmia. We have previously reported that the preservation of phosphorylated Cx43 plays an important role in the maintenance of sinus rhythm. In addition, Cx43 gene therapy was noted to recover the cardiac conduction system and prevent ventricular tachycardia in a healed myocardial infarction.

We hypothesized that acute exposure to toluene and xylene would affect the cardiac conduction system in human cardiac myocytes (HCMs). Therefore, we exposed HCMs to different doses of toluene and xylene in order to evaluate the relationship between the cardiotoxicity of each organic solvent and the expression of gap junction proteins.

2. Materials and methods

2.1. Study design

HCMs (PromoCell, Heidelberg, Germany) were plated in a 6-mm well plate according to the manufacturer's instructions. The following day, the cells were exposed to different concentrations of toluene (Nacalai Tesque, Kyoto, Japan) , xylene (Nacalai Tesque), and dimethyl sulfoxide (DMSO), and maintained in 5% CO_2 at 37°C for 3h, 6h, 12h, and 24h. The supernatants were subjected to a cytotoxicity assay, whereas the whole cells were

subjected to western blotting and immunohistochemistry analysis. Toluene and xylene were dissolved in DMSO immediately before use.

2.2. Cytotoxicity assay

The supernatants obtained after exposing the HCMs to the solvents were collected and purified by centrifugation (3000× g for 10 minutes at 20°C). The cytotoxicity assay was performed on the supernatant using ToxiLight® (Lonza, Basel, Switzerland) according to the manufacturer's instructions. Assay of luciferase activity showed a high extracellular level of adenylate kinase, indicating leakage of the latter from the HCMs.

2.3. Western blot analysis

The cardiomyocytes were harvested, homogenized, and dissolved in 0.3 M sucrose/10 mM sodium phosphate buffer containing a protease inhibitor (Roche, Indianapolis, IN, USA) and a phosphatase inhibitor (Sigma, St. Louis, MO, USA). Next, centrifugation (3000× g for 10 minutes at 4°C) was performed to obtain the cell lysates. Protein concentrations were then determined by the bicinchoninic acid assay (Thermo Scientific, Rockford, IL, USA). The proteins were fractionated by sodium dodecyl sulfate polyacrylamide gel electrophoresis, transferred to nitrocellulose membranes, blocked with 3% non-fat dry milk, and blotted with anti-Cx43 (Thermo Scientific), anti-human ether-a-go-go related gene (HERG) (Invitrogen,

Carlsbad, CA, USA), anti-Nav1.5 (Santa Cruz Biotechnology, Dallas, TX, USA), anti-L-type Ca^{2+} (Santa Cruz Biotechnology), and anti-actin (Santa Cruz Biotechnology) at 4°C overnight. The following day, the membranes were washed with blocking buffer and incubated with secondary antibodies conjugated with horseradish peroxidase. Protein bands were detected by enhanced chemiluminescence (Thermo Scientific) and quantified using the ImageJ software (National Institutes of Health (NIH), Bethesda, MD, USA). The band intensity for each protein was normalized to the intensity of actin in its lane.

2.4. Immunohistochemical analysis

Cover glasses were placed on the bottoms of 6-well plates before plating the HCMs. Twenty four hours after exposing the cells to toluene and xylene, the HCMs on the cover glasses were subjected to an immunohistochemical study. The HCMs were fixed in 2% formalin, followed by washing with phosphate-buffered saline (3 times, 5 minutes each). The cells were then incubated overnight with anti-Cx43 antibodies (1:400 dilution, Invitrogen) at 4°C overnight. The following day, the cells were incubated with fluorescein isothiocyanate-conjugated goat anti-rabbit IgG (1:400 dilution; Jackson ImmunoResearch Laboratories, Inc., West Grove, PA) before being examined by laser microscopy (×20 magnification; Axio; Carl Zeiss, Oberkochen, Germany). The signal intensities of the connexin proteins in the IC-D and lateral membrane were digitized and quantified using the Image-J software.

2.5. Statistical analysis

Statistical differences were determined by repeated measures analysis of variance. All the analyses were conducted at a 0.05 significance level. Data are presented as mean ± standard deviation.

3. Results

3.1. Cytotoxic effects of toluene and xylene on HCMs

The HCMs were exposed to 0μM, 3.1μM, 6.3μM, 12.5μM, 25.0μM, and 50.0μM of toluene and xylene for 24 hours and subjected to a cytotoxicity assay as described above. The supernatants from the HCMs were used in a cytotoxicity evaluation according to the ToxiLight® assay. We found that the cytotoxicity of each solvent increased in a concentration-dependent manner (Fig. 1). In addition, the two solvents were significantly and more cytotoxic to the HCMs [xylene at 25 μM (24.3 ± 19.5 IU, $p < 0.01$) and 50 μM (288.7 ±13.5 IU, $p < 0.01$), toluene at 50 μM (250.3 ± 8.39 IU, $p < 0.01$)] than DMSO was. Overall, xylene showed a higher cytotoxic effect than toluene did (half maximal inhibitory concentration values: xylene, 21 μM; toluene, 38 μM). Therefore, we used toluene and xylene at 10 μM and 20 μM, respectively, for the subsequent western blotting and immunohistochemical studies.

3.2. Western blot analyses of Cx43 expression in HCMs exposed to toluene and xylene

We assessed Cx43 expression by western blot analysis using an anti-Cx43 antibody that recognized total Cx43. The expression of Cx43 was decreased in a dose-dependent manner after exposure of the cells to toluene and xylene (Fig. 2A). The signal intensity was quantified using the ImageJ software and normalized to the expression of actin in the non-treated cells. We found that there were significant reductions in Cx43 expression when toluene was used at concentrations of 2 μM (0.58 ± 0.03 AU, $p < 0.05$) and 20 μM (0.38 ± 0.04 AU, $p < 0.01$) and xylene was used at 1 μM (0.59±0.12 AU, $p < 0.01$) and 10 μM (0.49 ± 0.07 AU, $p < 0.01$) (Fig. 2B). Next, we performed a time-course cytotoxic evaluation of the organic solvents. It was observed that the expression of Cx43 decreased in a time-dependent manner after the cells were exposed to either toluene or xylene (Fig. 3A). Furthermore, we found that, compared to the non-treated cells, there were significant reductions in Cx43 expression after incubation of the cells with toluene for 12 hours (0.56 ± 0.05 AU, $p < 0.05$) or 24 hours (0.42 ± 0.03 AU, $p < 0.01$), as well as with xylene for 12 hours (0.46 ± 0.02 AU, $p < 0.01$) or 24 hours (0.51 ± 0.07 AU, $p < 0.01$) (Fig. 3B).

3.3. Immunohistochemical analyses of Cx43 expression in HCMs exposed to toluene and xylene

We evaluated the percentage expression of Cx43 in the IC-Ds using immunohistochemistry. Representative pictures showing cells stained with Cx43 antibody are

shown in Fig. 4A. We found that there were significant reductions in Cx43 expression in the IC-Ds when toluene was used at concentrations of 0.2 μM (0.73 ± 0.06 AU, $p < 0.05$), 2 μM (0.64 ± 0.04 AU, $p < 0.05$), and 20 μM (0.45 ± 0.14 AU, $p < 0.01$), and xylene was used at 1 μM (0.65 ± 0.06 AU, $p < 0.05$) and 10 μM (0.59 ± 0.07 AU, $p < 0.05$). This suggests that the organic solvents possibly affect the trafficking pathway of Cx43 proteins (Fig. 4B).

3.4. Western blot analyses of HERG, Nav1.5, and L-type Ca^{2+} channel expressions in HCMs exposed to toluene and xylene

We also assessed the expression of major cardiac channels such as HERG, Nav1.5, and L-type Ca^{2+} using western blot analysis, because these channel proteins play an important role in action potential duration. We found that the expressions of the channels before and after exposure of the cells to toluene or xylene for 24 hours were the same (Fig. 5).

4. Discussion

The National Institute for Occupational Safety and Health has declared the criteria for the use of organic solvents in order to prevent disease and hazardous conditions at the workplace (https://www.cdc.gov/niosh/topics/organsolv/). The criteria include all the information on an organic solvent, which is necessary to know at the workplace. Although the usage of organic solvents are strictly controlled by official guidelines, workers are likely to be exposed to high

concentrations of organic solvents, especially in a narrow space. The inhalation of organic solvents sometimes causes sudden death. The main mechanism underling the lethality of organic solvents is considered to be oxygen deficiency in cardiomyocytes (Harrison et al., 2016); however, the detailed mechanism remains unknown. Butane is a typical organic solvent used in industries and that sometimes causes sudden death (Celinski et al., 2013; Novosel et al., 2011). According to our cytotoxicity assay, toluene and xylene showed cytotoxic effects on the HCMs in dose-dependent and time-dependent manners, which suggests that the organic solvents have acute cytotoxic effects on human cardiomyocytes. Furthermore, environmental chemical contamination is a risk factor for congenital heart disease, which indicates that exposure to chemicals poses a risk for defective heart function during the embryonic stage (Rufer et al., 2010; Tikkanen and Heinonen, 1991). Although several epidemiological studies have been focused on the effects of chronic or constant exposure to organic solvents at the workplace (Kotseva and Popov, 1998; Tibon-Fisher et al., 1992), it would also be highly important to assess acute cell damage in the human heart caused by such exposures. The next step would then be an animal experiment to reveal how organic solvents might affect the conduction system in the heart *in vivo*. Several studies have reported that nanoparticles showed direct and indirect toxic effects on the cardiovascular system and increased the risks of ischemic heart disease or cerebrovascular disease (Chen et al., 2015; Nelin et al., 2012; Polichetti et al., 2009), and furthermore demonstrated that

mortality would be decreased at workplaces where workers are constantly exposed to small particles in the air (Stephan et al., 2014; Toren et al., 2007). However, little is known about the mortality of workers at places where high concentrations of organic solvents are used. According to our results, toluene and xylene are toxic to HCMs, however, it is quite important to evaluate the mechanism of cytotoxic effects of organic solvents on HCMs.

Furthermore, we assessed the relationship between exposure to organic solvent and connexin expression in HCMs. According to our results, toluene and xylene decreased the expression of gap junction proteins, increased the heterogeneity of cardiac propagation, and caused reentrant arrhythmias such as ventricular tachycardia and ventricular fibrillation. Imbalance in autonomic nerve activities has been stated as another important factor that increases the risk of arrhythmia (Matikainen and Juntunen, 1985; Morrow and Steinhauer, 1995; Murata et al., 1994). Since autonomic nerve activities are influenced by organic solvents following a long-term occupational exposure (Morrow and Steinhauer, 1995), high concentrations of organic solvents might drive sympathetic nerve activities. We have previously shown that an altered expression of Cx43 is strongly associated with heterogeneity of cardiac impulse propagation in atrial fibrillation (AF) in healed myocardial infarction models (Bikou et al., 2011; Greener et al., 2012; Igarashi et al., 2012). In the present study, we found that the expression of Cx43 was significantly decreased by toluene and xylene in dose-dependent and time-dependent manners after exposing HCMs to the solvents. These

results imply that a decreased expression of Cx43 slows impulse propagation in cardiomyocytes and increases the risk of arrhythmia.

Connexin proteins are folded in the Golgi system, which are phosphorylated and trafficked to the plasma membrane surface (Basheer and Shaw, 2016; Falk et al., 2016; Zhang and Shaw, 2014). We have previously shown that the expression of connexin proteins is significantly decreased in AF induced by atrial burst-pacing in animal models (Igarashi et al., 2012). According to our immunohistochemical analyses, lateralized expression of Cx43 was significantly increased after exposing the cells to toluene and xylene, indicating that the organic solvents affect the intracellular trafficking of connexin proteins. Since we observed that the expression of connexin proteins in the IC-D was decreased by the organic solvents, there are possibilities that the organic solvents would affect the phosphorylation status of connexin proteins. Several previous studies have reported that chemical agents affect the trafficking of proteins such as sodium and potassium channels (Abriel et al., 2015; Basheer and Shaw, 2016; Steffensen et al., 2015). However, no organic solvents have been reported to affect the expression of gap junction proteins. Another concern is whether organic solvents might affect the functions of phosphatases and/or phosphatase inhibitors in cardiomyocytes. Therefore, further investigations are necessary to assess the relationship between exposure to organic solvents and the phosphorylation system in cardiomyocytes.

According to official reports from the Centers for Disease Control and Prevention, nine

sudden deaths have been caused by inhalation of hydrocarbon gases and oxygen deficiency at specific locations such as catwalk or in front of an open hatch, where the oxygen level might have been low (Harrison et al., 2016). Most of the reasons for sudden deaths in such places are due to oxygen deficiency; however, a direct effect of organic solvents on HCMs can cause sudden death especially at workplaces where organic solvents are used. We have shown that toluene and xylene had cytotoxic effects on the HCMs in the acute phase; however, further studies should be carried out to assess the effects of long-term continuous exposure to organic solvents at low concentrations. Since the concentration of organic solvents in the air is strictly controlled by official guidelines, it is highly unlikely that workers would inhale high concentrations of organic solvents for long periods. Moreover, organic solvents can directly decrease the expression of Cx43, as well as decrease impulse propagation and increase the risk of arrhythmia. AF is the most common arrhythmia in clinical practice with a prevalence rate of about 10% in individuals aged > 80 years old (Alonso and Norby, 2016; Ko et al., 2016). The major contributing factor to AF is thought to be the age of patients; however, other risk factors for AF include hypertension, dyslipidemia, and diabetes mellitus. In clinical medical practice, little is known about the relationship between continuous exposure to organic solvents and the occurrence of AF. Since the prevalence of AF is strongly correlated with patient age, we have not assessed to the working history or working environmental aspects when patients with AF come to the hospital. Therefore, the work history and working

conditions of a patient who presents with AF must be evaluated. Furthermore, the direct effects of continuous and low-dose exposure of organic solvents on the human heart have to be evaluated in large animal models. This will allow for the investigation of exposure to low doses of organic solvents and the resulting long-term effects on cardiomyocytes.

In conclusion, toluene and xylene showed cytotoxic effects on HCMs in dose-dependent and time-dependent manners. In addition, toluene and xylene decreased the expression of Cx43, especially that in the IC-Ds of the HCMs. An *in vivo* electrophysiological study would be necessary to understand the mechanism underlying the toxicities of the organic solvents and how they increase susceptibility to arrhythmia.

Acknowledgements

We thank Rie Yukiya for secretarial assistance.

Conflict of interest

The authors declare that there are no conflicts of interest.

Funding information

This work was funded by the Occupational Research Fund of the University of Occupational and Environmental Health, School of Medicine, Japan.

References

Abriel, H., Rougier, J.S., Jalife, J., 2015. Ion channel macromolecular complexes in cardiomyocytes: roles in sudden cardiac death. Circ. Res. 116, 1971–1988.

Alonso, A., Norby, F.L., 2016. Predicting atrial fibrillation and its complications. Circ. J. 80, 1061–1066.

Basheer, W.A., Shaw, R.M., 2016. Connexin 43 and CaV1.2 ion channel trafficking in healthy and diseased myocardium. Circ. Arrhythm. Electrophysiol. 9, e001357.

Bikou, O., Thomas, D., Trappe, K., Lugenbiel, P., Kelemen, K., Koch, M., Soucek, R., Voss, F., Becker, R., Katus, H.A., Bauer, A., 2011. Connexin 43 gene therapy prevents persistent atrial fibrillation in a porcine model. Cardiovasc. Res. 92, 218–225.

Celiński, R., Skowronek, R., Uttecht-Pudełko, A., 2013. [Atypical case of teenager fatal poisoning by butane as a result of gas for lighters inhalation against his will]. Przegl. Lek. 70, 473–475.

Chen, Z., Wang, Y., Zhuo, L., Chen, S., Zhao, L., Luan, X., Wang, H., Jia, G., 2015. Effect of titanium dioxide nanoparticles on the cardiovascular system after oral administration. Toxicol. Lett. 239, 123–130.

Falk, M.M., Bell, C.L., Kells Andrews, R.M., Murray, S.A., 2016. Molecular mechanisms regulating formation, trafficking and processing of annular gap junctions. BMC Cell Biol. 17 Suppl 1, S22.

Greener, I.D., Sasano, T., Wan, X., Igarashi, T., Strom, M., Rosenbaum, D.S., Donahue, J.K., 2012. Connexin43 gene transfer reduces ventricular tachycardia susceptibility after myocardial infarction. J. Am. Coll. Cardiol. 60, 1103–1110.

Harrison, R.J., Retzer, K., Kosnett, M.J., Hodgson, M., Jordan, T., Ridl, S., Kiefer, M., 2016. Sudden deaths among oil and gas extraction workers resulting from oxygen deficiency and inhalation of hydrocarbon gases and vapors - United States, January 2010-March 2015. MMWR Morb. Mortal. Wkly. Rep. 65, 6–9.

Igarashi, T., Finet, J.E., Takeuchi, A., Fujino, Y., Strom, M., Greener, I.D., Rosenbaum, D.S., Donahue, J.K., 2012. Connexin gene transfer preserves conduction velocity and prevents atrial fibrillation. Circulation 125, 216–225.

Ko, D., Rahman, F., Schnabel, R.B., Yin, X., Benjamin, E.J., Christophersen, I.E., 2016. Atrial fibrillation in women: epidemiology, pathophysiology, presentation, and prognosis. Nat. Rev. Cardiol. 13, 321–332.

Kotseva, K., Popov, T., 1998. Study of the cardiovascular effects of occupational exposure to organic solvents. Int. Arch. Occup. Environ. Health. 71 Suppl, S87–S91.

Kurppa, K., Hietanen, E., Klockars, M., Partinen, M., Rantanen, J., Rönnemaa, T., Viikari, J., 1984. Chemical exposures at work and cardiovascular morbidity. Atherosclerosis, ischemic heart disease, hypertension, cardiomyopathy and arrhythmias. Scand. J. Work Environ. Health 10, 381–388.

Kurppa, K., Holmberg, P.C., Hernberg, S., Rantala, K., Riala, R., Nurminen, T., 1983. Screening for occupational exposures and congenital malformations. Scand. J. Work Environ. Health 9, 89–93.

Makwana, O., Ahles, L., Lencinas, A., Selmin, O.I., Runyan, R.B., 2013. Low-dose trichloroethylene alters cytochrome P450-2C subfamily expression in the developing chick heart. Cardiovasc. Toxicol. 13, 77–84.

Matikainen, E., Juntunen, J., 1985. Autonomic nervous system dysfunction in workers exposed to organic solvents. J. Neurol. Neurosurg. Psychiatry 48, 1021–1024.

Morrow, L.A., Steinhauer, S.R., 1995. Alterations in heart rate and pupillary response in persons with organic solvent exposure. Biol. Psychiatry 37, 721–730.

Murata, K., Araki, S., Yokoyama, K., Yamashita, K., Okajima, F., Nakaaki, K., 1994. Changes in autonomic function as determined by ECG R-R interval variability in sandal, shoe and leather workers exposed to n-hexane, xylene and toluene. Neurotoxicology 15, 867–875.

Nelin, T.D., Joseph, A.M., Gorr, M.W., Wold, L.E., 2012. Direct and indirect effects of particulate matter on the cardiovascular system. Toxicol. Lett. 208, 293–299.

Novosel, I., Kovačić, Z., Gusić, S., Batelja, L., Nestić, M., Seiwerth, S., Skavić, J., 2011. Immunohistochemical detection of early myocardial damage in two sudden deaths due to intentional butane inhalation. Two case reports with review of literature. J.

Forensic Leg. Med. 18, 125–131.

Polichetti, G., Cocco, S., Spinali, A., Trimarco, V., Nunziata, A., 2009. Effects of particulate matter (PM(10), PM(2.5) and PM(1)) on the cardiovascular system. Toxicology 261, 1–8.

Rufer, E.S., Hacker, T.A., Flentke, G.R., Drake, V.J., Brody, M.J., Lough, J., Smith, S.M., 2010. Altered cardiac function and ventricular septal defect in avian embryos exposed to low-dose trichloroethylene. Toxicol. Sci. 113, 444–452.

Steffensen, A.B., Refaat, M.M., David, J.P., Mujezinovic, A., Calloe, K., Wojciak, J., Nussbaum, R.L., Scheinman, M.M., Schmitt, N., 2015. High incidence of functional ion-channel abnormalities in a consecutive long QT cohort with novel missense genetic variants of unknown significance. Sci. Rep. 5, 10009.

Stephan, C., Schlawne, C., Grass, S., Waack, I.N., Ferenz, K.B., Bachmann, M., Barnert, S., Schubert, R., Bastmeyer, M., de Groot, H., Mayer, C., 2014. Artificial oxygen carriers based on perfluorodecalin-filled poly(n-butyl-cyanoacrylate) nanocapsules. J. Microencapsul. 31, 284–292.

Tibon-Fisher, O., Heller, E., Ribak, J., 1992. [Occupational scleroderma due to organic solvent exposure]. Harefuah 122, 530-2, 551.

Tikkanen, J., Heinonen, O.P., 1991. Risk factors for ventricular septal defect in Finland. Public Health 105, 99–112.

Torén, K., Bergdahl, I.A., Nilsson, T., Järvholm, B., 2007. Occupational exposure to particulate air pollution and mortality due to ischaemic heart disease and cerebrovascular disease. Occup. Environ. Med. 64, 515–519.

Watson, R.E., Jacobson, C.F., Williams, A.L., Howard, W.B., DeSesso, J.M., 2006. Trichloroethylene-contaminated drinking water and congenital heart defects: a critical analysis of the literature. Reprod. Toxicol. 21, 117–147.

Zhang, S.S., Shaw, R.M., 2014. Trafficking highways to the intercalated disc: new insights unlocking the specificity of connexin 43 localization. Cell Commun. Adhes. 21, 43–54.

Zhou, Y., Wu, H.J., Zhang, Y.H., Sun, H.Y., Wong, T.M., Li, G.R., 2011. Ionic mechanisms underlying cardiac toxicity of the organochloride solvent trichloromethane. Toxicology. 290, 295–304.

Figure legends

Fig. 1. Evaluation of the cytotoxic effects of toluene and xylene on human cardiac myocytes (HCMs).

HCMs were exposed to different concentrations of toluene, xylene, and dimethyl sulfoxide (DMSO). Luciferase activity was used to evaluate the cytotoxicities of the solvents using ToxiLight® assay.

Fig. 2. Western blot analysis of connexin43 (Cx43) expression in human cardiac myocytes (HCMs) exposed to toluene and xylene.

HCMs were exposed to different concentrations of toluene and xylene for 24 hours. (A) Whole cell lysates were then harvested and subjected to western blot analysis. (B) The expression levels of Cx43 and actin were quantified and normalized to the expression level of actin in control cells.

Fig. 3. Time-course evaluation of connexin43 (Cx43) expression in human cardiac myocytes (HCMs) exposed to toluene and xylene using western blot analysis.

HCMs were exposed to toluene (20 μM) or xylene (10 μM) for 3, 6, 12, or 24 hours. (A) Whole cell lysates were harvested and subjected to western blot analysis. (B) The expression levels of Cx43 and actin were quantified and normalized to the expression level of actin in

control cells.

Fig. 4. Immunohistochemical analysis of connexin43 (Cx43) expression in human cardiac myocytes (HCMs) exposed to toluene and xylene.

HCMs were exposed to different concentrations of toluene and xylene for 24 hours. (A) Representative images of cells stained with Cx43 antibody. The yellow boxes are magnified images of intercalated discs (IC-Ds) located between neighboring cardiomyocytes. The red arrow indicates Cx43 expressed in the IC-Ds. The expression of Cx43 in all fields and IC-Ds was quantified using the ImageJ software. (B) The expression level of Cx43 in the IC-Ds.

Fig. 5. Western blot analysis of human ether-a-go-go related gene (HERG), Nav1.5, and L-type Ca^{2+} channel expressions in human cardiac myocytes (HCMs) exposed to toluene and xylene.

HCMs were exposed to toluene (20 μM) or xylene (10 μM) for 24 hours. Whole cell lysates were then harvested and subjected to western blot analysis using primary antibodies against HERG, Nav1.5, L-type Ca^{2+}, and actin.

Endocrine Journal

Advance Publication
doi:10.1507/endocrj.EJ16-0431

NOTE

Association of common polymorphisms with gestational diabetes mellitus in Japanese women: A case-control study

Yoshifumi Kasuga[1), 2)], Kenichiro Hata[2)], Atsushi Tajima[3)], Daigo Ochiai[1)], Yoshifumi Saisho[4)], Tadashi Matsumoto[1)], Naoko Arata[5)], Kei Miyakoshi[1)] and Mamoru Tanaka[1)]

[1)] *Department of Obstetrics and Gynecology, Keio University School of Medicine, Tokyo 160-8582, Japan*
[2)] *Department of Maternal-Fetal Biology, National Research Institute for Child Health and Development, Tokyo 157-8583, Japan*
[3)] *Department of Bioinformatics and Genomics, Graduate School of Advanced Preventive Medical Sciences, Kanazawa University, Kanazawa 920-8640, Japan*
[4)] *Department of Internal Medicine, Keio University School of Medicine, Tokyo 160-8582, Japan*
[5)] *Department of Women's Health, National Center for Child Health and Development, Tokyo 157-8583, Japan*

Abstract. Gestational diabetes (GDM) and type 2 diabetes (T2DM) share part of pathomechanism and several T2DM susceptibility genes are demonstrated to be associated with GDM. No information on the genetics of GDM, however, was available in Japanese women. In this study, T2DM risk variants (45 single nucleotide polymorphisms [SNPs] from 36 genes) identified in previous studies were genotyped using matrix-assisted laser desorption/ionization time-of-flight mass spectrometry in a cohort of 171 Japanese women with GDM and 128 normal glucose tolerance (NGT) diagnosed by the new International Association of Diabetes in Pregnancy Study Group criteria. Of 45 SNPs, three genetic variants were nominally associated with the development of GDM: rs266729 ($p = 0.013$, odds ratio [OR]: 1.56, 95% confidence interval [CI]: 1.10–2.23) in *ADIPOQ*, rs10811661 ($p = 0.035$, OR: 1.46, 95% CI: 1.03–2.08) in *CDKN2A/2B*, and rs9505118 ($p = 0.046$, OR: 1.41, 95% CI: 1.01–1.97) in *SSR1-RREB1*. There was a significant difference in the number of risk alleles of three variants between women with GDM and NGT (3.79 ± 1.33 *vs.* 3.05 ± 1.41, $p = 6.0 \times 10^{-6}$). In combined analysis of three genetic variants, women with five or more risk alleles had a 7.32-fold increased risk of GDM ($p = 5.6 \times 10^{-5}$, 95% CI: 4.54–11.96), compared with those having no more than one risk allele. Our results suggest several risk variants of T2DM had cumulative effects on the development of GDM in Japanese women.

Key words: Gestational diabetes mellitus, Single nucleotide polymorphism, Japanese women

GESTATIONAL DIABETES MELLITUS (GDM), defined as glucose intolerance with onset or first recognition during pregnancy, is a multifactorial disease that is similar to type 2 diabetes mellitus (T2DM): glucose intolerance is likely to be caused by the combination of environmental and genetic effects [1, 2]. With the recent advances in high-throughput genotyping technologies, the genetics of GDM as well as T2DM has been investigated over the past decade. For instance, genetic variants associated with insulin sensitivity and beta cell function have been related to T2DM in various racial or ethnic groups including Japanese population by the linkage analysis, the candidate gene approach, and the genome-wide association studies (GWAS) [3-6]. In particular, several T2DM susceptibility genes were related to the development of GDM in Caucasians [7-11]. Since the susceptibility to glucose intolerance depends on racial or ethnic groups, the effect of T2DM risk genetic variants on GDM might be different between Caucasian and Japanese women. To date, however, no information on risk variants of GDM was available in Japanese women.

Women with GDM are at a high risk of developing future T2DM as well as perinatal complications (i.e. pregnancy-induced hypertension and macrosomia) [2, 12]. Offspring born to mother with GDM carries a risk of early onset obesity and glucose intolerance [12, 13]. Therefore, the optimal management of GDM is important not only to perinatal care, but also to maternal and

Submitted Sep. 14, 2016; Accepted Dec. 6, 2016 as EJ16-0431
Released online in J-STAGE as advance publication Feb. 16, 2017
Correspondence to: Kenichiro Hata, M.D., Ph.D., Department of Maternal-Fetal Biology, National Research Institute for Child Health and Development, 2-10-1 Okura, Setagaya-ku, Tokyo 157-8583, Japan. E-mail: hata-k@ncchd.go.jp
Co-correspondence to: Kei Miyakoshi, M.D., Department of Obstetrics and Gynecology, Keio University School of Medicine, 35 Shinanomachi, Shinjuku-ku, Tokyo 160-8582, Japan.
E-mail: kei.z7@keio.jp

children's healthcare. In general, Asians are classified as a highly susceptible to glucose intolerance [14-16]. This means that genetic information would contribute to the identification of women at highest risk of T2DM as well as the understanding of the pathophysiology of GDM in Japanese women.

With this background, the current study was designed to examine the association between T2DM or GDM susceptibility genes previously reported and the development of GDM in Japanese women. Especially, in the present study, glucose tolerance status was evaluated by a single criterion (i.e. the new criteria proposed by International Association of Diabetes in Pregnancy Study Group [IADPSG]) and pregnant women with normal glucose tolerance (NGT) were considered as control to account for the environmental influence (i.e. pregnancy).

Materials and Methods

Subjects

We recruited a total of 299 Japanese women with singleton pregnancies who underwent the diagnostic 75g oral glucose tolerance test (75g-OGTT) at 24–32 gestational weeks at Keio University Hospital or at the National Center for Child Health and Development from April 2011 until December 2014. Gestational age was confirmed by crown-rump length measurements in the first trimester. Women with multi-fetal pregnancies, fetal congenital anomalies, overt diabetes in pregnancy, pre-gestational diabetes mellitus (i.e. type 1 diabetes and T2DM), and hypertensive disorders in pregnancy, chronic hypertension, and the use of medications known to affect glucose metabolism were excluded. This research was performed in accordance with the Declaration of Helsinki and informed consent was obtained from patients, where appropriate. The study was approved by Keio University School of Medicine Ethics Committee (No. 20100154) and the institutional review board of National Research Institute for Child Health and Development (No. 406).

According to IADPSG criteria, GDM was diagnosed if one or more values reached or exceeded the following thresholds: fasting plasma glucose level (FPG), 92 mg/dL (5.1 mmol/L); 1h-plasma glucose level during 75g-OGTT (1h-PG), 180 mg/dL (10.0 mmol/L); and 2h-plasma glucose level during 75g-OGTT (2h-PG), 153 mg/dL (8.5 mmol/L). Overt diabetes in pregnancy was defined as HbA1c > 6.5%, FPG ≥ 126 mg/dL (7.0 mmol/L), or random plasma glucose level ≥ 200 mg/dL (11.1 mmol/L): the latter needing to be confirmed by one of the former [17]. Women with normal OGTT results were considered as NGT (i.e. control) in this study. As a result, there were 171 women with GDM and 128 with NGT in this study cohort. Statistical power of the current analysis using 171 GDM and 128 NGT was calculated using Genetic Power Calculator in the GDM prevalence rate of 10% [18]. The current study had 57% or 85% power to detect a GDM-susceptible allele with a genotype relative risk (GRR) of 1.4 or 1.6 (under an additive model in log-odds scale), respectively, assuming that the type I error rate was 0.05 and the susceptible allele frequency was 0.3.

Assessment of insulin sensitivity, insulin secretion, and beta cell function

Insulin sensitivity and insulin secretion were evaluated by parameters calculated using the diagnostic 75g-OGTT. The insulin sensitivity was estimated by the whole-body insulin sensitivity index derived from the OGTT (IS_{OGTT}) and the homeostasis model assessment of insulin resistance (HOMA-IR), and Quantitative insulin sensitivity check index (QUICKI). The IS_{OGTT} was calculated by the following formula: 10,000 / square root $\{PG_0 \times Ins_0 \times (PG_0 + PG_{60} \times 2 + PG_{120}) / 2 \times (Ins_0 + Ins_{60} \times 2 + Ins_{120}) / 2\}$, where PG_y and Ins_y represent plasma glucose (mg/dL) and insulin values (mU/L), respectively, at time y min during the OGTT [19]. The HOMA-IR was calculated as $(PG_0 \times Ins_0) / 405$ [20]. The QUICKI was estimated as follows: $1 / [\log (Ins_0) + \log (PG_0)]$ [21]. Insulin secretion was assessed by the Insulinogenic Index (IGI: $\{Ins_{30} - Ins_0\} / \{PG_{30} - PG_0\}$) during the OGTT [22]. To evaluate beta cell function, we calculated the OGTT-derived disposition index using the following measures: Insulin Secretion-Sensitivity Index-2 (ISSI-2: IS_{OGTT} × the ratio of the total area under the insulin curve to the total area under the glucose curve during the OGTT) [23].

SNP selection and genotyping

A PubMed search was performed in October 2014 and we retrieved 151 SNPs from 88 genes, previously reported to be associated with T2DM or GDM (Supplementary Table 1). It is well known that an impaired insulin secretion plays a critical role in the development of T2DM or GDM in east Asian

including Japanese [24, 25]. Therefore, most of SNPs analyzed were insulin secretion candidate SNPs. Several T2DM susceptibility genes were identified in Japanese as well as Caucasian. All GDM risk gene variants examined were found in subjects other than Japanese. We selected the SNPs based on the criterion of the minor allele frequency (MAF) > 30% in Japanese population because this selection could provide adequate statistical power to detect SNPs with GRR ≥ 1.4 in our study cohort, as was described above. Additionally, gene-based tag SNPs (pairwise $r^2 < 0.8$) using HapMap-JPT in this study and several SNPs were excluded because of technical reasons (e.g. polymerase chain reaction failures). Finally, we investigated the association between 45 SNPs from 36 genes and the development of GDM. All polymorphisms analyzed in this study were in Hardy-Weinberg equilibrium.

Maternal peripheral blood samples were collected after delivery and genomic DNA was extracted using QIAsymphony DNA Midi Kit (96) (Qiagen, Valencia, CA, USA). Genotyping was performed using high-throughput genotyping MassARRAY® platform (Sequenom, Inc, San Diego, CA, USA). The primers including amplification and extension were designed using Assay Design Suite® (Sequenom, https://seqpws1.sequenom.com/AssayDesignerSuite.html) (Supplementary Table 2). Negative controls, at least quadruplicate, were placed at all 384 plates as quality controls. SNP genotyping success rate was > 94% and the concordance rate for genotyping was > 99.8% in this study.

Statistical analysis

Per-allele odd ratios (ORs) and their 95% confidence intervals (CIs) for the association between SNPs and GDM were estimated by logistic regression analysis. The possibility of multiple testing was avoided by Bonferroni correction. Therefore, we examined the combined effects of genetic variants on Japanese GDM and the cumulative effects of risk alleles at GDM-associated SNPs having lower *p*-value (pre-Bonferroni correction) [26]. Data are presented as mean ± SD or the number of cases (percent). Continuous data were compared between the GDM and NGT groups by Student's *t*-test. The frequencies of SNPs between the two groups were evaluated by logistic regression analysis. Categorical variables were analyzed by the Fisher's exact test. Statistical analyses were performed using SPSS v.22 (IBM, Chicago, IL, USA). A p-value < 0.05 was considered statistically significant. The calculation of linkage disequilibrium (LD) among SNPs and construction of a forest plot of per-allele ORs were done with R (version 3.3.1).

Results

Maternal characteristics

Maternal characteristics and metabolic measurements of the GDM and NGT (i.e. control) groups are shown in Table 1. There were no notable differences in maternal age at delivery, pregravid BMI, and the rate of overweight or nulliparous between the GDM and NGT groups. A first-degree family history of T2DM was more prevalent women with GDM, compared with NGT. With regard to metabolic measurements, FPG, 1h-PG, 2h-PG, and HOMA-IR were significantly higher in the GDM group compared with those in the NGT group. Women with GDM showed significantly lower levels of IS_{OGTT}, QUICKI, IGI, and ISSI-2, compared with NGT ($p < 0.05$).

Table 1 Comparison of maternal characteristics between the gestational diabetes mellitus and normal glucose tolerance groups

	GDM (n = 171)	NGT (n = 128)	*p*-value
Maternal age at delivery (years)	36.1 ± 4.6	36.6 ± 4.3	0.36
Pre-pregancy BMI (kg/m^2)	21.4 ± 3.3	20.7 ± 2.5	0.05
Pre-pregancy overweight	24 (14.0)	10 (7.8)	0.18
Nulliparous	111 (64.9)	79 (61.7)	0.63
A first-degree family history of diabetes	33 (19.3)	9 (7.0)	0.002
Prior miscarriage	57 (33.3)	58 (45.3)	0.04
Gestational week at OGTT (weeks)	27.5 ± 3.1	27.8 ± 2.8	0.36
Plasma glucose of OGTT			
0 min (mg/dL)	85.9 ± 7.5	82.3 ± 4.8	2.0×10^{-6}
60 min (mg/dL)	174.1 ± 25.0	141.4 ± 21.0	4.1×10^{-28}
120 min (mg/dL)	154.7 ± 25.6	121.0 ± 17.1	2.2×10^{-30}
IS_{OGTT}	5.09 ± 2.46	7.79 ± 3.51	6.5×10^{-12}
HOMA-IR	1.88 ± 1.68	1.14 ± 0.62	6.0×10^{-6}
QUICKI	0.36 ± 0.03	0.38 ± 0.04	9.1×10^{-9}
Insulinogenic index	0.78 ± 0.49	1.03 ± 0.99	0.01
ISSI-2	1.75 ± 0.54	2.46 ± 0.70	1.3×10^{-13}

BMI, body mass index; overweight, BMI ≥25kg/m^2; OGTT, oral glucose tolerance test; IS_{OGTT}, Insulin sensitivity index from OGTT; HOMA-IR, homeostasis model assessment for insulin resistance; QUICKI, quantitative insulin sensitivity check index; ISSI-2, Insulin Secretion-Sensitivity Index-2; Data, mean ± SD or N (%).

Case-control study

In this study, we evaluated the frequencies of 45 SNPs in the GDM and NGT groups using logistic regression analysis. The individual allele odds ratio (OR) is shown in Fig. 1 and Supplementary Table 3. Three genetic variants had nominal associations with GDM (rs266729 [$p = 0.013$, OR: 1.56, 95% CI: 1.10–2.23], rs10811661 [$p = 0.035$, OR: 1.46, 95% CI: 1.03–2.08], and rs9505118 [$p = 0.046$, OR: 1.41, 95% CI: 1.01–1.97]). Therefore, we examined the combined effects of the risk alleles from these three genetic variants (rs266729, rs10811661, and rs9505118). Taking into account these three variants, each individual could harbor between 0 and 6 possible risk alleles.

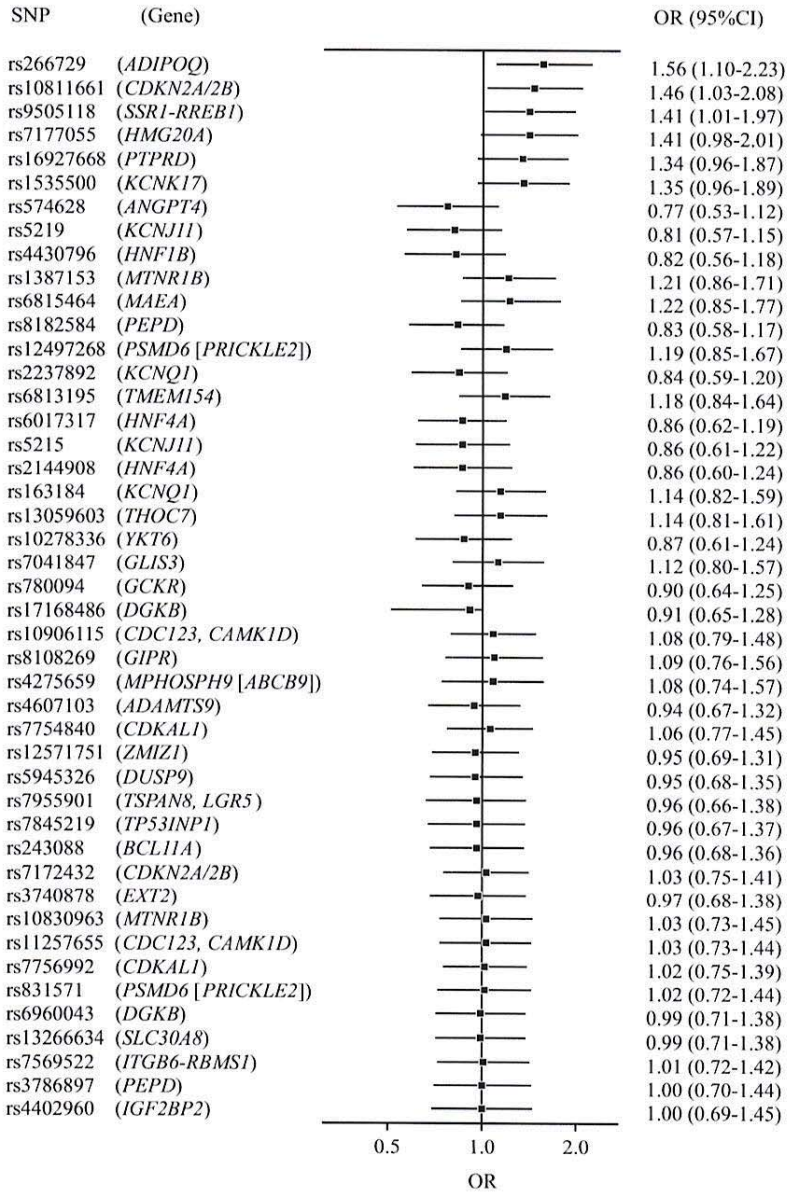

Fig. 1 A forest plot of per-allele odds ratio of 45 single nucleotide polymorphisms examined in this study
SNP, Single nucleotide polymorphism; OR, Odds ratio; CI, Confidence interval.

The distribution of risk alleles of the three genetic variants in the GDM and NGT groups are shown in Fig. 2A. The percentages of subjects with GDM increased in the subgroups with more risk alleles. Furthermore, there was a significant difference in the number of T2DM risk alleles between women with GDM and NGT (3.79 ± 1.33 *vs.* 3.05 ± 1.41, $p = 6.0 \times 10^{-6}$). Especially, women with five or more risk alleles showed a 7.32-fold increased risk of GDM ($p = 5.6 \times 10^{-5}$, 95% CI: 4.54–11.97), compared with those having no more than one risk allele (Fig. 2B). The LD values among three SNPs calculated using r^2 were under 0.02 in both GDM and NGT groups.

Discussion

With the development of genetic association studies, information on T2DM susceptibility genes has been accumulated in Japanese population. To date, however, no studies on GDM risk variants in Japanese women have been reported, although GDM may share genetic backgrounds with T2DM to some extent. In addition, there is a paucity of information on genetics of GDM by the new IADPSG criteria because the number of healthcare associations adopting the criteria is still limited [27]. Therefore, we designed the current study to examine the association of previously reported T2DM or GDM susceptibility genes with having GDM by the new IADPSG criteria in Japanese women.

It is demonstrated that the prevalence of GDM by the IADPSG criteria is 10-15% [28, 29]. When analyzing statistical power of our cohort (i.e. GDM, 171 women: NGT, 128 women) using Genetic Power Calculator in the GDM prevalence of 10%, SNPs with MAF > 30% could provide adequate statistical power to detect risk variants with GRR ≥ 1.4 in our study cohort. Of 45 SNPs examined, three genetic variants (rs266729, rs10811661, and rs9505118) were nominally associated with GDM in Japanese women. Since multiple genes would be involved in the development of GDM, we investigated the combined effects of three genetic variants on GDM. As a result, women with five or more risk alleles showed a 7.32-fold increased risk of GDM, compared with those having no more than one risk allele. Our results suggested the genetic background of GDM in a multigenetic manner in Japanese women.

Of the three genetic variants, rs266729 (*ADIPOQ*) is a gene involved in insulin sensitivity, while rs10811661 (*CDKN2A/2B*) and rs9505118 (*SSR1-RREB1*) play an important role in insulin secretion. Several studies have shown that a single polymorphism rs266729 is associated with decreased levels of serum adiponectin in GDM as well as T2DM [30, 31]. *CDKN2A/2B* is cyclin-dependent kinases 4 suppressor gene that contributes to the proliferation and maintenance of pancreatic β-cells. Based on previous studies, *CDKN2A/2B* is considered as one of the T2DM susceptibility genes in

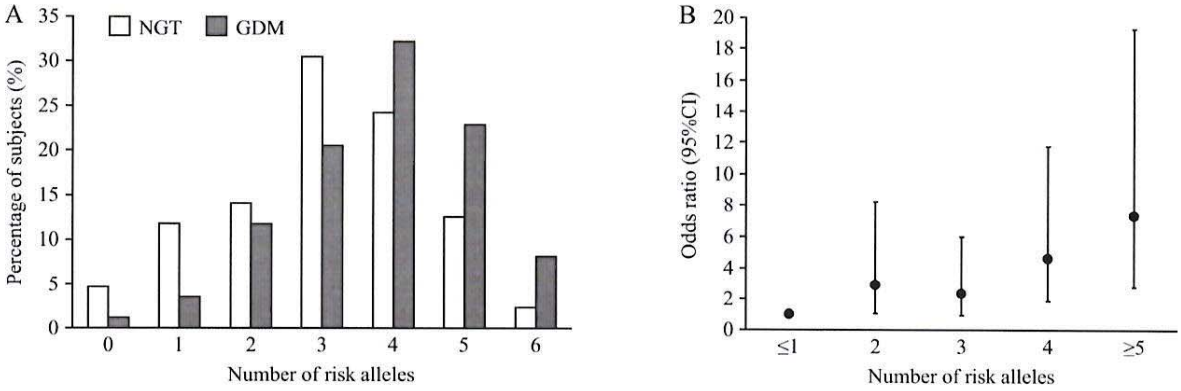

Fig. 2 Risk alleles of three genetic variants and the development of gestational diabetes mellitus

(**A**) Distribution of risk alleles of three genetic variants and in women with gestational diabetes mellitus (GDM) or normal glucose tolerance (NGT). Women with GDM presented significantly more T2DM risk alleles, compared with those with NGT. Black bars represent GDM (n = 171), while white bars represent NGT (n = 128). (**B**) Odds ratio for the risk of GDM according to the number of type 2 diabetes mellitus risk alleles carried. Women with five or more risk alleles showed a 7.32-fold increased risk of GDM ($p = 5.6 \times 10^{-5}$, 95% CI: 4.54–11.96), compared with those having no more than one risk allele.

Japanese as well as Europeans [3, 32]. With regard to *SSR1-RREB1*, it is demonstrated that the depletion of RAS-responsive element binding protein 1 (RREB1) encoded by *SSR1* reduces β-cell development and insulin secretion [33]. The meta-analysis of GWAS indicated that rs9505118 in *SSR1-RREB1* was associated with T2DM [34]. Therefore, the risk allele in *SSR1-RREB1* could be related to pancreatic β-cell dysfunction in T2DM. To the best of our knowledge, however, no association between *SSR1-RREB1* variants and risk of GDM has been demonstrated in previous reports. Our findings suggest that *SSR1-RREB1* might be one of risk variants associated with GDM in Japanese women.

It is demonstrated that a potential etiology for GDM is a limitation in beta cell reserves that manifests as maternal hyperglycemia when insulin secretion does not increase to match the escalated insulin needs during pregnancy. With regard to maternal characteristics, Asian women with GDM are less obese than Caucasian and Hispanic women [14, 16]. Thus, decreased insulin secretion in GDM might be more evident in Asians, compared with Caucasians and Hispanics [35]. Our previous investigation has shown that women with Japanese GDM have beta cell dysfunction irrespective of presence or absence of overweight [25]. Regarding the genetic background, several studies revealed risk variants related to insulin secretion in Korean and Chinese population [36-41]. Of the three genetic variants found in this study, two are related to the regulation of insulin secretion (i.e. beta cell function). Taken together, beta cell dysfunction might be the core pathophysiology of GDM in Japanese women.

The strength of the present study is that we performed the association analysis using SNPs more than ever before. Most previous studies on GDM risk variants were candidate gene approach using no more than ten variants [42], whereas we used 45 SNPs from 36 genes for analysis. In addition, women with GDM were diagnosed by a single criterion, and those with NGT were fully evaluated for the glucose tolerance status. All women in our cohort were taken care, based on the clinical recommendation by the Japan Society of Obstetrics and Gynecology [17]. The findings that maternal age at delivery, pre-pregnancy BMI and the rate of overweight were comparable between the GDM and NGT groups are important. Therefore, our study cohort is suitable to investigate GDM risk genes, as were suggested in previous reports [8, 40].

There are several limitations in this study. One of the limitations is that we focused on only SNPs with MAF > 30% since our study cohort was a relatively small panel. Therefore, we may have missed SNPs with MAF ≤ 30% that are associated with GDM in Japanese women because more than 80 susceptibility genes for T2DM have been were identified so far [43]. It is also important to replicate and evaluate the present findings in another independent case-control set. In this regard, the results of our study should be interpreted cautiously. In the future, we would conduct the multi-institutional collaborative genetic association study to investigate candidate gene variants for GDM. Ideally, GWAS should be performed to identify all candidate gene variants for GDM in Japanese women.

In conclusion, we performed the association analysis in the context of GDM in Japanese women for the first time and found that genetic variants in *ADIPOQ*, *CDKN2A/2B*, and *SSR1-RREB1* are nominally associated with the development of GDM in Japanese. Since women with GDM are at a high risk of future T2DM, genetic information on GDM would be useful for the T2DM risk classification [38, 41]. Further research using a larger cohort is warranted for better understanding the genetics of GDM in Japanese women.

Disclosure

The authors have no conflict of interest to declare in this study.

Funding

This study was supported by Japan Agency for Medical Research and Development Diseases (AMED, 16gm0510011h0205, 16ek0109067h0003, 16gk0110013s0801, 16gk0110018s0601), KAKENHI (26293365 and 26462500), Grants from the NCCHD of Japan (26-13), and a CREST Program of JST (Epigenomic analysis of the human placenta and endometrium constituting the fetal-maternal interface).

Acknowledgements

The authors are grateful to all medical staffs at Keio University Hospital for excellent patient care. We also appreciate medical staff in the perinatal unit of National Center for Child Health and Development.

Supplementary Table 1 Genotype information previously reported to be associated with type 2 diabetes or gestational diabetes mellitus

Chr	SNP	Nearby gene	Minor allele	MAF	Risk allele	Candidate gene for GDM	References on GDM	Candidate gene for T2DM	References on T2DM	Reasons for exclusion from our analysis
16	rs3785233	*A2BP1(RBFOX1)*	G	0.18	C			Yes	Miyake *et al.* J Hum Genet, 2009	
3	rs4607103	*ADAMTS9*	T	0.41	C			Yes	Zeggini *et al.* Nat Genet, 2008	
3	rs6795735	*ADAMTS9*	C	0.21	C			Yes	Voight *et al.* Nat Genet, 2010	
3	rs11717195	*ADCY5*	C	0	C			Yes	Saxena *et al.* Nat Genet, 2010	No variation in Japanese
3	rs11708067	*ADCY5*	G	0	A			Yes	Andersson *et al.* Diabetologia, 2010	No variation in Japanese
3	rs2241766	*ADIPOQ*	G	0.22	T	Yes	Beltcheva *et al.* Arch Gynecol Obstet, 2014			
3	rs266729	*ADIPOQ*	G	0.31	C	Yes	Beltcheva *et al.* Arch Gynecol Obstet, 2014	Yes	Han *et al.* Diabetelogia, 2011	
8	rs4994	*ADRB3*	G	0.19	G			Yes	Jing *et al.* Endocrine, 2012	
20	rs574628	*ANGPT4*	A	0.37	G			Yes	Miyake *et al.* J Hum Genet, 2009	
8	rs515071	*ANK1*	A	0.22	C			Yes	Imamura *et al.* Hum Mol Genet, 2012	
8	rs516946	*ANK1*	T	0.16	C			Yes	Morris *et al.* Nat Genet, 2012	
15	rs2028299	*AP3S2*	C	0.20	C			Yes	Kooner *et al.* Nat Genet, 2011	
11	rs1552224	*ARAP1*	C	0.04	A	Yes	Huerta-Chagoya A *et al.* PLoS One, 2015	Yes	Voight *et al.* Nat Genet, 2010	
5	rs702634	*ARL15*	C	0.12	A			Yes	DIAGRAM Nat Genet, 2014	
16	rs7202877	*BCAR1*	G	0.21	G			Yes	Morris *et al.* Nat Genet, 2012	
2	rs243019	*BCL11A*	T	0.27	C			Yes	Metabochip®	
2	rs243021	*BCL11A*	G	0.27	A			Yes	Voight *et al.* Nat Genet, 2010	
2	rs243088	*BCL11A*	T	0.44	T			Yes	Voight *et al.* Nat Genet, 2010	
15	rs7163757	*C2CD4A*	T	0.38	C			Yes	Yamauchi *et al.* Nat Genet, 2010	Gene-based genetic redundancy (pairwise $r^2 > 0.8$)
15	rs7172432	*C2CD4A, C2CD4B*	G	0.45	A			Yes	Yamauchi *et al.* Nat Genet, 2010	
10	rs10906115	*CDC123, CAMK1D*	G	0.49	A			Yes	Shu *et al.* PLoS Genet, 2010	
10	rs11257655	*CDC123, CAMK1D*	T	0.41	T			Yes	Voight *et al.* Nat Genet, 2010	
10	rs12779790	*CDC123, CAMK1D*	G	0.12	G			Yes	Zeggini *et al.* Nat Genet, 2008	
6	rs10440833	*CDKAL1*	A	0.40	A			Yes	Voight *et al.* Nat Genet, 2010	Gene-based genetic redundancy (pairwise $r^2 > 0.8$)
6	rs7754840	*CDKAL1*	C	0.41	C	Yes	Zhang *et al.* Hum Reprod Update, 2013	Yes	Scott *et al.* Science, 2007	
6	rs7756992	*CDKAL1*	G	0.46	G	Yes	Cho YM *et al.* Diabetologia, 2009	Yes	Voight *et al.* Nat Genet, 2010	
6	rs4712523	*CDKAL1*	G	0.41	G			Yes	Takeuchi *et al.* Diabetes, 2009	Gene-based genetic redundancy (pairwise $r^2 > 0.8$)
9	rs10811661	*CDKN2A, CDKN2B*	C	0.48	T	Yes	Cho YM *et al.* Diabetologia, 2009	Yes	Scott *et al.* Science, 2007	
9	rs10965250	*CDKN2A, CDKN2B*	A	0.43	G			Yes	Voight *et al.* Nat Genet, 2010	Gene-based genetic redundancy (pairwise $r^2 > 0.8$)
9	rs2383208	*CDKN2A, CDKN2B*	G	0.45	A	Yes	Wang Y *et al.* PLoS One, 2011	Yes	Takeuchi *et al.* Diabetes, 2009	Gene-based genetic redundancy (pairwise $r^2 > 0.8$)
9	rs13292136	*CHCHD9*	T	0.13	C			Yes	Voight *et al.* Nat Genet, 2010	
19	rs10401969	*CILP2(SUGP1)*	C	0.09	C			Yes	Morris *et al.* Nat Genet, 2012	
7	rs17168486	*DGKB*	T	0.41	T			Yes	Dupuis *et al.* Nat Genet, 2010	
7	rs2191349	*DGKB*	G	0.27	T			Yes	Dupuis *et al.* Nat Genet, 2010	
7	rs6960043	*DGKB*	C/T	0.50	C			Yes	Dupuis *et al.* Nat Genet, 2010	
X	rs5945326	*DUSP9*	G	0.38	A			Yes	Voight *et al.* Nat Genet, 2010	
11	rs3740878	*EXT2*	C	0.36	A			Yes	Takeuchi *et al.* Diabetes, 2009	
1	rs17106184	*FAF1*	A	0.06	G			Yes	DIAGRAM Nat Genet, 2014	
12	rs3741872	*FAM60A*	C	0.27	C			Yes	Miyake *et al.* J Hum Genet, 2009	
16	rs8050136	*FTO*	A	0.18	A			Yes	Scott *et al.* Science, 2007	
16	rs11642841	*FTO*	A	0.06	A			Yes	Voight *et al.* Nat Genet, 2010	
16	rs9936385	*FTO*	C	0.12	C			Yes	Voight *et al.* Nat Genet, 2010	
7	rs17867832	*GCC1*	G	0.05	T			Yes	Cho *et al.* Nat Genet, 2012	
7	rs6467136	*GCC1*	A	0.18	G			Yes	Cho *et al.* Nat Genet, 2012	
7	rs1799884	*GCK*	T	0.17	T	Yes	Zhang *et al.* Hum Reprod Update, 2013			
7	rs4607517	*GCK*	A	0.20	A	Yes	Mao *et al.* PLoS One, 2012	Yes	Dupuis *et al.* Nat Genet, 2010	
2	rs780094	*GCKR*	C	0.44	C	Yes	Huopio H *et al.* Eur J Endocrinol, 2013	Yes	Dupuis *et al.* Nat Genet, 2010	
19	rs8108269	*GIPR*	T	0.39	G			Yes	Morris *et al.* Nat Genet, 2012	
9	rs7041847	*GLIS3*	G	0.47	A			Yes	Cho *et al.* Nat Genet, 2012	
9	rs11787792	*GPSM1*	G	0.05	A			Yes	Hara *et al.* Hum Mol Genet, 2014	

Supplementary Table 1 Cont.

Chr	SNP	Nearby gene	Minor allele	MAF	Risk allele	Candidate gene for GDM	References on GDM	Candidate gene for T2DM	References on T2DM	Reasons for exclusion from our analysis
2	rs13389219	*GRB14*	T	0.08	C			Yes	Kooner *et al.* Nat Genet, 2011	
2	rs3923113	*GRB14*	C	0.09	A			Yes	Kooner *et al.* Nat Genet, 2011	
10	rs5015480	*HHEX*	C	0.20	C	Yes	Cho YM *et al.* Diabetologia, 2009	Yes	Voight *et al.* Nat Genet, 2010	
10	rs7923837	*HHEX*	G	0.20	G	Yes	Cho YM *et al.* Diabetologia, 2009	Yes	Qian *et al.* PLoS One, 2012	
15	rs7177055	*HMG20A*	A	0.41	A			Yes	Kooner *et al.* Nat Genet, 2011	
15	rs7178572	*HMG20A*	G	0.46	G			Yes	Fukuda *et al.* PLoS One, 2012	Polymerase chain reaction failures
12	rs2261181	*HMGA2(RPSAP52)*	T	0.15	T			Yes	Voight *et al.* Nat Genet, 2010	
12	rs1531343	*HMGA2(RPSAP52)*	C	0.13	C			Yes	Voight *et al.* Nat Genet, 2010	
12	rs2612035	*HMGA2(RPSAP52)*	G	0.13	G			Yes	Voight *et al.* Nat Genet, 2011	
12	rs12427353	*HNF1A*	C	0	G			Yes	Langenberg *et al.* PLoS Med, 2014	No variation in Japanese
17	rs11651755	*HNF1B*	C	0.29	C			Yes	Metabochip®	
17	rs11651052	*HNF1B*	A	0.30	A			Yes	Voight *et al.* Nat Genet, 2010	
17	rs4430796	*HNF1B*	G	0.36	G			Yes	Voight *et al.* Nat Genet, 2010	
20	rs2144908	*HNF4A*	A	0.42	A	Yes	Shaat N *et al.* Diabetologia, 2006	Yes	Chavali *et al.* J Hum Genet, 2011	
20	rs4812829	*HNF4A*	A	0.40	A			Yes	Kooner *et al.* Nat Genet, 2011	Gene-based genetic redundancy (pairwise $r^2 > 0.8$)
20	rs6017317	*HNF4A*	T	0.46	G			Yes	Cho *et al.* Nat Genet, 2012	
3	rs4402960	*IGF2BP2*	T	0.30	T	Yes	Mao *et al.* PLoS One, 2012	Yes	Voight *et al.* Nat Genet, 2010	
3	rs1470579	*IGF2BP2*	C	0.33	C			Yes	Saxena *et al.* Science, 2007	Gene-based genetic redundancy (pairwise $r^2 > 0.8$)
3	rs6769511	*IGF2BP2*	C	0.33	C			Yes	Long *et al.* Am J Epidemiol, 2012	Polymerase chain reaction failures
2	rs7578326	*IRS1*	G	0.18	A			Yes	Voight *et al.* Nat Genet, 2010	
2	rs1801278	*IRS1*	T	0.08	T	Yes	Zhang *et al.* Hum Reprod Update, 2013	Yes	Alharbi *et al.* Endocrine, 2014	
2	rs2943640	*IRS1*	A	0.07	C			Yes	Voight *et al.* Nat Genet, 2010	
2	rs2943641	*IRS1*	T	0.07	C			Yes	Rung *et al.* Nat Genet, 2009	
2	rs7593730	*ITGB6-RBMS1*	T	0.12	C			Yes	Qi *et al.* Hum Mol Genet, 2010	
2	rs7569522	*ITGB6-RBMS1*	A	0.38	A			Yes	Qi *et al* Hum Mol Genet, 2010	
7	rs849134	*JAZF1*	G	0.21	A			Yes	Voight *et al.* Nat Genet, 2010	
7	rs864745	*JAZF1*	C	0.21	T	Yes	Stuebe AM *et al.* Am J Perinatol, 2014	Yes	Zeggini *et al.* Nat Genet, 2008	
7	rs849135	*JAZF1*	A	0	G			Yes	Langenberg *et al.* PLoS Med, 2014	No variation in Japanese
11	rs5215	*KCNJ11*	C	0.34	C			Yes	Scott *et al.* Science, 2007	
11	rs5219	*KCNJ11*	T	0.35	T	Yes	Mao *et al.* PLoS One, 2012	Yes	Sokolova *et al.* PLoS One, 2014	
6	rs1535500	*KCNK17*	T	0.40	T			Yes	Cho *et al.* Nat Genet, 2012	
11	rs231362	*KCNQ1*	T	0.13	G			Yes	Voight *et al.* Nat Genet, 2010	
11	rs163184	*KCNQ1*	G	0.42	G	Yes	Huerta-Chagoya A *et al.* PLoS One, 2015	Yes	Voight *et al.* Nat Genet, 2010	
11	rs2237892	*KCNQ1*	T	0.36	C	Yes	Mao *et al.* PLoS One, 2012	Yes	Yasuda *et al.* Nat Genet, 2008	
11	rs231361	*KCNQ1*	C	0.17	A			Yes	Voight *et al.* Nat Genet, 2010	
11	rs2237895	*KCNQ1*	C	0.3	C	Yes	Mao *et al.* PLoS One, 2012	Yes	Unoki *et al.* Nat Genet, 2008	Unique primer design failure
7	rs13233731	*KLF14*	A	0.29	G			Yes	Voight *et al.* Nat Genet, 2010	
7	rs972283	*KLF14*	A	0.29	G			Yes	Voight *et al.* Nat Genet, 2010	
12	rs10842994	*KLHDC5*	T	0.21	T			Yes	Morris *et al.* Nat Genet, 2012	
12	rs2307027	*KRT4*	C	0.17	C			Yes	Miyake *et al.* J Hum Genet, 2009	
4	rs6819243	*MAEA*	C	0.36	T			Yes	Cho *et al.* Nat Genet, 2012	Gene-based genetic redundancy (pairwise $r^2 > 0.8$)
4	rs6815464	*MAEA*	G	0.36	C			Yes	Cho *et al.* Nat Genet, 2012	
18	rs12970134	*MC4R*	A	0.19	A			Yes	Morris *et al.* Nat Genet, 2012	
7	rs791595	*MIR129-LEP*	A	0.10	A			Yes	Hara *et al.* Hum Mol Genet, 2014	
12	rs4275659	*MPHOSPH9(ABCB9)*	T	0.33	C			Yes	DIAGRAM Nat Genet, 2014	
11	rs10830963	*MTNR1B*	G	0.47	G	Yes	Mao *et al.* PLoS One, 2012	Yes	Dupuis *et al.* Nat Genet, 2010	
11	rs1387153	*MTNR1B*	T	0.48	T	Yes	Zhang *et al.* Hum Reprod Update, 2013	Yes	Voight *et al.* Nat Genet, 2010	
1	rs10923931	*NOTCH2*	T	0.02	T			Yes	Zeggini *et al.* Nat Genet, 2008	
19	rs8182584	*PEPD*	G	0.36	T			Yes	Cho *et al.* Nat Genet, 2012	
19	rs3786897	*PEPD*	G	0.45	A			Yes	Cho *et al.* Nat Genet, 2012	

Supplementary Table 1 Cont.

Chr	SNP	Nearby gene	Minor allele	MAF	Risk allele	Candidate gene for GDM	References on GDM	Candidate gene for T2DM	References on T2DM	Reasons for exclusion from our analysis
19	rs10425678	*PEPD*	C	0.27	C			Yes	Cho *et al.* Nat Genet, 2012	Polymerase chain reaction failures
6	rs3130501	*POU5F1*	A	0.45	G			Yes	Nair *et al.* Diabetologia, 2014	Unique primer design failure
3	rs1801282	*PPARG*	G	0.06	C	Yes	Wu L *et al.* Sci Rep, 2016	Yes	Saxena *et al.* Science, 2007	
3	rs13081389	*PPARG*	G	0.04	A			Yes	Voight *et al.* Nat Genet, 2010	
15	rs12899811	*PRC1*	A	0.01	G			Yes	Voight *et al.* Nat Genet, 2010	
15	rs8042680	*PRC1-AS1*	C	0	A			Yes	DIAGRAM Nat Genet, 2014	No variation in Japanese
1	rs2075423	*PROX1*	T	0.14	G			Yes	Dupuis *et al.* Nat Genet, 2010	
1	rs340874	*PROX1-AS1*	C	0.33	C			Yes	Hu *et al.* PLoS One, 2010	Polymerase chain reaction failures
3	rs12497268	*PSMD6(PRICKLE2)*	C	0.39	G			Yes	Cho *et al.* Nat Genet, 2012	
3	rs831571	*PSMD6(PRICKLE2)*	T	0.31	C			Yes	Cho *et al.* Nat Genet, 2012	
3	rs13059603	*PSMD6(THOC7)*	G	0.32	A			Yes	Cho *et al.* Nat Genet, 2012	
9	rs16927668	*PTPRD*	T	0.43	T			Yes	Tsai *et al.* PLoS One, 2010	
9	rs17584499	*PTPRD*	T	0.15	T			Yes	Tsai *et al.* PLoS One, 2010	
2	rs7560163	*RBM43, RND3*	G	0.19	C			Yes	Palmer *et al.* PLoS One, 2012	
2	rs4410242	*RBMS1*	A	0.17	G			Yes	Metabochip®	
17	rs312457	*SLC16A13*	C	0.07	G			Yes	Hara *et al.* Hum Mol Genet, 2014	Unique primer design failure
8	rs13266634	*SLC30A8*	T	0.44	C	Yes	Cho YM *et al.* Diabetologia, 2009	Yes	Sladek *et al.* Science, 2007	
8	rs3802177	*SLC30A8*	A	0.45	G	Yes	Liang Z *et al.* Diabetes Res Clin Pract, 2010	Yes	Voight *et al.* Nat Genet, 2010	Gene-based genetic redundancy (pairwise $r^2 > 0.8$)
17	rs391300	*SRR*	T	0.22	G	Yes	Wang Y *et al.* PLoS One, 2011	Yes	Tsai *et al.* PLoS One, 2010	
6	rs9505118	*SSR1-RREB1*	G	0.41	A			Yes	DIAGRAM Nat Genet, 2014	
3	rs16861329	*ST6GAL1*	T	0.24	G			Yes	Kooner *et al.* Nat Genet, 2011	
3	rs17301514	*ST6GAL1*	A	0.04	A			Yes	Kooner *et al.* Nat Genet, 2011	
10	rs12255372	*TCF7L2*	T	0.02	T	Yes	Zhang *et al.* Hum Reprod Update, 2013	Yes	Tabara *et al.* Diabetes, 2009	
10	rs7901695	*TCF7L2*	C	0.04	C	Yes	Huerta-Chagoya A *et al.* PLoS One, 2015	Yes	Yamauchi *et al.* Nat Genet, 2010	
2	rs10203174	*THADA*	T	0.02	C			Yes	Voight *et al.* Nat Genet, 2010	
2	rs7578597	*THADA*	C	0.01	T			Yes	Zeggini *et al.* Nat Genet, 2008	
2	rs11899863	*THADA*	C	0	C			Yes	Mercader *et al.* PLoS Genet, 2012	No variation in Japanese
9	rs17791513	*TLE4*	G	0.08	A			Yes	Voight *et al.* Nat Genet, 2010	
4	rs6813195	*TMEM154*	T	0.46	C			Yes	DIAGRAM Nat Genet, 2014	
6	rs1800629	*TNF*	A	0.02	G	Yes	Wu L *et al.* Sci Rep, 2016	Yes	Boraska *et al.* BMC Med Genet, 2010	Unique primer design failure
8	rs7845219	*TP53INP1*	T	0.46	T			Yes	Voight *et al.* Nat Genet, 2010	
12	rs4760790	*TSPAN8, LGR5*	A	0.24	A			Yes	Voight *et al.* Nat Genet, 2010	
12	rs7961581	*TSPAN8, LGR5*	C	0.23	C	Yes	Stuebe AM *et al.* Am J Perinatol, 2014	Yes	Zeggini *et al.* Nat Genet, 2008	
12	rs4760915	*TSPAN8, LGR5*	T	0.27	T			Yes	Metabochip®	
12	rs7955901	*TSPAN8, LGR5*	T	0.30	C			Yes	Voight *et al.* Nat Genet, 2010	
3	rs7612463	*UBE2E2*	A	0.15	C	Yes	Kim JY *et al.* Gynecol Endocrinol, 2013	Yes	Yamauchi *et al.* Nat Genet, 2010	
3	rs1496653	*UBE2E2*	G	0.15	A			Yes	Yamauchi *et al.* Nat Genet, 2010	
3	rs6780569	*UBE2E2*	A	0.15	G			Yes	Yamauchi *et al.* Nat Genet, 2010	
10	rs1802295	*VPS26A*	T	0.12	A			Yes	Kooner *et al.* Nat Genet, 2011	
10	rs12242953	*VPS26A*	A	0.05	G			Yes	Kooner *et al.* Nat Genet, 2011	
4	rs4458523	*WFS1*	T	0.02	G			Yes	Voight *et al.* Nat Genet, 2010	
4	rs4689388	*WFS1*	G	0.02	T			Yes	Rung *et al.* Nat Genet, 2009	
4	rs1801214	*WFS1*	C	0	T			Yes	Long *et al.* Am J Epidemiol, 2013	No variation in Japanese
16	rs17797882	*WWOX*	T	0.21	C			Yes	Sakai *et al.* PLoS One, 2013	
7	rs10278336	*YKT6*	G	0.43	A			Yes	Dupuis *et al.* Nat Genet, 2010	
5	rs4457053	*ZBED3*	G	0.03	G			Yes	Voight *et al.* Nat Genet, 2010	
5	rs6878122	*ZBED3*	G	0.02	G			Yes	Voight *et al.* Nat Genet, 2010	
6	rs9470794	*ZFAND3*	C	0.20	C			Yes	Cho *et al.* Nat Genet, 2012	
6	rs4299828	*ZFAND3(BTBD9)*	G	0.06	A			Yes	Cho *et al.* Nat Genet, 2012	
15	rs11634397	*ZFAND6*	G	0.09	G			Yes	Voight *et al.* Nat Genet, 2010	
10	rs12571751	*ZMIZ1*	G	0.42	G			Yes	Morris *et al.* Nat Genet, 2012	

The information was retrieved from HapMap JPT as well as previous studies. Chr, Chromosome; SNP, Single nucleotide polymorphism; MAF, Minor allele frequency; T2DM, Type 2 diabtes mellitus; GDM, Gestational diabetes mellitus.

Supplementary Table 2 Primers designed by Assay Design Suite in this study

SNP	Forward primer sequence	Reverse primer sequence	Extension primer sequence
rs10278336	ACGTTGGATGGAACAATCCTGTGGATTGTG	ACGTTGGATGGCACTGTGCTAAAATCCTC	AATCCTCATATGATTGAAAGG
rs10811661	ACGTTGGATGGTCAATAAGCGTTCTTGCCC	ACGTTGGATGGATCAGGAGGGTAATAGAC	cccgtAGGGTAATAGACTTACTGTCATG
rs10830963	ACGTTGGATGAGGTCACTCTGTCTATGCTG	ACGTTGGATGCCAGGCAGTTACTGGTTCT	gggcGGCAGTTACTGGTTCTGGATAG
rs10906115	ACGTTGGATGATTGAGGACTCCGTTTTGGC	ACGTTGGATGGTTACGTGTATGCGATCCC	cgggACGTGTATGCGATCCCAAGTTTG
rs11257655	ACGTTGGATGTGCAAAGCACCTACTGCTTC	ACGTTGGATGCCACGGAGATGGTTTCATGC	ttaaGGTTTCATGCCCAGTA
rs12497268	ACGTTGGATGAGGCACCCCCTTGAAAAACA	ACGTTGGATGGAAACTGATAGTAGATGCTG	GCTTGATCAGAGCAGGA
rs12571751	ACGTTGGATGGGTGTGTGCATGGTACGTAT	ACGTTGGATGAAACACCTACAGACCCGAG	ttgGGAGGAGGAAAACAGTG
rs13059603	ACGTTGGATGTGACAGACTGCTCAAGCTAC	ACGTTGGATGGTCTCAGTCTCTTCAGATAA	cTTTAAAAATACAAACTAATGCTTTC
rs13266634	ACGTTGGATGGCAATCAGTGCTAATCTCCC	ACGTTGGATGTTTCTCTCCGAACCACTTG	tctccCCACTTGGCTGTCCC
rs1387153	ACGTTGGATGCTCTCTCTAGAGCTCACAAC	ACGTTGGATGTGTCTGTGGAATGCTAGCAA	CTTTTACAGATAAGAAAATTGAGTT
rs1535500	ACGTTGGATGAGAGATGGGGATCTTCTGAG	ACGTTGGATGAGCTCTGGCTGCTCAGTAGG	aGCGTCAAGGATGGGG
rs163184	ACGTTGGATGTTTGCTCAGTAACGGACTGG	ACGTTGGATGGGTAAAGTGTCTGTGGAAAG	ccGGGGCAAGGGTGGAG
rs16927668	ACGTTGGATGCCATTTTAGTGGCCTGTTGG	ACGTTGGATGCACTCTTCAGAACTGGAAGG	gaagaTTCAGAACTGGAAGGAATAGG
rs17168486	ACGTTGGATGGCACCGTGAGGGATATTAAG	ACGTTGGATGCTGCTGATCTGGTTGATCTT	cctgcTCTCTTGCCATTTGACACC
rs2144908	ACGTTGGATGACCACGTGCATTGCAAAGAC	ACGTTGGATGCCTGACTAGAGTCAGGAGAT	TCTGTCATTCCCTGGC
rs2237892	ACGTTGGATGCAGATGATGGGAGCTGTCAC	ACGTTGGATGTAAGGCATCTGGTGGAGAGG	CTAGGCCCCTCACCCC
rs243088	ACGTTGGATGTGAGAGTAGGGTAGGAACAC	ACGTTGGATGTGTGGAAAAGGGTAGCTCCG	tGGTAGCTCCGAGAAGA
rs266729	ACGTTGGATGATGTGTGGCTTGCAAGAACC	ACGTTGGATGTGGACTTTCTTGGCACGCTC	CGCTCATGTTTTGTTTTTGAAG
rs3740878	ACGTTGGATGCAAAAACATACCTGGCTGTC	ACGTTGGATGCACAAAAGAATGCAGTGTGG	ccggCACAAGCATGATTTTATTGTCCT
rs3786897	ACGTTGGATGAAGCCATCCTGGAAGACCTG	ACGTTGGATGATCTGCATAGGACAGCCCCA	ggagGCCTGGGCTGAGCCCTGAG
rs4275659	ACGTTGGATGAGAGGTGATAAGACTGCTG	ACGTTGGATGTGCTGACGCATGTAAGTGCC	AGACTGCTGAGGCTAA
rs4402960	ACGTTGGATGAGCAGTAAGGTAGGATGGAC	ACGTTGGATGTGGGGCATGTTTGCAAACAC	ggtggGCAAACACAATCAGTATCTT
rs4430796	ACGTTGGATGTGAATACAGAGAGGCAGCAC	ACGTTGGATGCAAAGACCCAACAACGCTTG	gggatAGGCAGCACAGACTGGA
rs4607103	ACGTTGGATGTCATAATTCCTCAGGCCCAG	ACGTTGGATGGTGTGTACCAAGGACATCCA	AGGCCCAGCAGGTTT
rs5215	ACGTTGGATGCTGTGGTCCTCATCAAGCTG	ACGTTGGATGACGGACGTTACTCTGTGGAC	GTGTGGGCACTTTGA
rs5219	ACGTTGGATGTGTTCTTGTGGGCCACGTTG	ACGTTGGATGGCATCATCCCCGAGGAATA	gagaCACGGTACCTGGGCT
rs574628	ACGTTGGATGCTCTTGACCCCACATCAAAG	ACGTTGGATGTCTCAGTGCCTAATCCGGAG	CCACATCAAAGGTCAGG
rs5945326	ACGTTGGATGCAGGGATCTCAGGCTCTTTA	ACGTTGGATGTGTCTCCAGGGCTTTGCAC	GGGGCCGTAGCAATG
rs6017317	ACGTTGGATGAAGAAAAGGCAAAGGATCTG	ACGTTGGATGTGGCCATTTCTATGTTGTC	TCTATGTTGTCTTGTTTTGAG
rs6813195	ACGTTGGATGGGGAGAGGAAGCAAGTAAAC	ACGTTGGATGATGGCAACCACACTCCTGCT	gaggGTAAATACTGGCCTTGC
rs6815464	ACGTTGGATGTCTGCACACATCCTGCTTAG	ACGTTGGATGAGCTCTCACGAGGAAGCAAT	cggaCCGATACCTGTACCCCGGGTTTTG
rs6960043	ACGTTGGATGCCCTTTTGGACTAATAGCTG	ACGTTGGATGGCCCTTGAATGTGAGGTTTA	AACCTGCTGTCCTCA
rs7041847	ACGTTGGATGGATGCCGGGTTGTAAATCAC	ACGTTGGATGCCACCTCATCGCATACATTT	TCCTTCCCTTGACCA
rs7172432	ACGTTGGATGCTTTGGGAGATAGGTTCTGC	ACGTTGGATGGCTTAAAAGAGGGCTTGGG	AGACAGTTTCTTTGGGAA
rs7177055	ACGTTGGATGCACAGCTTCTACCTTACGTG	ACGTTGGATGCTAGGAGGACATCTTACCTG	ccccCCTTACGTGCTGAGAC
rs7569522	ACGTTGGATGCTGTCCCAAATTGCTTTCAG	ACGTTGGATGGCCAGTGCATGTATGTAAAT	GTAAATAGTTATGGGGATTGAAATA
rs7754840	ACGTTGGATGATCAACTGCTTGCTGTTGGG	ACGTTGGATGCAGAGACATCACTGTCCTTT	AAATCCTCTATCAAGTCAAC
rs7756992	ACGTTGGATGGACAATTAATATTCCCCCCTG	ACGTTGGATGATGCAACCAAGAGAGGTCTG	cattaCCCCCTGTATTTTAGTTTT
rs780094	ACGTTGGATGAGGGCCCCAGTTTTTTAGAC	ACGTTGGATGCCCGGCCTCAACAAATGTAT	cttgTAGACCATGACTGACACAT
rs7845219	ACGTTGGATGTTCTTTGGGCTTCGTGTTCC	ACGTTGGATGACCCCTATTGTGGAGCTCTA	CTTCGTGTTCCATTATTCTGAA
rs7955901	ACGTTGGATGATGCATTCATAGACACCACC	ACGTTGGATGTGTTGTGTACATGCACTGGG	gggagGGGAGCCCAAGTGGTT
rs8108269	ACGTTGGATGGGGTCCTGATTTCAACACCT	ACGTTGGATGCCCCATTTTCTGGATAGGGA	ttAGACATGTCACCCTGA
rs8182584	ACGTTGGATGGCATGACGACAAACACAGAC	ACGTTGGATGTTGCTCATTTCAGGCACTCG	GCACTCGGAGCCTCAG
rs831571	ACGTTGGATGGACAAGGCTATTCCATCCTC	ACGTTGGATGGTGACCTAGAGATAGGGCTG	TCTTGACAACAAGATAGGCTTTA
rs9505118	ACGTTGGATGACTTGGTTATTGTACTGCTG	ACGTTGGATGCAGCAGTTTTTAAGCGTTTAC	ACTGCTGAAGACACC

SNP, Single nuchreotude polymorphism.

Supplementary Table 3 Association analysis results between single nucleotide polymorphisms and the risk of gestational diabetes mellitus

	SNP	Chr	Nearby gene	Insulin sensitivity	Insulin secretion	Risk allele	Japanese major allele	Japanese minor allele	RAF in this study		The present study	
									GDM	NGT	*p*-value	OR (95%CI)
1	rs266729	3	*ADIPOQ*	Yes		C	C	G	0.79	0.69	0.013	1.56 (1.10-2.23)
2	rs10811661	9	*CDKN2A/2B*		Yes	T	T	C	0.58	0.49	0.035	1.46 (1.03-2.08)
3	rs9505118	6	*SSR1-RREB1*		Yes	A	A	G	0.58	0.50	0.046	1.41 (1.01-1.97)
4	rs7177055	15	*HMG20A*		Yes	A	G	A	0.39	0.32	0.064	1.41 (0.98-2.01)
5	rs16927668	9	*PTPRD*	Yes		T	T	C	0.55	0.48	0.083	1.34 (0.96-1.87)
6	rs1535500	6	*KCNK17*			T	G	T	0.38	0.31	0.087	1.35 (0.96-1.89)
7	rs574628	20	*ANGPT4*	Yes		G	G	A	0.59	0.64	0.165	0.77 (0.53-1.12)
8	rs5219	11	*KCNJ11*		Yes	T	C	T	0.36	0.41	0.245	0.81 (0.57-1.15)
9	rs4430796	17	*HNF1B*		Yes	G	A	G	0.31	0.35	0.279	0.82 (0.56-1.18)
10	rs1387153	11	*MTNR1B*		Yes	T	C	T	0.49	0.45	0.280	1.21 (0.86-1.71)
11	rs6815464	4	*MAEA*	Yes		C	C	G	0.68	0.64	0.282	1.22 (0.85-1.77)
12	rs8182584	19	*PEPD*	Yes		T	T	G	0.62	0.67	0.284	0.83 (0.58-1.17)
13	rs12497268	3	*PSMD6(PRICKLE2)*			G	G	C	0.65	0.60	0.312	1.19 (0.85-1.67)
14	rs2237892	11	*KCNQ1*		Yes	C	C	T	0.63	0.67	0.326	0.84 (0.59-1.20)
15	rs6813195	4	*TMEM154*		Yes	C	T	C	0.48	0.44	0.341	1.18 (0.84-1.64)
16	rs6017317	20	*HNF4A*		Yes	G	G	T	0.52	0.56	0.357	0.86 (0.62-1.19)
17	rs5215	11	*KCNJ11*		Yes	C	T	C	0.38	0.42	0.393	0.86 (0.61-1.22)
18	rs2144908	20	*HNF4A*		Yes	A	G	A	0.46	0.48	0.425	0.86 (0.60-1.24)
19	rs163184	11	*KCNQ1*		Yes	G	T	G	0.48	0.45	0.430	1.14 (0.82-1.59)
20	rs13059603	3	*THOC7*			A	A	G	0.66	0.63	0.446	1.14 (0.81-1.61)
21	rs10278336	7	*YKT6*			A	A	G	0.67	0.70	0.446	0.87 (0.61-1.24)
22	rs7041847	9	*GLIS3*		Yes	A	G	A	0.47	0.44	0.506	1.12 (0.80-1.57)
23	rs780094	2	*GCKR*	Yes		G	A	G	0.44	0.47	0.512	0.90 (0.64-1.25)
24	rs17168486	7	*DGKB*		Yes	T	C	T	0.39	0.41	0.598	0.91 (0.65-1.28)
25	rs10906115	10	*CDC123, CAMK1D*		Yes	A	A	G	0.58	0.56	0.642	1.08 (0.79-1.48)
26	rs8108269	19	*GIPR*	Yes		G	G	T	0.68	0.66	0.645	1.09 (0.76-1.56)
27	rs4275659	12	*MPHOSPH9(ABCB9)*			C	C	T	0.71	0.70	0.687	1.08 (0.74-1.57)
28	rs4607103	3	*ADAMTS9*	Yes		C	C	T	0.61	0.62	0.716	0.94 (0.67-1.32)
29	rs7754840	6	*CDKAL1*		Yes	C	G	C	0.45	0.44	0.737	1.06 (0.77-1.45)
30	rs12571751	10	*ZMIZ1*			G	A	G	0.45	0.46	0.738	0.95 (0.69-1.31)
31	rs5945326	X	*DUSP9*	Yes		A	A	G	0.65	0.66	0.769	0.95 (0.68-1.35)
32	rs7955901	12	*TSPAN8, LGR5*		Yes	C	C	T	0.68	0.69	0.807	0.96 (0.66-1.38)
33	rs7845219	8	*TP53INP1*		Yes	T	C	T	0.31	0.32	0.814	0.96 (0.67-1.37)
34	rs243088	2	*BCL11A*	Yes		T	A	T	0.32	0.33	0.830	0.96 (0.68-1.36)
35	rs7172432	15	*C2CD4A/4B*		Yes	A	A	G	0.59	0.58	0.852	1.03 (0.75-1.41)
36	rs3740878	11	*EXT2*		Yes	A	A	G	0.63	0.64	0.876	0.97 (0.68-1.38)
37	rs10830963	11	*MTNR1B*		Yes	G	C	G	0.48	0.47	0.880	1.03 (0.73-1.45)
38	rs11257655	10	*CDC123, CAMK1D*		Yes	T	C	T	0.47	0.46	0.882	1.03 (0.73-1.44)
39	rs7756992	6	*CDKAL1*		Yes	G	A	G	0.49	0.48	0.893	1.02 (0.75-1.39)
40	rs831571	3	*PSMD6(PRICKLE2)*			C	C	T	0.67	0.32	0.918	1.02 (0.72-1.44)
41	rs6960043	7	*DGKB*		Yes	C	C	T	0.51	0.51	0.931	0.99 (0.71-1.38)
42	rs13266634	8	*SLC30A8*		Yes	C	C	T	0.61	0.61	0.961	0.99 (0.71-1.38)
43	rs7569522	2	*ITGB6-RBMS1*	Yes		A	G	A	0.34	0.34	0.963	1.01 (0.72-1.42)
44	rs3786897	19	*PEPD*	Yes		A	A	G	0.58	0.58	0.982	1.00 (0.70-1.44)
45	rs4402960	3	*IGF2BP2*		Yes	T	G	T	0.32	0.31	0.987	1.00 (0.69-1.45)

SNP, Single nucleotide polymorphism; Chr, Chromosome; GDM, Gestational diabetes mellitus; RAF, Risk allele frequency; OR, Odds ratio; CI, confidence interval.

References

1. Reece EA, Leguizamon G, Wiznitzer A (2009) Gestational diabetes: the need for a common ground. *Lancet* 373: 1789-1797.
2. Buchanan TA, Xiang AH, Page KA (2012) Gestational diabetes mellitus: risks and management during and after pregnancy. *Nat Rev Endocrinol* 8: 639-649.
3. Imamura M, Maeda S (2011) Genetics of type 2 diabetes: the GWAS era and future perspectives [Review]. *Endocr J* 58: 723-739.
4. Imamura M, Maeda S, Yamauchi T, Hara K, Yasuda K, *et al.* (2012) A single-nucleotide polymorphism in ANK1 is associated with susceptibility to type 2 diabetes in Japanese populations. *Hum Mol Genet* 21: 3042-3049.
5. Fukuda H, Imamura M, Tanaka Y, Iwata M, Hirose H, *et al.* (2012) A single nucleotide polymorphism within DUSP9 is associated with susceptibility to type 2 diabetes in a Japanese population. *PLoS One* 7: e46263.
6. Imamura M, Iwata M, Maegawa H, Watada H, Hirose H, *et al.* (2011) Genetic variants at CDC123/CAMK1D and SPRY2 are associated with susceptibility to type 2 diabetes in the Japanese population. *Diabetologia* 54: 3071-3077.
7. Lauenborg J, Grarup N, Damm P, Borch-Johnsen K, Jorgensen T, *et al.* (2009) Common type 2 diabetes risk gene variants associate with gestational diabetes. *J Clin Endocrinol Metab* 94: 145-150.
8. Zhang C, Bao W, Rong Y, Yang H, Bowers K, *et al.* (2013) Genetic variants and the risk of gestational diabetes mellitus: a systematic review. *Hum Reprod Update* 19: 376-390.
9. Zhang Y, Sun CM, Hu XQ, Zhao Y (2014) Relationship between melatonin receptor 1B and insulin receptor substrate 1 polymorphisms with gestational diabetes mellitus: a systematic review and meta-analysis. *Sci Rep* 4: 6113.
10. Watanabe RM, Black MH, Xiang AH, Allayee H, Lawrence JM, *et al.* (2007) Genetics of gestational diabetes mellitus and type 2 diabetes. *Diabetes Care* 30: S134-140.
11. Robitaille J, Grant AM (2008) The genetics of gestational diabetes mellitus: evidence for relationship with type 2 diabetes mellitus. *Genet Med* 10: 240-250.
12. Hillier TA, Pedula KL, Schmidt MM, Mullen JA, Charles MA, *et al.* (2007) Childhood obesity and metabolic imprinting: the ongoing effects of maternal hyperglycemia. *Diabetes Care* 30: 2287-2292.
13. Clausen TD, Mathiesen ER, Hansen T, Pedersen O, Jensen DM, *et al.* (2008) High prevalence of type 2 diabetes and pre-diabetes in adult offspring of women with gestational diabetes mellitus or type 1 diabetes: the role of intrauterine hyperglycemia. *Diabetes Care* 31: 340-346.
14. Ramachandran A, Ma RC, Snehalatha C (2010) Diabetes in Asia. *Lancet* 375: 408-418.
15. Tutino GE, Tam WH, Yang X, Chan JC, Lao TT, *et al.* (2014) Diabetes and pregnancy: perspectives from Asia. *Diabet Med* 31: 302-318.
16. Hedderson M, Ehrlich S, Sridhar S, Darbinian J, Moore S, *et al.* (2012) Racial/ethnic disparities in the prevalence of gestational diabetes mellitus by BMI. *Diabetes Care* 35: 1492-1498.
17. Minakami H, Maeda T, Fujii T, Hamada H, Iitsuka Y, *et al.* (2014) Guidelines for obstetrical practice in Japan: Japan Society of Obstetrics and Gynecology (JSOG) and Japan Association of Obstetricians and Gynecologists (JAOG) 2014 edition. *J Obstet Gynaecol Res* 40: 1469-1499.
18. Purcell S, Cherny SS, Sham PC (2003) Genetic Power Calculator: design of linkage and association genetic mapping studies of complex traits. *Bioinformatics* 19: 149-150.
19. Matsuda M, DeFronzo RA (1999) Insulin sensitivity indices obtained from oral glucose tolerance testing: comparison with the euglycemic insulin clamp. *Diabetes Care* 22: 1462-1470.
20. Matthews DR, Hosker JP, Rudenski AS, Naylor BA, Treacher DF, *et al.* (1985) Homeostasis model assessment: insulin resistance and beta-cell function from fasting plasma glucose and insulin concentrations in man. *Diabetologia* 28: 412-419.
21. Katz A, Nambi SS, Mather K, Baron AD, Follmann DA, *et al.* (2000) Quantitative insulin sensitivity check index: a simple, accurate method for assessing insulin sensitivity in humans. *J Clin Endocrinol Metab* 85: 2402-2410.
22. Kosaka K, Hagura R, Kuzuya T, Kuzuya N (1974) Insulin secretory response of diabetics during the period of improvement of glucose tolerance to normal range. *Diabetologia* 10: 775-782.
23. Retnakaran R, Qi Y, Goran MI, Hamilton JK (2009) Evaluation of proposed oral disposition index measures in relation to the actual disposition index. *Diabet Med* 26: 1198-1203.
24. Yabe D, Seino Y (2016) Type 2 diabetes via beta-cell dysfunction in east Asian people. *Lancet Diabetes Endocrinol* 4: 2-3.
25. Saisho Y, Miyakoshi K, Tanaka M, Shimada A, Ikenoue S, *et al.* (2010) Beta cell dysfunction and its clinical significance in gestational diabetes. *Endocr J* 57: 973-980.
26. Qian Y, Lu F, Dong M, Lin Y, Li H, *et al.* (2015) Cumulative effect and predictive value of genetic variants associated with type 2 diabetes in Han Chinese: a case-control study. *PLoS One* 10: e0116537.
27. Freathy RM, Hayes MG, Urbanek M, Lowe LP, Lee H, *et al.* (2010) Hyperglycemia and Adverse Pregnancy Outcome (HAPO) study: common genetic variants

in GCK and TCF7L2 are associated with fasting and postchallenge glucose levels in pregnancy and with the new consensus definition of gestational diabetes mellitus from the International Association of Diabetes and Pregnancy Study Groups. *Diabetes* 59: 2682-2689.
28. Laafira A, White SW, Griffin CJ, Graham D (2016) Impact of the new IADPSG gestational diabetes diagnostic criteria on pregnancy outcomes in Western Australia. *Aust N Z J Obstet Gynaecol* 56: 36-41.
29. Mayo K, Melamed N, Vandenberghe H, Berger H (2015) The impact of adoption of the international association of diabetes in pregnancy study group criteria for the screening and diagnosis of gestational diabetes. *Am J Obstet Gynecol* 212: 224.e1-e9.
30. Hivert MF, Manning AK, McAteer JB, Florez JC, Dupuis J, *et al.* (2008) Common variants in the adiponectin gene (ADIPOQ) associated with plasma adiponectin levels, type 2 diabetes, and diabetes-related quantitative traits: the Framingham Offspring Study. *Diabetes* 57: 3353-3359.
31. Beltcheva O, Boyadzhieva M, Angelova O, Mitev V, Kaneva R, *et al.* (2014) The rs266729 single-nucleotide polymorphism in the adiponectin gene shows association with gestational diabetes. *Arch Gynecol Obstet* 289: 743-748.
32. Zeggini E, Weedon MN, Lindgren CM, Frayling TM, Elliott KS, *et al.* (2007) Replication of genome-wide association signals in UK samples reveals risk loci for type 2 diabetes. *Science* 316: 1336-1341.
33. Ray SK, Li HJ, Metzger E, Schule R, Leiter AB (2014) CtBP and associated LSD1 are required for transcriptional activation by NeuroD1 in gastrointestinal endocrine cells. *Mol Cell Biol* 34: 2308-2317.
34. DIAbetes Genetics Replication And Meta-analysis (DIAGRAM) Consortium, Asian Genetic Epidemiology Network Type 2 Diabetes (AGEN-T2D) Consortium, South Asian Type 2 Diabetes (SAT2D) Consortium, Mexican American Type 2 Diabetes (MAT2D) Consortium, Type 2 Diabetes Genetic Exploration by Next-generation sequencing in multi-Ethnic Samples (T2D-GENES) Consortium, *et al.* (2014) Genome-wide trans-ancestry meta-analysis provides insight into the genetic architecture of type 2 diabetes susceptibility. *Nat Genet* 46: 234-244.
35. Morkrid K, Jenum AK, Sletner L, Vardal MH, Waage CW, *et al.* (2012) Failure to increase insulin secretory capacity during pregnancy-induced insulin resistance is associated with ethnicity and gestational diabetes. *Eur J Endocrinol* 167: 579-588.
36. Wu Y, Li H, Loos RJ, Yu Z, Ye X, *et al.* (2008) Common variants in CDKAL1, CDKN2A/B, IGF2BP2, SLC30A8, and HHEX/IDE genes are associated with type 2 diabetes and impaired fasting glucose in a Chinese Han population. *Diabetes* 57: 2834-2842.
37. Cho YS, Chen CH, Hu C, Long J, Ong RT, *et al.* (2012) Meta-analysis of genome-wide association studies identifies eight new loci for type 2 diabetes in east Asians. *Nat Genet* 44: 67-72.
38. Kwak SH, Choi SH, Jung HS, Cho YM, Lim S, *et al.* (2013) Clinical and genetic risk factors for type 2 diabetes at early or late post partum after gestational diabetes mellitus. *J Clin Endocrinol Metab* 98: E744-752.
39. Ao D, Wang HJ, Wang LF, Song JY, Yang HX, *et al.* (2015) The rs2237892 Polymorphism in KCNQ1 Influences Gestational Diabetes Mellitus and Glucose Levels: A Case-Control Study and Meta-Analysis. *PLoS One* 10: e0128901.
40. Kwak SH, Kim SH, Cho YM, Go MJ, Cho YS, *et al.* (2012) A genome-wide association study of gestational diabetes mellitus in Korean women. *Diabetes* 61: 531-541.
41. Kwak SH, Choi SH, Kim K, Jung HS, Cho YM, *et al.* (2013) Prediction of type 2 diabetes in women with a history of gestational diabetes using a genetic risk score. *Diabetologia* 56: 2556-2563.
42. Wang Y, Nie M, Li W, Ping F, Hu Y, *et al.* (2011) Association of six single nucleotide polymorphisms with gestational diabetes mellitus in a Chinese population. *PLoS One* 6: e26953.
43. Imamura M, Takahashi A, Yamauchi T, Hara K, Yasuda K, *et al.* (2016) Genome-wide association studies in the Japanese population identify seven novel loci for type 2 diabetes. *Nat Commun* 7: 10531.

PLOS ONE

RESEARCH ARTICLE

Potential roles of DNA methylation in the initiation and establishment of replicative senescence revealed by array-based methylome and transcriptome analyses

Mizuho Sakaki[1,2]*, Yukiko Ebihara[1], Kohji Okamura[3], Kazuhiko Nakabayashi[1], Arisa Igarashi[4], Kenji Matsumoto[4], Kenichiro Hata[1], Yoshiro Kobayashi[2]*, Kayoko Maehara[5]*

1 Department of Maternal-Fetal Biology, National Research Institute for Child Health and Development, Setagaya, Tokyo, Japan, **2** Department of Biomolecular Science, Graduate School of Science, Toho University, Funabashi, Chiba, Japan, **3** Department of Systems BioMedicine, National Research Institute for Child Health and Development, Setagaya, Tokyo, Japan, **4** Department of Allergy and Clinical Immunology, National Research Institute for Child Health and Development, Setagaya, Tokyo, Japan, **5** Department of Nutrition, Graduate School of Health Science, Kio University, Kitakatsuragi, Nara, Japan

* sakaki-m@ncchd.go.jp (MS); yoshiro@biomol.sci.toho-u.ac.jp (YK); k.maehara@kio.ac.jp (K. Maehara)

OPEN ACCESS

Citation: Sakaki M, Ebihara Y, Okamura K, Nakabayashi K, Igarashi A, Matsumoto K, et al. (2017) Potential roles of DNA methylation in the initiation and establishment of replicative senescence revealed by array-based methylome and transcriptome analyses. PLoS ONE 12(2): e0171431. doi:10.1371/journal.pone.0171431

Editor: Robert Dante, Centre de Recherche en Cancerologie de Lyon, FRANCE

Received: August 29, 2016

Accepted: January 20, 2017

Published: February 3, 2017

Data Availability Statement: Most relevant data are within the paper and its Supporting Information files. The microarray data for gene expression have been deposited in GEO (GSE81798). The microarray data for methylation have been deposited in GEO (GSE81788 and GSE81797). The microarray data for miRNA expression have been deposited in the GEO (GSE90942).

Funding: This work was supported by the Takeda Science Foundation (http://www.takeda-sci.or.jp/)

Abstract

Cellular senescence is classified into two groups: replicative and premature senescence. Gene expression and epigenetic changes are reported to differ between these two groups and cell types. Normal human diploid fibroblast TIG-3 cells have often been used in cellular senescence research; however, their epigenetic profiles are still not fully understood. To elucidate how cellular senescence is epigenetically regulated in TIG-3 cells, we analyzed the gene expression and DNA methylation profiles of three types of senescent cells, namely, replicatively senescent, *ras*-induced senescent (RIS), and non-permissive temperature-induced senescent SVts8 cells, using gene expression and DNA methylation microarrays. The expression of genes involved in the cell cycle and immune response was commonly either down- or up-regulated in the three types of senescent cells, respectively. The altered DNA methylation patterns were observed in replicatively senescent cells, but not in prematurely senescent cells. Interestingly, hypomethylated CpG sites detected on non-CpG island regions ("open sea") were enriched in immune response-related genes that had non-CpG island promoters. The integrated analysis of gene expression and methylation in replicatively senescent cells demonstrated that differentially expressed 867 genes, including cell cycle- and immune response-related genes, were associated with DNA methylation changes in CpG sites close to the transcription start sites (TSSs). Furthermore, several miRNAs regulated in part through DNA methylation were found to affect the expression of their targeted genes. Taken together, these results indicate that the epigenetic changes of DNA methylation regulate the expression of a certain portion of genes and partly contribute to the introduction and establishment of replicative senescence.

to KMae, a grant from Kio University (http://www.kio.ac.jp/) to KMae, grant 24-3 from the National Research Institute for Child Health and Development to KN and KMat, and Grant-in-Aid for Young Scientists (B 15K19439) from JSPS KAKENHI to AI. The funders had no role in study design, data collection and analysis, decision to publish, or preparation of the manuscript.

Competing Interests: The authors have declared that no competing interests exist.

Introduction

Cellular senescence is the irreversible cessation of cell proliferation [1] and is classified into two groups: replicative senescence and premature senescence [2]. Replicative senescence is caused by telomere shortening due to repeated DNA replication [3], while premature senescence is caused by stress, such as oncogene activation [4] and reactive oxygen species (ROS) [5], without apparent loss of telomere length and function. Although cellular senescence has been shown to be associated with tumor suppression in several cancers [2, 6, 7], it has been reportedly involved in cancer progression through the induction of epithelial-mesenchymal transitions and tumor invasion [8]. In addition, senescent cells secrete several factors associated with inflammation such as interleukin (IL)-6 and IL-8 [9], which are referred to as senescence-associated secretory phenotypes (SASP). Recently, SASP has been implicated in the pathogenesis of age-related diseases such as rheumatoid arthritis, periodontitis and Alzheimer's disease [8, 10]. Therefore, elucidation of the mechanism contributing to induction and establishment of the senescent state will help overcome such age-related diseases.

Epigenetic regulation such as histone modification, DNA methylation and interference with micro RNA (miRNA) is one of the mechanisms that modulate gene expression. Alteration of the chromatin structure occurs in human senescent fibroblasts, where epigenetic regulation contributes to the establishment of the senescent state partly through the $p16^{INK4A}$ / retinoblastoma (RB) protein pathway [11]. Modification of histones, trimethylated histone H3 at lysine9 (H3K9me3) and trimethylated histone H3 at lysine 27 (H3K27me3) is enriched in the senescent-associated heterochromatic foci (SAHF), although the spreading of repressive histone marks is not necessary for SAHF formation [12]. So far as known, histone modification is reportedly involved in expression of key molecules of senescence, such as $p16^{INK4A}$, $p14^{ARF}$ and p53. Loss of H3K27me3 is involved in expression of $p16^{INK4A}$ and $p14^{ARF}$, whereas H4 acetylation and trimethylation of histone H3 at lysine 4 (H3K4me3) are involved in expression of p53 [13–16]. Furthermore, Takahashi, A. *et al.* [17] showed that the expression levels of SASP factors, IL-6 and IL-8, are regulated by demethylation of H3K9 through the APC/C^{Cdh1}-G9a/GLP pathway.

DNA methylation changes have also been observed during cellular senescence and individual aging. Many studies have elucidated the role of epigenetics in senescence using various approaches such as pyrosequencing, array-based methylome and combined bisulfite restriction analysis (COBRA), as well as using various types of cells and different tissues derived from genetically different individuals [18–21]. These studies have shown that DNA methylation profiles are tissue- and cell-type specific, and the epigenetic control of gene expression seems to promote in part tissue- and cell-type specific differentiation in addition to cellular senescence. For instance, the DNA methylation profile of fibroblast cells is different to that of mesenchymal stromal cells [22]. Moreover, principal component analysis showed that the methylation pattern of fibroblast cells from one dermal region is different to that from other dermal regions [23]. Christensen *et al.* also showed interindividual variation in methylation profiles among 11 tissues, including blood and brain [24]. In contrast to the studies using genetically different tissues and cells derived from individuals, age-related changes in DNA methylation between monozygotic twins were reported to arise with chronological time, indicating that the differences in genetically identical individuals are driven by different cellular responses to environmental changes [25]. Therefore, we hypothesized that a specific type of cultured cell leading to senescent states induced by different methods and demonstrating differences in methylation profiles will allow us to characterize in detail the role of epigenetic regulation in response to cellular senescence.

The effects of DNA methylation on gene transcription have been extensively studied in relation to the states of CpG islands (CGIs) near the transcription start sites (TSS). According to recent studies examining the relationship between gene body methylation and gene expression, hypermethylation correlated to not only high gene expression but also low gene expression [26], suggesting a more complex regulation. Varley *et. al.* also reported that the relationship between methylation and gene expression is context-dependent, although the current models reported by several groups indicate that methylation in the promoter regions is associated with gene silencing, and gene body methylation is associated with expression [20].

Furthermore, some senescence-associated genes are regulated in part by miRNA [27–31]. MiR-34 has been well known as a tumor suppressor and its targeted genes encode the cell cycle regulators including E2F, c-Myc, cyclin D1, cyclin E2, cdk4, and cdk6 [32–34]. Recent studies on cancers have revealed that the expression of some tumor suppressive miRNAs is regulated by DNA methylation in the miRNA promoter regions [35–37]. Despite these recent advances, much of the relationship between DNA methylation and miRNA expression and how this relates to senescence genes remains unclear.

In this study, we examined characteristic features of DNA methylation during cellular senescence using TIG-3 cells established from fetal lung fibroblasts. Although such TIG-3 cells have been a common focus in senescence research, much of the epigenetics remains unexplored. To test the hypothesis that the differences in genetically identical cells are driven by different cellular responses to senescence, we examined array-based gene expression and DNA methylation profiles using genetically identical TIG-3 cells which had been induced to a senescent state by three different methods, namely, replicatively senescent, *ras*-induced senescent (RIS), and senescent SVts8 cells. Originally derived from TIG-3 cells, SVts8 cells can induce senescence under non-permissive temperature by inactivation of the temperature-sensitive SV40 large T antigen. We then searched for the positional trend of methylation changes and the possible effects of DNA methylation changes on gene expression using integrated analysis.

Materials and methods

Cells and cell culture

Normal human diploid fibroblast TIG-3 cells (obtained from the Health Science Research Resources Bank, Japan) were cultured in DMEM+GlutaMAX-I (GIBCO) supplemented with 10% fetal bovine serum (FBS) (HyClone) and 1% penicillin/streptomycin (Nacalai Tesque) at 37˚C under a 5% CO_2 atmosphere. TIG-3 cells were cultured until they senesced at population doubling level (PDL) 85. The TIG-3 cells were harvested for DNA extraction at PDL 36, 49, 69 and 85, for RNA extraction to analyze gene expression at PDL 36 and 84, and for RNA extraction to analyze miRNA expression at PDL 44, 60, 78 and 80.

To prepare RIS cells, retroviral infection was performed as reported previously [38]. Briefly, Phoenix-Eco cells (obtained from Dr. G. P. Nolan, Stanford University, CA, USA) were transfected with the pBabe-puro-H-Ras-V12 or pBabe-puro plasmid by the Chen-Okayama method [39]. Viral supernatants were prepared from the cells after transfection, passed through a 0.45-μm-pore-size syringe filter, and pooled. The supernatant and 8 μg/mL hexadimethrine bromide (Sigma-Aldrich) were added to TIG-3 cells expressing an ecotropic receptor at a proliferating phase. After infection, the cells were selected with growth medium containing 300 μg/mL G418 and 2 μg/mL puromycin for 9 days before being harvested.

SVts8 cells (obtained from the Health Science Research Resources Bank, Japan) [40] continued to proliferate at a permissive temperature (33.5˚C), because of suppression of RB and p53 through induction of a temperature-sensitive mutant of the simian virus (SV) 40 large T

antigen to TIG-3 cells and the high ability of telomere maintenance. Senescent SVts8 cells were obtained by culturing SVts8 cells at a non-permissive temperature (38˚C) for 6 days.

Microarray assays

Gene expression. Total RNA was isolated with a ReliaPrep RNA Cell MiniPrep System (Promega) according to the manufacturer's instructions. Starting with 200 ng of the isolated RNA for each sample, double stranded cDNA and cyanine 3 labeled cRNA were synthesized using a low input quick amp labeling kit (one-color) and RNA spike-in kit (Agilent). The labeled cRNA was purified with an RNeasy mini kit (Qiagen), and hybridized to a SurePrint G3 Human GE microarray 8×60K Ver. 2.0 (Agilent). After washing the microarray to remove unhybridized cRNA, the microarray was scanned with an Agilent DNA microarray scanner G2505B, and then feature extraction was performed using the GE1_QCMT_Sep09 protocol.

DNA methylation. Genomic DNA was isolated using DNeasy Blood & Tissue (Qiagen) according to the manufacturer's instructions. Genomic DNA (1.5 μg) was bisulfite-converted using the EpiTec Plus DNA Bisulfite Kit (Qiagen). From each sample, 300 ng of bisulfite-treated DNA was subjected to DNA methylation profiling using an Infinium HumanMethylation27 or HumanMethylation450 BeadChip array (Illumina) according to the manufacturer's standard protocol. The array slides were scanned with an iScan system (Illumina).

MicroRNA (miRNA) expression. Total RNA including miRNA was isolated with a ReliaPrep miRNA Cell and Tissue MiniPrep System (Promega) according to the manufacturer's instructions. Approximately 100 ng of the isolated RNA for each sample was labeled with cyanine 3 using miRNA Complete Labelling and Hyb Kit (Agilent) according to the manufacturer's protocols. The labeled RNA was hybridized to a SurePrint G3 Human miRNA Microarray (Release 21.0) (Agilent). After washing, the microarray was immediately scanned using one color scan setting for 8×60k array slides with an Agilent DNA microarray scanner G2505C. The images were extracted with Feature Extraction Software 10.7.3.1 (Agilent) using default parameters.

Data analysis

Gene expression. The SurePrint G3 Human GE microarray data were analyzed using the Subio Platform (Ver. 1.18.4625). The data were normalized as to low signal cutoff (cutoff 1.0 and replace), log transformation (base 2), and global normalization (percentile 75), and then the ratios to those of the control sample (mean) were obtained. In this study, $>=$ 2-fold and $=<$ 0.5-fold changes were regarded as up- and down-regulated gene expression, respectively. In order to calculate fold-change differences and construct a heatmap, each gene expression level in the senescent cells was compared with that in the control cells, namely replicative senescent cells versus proliferating cells, RIS cells versus cells infected with the empty vector, and senescent SVts8 cells versus proliferating SVts8 cells. The heatmap with sample clustering was drawn using Subio Platform with Uncentered Correlation. The microarray data for gene expression have been deposited in the GEO (GSE81798).

DNA methylation. The Infinium HumanMethylation27 BeadChip includes probes for 27,578 CpG sites [41]. The Infinium HumanMethylation450 BeadChip includes probes for 485,577 CpG sites covering 21,231 RefSeq genes (99%), and 26,658 CGIs (96%), and 3,091 probes for non-CpG loci [42]. The image data obtained by the iScan system were subjected to background subtraction and control normalization using GenomeStudio V2011.1 (Illumina). Methylation levels were calculated as β values (= intensity of the methylation allele / [intensity of the unmethylated allele + intensity of the methylated allele +100]), which ranged from 0 (0% methylation) to 1 (100% methylation). Probes for CpG sites with a detection p-value

of > 0.05 or a blank β value were eliminated from further analysis. The β values of control cells were subtracted from those of senescent cells (Δβ). Δβ > = 0.2 and Δβ = < −0.2 were regarded as hyper- and hypomethylation in this study. TIG-3 cells at PDL 36 were regarded as control cells for those at higher PDLs (49, 69, and 85). An Infinium HumanMethylation27 BeadChip was used to obtain methylation profiles for all samples (TIG-3, RIS, and SVts8 cells). An Infinium HumanMethylation450 BeadChip was used to obtain more comprehensive methylation profiles of TIG-3 cells at PDL 36 and PDL 85, and RIS cells. The BeadChip data have been deposited in the GEO (GSE81788 and GSE81797). Scatter plots for β values were drawn using Genome Studio. Hyper- and hypo-methylated CpG sites were classified into six CpG subcategories depending on the location relative to the CpG island (CpG island, N_Shore, S_Shore, N_Shelf, S_Shelf, and the open sea) and into seven gene feature subcategories (− 1500 to − 200 bp upstream of the TSS (TSS1500), − 200 bp to 0 bp upstream of TSS (TSS200), 5' untranslated region (5'UTR), first exon (1st exon), gene body, 3' untranslated region (3'UTR), and intergenic region), according to the probe annotation (HumanMethylation450_15017482_v.1.1.csv) provided by Illumina [43].

Integrated analysis of DNA methylation and gene expression. Normalized gene expression and DNA methylation array data were integrated based on the genomic locations of the RefSeq genes' TSS composed in the expression array and the genomic location of the CpG sites placed in the BeadChip array using custom perl scripts. RefSeq information was retrieved from http://hgdownload.cse.ucsc.edu/goldenPath/hg19/database/refGene.txt.gz. We assessed Δβ values for the CpG sites located within 8 kb distance from the closest TSS of the RefSeq genes and the fold-change value of the corresponding gene expression. The gene expression data were obtained from probes annotated by the RefSeq ID for mRNA. When multiple expression probes existed in the same RefSeq ID, the mean of multiple intensities was calculated for the RefSeq ID. The distance from the methylation site to the TSS was calculated with a computer using the location information on the methylation probes and RefSeq (as described above). Promoters registered in RefSeq were classified into two classes, CGI and non-CGI promoters, using the following criteria: > = 50% GC content and observed-to-expected ratio of CpG > = 0.6.

Gene ontology (GO) analysis. GO analysis was performed using the Database for Annotation, Visualization and Integrated Discovery (DAVID) v6.7 (http://david.abcc.ncifcrf.gov/) [15–17] with GOTERM_BP_ALL and functional annotation clustering. The genes for GO analysis were extracted according to each cut-off value given in the methylation and integrated analysis section. For GO analysis using only gene expression data, genes exhibiting a more than 3-fold change of expression were used due to the limited gene numbers loaded onto the annotation tool. The top 10 represented GO terms are shown in some tables. Enrichment scores of more than 1.3 gave p-values of less than 0.05.

To conduct GO analysis on gene feature- and CpG site-categories, the genes related to differentially methylated CpG sites on the gene-coding region based on the probe annotation were analyzed with GOTERM_BP_ALL and a functional annotation chart due to the small numbers of extracted genes. The ratios of the number of genes with similar functions were calculated for all gene feature- and CpG site-subcategories.

miRNA expression regulated by DNA methylation and its targeted genes. To measure the expression level of miRNAs during replicative senescence, the Human miRNA microarray data were analyzed using GeneSpring (Ver. 12.5). The data were normalized by a 90-percentile shift, and then the ratios to those of the control sample (PDL 44) were obtained. The cut-off for miRNA expression change used in this study was a ±1.5-fold change. The microarray data for miRNA expression have been deposited in the GEO (GSE90942). miRNAs exhibiting methylation changes were obtained from HumanMethylation450 BeadChip data using the

"MIR" keyword in the "UCSC_REFGENE_NAME" column provided by Illumina. We searched for miRNAs with hypermethylated promoter regions and down-regulated expression, and vice versa, by comparing methylation changes (Δβ cut-off was ±0.2) with expression changes (fold-change cut-off, ±1.5). Genes targeted by those miRNAs for which expression seemed to be regulated by DNA methylation were picked up by TargetScanHuman Release 7.0. The resulting genes were then further filtered by more than two miRNAs and the gene expression levels based on our microarray data.

Results

Similar biological outcomes, but different gene expression patterns were detected in three types of senescent cells

We prepared three types of senescent cells, namely, replicatively senescent, RIS and senescent SVts8 cells. The senescence state in SVts8 cells was rapidly induced by the inactivation of the temperature-sensitive mutant of the SV40 large T antigen under non-permissive temperature. Senescence was confirmed by the growth arrest, appearance (a large flat morphology), senescence-associated beta-galactosidase (SA-β-Gal) activity, and protein and mRNA levels of $p16^{INK4A}$ and $p21^{Cip1/Waf1}$ (S1 Fig). Gene expression data for senescent cells obtained with SurePrint G3 Human GE microarrays (Agilent) showed that less than 10% of the probes tended to show similar changes in the three types of senescent cells (up-regulated: 358 of 4,355 probes in replicatively senescent cells, 3,927 probes in RIS cells and 5,124 probes in senescent SVts8 cells; down-regulated: 278 of 4,679 probes in replicatively senescent cells, 4,557 probes in RIS cells and 3,823 probes in senescent SVts8 cells), whereas more than 50% of the probes showed changes specific to each type of senescent cell (up-regulated: 2,396 of 4,355 probes in replicatively senescent cells, 2,384 of 3,927 probes in RIS cells, and 3,408 of 5,124 probes in senescent SVts8 cells; down-regulated: 2,561 of 4,679 probes in replicatively senescent cells, 2,750 of 4,557 probes in RIS cells, and 2,840 of 3,823 probes in senescent SVts8 cells) (Fig 1). A heatmap also showed different patterns of gene expression among the three types of senescent cells, even though sample clustering indicated that replicatively senescent cells and RIS cells were closer than senescent SVts8 cells (Fig 2).

According to the GO analysis of more than 3-fold changed genes, the down-regulated genes in the replicatively senescent, RIS and senescent SVts8 cells were mostly related to the "cell cycle" (S1 Table). On the other hand, the up-regulated genes were related to "immune response", "locomotion", and "cell migration" in all three types of senescent cells that we examined. Both up-regulated and down-regulated genes included "developmental process" genes. The results suggest that different genes with similar functions contributed to the senescent process, although the biological outcomes were similar among the three types of senescent cells.

Replicatively senescent cells showed DNA methylation changes

The DNA methylation profiles of senescent and proliferating cells were obtained using the Infinium HumanMethylation27 BeadChip. Among the three types of senescent cells examined, only the replicatively senescent cells (TIG-3 at PDL 85) were notably differentially methylated compared to the proliferating control cells (TIG-3 at PDL 36), whereas prematurely senescent cells (RIS and SVts8) were not (Fig 3, upper panels). Among the 629 and 366 CpG sites that were hyper- and hypo-methylated, respectively, in TIG-3 at PDL 85 (Fig 3, lower table), 565 (89.8%) and 310 (84.7%) sites showed a stepwise increase and decrease, respectively, of DNA methylation along with the progression of PDLs (36, 49, 69, and 85) (Table 1). Genes

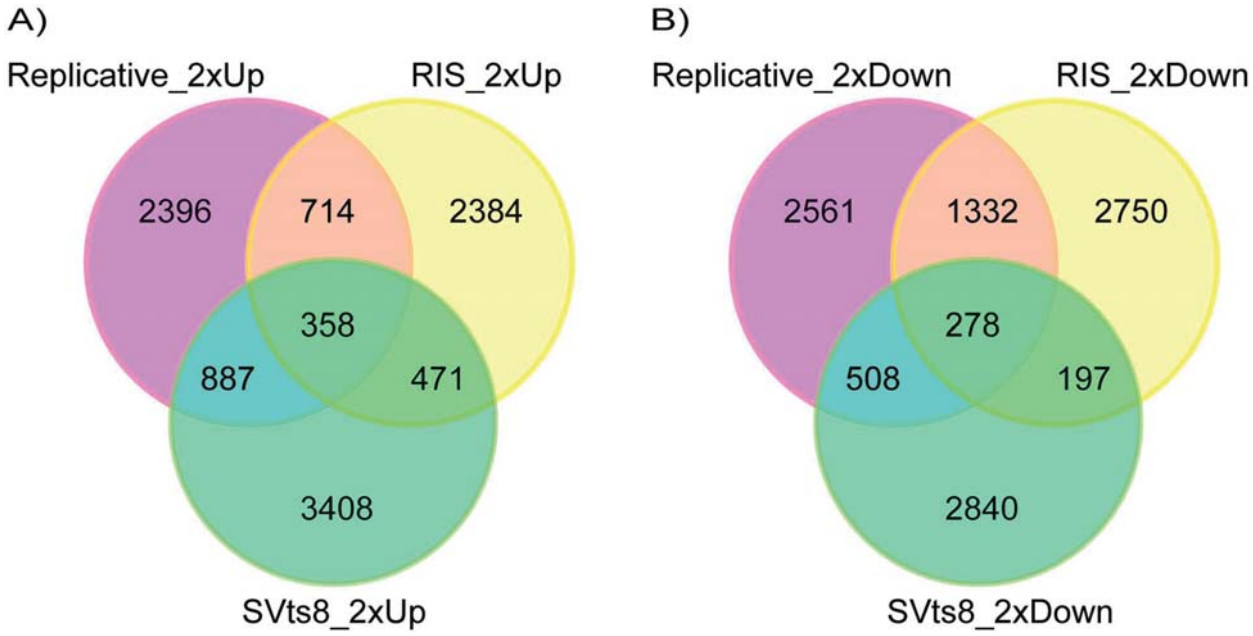

Fig 1. The number of probes indicating up- or down-regulated genes in three types of senescent cells. The number of up-regulated (A) or down-regulated probes (B) are shown in three types of senescent cells. The probes exhibiting a more than 2-fold change were counted. Purple circles, replicatively senescent cells; yellow circles, RIS cells; green circles, senescent SVts8 cells.

doi:10.1371/journal.pone.0171431.g001

hosting the differentially methylated CpG sites detected in TIG-3 at PDL 85 were subjected to GO analysis using DAVID. Genes associated with hypomethylated CpG sites were found to be most enriched in the term "immune response" (enrichment score 7.86) and its related terms (S2 Table). On the other hand, genes associated with hypermethylated CpG sites were enriched in a wider variety of terms such as regulation of biological and developmental processes with lower enrichment scores (4.24 or lower).

To more comprehensively examine the alteration of DNA methylation upon senescence, we obtained the DNA methylation profiles of TIG-3 cells at PDL 36 and PDL 85, and RIS cells using the Infinium HumanMethylation450 BeadChip. Again, replicatively senescent TIG-3 cells were differentially methylated compared to the proliferating control cells, whereas RIS cells were not (Fig 3D and 3E). Among 484,662 probes that passed quality control procedures, 14,214 and 12,727 probes were hyper- and hypo-methylated, respectively, in TIG-3 cells at PDL 85 as compared with TIG-3 cells at PDL 36 (Fig 3F). The ratios of differentially methylated probes were determined for each of the seven gene features and six CpG subcategories (Fig 4). The frequency of hypermethylated CpG sites was higher than that of hypomethylated CpG sites in TSS1500 (1.6 fold), TSS200 (2.1 fold), 5'UTR (1.5 fold), 1st exon (2.0 fold) and gene body (1.2 fold) subcategories (Fig 4A). As shown in Fig 4B, the frequency of hypermethylated CpG sites was higher in CGI (16.0 fold), N_Shore (2.2 fold), and S_shore (2.4 fold) subcategories, but was lower in N_Shelf (0.44 fold), S_Shelf (0.39 fold), and the open sea (0.51 fold) subcategories. We applied GO analyses to genes hosting the differentially methylated CpG sites to characterize the features of the genes that were supposed to be regulated in part by DNA methylation in each gene feature- and CpG site-subcategories. A total of 8,114 genes hosting the differentially methylated CpG sites were classified by GO terms into the subcategories. The GO terms obtained from functional annotation charts using DAVID were further categorized into seven groups: "immune response", "metabolic process", "transport", "cell

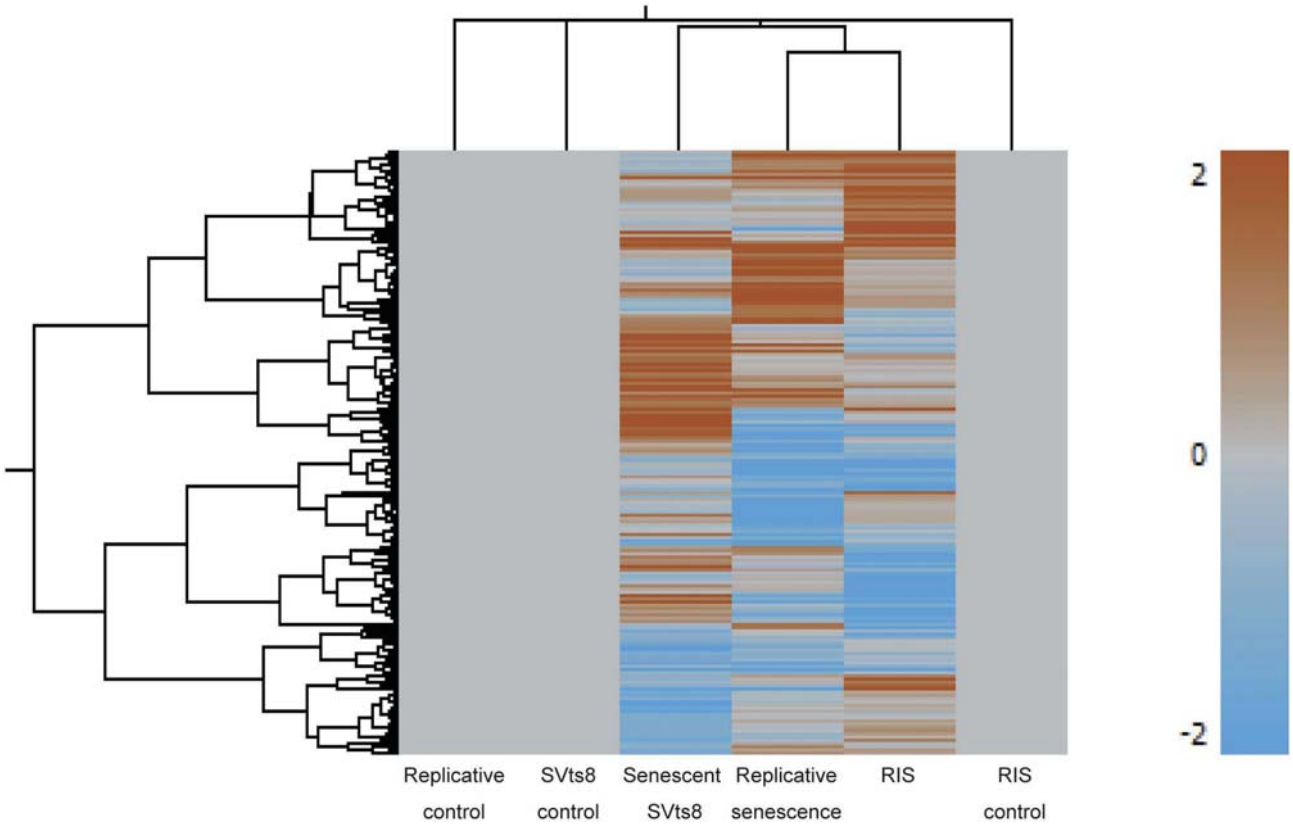

Fig 2. Heatmap of gene expression in three types of senescent cells. Gene expression patterns in three types of senescent cells are shown as a heatmap with sample clustering using uncentered correlation.

doi:10.1371/journal.pone.0171431.g002

adhesion", "development", "signal transduction", and "transcription", plus an additional group, others (Figs 5A–5H and 6A–6H and S3 Table). The "immune response"-related genes hosting hypomethylated CpG sites were enriched in all of the gene feature subcategories, whereas a small portion of those hosting hypermethylated sites were located in the TSS1500, 5'UTR, 1st exon and gene body subcategories (Fig 5A). Interestingly, in the region from − 200 bp to 0 bp upstream of TSS (TSS200), all of the classified 63 genes related to "immune response" consisted of the hypomethylated CpG sites. Consistent with the results of GO analyses using HumanMethylation27 data (S2 Table), the genes hosting hypomethylated CpG sites were found to be markedly enriched with the genes involved in "immune response". In sharp contrast, the "transcription"-related genes hosting hypermethylated CpG sites were enriched in all of the gene feature subcategories except for "1st exon", whereas no "transcription"-related genes hosting the hypomethylated ones were located in the gene feature subcategories except "gene body" (Fig 5G). The results of the GO analyses conducted on the CpG site subcategories are shown in Fig 6. Genes related to "immune response" were enriched only in the genes hosting hypomethylated CpG sites in the "open sea", but not those in other subcategories (islands, shores, and shelves) (Fig 6A). In addition, genes related to "transcript" were enriched in the genes hosting hypomethylated CpG sites in the "CpG islands" (Fig 6G). However, genes related to the other six groups of GO terms were enriched in the genes hosting hypomethylated CpGs in several CpG subcategories (Fig 6B–6F and 6H). When we focused on the genes hosting hypermethylated CpG sites, genes related to "immune response" were enriched in

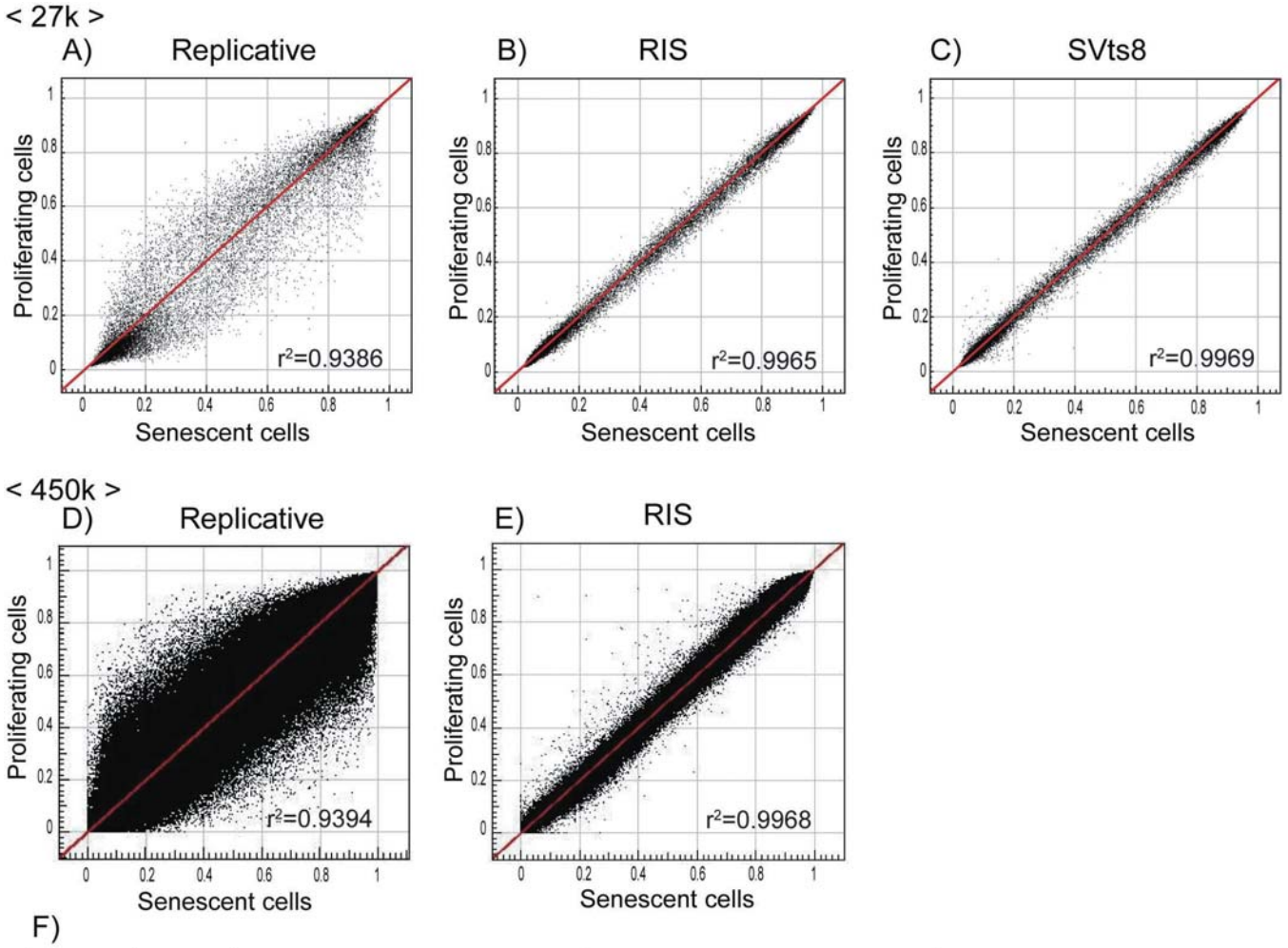

F)

BeadChip type	Total probe number	Replicative senescence		RIS		Senescent SVts8	
		Changed probe number and ratio		Changed probe number and ratio		Changed probe number and ratio	
		Hypo	Hyper	Hypo	Hyper	Hypo	Hyper
27k	27567	366 (1.328%)	629 (2.282%)	0 (0.000%)	0 (0.000%)	2 (0.007%)	1 (0.004%)
450k	484662	12727 (2.626%)	14214 (2.933%)	67 (0.014%)	6 (0.001%)	NA	NA

Fig 3. Comparison of DNA methylation profiles in three types of senescent cells. DNA methylation β values of senescent (x-axis) and proliferating control (y-axis) cells in the three types of senescent models are shown in scatter plots. The data were obtained by Infinium HumanMethylation27 (upper panels, A–C) and HumanMethylation450 BeadChip (middle panels, D–E). The correlation coefficient (r^2) is shown in each plot. The lower table (F) shows the numbers of CpG sites that were hyper- ($\Delta\beta >= 0.2$) and hypo-methylated ($\Delta\beta =< -0.2$) upon senescence.

doi:10.1371/journal.pone.0171431.g003

"N_shore" rather than in the "open sea". In addition, genes related to other groups were enriched in the genes hosting hypermethlated CpG sites regardless of the CpG site locations (islands, shores, shelves, and the open sea) (Fig 6B–6G). Thus, a certain portion of "immune response"-related genes might be regulated in part by DNA methylation via CpG sites being outside of the CpG islands.

Table 1. Sequential changes of DNA methylation during replicative senescence.

		PDL 49 vs PDL 36	PDL 69 vs PDL 36	PDL 85 vs PDL36
Hypomethylated CpG sites	Total number	64	165	366
	Number of sites with sequential change	–	156 (94.5%)	310(84.7%)
Hypermethylated CpG sites	Total number	76	277	629
	Number of sites with sequential change	–	273 (98.6%)	565 (89.8%)

doi:10.1371/journal.pone.0171431.t001

Hypomethylation observed in the open sea was frequently associated with the up-regulation of genes related to immune response

Next, we performed an integrated analysis of HumanMethylation450 BeadChip and gene expression profiles to investigate potential functional effects of DNA methylation on gene expression in replicative senescence. Most methylation changes were unlikely to have a significant impact on gene expression (S2 Fig). Out of 212,885 probes located within 8 kb distance from a TSS of RefSeq genes, 1,596 CpG sites were differentially methylated along with the altered expression of the nearest genes to these CpG sites: 1,101 hyper- and 495 hypo-methylated CpG sites for which the nearest genes were down- and up-regulated, respectively, upon senescence (S4 Table). The genes nearest to these 1,596 differentially methylated CpG sites were subjected to GO analysis using DAVID. Those genes with up-regulated expression that were in a hypomethylated state in close proximity (within 8 kb) to their TSS were involved in "immune response" and "cell death" as ranked in the top 10 terms (Table 2). The immune response-related genes included *MHC II*, and the cell death-related genes included *FAS* and *oxidized low density lipoprotein receptor 1 (OLR1)*. In contrast, those genes with down-regulated expression that were in a hypermethylated state in close proximity to their TSS were categorized into several categories such as "development" and "cell cycle".

We also assessed the distribution of the distances between each of the 1,596 differentially methylated CpG sites and the nearest TSS. In this analysis, we classified genes into two subcategories based on promoter types, CGI and non-CGI promoters. The number of probes for all CpG sites within CGI and non-CGI promoters on the array were 204,829 and 94,432 respectively (Fig 7A). The number of probes located within 1 kb distance to the TSS was 186,998 (62%). The 1,101 hypermethylated CpG sites for which the nearest gene was down-regulated upon replicative senescence consisted of 744 and 357 CpG sites within CGI and non-CGI promoters, respectively. The hypermethylated CpG sites tended to be located more frequently in CGI promoters than in non-CGI promoters, and located close to the TSS: 630 out of 1,101 (57%) within 1 kb distance (Fig 7B). The distribution patterns were similar between all CpG sites (Fig 7A) and 1,101 hypermethylated CpG sites (Fig 7B). In sharp contrast, 495 hypomethylated CpG sites for which the nearest gene was up-regulated were mainly located in non-CGI promoters (Fig 7C). Within 1 kb distance of the TSS, 202 hypomethylated CpG sites, for which the nearest gene was up-regulated upon replicative senescence, consisted of 36 and 166 CpG sites within CGI and non-CGI promoters, respectively (Fig 7C). This distribution pattern was similar to that of a subset of hypomethylated CpG sites, for which the nearest gene was up-regulated and related to "immune response" (Fig 7D). This result suggests the possibility that DNA methylation on the promoter modulates the expression of a subset of "immune response" genes in replicative senescence.

DNA methylation affected the expression of miRNAs and the target genes during replicative senescence

A HumanMethylation450 BeadChip includes 3,436 probes related to miRNA. In replicatively senescent TIG-3 cells, 98 CpG sites corresponding to 66 miRNAs were hypomethylated,

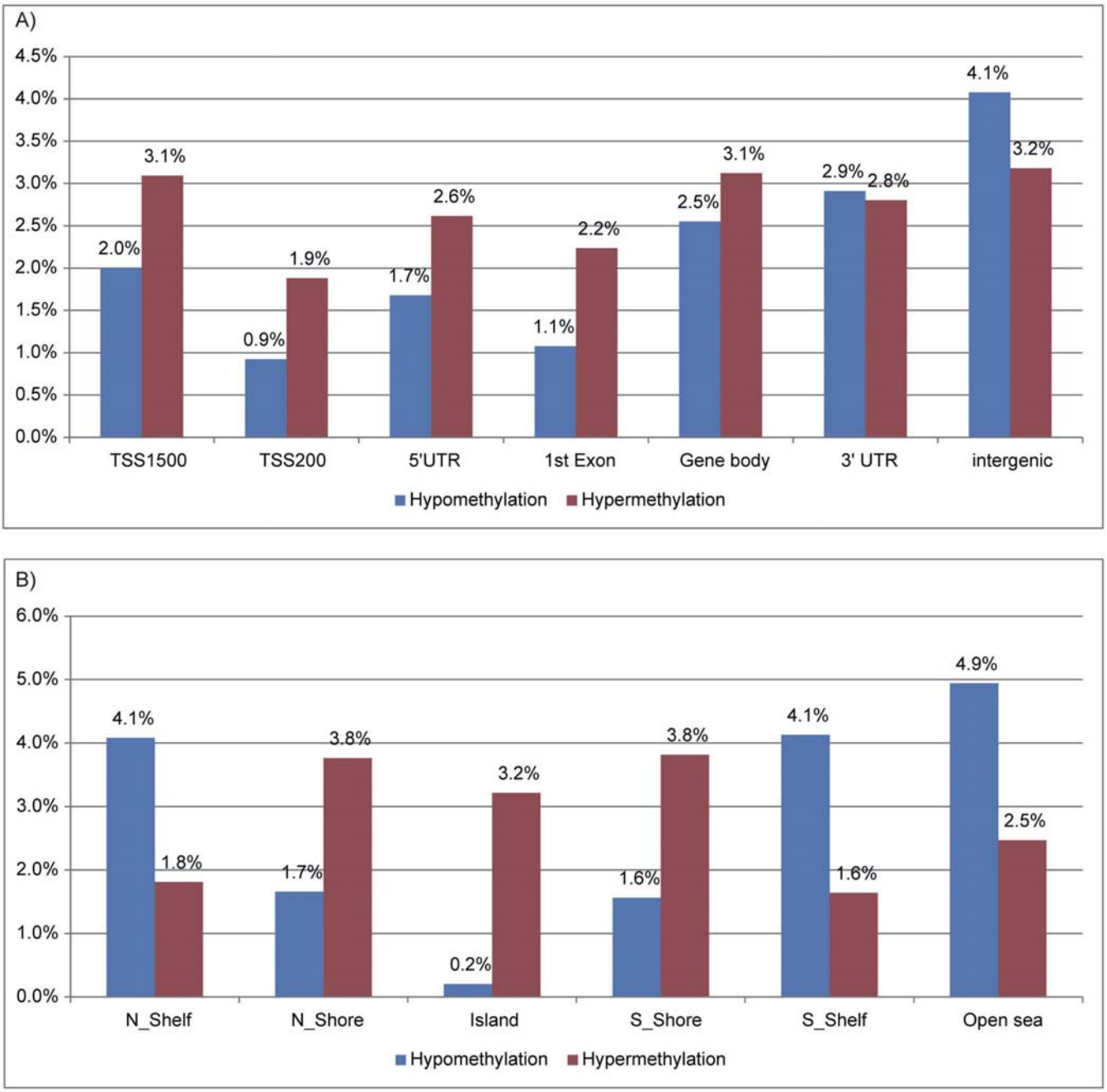

Fig 4. Rates of differentially methylated CpG sites in replicatively senescent TIG-3 cells in seven gene- feature (A) and six CpG- site (B) subcategories. CpG sites showing Δβ > = 0.2 and Δβ = < −0.2 in senescent TIG-3 cells (at PDL 85) compared to those at PDL 36 were regarded as hyper- and hypo-methylated, respectively. Seven gene-feature subcategories: TSS1500, TSS200, 5'UTR, 1st exon, gene body, 3'UTR, and intergenic region. Six CpG subcategories: CpG island, N_Shore, S_Shore, N_Shelf, S_Shelf, and the open sea.

doi:10.1371/journal.pone.0171431.g004

whereas 102 CpG sites corresponding to 62 miRNAs were hypermethylated (S5 Table). The expression levels of miRNAs were examined using Human miRNA microarray (Release 21.0), where 2,549 human miRNAs were represented. During replicative senescence, 178 miRNAs (fold-change > = ±1.5) showed up- or down-regulated (data not shown). To select miRNAs

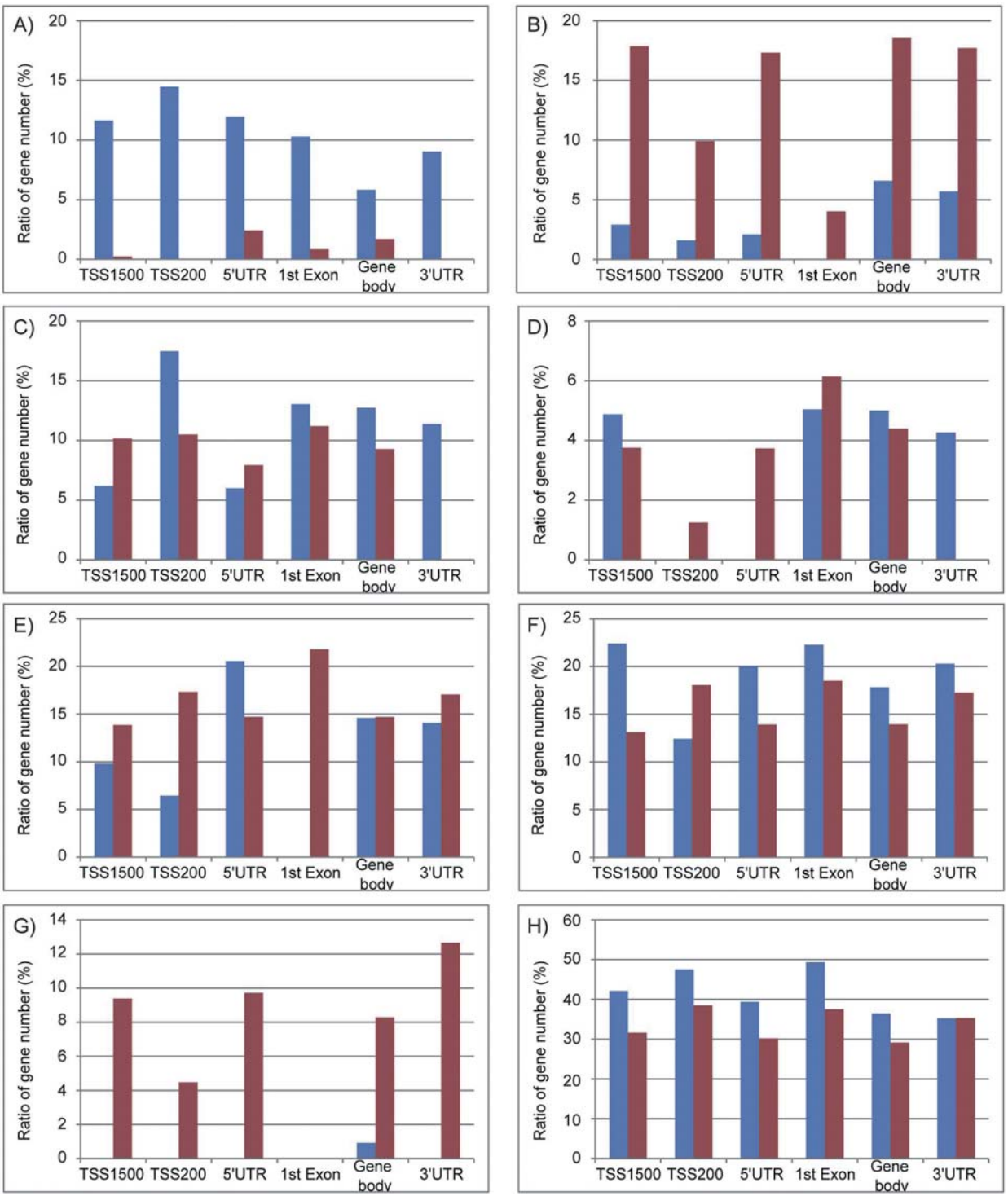

Fig 5. The characterization of genes hosting differentially methylated CpG sites in the gene feature subcategories. GO analyses for gene hosting differentially methylated CpG sites were performed using DAVID (functional annotation chart and GOTERM_BP_ALL). The genes hosting hypermethylated (red) or hypomethylated (blue) CpG sites were classified into six gene feature categories (TSS1500, TSS200, 5'UTR, 1st exon, gene body and 3'UTR). Using the GO terms detected to be enriched (p-value = < 0.05) by DAVID, genes with similar functions were classified into seven groups: immune response (A), metabolic process (B), transport (C), cell adhesion (D), development (E), signal transduction (F), and transcription (G), plus an additional group, others (H). Histograms (A–H) show the ratio of the number of genes classified by GO terms in gene features subcategories (S3 Table shows the number of genes analyzed and classified).

doi:10.1371/journal.pone.0171431.g005

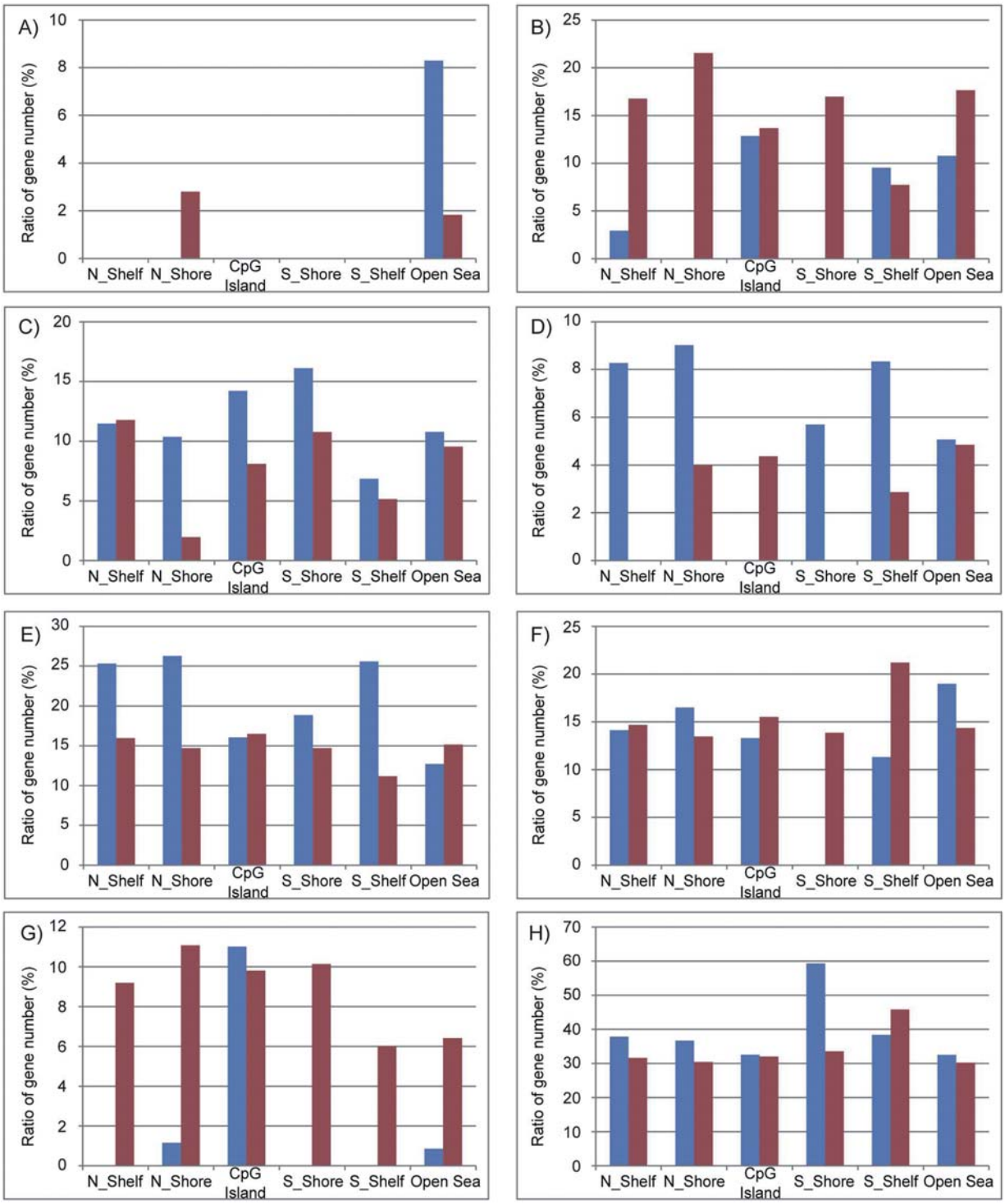

Fig 6. The characterization of genes hosting differentially methylated CpG sites in the CpG site subcategories. The same type of GO analyses shown in Fig 5 was applied to six CpG subcategories (N_Shelf, N_Shore, CpG island, S_Shore, S_Shelf, and the open sea). S3 Table shows the number of genes analyzed and classified.

doi:10.1371/journal.pone.0171431.g006

Table 2. GO analysis of genes showing the relationship between methylation and gene expression level in replicative senescence.

Rank	Hypomethylation & up-regulated gene expression (n = 351)		Hypermethylation & down-regulated gene expression (n = 516)	
	GO term categories	Enrichment Score	GO term categories	Enrichment Score
1	Response to stimulus	3.20	Developmental process	7.08
2	Immune response	3.19	Organ development	5.14
3	Inflammatory response	2.73	Lung alveolus development	3.69
4	Response to hormone stimulus, Response to corticosteroid stimulus	2.50	Embryonic development	3.64
5	Response to nutrient levels, Response to extracellular stimulus	2.30	Cell cycle	3.16
6	Regulation of transport	1.69	Negative regulation of transcription	3.11
7	Developmental process	1.62	Epithelial tube morphogenesis	2.70
8	Cell death	1.37	Mesenchymal cell development	2.47
9	Actin cytoskeleton organization	1.26	Ear development	2.46
10	Negative/positive regulation of kinase activity	1.25	Positive regulation of transcription, DNA-dependent, positive regulation of metabolic process	2.34

* More than 1.3 of enrichment scores gave less than 0.05 p-value.

doi:10.1371/journal.pone.0171431.t002

for which expression seemed to be regulated by DNA methylation, we compared the methylation changes of CpG sites related to miRNA with the miRNA expression changes. Among 18 miRNAs selected, seven miRNAs showed a decrease in expression accompanied with a hypermethylated CpG site in the promoters (S6 Table). This result was consistent with a previous report using IMR 90 cells, where the expression levels of six of the seven miRNAs were down-regulated during replicative senescence [27]. In contrast, no miRNAs showed an increase in expression along with a hypomethylated CpG site in the promoters. We next searched for candidate genes targeted by the seven miRNAs using TargetScan Human Release 7.0, and these genes were further selected by more than two miRNAs and the targeted gene expression levels based on our microarray data. As a result, we identified 27 genes for which expression seemed to be indirectly regulated by DNA methylation on the promoters of targeting miRNAs (Table 3). The genes encoding IL-6 signal transducer (*IL6ST*) and Zinc finger matrin-type 3 (*ZMAT3*) were included in the targeted genes.

Discussion

In this study, we examined DNA methylation levels in three types of senescent cells and found that only replicatively senescent cells were differentially methylated, whereas prematurely senescent ones (RIS and SVts8) were not (Fig 3 and Table 1). These results were in good agreement with previous studies showing DNA methylation changes in aged tissues and cells [16, 21, 24, 44]. There are several reasons why the DNA methylation profile is strongly modified during replicative senescence and not during premature senescence. Firstly, errors may accumulate due to repeated cell division. Laird *et al.* evaluated the fidelity of transmission of the DNA methylation state in the CpG island of the *FMR1* gene in normal human lymphocytes using hairpin-bisulfite PCR [45]. Although the high fidelity of inheritance of the methylated state of cytosine was estimated, the results clearly showed that errors in maintaining DNA methylation occurred to some extent in every DNA replication. When culturing TIG-3 cells from PDL 36 to PDL 85, the cells would be divided approximately 2^50 times. In contrast, as RIS and senescent SVts8 cells were rapidly induced to a senescent state, prematurely senescent

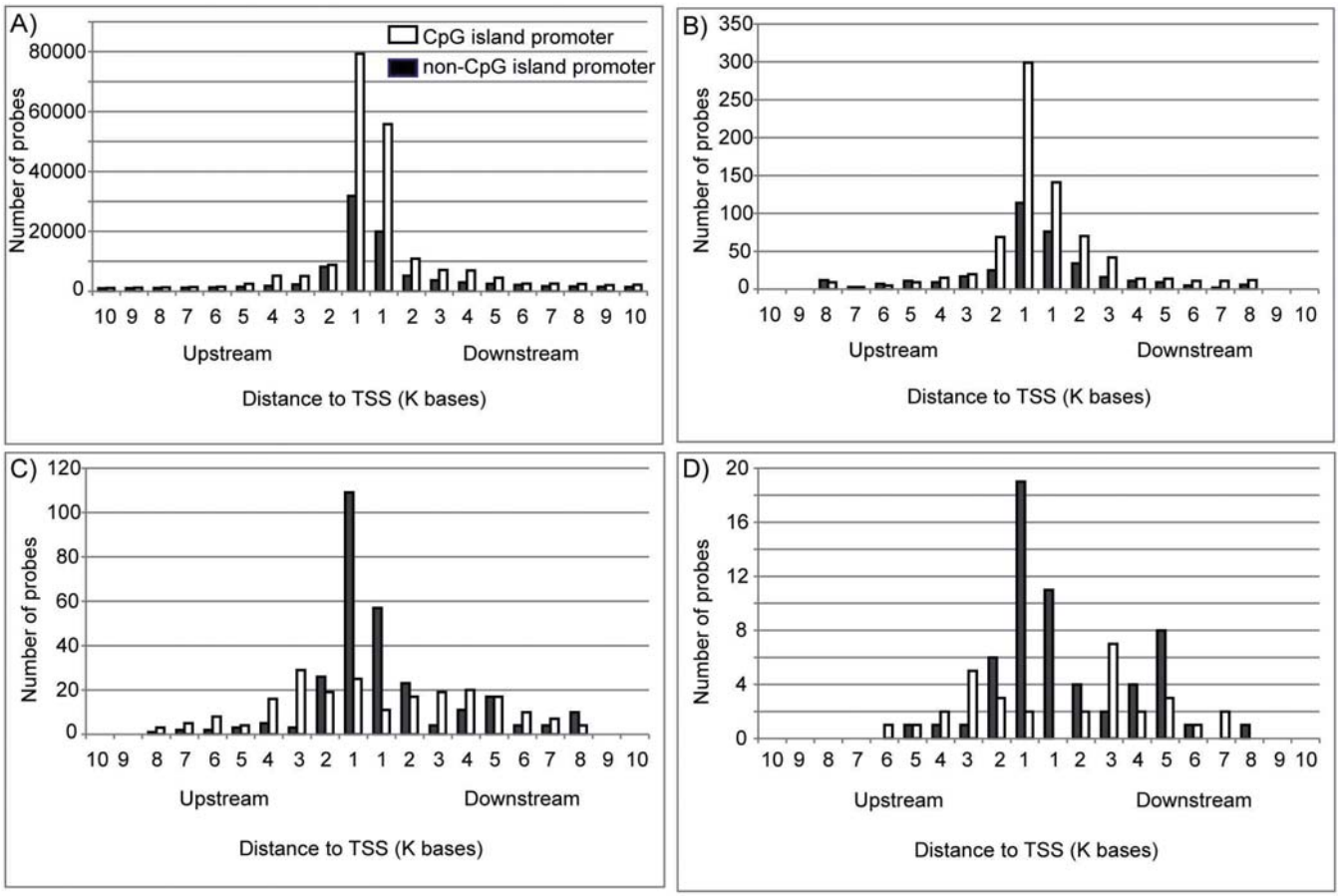

Fig 7. Distribution patterns of the distances between CpG sites and the nearest TSS. Distribution patterns for all 299,261 CpG probes on the HumanMethylation450 BeadChip (A), 1,101 hypermethylated CpG sites for which the nearest gene was down-regulated upon replicative senescence (B), 495 hypomethylated CpG sites for which the nearest gene was up-regulated upon replicative senescence (C), and 90 hypomethylated CpG sites for which the nearest gene was up-regulated upon replicative senescence and related to immune response (D) are shown.

doi:10.1371/journal.pone.0171431.g007

cells would not have enough rounds of cell division to accumulate any errors. Secondly, reduced activity of DNA methyltransferase 1 (DNMT1), which primarily maintains DNA methylation patterns during replication, may increase the incidence of errors. The expression profiles in this study exhibited a marked decrease in *DNMT1* in replicatively senescent cells (0.23-fold reduction, data not shown), whereas the expression levels of *DNMT1* in RIS (0.70-fold reduction, data not shown) and senescent SVts8 (0.80-fold reduction, data not shown) were slightly reduced. This is consistent with the results reported by Kaneda *et al.*, who reported that DNA methylation was not altered in RIS using methylated DNA immunoprecipitation (MeDIP) sequencing and bisulfite sequencing, and the *Dnmt1* expression level was not altered in RIS, or during 3 passages (passage 2 to 5) using mouse embryonic fibroblasts [16]. Thirdly, a marked decrease in Ten-eleven translocation 1 (TET1) expression could alter DNA methylation patterns. Recent studies have suggested active DNA demethylation is mediated by TET, the enzyme that converts 5-methylcytosine (5mC) to 5-hydroxymethylcytosine (5hmC), 5-formylcytosine (5fc), and 5-carboxylcytosine (5caC) [46–49]. There are three TET proteins: TET1, TET2 and TET3. The expression levels of *TET1* and *TET3* genes, but not *TET2*, reportedly decrease along with aging, and *TET3* expression is important for decreasing genomic

Table 3. Targeted genes mediated in part by miRNAs, with miRNA expression regulated via methylation in the promoter regions.

Targeted gene symbol	Gene expression (fold-change)	miRNAs of regulating targeted gene		
EIF4EBP2	3.0	hsa-miR-7-5p	hsa-miR-193a-5p	hsa-miR-335-5p
HECW2	4.2	hsa-miR-7-5p	hsa-miR-25-3p	hsa-miR-505-3p
CADM1	8.2	hsa-miR-7-5p	hsa-miR-505-3p	
CNNM2	2.9	hsa-miR-335-5p	hsa-miR-505-3p	
CPEB2	2.6	hsa-miR-7-5p	hsa-miR-505-3p	
CRY2	2.2	hsa-miR-7-5p	hsa-miR-17-5p	
DAAM1	2.5	hsa-miR-130b-3p	hsa-miR-335-5p	
DGKH	2.5	hsa-miR-130b-3p	hsa-miR-505-3p	
DOK6	2.2	hsa-miR-17-5p	hsa-miR-335-5p	
EGR2	2.8	hsa-miR-17-5p	hsa-miR-25-3p	
FAM134C	2.2	hsa-miR-17-5p	hsa-miR-335-5p	
GRIN2A	2.0	hsa-miR-7-5p	hsa-miR-130b-3p	
HPCAL4	7.6	hsa-miR-7-5p	hsa-miR-335-5p	
IL6ST	2.2	hsa-miR-130b-3p	hsa-miR-505-3p	
KLHL28	2.4	hsa-miR-7-5p	hsa-miR-335-5p	
MEF2D	2.7	hsa-miR-335-5p	hsa-miR-505-3p	
MYO1D	5.9	hsa-miR-193a-5p	hsa-miR-335-5p	
NR4A3	2.1	hsa-miR-7-5p	hsa-miR-335-5p	
OXR1	2.9	hsa-miR-7-5p	hsa-miR-17-5p	
PGM2L1	4.8	hsa-miR-17-5p	hsa-miR-130b-3p	
PIP4K2C	2.1	hsa-miR-25-3p	hsa-miR-505-3p	
PPARGC1B	2.6	hsa-miR-7-5p	hsa-miR-505-3p	
RAB11FIP5	2.8	hsa-miR-7-5p	hsa-miR-17-5p	
RNF141	2.4	hsa-miR-7-5p	hsa-miR-335-5p	
SEMA6D	5.9	hsa-miR-7-5p	hsa-miR-193a-5p	
ZDHHC8	5.2	hsa-miR-17-5p	hsa-miR-335-5p	
ZMAT3	3.4	hsa-miR-7-5p	hsa-miR-130b-3p	

doi:10.1371/journal.pone.0171431.t003

5hmC during aging in human T cells [50]. In replicatively senescent TIG-3 cells, the expression levels of the *TET1* gene were drastically decreased, although we have no expression data for the TET3 gene due to a lack of TET3 probes in the expression array. A recent study showed that *Tet1*/*Tet2* double-knockout mouse embryonic fibroblasts (MEFs) had defects in maintaining hypomethylation and resulted in hypermethylation of DNA methylation canyons where developmental genes are associated [51]. Taken togather, methylation changes during senescence would be required for many rounds of cell division and the decreased activities of DNA methyltransferase and methylcytsine deoxygenase, such as DNMT1 and TET1, might produce the altered methylation patterns within long-term culture.

We found that hypomethylation observed in the open sea was frequently associated with the up-regulation of genes related to immune response. When the genes hosting hypomethylated CpG sites were classified into six CpG subcategories using annotated GO terms, genes related to "immune response" were enriched only in the genes hosting hypomethylated CpG sites in the "open sea" (Fig 6A). Consistent with the results, the promoter types of genes categorized as "immune response" were mainly non-CGI promoters (Fig 7D). Nevertheless, the probes in the HumanMethylation450 BeadChip covered much more CpG island promoter genes than non-CpG island promoter genes (Fig 7A). In contrast, genes categorized into other groups, namely "metabolic process", "transport", "cell adhesion", "development", "signal

transduction", and "transcription", exhibited hypermethylation rather than hypomethylation in the CpG sites close to the TSS (S3 Table). Furthermore, integrated analyses showed that "immune response" was ranked in GO terms of genes up-regulated and concomitantly hypomethylated in close proximity to their TSS (Table 2). These results suggest that hypomethylation in the open sea may increase the expression of the "immune response"-related genes during replicative senescence. For example, *MHC II* has non-CGI promoters exhibiting hypomethylated CpG sites and its expression was up-regulated during replicative senescence. Several studies also indicated the effects of DNA methylation in the promoter regions on the expression of inflammatory genes [52–54].

Currently we cannot explain the mechanism by which hypomethylation in the non-CpG promoter increases the expression of a certain portion of the "immune response"-related genes during replicative senescence. We speculate that TET2 may play a role in this regulation. As mentioned above, TET proteins contribute to active DNA demethylation. In our data, the expression levels of one of the *TET2* probes showed a 2-fold increase in replicatively senescent cells and senescent SVts8 cells, whereas no increase in *TET2* expression was detected in the RIS cells. Unlike TET1 and TET3, TET2 does not have a CXXC domain, which is required for binding to the CpG site [55, 56]. These results suggest that collaboration between TET2 and its associated factor(s) may be required for DNA binding and demethylation. In fact, TET2 was reported to need a cofactor for binding to DNA [49]. During differentiation of helper T (Th) cells, TET2 induced DNA demethylation at the loci of key cytokine genes in a lineage-specific transcription factor-dependent manner and promoted signature cytokine expression in Th1 and Th17 cells [57]. Depending on the cofactor, TET2 may bind to non-CGI promoters in senescence-associated genes, and increase gene expression. Further studies are needed to investigate the effects of TET2 on hypomethylation at the specific CpG sites and its interacting factor(s) during senescence.

Recently, senescence-associated miRNAs (SA-miRNAs) have been reported to regulate genes associated with senescence [27–31]. We examined the effects of DNA methylation in the promoter regions of miRNAs on miRNA expression using human miRNA expression microarray and further selected miRNAs that likely affected the predicted gene expression. As a result, we identified seven miRNAs and 27 targeted genes (Table 3). These genes included eukaryotic translation initiation factor 4E binding protein 2 (*EIF4EBP2*), which inhibits translation initiation [58], and cryptochrome circadian clock 2 (*CRY2*), which is a key component in regulating circadian rhythm [59]. Among the 27 genes, the IL-6 signal transducer (*IL6ST*) and zinc finger matrin-type 3 (*ZMAT3*) are involved in immune response. *IL6ST*, which is supposed to be up-regulated by decreased levels of has-miR-130b-3p and has-miR-505-3p, encodes glycoprotein 130 (gp130) [60]. The protein gp130 is a signal transducer shared by many cytokines including IL-6, one of the SASP factors [61], IL-11, IL-27, and oncostatin-M [62–64]. In addition, *ZMAT3*, a predicted gene regulated by has-miR-7-5p and has-miR-130b-3p, encodes a double-stranded-RNA-binding zinc finger protein Wig-1 (for wild-type p53-induced gene 1). Wig-1, a transcriptional target of p53, stabilizes p53 by binding to the 3' UTR of p53 mRNA and protecting it from deadenylation [65]. A high level of p53 triggers cell cycle arrest, senescence and apoptosis, and efficiently inhibits tumor development [7, 66, 67]. In addition to the p53 transcription factor, miRNAs with expression regulated by DNA methylation via their promoter regions may also contribute to *ZMAT3* expression. MiR-34 is one of the SA-miRNAs and is up-regulated by p53 [27, 28, 32, 33, 68, 69]. Although increased levels of miRNA-34 were detected upon replicative senescence, the methylation changes (Δβ cut-off was ±0.2) in the promoter regions of miRNA-34 were not included in our data (data not shown).

In this study, we investigated the possibility of regulation by DNA methylation during senescence. We found that hypomethylation in the open sea may contribute to the up-

regulation of genes related to immune response. Several miRNAs targeting genes associated with a senescent state seem to regulate expression by DNA methylation in the promoter regions. However, we have to consider the possibility that DNA methylation results from alteration of gene expression. To investigate this possibility, we need to collect more data and explore the mechanism of methylation and demethylation change. Moreover, in order to reveal the whole mechanism of DNA methylation, we also need to focus on the methylation profile in hypomethylation and outside of the TSS and CpG islands.

Conclusion

Three types of senescent TIG-3 cells showed similar biological outcomes, but the regulatory mechanisms were different. Replicatively senescent cells showed sequential DNA methylation changes, but prematurely senescent RIS and SVts8 cells did not. In replicative senescence, hypomethylation with up-regulated gene expression often occurred in the open sea. Moreover, hypomethylation was observed in non-CGI promoters of genes related to the immune response. These results suggested that hypomethylation in the open sea regulates the expression of a certain portion of immune-related genes in replicative senescence. In addition, several miRNAs that seemed to have expression levels regulated in part by DNA methylation may also contribute to the expression of senescence-associated genes.

Supporting information

S1 Fig. Confirmation of senescence. Senescent cells were subjected to senescence-associated beta-galactosidase (SA-β-Gal) staining, qRT-PCR and immunoblotting. SA-β-Gal staining of the control A), C), E), replicatively senescent B), RIS D), and senescent SVts8 cells F). The percentages of SA-β-Gal-positive cells are shown at the bottom of each picture. Bar, 200 μm. Objective, ×10. G) The expression levels of $p16^{INK4A}$ and $p21^{Cip1/Waf1}$ obtained with SurePrint G3 Human GE microarrays and qRT-PCR. H) Representative western blotting of $p16^{INK4A}$ and $p21^{Cip1/Waf1}$, Ras, and loading control (actin). Images of $p16^{INK4A}$ are shown separately shown due to different exposure time.
(TIF)

S2 Fig. Integrated analysis of methylation and gene expression in replicative senescence. Each plot represents the values obtained from a single gene using integrated analyses. DNA methylation β values and gene expression levels are plotted along the abscissa and the ordinate, respectively. Red lines show the cut-off border. For methylation, Δβ for hypermethylation is $>= 0.2$, Δβ for hypomethylation is $=< -0.2$. For gene expression, the cut-off for increased/decreased expression was a ±2-fold change.
(TIF)

S1 Table. GO terms for up- or down-regulated genes in three types of senescent cells.
(XLSX)

S2 Table. GO terms for hypo- or hyper-methylated genes in replicatively senescent cells.
(XLSX)

S3 Table. The number of genes hosting differentially methylated CpG sites in the gene feature- and the CpG site- subcategories.
(XLSX)

S4 Table. Integrated analysis of gene expression and methylation changes in replicatively senescent cells.
(ZIP)

S5 Table. Hypo- or hyper-methylated miRNAs in the promoter regions of replicatively senescent cells.
(XLSX)

S6 Table. miRNA expression regulated by DNA methylation in the promoter region.
(XLSX)

Acknowledgments

We thank Dr. Takao Yokoyama for assisting with the data analysis and Ms. Emma L. Barber (National Research Institute for Child Health and Development, Japan) for editing the manuscript.

Author contributions

Conceptualization: MS KH K. Maehara.

Data curation: MS KO KN.

Formal analysis: MS AI KN KO.

Funding acquisition: AI KN K. Matsumoto K. Maehara.

Investigation: MS YE AI K. Matsumoto K. Maehara.

Methodology: KO KN.

Project administration: K. Maehara.

Resources: K. Matsumoto KH K. Maehara.

Software: KO.

Supervision: KH YK K. Maehara.

Validation: MS KN KO AI K. Maehara.

Visualization: MS.

Writing – original draft: MS.

Writing – review & editing: KN YK K. Maehara.

References

1. Hayflick L. The limited in vitro lifetime of human diploid cell strains. Exp Cell Res. 1965; 37:614–636. PMID: 14315085
2. Kuilman T, Michaloglou C, Mooi WJ, Peeper DS. The essence of senescence. Genes Dev. 2010; 24 (22):2463–2479. doi: 10.1101/gad.1971610 PMID: 21078816
3. Harley CB, Futcher AB, Greider CW. Telomeres shorten during ageing of human fibroblasts. Nature. 1990; 345(6274):458–460. doi: 10.1038/345458a0 PMID: 2342578
4. Serrano M, Lin AW, McCurrach ME, Beach D, Lowe SW. Oncogenic ras provokes premature cell senescence associated with accumulation of p53 and p16INK4a. Cell. 1997; 88(5):593–602. PMID: 9054499
5. Takahashi A, Ohtani N, Yamakoshi K, Iida S, Tahara H, Nakayama K, et al. Mitogenic signalling and the p16INK4a-Rb pathway cooperate to enforce irreversible cellular senescence. Nat Cell Biol. 2006; 8 (11):1291–1297. doi: 10.1038/ncb1491 PMID: 17028578
6. Collado M, Blasco MA, Serrano M. Cellular senescence in cancer and aging. Cell. 2007; 130(2):223–233. doi: 10.1016/j.cell.2007.07.003 PMID: 17662938

7. Campisi J. Cellular senescence as a tumor-suppressor mechanism. Trends Cell Biol. 2001; 11(11): S27–31. PMID: 11684439
8. Campisi J. Aging, cellular senescence, and cancer. Annu Rev Physiol. 2013; 75:685–705. doi: 10.1146/annurev-physiol-030212-183653 PMID: 23140366
9. Coppe JP, Patil CK, Rodier F, Sun Y, Munoz DP, Goldstein J, et al. Senescence-associated secretory phenotypes reveal cell-nonautonomous functions of oncogenic RAS and the p53 tumor suppressor. PLoS Biol. 2008; 6(12):2853–2868. doi: 10.1371/journal.pbio.0060301 PMID: 19053174
10. Wu Z, Nakanishi H. Lessons from Microglia Aging for the Link between Inflammatory Bone Disorders and Alzheimer's Disease. J Immunol Res. 2015; 2015:1–9.
11. Narita M, Nunez S, Heard E, Narita M, Lin AW, Hearn SA, et al. Rb-mediated heterochromatin formation and silencing of E2F target genes during cellular senescence. Cell. 2003; 113(6):703–716. PMID: 12809602
12. Narita M, Narita M, Krizhanovsky V, Nunez S, Chicas A, Hearn SA, et al. A novel role for high-mobility group a proteins in cellular senescence and heterochromatin formation. Cell. 2006; 126(3):503–514. doi: 10.1016/j.cell.2006.05.052 PMID: 16901784
13. Zhang W, Hu D, Ji W, Yang L, Yang J, Yuan J, et al. Histone modifications contribute to cellular replicative and hydrogen peroxide-induced premature senescence in human embryonic lung fibroblasts. Free Radic Res. 2014; 48(5):550–559. doi: 10.3109/10715762.2014.893580 PMID: 24528089
14. Shah PP, Donahue G, Otte GL, Capell BC, Nelson DM, Cao K, et al. Lamin B1 depletion in senescent cells triggers large-scale changes in gene expression and the chromatin landscape. Genes Dev. 2013; 27(16):1787–1799. doi: 10.1101/gad.223834.113 PMID: 23934658
15. Bracken AP, Kleine-Kohlbrecher D, Dietrich N, Pasini D, Gargiulo G, Beekman C, et al. The Polycomb group proteins bind throughout the INK4A-ARF locus and are disassociated in senescent cells. Genes Dev. 2007; 21(5):525–530. doi: 10.1101/gad.415507 PMID: 17344414
16. Kaneda A, Fujita T, Anai M, Yamamoto S, Nagae G, Morikawa M, et al. Activation of Bmp2-Smad1 signal and its regulation by coordinated alteration of H3K27 trimethylation in Ras-induced senescence. PLoS Genet. 2011; 7(11):e1002359. doi: 10.1371/journal.pgen.1002359 PMID: 22072987
17. Takahashi A, Imai Y, Yamakoshi K, Kuninaka S, Ohtani N, Yoshimoto S, et al. DNA damage signaling triggers degradation of histone methyltransferases through APC/C(Cdh1) in senescent cells. Mol Cell. 2012; 45(1):123–131. doi: 10.1016/j.molcel.2011.10.018 PMID: 22178396
18. Zhang Y, Elgizouli M, Schottker B, Holleczek B, Nieters A, Brenner H. Smoking-associated DNA methylation markers predict lung cancer incidence. Clin Epigenetics. 2016; 8(127):1–12.
19. Asada K, Kotake Y, Asada R, Saunders D, Broyles RH, Towner RA, et al. LINE-1 hypomethylation in a choline-deficiency-induced liver cancer in rats: dependence on feeding period. J Biomed Biotechnol. 2006; 2006(1):1–6.
20. Varley KE, Gertz J, Bowling KM, Parker SL, Reddy TE, Pauli-Behn F, et al. Dynamic DNA methylation across diverse human cell lines and tissues. Genome Res. 2013; 23(3):555–567. doi: 10.1101/gr.147942.112 PMID: 23325432
21. Horvath S, Zhang Y, Langfelder P, Kahn RS, Boks MP, van Eijk K, et al. Aging effects on DNA methylation modules in human brain and blood tissue. Genome Biol. 2012; 13(10):1–18.
22. Koch CM, Wagner W. Epigenetic biomarker to determine replicative senescence of cultured cells. Methods Mol Biol. 2013; 1048:309–321. doi: 10.1007/978-1-62703-556-9_20 PMID: 23929112
23. Koch CM, Suschek CV, Lin Q, Bork S, Goergens M, Joussen S, et al. Specific age-associated DNA methylation changes in human dermal fibroblasts. PLoS One. 2011; 6(2):e16679. doi: 10.1371/journal.pone.0016679 PMID: 21347436
24. Christensen BC, Houseman EA, Marsit CJ, Zheng S, Wrensch MR, Wiemels JL, et al. Aging and environmental exposures alter tissue-specific DNA methylation dependent upon CpG island context. PLoS Genet. 2009; 5(8):e1000602. doi: 10.1371/journal.pgen.1000602 PMID: 19680444
25. Fraga MF, Ballestar E, Paz MF, Ropero S, Setien F, Ballestar ML, et al. Epigenetic differences arise during the lifetime of monozygotic twins. Proc Natl Acad Sci U S A. 2005; 102(30):10604–10609. doi: 10.1073/pnas.0500398102 PMID: 16009939
26. Jjingo D, Conley AB, Yi SV, Lunyak VV, Jordan IK. On the presence and role of human gene-body DNA methylation. Oncotarget. 2012; 3(4):462–474. doi: 10.18632/oncotarget.497 PMID: 22577155
27. Dhahbi JM, Atamna H, Boffelli D, Magis W, Spindler SR, Martin DI. Deep sequencing reveals novel microRNAs and regulation of microRNA expression during cell senescence. PLoS One. 2011; 6(5): e20509. doi: 10.1371/journal.pone.0020509 PMID: 21637828
28. Lafferty-Whyte K, Cairney CJ, Jamieson NB, Oien KA, Keith WN. Pathway analysis of senescence-associated miRNA targets reveals common processes to different senescence induction mechanisms. Biochim Biophys Acta. 2009; 1792(4):341–352. doi: 10.1016/j.bbadis.2009.02.003 PMID: 19419692

29. Taguchi YH. Inference of Target Gene Regulation via miRNAs during Cell Senescence by Using the MiRaGE Server. Aging Dis. 2012; 3(4):301–306. PMID: 23185711

30. Overhoff MG, Garbe JC, Koh J, Stampfer MR, Beach DH, Bishop CL. Cellular senescence mediated by p16INK4A-coupled miRNA pathways. Nucleic Acids Res. 2014; 42(3):1606–1618. doi: 10.1093/nar/gkt1096 PMID: 24217920

31. Li CW, Wang WH, Chen BS. Investigating the specific core genetic-and-epigenetic networks of cellular mechanisms involved in human aging in peripheral blood mononuclear cells. Oncotarget. 2016; 7 (8):8556–8579. doi: 10.18632/oncotarget.7388 PMID: 26895224

32. Tazawa H, Tsuchiya N, Izumiya M, Nakagama H. Tumor-suppressive miR-34a induces senescence-like growth arrest through modulation of the E2F pathway in human colon cancer cells. Proc Natl Acad Sci U S A. 2007; 104(39):15472–15477. doi: 10.1073/pnas.0707351104 PMID: 17875987

33. He X, He L, Hannon GJ. The guardian's little helper: microRNAs in the p53 tumor suppressor network. Cancer Res. 2007; 67(23):11099–11101. doi: 10.1158/0008-5472.CAN-07-2672 PMID: 18056431

34. Christoffersen NR, Shalgi R, Frankel LB, Leucci E, Lees M, Klausen M, et al. p53-independent upregulation of miR-34a during oncogene-induced senescence represses MYC. Cell Death Differ. 2010; 17 (2):236–245. doi: 10.1038/cdd.2009.109 PMID: 19696787

35. Ayala-Ortega E, Arzate-Mejia R, Perez-Molina R, Gonzalez-Buendia E, Meier K, Guerrero G, et al. Epigenetic silencing of miR-181c by DNA methylation in glioblastoma cell lines. BMC Cancer. 2016; 16 (226):1–12.

36. Asuthkar S, Velpula KK, Chetty C, Gorantla B, Rao JS. Epigenetic regulation of miRNA-211 by MMP-9 governs glioma cell apoptosis, chemosensitivity and radiosensitivity. Oncotarget. 2012; 3(11):1439–1454. doi: 10.18632/oncotarget.683 PMID: 23183822

37. Yin H, Song P, Su R, Yang G, Dong L, Luo M, et al. DNA Methylation mediated down-regulating of MicroRNA-33b and its role in gastric cancer. Sci Rep. 2016; 6(18824):1–12.

38. Maehara K, Takahashi K, Saitoh S. CENP-A reduction induces a p53-dependent cellular senescence response to protect cells from executing defective mitoses. Mol Cell Biol. 2010; 30(9):2090–2104. doi: 10.1128/MCB.01318-09 PMID: 20160010

39. Chen C, Okayama H. High-efficiency transformation of mammalian cells by plasmid DNA. Mol Cell Biol. 1987; 7(8):2745–2752. PMID: 3670292

40. Tsuyama N, Miura M, Kitahira M, Ishibashi S, Ide T. SV40 T-antigen is required for maintenance of immortal growth in SV40-transformed human fibroblasts. Cell Struct Funct. 1991; 16(1):55–62. PMID: 1851674

41. Bibikova M, Le J, Barnes B, Saedinia-Melnyk S, Zhou L, Shen R, et al. Genome-wide DNA methylation profiling using Infinium(R) assay. Epigenomics. 2009; 1(1):177–200. doi: 10.2217/epi.09.14 PMID: 22122642

42. Bibikova M, Barnes B, Tsan C, Ho V, Klotzle B, Le JM, et al. High density DNA methylation array with single CpG site resolution. Genomics. 2011; 98(4):288–295. doi: 10.1016/j.ygeno.2011.07.007 PMID: 21839163

43. Price ME, Cotton AM, Lam LL, Farre P, Emberly E, Brown CJ, et al. Additional annotation enhances potential for biologically-relevant analysis of the Illumina Infinium HumanMethylation450 BeadChip array. Epigenetics Chromatin. 2013; 6(4):1–15.

44. Hannum G, Guinney J, Zhao L, Zhang L, Hughes G, Sadda S, et al. Genome-wide methylation profiles reveal quantitative views of human aging rates. Mol Cell. 2013; 49(2):359–367. doi: 10.1016/j.molcel.2012.10.016 PMID: 23177740

45. Laird CD, Pleasant ND, Clark AD, Sneeden JL, Hassan KM, Manley NC, et al. Hairpin-bisulfite PCR: assessing epigenetic methylation patterns on complementary strands of individual DNA molecules. Proc Natl Acad Sci U S A. 2004; 101(1):204–209. doi: 10.1073/pnas.2536758100 PMID: 14673087

46. Chen ZX, Riggs AD. DNA methylation and demethylation in mammals. J Biol Chem. 2011; 286 (21):18347–18353. doi: 10.1074/jbc.R110.205286 PMID: 21454628

47. Wu SC, Zhang Y. Active DNA demethylation: many roads lead to Rome. Nat Rev Mol Cell Biol. 2010; 11(9):607–620. doi: 10.1038/nrm2950 PMID: 20683471

48. Weber AR, Krawczyk C, Robertson AB, Kusnierczyk A, Vagbo CB, Schuermann D, et al. Biochemical reconstitution of TET1-TDG-BER-dependent active DNA demethylation reveals a highly coordinated mechanism. Nat Commun. 2016; 7(10806):1–13.

49. Pastor WA, Aravind L, Rao A. TETonic shift: biological roles of TET proteins in DNA demethylation and transcription. Nat Rev Mol Cell Biol. 2013; 14(6):341–356. doi: 10.1038/nrm3589 PMID: 23698584

50. Truong TP, Sakata-Yanagimoto M, Yamada M, Nagae G, Enami T, Nakamoto-Matsubara R, et al. Age-Dependent Decrease of DNA Hydroxymethylation in Human T Cells. J Clin Exp Hematop. 2015; 55 (1):1–6. doi: 10.3960/jslrt.55.1 PMID: 26105999

51. Wiehle L, Raddatz G, Musch T, Dawlaty MM, Jaenisch R, Lyko F, et al. Tet1 and Tet2 Protect DNA Methylation Canyons against Hypermethylation. Mol Cell Biol. 2015; 36(3):452–461. doi: 10.1128/MCB.00587-15 PMID: 26598602

52. Oliveira NF, Damm GR, Andia DC, Salmon C, Nociti FH Jr., Line SR, et al. DNA methylation status of the IL8 gene promoter in oral cells of smokers and non-smokers with chronic periodontitis. J Clin Periodontol. 2009; 36(9):719–725. doi: 10.1111/j.1600-051X.2009.01446.x PMID: 19659670

53. Rusiecki JA, Byrne C, Galdzicki Z, Srikantan V, Chen L, Poulin M, et al. PTSD and DNA Methylation in Select Immune Function Gene Promoter Regions: A Repeated Measures Case-Control Study of U.S. Military Service Members. Front Psychiatry. 2013; 4:1–12.

54. Ushijima T. Epigenetic field for cancerization. J Biochem Mol Biol. 2007; 40(2):142–150. PMID: 17394762

55. Lee JH, Voo KS, Skalnik DG. Identification and characterization of the DNA binding domain of CpG-binding protein. J Biol Chem. 2001; 276(48):44669–44676. doi: 10.1074/jbc.M107179200 PMID: 11572867

56. Williams K, Christensen J, Helin K. DNA methylation: TET proteins-guardians of CpG islands? EMBO Rep. 2012; 13(1):28–35.

57. Ichiyama K, Chen T, Wang X, Yan X, Kim BS, Tanaka S, et al. The methylcytosine dioxygenase Tet2 promotes DNA demethylation and activation of cytokine gene expression in T cells. Immunity. 2015; 42(4):613–626. doi: 10.1016/j.immuni.2015.03.005 PMID: 25862091

58. Banko JL, Poulin F, Hou L, DeMaria CT, Sonenberg N, Klann E. The translation repressor 4E-BP2 is critical for eIF4F complex formation, synaptic plasticity, and memory in the hippocampus. J Neurosci. 2005; 25(42):9581–9590. doi: 10.1523/JNEUROSCI.2423-05.2005 PMID: 16237163

59. van der Horst GT, Muijtjens M, Kobayashi K, Takano R, Kanno S, Takao M, et al. Mammalian Cry1 and Cry2 are essential for maintenance of circadian rhythms. Nature. 1999; 398(6728):627–630. doi: 10.1038/19323 PMID: 10217146

60. Rose-John S, Heinrich PC. Soluble receptors for cytokines and growth factors: generation and biological function. Biochem J. 1994; 300:281–290. PMID: 8002928

61. Freund A, Orjalo AV, Desprez PY, Campisi J. Inflammatory networks during cellular senescence: causes and consequences. Trends Mol Med. 2010; 16(5):238–246. doi: 10.1016/j.molmed.2010.03.003 PMID: 20444648

62. Baumann H, Schendel P. Interleukin-11 regulates the hepatic expression of the same plasma protein genes as interleukin-6. J Biol Chem. 1991; 266(30):20424–20427. PMID: 1718962

63. Heinrich PC, Behrmann I, Haan S, Hermanns HM, Muller-Newen G, Schaper F. Principles of interleukin (IL)-6-type cytokine signalling and its regulation. Biochem J. 2003; 374(Pt 1):1–20. doi: 10.1042/BJ20030407 PMID: 12773095

64. Pflanz S, Hibbert L, Mattson J, Rosales R, Vaisberg E, Bazan JF, et al. WSX-1 and glycoprotein 130 constitute a signal-transducing receptor for IL-27. J Immunol. 2004; 172(4):2225–2231. PMID: 14764690

65. Vilborg A, Glahder JA, Wilhelm MT, Bersani C, Corcoran M, Mahmoudi S, et al. The p53 target Wig-1 regulates p53 mRNA stability through an AU-rich element. Proc Natl Acad Sci U S A. 2009; 106(37):15756–15761. doi: 10.1073/pnas.0900862106 PMID: 19805223

66. Beausejour CM, Krtolica A, Galimi F, Narita M, Lowe SW, Yaswen P, et al. Reversal of human cellular senescence: roles of the p53 and p16 pathways. EMBO J. 2003; 22(16):4212–4222. doi: 10.1093/emboj/cdg417 PMID: 12912919

67. Vousden KH. Outcomes of p53 activation—spoilt for choice. J Cell Sci. 2006; 119(Pt 24):5015–5020. doi: 10.1242/jcs.03293 PMID: 17158908

68. Disayabutr S, Kim EK, Cha SI, Green G, Naikawadi RP, Jones KD, et al. miR-34 miRNAs Regulate Cellular Senescence in Type II Alveolar Epithelial Cells of Patients with Idiopathic Pulmonary Fibrosis. PLoS One. 2016; 11(6):e0158367. doi: 10.1371/journal.pone.0158367 PMID: 27362652

69. Harries LW. MicroRNAs as Mediators of the Ageing Process. Genes (Basel). 2014; 5(3):656–670.

J. Neurovirol. (2017) 23:79–86
DOI 10.1007/s13365-016-0475-y

Human cytomegalovirus downregulates *SLITRK6* expression through IE2

Huanan Liao[1] · Haruna Sato[1] · Ryosuke Chiba[1] · Tomoko Kawai[2] · Kazuhiko Nakabayashi[2] · Kenichiro Hata[2] · Hidenori Akutsu[3] · Shigeyoshi Fujiwara[1] · Hiroyuki Nakamura[1]

Received: 9 March 2016 / Revised: 7 June 2016 / Accepted: 1 August 2016 / Published online: 16 August 2016

Abstract Congenital human cytomegalovirus (HCMV) infection causes sensorineural hearing loss (SNHL) and other neurological disorders, although the neuropathogenesis of HCMV infection is not well understood. Here, we show that the expression of *SLITRK6*, one of causative genes for hereditary SNHL, was robustly downregulated by HCMV infection in cultured neural cells. We also show that HCMV-encoded immediate-early 2 (IE2) proteins mediate this downregulation and their carboxy-terminal region, especially amino acid residue Gln^{548}, has a critical role. These findings suggest that the downregulation of *SLITRK6* expression by IE2 may have a role in HCMV-induced SNHL and other neurological disorders.

Keywords Human cytomegalovirus · IE2 · *SLITRK6* · Hearing loss

Introduction

Congenital human cytomegalovirus (HCMV) infection is the most common congenital viral infection, affecting 0.2 to 2.5 % of all live-born neonates (Cheeran et al. 2009; Ornoy and Diav-Citrin 2006). Approximately 10 % of neonates with congenital HCMV infection are estimated to be symptomatic at birth and often manifest severe damages in various organs including the central nervous system (CNS) and the inner ear. A recent large-scale screening in Japan demonstrated that approximately 30 % of congenitally HCMV-infected newborns had some clinical manifestations at birth if abnormal findings of brain MRI are included (Koyano et al. 2011). Although the vast majority of neonates with congenital HCMV infection are thus asymptomatic at birth, approximately 10 % of these asymptomatic children will develop delayed sequelae caused by HCMV-induced nervous system damages, such as sensorineural hearing loss (SNHL), vestibular symptoms, and behavioral abnormalities (Bernard et al. 2015; Karltorp et al. 2014). Congenital HCMV infection is the leading cause of nongenetic congenital SNHL; 22 to 65 % of children that were symptomatic at birth and 6 to 23 % of children that were asymptomatic at birth develop SNHL (Fowler and Boppana 2006; Morton and Nance 2006).

Although HCMV infection and gene expression in the inner ear as well as various parts of the CNS have been analyzed in a limited number of congenitally infected children, the exact nature of HCMV infection in the human nervous system has not been well characterized. The mechanism of HCMV-induced neuropathogenesis therefore remains largely unknown. To get a new insight into HCMV-induced neuropathogenesis, we have been analyzing the effect of HCMV infection on the expression of cellular genes involved in the development and function of the CNS and/or auditory system. In this report, we demonstrate that the expression of *SLITRK6*, an etiologic gene for a group of hereditary SNHL (Morlet et al. 2014; Tekin et al. 2013), is robustly downregulated by HCMV infection in cultured neural cells. Further, we demonstrate that HCMV-encoded immediate-early 2 (IE2) proteins are involved in this *SLITRK6* downregulation.

✉ Hiroyuki Nakamura
nakamura-hry@ncchd.go.jp

[1] Department of Allergy and Clinical Immunology, National Research Institute for Child Health and Development, 2-10-1 Okura, Setagaya-ku, Tokyo 157-8535, Japan

[2] Department of Maternal-Fetal Biology, National Research Institute for Child Health and Development, Tokyo, Japan

[3] Department of Reproductive Biology, Center for Regenerative Medicine, National Research Institute for Child Health and Development, Tokyo, Japan

Materials and methods

Cells and viruses

The human glioblastoma-astrocytoma cell lines U373 MG and Hs 683 were grown in Dulbecco's modified Eagle's medium (DMEM; Nacalai Tesque, Kyoto, Japan) supplemented with 10 % fetal bovine serum (FBS; Biowest, France), penicillin (200 U/mL), and streptomycin (200 μg/mL) at 37 °C in 5 % CO_2 atmosphere. The human neuroblastoma cell line SH-SY5Y was grown in DMEM/F-12 (Nacalai Tesque) supplemented with 10 % FBS and the antibiotics. The human foreskin fibroblast cell line hTERT-BJ1 (Clontech, Palo Alto, CA) was grown in a medium consisting of DMEM/medium 199 (Sigma-Aldrich, St. Louis, MO) (4:1) supplemented with 10 % FBS, 1 mM sodium pyruvate (Nacalai Tesque), 2 mM glutamine (Thermo Fisher Scientific; Madison, WI), and the antibiotics. The HCMV laboratory strains Towne (ATCC VR-977) and AD169 (ATCC VR-538) were propagated in cultured hTERT-BJ1 cells. Heat-inactivated (HI) HCMV was prepared by heating HCMV-containing culture media at 63 °C for 60 min. The Gibco episomal human iPSC line (Thermo Fisher Scientific), an induced pluripotent stem cell (iPSC) line generated using cord blood-derived CD34+ progenitors, was grown under feeder-free conditions in complete Essential 8 medium (Thermo Fisher Scientific) on vessels coated with vitronectin (Thermo Fisher Scientific). The iPSCs were differentiated into neural stem/progenitor cells (NSPCs) using PSC Neural Induction Medium (Thermo Fisher Scientific) according to manufacturer's instructions.

Antibodies and reagents

The antibodies used were as follows: sheep anti-SLITRK6 (R&D Systems, Minneapolis, MN); mouse anti-CMV IE1/IE2 (8B1.2, Merck Millipore, Bedford, MA); mouse anti-IE2 (5A8.2, Merck Millipore); mouse anti-IE2 (12E2, Santa Cruz Biotechnology, Santa Cruz, CA); mouse anti-IE1 (6E1, Santa Cruz Biotechnology); mouse anti-CMV gB (2F12, Abcam, Cambridge, MA); mouse anti-pp65 (3A12, Abcam); mouse anti-nestin (10C2, Merck Millipore), horseradish peroxidase (HRP)-conjugated mouse anti-β-actin (Wako Chemical, Osaka, Japan); Alexa Fluor 488-conjugated goat anti-mouse immunoglobulin G (IgG) (Thermo Fisher Scientific); HRP-conjugated donkey anti-sheep IgG (R&D Systems); and HRP-conjugated sheep anti-mouse IgG (GE Healthcare, Little Chalfont, Buckinghamshire, UK). Cellstain-DAPI solution was obtained from Dojindo Molecular Technologies (Kumamoto, Japan).

Plasmid constructs and the Flp-In/TREx expression system

HCMV-encoded genes and deletion mutants were generated by PCR with primers shown in Table 1. The PCR products were cloned into the pcDNA5/FRT/TO vector (Thermo Fisher Scientific) to construct pcDNA5/FRT/TO-IE1 72, pcDNA5/FRT/TO-IE2 86, pcDNA5/FRT/TO-IE2 60, pcDNA5/FRT/TO-IE2 40, and pcDNA5/FRT/TO-pp65. To construct pcDNA5/FRT/FRT-IE2 (Q548R), site-directed mutagenesis was performed using QuikChange II site-directed mutagenesis kit (Agilent Technologies, Santa Clara, CA) with the following primers: forward 5′-GGCCTACGCCGTCG GCCGGTTTGAGCAGCCC-3′, reverse 5′-GGGC TGCTCAAACCGGCCGACGGCGTAGGCC-3′ as described previously (Petrik et al. 2006). To establish U373 MG cells expressing HCMV-encoded genes in a tetracycline-inducible manner, pFRT/lacZeo (Thermo Fisher Scientific) containing a Flp recombination target site and a lacZ-Zeocin fusion gene and pcDNA6/TR (Thermo Fisher Scientific) containing tetracycline repressor gene were sequentially transduced into U373 MG cells, and transfected cells were selected with zeocin (InvivoGen, San Diego, CA) and blasticidin (InvivoGen), respectively, as described previously (Nakamura et al. 2003). The resultant cells were co-transfected with pOG44 (Thermo Fisher Scientific) expressing Flp recombinase combined with pcDNA5/FRT/TO-IE1, pcDNA5/FRT/TO-IE2, pcDNA5/FRT/TO-pp65, or pcDNA5/FRT/TO, and selected with 500 μg/mL of hygromycin B (Wako Chemical) for 6 weeks. These cells were designated as Flp-In/TREx U373 MG-IE1, Flp-In/TREx U373 MG-IE2, Flp-In/TREx U373 MG-pp65, and Flp-In/TREx U373 MG-pcDNA5/FRT/TO cells, respectively. To induce viral gene expression, cells were treated with 3 μg/mL of doxycycline (Takara Bio, Shiga, Japan).

Reverse transcription PCR, real-time quantitative RT-PCR

Total RNA was extracted from cells using ReliaPrep RNA Cell Miniprep System (Promega, Madison, WI). First-strand complementary DNAs (cDNAs) were synthesized using a PrimeScript II 1st strand cDNA Synthesis Kit (Takara Bio). The resultant cDNAs were analyzed by either reverse transcription (RT)-PCR or real-time quantitative RT-PCR (RT-qPCR). RT-PCR was performed in a total volume of 50 μL for 30 cycles using the GeneAmp PCR System 9700 thermocycler (Thermo Fisher Scientific), and then the PCR products were analyzed by 1–2 % agarose gel electrophoresis. RT-qPCR was performed with pre-designed TaqMan probe and primer sets specific for human *SLITRK6* (TaqMan Gene Expression Assay, assay identification Hs00536106_s1; Thermo Fisher Scientific) and human TATA box-binding protein (*TBP*) (assay identification Hs00427620_m1) in a StepOne Plus System (Thermo Fisher Scientific). The relative quantification of gene expression was calculated using the ΔΔCt method and normalized to *TBP* messenger RNA (mRNA).

Table 1 Primers used for molecular cloning and RT-PCR analysis

Gene	Forward primer	Reverse primer
Cloning		
IE1 72	CGCAAGCTTGCCGCCACCATGGAGTCCTCTGCCAAGAGAAAG	CGCGGATCCTTACTGGTCAGCCTTGCTTCTAG
IE2 86	CGCAAGCTTGCCGCCACCATGGAGTCCTCTGCCAAGAGAAAG	CGCGGATCCTTACTGAGACTTGTTCCTCAGG
pp65	CGCGGATCCAGCATGGAGTCGCGCGGTCGC	CGCCTCGAGTCAACCTCGGTGCTTTTTGGGC
IE2 (1–550)	CGCAAGCTTGCCGCCACCATGGAGTCCTCTGCCAAGAGAAAG	CGCGGATCCTTACTCAAACTGCCCCACGGCGTAG
IE2 (1–547)	CGCAAGCTTGCCGCCACCATGGAGTCCTCTGCCAAGAGAAAG	CGCGGATCCTTACCCCACGGCGTAGGCCTTCGC
IE2 (1–543)	CGCAAGCTTGCCGCCACCATGGAGTCCTCTGCCAAGAGAAAG	CGCGGATCCTTAGGCCTTCGCGGCCGTCTCGTAG
IE2 60	CGCAAGCTTGCCGCCACCATGCTGCCCCTCATCAAACAGG	CGCGGATCCTTACTGAGACTTGTTCCTCAGG
IE2 40	CGCAAGCTTGCCGCCACCATGAACCACCCTCCTCTTCCCGA	CGCGGATCCTTACTGAGACTTGTTCCTCAGG
RT-PCR		
SLITRK6	CAGCAGCTTGCAAATGGTTA	GAGCCTCTGGATGAGAGCAC
IE1	ATGGAGTCCTCTGCCAAGAG	ATTCTATGCCGCACCATGTCC
IE2	ATGGAGTCCTCTGCCAAGAG	CTGAGACTTGTTCCTCAGGTCCTG
pp65	CGCAACCTGGTGCCCATGG	CGTTTGGGTTGCGCAGCGGG
β-actin	ACCATGGATGATGATATCGC	TCATTGTAGAAGGTGTGGTG
TBP	TTCGGAGAGTTCTGGGATTGTA	TGGACTGTTCTTCACTCTTGGC

Underlined letters indicate restriction enzyme recognition sites

Immunoblot analysis

Cellular proteins extracted with a sodium dodecyl sulfate (SDS) sample buffer (50 mM Tris-HCl, pH 6.8, 2 % SDS, 10 % glycerol, 6 % 2-mercaptoethanol, 0.1 % bromophenol blue) were subjected to sodium dodecyl sulfate-polyacrylamide gel electrophoresis (SDS-PAGE). Proteins were transferred to Immobilon-P transfer membranes (Merck Millipore). Membranes were blocked with 5 % non-fat milk (Nacalai Tesque) and then incubated with a primary antibody overnight at 4 °C in TBS-T (20 mM Tris, pH 7.6, 137 mM NaCl, 0.1 % Tween-20). Membranes were then incubated with a HRP-conjugated secondary antibody, and antigen proteins were visualized with ImmunoStar Zeta (Wako Chemicals) and detected by the GE LAS4000 Phosphor Imager (GE Healthcare Life Sciences).

Results

HCMV infection robustly downregulates *SLITRK6* expression

A variety of cellular genes have been identified as the causes of hereditary neurodevelopmental diseases (Mitchell 2011), and we speculated that HCMV infection may affect the expression of such genes to induce neurodevelopmental diseases. Among those genes, we focused on *SLITRK6*, since it has been recently demonstrated as a causative gene of hereditary SNHL and myopia in mice and humans (Katayama et al. 2009; Matsumoto et al. 2011; Morlet et al. 2014; Tekin et al. 2013). RT-PCR analysis showed that the *SLITRK6* mRNA expression was clearly and robustly downregulated in HCMV-infected SH-SY5Y cells compared to mock-infected cells (Fig. 1(a)). This downregulation of *SLITRK6* mRNA expression was not observed following infection with heat-inactivated HCMV, indicating that viable HCMV is required. The downregulation of *SLITRK6* mRNA was also detected in U373 MG cells (Fig. 1(d)) and Hs 683 cells (data not shown) following HCMV infection. To confirm the results and obtain more quantitative data, we performed real-time quantitative RT-PCR (RT-qPCR) and the results demonstrated that *SLITRK6* mRNA expression in HCMV-infected SH-SY5Y cells (Fig. 1(b)) and U373 MG cells (Fig. 1(e)) was decreased 21–183-fold and 41–46-fold, respectively, compared to those cells infected with heat-inactivated HCMV. Immunoblot analysis showed that the downregulation of *SLITRK6* mRNA levels was reflected at the protein level; the SLITRK6 protein expression was apparently abolished in SH-SY5Y (Fig. 1(c)), U373 MG cells (Fig. 1(f)), and Hs 683 cells (data not shown) following HCMV infection.

We previously demonstrated that neural stem/progenitor cells (NSPCs) derived from human induced pluripotent stem cells (iPSCs) can be infected with HCMV (Nakamura et al. 2013). Therefore, we examined whether

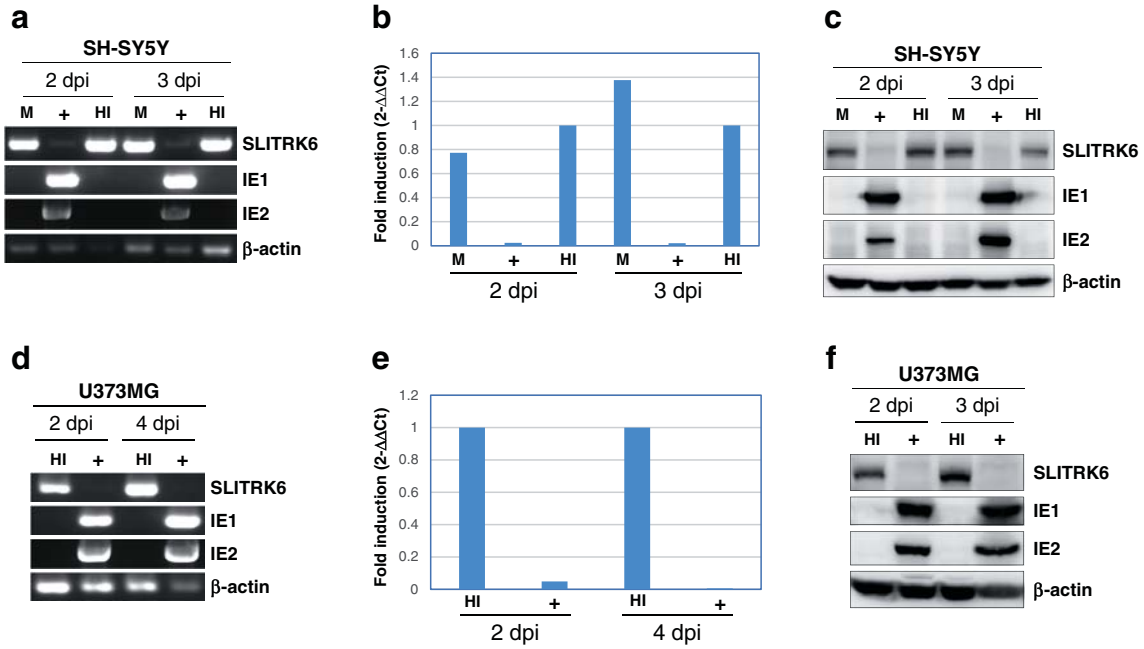

Fig. 1 HCMV infection robustly downregulates SLITRK6 expression in neural cell lines. RT-PCR analysis of SLITRK6 mRNA expression in the HCMV-infected cell lines SH-SY5Y (**a**) and U373 MG (**d**). Total RNAs isolated from cells infected with Towne HCMV (+), heat-inactivated Towne HCMV (*HI*), or mock-infected (*M*, culture media from HCMV-uninfected hTERT-BJ1 cells) at indicated days post-infection (*dpi*) were subjected to RT-PCR assays with SLITRK6-specific primers. RT-PCR assays with IE1- and IE2-specific primers were also performed. β-actin was used as an internal control. RT-qPCR analysis of SLITRK6 mRNA expression in the HCMV-infected cell lines SH-SY5Y (**b**) and U373 MG (**e**). RT-qPCR data was analyzed by the 2-ΔΔCt method. The mRNA expression was normalized to that of TBP. The fold induction was calculated as the ratio of mRNA levels. Immunoblot analysis of SLITRK6 protein expression in the HCMV-infected cell lines SH-SY5Y (**c**) and U373 MG (**f**). Whole-cell lysates of cells infected with Towne HCMV (+), heat-inactivated Towne HCMV (*HI*), or mock-infected (*M*) were extracted at indicated dpi and separated by SDS-PAGE and analyzed by immunoblotting with antibodies against SLITRK6, IE1, or IE2. Equal protein loading was established with anti-β-actin antibody

the expression of *SLITRK6* is downregulated by HCMV infection also in NSPCs derived from human iPSCs. RT-PCR (Fig. 2(a)), RT-qPCR (Fig. 2(b)), and immunoblot analyses (Fig. 2(c)) showed that *SLITRK6* was highly expressed in iPSC-derived NSPCs compared to parental iPSCs, suggesting that differentiation of iPSCs into NSPCs induced *SLITRK6* expression. In NSPCs derived from human iPSCs, the expression of *SLITRK6* was robustly downregulated by HCMV infection (Fig. 2(d–f)). These results indicated that the *SLITRK6* downregulation by HCMV is commonly observed in a variety of human neural cell lines.

IE2 mediates the downregulation of *SLITRK6* expression by HCMV

To clarify the mechanism of the *SLITRK6* downregulation by HCMV, we explored which viral gene is responsible for this downregulation. We initially examined whether HCMV-encoded immediate-early proteins IE1 72 and IE2 86 and viral tegument protein pp65 can affect *SLITRK6* expression. Using U373 MG cells, we established cell lines in which these individual viral genes were expressed in a tetracycline-inducible manner. The cell lines were designated Flp-In/TREx U373 MG-IE1 72, Flp-In/TREx U373 MG-IE2 86, and Flp-In/TREx U373 MG-pp65, respectively. Flp-In/TREx U373 MG-pcDNA5/FRT/TO was used as a negative control. When these cells were treated with doxycycline (Dox) for 2 or 4 days, the synthesis of IE1 72, IE2 86, and pp65 proteins was induced (Fig. 3(B)). RT-PCR assay at 2 or 4 days after the addition of Dox demonstrated the downregulation of *SLITRK6* mRNA expression by IE2 86 (Fig. 3(A-b)) but not by IE1 72 (Fig. 3(A-a)) and pp65 (Fig. 3(A-c)). As expected, the control Flp-In/TREx U373 MG-pcDNA5/FRT/TO cells showed similar levels of *SLITRK6* mRNA with or without Dox treatment (Fig. 3(A-d)). In accordance with these mRNA data, SLITRK6 protein levels were clearly reduced by Dox treatment in Flp-In/TREx U373 MG-IE2 86 cells (Fig. 3(B), lanes 5–8). In contrast, SLITRK6 protein levels were not significantly reduced in Flp-In/TREx U373 MG-IE1 72 (Fig. 3(B), lanes 1–4), Flp-In/TREx U373 MG-pp65 (Fig. 3(B), lanes 13–16), or Flp-In/TREx U373 MG-pcDNA5/FRT/TO cells (Fig. 3(B), lanes 9–12) following treatment with Dox. These results clearly indicate that IE2 86 is involved in the HCMV-induced downregulation of *SLITRK6* expression.

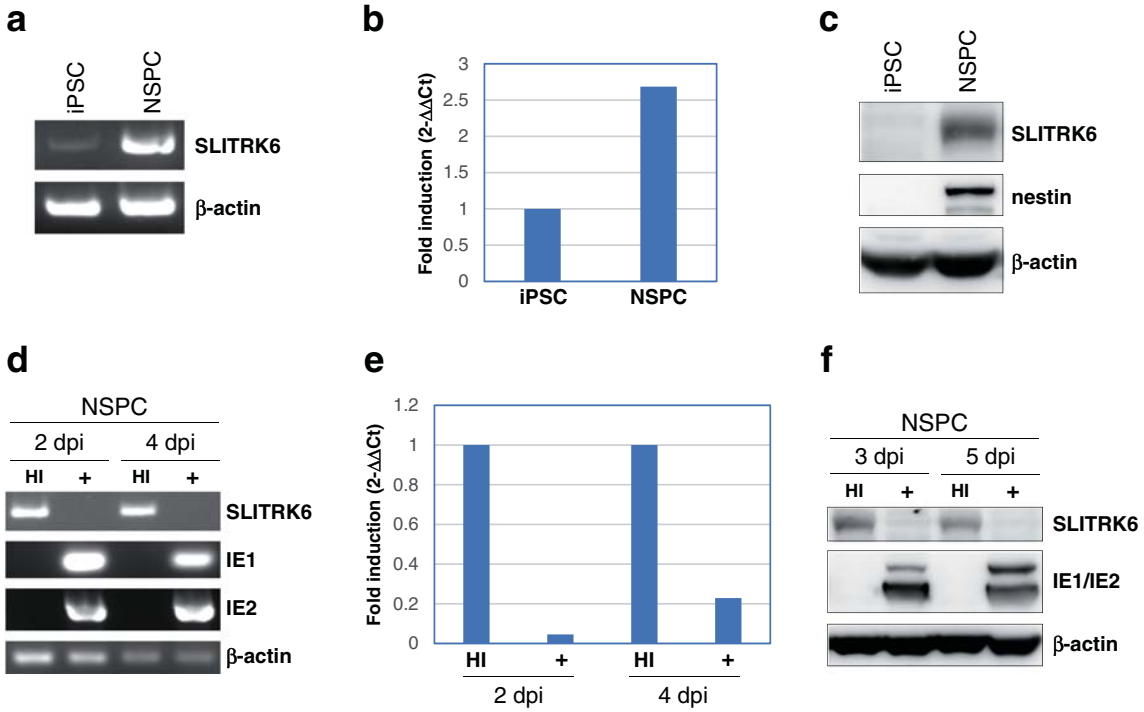

Fig. 2 SLITRK6 expression in iPSCs and iPSC-derived NSPCs. (**a**) Total RNAs extracted from iPSCs and iPSC-derived NSPCs were analyzed by RT-PCR for the expression of SLITRK6 and β-actin. (**b**) SLITRK6 mRNA expression in iPSCs and NSPCs was analyzed by RT-qPCR. RT-qPCR data was analyzed by the 2-ΔΔCt method. The mRNA expression was normalized to that of TBP. The fold induction was calculated as the ratio of mRNA levels. (**c**) Whole-cell lysates of iPSCs and NSPCs were analyzed by immunoblotting with antibodies against SLITRK6 or nestin. Equal protein loading was established with anti-β-actin antibody. (**d**) RT-PCR analysis of SLITRK6 mRNA expression in the HCMV-infected NSPCs. Total RNAs isolated from NSPCs infected with AD169 HCMV (+) or heat-inactivated AD169 HCMV (*HI*) at indicated days post-infection (*dpi*) were subjected to RT-PCR assays for the expression of SLITRK6, IE1, and IE2. β-actin was used as an internal control. (**e**) RT-qPCR analysis of SLITRK6 mRNA expression in the HCMV-infected NSPCs. (**f**) Immunoblot analysis of SLITRK6 protein expression in the HCMV-infected NSPCs. Whole-cell lysates of cells infected with AD169 HCMV (+) or heat-inactivated AD169 HCMV (*HI*) were extracted at indicated dpi and separated by SDS-PAGE and analyzed by immunoblotting with antibodies against SLITRK6 and IE1/ IE2. Equal protein loading was established with anti-β-actin antibody

Carboxy-terminal region of IE2 86 is required for the downregulation of *SLITRK6* expression by HCMV

To address which region of IE2 86 is required for the *SLITRK6* downregulation, we compared the wild-type IE2 86 (designated as IE2 (1–579)) and its several deletion mutants (Fig. 4(C)) in terms of the ability of the *SLITRK6* downregulation. The deletion mutants IE2 (1–550), IE2 (1–547), and IE2 (1–543) were expressed in Flp-In/TREx U373 MG cells in a Dox-inducible manner as described above. RT-PCR analysis confirmed that IE2 (1–550) suppressed the *SLITRK6* mRNA level markedly (Fig. 4(A-a)), whereas IE2 (1–547) (Fig. 4(A-b)) and IE2 (1–543) (Fig. 4(A-c)) had little or no effect. Immunoblot analyses demonstrated that individual deletion mutants were expressed at comparable levels, and immunofluorescence analysis showed that these deletion mutants localize in the nucleus. Immunoblot analyses demonstrate that the expression levels of the SLITRK6 protein was reduced by IE2 (1–550) (Fig. 4(A-g)), but not by IE2 (1–547) (Fig. 4(A-h)) or IE2 (1–543) (Fig. 4(A-i)). Collectively, these results indicate that the carboxy-terminal region (548 to 550 a.a.) of IE2 86 is critically important for the downregulation of *SLITRK6*. Since these data suggested that the amino acid residues 548 to 550 of IE2 86 is involved in the downregulation of *SLITRK6* expression, IE2 (Q548R), in which the glutamine residue at a.a. 548 was mutated to arginine, was expressed in U373 MG cells and *SLITRK6* expression was analyzed. Remarkably, the downregulation of *SLITRK6* was not seen with IE2 (Q548R) both by RT-PCR (Fig. 4(A-d)) and by immunoblotting (Fig. 4(A-j)). These results clearly show that glutamine residue at a.a. 548 has a critical role in the downregulation of *SLITRK6* expression.

Internal methionine codons in the exon 5 of IE2 86 generates the IE2 isoforms IE2 60 and IE2 40 (Plachter et al. 1993; Puchtler and Stamminger 1991; Stenberg et al. 1989). To test whether these isoforms can induce the *SLITRK6* downregulation, we established the Flp-In/TREx U373 MG-IE2 60 and Flp-In/TREx U373 MG-IE2 40 cells in which the individual isoforms are synthesized in a Dox-dependent manner. Both IE2 60 and IE2 40 proteins were detected in the nucleus in these cells by

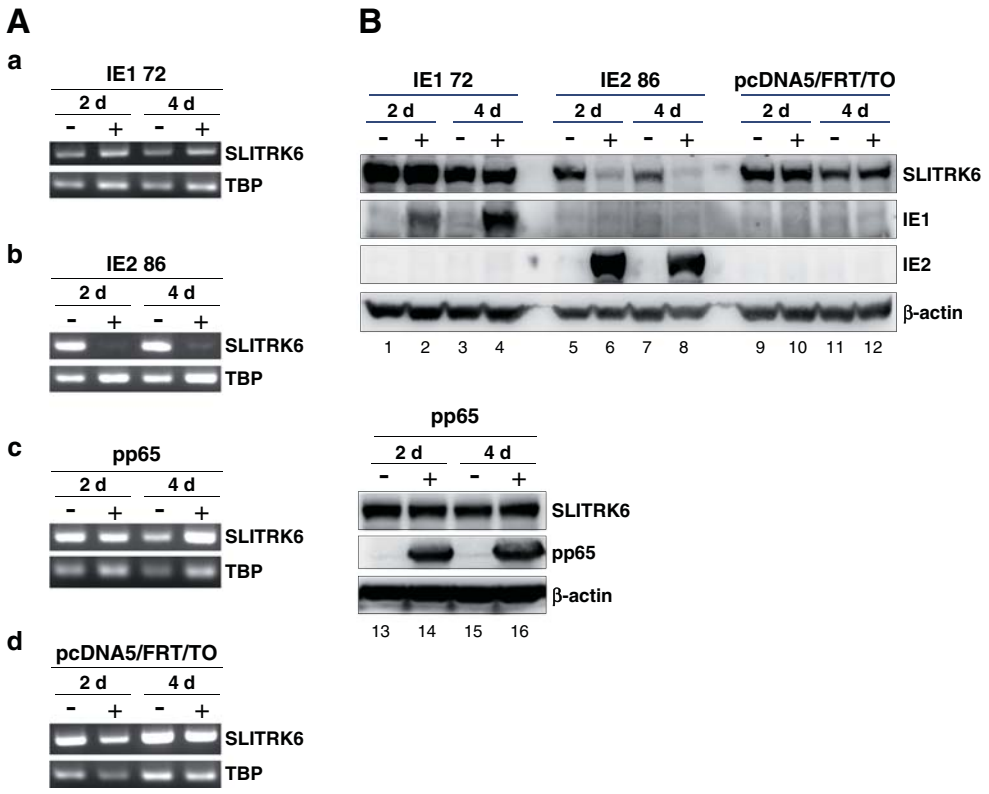

Fig. 3 Downregulation of SLITRK6 expression by IE2. **A** Total RNAs extracted from Flp-In/TREx U373 MG-IE1 72 (*a*), Flp-In/TREx U373 MG-IE2 86 (*b*), Flp-In/TREx U373 MG-pp65 (*c*), and Flp-In/TREx U373 MG-pcDNA5/FRT/TO cells (*d*) were subjected to RT-PCR analysis. RNAs isolated from the cells harvested at the indicated time points were subjected to RT-PCR assays. TATA-binding protein (*TBP*) was used as an internal control. Total RNA was isolated from the cells treated with (+) or without (−) 3 μg/mL Dox and harvested after indicated periods of Dox treatment. **B** Flp-In/TREx U373 MG-IE1 72 (lanes 1–4), Flp-In/TREx U373 MG-IE2 86 (lanes 5–8), Flp-In/TREx U373 MG-pp65 (lanes 13–16), and Flp-In/TREx U373 MG-pcDNA5/FRT/TO cells (lanes 9–12) were treated with (+) or without (−) 3 μg/mL doxycycline (Dox) and harvested after 2 days (*2 d*) and 4 days (*4 d*) post-induction by Dox treatment. Whole-cell lysates were prepared and used for immunoblot assays with the indicated antibodies. An anti-β-actin antibody was used to monitor general protein levels

immunofluorescence analysis (Fig. 4(B)). Both IE2 60 (Fig. 4(A-e)) and IE2 40 (Fig. 4(A-f)) clearly downregulated *SLITRK6* mRNA expression by RT-PCR assays. Immunoblot analyses also showed that IE2 60 (Fig. 4(A-k)) and IE2 40 (Fig. 4(A-l)) downregulate SLITRK6 protein expression.

Discussion

In this study, we demonstrate that HCMV infection robustly downregulates the expression of *SLITRK6* in cultured neural cells such as SH-SY5Y, U373 MG, Hs 683, and NSPCs derived from iPSCs. HCMV-encoded IE2 86, IE2 60, and IE2 40 were shown responsible for this downregulation. Analyses of IE2 86 mutants showed that the carboxy-terminal region, especially Gln^{548}, has a critical role in the *SLITRK6* downregulation. The Gln^{548} residue of IE2 has been shown to have a critical role in its association with p150, a component of chromatin assembly factor 1 (Lee et al. 2011). It is therefore speculated that similar association of IE2 with other cellular proteins via Gln^{548} may be involved in the IE2-mediated *SLITRK6* downregulation.

Human *SLITRK6* encodes a type I transmembrane protein highly expressed in the brain of first-trimester human fetuses (Iruretagoyena et al. 2014). Homozygous nonsense mutations of *SLITRK6* were identified in Amish, Turkish, and Greek cases of familial myopia and SNHL (Tekin et al. 2013) and in nine cases of progressive auditory neuropathy in an endogamous Amish community (Morlet et al. 2014). In mice, *Slitrk6* expression is detected in the thalamus, lateral geniculate nucleus, and developing cochlear organs (Aruga 2003; Aruga and Mikoshiba 2003; Beaubien and Cloutier 2009; Katayama et al. 2009), and *Slitrk6* knock-out mice showed SNHL (Matsumoto et al. 2011). In *Slitrk6* knock-out mice, cell death in the spiral and vestibular ganglia was observed and innervation and survival of inner ear sensory neurons were disturbed (Katayama et al. 2009). *Slitrk6* is thus considered to play critical roles in auditory and vestibular functions, and suppression of its expression in the developing nervous system is expected to cause serious defects in the auditory and nervous systems.

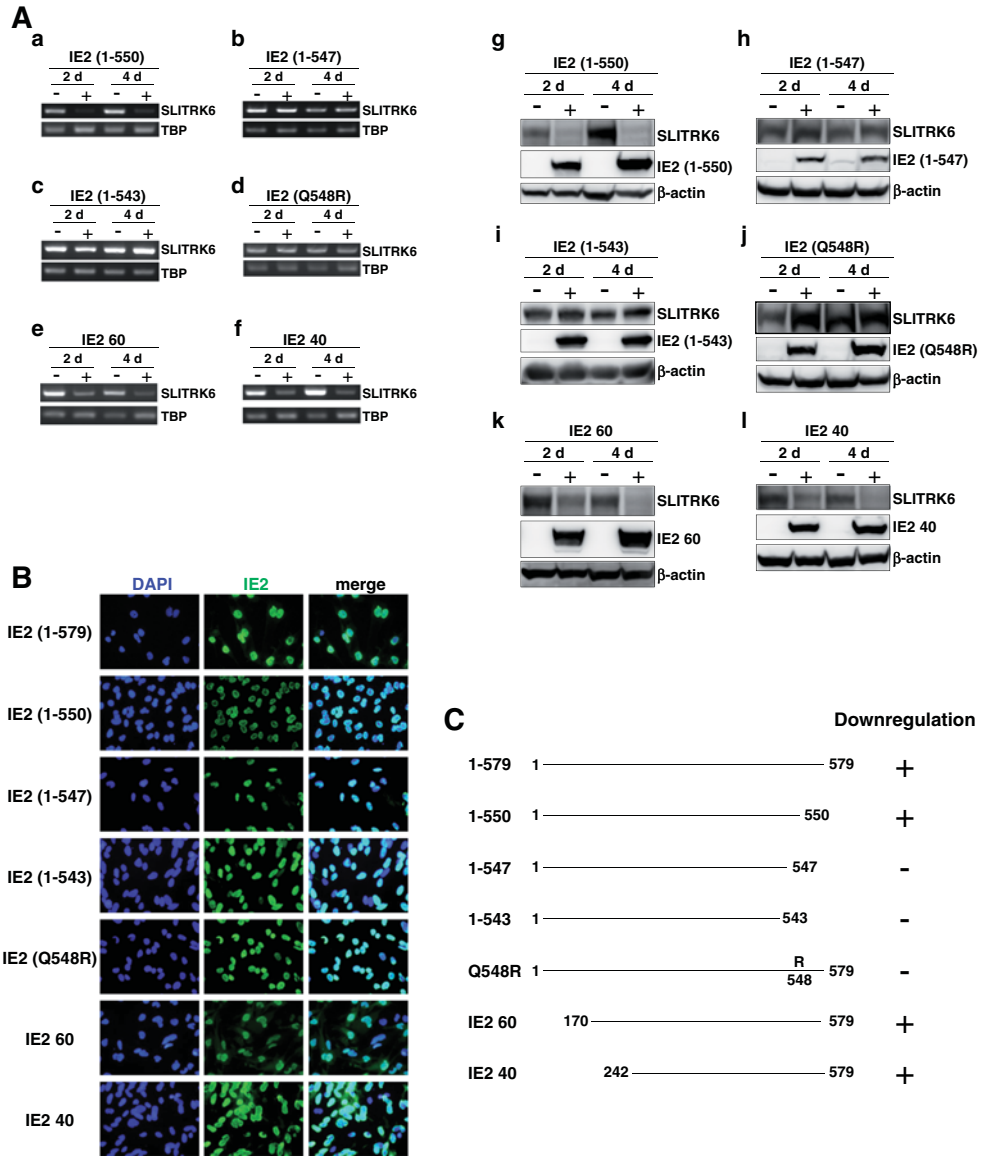

Fig. 4 Carboxy-terminal region of IE2 86 is required for the SLITRK6 downregulation. **A** RT-PCR analysis of the SLITRK6 mRNA expression in Flp-In/TREx U373 MG cells expressing IE2 (1–550) (*a*), IE2 (1–547) (*b*), IE2 (1–543) (*c*), IE2 (Q548R) (*d*), IE2 60 (*e*), and IE2 40 (*f*). Immunoblot analysis of the SLITRK6 protein expression in Flp-In/TREx U373 MG cells expressing IE2 (1–550) (*g*), IE2 (1–547) (*h*), IE2 (1–543) (*i*), IE2 (Q548R) (*j*), IE2 60 (*k*), and IE2 40 (*l*). Individual IE2 mutants were detected anti-IE2 antibody. **B** IE2 deletion mutant proteins induced by Dox in Flp-In/TREx U373 MG cells were detected by immunofluorescence analysis with anti-IE2 antibody. Nuclei were stained by DAPI. **C** Schematic diagram of IE2 86 and its deletion mutants, IE2 60, and IE2 40 and summary of the downregulation of SLITRK6 expression by IE2 86 and its derivatives

The exact mechanism of HCMV neuropathogenesis including SNHL is not known. Although histological studies of patients with congenital HCMV infection have detected viral proteins in various parts of the nervous system, including the inner ear (Davis et al. 1981; Gabrielli et al. 2012, 2013; Stagno et al. 1977; Teissier et al. 2011), the exact nature and outcome of HCMV infection in the neural tissues remain largely unknown. The results obtained in this study imply that the downregulation of *SLITRK6* expression by HCMV-encoded IE2 may have some role in neurological dysfunctions, especially SNHL, induced by congenital HCMV infection. Abortive HCMV infection of neural cells at their critical period of development may result in the expression of a limited number of HCMV genes including *IE2* and eventually induce a serious dysfunction of the auditory system through downregulation of *SLITRK6*. It should be noted that children with homozygous *SLITRK6* mutation, *Slitrk6* knock-out mice, and children with congenital HCMV infection exhibit not only SNHL but also other neurological problems in common, such as vestibular symptoms and behavioral problems, implying that the *SLITRK6* downregulation plays an important role in these conditions. Further investigation into the effect of the HCMV-induced downregulation of *SLITRK6* expression on the development of the nervous system may give a new insight into the neuropathogenesis of congenital HCMV infection.

Acknowledgments We thank M. Iikura for the excellent technical assistance. We also thank N. Inoue for providing the reagents.

This work was partly supported by Grants-in-Aid for Scientific Research from the Ministry of Education, Culture, Sports, Science and Technology of Japan (24591616) to H.N., the Ministry of Health, Labour and Welfare of Japan (H23-Jisedai-Ippan-001) to H.N., and the Grants of National Center for Child Health and Development (24-17 and 27-18 to H.N., 25-9 to S.F.).

Compliance with ethical standards

Conflict of interest The authors declare that they have no conflict of interest.

References

Aruga J (2003) Slitrk6 expression profile in the mouse embryo and its relationship to that of Nlrr3. Gene Expr Patterns 3:727–733

Aruga J, Mikoshiba K (2003) Identification and characterization of Slitrk, a novel neuronal transmembrane protein family controlling neurite outgrowth. Mol Cell Neurosci 24:117–129

Beaubien F, Cloutier JF (2009) Differential expression of Slitrk family members in the mouse nervous system. Dev Dyn 238:3285–3296

Bernard S, Wiener-Vacher S, Van Den Abbeele T, Teissier N (2015) Vestibular disorders in children with congenital cytomegalovirus infection. Pediatrics 136:e887–e895

Cheeran MC, Lokensgard JR, Schleiss MR (2009) Neuropathogenesis of congenital cytomegalovirus infection: disease mechanisms and prospects for intervention. Clin Microbiol Rev 22:99–126 Table of Contents

Davis LE, Johnsson LG, Kornfeld M (1981) Cytomegalovirus labyrinthitis in an infant: morphological, virological, and immunofluorescent studies. J Neuropathol Exp Neurol 40:9–19

Fowler KB, Boppana SB (2006) Congenital cytomegalovirus (CMV) infection and hearing deficit. J Clin Virol 35:226–231

Gabrielli L, Bonasoni MP, Santini D, Piccirilli G, Chiereghin A, Guerra B, Landini MP, Capretti MG, Lanari M, Lazzarotto T (2013) Human fetal inner ear involvement in congenital cytomegalovirus infection. Acta Neuropathol Commun 1:63

Gabrielli L, Bonasoni MP, Santini D, Piccirilli G, Chiereghin A, Petrisli E, Dolcetti R, Guerra B, Piccioli M, Lanari M, Landini MP, Lazzarotto T (2012) Congenital cytomegalovirus infection: patterns of fetal brain damage. Clin Microbiol Infect 18:E419–E427

Iruretagoyena JI, Davis W, Bird C, Olsen J, Radue R, Teo Broman A, Kendziorski C, Splinter BonDurant S, Golos T, Bird I, Shah D (2014) Differential changes in gene expression in human brain during late first trimester and early second trimester of pregnancy. Prenat Diagn 34:431–437

Karltorp E, Lofkvist U, Lewensohn-Fuchs I, Lindstrom K, Westblad ME, Fahnehjelm KT, Verrecchia L, Engman ML (2014) Impaired balance and neurodevelopmental disabilities among children with congenital cytomegalovirus infection. Acta Paediatr 103:1165–1173

Katayama K, Zine A, Ota M, Matsumoto Y, Inoue T, Fritzsch B, Aruga J (2009) Disorganized innervation and neuronal loss in the inner ear of Slitrk6-deficient mice. PLoS One 4:e7786

Koyano S, Inoue N, Oka A, Moriuchi H, Asano K, Ito Y, Yamada H, Yoshikawa T, Suzutani T (2011) Screening for congenital cytomegalovirus infection using newborn urine samples collected on filter paper: feasibility and outcomes from a multicentre study. BMJ Open 1:e000118

Lee SB, Lee CF, Ou DS, Dulal K, Chang LH, Ma CH, Huang CF, Zhu H, Lin YS, Juan LJ (2011) Host-viral effects of chromatin assembly factor 1 interaction with HCMV IE2. Cell Res 21:1230–1247

Matsumoto Y, Katayama K, Okamoto T, Yamada K, Takashima N, Nagao S, Aruga J (2011) Impaired auditory-vestibular functions and behavioral abnormalities of Slitrk6-deficient mice. PLoS One 6:e16497

Mitchell KJ (2011) The genetics of neurodevelopmental disease. Curr Opin Neurobiol 21:197–203

Morlet T, Rabinowitz MR, Looney LR, Riegner T, Greenwood LA, Sherman EA, Achilly N, Zhu A, Yoo E, O'Reilly RC, Jinks RN, Puffenberger EG, Heaps A, Morton H, Strauss KA (2014) A homozygous SLITRK6 nonsense mutation is associated with progressive auditory neuropathy in humans. Laryngoscope 124:E95–103

Morton CC, Nance WE (2006) Newborn hearing screening—a silent revolution. N Engl J Med 354:2151–2164

Nakamura H, Liao H, Minami K, Toyoda M, Akutsu H, Miyagawa Y, Okita H, Kiyokawa N, Umezawa A, Imadome K, Inoue N, Fujiwara S (2013) Human cytomegalovirus induces apoptosis in neural stem/progenitor cells derived from induced pluripotent stem cells by generating mitochondrial dysfunction and endoplasmic reticulum stress. Herpesviridae 4:2

Nakamura H, Lu M, Gwack Y, Souvlis J, Zeichner SL, Jung JU (2003) Global changes in Kaposi's sarcoma-associated virus gene expression patterns following expression of a tetracycline-inducible Rta transactivator. J Virol 77:4205–4220

Ornoy A, Diav-Citrin O (2006) Fetal effects of primary and secondary cytomegalovirus infection in pregnancy. Reprod Toxicol 21:399–409

Petrik DT, Schmitt KP, Stinski MF (2006) Inhibition of cellular DNA synthesis by the human cytomegalovirus IE86 protein is necessary for efficient virus replication. J Virol 80:3872–3883

Plachter B, Britt W, Vornhagen R, Stamminger T, Jahn G (1993) Analysis of proteins encoded by IE regions 1 and 2 of human cytomegalovirus using monoclonal antibodies generated against recombinant antigens. Virology 193:642–652

Puchtler E, Stamminger T (1991) An inducible promoter mediates abundant expression from the immediate-early 2 gene region of human cytomegalovirus at late times after infection. J Virol 65:6301–6306

Stagno S, Reynolds DW, Amos CS, Dahle AJ, McCollister FP, Mohindra I, Ermocilla R, Alford CA (1977) Auditory and visual defects resulting from symptomatic and subclinical congenital cytomegaloviral and toxoplasma infections. Pediatrics 59:669–678

Stenberg RM, Depto AS, Fortney J, Nelson JA (1989) Regulated expression of early and late RNAs and proteins from the human cytomegalovirus immediate-early gene region. J Virol 63:2699–2708

Teissier N, Delezoide AL, Mas AE, Khung-Savatovsky S, Bessieres B, Nardelli J, Vauloup-Fellous C, Picone O, Houhou N, Oury JF, Van Den Abbeele T, Gressens P, Adle-Biassette H (2011) Inner ear lesions in congenital cytomegalovirus infection of human fetuses. Acta Neuropathol 122:763–774

Tekin M, Chioza BA, Matsumoto Y, Diaz-Horta O, Cross HE, Duman D, Kokotas H, Moore-Barton HL, Sakoori K, Ota M, Odaka YS, Foster J 2nd, Cengiz FB, Tokgoz-Yilmaz S, Tekeli O, Grigoriadou M, Petersen MB, Sreekantan-Nair A, Gurtz K, Xia XJ, Pandya A, Patton MA, Young JI, Aruga J, Crosby AH (2013) SLITRK6 mutations cause myopia and deafness in humans and mice. J Clin Invest 123:2094–2102

Original Article

Gynecologic and Obstetric Investigation

Gynecol Obstet Invest
DOI: 10.1159/000441780

Received: November 25, 2014
Accepted after revision: October 15, 2015
Published online: November 26, 2015

Novel Nonsense Mutation in the *NLRP7* Gene Associated with Recurrent Hydatidiform Mole

Yuki Ito[a, c] Kayoko Maehara[a] Eisuke Kaneki[d] Kentaro Matsuoka[b] Naoko Sugahara[a] Tomoko Miyata[a] Hiromi Kamura[a] Yuko Yamaguchi[a] Ayako Kono[a] Kazuhiko Nakabayashi[a] Ohsuke Migita[a] Ken Higashimoto[e] Hidenobu Soejima[e] Aikou Okamoto[c] Hitomi Nakamura[f] Tadashi Kimura[f] Norio Wake[d] Takeshi Taniguchi[g] Kenichiro Hata[a]

[a]Department of Maternal-Fetal Biology, National Research Institute for Child Health and Development, [b]Department of Pathology, National Center for Child Health and Development, and [c]Department of Obstetrics and Gynecology, The Jikei University School of Medicine, Tokyo, [d]Department of Obstetrics and Gynecology, Graduate School of Medical Science, Kyushu University, Fukuoka, [e]Division of Molecular Genetics and Epigenetics, Department of Biomolecular Sciences, Faculty of Medicine, Saga University, Saga, [f]Department of Obstetrics and Gynecology, Osaka University Graduate School of Medicine, and [g]Taniguchi Hospital, Osaka, Japan

Key Words
Recurrent hydatidiform mole · DNA methylation · *NLRP7* · Genomic imprinting

Abstract
Aim: This study aimed to clarify the genetic and epigenetic features of recurrent hydatidiform mole (RHM) in Japanese patients. ***Methods:*** Four Japanese isolated RHM cases were analyzed using whole-exome sequencing. Villi from RHMs were collected by laser microdissection for genotyping and DNA methylation assay of differentially methylated regions (DMRs). Single nucleotide polymorphisms of *PEG3* and *H19* DMRs were used to confirm the parental origin of the variants. ***Results:*** A novel homozygous nonsense mutation in *NLRP7* (c.584G>A; p.W195X) was identified in 1 patient. Genotyping of one of her molar tissue revealed that it was biparental but not androgenetic in origin. Despite the fact that the RHM is biparental, maternally methylated DMRs of *PEG3*, *SNRPN* and *PEG10* showed complete loss of DNA methylation. A paternally methylated DMR of *H19* retained normal methylation. ***Conclusions:*** This is the first Japanese case of RHM with a novel homozygous nonsense *NLRP7* mutation and a specific loss of maternal DNA methylation of DMRs. Notably, the mutation was identified in an isolated case of an ethnic background that has not previously been studied in this context. Our data underscore the involvement of *NLRP7* in RHM pathophysiology and confirm that DNA methylation of specific regions is critical.

Y. Ito and K. Maehara contributed equally to this work.

Kenichiro Hata, MD, PhD
Director, Department of Maternal-Fetal Biology
National Research Institute for Child Health and Development
2-10-1 Setagaya-ku, Tokyo 157-8535 (Japan)
E-Mail hata-k@ncchd.go.jp

Introduction

Complete hydatidiform mole (CHM) is an abnormal pregnancy that typically arises from an androgenote (diploid conception without maternal chromosomes) and predominantly gives rise to the development of only trophoblastic tissues [1, 2]. Recent studies of rare familial cases with recurrent molar pregnancies have shown that mutations of *NLRP7* and *KHDC3L (C6orf221)* are associated with recurrent hydatidiform moles (RHMs) [3, 4]. However, more than 20% of RHM cases have no mutations in these genes [5], and the mechanism underlying the occurrence of molar pregnancy associated with *NLRP7* and *KHDC3L (C6orf221)* mutation remains unknown. To clarify the genetic etiology of RHMs, further comprehensive genetic screening in various ethnic backgrounds is important.

In Japan, the incidence of CHM has become as low as that in western countries. The incidence of CHM per 1,000 live births was 0.49 in 2,000, with a recurrence rate of 1.3% [6, 7]. Nonetheless, a genetic and epigenetic analysis of RHM in Japan has not been performed previously.

CHM conceptions exhibit abnormal genomic imprinting. Although some villi of RHM possess normal biparental alleles, they exhibit loss of maternal DNA methylation of differentially methylated regions (DMRs) within imprinted loci, and thus have aberrant genomic imprinting [8, 9]. Because the histopathological findings of diploid biparental RHM are identical to those of diploid androgenetic CHM, diploid biparental RHM cannot be distinguished from typical CHM without a genetic and epigenetic diagnosis. To clarify the molecular mechanisms of RHM, we performed comprehensive genetic and epigenetic analyses of isolated Japanese RHM cases and in doing so, we identified a novel nonsense *NLRP7* mutation. The RHM tissue contained biparental alleles and showed a loss of maternal DNA methylation of imprinted genes. This evidence strongly supports the role for *NLRP7* in maternal DNA methylation of imprinted genes and the involvement of *NLRP7* in RHM.

Materials and Methods

Study Participants and Samples

Patients with RHM (n = 5) and CHM (n = 9) were included in this study. The profiles of the 5 RHM patients are shown in table 1. Each sample was histopathologically diagnosed as CHM or partial hydatidiform mole and previously genetically diagnosed as an androgenote or a triploid, with the exception of Patients 1, 2, 4 and 5 [10]. All the villi of the 9 CHM conceptions were androgenote. None of the CHM patients had a family history of the condition. Genomic DNA was extracted from peripheral blood cells and molar tissues. This study was approved by the Institutional Review Board Committee at the National Center for Child Health and Development, Tokyo, Japan (approval number 234), and written informed consent was obtained from all patients.

Table 1. Profiles of 5 patients with RHM

Patient ID	Pathological diagnosis	Genetic diagnosis	Familial history
1	5 CHM	This study	No
2	2 CHM	No samples	No
3	PHM, NP, SA, CHM	Triploid[1]	No
4	CHM, PHM	No samples	No
5	SA, PHM, NP, PHM	No samples	No

PHM = Partial hydatidiform mole; NP = normal pregnancy; SA = spontaneous abortion.

[1] Genetic diagnosis of the first molar pregnancy (PHM).

Whole-Exome Sequencing

The whole-exome library was prepared from the peripheral blood cells of 4 RHM patients (Patients 1–4 in table 1) by using Agilent SureSelect Human All Exon V3 capture reagent (Agilent Technologies, Inc., Santa Clara, Calif., USA), and sequenced using the Illumina HiSeq1000 platform. Data analysis procedures are described in the online supplementary materials and methods (for all online suppl. material, see www.karger.com/doi/10.1159/000441780).

NLRP7 Mutation Analysis

The mutations were confirmed by direct sequencing [11]. Ten coding exons and 1 non-coding exon of *NLRP7* were amplified using primers and PCR conditions that were previously described [12].

Genotyping of Molar Tissue

The molar tissue of Patient 1 was genotyped. The villi were selectively laser microdissected using an LMD7000 (Leica Microsystems GmbH, Wetzlar, Germany), and genomic DNA was extracted using the QIAamp DNA FFPE Tissue Kit (Qiagen, Hilden, Germany). The refSNP(rs) numbers of the 8 genotyped loci are shown in online supplementary table S1.

DNA Methylation Assay

The villi of a CHM from a patient with RHM (Patient 1), an androgenetic CHM and normal placenta were examined for *PEG3*, *SNRPN*, *PEG10* and *H19* gene methylation by bisulfite sequencing [13]. Bisulfite conversion was performed using the EpiTect Bisulfite kit (Qiagen, Hilden, Germany) with primers listed in online supplementary table S2.

Results

RHM is most likely caused by genetic factors, and 2 candidate genes have been previously reported [3, 4]. To search for additional mutations in genes that have not

Table 2. SNVs detected by whole-exome sequencing

Chromosome[1]	Position	Gene	Location	SNV	Protein alteration	RefSNP	Allele frequency in HGVB	Patient 1	Patient 2	Patient 3	Patient 4
1	52828383	*CC2D1B*[1]	Exon 3	c.G105A	p.M35I	rs183845075	0.02	G/G	G/G	G/G	A/A
3	10452493	*ATP2B2*[1]	Exon 3	c.C206T	p.P69L	N/A	N/A	T/T	C/C	C/C	C/C
3	16254129	*GALNT15*[1]	Exon 6	c.C1251A	p.H417Q	rs185944497	0.008	A/A	C/C	C/C	C/C
9	140007466	*DPP7*[1]	Exon 7	c.C809T	p.A270V	rs181036640	0.013	T/T	C/C	C/C	C/C
11	69063476	*MYEOV*[1]	Exon 3	c.C559T	p.R187W	rs116926312	0.044	C/C	C/C	C/C	T/T
13	41835028	*MTRF1*[1]	Exon 2	c.T16C	p.C6R	N/A	0.009	T/T	C/C	T/T	T/T
16	30735148	*SRCAP*[1]	Exon 25	c.C4403T	p.S1468L	rs75035256	0.019	T/T	C/T	C/C	C/C
17	27030713	*PROCA1*[1]	Exon 4	c.G874A	p.E292K	rs3744637	0.043	C/C	C/C	C/C	A/A
19	55451603	*NLRP7*	Exon 4	c.G584A	p.W195X	N/A	N/A	A/A	G/G	G/G	G/G
21	38439597	*PIGP*[1]	Exon 4	c.G239A	p.S80N	rs114319840	0.004	A/A	G/G	G/G	G/G

HGVB = Human Genetic Variation Browser; N/A = not available.
[1] Except for *NLRP7*, the 10 SNVs detected have no particular reported/predicted pathogenic features in the reproduction system.

Table 3. Summary of the SNVs found in *ZFP57*, *NLRP7* and *NLRP2* in 4 patients with RHM by whole-exome sequencing

Chromosome	Position	Gene	Location	SNV	Protein	RefSNP	Patient 1	Patient 2	Patient 3	Patient 4
6	29644668	*ZFP57*	Exon 14	c.G113>A	p.R38Q	rs142917604	G/G	G/G	G/A	A/A
19	55441902	*NLRP7*	Exon 9	c.A2775>G	p.A925A	rs269950	G/G	G/G	G/G	A/G
19	55441995	*NLRP7*	Exon 9	c.T2682>C	p.Y894Y	rs269951	G/G	G/G	G/G	A/G
19	55451050	*NLRP7*	Exon 4	c.G1137>A	p.K379K	rs10418277	A/A	G/G	G/G	G/G
19	55451232	*NLRP7*	Exon 4	c.G955>A	p.V319I	rs775882	A/A	G/G	G/G	G/G
19	55451603	*NLRP7*	Exon 4	c.G584>A	p.W195X	N/A	A/A	G/G	G/G	G/G
19	55451797	*NLRP7*	Exon 4	c.G390>A	p.Q130Q	rs775883	A/A	G/G	G/G	G/G
19	55485899	*NLRP2*	Exon 4	c.G312>A	p.K104K	rs2217659	G/G	A/A	G/G	A/A
19	55494881	*NLRP2*	Exon 7	c.C1815>G	p.L605L	rs11672113	G/G	C/C	G/G	C/C
19	55512137	*NLRP2*	Exon 14	c.C3060>A	p.I1020I	rs12768	A/A	C/A	A/A	A/A
19	55512232	*NLRP2*	Exon 14	c.C3155>A	p.A1052E	rs1043673	C/C	C/C	A/A	C/C

N/A = Not available.
[1] A novel homozygous nonsense mutation of *NLRP7* (c.584G>A; p.W195X) was found in Patient 1. Other SNVs are all commonly known SNPs with RefSNP(rs) numbers.

been previously associated with RHM, we performed whole-exome sequencing using peripheral blood cells from 4 RHM patients (Patients 1–4 in table 1). Quality filtering in the patients resulted in a set of 176,663 single nucleotide variations (SNVs) in coding regions. We excluded all non-coding SNVs and SNVs with more than 5% frequency in the 1000 Genomes database (http://www.1000genomes.org/, May 5, 2013) or the Human Genetic Variation Browser (http://www.genome.med.kyoto-u.ac.jp/SnpDB/). The remaining 10 SNVs (table 2) contained no particular potential pathogenic genes involved in the reproduction process except for an *NLRP7* mutation, as described later.

Next, we focused on *NLRP7*, *NLRP2*, *ZFP57* and *KHDC3L (C6orf221)*, which were previously reported as candidate genes for RHM or were associated with DNA methylation defects [3, 4, 14, 15]. Based on the minor allele frequency information of the 1000 Genomes database and other reports [3, 5, 9, 12, 16], the homozygous nonsense mutation of *NLRP7* (c.584G>A; p.W195X) identified in Patient 1 is considered a mutation, which was not previously reported (table 3). Other SNVs found in *ZFP57*, *NLRP7* and *NLRP2* are common variants. Sanger sequencing of genomic DNA from 5 RHM patients (Patients 1–5 in table 1), 9 patients with typical androgenetic CHM and 86 controls confirmed that the *NLRP7* muta-

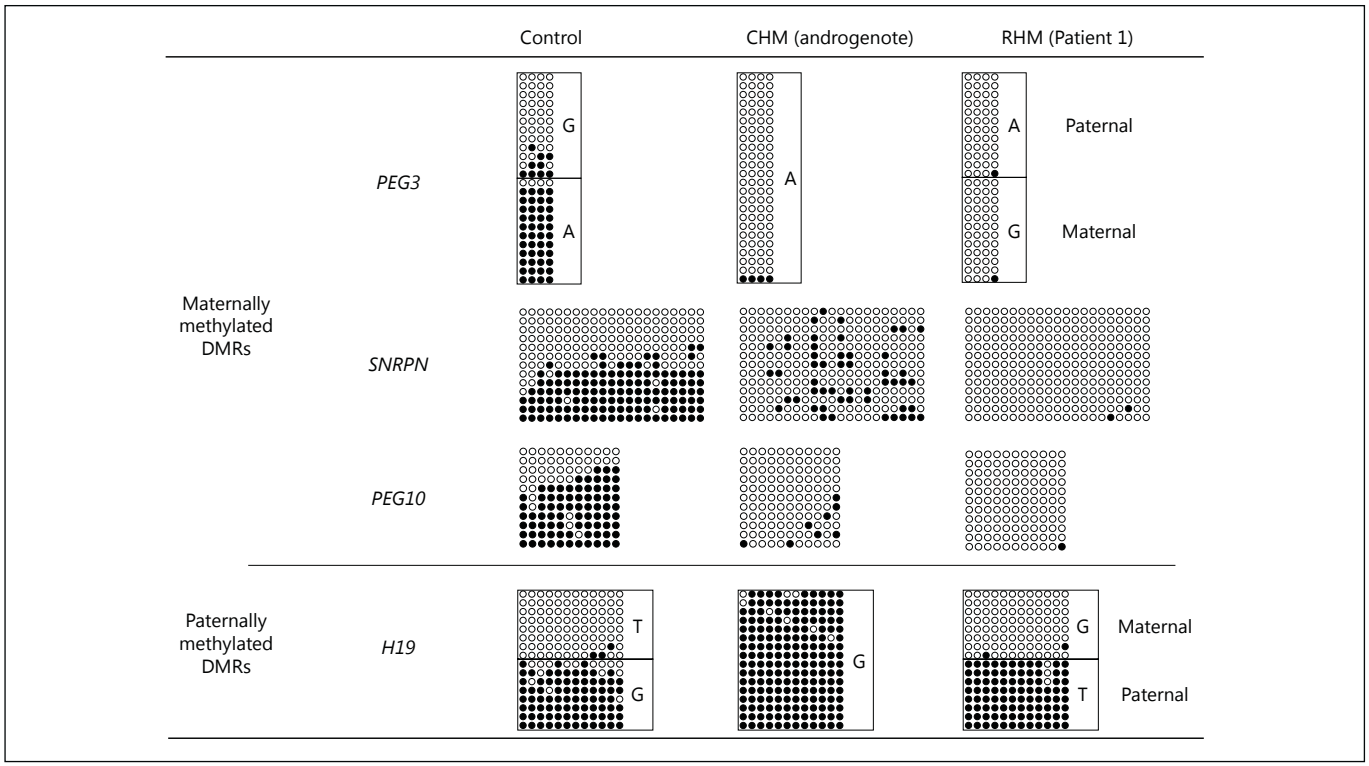

Fig. 1. DNA methylation assay of DMRs. Bisulfite sequencing was performed for 3 maternal DMRs (*PEG3*, *SNRPN* and *PEG10*) and 1 paternal DMR *(H19)*. Each line indicates a single clone, and each circle denotes a CpG; filled and open circles represent methylated and unmethylated cytosine residues, respectively. Allele-specific methylation was definitively diagnosed by SNPs in *PEG3* and *H19* DMRs. All maternally methylated DMRs (*PEG3*, *SNRPN* and *PEG10*) showed loss of DNA methylation in the villi of RHM (Patient 1). In contrast, paternal methylation of the *H19* DMR was maintained normally, even in the villi of RHM. Methylation defects were observed only in maternally methylated DMRs.

tion (c.584G>A; p.W195X) was observed only in 1 RHM (Patient 1; online suppl. table S3, fig. S1).

Previous reports have shown that the origin of a subset of RHM is not androgenic but biparental [12–14]. To precisely confirm the genotype of the villi of RHM Patient 1, the villi were selectively collected by laser microdissection, and a small amount of genomic DNA was obtained. Since the extracted DNA was fragmented and of low quality, analysis of polymorphic DNA markers was inconclusive. We then performed a comprehensive SNP analysis of the biological parents to confirm the origin of the villi of RHM Patient 1. Eight loci in which each parent (Patient 1 and her husband) possesses the opposite major or minor homozygous allele were genotyped, and all showed heterozygous genotypes in the villi (online suppl. table S1). These results clearly show that the villi of RHM Patient 1 contain both parental alleles and thus it is not androgenic, but biparental.

To clarify epigenetic abnormalities in the villi of Patient 1 RHM, DNA methylation analysis of DMRs of imprinted genes was performed using bisulfite sequencing (fig. 1). Three maternally methylated DMRs in *PEG3*, *SNRPN* and *PEG10* and a paternally methylated DMR in *H19* were analyzed. SNPs of *PEG3* and *H19* were used to distinguish between paternal and maternal alleles, enabling specific estimations of allele-specific DNA methylation defects of DMRs. The villi of RHM Patient 1 showed a loss of methylation in all the analyzed maternal DMRs and retained completely normal methylation in the paternal DMR.

Discussion

It is currently not possible to distinguish diploid biparental RHM from typical diploid androgenetic CHM with conventional pathological criteria. In fact, the RHM of Patient 1 and control CHM are histopathologically identical and were both p57KIP2-negative upon immunohistochemical analysis (online suppl. fig. S2). Though striking features of RHM are being revealed with genetic and epi-

genetic analyses [3, 8, 17–19], there is no clear mechanistic understanding as to why certain candidate genes are associated with the condition. Furthermore, no candidate genes have been identified in approximately 20% of all cases [5]. Thus, there is a clear need to explore genetic mutations and epigenetic aberrations in different genetic backgrounds. Additionally, whole-exome sequencing is a potentially promising approach to identifying unknown genetic factors [20]; however, to our knowledge, this is the first report of whole-exome sequencing in RHM patients.

To clarify the features of these Japanese isolated RHM cases, we performed comprehensive genetic and epigenetic analyses. We successfully detected a novel pathogenic homozygous nonsense *NLRP7* mutation (c.584G>A; p.W195X). Since we could not obtain genomic DNA to confirm the mutation in the parents of Patient 1, the parental origin of the mutation is unknown. The approximate 1-Mb region around the *NLRP7* mutation (c.584G>A) shows copy neutral loss of heterozygosity (data not shown). Although the parents of the Patient 1 do not appear to be consanguineous, we speculate that the *NLRP7* region of Patient 1 most likely has alleles identical by descent.

The examination of DNA methylation abnormalities is indispensable for a definitive diagnosis of epigenetic mutations specifically observed in diploid biparental RHMs. In this study, the parental origin of the *PEG3* and *H19* DMRs were definitively confirmed by SNP analysis. The villi of RHM Patient 1 clearly showed complete loss of DNA methylation of maternally methylated DMRs (*PEG3*, *SNRPN* and *PEG10*) but retained methylation of a paternally methylated DMR *(H19)*. Although the villi of the RHM were genetically normal, they showed abnormal DNA methylation and their DNA methylation profile was quite similar to that in a typical androgenetic CHM. This is in contrast to previous studies, in which patterns including hypermethylation of *H19* DMR [21] and retention of methylation at *PEG10* DMR were observed [12]. These differences are likely due to the multifactorial nature in which the DNA methylation machinery is regulated; this would account for the variable methylation changes within DMRs, as we previously reported in our study of *Dnmt3L* knockout mice [22].

RHM patients with *NLRP7* mutations are most likely to have failed in the establishment of methylation of maternal DMRs during oogenesis. The p.W195X mutation in Patient 1 is located upstream of the known nonsense mutations in RHM patients [5]. It is, therefore, expected that RHM from Patient 1 would exhibit the typical phenotype, and indeed this patient had 5 molar pregnancies. Some reported missense mutations could be hypomorphic and show stochastic effects on the methylation of DMRs [9, 12]. If DMR methylation defects are partial, they may cause ordinary abortion or may be sufficiently mild so as to allow normal pregnancy rather than cause molar pregnancy [21]. In fact, patients with *NLRP7* missense mutations have a mixed reproductive history of molar pregnancy and abortion or normal pregnancy [23]. Thus, some unexplained cases of infertility might be attributed to such stochastic epigenetic aberrations.

The NLR family proteins have roles in inflammation and apoptosis [24]. *NLRP7* is involved in the secretion of IL-1β [25–27], but there is no direct evidence that perturbations to the NLRP7-IL-1β axis cause loss of DNA methylation and molar pregnancy. Since *NLRP7* is present in oocytes [16] and preimplantation embryos [28], it could be involved in the hypomethylation of DMRs observed in the villi of RHMs. However, because *NLRP7* has no ortholog in mice [24], evaluation of its function in oogenesis and early embryogenesis is challenging. Therefore, identification of genetic and/or epigenetic mutations in isolated cases and in different genetic backgrounds remains an important aspect of studies designed to unravel the mechanisms underlying RHM pathogenesis.

In conclusion, we have, for the first time, identified a novel nonsense homozygous mutation of *NLRP7* in a Japanese RHM patient. Our study is the first to report an isolated RHM case in a previously unreported ethnic background. This comprehensive genetic and epigenetic analysis approach can facilitate the definitive molecular diagnosis of diploid biparental RHM in isolated cases and can be performed using fragmented DNA extracted from formaldehyde-fixed and paraffin-embedded tissue samples. *NLRP7* mutations cause abnormal DNA methylation in DMRs [21]. However, the mechanisms underlying region-specific DNA methylation remain unknown. Further analysis of RHM will shed light on the unknown etiology of infertility and the mechanisms that control region-specific DNA methylation.

Acknowledgments

This research has been conducted using the National Central Biobank Network (NCBN), Japan.

Funding Sources

This study was supported by a grant from the Ministry of Health, Labor and Welfare, Japan (H26-082, H26-001, H25-001), the CREST Program of the Japan Science and Technology Agency (JST), a grant from the Ministry of Education, Culture, Sports, Sci-

ence and Technology (MEXT), Japan (grant numbers: 26670734, 26293365), and a grant from the National Center for Child Health and Development (NCCHD), Japan (26-13). The study sponsors had no involvement in study design, in the collection, analysis and interpretation of data, in the writing of the report and in the decision to submit the report for publication.

Disclosure Statement

None to declare.

References

1 Kajii T, Ohama K: Androgenetic origin of hydatidiform mole. Nature 1977;268:633–634.
2 Sánchez-Ferrer ML, Hernández-Martínez F, Machado-Linde F, Ferri B, Carbonel P, Nieto-Diaz A: Uterine rupture in twin pregnancy with normal fetus and complete hydatidiform mole. Gynecol Obstet Invest 2014;77:127–133.
3 Murdoch S, Djuric U, Mazhar B, Seoud M, Khan R, Kuick R, Bagga R, Kircheisen R, Ao A, Ratti B, Hanash S, Rouleau GA, Slim R: Mutations in NALP7 cause recurrent hydatidiform moles and reproductive wastage in humans. Nat Genet 2006;38:300–302.
4 Parry DA, Logan CV, Hayward BE, Shires M, Landolsi H, Diggle C, Carr I, Rittore C, Touitou I, Philibert L, Fisher RA, Fallahian M, Huntriss JD, Picton HM, Malik S, Taylor GR, Johnson CA, Bonthron DT, Sheridan EG: Mutations causing familial biparental hydatidiform mole implicate c6orf221 as a possible regulator of genomic imprinting in the human oocyte. Am J Hum Genet 2011;89:451–458.
5 Nguyen NM, Slim R: Genetics and epigenetics of recurrent hydatidiform moles: basic science and genetic counselling. Curr Obstet Gynecol Rep 2014;3:55–64.
6 Matsui H, Iitsuka Y, Suzuka K, Seki K, Sekiya S: Subsequent pregnancy outcome in patients with spontaneous resolution of HCG after evacuation of hydatidiform mole: comparison between complete and partial mole. Hum Reprod 2001;16:1274–1277.
7 Matsui H, Iitsuka Y, Yamazawa K, Tanaka N, Seki K, Sekiya S: Changes in the incidence of molar pregnancies. A population-based study in Chiba prefecture and Japan between 1974 and 2000. Hum Reprod 2003;18:172–175.
8 Judson H, Hayward BE, Sheridan E, Bonthron DT: A global disorder of imprinting in the human female germ line. Nature 2002;416:539–542.
9 Kou YC, Shao L, Peng HH, Rosetta R, del Gaudio D, Wagner AF, Al-Hussaini TK, Van den Veyver IB: A recurrent intragenic genomic duplication, other novel mutations in NLRP7 and imprinting defects in recurrent biparental hydatidiform moles. Mol Hum Reprod 2008;14:33–40.
10 Kaneki E, Kobayashi H, Hirakawa T, Matsuda T, Kato H, Wake N: Incidence of postmolar gestational trophoblastic disease in androgenetic moles and the morphological features associated with low risk postmolar gestational trophoblastic disease. Cancer Sci 2010;101:1717–1721.
11 Li C, Qiao B, Zhan Y, Peng W, Chen ZJ, Sun L, Zhang J, Zhao L, Gao Q: Association between genetic variations in MTNR1A and MTNR1B genes and gestational diabetes mellitus in Han Chinese women. Gynecol Obstet Invest 2013;76:221–227.
12 Hayward BE, De Vos M, Talati N, Abdollahi MR, Taylor GR, Meyer E, Williams D, Maher ER, Setna F, Nazir K, Hussaini S, Jafri H, Rashid Y, Sheridan E, Bonthron DT: Genetic and epigenetic analysis of recurrent hydatidiform mole. Hum Mutat 2009;30:E629–E639.
13 Clark SJ, Harrison J, Paul CL, Frommer M: High sensitivity mapping of methylated cytosines. Nucleic Acids Res 1994;22:2990–2997.
14 Meyer E, Lim D, Pasha S, Tee LJ, Rahman F, Yates JR, Woods CG, Reik W, Maher ER: Germline mutation in NLRP2 (NALP2) in a familial imprinting disorder (Beckwith-Wiedemann Syndrome). PLoS Genet 2009;5:e1000423.
15 Li X, Ito M, Zhou F, Youngson N, Zuo X, Leder P, Ferguson-Smith AC: A maternal-zygotic effect gene, zfp57, maintains both maternal and paternal imprints. Dev Cell 2008;15:547–557.
16 Wang CM, Dixon PH, Decordova S, Hodges MD, Sebire NJ, Ozalp S, Fallahian M, Sensi A, Ashrafi F, Repiska V, Zhao J, Xiang Y, Savage PM, Seckl MJ, Fisher RA: Identification of 13 novel NLRP7 mutations in 20 families with recurrent hydatidiform mole; missense mutations cluster in the leucine-rich region. J Med Genet 2009;46:569–575.
17 Moglabey YB, Kircheisen R, Seoud M, El Mogharbel N, Van den Veyver I, Slim R: Genetic mapping of a maternal locus responsible for familial hydatidiform moles. Hum Mol Genet 1999;8:667–671.
18 Helwani MN, Seoud M, Zahed L, Zaatari G, Khalil A, Slim R: A familial case of recurrent hydatidiform molar pregnancies with biparental genomic contribution. Hum Genet 1999;105:112–115.
19 Fisher RA, Khatoon R, Paradinas FJ, Roberts AP, Newlands ES: Repetitive complete hydatidiform mole can be biparental in origin and either male or female. Hum Reprod 2000;15:594–598.
20 Rabbani B, Tekin M, Mahdieh N: The promise of whole-exome sequencing in medical genetics. J Hum Genet 2014;59:5–15.
21 El-Maarri O, Seoud M, Coullin P, Herbiniaux U, Oldenburg J, Rouleau G, Slim R: Maternal alleles acquiring paternal methylation patterns in biparental complete hydatidiform moles. Hum Mol Genet 2003;12:1405–1413.
22 Henckel A, Nakabayashi K, Sanz LA, Feil R, Hata K, Arnaud P: Histone methylation is mechanistically linked to DNA methylation at imprinting control regions in mammals. Hum Mol Genet 2009;18:3375–3383.
23 Deveault C, Qian JH, Chebaro W, Ao A, Gilbert L, Mehio A, Khan R, Tan SL, Wischmeijer A, Coullin P, Xie X, Slim R: NLRP7 mutations in women with diploid androgenetic and triploid moles: a proposed mechanism for mole formation. Hum Mol Genet 2009;18:888–897.
24 Tian X, Pascal G, Monget P: Evolution and functional divergence of NLRP genes in mammalian reproductive systems. BMC Evol Biol 2009;9:202.
25 Kinoshita T, Wang Y, Hasegawa M, Imamura R, Suda T: PYPAF3, a PYRIN-containing APAF-1-like protein, is a feedback regulator of caspase-1-dependent interleukin-1beta secretion. J Biol Chem 2005;280:21720–21725.
26 Messaed C, Akoury E, Djuric U, Zeng J, Saleh M, Gilbert L, Seoud M, Qureshi S, Slim R: NLRP7, a nucleotide oligomerization domain-like receptor protein, is required for normal cytokine secretion and co-localizes with Golgi and the microtubule-organizing center. J Biol Chem 2011;286:43313–43323.
27 Khare S, Dorfleutner A, Bryan NB, Yun C, Radian AD, de Almeida L, Rojanasakul Y, Stehlik C: An NLRP7-containing inflammasome mediates recognition of microbial lipopeptides in human macrophages. Immunity 2012;36:464–476.
28 Zhang P, Dixon M, Zucchelli M, Hambiliki F, Levkov L, Hovatta O, Kere J: Expression analysis of the NLRP gene family suggests a role in human preimplantation development. PLoS One 2008;3:e2755.

Research article

Journal of Applied Toxicology

Received: 22 January 2015, Revised: 13 February 2015, Accepted: 17 February 2015 Published online in Wiley Online Library: 30 March 2015

(wileyonlinelibrary.com) DOI 10.1002/jat.3149

Augmenting effects of gestational arsenite exposure of C3H mice on the hepatic tumors of the F_2 male offspring via the F_1 male offspring

Keiko Nohara[a]*, Kazuyuki Okamura[a], Takehiro Suzuki[a], Hikari Murai[a], Takaaki Ito[b], Keiko Shinjo[c], Shota Takumi[d], Takehiro Michikawa[a], Yutaka Kondo[c] and Kenichiro Hata[e]

ABSTRACT: Gestational exposure can affect the F_2 generation through exposure of F_1 germline cells. Previous studies reported that arsenite exposure of only F_0 females during their pregnancy increases hepatic tumors in the F_1 males in C3H mice, whose males are predisposed spontaneously to develop hepatic tumors later in life. The present study addressed the effects of gestational arsenite exposure on tumorigenesis of the F_2 males in C3H mice. Expression analysis of several genes in the normal livers at 53 and 80 weeks of age clearly showed significant changes in the F_2 males obtained by crossing gestational arsenite-exposed F_1 (arsenite-F_1) males and females compared to the control F_2 males. Some of the changes were shown to occur in a late-onset manner. Then the tumor incidence was assessed at 75–82 weeks of age in the F_2 males obtained by reciprocal crossing between the control and arsenite-F_1 males and females. The results demonstrated that the F_2 males born to arsenite-F_1 males developed tumors at a significantly higher rate than the F_2 males born to the control F_1 males, irrespective of exposure of F_1 females. Gene expressions of hepatocellular carcinoma markers β-catenin (CTNNB1) and interleukin-1 receptor antagonist in the tumors were significantly upregulated in the F_2 males born to arsenite-F_1 males compared to those born to the control F_1 males. These results show that arsenite exposure of only F_0 pregnant mice causes late-onset changes and augments tumors in the livers of the F_2 males by affecting the F_1 male offspring. Copyright © 2015 John Wiley & Sons, Ltd.

Keywords: arsenic; gestational exposure; hepatic tumor; transgenerational; gene expression

Introduction

Gestation is known to be vulnerable to a variety of environmental conditions, including chemical exposure and nutritional imbalances, and the adverse effects of environmental conditions in this period can lead to a number of adult-onset diseases in the F_1 offspring and in subsequent multiple generations (Aiken and Ozanne, 2014; Guerrero-Bosagna and Skinner, 2012; Perera and Herbstman, 2011). A possible causative route of the effects on the F_2 and subsequent generations by gestational chemical exposure is through direct exposure of germline cells in the F_1 fetuses and the responsible germ cells can be those of male, female, or both (Aiken and Ozanne, 2014; Guerrero-Bosagna and Skinner, 2012; Perera and Herbstman, 2011).

Naturally occurring inorganic arsenic, which is known as a human carcinogen, is causing serious health problems, including cancer, in many areas in the world (Hughes *et al*., 2011). Although animal models are pivotal to elucidate the mechanism of arsenic toxicity, it has been difficult to verify the carcinogenicity of arsenic in rodents (Rossman *et al*., 2002). Pioneering studies by Waalkes and colleagues showed that exposure of pregnant C3H mice (F_0) from gestational day (GD) 8–18 to inorganic arsenite results in an increase in tumors in the liver and adrenal gland of their F_1 male offspring at 74 weeks of age (Waalkes *et al*., 2003). As male C3H mice are predisposed to spontaneously develop hepatic tumors in adulthood (Köhle *et al*., 2008; Maronpot *et al*., 1995), the finding by Waalkes and colleagues supports the notion that arsenic acts in combination with other tumor promoting factors or dispositions (Klein *et al*., 2007). The results obtained by Waalkes *et al*. (2003) also indicate that gestation is a vulnerable period for arsenic carcinogenicity. Epidemiological studies have reported that gestational exposure to arsenite is associated with increased cancers in adulthood (Smith *et al*., 2006; Yuan *et al*., 2010). These findings on the sensitivity of gestational period against arsenic imply the possibility that gestational arsenic exposure may also affect F_1 germline cells and have an impact on late-onset tumorigenesis in the F_2 and subsequent generations, while those issues have not been addressed.

*Correspondence to: Keiko Nohara, Center for Environmental Health Sciences, National Institute for Environmental Studies, Tsukuba 305-8506, Japan.
E-mail: keikon@nies.go.jp

[a]Center for Environmental Health Sciences, National Institute for Environmental Studies, Tsukuba, Japan

[b]Department of Pathology and Experimental Medicine, Kumamoto University Graduate School of Medical Sciences, Kumamoto, Japan

[c]Department of Epigenomics, Nagoya City University Graduate School of Medical Sciences, Nagoya, Japan

[d]Department of Public Health and Environmental Medicine, The Jikei University School of Medicine, Tokyo, Japan

[e]Department of Maternal-Fetal Biology, National Research Institute for Child Health and Development, Tokyo, Japan

We previously investigated the causal factors of hepatic tumor augmentation in the F_1 male offspring by gestational arsenite exposure in the experimental model reported by Waalkes *et al.* (2003) Nohara *et al.*, 2012). The results showed several characteristic changes, such as late-onset gene expression changes in the normal livers and an increase in hepatic tumors, particularly those having a C to A somatic mutation at codon 61 in oncogene Ha-*ras*, in the F_1 offspring by gestational arsenite exposure (Nohara *et al.*, 2012). In the present study, we addressed the effects of gestational arsenite exposure on the F_2 males of C3H mice by investigating gene expression changes in the normal livers, the hepatic tumor incidence, and the incidence of Ha-*ras* mutation at codon 61 in the tumors. In the assessment of tumor incidence, we performed a reciprocal crossing experiment between the control and arsenite-F_1 males and females to clarify the F_1 sex responsible for the tumor augmentation in the F_2 males. We also measured gene expression of several human hepatocellular carcinoma markers in the tumors of the F_2 males for confirmation of the tumor augmenting effects of gestational arsenite exposure.

The results of the present study made the novel findings on the tumor augmenting effects of gestational arsenite exposure on the F_2 generation.

Materials and methods

Design of Animal Experiments

Pregnant C3H/HeN mice (F_0) were purchased from CLEA Japan (Tokyo, Japan) and given free access to a standard diet (CA-1; CLEA Japan) and tap water (control mice) or tap water containing 85 ppm sodium arsenite (Sigma, St. Louis, MO, USA) from day 8 to 18 of gestation as described previously (Nohara *et al.*, 2012). Throughout the experiments, arsenite was only given to F_0 pregnant mice and not to F_1 or F_2 mice. To assess the tumor incidence and the F_1 sex responsible for the F_2 tumor augmentation, we did a reciprocal crossing experiment among the control F_1 males and females and arsenite-F_1 males and females, which originated from 22 control F_0 females and 29 arsenite-F_0 females. Male and female mice were mated at 10 weeks of age. The resulting F_2 males were reared until 75–82 weeks (17.5–19 months) of age and used for the assessment. Hepatic tumors were examined macroscopically (Nohara *et al.*, 2012) and some were subjected to histological analysis as described below.

The animals were handled in accordance with the National Institute for Environmental Studies guidelines for animal experiments.

Histological Analysis

Sections prepared from paraffin-embedded liver tissues were stained with hematoxylin and eosin as previously described (Nohara *et al.*, 2012). The histology of the liver neoplasms was classified as hepatocellular adenoma or hepatocellular carcinoma. Briefly, hepatocellular adenoma is characterized by a well-circumscribed lesion composed of well-differentiated hepatocytes, and hepatocellular carcinoma is characterized by an abnormal growth pattern and both cytological and nuclear atypia (Harada *et al.*, 1999).

cDNA Preparation and Real-Time Polymerase Chain Reaction

Total RNA of individual livers was prepared with an RNeasy Mini Kit (Qiagen, Valencia, CA, USA). After checking the quality of the RNA by electrophoresis, reverse transcription reactions were performed with an AMV Reverse Transcriptase XL (TaKaRa Bio, Shiga, Japan) using 100 ng of total RNA. Quantitative real-time polymerase chain reaction (PCR) analysis was performed on a LightCycler 480 instrument, version 1.5 (Roche Diagnostics, Basel, Switzerland) as described previously (Nohara *et al.*, 2006). The primer sequences and annealing temperatures used for real-time PCR are shown in Table 1.

Ha-*ras* Mutation

Ha-*ras* mutations at codon 61 were analyzed by the pyrosequencing method (Ogino *et al.*, 2005). The DNA region containing the sequence coding codon 61 in the Ha-*ras* gene was amplified by PCR using the biotinylated primers (5′-cggaaacaggtggtcattgat-3′ and biotin-5′-tgatggcaaatacacagaggaag-3′) and a PyroMark PCR kit (Qiagen). Amplification was achieved by heating at 95 °C for 5 min, cycling at 95 °C for 30 s, 55 °C for 30 s and 72 °C for 45 s, and was followed by extension at 72 °C for 10 min after the final cycle. The biotinylated PCR product was captured on streptavidin-coated beads (GE Healthcare Bio-Science, Little Chalfont, UK), denatured and washed. The sequence primer for codon 61 (5′-ggacatcttagacacagca-3′) was annealed to the biotinylated PCR product and pyrosequencing analysis was performed by using a

Table 1. Primers for real-time polymerase chain reaction analysis

Gene	Forward primer 5′-3′	Reverse primer 5′-3′	Annealing temp. (°C)
Creld2	gcagacagcagaaggcaaa	tgcccgtcacaaatcctc	60
Slc25a30	gaacgcccagaagatgaaac	ctgttctgtgcttgcattcg	60
Ell3	ccagaaacgcctggacaa	cttgaggctagaggcagagc	64
Fabp4	cagcctttctcacctggaag	ttgtggcaaagcccactc	60
Gpat-1	agcaagtcctgcgctatcat	ctcgtgtgggtgattgtgac	64
Afp	cccaaccttcctgtctcagt	tggctctcctcgatgtgttt	64
Il-1rn	tgcacaacactagaggctga	agtgatcaggcagttggtga	64
Ctnnb1	ccctgagacgctagatgagg	tgtcagctcaggaattgcac	64
Cpb	agactgttccaaaaacagtgga	gatgctctttcctcctgtgc	64
rRNA	tgcgaatggctcattaaatcagtt	ccgtcggcatgtattagctctag	64

Journal of Applied Toxicology

PyroMark Q96 ID system (Qiagen) and PyroMark Q96 ID Software 2.5 (Qiagen) according to the manufacturer's instructions.

Western Blotting

Tissues were homogenized in ice-cold lysis buffer (1% Triton X-100, 0.1% sodium dodecyl sulfate [SDS], 0.5% deoxycholic acid, 1 mM EDTA, 1 mM EGTA, 2.5 mM sodium pyrophosphate, 1 mM β-glycerophosphate, 1 mM sodium orthovanadate, 1 mM phenylmethylsulfonyl fluoride, 50 mM Tris–HCl [pH 7.5] and 150 mM NaCl) with a pellet mixer and then with a Bioruptor UCD-200TM (Cosmo Bio, Tokyo, Japan). The supernatant was boiled with the same volume of × 2 SDS sample buffer (100 mM Tris–HCl [pH 6.8], 4% SDS, 20% glycerol, 200 mM DTT, 0.002% bromophenol blue), and subjected to SDS-polyacrylamide gel electrophoresis. The first antibodies used were anti-p44/42 MAPK (Cell Signaling Technology, Danvers, MA, USA; 9102), anti-phospho-p44/42 MAPK (Cell Signaling Technology; 9101) and anti-β-actin (Sigma; A5441). The second antibodies were horseradish peroxidase-conjugated anti-rabbit IgG (Sigma) and antimouse IgG (Sigma). The membranes were developed using the ECL Prime Western Blotting Detection System (GE Healthcare) and the images were captured using a VersaDoc imaging system (Bio Rad, Hercules, CA, USA).

Statistical Analysis

The difference in the tumor incidence between the two groups was analyzed by a chi-squared test. The difference in gene expression between the two groups was analyzed by Student's *t*-test. Those analyses were conducted with Stata11 (Stata Corporation, College Station, TX, USA).

Results

Late-Onset Gene Expression Changes Detected in the Normal Liver of the F_2 Generation

Analyses of mouse livers with Affymetrix GeneChips in our previous study showed that expression of two genes, *Creld2* and *Slc25a30*, was upregulated more than twofold and expression of another two genes, *Fabp4* and *Ell3*, was downregulated more than twofold in the normal livers of arsenite-F_1 males in comparison with those of the control males at 74 weeks of age (Nohara *et al.*, 2012). The expression changes of these genes were found to occur in an adult-onset manner (Nohara *et al.*, 2012). To examine whether arsenite exposure of F_0 pregnant mice has any effect on the F_2 offspring, we measured the expression of these four genes in the normal livers of the control F_2 males and the F_2 males obtained by crossing arsenite-F_1 males and females (arsenite-F_2) at 53 weeks and 80 weeks of age.

The results of the measurements showed significant downregulation of *Creld2* from 53 weeks of age and late-onset downregulation of *Slc25a30* at 80 weeks of age in arsenite-F_2 males in comparison with the control F_2 males. On the other hand, those genes were upregulated in arsenite-F_1 males in comparison with the control F_1 males at 49 and/or 74 weeks of age. Thus, direction of the changes by gestational arsenite exposure in the arsenite-F_1 and arsenite-F_2 males was the opposite (Fig. 1). Expression of *Ell3* was significantly upregulated in arsenite-F_2 males in comparison

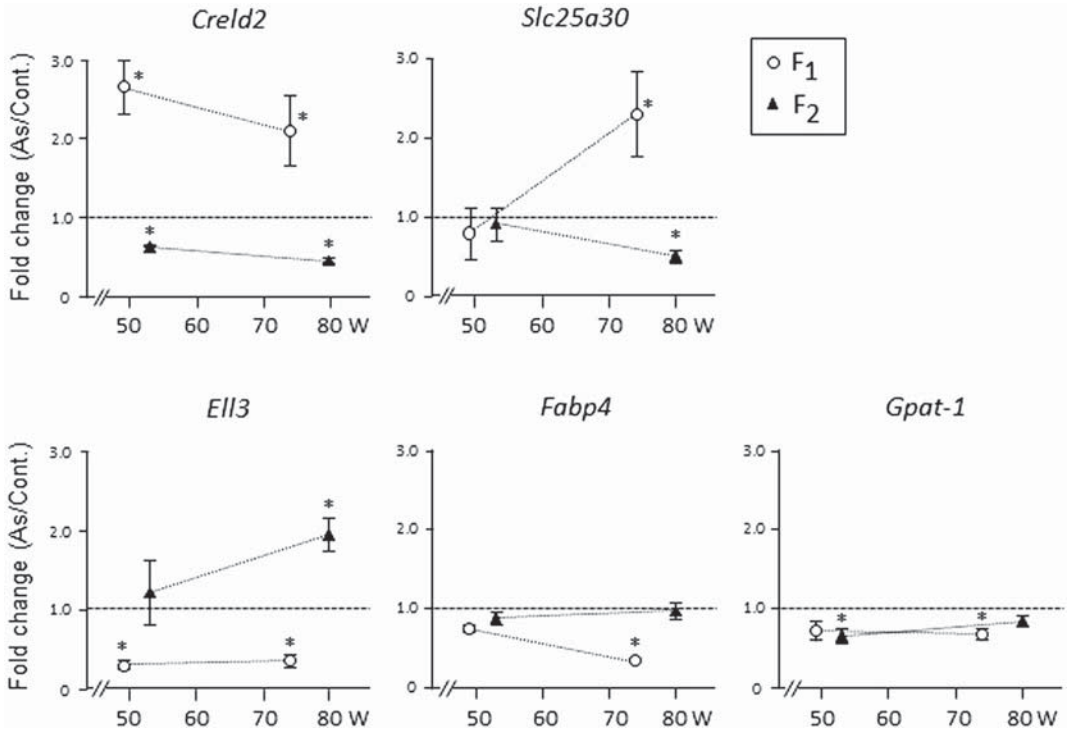

Figure 1. The changes in hepatic gene expression in the arsenite-F_1 males and arsenite-F_2 males in comparison with their control males. The expressions of five genes in the livers of the control F_2 males and arsenite-F_2 males were measured by real-time polymerase chain reaction at 53 weeks of age ($n = 4$ in each group) and 80 weeks of age ($n = 6$ in each group) and normalized to expression of *Cpb*. For the gene expressions in the F_1 generation, data obtained at 49 weeks of age ($n = 4$ in each group) and 74 weeks of age ($n = 8$ in each group) in our previous study (Nohara *et al.*, 2012) were used. The graphs show the ratios of the expression in the arsenite-exposed group normalized to the expression in the control group. The error bar shows the standard error. *Significant difference ($P < 0.05$) between the offspring of the control females and the offspring of the arsenite-exposed females.

with the control F_2 males also in a late-onset manner. The effect of gestational arsenite exposure on *Ell3* expression in the F_2 males was again the opposite of its effect in the F_1 males. Downregulation of *Fabp4*, which was detected in the arsenite-F_1 males, was not detected in the F_2 generation (Fig. 1).

In our previous study, we also observed downregulation of a lipid metabolism-related gene *Gpat-1* at 74 weeks of age in the normal livers of arsenite-F_1 males in comparison with the control males (Nohara *et al.*, 2012). This gene was downregulated in arsenite-F_2 males in comparison with the control F_2 males at 53 weeks of age (Fig. 1).

These changes in gene expression clearly showed significant effects of gestational arsenite exposure on the F_2 males, and the effects on the F_1 and the F_2 were varied.

Increased Hepatic Tumors in the F_2 Males Born to the Arsenite-F_1 Males

We performed the reciprocal crossing experiment with the control and arsenite-F_1 males and females as shown in Fig. 2 to assess the effects of gestational arsenite exposure on tumorigenesis in the F_2 males and determine the F_1 sex responsible for the F_2 tumor augmentation.

The tumor incidences in each F_2 group were 33.8% in CC, 34.3% in CA, 49.2% in AC and 43.6% in AA (Fig. 2A). Comparison of the tumor incidence between the F_2 male offspring of arsenite-F_1 males (AC and AA) and the control F_1 males (CC and CA) showed a significantly higher tumor incidence in the F_2 offspring of arsenite-F_1 males (45.9% in AC and AA vs 34.1% in CC and CA) (Fig. 2B). On the other hand, the tumor incidence of the F_2 male offspring of arsenite-F_1 females (39.9% in CA and AA) and the control F_1 females (41.1% in CC and AC) were not different (Fig. 2B). These results showed that the tumor-augmenting effect of gestational arsenite exposure is transmitted to the F_2 males via the F_1 male offspring, but not via the F_1 female offspring.

Pathological examination of tumor tissues from the control F_2 and arsenite-F_2 males (10 samples from each group) showed that hepatocellular adenoma was the predominant histological tumor type (Fig. 3). This finding was consistent with the observation of the hepatic tumors of the control mice and arsenite-F_1 mice in our previous study (Nohara *et al.*, 2012).

Ha-*ras* Mutation in the Tumors of the F_2 Generation

Our previous study showed that gestational arsenite exposure particularly increased the percentage of hepatic tumors containing

A)

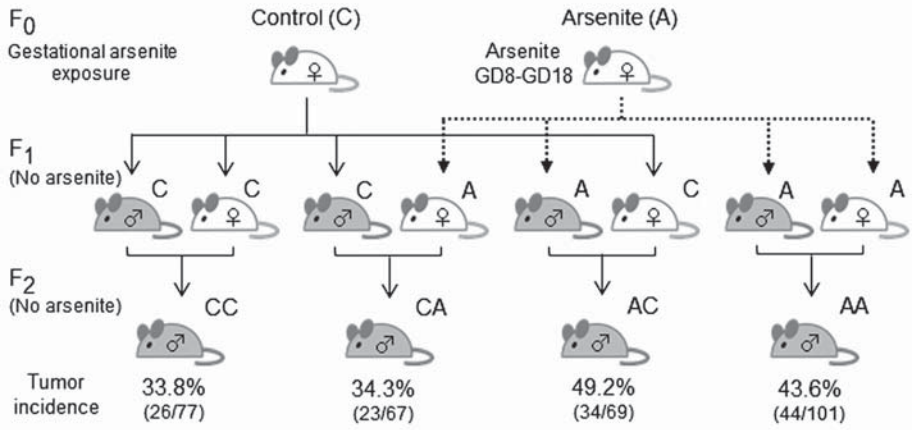

B)

Comparison to assess the F_1 sex responsible for the F_2 tumor augmentation

	Tumor incidence		p value
F_2 group	Offspring of control F_1 male (CC, CA)	Offspring of arsenite-F_1 male (AC, AA)	
	34.1% (49/144)	45.9% (78/170)	0.033
F_2 group	Offspring of control F_1 female (CC, AC)	Offspring of arsenite-F_1 female (CA, AA)	
	41.1% (60/146)	39.9% (67/168)	0.827

Figure 2. Increase in the tumor incidence in the F_2 male offspring born to arsenite-F_1 males but not to arsenite-F_1 females. (A) The F_2 males were obtained by reciprocally crossing the control and arsenite-F_1 males and females as shown in the figure. The F_2 mice were macroscopically examined for hepatic tumors at 75–82 weeks of age I n an age-matched manner. Small lesions (≤1 mm in diameter) were omitted. The number in parenthesis is that of mice bearing hepatic tumors/the number of mice investigated. (B) The difference between the tumor incidences in the two groups was analyzed by chi-squared test. GD, gestational day.

Journal of Applied Toxicology

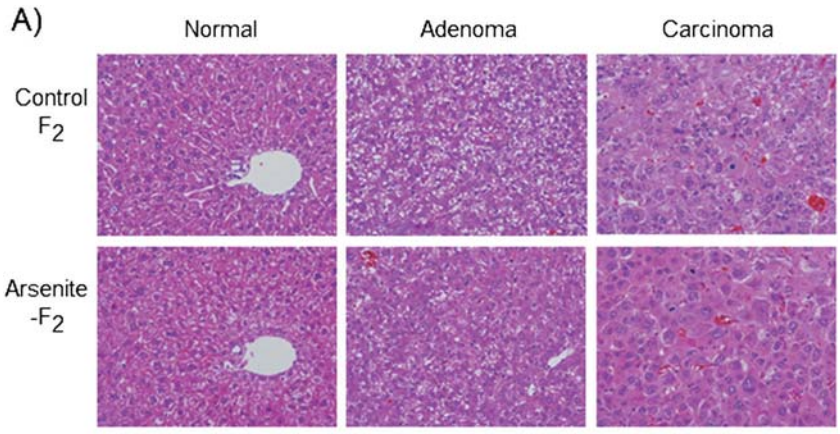

B)

Occurrence of hepatocellular adenoma and hepatocellular carcinoma

	Number of tumors	
	Adenoma	Carcinoma
Control F_2 (n=10)	8	2
Arsenite-F_2 (n=10)	7	3

Figure 3. Histological analysis of the hepatic tumors of the control and arsenite-F_2 males. (A) Representative sections of hepatocellular adenoma and hepatocellular carcinoma of the control F_2 males and arsenite-F_2 males. (B) Occurrence of hepatocellular adenoma and hepatocellular carcinoma.

the Ha-*ras* C61A somatic mutation in the F_1 males (Nohara *et al.*, 2012). Ha-*ras* mutation is thought to be involved in carcinogenesis by activating several signaling pathways, including the RAF/MEK/ERK cascade (Pylayeva-Gupta *et al.*, 2011). The investigation in the present study confirmed that the Ha-*ras* mutations increase the activating phosphorylated forms of ERKs, ERK1 (p44 MAPK) and ERK2 (p42 MAPK) in the tumor tissues harboring codon 61 Ha-*ras* mutations in both the control F_2 males and arsenite-F_2 males (Fig. 4A). p44/p42 MAPK was shown to be hypophosphorylated in the non-tumor tissues of tumor-bearing livers, which do not contain mutated Ha-*ras* (Fig. 4B).

On the other hand, Ha-*ras* C61A mutation or the total Ha-*ras* mutations in codon 61 in the tumor tissues was shown not to be increased in the F_2 males born to arsenite-F_1 males (AC and AA) in comparison with the F_2 males born to the control males (CC and CA) (Table 2). Thus, the existence of Ha-*ras* mutations seems not to be the major causation of the increased hepatic tumor incidence in the F_2 males born to arsenite-F_1 males.

Upregulation of Cancer Related Genes in the Tumor Tissues of F_2 Males Born to the Arsenite-F_1 Males

In an effort to establish early diagnostic markers for detecting human hepatocellular carcinoma, increases in several serum proteins, including α-fetoprotein, β-catenin (CTNNB1) and interleukin-1 receptor antagonist (IL1-RN), were shown to be closely associated with hepatocellular carcinoma (Sun *et al.*, 2008). The expression of those genes was shown to be higher in the tumor tissues compared to the normal tissues or the non-tumor tissues of tumor-bearing livers, while the expression of *Afp* is varied widely among samples (Fig. 5). The expressions of *Ctnnb1* and *Il1rn* genes were significantly higher in the F_2 males born to arsenite-F_1 males (AC and AA) than those born to the control males (CC and CA) (Fig. 5).

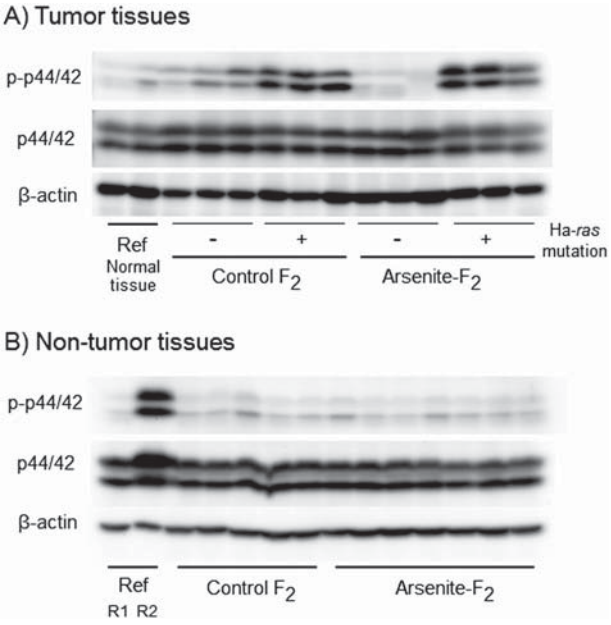

Figure 4. p44/42 MAP kinases activation as a result of Ha-*ras* mutation in the hepatic tumors of C3H males. Western blots of hepatic tumor tissues (A) and non-tumor tissues in the tumor-bearing livers (B) of the control F_2 and arsenite-F_2 males were prepared as described in the Materials and methods section. Labels in (B) are R1, normal tissue and R2, tumor tissue with a Ha-*ras* mutation.

Interestingly, when the gene expression was assessed separately in tumor tissues with and without Ha-*ras* mutation, the expression of *Il-1rn* seemed to be upregulated by Ha-*ras* mutation (Fig. 5).

Table 2. Spectra of Ha-*ras* codon 61 mutations in the hepatic tumors of the F_2 males

F_2 group (*n*)		Ha-*ras* codon 61 type (%)			
		CAA wild-type	AAA	CTA	CGA
CC	(29)	31	41	7	7
CA	(33)	61	18	3	3
AC	(34)	38	35	3	3
AA	(49)	39	45	6	6

The hepatic tumor tissues were obtained in the reciprocal crossing experiment (Fig. 2) and analyzed for mutations in Ha-*ras* codon 61 by a pyrosequencing method.

Discussion

The earliest studies carried out primarily in the middle 1900s reported that maternal exposure or germ cell exposure to radiation and some carcinogenic chemicals transgenerationally affect the susceptibility of the progeny to cancer (Tomatis, 1994). The transgenerational effects of radiation, chemicals and nutritional imbalances on cancers and other disorders have been reported to be transmitted paternally, maternally, or both paternally and maternally (Aiken and Ozanne, 2014; Anway *et al.*, 2005; Barber *et al.*, 2002; Mohamed *et al.*, 2010; Tomatis, 1994). The individual molecular mechanisms of the transmission are yet to be clarified.

The present study showed that gestational arsenite exposure of pregnant C3H mice from GD8 to GD18 increases the incidence of hepatic tumors in the F_2 males born to arsenite-F_1 males (AC and AA in Fig. 2) compared to the F_2 males born to the control males (CC and CA in Fig. 2), irrespective of exposure of the F_1 females. These results showed that tumor augmenting effects by gestational arsenite exposure is transmitted to the F_2 males through the F_1 males. We also detected significant late-onset changes in gene expression in the normal livers of arsenite-F_2 (AA F_2) males compared to those of the control F_2 males (Fig. 1), indicating that transient gestational arsenite exposure of pregnant females causes a significant impact on the F_2 generation. Furthermore, the cancer-related genes *Ctnnb1* and *Il1rn* were shown to be upregulated in the hepatic tumors of the F_2 males born to arsenite-F_1 males (AC and AA) compared to those born to the control males (CC and CA) (Fig. 5). These results show the augmenting effects of gestational arsenite exposure on the hepatic tumors of the F_2 male offspring.

The F_1 male fetuses in the present study were exposed from GD8 to GD18, when the primordial germ cells appear and differentiate into the sperm precursor cells (Sasaki and Matsui, 2008). The epigenetic profile of the primordial germ cells undergoes dynamic alterations, including imprint erasure, during the development stage, and disruption of the epigenetic profile during this stage has been implicated in transgenerational effects of F_0 gestational exposure (Aiken and Ozanne, 2014; Guerrero-Bosagna and Skinner, 2012; Perera and Herbstman, 2011). A previous study (Devesa *et al.*, 2006) reported the concentrations of inorganic arsenic and methylated arsenic at GD18 in the fetus organs, including

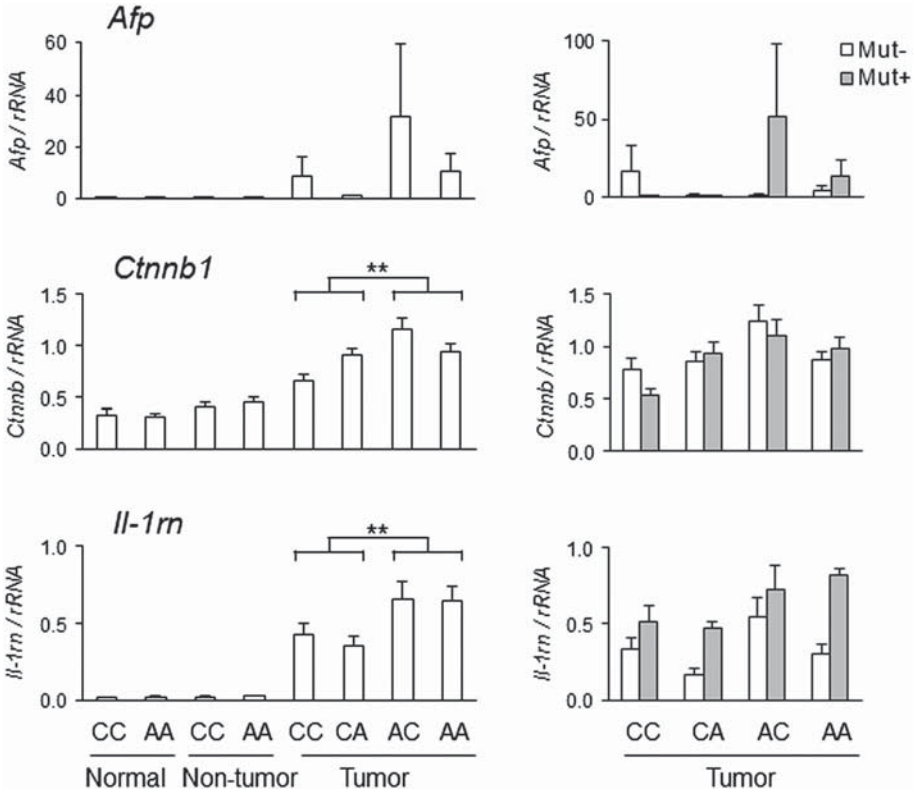

Figure 5. Expression of cancer-related genes in the hepatic tissues in the F_2 mice. The expressions of *Afp*, *Ctnnb* and *Il-1rn* were measured by real-time PCR for the normal livers ($n = 6$), non-tumor tissues from tumor-bearing livers ($n = 6$) and tumor tissues ($n = 9$–11) from the F_2 males and normalized to the expression of rRNA. The difference in the gene expressions in the tumor tissues between the F_2 males born to the control F_1 males (CC and CA) and those born to arsenite-F_1 males (CA and AA) was analyzed by Student's *t*-test. $^{**}P < 0.01$.

the liver and blood in the same gestational arsenite exposure model of C3H mice we used. The study showed that fetus organs are directly exposed upon gestational arsenite exposure. As arsenic has been reported to induce epigenetic changes, particularly DNA methylation changes (Reichard and Puga, 2010; Ren *et al*., 2011; Suzuki *et al*., 2013), the gestational arsenite exposure may alter the phenotype of the F_2 generation by affecting the epigenetic profile of genes, possibly including imprinted genes, in the F_1 male germ cells.

Arsenic has been thought to be a weak mutagen or not a mutagen based on the results of assays using bacteria and mammalian cells *in vitro* (reviewed by Rossman, 2003). Our recent study using *gpt* delta transgenic mice clarified that arsenite exposure greatly increases the incidence of G:C to T:A transversion *in vivo* (Takumi *et al*., 2014). Thus, mutation in the proliferating and differentiating primordial germ cells might be another possible causation of the F_2 effect by arsenite exposure of F_0 pregnant mice.

In the present study, we found that gestational arsenite exposure significantly affects hepatic expression of *Creld2*, *Slc25a30* and *Ell3* even in the F_2 generation, but the effect of the exposure was the opposite of its effect on the F_1 generation (Fig. 1). The difference seems to be attributable to the fact that exposure of the F_1 and F_2 mice occurred in a different manner, e.g., the fetal liver is directly exposed in the F_1 and F_2 is exposed at the germ cell stage. On the other hand, *Gpat-1* was significantly downregulated in the liver of the F_2 generation, as was also observed in the F_1 generation (Nohara *et al*., 2012) (Fig. 1). *Gpat-1* is one of the target genes of sterol regulatory element-binding protein 1, a member of the central transcription factors that control intracellular cholesterol and fatty acid levels (Raghow *et al*., 2008; Wendel *et al*., 2010). Lipid accumulation in the liver has been implicated in hepatic carcinogenesis through an increase in oxidative stress (Ziech *et al*., 2011). The change in *Gpat-1* expression in the liver of the F_1 and F_2 mice may indicate involvement of lipid metabolism changes in the increase in hepatic tumors.

We previously found a higher proportion of C61A Ha-*ras* mutation in the hepatic tumors of arsenite-F_1 males (Nohara *et al*., 2012). In the present study, we confirmed that Ha-*ras* mutation increases activated forms of ERKs in the hepatic tumors of C3H mice (Fig. 4). However, the percentage of Ha-*ras* mutation in the tumors was not increased in the F_2 males born to arsenite-F_1 males (Table 2), which indicated that the tumor increase in the exposed F_2 males could not be attributed to the increase in Ha-*ras* codon 61 mutation 1.

In summary, we demonstrated the novel finding that gestational arsenite exposure of F_0 pregnant mice increases hepatic tumor incidence in the F_2 male offspring through the impact on the F_1 males. Further studies will be required to identify the factors that cause tumor augmentation in the liver of the F_2 generation by arsenite exposure of F_0 pregnant mice and to explore changes in the F_1 male germ cells that induce such tumor-augmenting factors in the liver of the F_2 generation.

Acknowledgments

We wish to thank Dr. A. Furuyama, Dr. Y. Aoki, Dr. H. Nitta (National Institute for Environmental Studies) and Dr. Kayo Ueda (Kyoto University) for their useful discussions, M. Owada and F. Ishitsuka for their excellent technical assistance and S. Itaki, Y. Yamazaki and S. Umehara for their helpful secretarial assistance. The authors also wish to thank the staff of the Animal Care Company (Tokyo, Japan) for their excellent assistance in the maintenance of mice. This study was partly supported by the National Institute for Environmental Studies (1115AA082; 1315AT001 KN), and Grant-in-Aid for Scientific Research (B) (no. 23390166, 26293154, KN) from the Ministry of Education, Culture, Sports, Science and Technology of Japan.

References

Aiken CE, Ozanne SE. 2014. Transgenerational developmental programming. *Hum. Reprod. Update* **20**: 63–75.

Anway MD, Cupp AS, Uzumcu M, Skinner MK. 2005. Epigenetic transgenerational actions of endocrine disruptors and male fertility. *Science* **308**: 1466–1469.

Barber R, Plumb MA, Boulton E, Roux I, Dubrova Y. 2002. Elevated mutation rates in the germ line of first- and second-generation offspring of irradiated male mice. *Proc. Natl. Acad. Sci. U. S. A.* **99**: 6877–6882.

Devesa V, Adair BM, Liu J, Waalkes MP, Diwan BA, Styblo M, Thomas DJ. 2006. Arsenicals in maternal and fetal mouse tissues after gestational exposure to arsenite. *Toxicology* **224**: 147–155.

Guerrero-Bosagna C, Skinner MK. 2012. Environmentally induced epigenetic transgenerational inheritance of phenotype and disease. *Mol. Cell. Endocrinol.* **354**: 3–8.

Harada T, Enomoto A, Boorman GA, Maronpot RR. 1999. Liver and gallbladder. In *Pathology of the Mouse*, Maronpot RR, Boorman GA, Gaul BW (eds). Cache River Express: St. Louis, MO; 119–183.

Hughes MF, Beck BD, Chen Y, Lewis AS, Thomas DJ. 2011. Arsenic exposure and toxicology: a historical perspective. *Toxicol. Sci.* **123**: 305–332.

Klein CB, Leszczynska J, Hickey C, Rossman TG. 2007. Further evidence against a direct genotoxic mode of action for arsenic-induced cancer. *Toxicol. Appl. Pharmacol.* **222**: 289–297.

Köhle C, Schwarz M, Bock KW. 2008. Promotion of hepatocarcinogenesis in humans and animal models. *Arch. Toxicol.* **82**: 623–631.

Maronpot RR, Fox T, Malarkey DE, Goldsworthy TL. 1995. Mutations in the ras proto-oncogene: clues to etiology and molecular pathogenesis of mouse liver tumors. *Toxicology* **101**: 125–156.

Mohamed el-SA, Song WH, Oh SA, Park YJ, You YA, Lee S, Choi JY, Kim YJ, Jo I, Pang MG. 2010. The transgenerational impact of benzo(a)pyrene on murine male fertility. *Hum. Reprod.* **25**: 2427–2433.

Nohara K, Ao K, Miyamoto Y, Ito T, Suzuki T, Toyoshiba H, Tohyama C. 2006. Comparison of the 2,3,7,8-tetrachlorodibenzo-p-dioxin (TCDD)-induced CYP1A1 gene expression profile in lymphocytes from mice, rats, and humans: most potent induction in humans. *Toxicology* **225**: 204–213.

Nohara K, Tateishi Y, Suzuki T, Okamura K, Murai H, Takumi S, Maekawa F, Nishimura N, Kobori M, Ito T. 2012. Late-onset increases in oxidative stress and other tumorigenic activities and tumors with a Ha-ras mutation in the liver of adult male C3H mice gestationally exposed to arsenic. *Toxicol. Sci.* **129**: 293–304.

Ogino S, Kawasaki T, Brahmandam M, Yan L, Cantor M, Namgyal C, Mino-Kenudson M, Lauwers GY, Loda M, Fuchs CS. 2005. Sensitive sequencing method for KRAS mutation detection by pyrosequencing. *J. Mol. Diagn.* **7**: 413–421.

Perera F, Herbstman J. 2011. Prenatal environmental exposures, epigenetics, and disease. *Reprod. Toxicol.* **31**: 363–373.

Pylayeva-Gupta Y, Grabocka E, Bar-Sagi D. 2011. RAS oncogenes: weaving a tumorigenic web. *Nat. Rev. Cancer* **11**: 761–774.

Raghow R, Yellaturu C, Deng X, Park EA, Elam MB. 2008. SREBPs: the crossroads of physiological and pathological lipid homeostasis. *Trends Endocrinol. Metab.* **19**: 65–73.

Reichard JF, Puga A. 2010. Effects of arsenic exposure on DNA methylation and epigenetic gene regulation. *Epigenomics* **2**: 87–104.

Ren X, McHale CM, Skibola CF, Smith AH, Smith MT, Zhang L. 2011. An emerging role for epigenetic dysregulation in arsenic toxicity and carcinogenesis. *Environ. Health Perspect.* **119**: 11–19.

Rossman TG. 2003. Mechanism of arsenic carcinogenesis: an integrated approach. *Mutat. Res.* **533**: 37–65.

Rossman TG, Uddin AN, Burns FJ, Bosland MC. 2002. Arsenite cocarcinogenesis: An animal model derived from genetic toxicology studies. *Environ. Health Perspect.* **110**: S749–S752.

Sasaki H, Matsui Y. 2008. Epigenetic events in mammalian germ-cell development: reprogramming and beyond. *Nat. Rev.* **9**: 129–140.

Smith AH, Marshall G, Yuan Y, Ferreccio C, Steinmaus C. 2006. Increased mortality from lung cancer and bronchiectasis in young adults after exposure to arsenic in utero and in early childhood. *Environ. Health Perspect.* **114**: 1293–1296.

Sun H, Chua MS, Yang D, Tsalenko A, Peter BJ, So S. 2008. Antibody arrays identify potential diagnostic markers of hepatocellular carcinoma. *Biomark. Insights* **3**: 1–18.

Suzuki T, Yamashita S, Ushijima T, Takumi S, Sano T, Michikawa T, Nohara K. 2013. Genome-wide analysis of DNA methylation changes induced by gestational arsenic exposure in liver tumors. *Cancer Sci.* **104**: 1575–1585.

Takumi S, Aoki Y, Sano T, Suzuki T, Nohmi T, Nohara K. 2014. *In vivo* mutagenicity of arsenite in the livers of *gpt* dalta transgenic mice. *Mutation Res.* **760**: 42–47.

Tomatis L. 1994. Transgenerational carcinogenesis: A review of the experimental and epidemiological evidence. *Jpn. J. Cancer Res.* **85**: 443–454.

Waalkes MP, Ward JM, Liu J, Diwan BA. 2003. Transplacental carcinogenicity of inorganic arsenic in the drinking water: induction of hepatic, ovarian, pulmonary, and adrenal tumors in mice. *Toxicol. Appl. Pharmacol.* **186**: 7–17.

Wendel AA, Li LO, Li Y, Cline GW, Shulman GI, Coleman RA. 2010. Glycerol-3-phosphate acyltransferase 1 deficiency in ob/ob mice diminishes hepatic steatosis but does not protect against insulin resistance or obesity. *Diabetes* **59**: 1321–1329.

Yuan Y, Marshall G, Ferreccio C, Steinmaus C, Liaw J, Bates M, Smith AH. 2010. Kidney cancer mortality: fifty-year latency patterns related to arsenic exposure. *Epidemiology* **21**: 103–108.

Ziech D, Franco R, Pappa A, Panayiotidis MI. 2011. Reactive oxygen species (ROS)-induced genetic and epigenetic alterations in human carcinogenesis. *Mutat. Res.* **711**: 167–173.

V. 化学物質リスク研究事業・班会議資料

平成 28 年 9 月 2 日開催

平成28年度厚生労働科学研究費補助金(化学物質リスク研究事業)

「発達期における統合的な遅発性神経毒性試験法の開発」

(研究課題番号:H28-化学-一般-003)

平成 28 年度 第 1 回班会議 議事次第

日時:平成 28 年 9 月 2 日(金)13 時 30 分～18 時 15 分 (13:00 開場)

場所:八重洲倶楽部 第 7 会議室

(〒104-0028 東京都中央区八重洲 2-1)

http://www.yaechika.com/access.php

議事次第:

1. はじめに (13:30～14:00)

開会の挨拶

自己紹介

2. 本研究班の進め方(諫田) (14:00～14:30)

3. 各分担研究者より報告(14:30～18:00)

4. 連絡事項(18:00～18:15)

今後のスケジュール

閉会の挨拶

以上

平成28年9月2日

平成28年度厚生労働科学研究費補助金
（化学物質リスク研究事業）

発達期における統合的な遅発性神経毒性試験法の開発

国立医薬品食品衛生研究所
薬理部
諫田　泰成

新規試験法の提案を踏まえたロードマップ

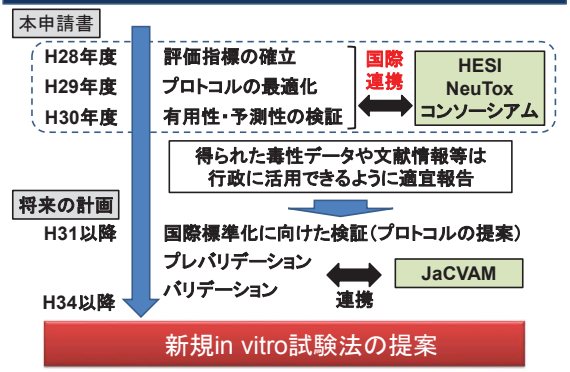

本研究班の特徴

1. in vitro試験法確立に向けて、一体となって取り組む
2. 国際的な協調を図る

これまでに確立した評価法の一覧

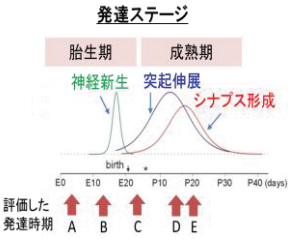

胎生・神経発達期の評価系
A: ヒトiPS細胞の神経系分化評価法
B: ラット神経堤細胞の遊送評価法
C: ラット生後初期の神経新生評価法

成熟期のシナプス機能評価系
D: ラット海馬の刺激応答評価法
E: ラット小脳の突起伸展評価法

※評価した発達時期は、左図のA～E。

※評価した陽性対照物質は、
1. バルプロ酸（VPA）
2. トリブチルスズ（TBT）
3. クロルピリホス（CPF）

同一の陽性対照物質に対して、胎生期と成熟期における作用を比較し、各発達段階において毒性評価できることを示した。

in vitro試験法の紹介

Embryo Stem cell Test

EST は 2001 年に ECVAM の諮問機関から生殖発生毒性の代替試験法として提案された。

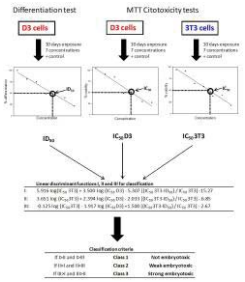

ES細胞の増殖阻害
ES細胞の分化能（拍動能）の阻害
3T3細胞の増殖阻害

各実験から算出したIC_{50}-3T3、IC_{50}-ES、ID_{50}-ESを決められた計算式で解析

被験物質の生殖発生毒性を評価

試験法の紹介

Embryo Stem cell Test

しかしながら、OECD のガイドライン化には至 らなかった。

その理由として、
①様々な毒性メカニズムをもつ多種類の被験物質の検証
②判定法の改良
③神経や骨など心筋以外の細胞への分化誘導系の導入
④代謝の評価の導入等の必要性
など。

EST法の改良

	Original EST	Hand1-Luc EST
細胞	ES-D3 細胞, balb/c 3T3 細胞	Hand1-ES 細胞
評価項目	ES-IC50 ES-ID50 3T3-IC50	ES-IC50 ES-ID50
測定指標	拍動（顕微鏡）	ルシフェラーゼ活性等
期間	10 日間（4 工程：0, 3, 5, 10 日目）	5 日間（2 工程：0, 5 日目）

TOXICOLOGICAL SCIENCES 124(2), 460–471 (2011)

予測性がまだ高いとはいえず、さらに改良する必要性

統合的なアプローチが必要

HESI Translation Biomarkers of Neurotoxicity (NeuTox) Committee

Activities and Accomplishments

2015-2016

ILSI Health and Environmental Sciences Institute

HESI Subcommittee: Pilot Study Protocol

Main objective: identify circulating biomarkers that predict central & peripheral neurotoxicity resulting from exposure to a known and well-characterized neurotoxic agent by correlating them with behavioral, imaging, morphometric and neuropathological endpoints.

- US FDA NCTR contributing rats, lab space and imaging – timeline Sept – Nov 2015.
- Prototypical compound trimethyltin (TMT).
- Time-course assessments of blood, CSF, CNS, urine and imaging (MRI, MRS) compared to traditional assessment (i.e. functional (behavioral), and histopathology)
- Dosing at 8 mg/kg
- Sample collection, behavioral analyses and MRI/MRS imaging at 2, 6, 10, 14, 21 days

Additional accomplishments

- Subteam formed to explore possible project to identify seizuregenic compounds using microelectrode array (MEA).
- Session planned at the 2015 Safety Pharmacology Society Annual Meeting in September.

Increases in Autism Spectrum Disorders in USA

Identified Prevalence of Autism Spectrum Disorders
ADDM Network 2000-2008
Combining Data from All Sites

Surveillance Year	Birth Year	Number of ADDM Sites Reporting	Prevalence per 1,000 Children (Range)	This is about 1 in X children...
2000	1992	6	6.7 (4.5-9.9)	1 in 150
2002	1994	14	6.6 (3.3-10.6)	1 in 150
2004	1996	8	8.0 (4.6-9.8)	1 in 125
2006	1998	11	9.0 (4.2-12.1)	1 in 110
2008	2000	14	11.3 (4.8-21.2)	1 in 88

(Data from CDC)

DNT testing

Developmental Neurotoxicity Testing for 2,863 Chemicals

Produced *Above 1 million pounds/year*

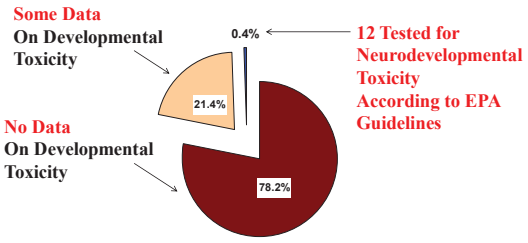

Environmental Health Perspectives, 117:17 (2009)

Current Status of DNT Testing

- Large numbers of chemicals identified for testing (e.g., pesticide) with no risk-based criteria for setting testing priorities
- Different regulatory authorities/different testing requirements with no scientific basis for flexible testing approach
- Current guideline testing is expensive, time consuming and requires large numbers of animals

Research Challenge

- Develop alternative testing approaches that are fast and efficient
  - Use *in vitro* cell culture or *in silico* models
  - Use alternative species (non-mammalian)
- Provide data for prioritization of chemicals for further testing (targeted?)
- Such an approach will:
  - Reduce costs and animal use
  - Facilitate screening of large numbers of chemicals *(high-throughput)*

Research Approach - In Vitro

- In vitro tests based on key events of CNS development
  - proliferation, differentiation, growth, synaptogenesis, myelination, apoptosis
- Endpoints amenable to high throughput testing
  - cell-based endpoints, biomarkers, molecular signaling
- Show predictive ability based on “training set” of developmental neurotoxicants

Key events of DNT at the cellular level

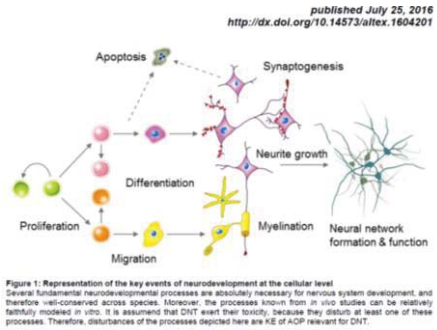

Figure 1: Representation of the key events of neurodevelopment at the cellular level
Several fundamental neurodevelopmental processes are absolutely necessary for nervous system development, and therefore well-conserved across species. Moreover, the processes known from *in vivo* studies can be relatively faithfully modeled *in vitro*. It is assumend that DNT exert their toxicity, because they disturb at least one of these processes. Therefore, disturbances of the processes depicted here are KE of AOP relevant for DNT.

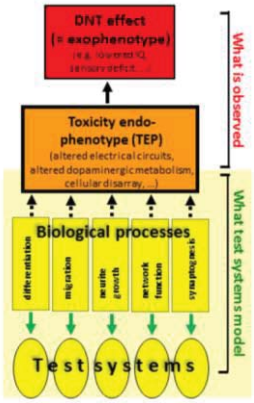

ヒトiPS細胞を用いた
発達神経毒性試験の可能性

1. Time, Cost-consuming
2. High Throughput screening
3. Species difference

in vitro test method using human iPS cells

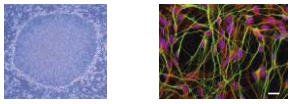

Neural differentiation by dual SMAD inhibition in human iPS cells

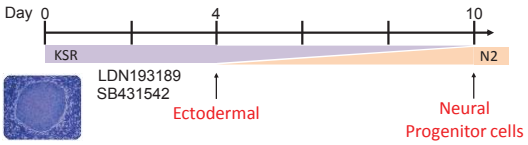

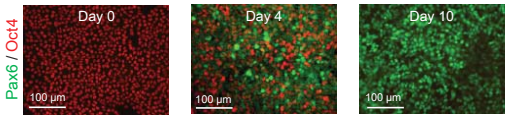

DNT compounds

2-Ethoxyethyl Acetate
Acibenzolar-S -methyl
Acrylamide
Aldicarb
Allethrin
Aluminum (cl or lactate)
Amino-nicotinamide(6-)
Aminopterin
Amphetamine(d-)
Arsenic
Aspartame
Azacytidine(5-)
Benomyl
Benzene
Bioallethrin
Bis(tri-n-butyltin)oxide
Bisphenol A
Bromodeoxyuridine(5-)
Butylated Hydroxy Anisol
Butylated hydroxytoluene
Cadmium
Caffeine
Carbamazepine
Carbaryl
Carbon monoxide
Chlordecone
Chlordiazepoxide
Chlorine dioxide
Chlorpromazine
Chlorpyrifos
Cocaine
Colcemid
Colchicine
Cypermethrin
Dexamethasone
Diamorphine hydrochloride
Diazepam
Cytosine Arabinoside
DEET
Deltamethrin
Diazinon
Dieldrin
Diethylstilbestrol
Diphenylhydantoin
Epidermal Growth Factor
Ethanol
Ethylene thiourea
Flourouracil(5-)
Fluazinam
Fluoride
Griseofulvin
Haloperiodol
Halothane
Heptachlor
Hexachlorobenzene
Hexachlorophene
Hydroxyurea
Imminodipropionitrile (IDPN)
Ketamine
Lead
Lindane
LSD
Maneb
Medroxyprogesterone
Mepivacaine
Methadone
Methanol
Methimazole
Methylparathion
Monosodium Glutamate
MPTP
Naloxone
Naltrexone
Nicotine
Methoxyethanol, 2-
Methylazoxymethanol
Methylmercury
Ozone
Paraquat
Parathion (ethyl)
PBDEs
PCBs (generic)
Penicillamine
Permethrin
Phenylacetate
Phenylalanine (d,l)
Phthalate, di-(2-ethylhexyl)
Propylthiouracil
Retinoids/vit.A/isotretinoin
Salicylate
Tebuconazole
Tellerium (salts)
Terbutaline
Thalidomide
THC
Toluene
Triamcinolone
Tributyltin chloride
Trichlorfon
Trichloroethylene
Triethyllead
Triethyltin
Trimethyltin
Trypan blue
Urethane
Valproate
Vincristine

From EPA database

Effect of TBT on neural differentiation

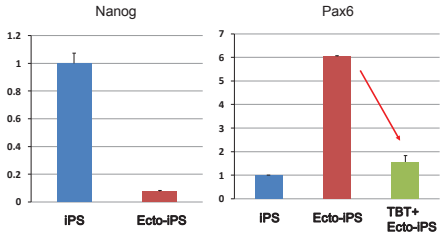

Effect of chlorpyrifos on neural differentiation

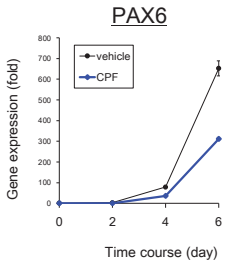

ミトコンドリア品質管理の制御

TCAサイクル
↓
膜間H⁺汲み出し・濃度勾配形成
↓
ミトコンドリア膜電位維持
↓
形態制御による品質管理

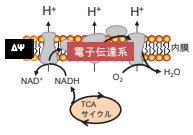

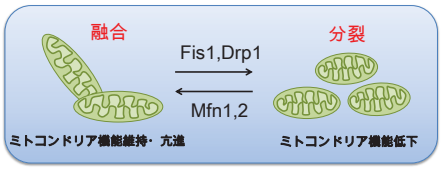

TBTによるミトコンドリア融合タンパク質の分解

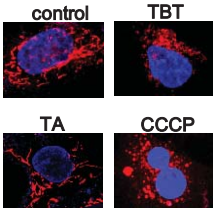

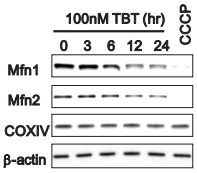

Yamada et al., Metallomics, 2015

ヒトiPS細胞のミトコンドリア形態に対するクロルピリホスの影響

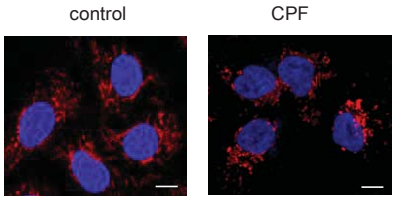

Bar = 10μm

Yamada et al., in preparation

ヒトiPS細胞の神経分化に対するMfn1の影響

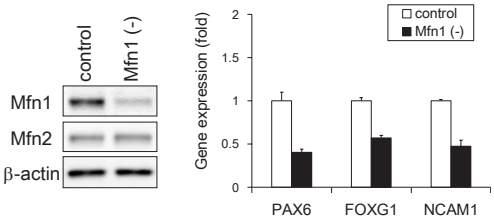

Yamada et al., in preparation

Summary

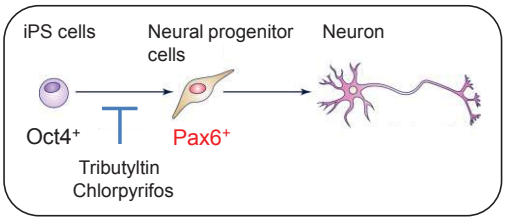

1. Capability of neural differentiation of human iPS cells can be used for assessment of chemicals with DNT.
2. This approach will reduce animal use and costs, facilitate screening of large numbers of chemicals and might provide data for prioritization of chemicals for further testing.

平成28年度厚生労働省科学研究費補助金
（化学物質リスク事業）
「発達期における統合的な遅発性神経毒性試験法の開発」
第1回　班会議　（2016年9月2日）

海馬ニューロンを用いた神経ネットワークによる評価法の開発

分担研究者：山崎　大樹（国立医薬品食品衛生研究所）
協力研究者：白尾　智明（群馬大学）

分担研究課題について

すでに開発した生後の発達神経毒性の評価手法に基づき、国際コンソーシアムとの協調、既存の毒性データとの比較により、試験法の有効性・予測性を検証し、統合的な試験法を確立する。

神経スパイクによる神経活動評価法（研究協力者：群馬大学・白尾）
白尾研より提供される凍結ラット海馬ニューロンを用いて、スパイクによるネットワーク活動評価プロトコルを整備し、再現性などを検証する。また、高スループットスクリーニング系の構築を進める。

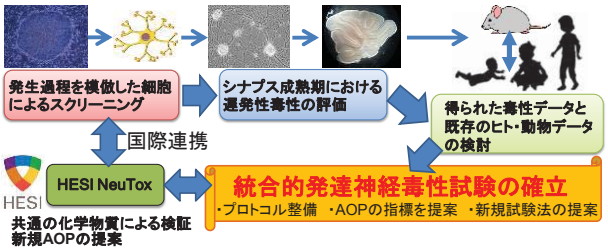

実験材料について

SKY Neuron

- 胎生18日のラット胎仔から海馬神経細胞を単離し、凍結したもの。
- 1 tubeあたり約80万個の細胞が入っている。
- 群馬大学・白尾研より提供いただいている。

21日間培養した際のMAP2とdrebrinの発現

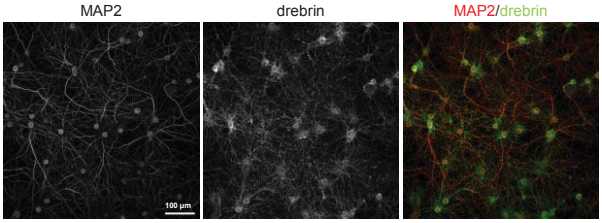

写真提供：白尾先生

SKY Neuronの解凍

1. 前日までにmestroプレートをPEIあるいはPLLでコーティング
2. 細胞の解凍1時間前に、5 μlのラミニン（plating mediumに溶解）を各ウェルの電極部分に乗せて1 hrインキュベーター内に静置
3. 3分間温浴で解凍
4. バイアル中の細胞懸濁液（1 ml）を50 mlコニカルチューブに移し、バイアルを1 ml plating mediumでリンスし、2～5sec/1滴ずつ添加
5. 2 ml plating mediumを2~3sec/1滴ずつ添加
6. 2 ml plating mediumを少しずつ添加し、ゆっくりと転倒混和・・・final vol. 6ml
7. 細胞懸濁液とトリパンブルーを1：1で混ぜ、適量を血球計算盤に添加し細胞数計測
8. 細胞懸濁液を15 mlコニカルチューブに移し細胞を遠心：↺180 x g, 5min, 室温
9. Sup捨て、タッピング3~4回してほぐす
10. カウントした生細胞数を元に懸濁する培地量を計算し、細胞を懸濁
11. 5 μlの細胞懸濁液をコートしたラミニン上に乗せる
12. プレートの周囲に乾燥を防止するための滅菌水を添加
13. 37℃, CO_2 incubate, 1 hr.
14. 各ウェルに500 μlのPlating mediumゆっくりと添加
16. Incubate, 37℃, 4days
17. Day4: Ara Cをculture mediumで溶解し培地交換を交換
19. Incubate, 37℃
20. Day7で培地交換、その後3-4日あるいは7日おきに培地交換
21. 測定

白尾研より提供されたプロトコルを改変

遠心条件の検討

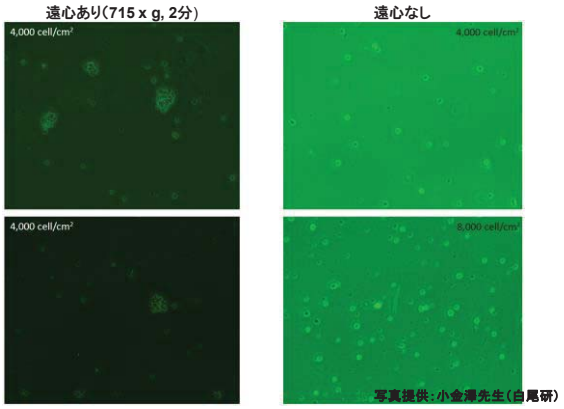

写真提供：小金澤先生（白尾研）

解凍時の細胞生存率

LOT #	細胞数	tube #	living cells	dead cells	Viability(%)	total cells
REH1004	1.3×10^6 cells/tube	3	-	-	-	-
REH1004	1.3×10^6 cells/tube	4	0.86 x 10^6 cells	0.66 x 10^6 cells	56.6	1.52 x 10^6 cells
REH1004	1.3×10^6 cells/tube	5	0.73 x 10^6 cells	0.85 x 10^6 cells	46.2	1.58 x 10^6 cells
REH1004	1.3×10^6 cells/tube	6	0.9 x 10^6 cells	0.7 x 10^6 cells	56.3	1.60 x 10^6 cells
REH1004	1.3×10^6 cells/tube	7	-	-	-	-
REH1006	1.21×10^6 cells/tube	5	1.05 x 10^6 cells	9.0 x 10^5 cells	53.8	1.95 x 10^6 cells
REH1006	1.21×10^6 cells/tube	6	2.2 x 10^6 cells	2.2 x 10^6 cells	50.0	4.4 x 10^6 cells
REH1006	1.21×10^6 cells/tube	7				
REH1006	1.21×10^6 cells/tube	8				
REH1006	1.21×10^6 cells/tube	9	1.9 x 10^6 cells	2.1 x 10^6 cells	47.5	4.0 x 10^6 cells
REH1006	1.21×10^6 cells/tube	10				
REH1009	7.13×10^5 cells/tube	4	0.78 x 10^6 cells	0.69 x 10^6 cells	53.1	1.47 x 10^6 cells
REH1009	7.13×10^5 cells/tube	5	1.56 x 10^6 cells	0.78 x 10^6 cells	66.7	2.34 x 10^6 cells
REH1009	7.13×10^5 cells/tube	6				
REH1010	8.1×10^5 cells/tube	6				
REH1010	8.1×10^5 cells/tube	7				
REH1010	8.1×10^5 cells/tube	8				

・生存率は毎回50%程度で安定している。
・白尾研での細胞数カウントとのギャップが大きい。

Maestro system 1

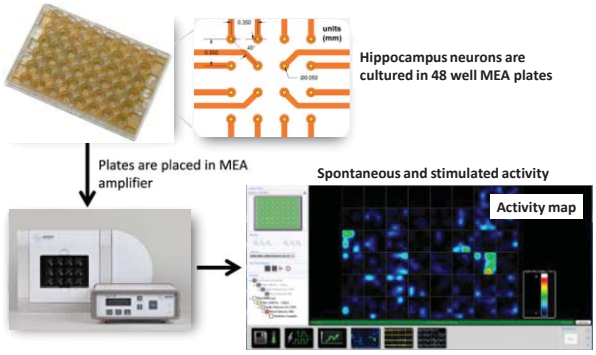

McConnell et al., *NeuroToxicology*, 2012を改変

Maestro system 2

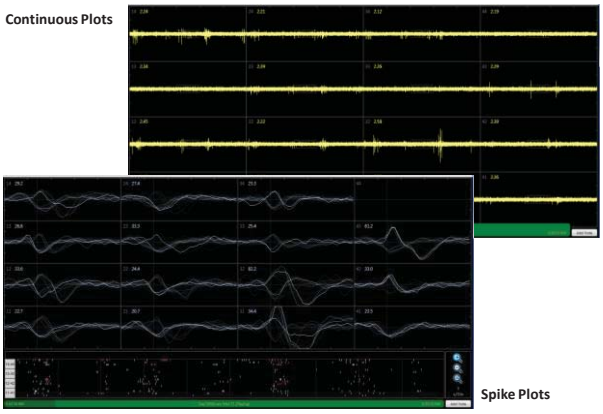

スパイクの評価系について

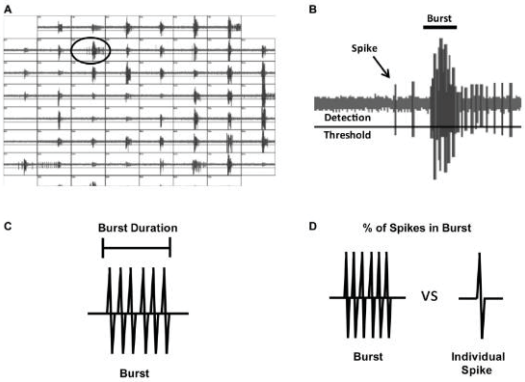

Mack et al., *NeuroToxicology*, 2014

実験のタイムスケジュール

DIV	曜日	作業項目
-3〜-1		コーティング(PLL or PEI)
Day 0	月 火	Lamininコーティング解凍・播種
4	金 土	AraC添加(0.5 or 1 μM)、(Maestro測定?)
7	月 火	Maestro測定、(培地交換)
10	木 金	Maestro測定、(培地交換)
14	月 火	Maestro測定、(培地交換)
17	木 金	Maestro測定、(培地交換)
21	月 火	Maestro測定、(培地交換)
24	木 金	Maestro測定、(培地交換)
28	月 火	Maestro測定、(培地交換)

・PLLあるいはPEIコーティングした後は乾燥させ冷蔵庫にて保存可能
・maestroプレートへ播種は生細胞数を採用している
・グリア細胞の増殖を抑制するためにAraCを添加している
・神経細胞は温度変化に対し弱いため、培養室から実験室への移動にはカルボックスを用いて温度変化を極力避けている

カルボックス

プロトコル整備

検討事項	Shafer's lab +Axion protocol (Cortical neuron)	条件① (Hippocampus)	条件② (Hippocampus)
コーティング	0.05% PEI⇒ 50 μg/ml laminin	0.05% PEI⇒ 50 μg/ml laminin	50 μg/ml PLL⇒ 50 μg/ml laminin
細胞播種密度	150,000 cells/25 μl	25,000 cells/5 μl	50,000 cells/5 μl
AraC濃度	5 μM	0.5 μM	1 μM
APV添加	無	無	有
培地交換量	半量交換	半量交換	全量交換
培地交換スケジュール	7日毎	3-4日毎	7日毎
投与方法	Acute(Day 12 to 22)	Acute	Chronic
電気刺激持続時間	ー	100 μS	200 μS
刺激電極の位置	ー	ウェルごとに変化	全ウェル同じ
検討濃度数	1濃度		
測定指標	Mean firing rate Active electrode (< 5 spikes/min) MFR on AE	Mean firing rate Active electrode(< 5 spikes/min) MFR on AE Spike counts at stimulation	

条件検討 ーコーティングー

検討事項	条件
コーティング	①PLL ②PEI
細胞播種密度	2.5x10^4 cells
AraC濃度	1 μM
APV添加	無
培地交換量	1/3量交換
培地交換	7日毎
電気刺激時間	100 μS
刺激電極	ウェルごとに変化

PEI
v
PLL

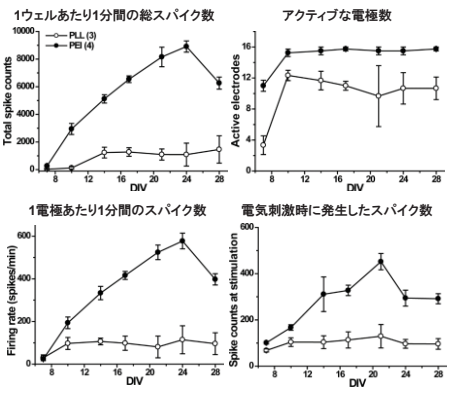

条件検討　ーコーティングー

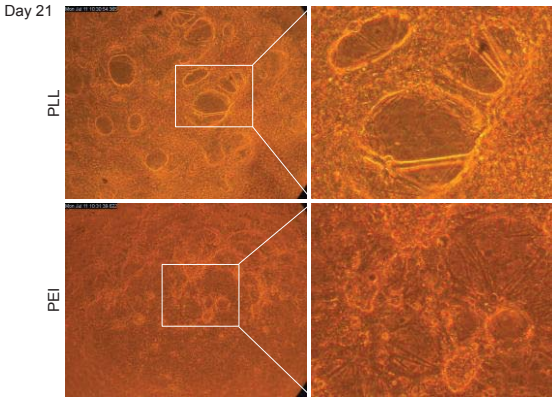

条件検討　ー細胞播種密度ー

検討事項	条件
コーティング	PEI
細胞播種密度	①2.5x10⁴ cells ②5.0x10⁴ cells
AraC濃度	0.5 μM
APV添加	無
培地交換量	1/3量交換
培地交換	7日毎
電気刺激時間	100 μS
刺激電極位置	ウェルごとに変化

2.5 x 10⁴ cells
v
5.0 x 10⁴ cells

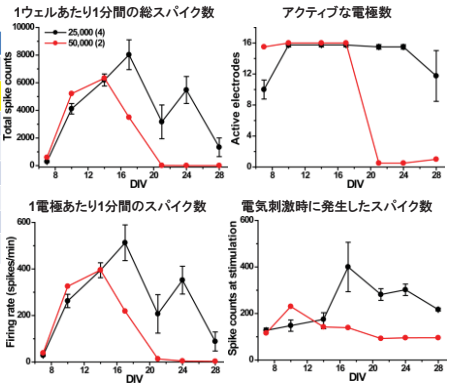

条件検討　ーAraC濃度ー

検討事項	条件
コーティング	PEI
細胞播種密度	2.5x10⁴ cells
AraC濃度	①0.5 μM ②1 μM
APV添加	無
培地交換量	全量交換
培地交換	3-4日毎
電気刺激時間	100 μS
刺激電極位置	ウェルごとに変化

0.5 μM AraC
v
1 μM AraC

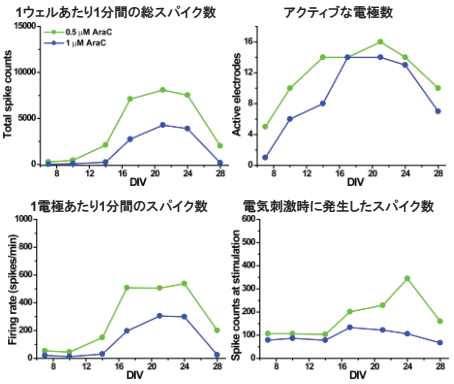

条件検討　ーAPV添加ー

検討事項	条件
コーティング	PEI
細胞播種密度	2.5x10⁴ cells
AraC濃度	0.5 μM
APV添加	①有 ②無
培地交換量	全量交換
培地交換	3-4日毎
電気刺激時間	100 μS
刺激電極位置	ウェルごとに変化

APV-
v
APV+

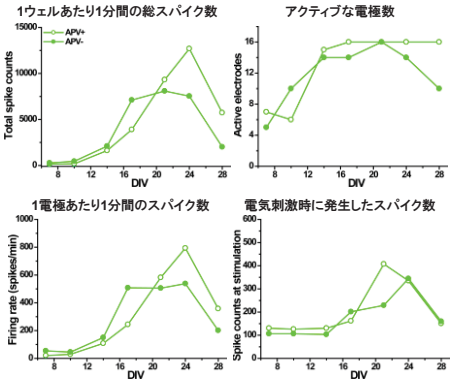

条件検討　ー培地交換量ー

検討事項	条件
コーティング	PEI
細胞播種密度	2.5x10⁴ cells
AraC濃度	0.5 μM
APV添加	無
培地交換量	①半量交換 ②全量交換
培地交換	3-4日毎
電気刺激時間	100 μS
刺激電極位置	ウェルごとに変化

半量交換
v
全量交換

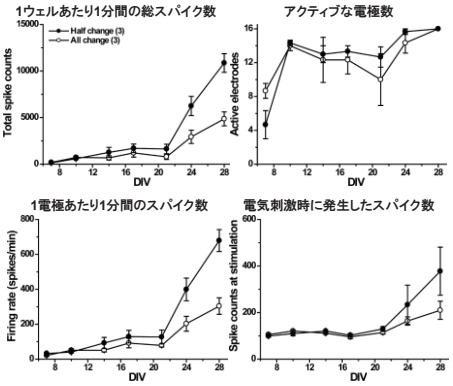

条件検討　ー電気刺激持続時間ー

検討事項	条件
コーティング	PLL
細胞播種密度	2.5 x 10⁴ cells
AraC濃度	1 μM
APV添加	無
培地交換量	1/3量交換
培地交換	7日毎
電気刺激時間	①100 μS ②200 μS
刺激電極位置	全ウェル同じ

100 μS
=
200 μS

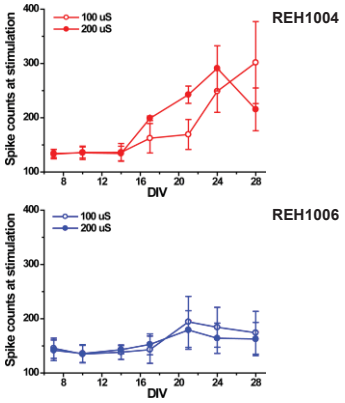

条件検討　－刺激電極位置－

検討事項	条件
コーティング	PLL
細胞播種密度	2.5 x 10^4 cells
AraC濃度	1 μM
APV添加	無
培地交換量	全量交換
培地交換	3-4日毎
電気刺激時間	100 μS
刺激電極位置	①ウェルごとに変化 ②全ウェル同じ

●：刺激電極

100us	A6				
	Day 7	Day10	Day21	Day24	Day28
Day7	97.2				
Day10	123.6	116.6			
Day14	127.8	109.2			
Day17	140.6	116.2			
Day21	174.6	211.2	188		
Day24	163.6	130.8	180.8	197.8	
Day28	144.8	191.2	245	145.8	173.2

2.5 x 10^4, PEI, APV+, 1 AraC

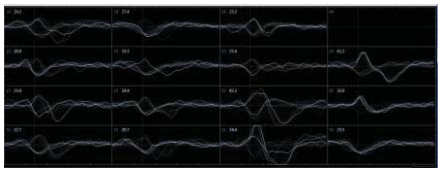

ウェルごとに変化
<
全ウェル同じ

・スパイクが出現していない電極は、細胞が乗っていないと判断されるため刺激をしても反応しないと考えられる。⇒ウェルごとに変えるべき。
・スパイク出現電極の刺激位置を変えても反応の程度は大きく変化しなかった。
⇒1度定めてしまえば、測定日毎に変える必要はないのではないか。

決定条件のまとめ

検討事項	Shafer's lab +Axion protocol (Cortical neuron)	条件① (Hippocampus)	条件② (Hippocampus)
コーティング	0.05% PEI⇒ 50 μg/ml laminin	0.05% PEI⇒ 50 μg/ml laminin	50 μg/ml PLL⇒ 50 μg/ml laminin
細胞播種密度	150,000 cells/25 μl	25,000 cells/5 μl	50,000 cells/5 μl
AraC濃度	5 μM	0.5 μM	1 μM
APV添加	無	無	有
培地交換量	半量交換	半量交換	全量交換
培地交換スケジュール	7日おき(1/2)	3-4日おき(1/2)	7日おき(1/2)
投与方法	Acute(Day14にて測定)	Acute	Chronic
電気刺激持続時間	ー	100 μS	200 μS
刺激電極の位置	ー	ウェルごとに変化	全ウェル同じ
検討濃度数	1濃度(Day14にて測定)		
測定指標	Mean firing rate Active electrode (< 5 spikes/min) MFR on AE	Mean firing rate Active electrode(< 5 spikes/min) MFR on AE Spike counts at stimulation	

今後の予定

・決定した条件にて、複数の化学物質を用いた評価を進める。

・評価する化学物質の選定・投与方法・濃度決定を行う。
（諫田班にて実績のある化学物質から実施するのが無難?）
（スライド22-23, HESI NeuTox化合物及びスライド24, Shaferらが採用している化合物リストも有り）

・maestroデータから得られる新たな指標による解析を行い、より精度・予測性の高い解析法を選定する。
（スライド25参照）

・EPAのDr. Timothy J. Shaferと実験系および実験データについての情報共有を行い、既存の毒性データとの比較を行う。
（9/30にEPAにて打ち合わせの予定）

・他分担者の結果等と統合的に理解できるよう連携して進める。

HESI NueToxにおける評価化合物

Neurotoxicants/ Dev. Neurotoxicants	Flame Retardants	Polycyclic Aromatic Hydrocarbons	Unknowns
1-methyl-4-phenylpyridinium iodide 2-Methoxyethanol 3,3'-Iminodipropionitrile 5-Fluorouracil 6-Hydroxydopamine hydrochloride 6-Propyl-2-thiouracil Acetic acid, manganese(2+) salt Acrylamide Aldicarb Bis(tributyltin)oxide Bisphenol A Captan Carbaryl Chlorpyrifos (Dursban) Colchicine Deltamethrin Di(2-ethylhexyl) phthalate Diazepam DDT Dieldrin Diethylstilbestrol Heptachlor Hexachlorophene Hydroxyurea Lindane Methyl mercuric (II) chloride n-Hexane Parathion Permethrin Phenobarbital sodium salt Rotenone Tebuconazole Tetraethylthiuram disulfide Thalidomide Toluene Valinomycin Valproic acid sodium salt	2- ethylhexyl diphenyl phosphate (EHDP) 2,2',4,4',5,5'-Hexabromodiphenyl ether 2,2',4,4'-Tetrabromodiphenyl ether 2,3,7,8-Tetrachlorodibenzo-p-dioxin 3,3',5,5'-Tetrabromobisphenol A Isodecyl diphenyl phosphate Phenol, isopropylated, phosphate (3:1) tert-Butylphenyl diphenyl phosphate Tricresyl phosphate Triphenyl phosphate Tris(2-chloroethyl) phosphate Bis(2-ethylhexyl) 3,4,5,6- tetrabromophthalate (TBPH) 2-ethylhexyl-2,3,4,5-tetrabromobenzoate (TBB) tris(2-Chloroisopropyl)phosphate, TCPP Firemaster-550	4-H-Cyclopenta[d,e,f]phenanthrene Acenaphthene Acenaphthylene Anthracene Benz[a]anthracene Benzo[a]pyrene Benzo[b]fluoranthene Benzo[e]pyrene Benzo[k]fluoranthene Benzo[g,h,i]perylene Chrysene Dibenz[a,h]anthracene Dibenz[a,c]anthracene Fluorene Naphthalene Phenanthrene Pyrene	1-ethyl-3-methylimidazolium diethylphosphate Berberine chloride Carbamic acid, butyl-, 3-iodo-2-propynyl ester Manganese, tricarbonyl[(1,2,3,4,5- eta.)- 1-methyl-2,4-cyclopentadien-1-yl]- **Other NTP Compounds** Bisphenol A Bisphenol AF Bisphenol S **Negative Controls** Acetaminophen Acetylsalicylic acid D-Glucitol L-Ascorbic acid Saccharin Sodium Salt hydrate

Neurotoxicants/Dev. Neurotoxicants in HESI NeuTox

1-methyl-4-phenylpyridinium iodide	Dieldrin
2-Methoxyethanol	Diethylstilbestrol
3,3'-Iminodipropionitrile	Heptachlor
5-Fluorouracil	Hexachlorophene
6-Hydroxydopamine hydrochloride	Hydroxyurea
6-Propyl-2-thiouracil	Lindane
Acetic acid, manganese(2+) salt	Methyl mercuric (II) chloride
Acrylamide	n-Hexane
Aldicarb	Parathion
Bis(tributyltin)oxide	Permethrin
Bisphenol A	Phenobarbital sodium salt
Captan	Rotenone
Carbaryl	Tebuconazole
Chlorpyrifos (Dursban)	Tetraethylthiuram disulfide
Colchicine	Thalidomide
Deltamethrin	Toluene
Di(2-ethylhexyl) phthalate	Valinomycin
Diazepam	Valproic acid sodium salt
DDT	

Shafer's labにて採用している化合物リスト

Details on the training set of chemicals used. 諫田班で使用実績あり　諫田班で使用実績はないが、極めて似た物質

Chemical positives	Chemical class	CAS #	Vehicle	Purity (%)	Source[c]	Previous data in MEAs
Bicuculline	$GABA_A$ antagonist	40709-69-1	DMSO/EtOH	≥90	Sigma	Gross et al. (1997)
Bifenthrin[a]	VGSC pesticide	82657-04-3	DMSO	89.0	Gift	Losa et al. (2009)
Carbaryl	AChE inhibitor	63-25-2	DMSO	99.8	Chem Service	Defranchi et al. (2011)
Chlorpyrifos oxon	AChE inhibitor	5598-15-2	DMSO	>98	Chem Service	Unpublished lab data
β-Cyfluthrin[a]	VGSC pesticide	68359-37-5	DMSO	99.2	Gift	Losa et al. (2009)
Deltamethrin	VGSC pesticide	52918-63-5	DMSO	99.5	Chem Service	Meyer et al. (2008)
Diazepam	$GABA_A$ modulator	439-14-5	DMSO	>98	Sigma	Novellino et al. (2011)
Domoic acid[b]	Glutamate R antagonist	14277-97-5	H_2O	≥90	Sigma	Hogberg et al. (2011)
Fipronil	$GABA_A$ antagonist	120068-37-3	DMSO	98.5	Chem Service	Defranchi et al. (2011)
Fluoxetine	SSRI	114247-09-5	DMSO	>98	Sigma	Novellino et al. (2011)
Imidacloprid	nAChR pesticide	138261-41-3	DMSO	99.5	Chem Service	–
Ketamine	NMDA R antagonist	31795-24-3	DMSO	>99	Sigma	Gross et al. (1995)
Lead[b]	Neurotoxic heavy metal	6080-56-4	H_2O	>98	Aldrich	–
L-Glutamate	Glutamate R agonist	19285-83-7	H_2O	≥98	Sigma	Frega et al. (2011)
Lindane	$GABA_A$ antagonist	58-89-9	DMSO	97	Aldrich	Unpublished lab data
Methylmercury[b]	Neurotoxic heavy metal	115-09-3	DMSO	93	Aldrich	van Vliet et al. (2007)
Muscimol	$GABA_A$ agonist	18174-72-6	H_2O	≥98	Sigma	Novellino et al. (2011)
Nicotine	nAChR agonist	54-11-5	DMSO	>99	Sigma	Defranchi et al. (2011)
Permethrin	VGSC pesticide	52645-53-1	DMSO	55	Chem Service	Meyer et al. (2008)
RDX[a]	$GABA_A$ antagonist	121-82-4	DMSO	>99.5	Gift	Williams et al. (2010)
Trimethyltin[b]	Neurotoxic heavy metal	56-24-6	H_2O	>95	ICN Biomedicals	Gramowski et al. (2000)
Valproic acid	Broad spectrum anticonvulsant	1069-66-5	DMSO	>98	Sigma	Gross et al. (1995)
Verapamil	VGSC blocker	152-11-4	DMSO	≥99.0	Sigma	Novellino et al. (2011)
Chemical negatives	**Chemical class**	**CAS #**	**Vehicle**	**Purity (%)**	**Source[c]**	**Reference**
Acetaminophen	Cox-2 inhibitor	103-90-2	DMSO	99	Sigma	Breier et al. (2008)
Amoxicillin	Antibiotic	26787-78-0	DMSO	N/A	Sigma	Breier et al. (2008)
Glyphosate	Herbicide	1071-83-6	H_2O	>99	Chem Service	Breier et al. (2008)
Paraquat	Herbicide	1910-42-5	H_2O	99.9	Sigma	Defranchi et al. (2011)
Saccharin	Sweetener	82385-42-0	DMSO	>99	Sigma	Breier et al. (2008)
Salicylic acid	Phytohormone	69-72-7	DMSO	≥99	Sigma	Defranchi et al. (2011)
D-Sorbitol	Sweetener	50-70-4	DMSO	>98	Sigma	Breier et al. (2008)

[a] Bifenthrin and cyfluthrin were graciously provided by Kevin Crofton at the US Environmental Protection Agency and were from the same stocks as used by Wolansky et al. (2006). RDX was provided by Dr. Larry Williams of the US Army Public Health Command.
[b] For domoic acid, methylmercury, and trimethyltin a 10 μM concentration was used. For lead a 30 μM concentration was used.
[c] Addresses: Sigma Aldrich Chemical Company, St. Louis, MO; Chem Service, West Chester, PA; ICN Biomedicals, Irvine, CA.

投与濃度：50 μM

McConnell et al., *NeuroToxicology*, 2012

新規評価指標の候補

Table 1. Features Used in Our Analysis and a Brief Description of How They Were Calculated.

Feature	Description
MFR	The MFR on each electrode was calculated. The well value was the median value of all active electrodes.
Burst rate	The number of bursts per minute on an electrode was calculated. The well value was the median value from all electrodes that exhibited bursting behavior.
Burst duration	The mean duration of all bursts on an electrode over the recording period was calculated. The well value was the median value from all electrodes that exhibited bursting behavior.
Fraction of bursting electrodes	An electrode was classified as bursting if the burst rate on the electrode was at least one per minute. The well value was the number of electrodes classified as bursting as a fraction of the total number of active electrodes on the well.
Within-burst firing rate	The mean firing rate within all bursts on an electrode was calculated. The well value was the median value from all electrodes that exhibited bursting behavior.
Percentage of spikes in bursts	The number of spikes on an electrode classified as being within bursts divided by the total number of spikes on the electrode. The well value was the median value from all electrodes that exhibited bursting behavior.
Coefficient of variation (CV) of IBI	The ratio of the standard deviation to the mean of the length of all IBIs on an electrode. The well value was the median value from all electrodes that exhibited bursting behavior.
CV of within-burst ISIs	The ratio of the standard deviation to the mean of the length of all ISIs within bursts on an electrode. The well value was the median value from all electrodes that exhibited bursting behavior.
Network spike rate	The well value was the number of network spikes on the well per minute of the recording period (see Methods section for definition of a network spike).
Network spike duration	The duration of a network spike was defined as the length of time during which the number of active electrodes on the well exceeded the threshold value (5). The well value was taken as the median duration of all network spikes on the well during the recording period.
Network spike peak	The maximum number of active electrodes during each network spike. The well value was taken as the median peak value of all network spikes on the well during the recording period.
Mean correlation	The correlation between every pairwise combination of electrodes on a well was calculated using the spike time tiling coefficient[25] with Δt = 50 ms (see Methods section for definition). The well value was the mean of the pairwise correlations between all distinct electrodes on the well.

Cotterill et al., *J Biomol Screen*, 2016

平成28年度厚生労働科学研究費補助金(化学物質リスク研究事業)
「発達期における統合的な遅発性神経毒性試験法の開発」
平成28年度 第1回班会議

研究分担者:上野　晋
(産業医大　産業生態科学研究所 職業性中毒学)
研究協力者:笛田由紀子
(産業医大　産業保健学部　作業環境計測制御学)

海馬とは

- 側頭葉の内部にある
- 記憶の司令塔
- 大脳皮質と神経連絡がある
  日常的な出来事や覚えた情報等は、海馬の中でいったんファイルされ整理整頓される。その後大脳皮質に蓄積されていく。
- 情動に関する脳内回路の一部
- ラットの海馬も記憶で重要

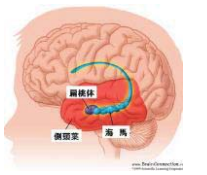

Craig Watson(山内昭雄 訳)「ワトソン神経解剖学アトラス」(1995)メディカル・サイエンス・インターナショナル
Paxinos, The Rat Nervous System Second Edition (1995) Academic Press

SCIENCE COUNCIL OF JAPAN

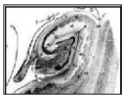

ヒトの海馬の断面図

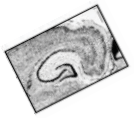

ラットの海馬の断面図

- 海馬の層構造は2つのU字が向き合った層構造(細胞密度が大きいので黒い線のように見える)。
- 海馬の層構造は、ヒトとラットでは似ている。

ラット海馬スライス標本

- 海馬は秩序だった細胞構築を持つ(ヒトと類似)
- 海馬内の神経ネットワークはすでに研究されている(下図)
  - おもな興奮性シナプス伝達物質はグルタミン酸(ヒトと類似)
  - おもな抑制性シナプス伝達物質はGABA(ヒトと類似)
  - 電気生理学的研究、薬理学的研究によく使用される

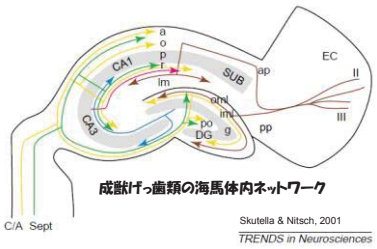

成獣げっ歯類の海馬体内ネットワーク

Skutella & Nitsch, 2001
TRENDS in Neuroscience

評価時期

生後13-18日齢のラット海馬

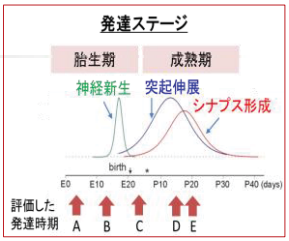

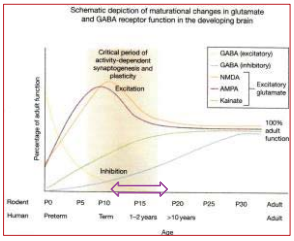

「Neural Circuit Development and Function in the Healthy and Diseased Brain」より

- シナプス形成期にあたる生後13-18日齢の脳はヒトでは生後1-2年に相当する。
- 部位による差があると思われるが、脳としては興奮系・抑制系がともに大きく変化する時期である。

研究の目的

- 胎生期に化学物質を投与した仔ラットについて、日齢13日から18日における海馬の神経回路機能を検討し、遅延性発達神経毒性の評価につながる指標を探索し、in vitro試験法での結果と合わせて新しい試験法の開発に結び付ける。

海馬神経ネットワーク：発達神経毒性評価のためのプロトコール

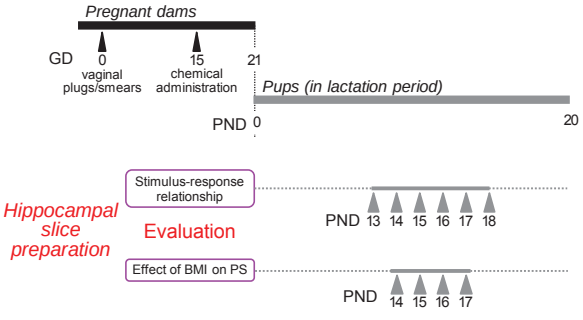

細胞外記録法の特徴

- 細胞外記録法とは、広義には神経細胞近傍に生じる微弱な電気的あるいは電気化学的変化を『電場電位』として調べる記録法。
- 目的の部位に測定電極（ガラス微小電極）を刺入し、十分に離れて電気的変動の少ない部位に基準電極（不関電極）を設けると、神経細胞の集団活動の結果生じる局所のフィールド電位を記録することができる。
- 特徴
  - ① 多くの神経細胞の電気的な変化を同時にとらえる（同期性）ことができるので、局所の電気的な性質がわかる。
  - ② 神経細胞膜を流れるイオン電流の総計を電場電位としてとらえる。海馬については生理学的な論理で解釈は可能で、薬理学的にも確認することができる。
  - ③ Intactなスライス標本を作成できれば、技術的な難易度は低い。

1個のシナプスから発生する電位や1個の神経細胞から発生する活動電位 → 神経細胞膜を流れる電流 → （細胞外）電場電位

単一神経細胞レベル　　神経細胞の集団

細胞外記録電位の生理学的解釈

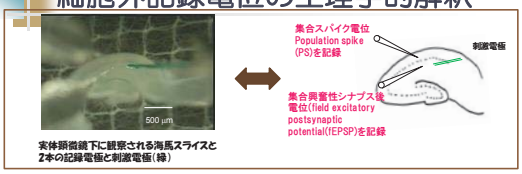

実体顕微鏡下に観察される海馬スライスと
2本の記録電極と刺激電極（緑）

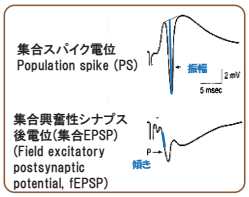

電位の解釈

1. 神経細胞からの出力特性
   - 集合スパイク電位を記録して、スパイク電位の振幅（青線）を解析する
   - 活動電位を発生している細胞の数を反映
2. 神経細胞への入力特性
   - 集合EPSPを記録して、その傾き（青線）を解析する
   - 『fEPSP slope』という
   - 興奮性シナプスの強さを反映

刺激応答性による評価

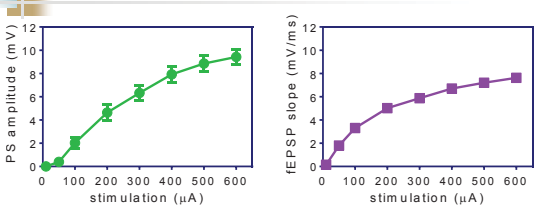

- PS振幅およびfEPEP slopeの大きさの電気刺激依存性を評価する。
- 例えば同じ電気刺激でも応答性が増大していれば、神経回路における興奮性入力（fEPSP slope）あるいは興奮性出力（PS振幅）が増強していることを示す。
- 生後13日齢から18日齢までの日齢ごとの刺激応答性、ならびにその生後発達に伴う変化を指標としている。

生後日齢毎に得られた集合EPSPとPSの刺激応答性

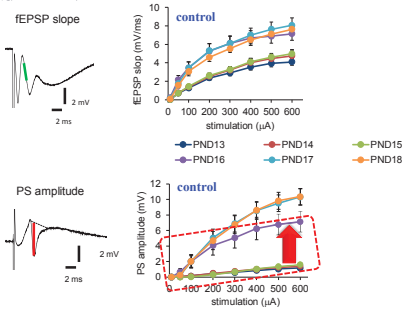

- PND15からPND16にかけて特にPS振幅の刺激応答性が一気に亢進する。

最近の知見：海馬CA1領域におけるspine densityの生後増加とその内因性神経活動依存性

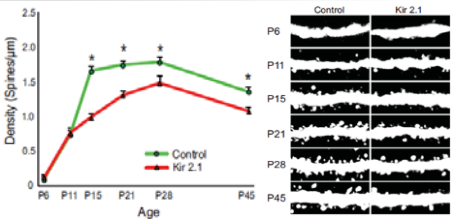

- CA1領域におけるspine densityは生後14日齢前後に急速に増加し最大となる。
- Kir2.1を過剰発現させ、内因性神経活動を抑制したマウスではdensityの増加が認められず、このdensityの増加が内因性神経活動に依存していることが示唆される。

Johnson-Venkatesh EM et al, Development 2015

内因性の興奮性活動を調節する“ambient” GABA

- “Ambient” GABAとは･･･
  - シナプス間隙から逸脱してきた神経伝達物質のspillover（溢流）
  - グリア細胞からのCa^{2+}非依存性/非小胞性のプロセスによる放出
  - トランスポーターを介した逆輸送

  などを供給源とするGABAのこと。
- この“ambient GABA”がもたらすものが“tonic inhibition”と呼ばれる持続的な抑制性調節機能であり、神経回路興奮性の調節に関与していると考えられている。
- PS振幅に対してambient GABAによる抑制性調節がどのように関与しているか、また胎生期曝露によりこの調節機能が影響を受けるのかどうかを検討することで評価指標に繋げる。

$GABA_A$受容体拮抗薬ビククリン(BMI、1μM)のPS振幅に対する影響

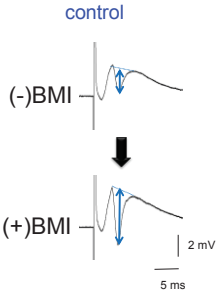

BMI比(BMI ratio)

$$= \frac{\text{(+)BMIにおけるPS振幅}}{\text{(-)BMIにおけるPS振幅}}$$

刺激応答性の亢進が出現する時期の前後で比較

PS振幅に対するBMIの効果：正常対照群の場合

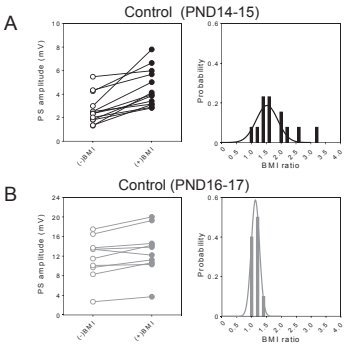

PS振幅におけるBMI比の分布

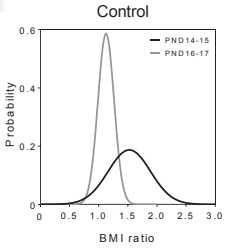

- PND14-15ではBMIによりPS振幅の増強が認められる
  → ambient GABAによる抑制性調節が関与している。
- PND16-17になるとBMIの効果はほとんど認められない。
  → ambient GABAによる抑制性調節の関与が消失している

- 刺激応答性に対してambient GABAによる抑制性調節が存在する。
- この調節機能が生後発達に伴い変化することが刺激応答性が一気に亢進することに関連している？

バルプロ酸(VPA)/トリブチルスズ(TBT)の胎生期曝露による影響

➢ **回路興奮性：PS振幅とfEPSP slopeにおける刺激応答性を指標とする評価**

評価プロトコール

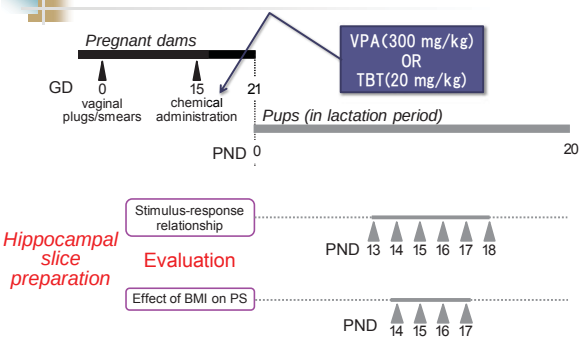

海馬スライス標本作成と誘発電位の指標

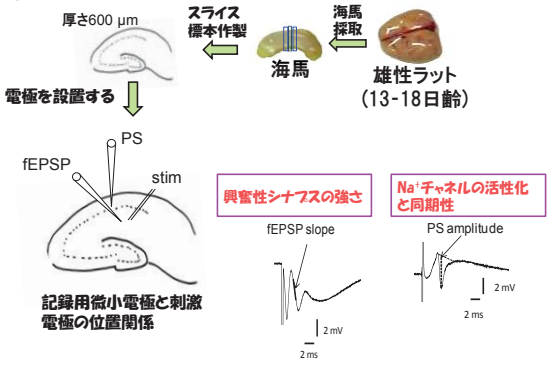

生後日齢毎に得られた集合EPSPと集合スパイク電位(PS)の刺激応答性：VPA

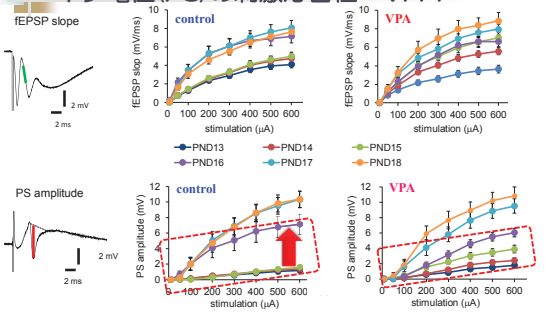

- 対照群ではPND15からPND16にかけて特にPS振幅の刺激応答性が一気に亢進した。
- しかしながらVPA群ではPND14からPND15の時期にかけて刺激応答性の亢進が徐々に出現し始めた。

VPA胎生期曝露における刺激応答性の発達に伴う変化

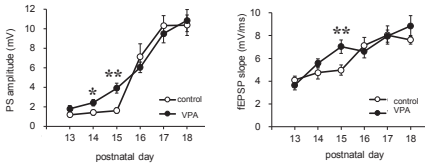

- 刺激電流600μAにおけるPS振幅とfEPSP slopeを、生後13日齢から18日齢にわたる変化として再度グラフ化し、対照群と比較した。
- VPA群のPS振幅では生後14日齢と15日齢で、fEPSP slopeでは生後15日齢で対照群に比べ刺激応答性が有意に増大していた(*p<0.05, **p<0.01)。

生後日齢毎に得られた集合EPSPと集合スパイク電位(PS)の刺激応答性：TBT

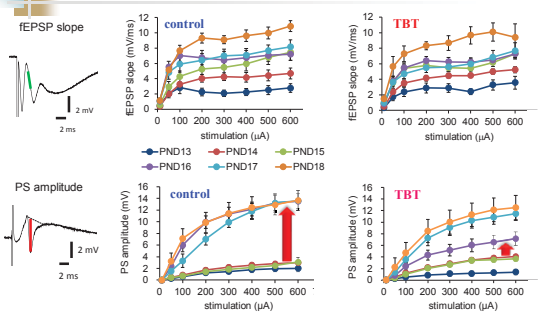

- 対照群と比較して、TBT群ではPND15からPND16に出現する刺激応答性の亢進が小さかった。

TBT胎生期曝露における刺激応答性の発達に伴う変化

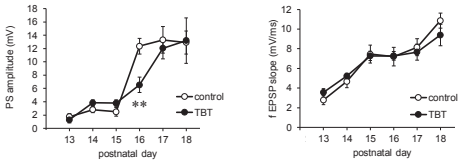

- 刺激電流600μAにおけるPS振幅とfEPSP slopeを、生後13日齢から18日齢にわたる変化として再度グラフ化し、対照群と比較した。
- TBT群ではPS振幅の方で生後16日齢における刺激応答性が低く、対照群と比べて有意差があった(**p<0.01)。

バルプロ酸(VPA)/トリブチルスズ(TBT)の胎生期曝露による影響

- 回路興奮性(PS振幅)に対する抑制性調節の生後発達を指標とする評価

$GABA_A$受容体拮抗薬ビククリン(BMI、1μM)のPS振幅に対する影響

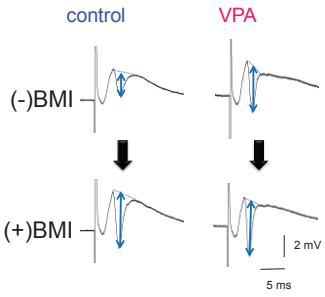

BMI比(BMI ratio)

$$= \frac{\text{(+)BMIにおけるPS振幅}}{\text{(-)BMIにおけるPS振幅}}$$

刺激応答性の亢進が出現する時期の前後で比較

- VPA胎生期曝露:
  - PND14-15と PND16-17
- TBT胎生期曝露:
  - PND14とPND16

PS振幅に対するBMIの効果：正常対照群の場合

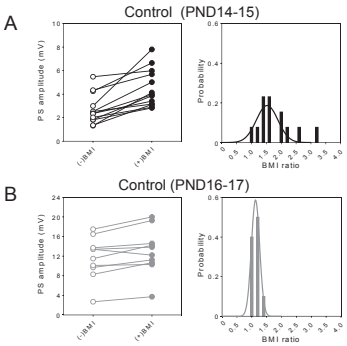

PS振幅に対するBMIの効果：VPA曝露群の場合

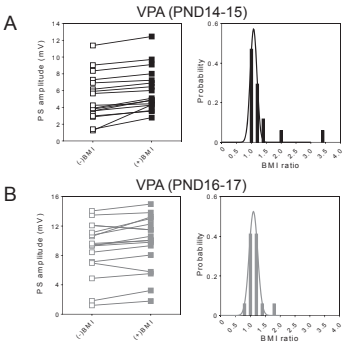

PS振幅におけるBMI比の分布：VPA

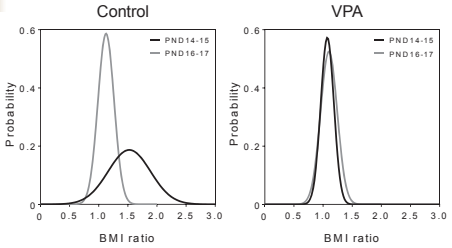

- 対照群で認められる発達に伴う分布の変化はVPA群で認められない。
- 対照群・PND16-17から得られたBMI比の分布はVPA群・PND16-17から得られた分布だけでなくPND14-15から得られた分布とほぼ一致している。

Ambient GABAによる抑制性調節の生後発達に伴う変化が**早期に出現(早熟)**している？

PS振幅に対するBMIの効果：TBT対照群の場合

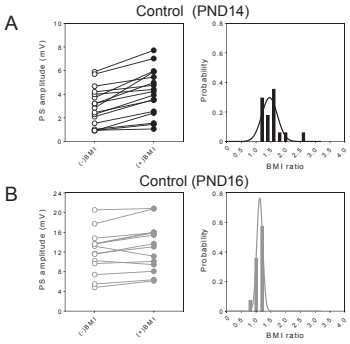

PS振幅に対するBMIの効果：TBT曝露群の場合

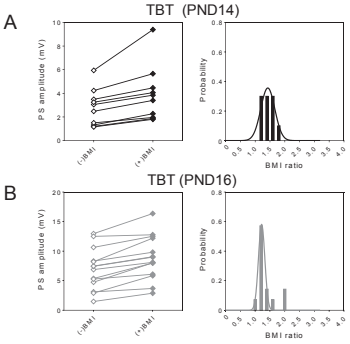

PS振幅におけるBMI比の分布：TBT

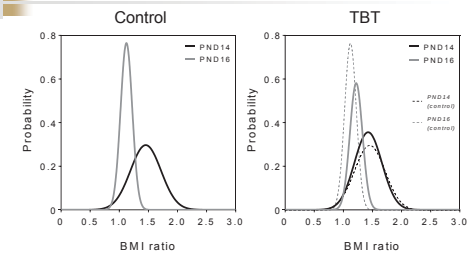

- 発達に伴うBMI比分布の変化はいずれの群でも認められる。
- TBT群・PND16の分布は対照群/TBT群・PND14の分布と対照群・PND16の分布との間に位置する。

Ambient GABAによる抑制性調節の生後発達に伴う変化が**停滞/遅延**している？

まとめ

- VPA胎生期曝露ラットでは回路興奮性、およびこれに対する抑制性調節の生後発達における早熟化
- TBT胎生期曝露ラットでは回路興奮性、およびこれに対する抑制性調節の生後発達における遅延(停滞？)

を見出した。

授乳期の海馬神経回路機能の発達を評価することが、発達神経毒性の早期スクリーニング手法の一つとして有用となる可能性が考えられた。

TOYOHASHI UNIVERSITY OF TECHNOLOGY

2016.9.2 八重洲クラブ

発達期における統合的な遅発性神経毒性試験法の開発

2016 Autumn

豊橋技術科学大学　環境・生命工学系
吉田祥子

TOYOHASHI UNIVERSITY OF TECHNOLOGY

自閉症・こころのもんだい

自閉症，　注意欠陥 多動性障害(ADHD),学習障害(LD)

自閉症スペクトラム障害(Autism Spectrum Disorder, ASD)
広 汎 性 発 達 障 害(Pervasive Developmental Disorder, PDD)

「三つ組の障害」
1. 対人関係の形成が難しい「社会性の障害」
2. ことばの発達に遅れがある「言語コミュニケーションの障害」
3. 想像力や柔軟性が乏しく、変化を嫌う「想像力の障害」

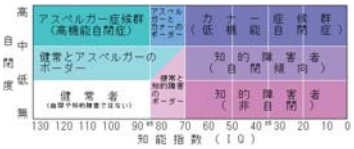

国立大学法人 豊橋技術科学大学

TOYOHASHI UNIVERSITY OF TECHNOLOGY

Contents lists available at ScienceDirect
Neuroscience and Biobehavioral Reviews
journal homepage: www.elsevier.com/locate/neubiorev

Review article

Autism spectrum disorder and attention-deficit/hyperactivity disorder in early childhood: A review of unique and shared characteristics and developmental antecedents

Janne C. Visser[a,*], Nanda N.J. Rommelse[a,b], Corina U. Greven[a,c,d], Jan K. Buitelaar[a,c]

[a] Karakter Child and Adolescent Psychiatry University Center, Nijmegen, The Netherlands
[b] Radboud University Medical Center, Donders Institute for Brain, Cognition and Behavior, Department of Psychiatry, Nijmegen, The Netherlands
[c] Radboud University Medical Center, Donders Institute for Brain, Cognition and Behavior, Department of Cognitive Neuroscience, Nijmegen, The Netherlands
[d] King's College London, Medical Research Council Social, Genetic & Developmental Psychiatry Centre, Institute of Psychiatry, Psychology & Neuroscience, London, UK

Table 1
Summary of findings on temperament in children with (traits of) ASD or ADHD.

Temperament dimension	6–11 months		1–2 years		2–3 years		3–4 years		4–5 years	
	ASD	ADHD	ASD	ADHD	ASD	ADHD	ASD	ADHD	ASD	ADHD
Approach/surgency										
Composite score	↓2,3,[ns]		↓[2]		↓[3,4] ns[12]		↓[6] ↑[5,12a]	↑[5]		↑[9]
Activity	↓2,3,[ns]	↑7,8	↓[3]	↑[8]	↑[3,4]	↑[8]			↓[6] ↓[12a]	↑[9]
Perceptual sensitivity	↓[2]	ns[7]	↑[2]	ns[7]		ns[7]				
High intensity pleasure	↓[2]							↑[10]		↑[10]
Positive affect			↓[2]							
Positive anticipation/ non-shyness [a]					↓[6]		↓[9] ↓[12a]	↑[10]	↓[12a]	↑[10]
Impulsivity										
Negative affect										
Composite score	ns[3a]		ns[3a]		ns[3a] ↑[12]		ns[3a]	↓[9,11]		↑[9]
Sadness/shyness [a] fear	↑[1]	ns[7]		ns[7]	↑[1,2,4] ns[12]	↑[8] ns[7]	↑[12]		↑[12] ↓[12]	
Anger		↑[7]		↑[8]	↑[4]	↑[8]				
Distress/discomfort reactions		↑[11]	↑[5]		↑[12]					
Effortful control										
Composite score			↓[2]		↓[3] ns[12]		ns[12]	↓[9,10]		↓[9,10]
Persistence/non-distractibility Vigilance/interest (ADHD)	↑[1] ns[3a]	↓[4,6]	ns[3a] ↓[7]	↓[8]	↑[3] ns[3]	↓[8]				
Cuddliness					↓[2]					
Low intensity pleasure					↓[4,5]					
Attention shifting		↓[8]	↓[5]	↓[8]			↓[12]		↓[12]	
Control of attention					↓[5]	↓[8]				
Inhibitory control					↓[5]	↓[8,14]	↓[12a]	↓[13]	↓[12a]	

国立大学法人 豊橋技術科学大学

TOYOHASHI UNIVERSITY OF TECHNOLOGY

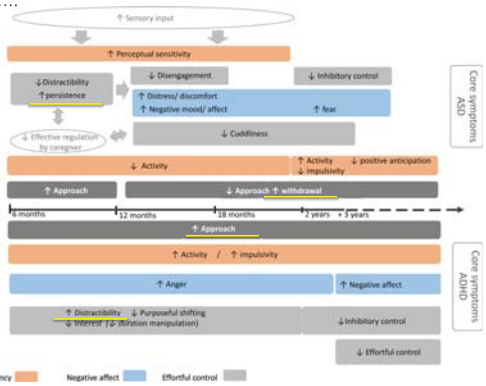

Fig. 1. Temperament traits in ASD and ADHD: ASD and ADHD share high levels of negative affect, but the underlying motivational and behavioral tendencies seem to differ, i.e. withdrawal vs approach in ASD vs ADHD, respectively. ASD and ADHD also share difficulties with control and shifting, but partly opposite behaviors seem to be involved, i.e. high persistence and low distractibility in ASD and poor sustained attention and high distractibility in ADHD.

国立大学法人 豊橋技術科学大学

TOYOHASHI UNIVERSITY OF TECHNOLOGY

高次機能に関わることから長く大脳の機能障害だと考えられてきた

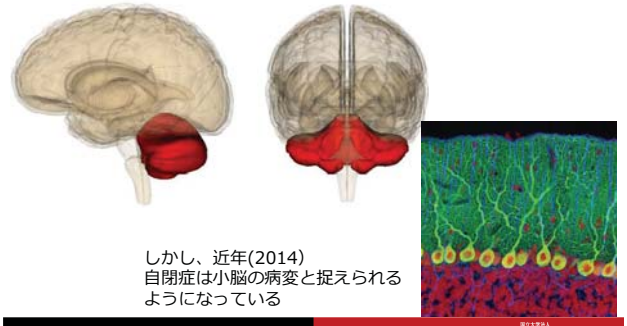

しかし、近年(2014)
自閉症は小脳の病変と捉えられる
ようになっている

国立大学法人 豊橋技術科学大学

TOYOHASHI UNIVERSITY OF TECHNOLOGY

小脳は認知の座：大脳の情報を受け取り、同様に処理する

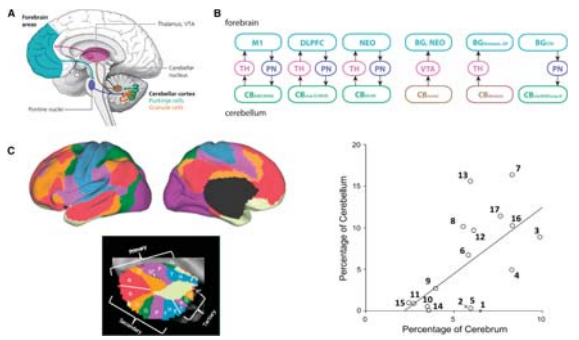

Figure 4. The Cerebellum and Forebrain Are Bidirectionally Linked in an Orderly Mapping

国立大学法人 豊橋技術科学大学

TOYOHASHI UNIVERSITY OF TECHNOLOGY

自閉症の進行（仮説）

小脳が過剰発達する
↓
神経細胞死がおこる
↓
機能障害の発症

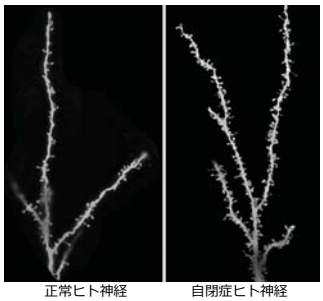

正常ヒト神経　　自閉症ヒト神経

Neurons in brains from people with autism do not undergo normal pruning during childhood and adolescence. The images show representative neurons from unaffected brains (left) and brains from autistic patients (right); the spines on the neurons indicate the location of synapses.

国立大学法人 豊橋技術科学大学

TOYOHASHI UNIVERSITY OF TECHNOLOGY

Investigation of the effects of environmental chemicals to cerebellar development

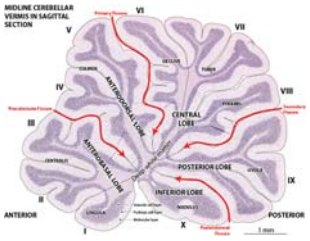

P60 rat cerebellum
from BrainDevelopmentMaps.org

The cerebellum is the center of motor coordination and motor learning, and also correlated with psychiatric disorder such as autism.

国立大学法人 豊橋技術科学大学

TOYOHASHI UNIVERSITY OF TECHNOLOGY

valproate

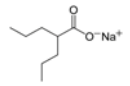

Popular antiepileptic drug
and
Major inducer of autism

VPA was administrated to E16 embryo (600mg/kg, p.o.)

Cerebellar development was checked during 2 weeks after birth.

国立大学法人 豊橋技術科学大学

TOYOHASHI UNIVERSITY OF TECHNOLOGY

Chlorpyrifos

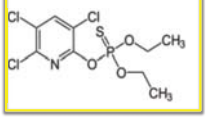

Widely used organophosphorus pesticide
and
inducer of autism

CPF was administrated to E16 embryo (10mg/kg, p.o.)

Cerebellar development was checked during 2 weeks after birth.

国立大学法人 豊橋技術科学大学

TOYOHASHI UNIVERSITY OF TECHNOLOGY

valproate

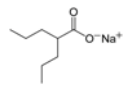

Class I HDAC inhibitor

suberoylanilide hydroxamic acid:SAHA (Vorinostat)

MS-275 (Entinostat)

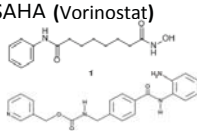

trichostatin A :TSA

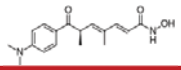

国立大学法人 豊橋技術科学大学

TOYOHASHI UNIVERSITY OF TECHNOLOGY

国立大学法人 豊橋技術科学大学

TOYOHASHI UNIVERSITY OF TECHNOLOGY

1. Alteration Purkinje cell differentiation

2. Alteration of glutamate-stimulated ATP release

3. Alteration of cerebellar gyrus

国立大学法人 豊橋技術科学大学

TOYOHASHI UNIVERSITY OF TECHNOLOGY

ブルキンエ細胞の突起進展異常

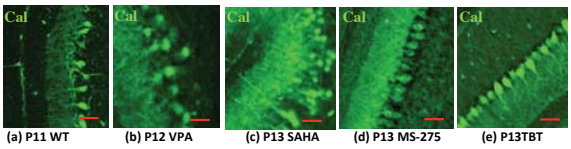

(a) P11 WT (b) P12 VPA (c) P13 SAHA (d) P13 MS-275 (e) P13TBT

Immunofluorescent antibody staining of Purkinje cell（Bar =100μm）

国立大学法人 豊橋技術科学大学

TOYOHASHI UNIVERSITY OF TECHNOLOGY

1. Alteration Purkinje cell differentiation

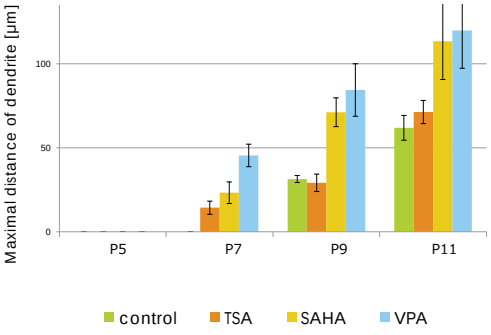

国立大学法人 豊橋技術科学大学

TOYOHASHI UNIVERSITY OF TECHNOLOGY

1. Alteration Purkinje cell differentiation

2. Alteration of glutamate-stimulated ATP release

3. Alteration of cerebellar gyrus

国立大学法人 豊橋技術科学大学

TOYOHASHI UNIVERSITY OF TECHNOLOGY

Enzyme-linked ATP detection

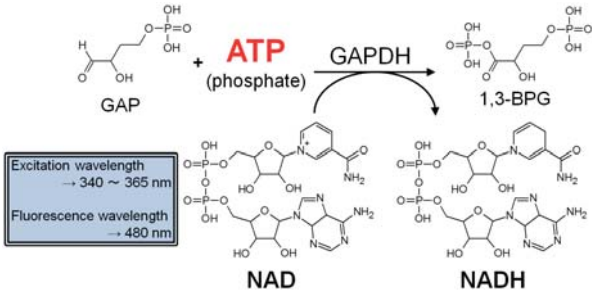

国立大学法人 豊橋技術科学大学

TOYOHASHI UNIVERSITY OF TECHNOLOGY

2. Alteration of glutamate-stimulated ATP release

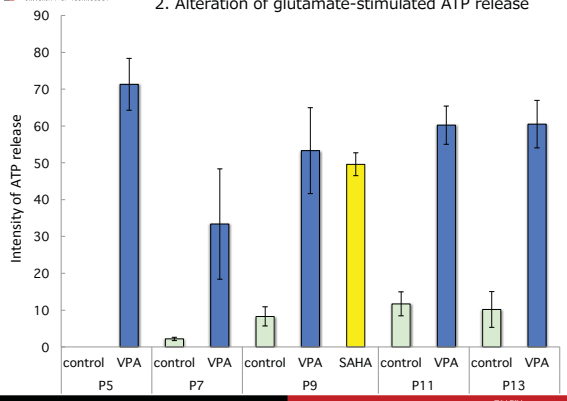

国立大学法人 豊橋技術科学大学

TOYOHASHI UNIVERSITY OF TECHNOLOGY

1. Alteration Purkinje cell differentiation

2. Alteration of glutamate-stimulated ATP release

3. Alteration of cerebellar gyrus

国立大学法人 豊橋技術科学大学

TOYOHASHI UNIVERSITY OF TECHNOLOGY

Cerebellar lobules and functions

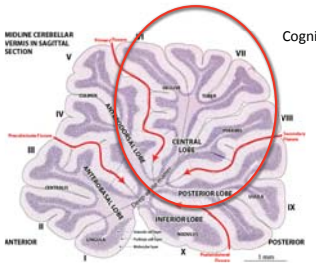

Cognition and emotion areas in cerebellum

P60 rat cerebellum
from BrainDevelopmentMaps.org

国立大学法人 豊橋技術科学大学

TOYOHASHI UNIVERSITY OF TECHNOLOGY

V/VI層における脳回形成異常

P18 Rat Cerebellum
VPA administrated

国立大学法人 豊橋技術科学大学

TOYOHASHI UNIVERSITY OF TECHNOLOGY

V/VI層における脳回形成異常

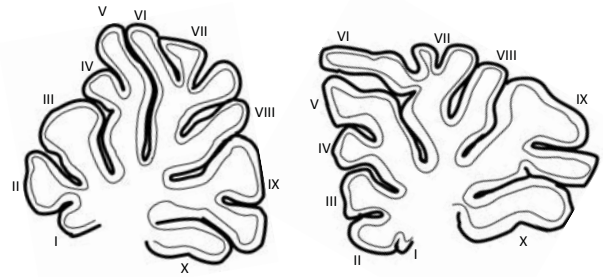

P10 control　　P10 VPA

国立大学法人 豊橋技術科学大学

TOYOHASHI UNIVERSITY OF TECHNOLOGY

V/VI層における脳回形成異常

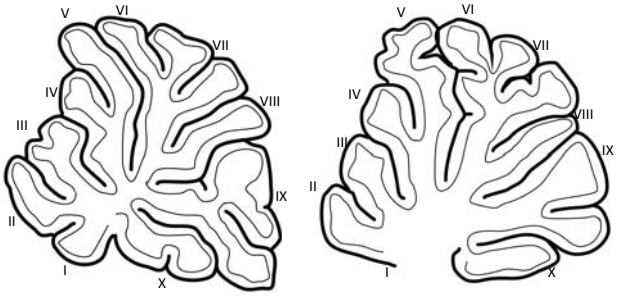

P16 control　　P16 VPA

国立大学法人 豊橋技術科学大学

TOYOHASHI UNIVERSITY OF TECHNOLOGY

VPA濃度依存性

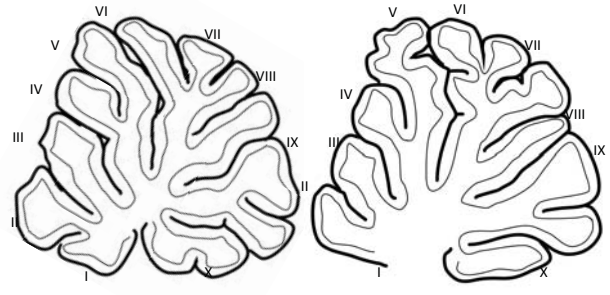

P16 VPA 200mg/kg　　P16 VPA 600mg/kg

国立大学法人 豊橋技術科学大学

TOYOHASHI UNIVERSITY OF TECHNOLOGY

VPA濃度依存性

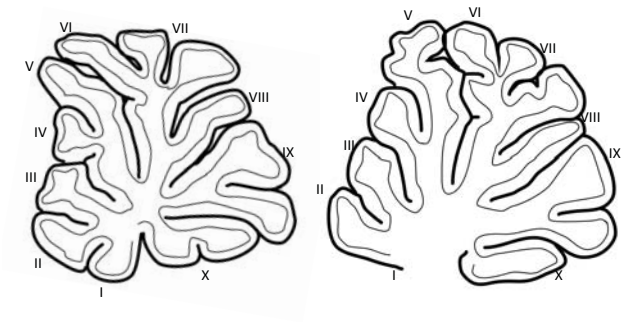

P16 VPA 400mg/kg　　P16 VPA 600mg/kg

豊橋技術科学大学

TOYOHASHI UNIVERSITY OF TECHNOLOGY

化学物質依存性

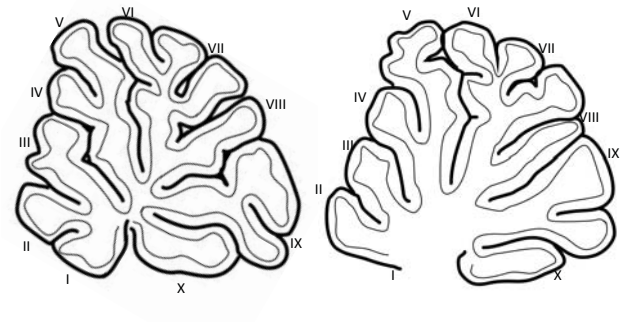

P15 CPF　　P16 VPA 600mg/kg

豊橋技術科学大学

TOYOHASHI UNIVERSITY OF TECHNOLOGY

化学物質依存性

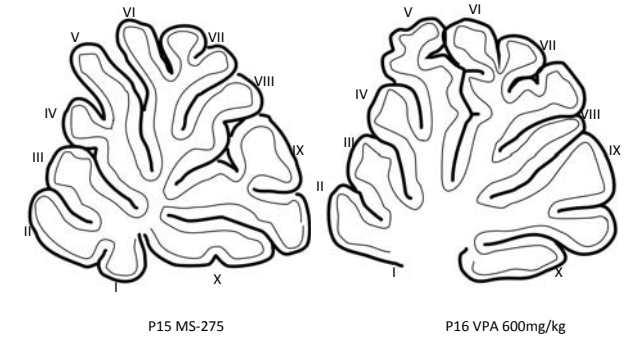

P15 MS-275　　P16 VPA 600mg/kg

豊橋技術科学大学

TOYOHASHI UNIVERSITY OF TECHNOLOGY

日齢による変化

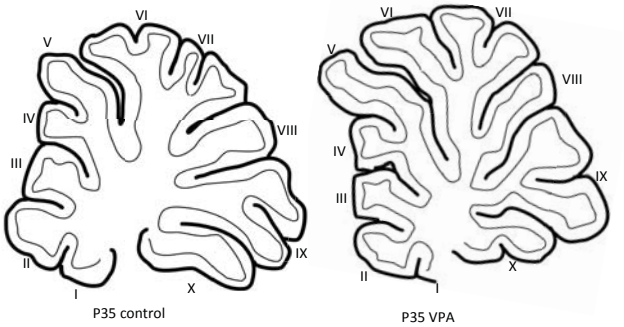

P35 control　　P35 VPA

豊橋技術科学大学

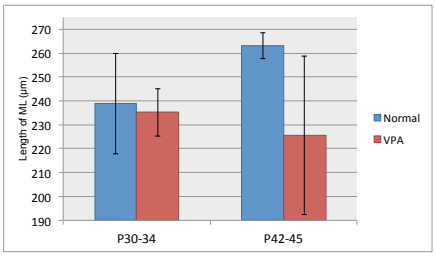

Thickness of Molecular Layer

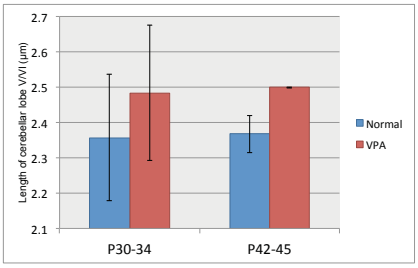

Length of Lobule V/VI

Conclusions

・自閉症誘導化学物質であるVPAで、小脳プルキンエ細胞の突起進展異常が見られた

・神経細胞の変化が小脳の神経活動の異常につながっていた

・小脳虫部V/VI層の脳回異常が観察された

・VPAの濃度依存性

・化学物質依存性　　が観察された

・これらの変化は成長により明瞭でなくなった
観察に適した時期は、生後1～3週間

さらに？

・行動への影響？

・エピジェネティックな影響？

・他の動物種での効果？

遺伝学と言えば…

優劣の法則
分離の法則
独立の法則

ビクトリア女王の家系と血友病

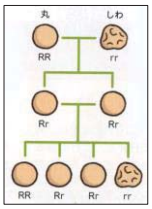

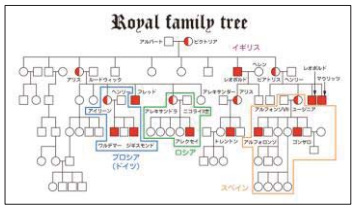

優性遺伝、劣性遺伝、浸透率、遺伝子座異質性、表現型異質性、等々、抽象的な難しい概念が・・・・.

デジタルカリオタイピングの例

正常な21番染色体　　21トリソミー

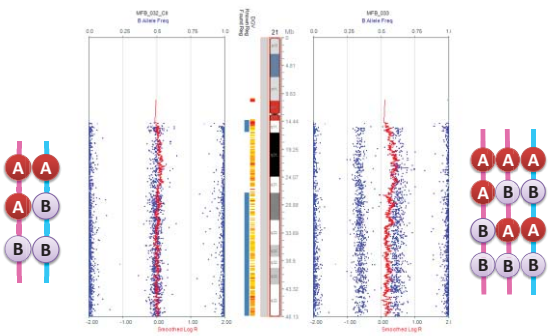

稀な初期発生異常の解析例

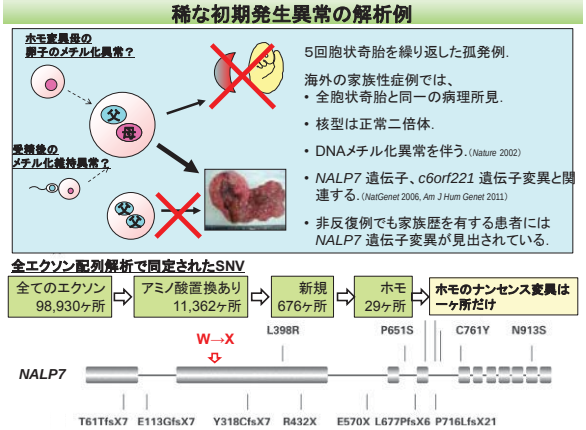

加齢の影響は母だけではない

Nature (2012) *488*, 471-475

- アイスランド78家系の全ゲノム配列解析結果.
- 一世代で平均約60個の新規変異.
- 父親の加齢とともに、子の新規変異数は増える(父20歳で15個、父40歳で65個).
- 母は、あまり加齢による変化はない(およそ15個くらい).
- 雄生殖細胞は、生涯にわたり体細胞分裂するため、エラーが蓄積する.

子への影響は、母由来の影響(胎児期の母体栄養状態や加齢)だけでなく、父の栄養状態や加齢も、エピゲノム・ゲノム双方の機構を通じて作用する.

家系サンプルでの解析が重要

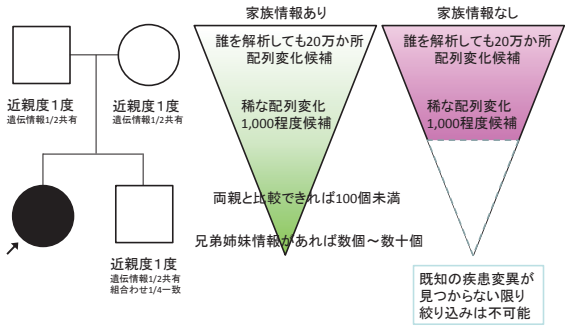

希少・未診断疾患イニシアチブ

http://nrichd.ncchd.go.jp/irud-p/

IRUD-

成育IRUD-P事務局：03－5494－8137
慶應IRUD-P事務局：03－5363－3906

国立成育医療研究センター・バイオバンク

- 臨床情報を伴う約7,000症例の既存検体
- 豊富な周産期・小児希少疾患
- 胎児期・出生時の正確な臨床情報と試料

日本人「正常」分娩集団データの有用性

「習慣流産特異的」として報告されたCNV17領域のうち8か所は、我々の独自データ日本人正常分娩歴集団でも観察されたことから、おそらく流産とは関係のないCNVと考えられた.

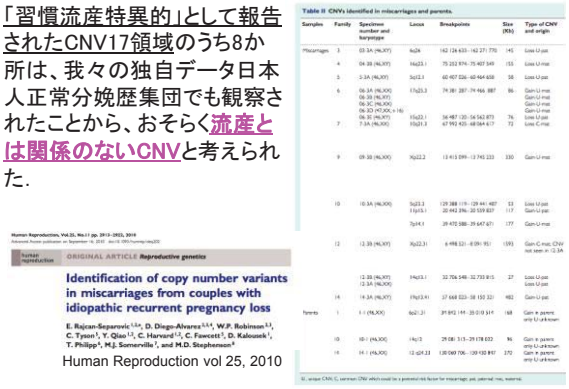

Identification of copy number variants in miscarriages from couples with idiopathic recurrent pregnancy loss

Human Reproduction vol 25, 2010

クロマチンとヒストン修飾

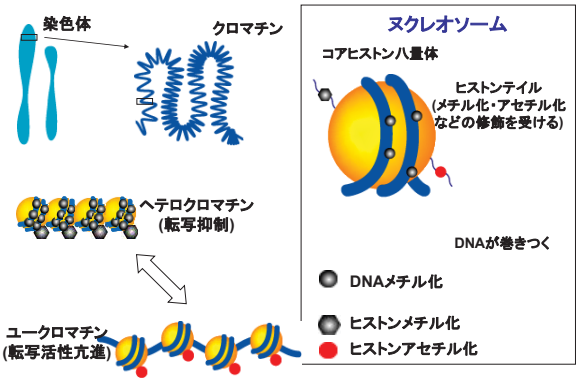

国際連携によるエピゲノムリファレンスデータ整備の試み

- 90%以上に純化した標的細胞
- DNAメチローム解析
- 6種のヒストン修飾解析
  （H3K4me3, H3K4me1, H3K27me3, H3K9me3, H3K36me3, H3K27ac）
- トランスクリプトーム、small RNA

クロマチンとヒストン修飾

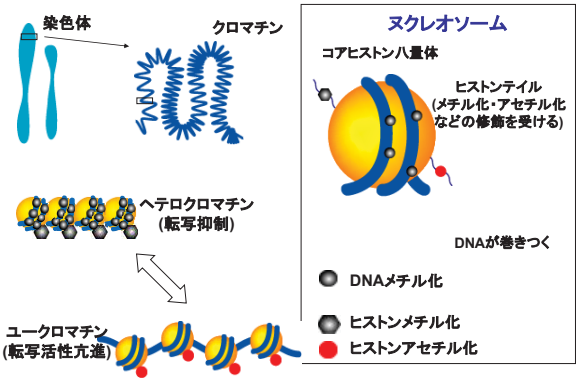

DNAのシトシンのメチル化によるエピジェネティックな遺伝子発現制御

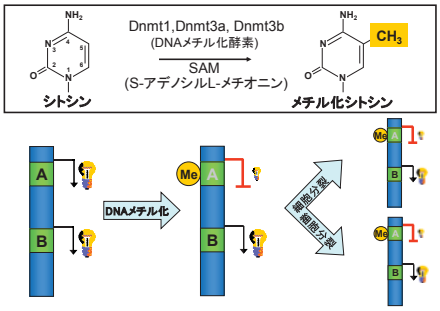

Epigenetics（エピジェネティクス）
– DNA配列を介さずに細胞分裂を経て安定に情報が「遺伝」する.

ゲノムインプリンティングの破綻と発生異常

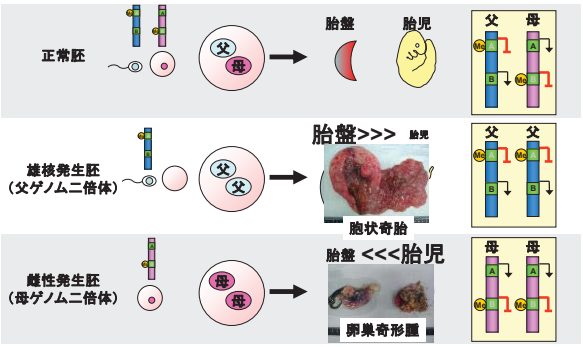

胎児期の栄養状態は一生を左右する？

Dutch famine（オランダ飢饉）の疫学研究

1944年秋から約半年間ナチスドイツによる出入港禁止措置のためオランダの一部の地域で極度の食料難に陥り1人当たり700キロカロリーまで栄養摂取が落ち込んだとされる。

この時期に胎児だった人々の数十年後を追跡調査すると・・・・

- 高血圧
- 2型糖尿病
- 高脂血症

（いわゆる生活習慣病の発症リスクが高い）

- 乳がん
- 精神疾患
- 次世代の低体重（親世代の環境適応が次世代に遺伝？）

Decreased birthweights in infants after maternal in utero exposure to the Dutch famine of 1944-1945. Lumey LH *Paediatr Perinat Epidemiol.* 1992, 6:240-53.

DOHaD学説（Developmental Origin of Health and Diseas）

DOHaD学説とは：
受精時、胎芽期、胎児期の子宮内及び乳幼児期の望ましくない環境がエピゲノム変化を起こし、それが疾病素因となり、出生後の環境との相互作用によって疾病が発症する. 生活習慣病等の多因子疾患はこの2段階を経て発症する.
DOHaD研究会ホームページより

「環境は遺伝する」

環境エピゲノム変化（モデル生物）

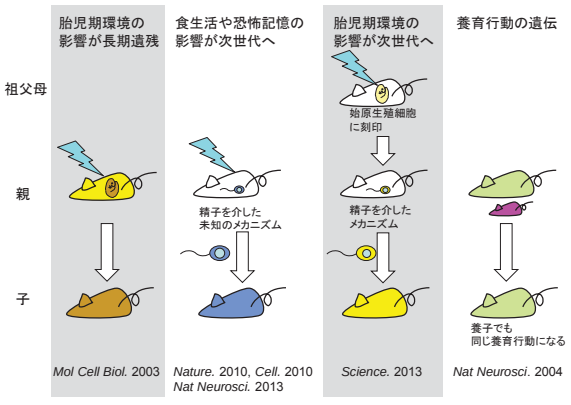

妊娠中の食事の影響

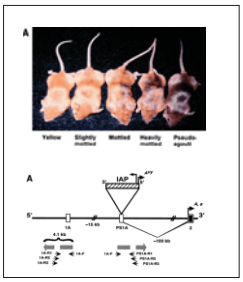

R. Waterland and R. Jirtle (2003)
Mol Cell Biol, **23**, 5293-5300.

妊娠中の食事で子供の毛色が変わる

・妊娠中、授乳中の母マウスに高メチル基質食
（高ビタミンB12、葉酸、コリン、ベタイン食）
↓
・A遺伝子上流のトランスポゾンのメチル化亢進
↓
・A遺伝子上流のトランスポゾンの転写抑制
↓
・A遺伝子本来の機能が回復
↓
・野生色マウスの数＞黄色マウスの数

妊娠中の食事の影響で、
胎児に偏ったエピゲノム情報が書き込まれ、
長期にわたり遺伝子発現に影響した例

母親の食事が胎児の遺伝情報を変化させるメカニズム

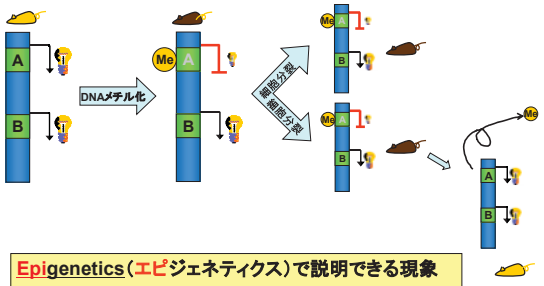

Epigenetics（エピジェネティクス）で説明できる現象
- DNA配列を介さずに情報が「遺伝」する.
- 安定であるとともに、可逆的.

環境エピゲノム変化（モデル生物）

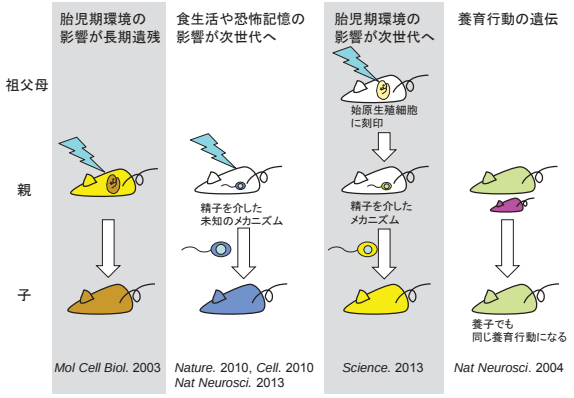

父親の若いころの食生活の影響が遺伝する？

LETTER
Chronic high-fat diet in fathers programs β-cell dysfunction in female rat offspring
Nature (2010) *467*, 963–966

Paternally Induced Transgenerational Environmental Reprogramming of Metabolic Gene Expression in Mammals
Cell (2010) *143*, 1084–1096

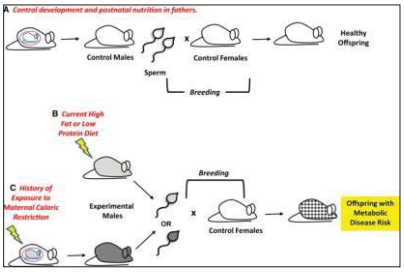

PPARα methylation
Wnt7 b methylation
glucose intolerance
reduced insulin secretion

恐怖記憶が遺伝する？？

Parental olfactory experience influences behavior and neural structure in subsequent generations
Brian G Dias[1,2] & Kerry J Ressler[1–3]
Nature Neuroscience (2013) *17*, 89-98

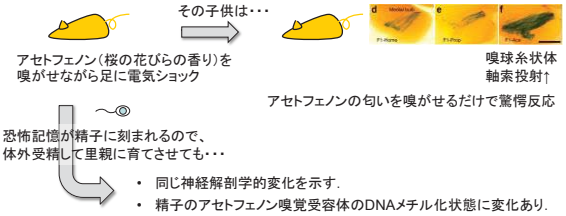

- 同じ神経解剖学的変化を示す.
- 精子のアセトフェノン嗅覚受容体のDNAメチル化状態に変化あり.

精子のエピジェネティックな変化を介した記憶の「遺伝」？

環境エピゲノム変化（モデル生物）

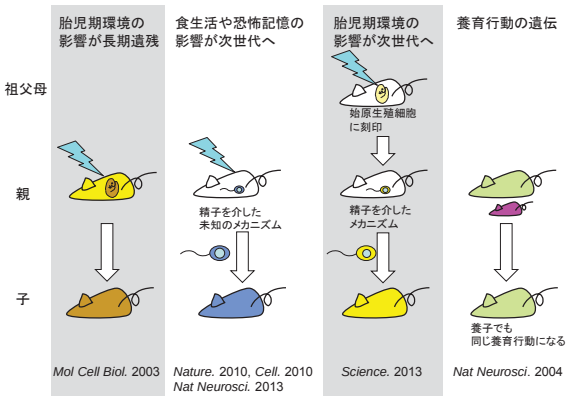

胎児期の影響が精子を介して次世代に伝わる？

RESEARCH ARTICLE

IN UTERO EFFECTS

Science (2014) ***245***, 786-793

In utero undernourishment perturbs the adult sperm methylome and intergenerational metabolism

胎児期に低栄養を経験したオスのDNAメチル化が変化し、その子供も代謝異常を呈した.

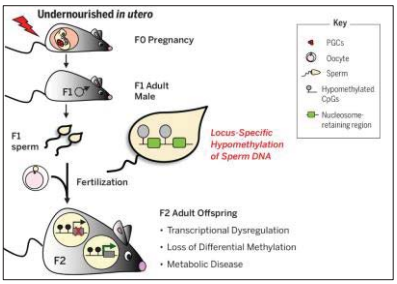

環境エピゲノム変化（モデル生物）

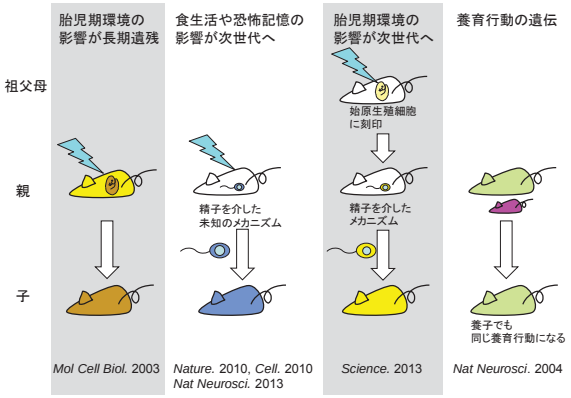

母親の養育行動が遺伝する例

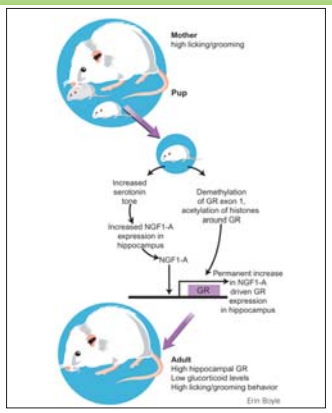

「養育行動の“非遺伝的”伝播」

Weaver IC, et al.
Nat Neurosci. 2004, 7:847-54.

周産期の分子疫学の必要性

1　14版　2011年(平成23年)12月24日　土曜日

体外受精児の健康追跡調査

厚労省 数千人を15年間

操作を加えるほど体重増

体外受精で生まれた赤ちゃんの体重は、凍結保存などで人工的な操作を加えるほど重くなることが、厚生労働省研究班の調査でわかった。遺伝子の働きを調整する仕組みに異常が出ている可能性もあり、将来、がんなどのリスクが高くならないか、15年間、数千人を対象に健康影響を調べていくことにしている。

研究班（主任研究者＝吉村泰典・慶応大教授）は2007～08年度に、体外受精により正常な過数で生まれた赤ちゃん約2万千人の出生時の体重を調べた。

その結果、受精卵をそのまま子宮に戻した場合は平均約3008グラムだったが、受精卵を凍結保存すると3302グラム、体外で培養すると3070グラム、凍結保存した後に戻した場合は3108グラムと、受精卵に操作を加えるほど重くなっていた。これらの操作は、妊娠率を高めるために行われるようになった。

この10年、生殖医療で生まれた子どもは遺伝子の働きを調整する仕組みに異常が出る「インプリンティング（刷り込み）異常症」を発症することが多い。（岡崎明子）

発生過程のエピジェネティックな制御

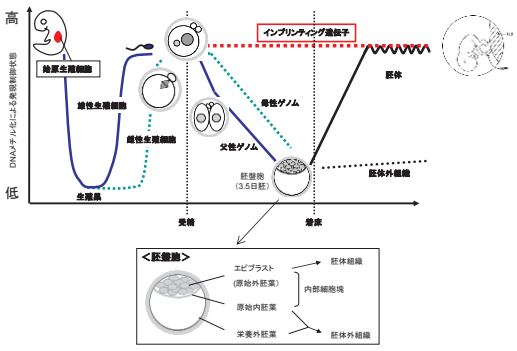

「小さく産んで大きく育てる」は誤り

Dutch famine（オランダ飢饉）の疫学研究からわかったこと

高血圧
糖尿病
高脂血症
乳がん
精神疾患
次世代の低体重

- 遺伝子に傷が入ることはあり得ない
- 細胞が数十年にわたり、胎児期の環境を憶えていた？？
- しかもそれが次の世代に伝わる？？

日本では低出生体重児が突出して増加しつつある

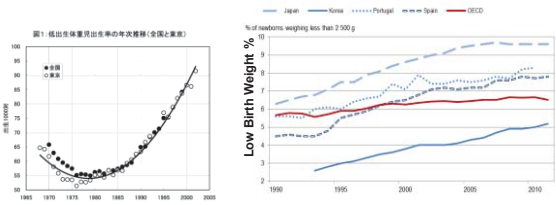

OECD Health Data 2013

もし体重減が胎児期低栄養に起因するならば、
出生児の長期予後は？　次々世代への影響は？

ヒトでも胎児期の栄養状態はエピゲノム変異を引き起こすか？

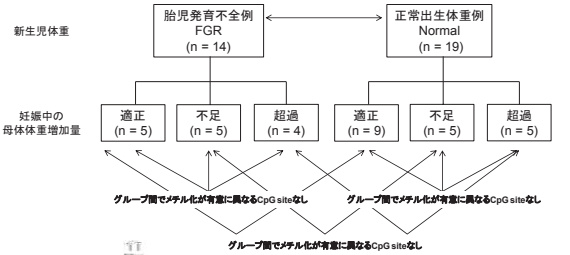

特定の領域にエピゲノム異常が起こりやすいのであれば、ケース・コントロール間で有意差が見つかるはず．しかし今回の症例群では、グループ間で特定領域のエピゲノム異常は検出されなかった．

周産期病態研究部　河合智子ら
北海道大学産婦人科　山田 崇弘先生、赤石理奈先生、水上 尚典先生

妊娠中の体重変化が胎盤DNAメチル化状態の「ばらつき」に及ぼす影響

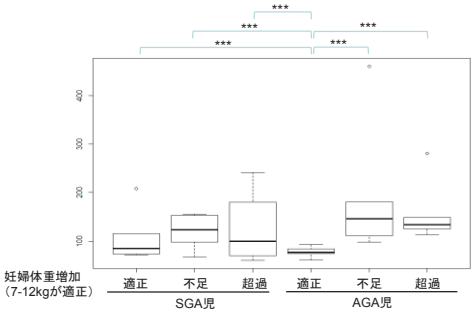

- ゲノム全領域（ほぼ全ての遺伝子領域）約45万か所のDNAメチル化アレイ解析
- 正常出生体重であっても、母体の体重増加が適正でないと、胎盤のDNAメチル化状態にばらつきが出る→潜在的なリスク群？

妊娠中の体重変化が胎盤DNAメチル化状態の「ばらつき」に及ぼす影響

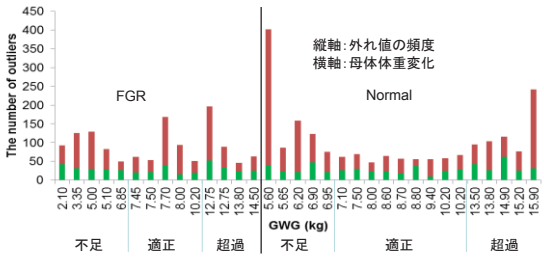

出生体重が正常であっても、母体体重増加が適正でないと、胎盤にランダムな異常DNAメチル化状態が観察される．

- ✓環境は遺伝する
- ✓DOHaD学説：胎児期新生児期の環境は、成人後の健康に影響する
- ✓生殖補助医療によるエピゲノム異常が心配されているが、はっきりしたエビデンスはないし、実験的にも懸念する情報は乏しい
- ✓出生体重が正常でも、お母さんの体重増加が十分でないと、エピゲノムの乱れが生じる